Advanced Drying Technologies

Tadeusz Kudra
Arun S. Mujumdar

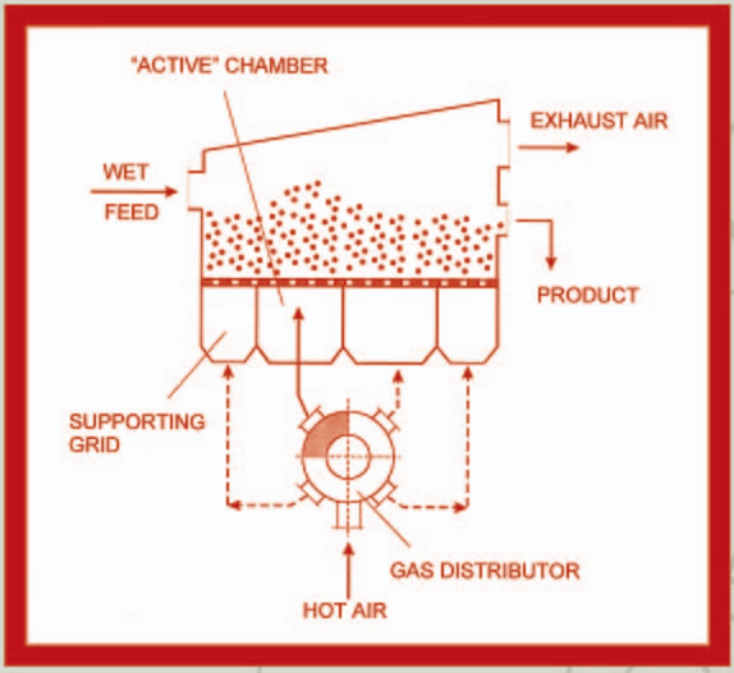

ISBN: 0-8247-9618-7

This book is printed on acid-free paper.

Headquarters
Marcel Dekker, Inc.
270 Madison Avenue, New York, NY 10016
tel: 212-696-9000; fax: 212-685-4540

Eastern Hemisphere Distribution
Marcel Dekker AG
Hutgasse 4, Postfach 812, CH-4001 Basel, Switzerland
tel: 41-61-261-8482; fax: 41-61-261-8896

World Wide Web
http://www.dekker.com

The publisher offers discounts on this book when ordered in bulk quantities. For more information, write to Special Sales/Professional Marketing at the headquarters address above.

Current printing (last digit):
10 9 8 7 6 5 4 3 2 1

PRINTED IN THE UNITED STATES OF AMERICA

Preface

Drying is a ubiquitous operation found in almost all industrial sectors, ranging from agriculture to pharmaceuticals. It is arguably the oldest, most common, most diverse, and most energy-intensive unit operation—and, coincidentally, is also one of the least understood at the microscopic level. Drying technology is an amalgamation of transport phenomena and material science since it deals not only with the removal of a liquid to produce a solid product but also with the extent to which the dried product meets the necessary quality criteria.

Until a little over two decades ago, developments in drying occurred at a remarkably slow pace. Indeed, one wondered if the field showed any visible signs of progress. Spurred by the energy crisis, consumer demand for better quality, and the initiation of the biennial International Drying Symposium series, advances on both the fundamental and applied fronts began by leaps and bounds. Literally thousands of technical papers of archival interest were published and made widely available. This had a synergistic effect of promoting further advances in the truly inter- and multidisciplinary field of drying technology.

This book is a direct outcome of the phenomenal growth in drying literature as well as new drying hardware. It is now virtually impossible for academic and industry personnel to keep abreast of the developments and evaluate

them logically. Therefore, the main objective of this book is to provide an evaluative overview of the new and emerging technologies in drying that are not readily accessible through conventional literature. We have attempted to provide a glimpse of the developments that have taken place in the past two decades and the direction toward which we see these technologies heading. We have included some well-established new technologies that are already commercialized, such as the superheated steam drying of pulp in flash or pressurized fluidized bed dryers, and laboratory curiosities, such as the displacement drying of wood (displacing water with the more volatile alcohol). Our hope is that some of the laboratory curiosities of today will lead to truly revolutionary drying technologies in the future; a systematic classification and evaluation of current technologies will hopefully lead to new ideas.

Innovation and knowledge are often called the flip sides of the same coin. It is important to know what drives innovative ideas to the marketplace. Here we also tried to look at the process of innovation and compare the innovative technologies with the more conventional ones, noting that novelty per se is not the goal of innovation.

As can be seen readily from a cursory look at the book's contents, we include dryers for all types of materials—from slurries and suspensions to continuous sheets such as paper and textiles. We cover low-tech, low-value products such as waste sludge to high-tech advanced materials, biotechnology products, and ceramics. We include production rates that range from fractions of a kilogram per hour (some pharmaceuticals) to tens of tons per hour (paper, milk, etc.). Further, we deal with drying processes that are completed in a fraction of a second (e.g., tissue paper) to several months (certain species of wood in large-dimension pieces). Thus, the scope is broad and, as the reader will find out, the range of innovations is truly breathtaking.

Finally, no new technology will see the light of day without appropriately supported R&D. We have therefore tried to identify holes in our current knowledge regarding drying and dryers that will provide new challenges to the new generation of academic and industrial researchers, eventually leading to better drying technologies.

Tadeusz Kudra
Arun S. Mujumdar

Contents

Part I

General Discussion: Conventional and Novel Drying Concepts

This part provides a general discussion of the need for new (advanced) drying technologies, objectives of drying R&D, classification and selection criteria for conventional and advanced drying technologies, as well as some thoughts on innovation and R&D needs. All of these topics are covered briefly; thus, the interested reader will need to refer to the literature cited for details. The objectives of this part of the book are to provide a concise introduction to our philosophy and to assist in using the information provided here.

1

The Need for Advanced Drying Technologies

1.1 WHY NEW DRYING TECHNOLOGIES?

Authors of a book such as this must honestly answer this fair question. It is true that we already have scores of conventional dryers with well-established records of performance for drying most materials. However, not all of these drying technologies are necessarily optimal in terms of energy consumption, quality of dried product, safety in operation, ability to control the dryer in the event of process upsets, ability to perform optimally even with large changes in throughput, ease of control, and minimal environmental impact due to emissions or combustion of fossil fuels used to provide energy for drying. Most drying technologies were developed empirically over sustained periods of time, often by small vendors of drying equipment with little access to R&D resources—human or financial. They were also designed at a time when energy and environmental considerations as well as quality demands were not very stringent. Indeed, many have been upgraded satisfactorily to meet legislative and competitive restrictions. Perhaps most are already designed and operated at their asymptotic limit of performance. However, if for any reason we wish to exceed their current performance in a cost-effective way, we need to

look for alternative technologies with a higher asymptotic limit to performance—which is necessarily below the maximum defined by thermodynamic constraints.

The majority of novel drying technologies, which evolved through a process of evolutionary incremental improvements, was built in to offset some or all of the limitations faced in operating conventional dryers. The benefits are typically also incremental rather than dramatic. Some of the new technologies may even start at a performance level below that of a conventional dryer. From this point of view it is not a fair comparison: novel versus conventional might be like comparing apples and oranges. We urge our readers not to be judgmental at this stage and rule on novel dryers simply because they do not have a significantly superior performance at this time, since not much effort has yet been devoted to a greater study of such technologies. Rather, they should study their potential and compare the predicted asymptotic limits of performance. Even on this scale some of these technologies may not turn out to be commercially successful in the long run and may disappear. However, we must give new ideas a chance—some of them definitely will emerge as victors and those choosing them will be the beneficiaries. Note that dryers have a lifetime of 30 to 40 years; a lifetime cost is the only way to really make a proper choice between conventional and new dryers. Novelty should not be the chief criterion in the selection of a dryer—it should be the last, if at all.

A conventional dryer may be admirably suited for a specific application while another may need one to look outside the conventional set of dryers. One must set the criteria for selection and then see which one meets them better and more cost effectively. There is a cost associated with the risk accompanying the technology not verified in pilot scale. Most companies shun this and are prepared to pay a higher cost for a conventional technology—the premium is often considered an insurance premium rather than a cost.

In some cases new drying technologies are sought simply because the current technologies have a limit in terms of the production rates possible. For example, today's modern newsprint machine is limited by the dryer speed. One can make the wet paper sheet faster than it can be dried cost effectively on the current multicylinder dryers. For higher speeds entirely new drying concepts are being evaluated.

In the following sections we will review two evolutionary types of advances in drying technologies, specifically the intensification of drying rates and multistaging of convective dryers.

1.2 INTENSIFICATION OF DRYING RATES

It is obvious that reduction of the size of the dryer will lead to a reduction in initial capital cost. Although this should not be a deciding factor in the selection of an individual dryer, since only 10 to 15 percent of the life-cycle cost of a direct dryer is due to the initial capital cost of the drying system, it is still an important consideration as it can reduce the space requirement, duct sizes, size of ancillary equipment, etc., as well. One must intensify the drying rates without adversely affecting product quality in order to make the equipment smaller.

Reduction of capital and operating costs of dryers clearly depends on the feasibility to enhance drying rates within the limits of product quality requirements. Higher drying rates translate into a smaller physical size of the dryer as well as the associated ancillary equipment. Generally, it is also reflected in lower running costs. An example is drying of liquid feeds in a fluidized or spouted bed of inert particles (see Chapter 4) where highly intensified heat and mass transfer results in high volumetric evaporation rates so the dryer volume can be reduced significantly as compared to the conventional spray dryer of the same throughput.

In general, the feedstock may contain both surface and internal moisture. The rate at which the surface moisture can be removed depends only on the external heat and mass transfer rates since the controlling resistance to drying rate lies outside the material being dried. Thus, enhancing external convective heat and mass transfer rates by increasing the gas velocity and gas temperature and/or reducing gas humidity will lead to increased drying rates for a purely convective (or direct) dryer. Any action that enhances external (gas-side) resistance will yield an increase in the drying rate. Thus, an increase of free-stream turbulence, application of mechanical vibration, or oscillation of the flow yields higher drying rates. Application of ultrasonic or sonic fields is also known to increase the drying rates, but the mechanisms responsible for the augmentation are different (see Chapter 13).

Above a critical temperature, commonly termed the ''inversion temperature,'' the rate of evaporation of the surface moisture is higher in superheated steam drying than in hot-air drying (see Chapter 7). This is due to the superior thermal properties of superheated steam. At lower temperatures the reduced temperature difference between the drying medium and the drying surface for superheated steam results in a lower drying rate for the latter. In purely convective air drying the surface temperature is equal to the wet bulb temperature corresponding to the air humidity and dry bulb temperature, whereas for super-

heated steam drying it is the saturation temperature of steam, i.e., 100°C for atmospheric pressure.

Enhancement of the falling rate period of drying, which requires faster transport of heat and moisture through the material, is more difficult to achieve. In general, attempts to do so result in a change in product quality. Application of an ultrasonic field can cause high-frequency pressure pulsation resulting in cavitation; the successive generation of high-pressure and low-pressure fields causes rapid vaporization and enhanced transport of the liquid through the material. The use of an electromagnetic field (e.g., microwave or radio-frequency radiation) can heat up volumetrically the polar liquid to be vaporized (e.g., water). This practically eliminates the resistance to transfer of heat into the material; the transport of moisture out through the material is also enhanced somewhat due to the higher mobility of moisture at higher temperatures as well as due to internal pressure gradient toward the material surface. The same mechanism is responsible for the marginally increased drying rates observed in superheated steam drying.

Another possible way of intensifying the drying rate involves increasing the effective interfacial areas for heat and mass transfer. For example, in an impinging stream configuration, the impingement zone generated by the collision of opposing gas–particle streams is one of high shear and high turbulence intensity (see Chapter 5). If a pasty or sludgelike wet material is dispersed in it, the turbulence field tends to deagglomerate the lumps and increase the interfacial area of drying. The drying rate is further intensified by the fact that the heat and mass transfer rates are nearly inversely proportional to the particle or droplet size, all other things being equal. When it is permissible, use of mechanical dispersers or mixers within the dryers results in more rapid drying.

An obvious means of intensifying drying rates is to increase the convective heat/mass transfer rate when feasible. Use of an impinging flow configuration rather than a parallel flow configuration can increase the evaporation rate several-fold when removing surface moisture. A gas–solid suspension flow yields higher heat transfer rate than a single-phase gas flow. For impinging gas–particle flows, the heat transfer rate is two to three times higher than for gas flow alone; the enhancement ratio depends on the flow and geometric parameters as well as particle loading in the gas. In spray drying, recirculation of fines can result in better drying rates.

Finally, since particle-to-particle heat transfer is more efficient (provided sufficient contact area) than between a gas and particles, the use of immersion drying (e.g., mixing hot inert particles with wet particles) can yield very high

TABLE 1.1 Techniques for Enhancement of Drying Rates

Drying period		
Constant rate only	Both	Falling rate period
Enhance free-stream turbulence	Increase interfacial area for heat and mass transfer	Apply ultrasonic field
Apply oscillation, vibration	Dielectric heating	Dielectric heating
Two-phase (gas–particle) drying medium	Superheated steam drying	Electrokinetic phenomena
Acoustic field of high sound pressure level		Synergistic effects

drying rates. It may be possible to use adsorbent particles so that the heat transfer medium can also effectively enhance the mass transfer potential by lowering the gas humidity concurrently (see Chapter 12).

Most of the drying-rate intensification concepts mentioned here have been tested. These are discussed in some detail in this book. It should be noted that not all ideas might be applicable in a given situation as most of these also result in changes in product quality. There is an increase in the complexity of the equipment as well. A careful technoeconomic evaluation is necessary before one may justify the use of enhancement techniques in a given application. The application areas for some of these enhancement techniques are given in Table 1.1.

1.3 MULTISTAGE DRYERS

If a material has both surface and internal moisture, i.e., both the so-called constant and falling rate periods exist in batch drying, it is logical to believe that for optimal drying the drying conditions, and even the type of dryer in some cases, should be different to remove these two distinctively different types of moisture. For cost reasons it is often preferable to choose a single dryer to accomplish the entire drying by varying the drying conditions spatially for continuous dryers and temporally for batch dryers, i.e., the dryer type is the same. Zoning of the dryers along their length is commonly used in conveyer, continuous fluidized beds, continuous vibrated beds, tunnel dryers, etc., to ensure optimal drying; this is especially true for heat-sensitive materials

that could be dried under intense conditions only while surface moisture is being removed. In the falling rate, the drying conditions must be made less intense to ensure that the material temperature remains below the critical temperature above which the material starts to deteriorate (change its color, texture, activity, solubility, etc.). However, for large production rates and for certain materials, it is cost-effective to employ two different dryer types for removal of surface and internal moistures.

Removal of surface moisture is generally a more rapid process requiring a shorter dwell time in the dryer, whereas internal moisture removal is a slower process requiring a longer dwell time and hence a larger dryer. Dryers suited for surface moisture removal are fluid bed, flash, spray dryers, etc. For longer residence times one could employ through circulation, fluid bed, packed bed (or tower), continuous tray dryers, etc. Relative to spray or flash dryers, which have residence times on the order of 1 to 45 seconds, fluid bed or vibrated bed dryers have much longer dwell times. Thus, a spray dryer can be followed with a fluid or vibro-fluidized bed dryer to reduce the overall cost of drying. Indeed, this is a well-established commercial process for drying coffee, detergents, skim milk, etc. Spray drying is an expensive drying process requiring a very large spray chamber size if the entire drying is to be accomplished in the spray dryer alone. On the other hand, if all of the surface moisture is removed along with a small part of the internal moisture in the spray chamber, one can employ a small fluid bed—even as an integral part of the conical bottom of the spray chamber—and the overall dryer becomes cost-effective. Indeed, the fluid bed (or vibrated bed) can be used to instantize (agglomerate) the fine powder produced by the spray dryer. Such hybrid dryers are presented briefly elsewhere in this book.

For successful multistage drying it is important that the wet feed material has both types of moisture in significant amounts and the drying times for the two-stage dryer concept become attractive. In some cases, the first stage may be used simply to remove the surface moisture so that the product becomes nonsticky and suitable for processing in a conventional fluid bed, for example. In some special cases such as tissue paper drying, a two-stage process with through drying as the first stage and hot-air impingement as the second stage is used to obtain softer paper although both stages have comparable drying rates and comparable drying times (in fractions of a second).

Sometimes, a long residence time is needed to accomplish some physical or chemical reactions, which are much slower than the drying kinetics, e.g., crystallization of PET (polyethylene terephthalate resin) is accomplished at a tall tower while the initial drying of surface moisture is done in a small fluid bed dryer in a two-stage drying–crystallization process.

TABLE 1.2 Selected Examples of Two-Stage Drying

Stage 1	Stage 2	Advantages	Applications
Spray dryer $t \approx$ O[a] (10) sec	Fluid bed dryer $t \approx$ O (10) min	Reduces overall size of dryer—hence better technoeconomics. Product is granulated (instantized), if necessary.	Spray fluidizer (Niro). Drying of slurries, e.g., coffee, detergents, milk, etc.
Spray dryer $t \approx$ O (10) sec	Vibrofluid bed dryer $t \approx$ O (10) min	As above.	Drying of coffee, milk, etc.
Spray dryer $t \approx$ O (10) sec	Through circulation conveyer dryer with temperature zoning	Drying at moderate conditions for heat-sensitive materials; high sugar content sticky solids.	Filtermat—commercial name—can handle drying of juices, e.g., orange.
Flash dryer $t \approx$ O (1)–O(10) sec	Fluid bed dryer $t \approx$ O (10) min	Surface moisture removed in flash dryer; internal moisture removed in long residence time fluid bed.	—
Fluid bed dryer $t \approx$ O (1) min	Tower/packed bed dryer $t \approx$ O (10) hr	Surface moisture removed fast in a fluid bed—long residence time obtained in a tall tower.	Suspension polymer.
Through dryer $t \approx$ O (0.1) sec	Impingement dryer $t \approx$ O (0.1) sec	Through dryer helps produce a structure of tissue paper that is ''soft.''	Drying of tissue paper—exceptional application for two-stage drying. The same order of residence times and drying rates in each stage.

[a] O: on the order of; t: dwell time in dryer

TABLE 1.3 Multistage Drying in the Dairy Industry: Combination of Conventional Technologies

Dryer	Energy savings	Powder characteristics
One-stage: spray dryer	Reference value	Nonagglomerated (≈0.2 mm) Wide size distribution Significant fraction of fines
Two-stage: spray dryer + internal fluid bed	≈18%	''Instantized'' agglomerated powder Small fines fraction Nondusting
Three-stage: spray dryer + fluid bed + external fluid bed	≈30%	Agglomerated and granulated Good flowability Narrow size distribution

Source: Mujumdar and Passos, 2000.

Table 1.2 lists selected commercially available two-stage drying technologies. Some of these technologies as well as three-stage dryers are covered elsewhere in this book. It is important to note that the multistage dryers represent nothing but an intelligent combination of well-established conventional technologies. However, such a combination usually offers unique advantages not possible with the component technologies separately (Table 1.3).

2

Classification and Selection Criteria: Conventional Versus Novel Technologies

2.1 INTRODUCTION

Mujumdar and Menon (1995) and Mujumdar (2000) provide detailed classification schemes for industrial dryers along with the numerous criteria that are important in making an appropriate selection. It is noted that one should select a drying system—including pre- and post-drying equipment—that can impact the choice of the dryer itself as well as its operating conditions.

Table 2.1 summarizes the key criteria often used in classifying dryers. A finer classification is also possible but is not relevant here.

Table 2.2 is a typical checklist for the selection of industrial dryers. In addition, the following information should be considered in specifying possible dryer types for a given application.

As a minimum, the following quantitative information is necessary to arrive at a suitable dryer:

Dryer throughput; mode of feedstock production (batch/continuous)
Physical, chemical, and biochemical properties of the wet feed as well as desired product specifications; expected variability in feed characteristics

TABLE 2.1 Classification of Dryers

Criterion	Types
Mode of operation	Batch
	Continuous[a]
Heat input-type	Convection,[a] conduction, radiation, electromagnetic fields, combination of heat transfer modes
	Intermittent or continuous[a]
	Adiabatic or non-adiabatic
State of material in dryer	Stationary
	Moving, agitated, dispersed
Operating pressure	Vacuum[a]
	Atmospheric
Drying medium (convection)	Air[a]
	Superheated steam
	Flue gases
Drying temperature	Below boiling temperature[a]
	Above boiling temperature
	Below freezing point
Relative motion between drying medium and drying solids	Cocurrent
	Countercurrent
	Mixed flow
Number of stages	Single[a]
	Multistage
Residence time	Short (<1 min)
	Medium (1–60 min)
	Long (>60 min)

[a] Most common in practice.

Upstream and downstream processing operations
Moisture content of the feed and product
Drying kinetics, sorption isotherms
Quality parameters (physical, chemical, biochemical)
Safety aspects, e.g., fire and explosion hazards, biohazard
Value of the product
Need for automatic control
Toxicological properties of the product
Turndown ratio, flexibility in capacity requirements
Type and cost of fuel, cost of electricity

TABLE 2.2 Typical Checklist for Selection of Industrial Dryers

Physical form of feed	Granular, particulate, sludge, crystalline, liquid, pasty, suspension, solution, continuous sheets, planks, odd shapes (small/large) Sticky, lumpy
Average throughput	kg/h (dry/wet); continuous kg per batch (dry/wet)
Expected variation in throughput (turndown ratio)	Small High
Fuel choice	Oil Gas Electricity
Pre- and post-drying operations (if any)	Preforming, backmixing, grinding, milling, screening, standardizing
For particulate feed products	Mean particle size Size distribution Particle density Bulk density Rehydration properties
Inlet/outlet moisture content	Dry basis Wet basis
Chemical/biochemical/microbiological activity	Active Inactive
Heat sensitivity	Melting point Glass transition temperature
Sorption/desorption isotherms	Shape, hysteresis Equilibrium moisture content
Drying time	Drying curves Effect of process variables
Special requirements	Material of construction Corrosion Toxicity Nonaqueous solution Flammability limits Fire hazard Color/texture/aroma requirements (if any)
Footprint of drying system	Space availability for dryer and ancillaries

Environmental regulations
Space in plant

Mujumdar (2000) presents cases where the choice of dryer is also governed by the quantity produced and the quality of the dried product.

Table 2.3 compares possible types of conventional and new drying technologies for various physical forms of wet products. This list is not all-inclusive; it is given only for illustrative purposes. One can arguably move some of the dryers from the new category to the conventional category, as their use becomes more commonplace.

As expected, there is a preference by industry to use conventional dryers due to their mature status and familiarity. Dryer vendors also prefer such technologies due to the low risk factor in design and scale-up. Also, the cost of developing new technologies may discourage offering quotes involving guar-

TABLE 2.3 Conventional vs. Innovative Drying Techniques

Feed type	Dryer type	New techniques[a]
Liquid suspension	Drum	Fluid/spouted beds of inert particles
	Spray	Spray/fluid bed combination
		Vacuum belt dryer
		Pulse combustion dryers
Paste/sludge	Spray	Spouted bed of inert particles
	Drum	Fluid bed (with solid backmixing)
	Paddle	Superheated steam dryers
Particles	Rotary	Superheated steam fluid bed dryer
	Flash	Vibrated bed
	Fluidized bed (hot air or combustion gas)	Ring dryer
		Pulsated fluid bed
		Jet-zone dryer
		Yamato rotary dryer
Continuous sheets (coated paper, paper, textiles)	Multicylinder contact dryers	Combined impingement/radiation dryers
	Impingement (air)	Combined impingement and through dryers (textiles, low basis weight paper)
		Impingement and microwave or radio-frequency

[a] New dryers do not necessarily offer better technoeconomic performance for all products.

TABLE 2.4 Fluidized Bed Dryers: Conventional vs. Innovative Concepts

Conventional	Innovative
Convective heat transfer	Convection + conduction (immersed heaters in bed)
Steady gas flow	Pulsed gas flow
Constant gas temperature	Variable gas temperature
Pneumatic fluidization	Mechanically assisted fluidization (vibration/agitation)
Used for drying of particles	Drying pastes, slurries using inert media
Air/combustion gas as drying medium	Superheated steam for fluidization/ drying
Air drag resisted by gravity	Centrifugal fluid beds (artificial gravity generated by rotation)
Single-stage/multistage fluid beds	Multistage with different dryer types
Simultaneous fluidization of entire bed	Moving fluidization zone (pulsating fluidized bed)

anteed performance. New drying technologies must offer significant advantages over existing ones to find industrial acceptance.

Legislative requirements may change this picture in the future in many parts of the world. For example, the imposition of carbon tax and severe restrictions on the emissions of greenhouse gases—particularly CO_2—will force industry to consider superheated steam drying where it is feasible. High fuel costs and high insurance rates reigning safe operation may also make steam drying more attractive in the future.

TABLE 2.5 Spouted Bed Dryers: Conventional vs. Innovative Concepts

Conventional	Innovative
Pneumatic spouting	Mechanical spouting (screw, vibration)
Single spout	Multiple spouts
Constant gas flow/continuous spouting	Variable gas flow/pulsed gas flow
Constant gas temperature	Variable gas temperature
Drying particles	Drying pastes, slurries using inert media
Spatially fixed spout	Moving spout (rotation, oscillation)
Convective drying	Combined convection and conduction
Axisymmetric	Two-dimensional, annular, hexagonal, etc.

TABLE 2.6 Conveyor (or Apron) Dryers: Conventional vs. Innovative Concepts

Conventional	Innovative
Fixed gas flow (within each zone)	Variable gas flow along length
Fixed layer thickness	Variable layer thickness along length (between zones)
Fixed (within each zone) temperature	Variable gas temperature
Hot air or flue gases as drying medium	Superheated steam as drying medium
Unidirectional gas flow	Reverse drying air flow direction between zones
Fixed bed—no mixing along bed depth	Mix or mechanically agitate bed, between fixed bed zones (e.g., vibrated or fluid bed between two fixed zones)
Air flow in bed thickness direction only	Air flow in cross-flow direction between zones of conventional axial flow (to reduce nonhomogeneity in drying rates)
Single-stage conveyor dryer	Use of flash or fluid bed to remove surface moisture followed by conveyor dryer (reduce attrition, etc.)
Continuous heating	Tempering zone between heating zones (interrupted drying when internal heat/mass transfer resistance is high)
Purely convective heating	Combined convective and microwave heating to reduce drying time
Atmospheric pressure	Vacuum or high pressure (with steam drying)
Fixed total pressure	Oscillating pressure between low and atmospheric (when convective heat is supplied)

New technologies that are likely to find acceptance over shorter time frames include combinations of well-known conventional technologies as noted earlier. Use of heat pumps, multistage operation, better control at optimum conditions, etc., will find—and indeed have already found—many applications.

The selection criteria for new technologies remain the same as those for conventional ones with the possible exception of risk management. In time the risk factor will decrease and such technologies will become mainstream.

Tables 2.4 and 2.5 compare the features of conventional and modified fluid bed and spouted bed dryers, respectively. In order to choose between them, one must know and compare the specific merits and demerits of each type of gas–solids contactor. With the new devices often the data available in the literature is obtained at laboratory scale—only in a few cases it may be pilot scale. The scale-up is, therefore, difficult and uncertain. One must objectively evaluate the potential offered by the new technology and, if justified, carry out a systematic pilot scale study. Often it may be possible to scale up the heat and mass transfer characteristics. However, the quality of the dried product is difficult to predict: actual experimental testing is therefore a necessity.

Finally, Table 2.6 lists the attributes of the conventional conveyor (or apron) dryer and compares them with some innovative concepts. Note that many of the new concepts are proposed here for the first time; they do provide some potential advantages, but they need to be tested at both laboratory and pilot scales. For a more detailed discussion, the reader is referred to Mujumdar (2000).

3

Innovation and Trends in Drying Technologies

3.1 INTRODUCTION

As an operation of prehistoric origin, drying is not normally associated with innovation. Since whatever products need to be dried currently are being dried with existing technology, it is often hard to justify the need for innovation and the concomitant need for R&D in drying and dewatering. This is reflected in the relatively low level of R&D resources that drying is able to attract as opposed to some of the exotic bioseparation processes, which on an economic scale may be an order of magnitude less significant. It is interesting to note, however, that some 250 patents—the titles of which contain the word ''dryer,'' ''drier,'' or ''drying''—are issued by the U.S. Patent Office each year. Only 10% or less of this number of U.S. patents is being issued per year in some of the other key unit operations, such as membrane separations, crystallization, adsorption, and distillation. A negative correlation appears to exist between the current level of industrial interest and the level of academic research activity, at least as measured by the number of publications in the archives of literature.

It is instructive to start this discussion by giving a definition of innovation, describing types of innovation, and then identifying the need for innova-

tion in drying as well as the features common to some of the novel drying technologies. At the outset, it is important to recognize that novelty per se is not adequate justification for embracing new technology; it must be technically superior and cost-effective compared to the current technology. In some instances the newer technologies may offer advantages over the conventional ones only for specific products or for specific rates of production.

3.2 INNOVATION: TYPES AND COMMON FEATURES

It is interesting to begin with *Webster's Dictionary*'s meaning of innovation, which is as follows:

> *Innovation*, n.:
> – The introduction of something new.
> – A new idea, method, or device.

Notice that the definition does not use adjectives like ''better,'' ''superior,'' ''improved,'' ''more cost-effective,'' ''higher quality,'' etc., to qualify as an innovation. In our vocabulary, however, we are not interested in innovation for the sake of novelty or even originality of concept but for the sake of some other positive technoeconomic attributes.

The following definition given by Howard and Guile (1992) appears to be more appropriate here: ''A process that begins with an invention, proceeds with development of the invention, and results in the introduction of the new product, process or service in the marketplace.''

To make it into a free marketplace, the innovation must be cost-effective. What are the motivating factors for innovation? For drying technologies, one or more of the following attributes may call for an innovative replacement of existing products, operations, or processes:

New product or process not made or invented heretofore
Higher capacities than current technology permits
Better quality and quality control than currently feasible
Reduced environmental impact
Safer operation
Better efficiency (resulting in lower cost)
Lower cost (overall)
Better control, more flexibility, ability to handle different products, etc.

Innovation is crucial for the survival of industries with short time scales (or life cycles) of products/processes, i.e., a short half-life (less than one year,

as in the case of most electronic and computer products). For longer half-lives (e.g., 10 to 20 years—typical of drying technologies) innovations come slowly and are less readily accepted.

The management of innovation depends on the ''stage'' it is at. Thus,

Initially, value comes from rapid commercialization.
Later, value comes from enhancing the product, process, or service.
At maturity, value may come from discontinuing and embracing newer technology. It is important to recognize when a current technology is due for replacement.

Note that management must be agreeable to discontinuing a currently viable technology in the interest of the company's future if the technology has reached its asymptotic limit of performance. This principle applies to all technologies.

Numerous studies have appeared in the literature on the fundamental aspects of the process of innovation. One of the models of the innovation process assumes a linear progress from (a) discovery of laws of nature to (b) invention to (c) development of a marketable product or process in this order. It is well known, however, that some of the truly remarkable revolutionary technologies evolved well before the fundamental physics or chemistry responsible for their success was worked out. True innovation is most likely to be a nonlinear— even chaotic—trial-and-error, serendipitous process. Therefore, it is difficult to teach innovation in a logical sense although one could presumably encourage creativity or try to remove blockages in the process of creativity.

What may be classified as innovation can represent different characteristics. Following is a list of the quality parameters of innovations in general (Howard and Guile, 1992):

Innovation establishes an entirely new product category.
Innovation is the first of its type in a product category already in existence.
Innovation represents a significant improvement in existing technology.
Innovation is a modest improvement in existing product/process.

Innovations trigger technological changes, which may be revolutionary or evolutionary. From our experience, we know that the latter are more common. They are often based on adaptive designs, have shorter gestation periods, have shorter times for market acceptance, and are typically a result of ''market-pull''—something the marketplace demands, i.e., a need exists currently for the product or process. These usually result from a linear model

of the innovation process (an intelligent modification of the dominant design is an example). Revolutionary innovations, on the other hand, are few and far between, have longer gestation periods, may have larger market resistance, and are often a result of ''technology-push,'' where the development of a new technology elsewhere prompts design of a new product or process for which market demand may have to be created. They are riskier and often require larger R&D expenditures as well as sustained marketing efforts. The time from concept to market can be very long for some new technologies. It is well known that the concept of a helicopter appeared some 500 years before the first helicopter took to the air. The idea of using superheated steam as the drying medium was well publicized over 100 years ago, yet its real commercial potential was first realized only about 50 years ago and that too not fully. In fact, it is not fully understood even today. A recent example of this long gestation period is the Condebelt drying process for high basis weight (thick grades) paperboard proposed and developed by the late Dr. Jukka Lehtinen of Valmet Oy of Finland (Lehtinen, 1998). It took a full 20 years of patient, expensive, and high-quality R&D before the process was first deployed successfully. The vision required by the management teams of such organizations must be truly farsighted to permit successful implementation of a revolutionary process.

It is natural to inquire if it is possible to predict or even estimate the best time when the marketplace requires an innovative technology or if the mature technology of the day is ripe for replacement. Foster's well-known ''S''-curve shown in Figure 3.1 (Foster, 1986), which gives a sigmoid relationship between product or process performance indicators and resources devoted to develop the corresponding technology, is a valuable tool for such tasks. When the technology matures (or is ''saturated'' in some sense), no amount of further infusion of R&D resources can enhance the performance level of that technology. When this happens (or even somewhat sooner), the time is right to look for alternate technologies—which should not be incremental improvements on the dominant design but truly new concepts—that, once developed to their full potential, will yield a performance level well above that of the current one. As proven by Foster with the help of real-world examples, the performance-versus-effort (resources) curve occurs in pairs when one technology is replaced by another. They represent discontinuity when one technology replaces another and industry moves from one S-curve onto another. As indicated in Figure 3.1, most well-established drying technologies are very close to their asymptotic performance level if they are well designed and operated under optimal conditions.

Table 3.1 lists examples of some new drying technologies that were developed via technology-push versus market-pull. In some cases, a sharp

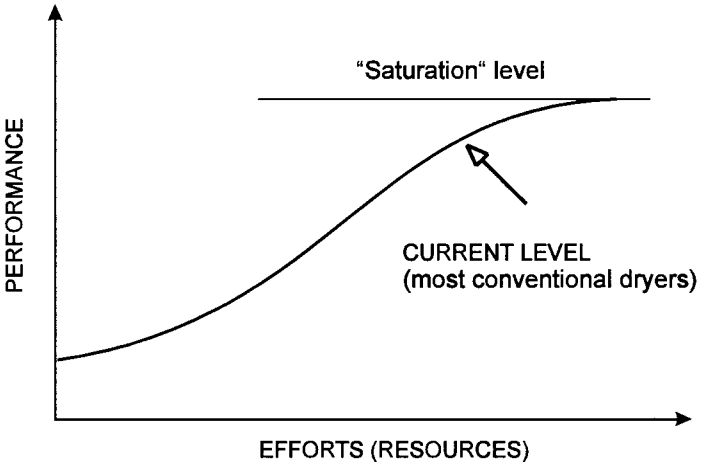

FIGURE 3.1 Foster's S-curve.

TABLE 3.1 Examples of New Drying Technologies Developed Through Technology-Push and Market-Pull

Technology-push[a]	Market-pull[b]
Microwave/RF/induction/ultrasonic drying	Superheated steam dryers—enhanced energy efficiency, better-quality product, reduced environmental impact, safety, etc.
Pulse combustion drying—PC developed for propulsion and later for combustion applications	Impulse drying/Condebelt drying of paper (also need technology-push)
Vibrating bed dryers—originally developed for solids conveying	Combined spray-fluid bed dryers—to improve economics of spray drying
Impinging streams (opposing jets)—originally developed for mixing, combustion applications	Intermittent drying—enhance efficiency

[a] Technology originally developed for other applications applied to drying.
[b] Developed to meet current or further market demand.

distribution of grouping in just two types is not possible since a ''market-pulled'' development may require a ''technology-push''to succeed.

3.3 DEVELOPMENT OF IMPROVED DRYING TECHNOLOGIES

New developments in any field may occur as a result of either an evolutionary or revolutionary process. Most developments follow the evolutionary path involving incremental improvements to offset one or more of the limitations of the contemporary technology. Such technologies are more readily accepted by industry since the risk associated with the adoption of such technologies is generally minimal and the cost-to-benefit ratio is favorable. Often the new technologies are intelligent combinations of traditional technologies necessitated by changes in the marketplace.

The following list illustrates the evolutionary developments that have occurred over the past five decades in two commonly used industrial dryers: rotary and flash dryers. Similar evolutionary development trends can be traced for most other dryer types as well.

Rotary dryer:

1. Purely convective, axial gas flow
2. Internal heaters (tubes or coils) or external heating of the shell to improve efficiency and capacity
3. Direct drying by air injection into the rolling bed of particles in the rotating shell via tubes connected to a central header (Yamato dryer)

Flash dryer:

1. Single-pass, vertical round insulated tube (adiabatic)
2. Single-pass, jacketed tube for increases in heat input, faster drying (nonadiabatic)
3. Flash dryer tubes of variable cross sections along its length (with delayed chambers)
4. Multipass, automatic aerodynamic classification in ''ring''-shaped dryer tubes to process particles with broader size distribution and cohesive particles prone to form lumps
5. Use of superheated steam as carrier gas-adiabatic/nonadiabatic designs
6. Use of inert carrier particles in a pneumatic tube to dry slurries

3.4 TRENDS IN DRYING RESEARCH AND DEVELOPMENT

It is extremely difficult, if not impossible, to make definitive statements about the direction drying technologies will take in the next several decades. Most of the developments in this field have occurred in the last three or four decades. As the general standard of living around the world rises along with the population of the world, it is obvious that the need for drying technologies will increase. New demands will be made on better energy efficiency, lower environmental impact via legislative measures, utilization of renewable energy for drying, better-quality products at lower total costs. Currently the major driving force for innovative drying techniques is the need to produce better-quality products at higher throughputs. If the price of fossil fuels rises rapidly and the various scenarios proposed regarding the impending shortage of oil and the resulting skyrocketing price of oil, then the R&D in drying will again be driven by the need to enhance efficiency. Some of the energy savings measures that are not cost-effective now would become very attractive if the price of oil doubles or triples in the next one or two decades.

In general, drying techniques designed to enhance quality are very product-specific. For example, high-valued, heat-sensitive products (e.g., pharmaceuticals, nutraceuticals, some foods, etc.) can be dried at low temperatures and under vacuum albeit at higher costs. As noted elsewhere in this book, two-stage, hybrid heat pump dryers or microwave-assisted vacuum dryers can compete with freeze-drying processes to produce a high-quality dried product at a lower cost. These processes are still very expensive for drying of low-value products, however. Also, scale-up to very high production rates is difficult at this time.

This book focuses on new drying technologies. Where possible, the merits and limitations of various new technologies are proposed in the literature and novel technologies marketed by vendors around the world are evaluated as objectively as possible. For proprietary reasons, some key details could not be located in some instances. Almost without exception, one key piece of information is not reported by most authors, that is, the cost-effectiveness of their proposed innovations and the objective comparison with competing current technologies. Readers will have to make such judgments carefully if they wish to use this information in practice. Many of the processes may be protected by patents as well.

The main goals of new drying technologies are to

Produce better-quality product.
Operate at higher capacities, safely, and with good control.

Operate at lower total cost by lowering capital as well as running costs (energy, maintenance, emissions, etc.).

One or more of these objectives can be reached in several possible ways. The following is a short list:

Use of indirect heating mode, where feasible
Use of heat pumps to save energy
Use of hybrid dryers
Use of multistage dryers
Use of new gas–solids contactors
Use of superheated steam as drying medium where possible
Use of enhancement techniques such as application of acoustic or ultrasonic fields
Use of better combustion techniques (e.g., pulse combustion)

Note that there is a cost associated with any additional complexity in the drying process. It is imperative to make a technoeconomic evaluation of conventional but more complex as well as newer (advanced) drying technologies before a final choice is made. The outcome will often depend on

Value and production rate of the product
Cost of electricity/fossil fuels (depends on time and geographic location of the plant)
Risk assessment due to uncertainties of scale-up, life-cycle cost evaluation
Choice of vendors, delivery times, and performance guarantees
Expected variability in product characteristics as well as production rates as some techniques are not flexible as far as capacities are concerned

Other factors may also need to be considered for specific applications.

Part II

Selected Advanced Drying Technologies

This section covers a number of relatively new but not commonly used drying techniques and technologies. Most have found commercial application for selected products in some countries. These technologies have demonstrated their potential to compete with conventional technologies and surpass them in performance in many instances, e.g., superheated steam drying, drying of suspensions on inert particles, heat pump drying, etc. With greater awareness and industrial interest, several of these will become common technologies within the next decade or two.

4

Drying on Inert Particles

4.1 INTRODUCTION

Drying of liquid materials on inert solid carriers is a relatively new commercial technology to produce powders from solutions, suspensions, slurries, and pastes. Although this technique was developed in the former USSR in the 1950s and used for industrial drying of pigments, fine chemicals, pharmaceuticals, and certain materials of biological origin (e.g., Kutsakova et al., 1964; Reger et al., 1967; Minchev et al., 1968, Anon, 1992a), it was not widespread, mostly because of the language barrier. Over the past two decades, however, drying on inert particles has found a renewed interest mainly because of its ability to produce powders even from the coarsely dispersed liquid feed at evaporation rates competitive to spray, drum, and film-rotary dryers (Strumillo et al., 1983; Adamiec et al., 1995; Kudra and Mujumdar, 1995). Extensive studies carried out in Poland, Brazil, England, New Zealand, and Australia have resulted in several pilot units and custom-made installations (e.g., Anon, 1986; Grbavcic et al., 1998). In addition, fluid bed dryers with inert particles have recently been marketed by such companies as Carrier Vibrating Equipment Co., USA, and Euro-Vent, England, as well as PROKOP INOVA in

Czech Republic which offers a dryer utilizing a swirling bed of inert particles (Kutsakova et al., 1990; Kutsakova et al., 1991).

4.2 DRYING MECHANISM AND PROCESS CONSIDERATIONS

Drying on inert particles is typically performed in a variety of fluid beds (classical fluid bed, spouted bed, spout–fluid bed, jet-spouted bed, vibrated fluid bed, cyclone dryer, etc.) as well as in other dryers for dispersed materials such as swirling stream dryers, impinging stream dryers, or pneumatic dryers (Figure 4.1). Independently of the hydrodynamic configuration, the principle behind this technology lies in dispersing the liquid feed over the surface of an inert solid carrier. This carrier is ''fluidized'' either by the sole hydrodynamic impact of the hot-air stream or by the combined impact of an air stream and a mechanical device such as a screw conveyor, a vibrator, or lifters (Flick et al., 1990; Kudra et al., 1989; Pallai et al., 1995; Erdesz and Ormos, 1986; Kudra and Mujumdar, 1989; Kudra and Mujumdar, 1995; Pan et al., 2000; Limaverde et al., 2000). Particles can also be ''fluidized'' by an external magnetic field if they are made of ferromagnetic material such as barium ferrite, for example (Kovalev et al., 1989).

Depending on the hydrodynamic conditions, the liquid coat on the particle surface dries by convective heat transfer from hot air and contact heat transfer due to sensible heat stored in the inert particles. When the coat is dry enough to be brittle, it cracks because of particle-to-particle and particle-to-wall collisions and peels off from the surface of inert particles. Because of intense attrition, dry product is discharged from the dryer with the exhaust air as a fine powder of rounded particles. When chipping due to the impact of inert particles prevails attrition, small flakes are produced especially when drying brittle materials of biological origin. Small flakes can also be obtained when using inert particles with a corrugated surface. The size of flakes is then proportional to the size of grooves on the particle surface (Kutsakova et al., 1985).

Figure 4.2 presents the idealized mechanism of drying on inert particles, which boils down to the following sequence of kinetic processes: heating of inert particles, coating with dispersed liquid, drying of the coat, and cracking and peeling-off the dry product. Because of continuous supply of the liquid feed and definite material residence time, the liquid spray coats at the same time not only the material-free particles but also particles with a dry but not peeled-off material, and particles with a partially dry layer. Thus, quasi-equilibrium is established among individual rates of the component processes. Sta-

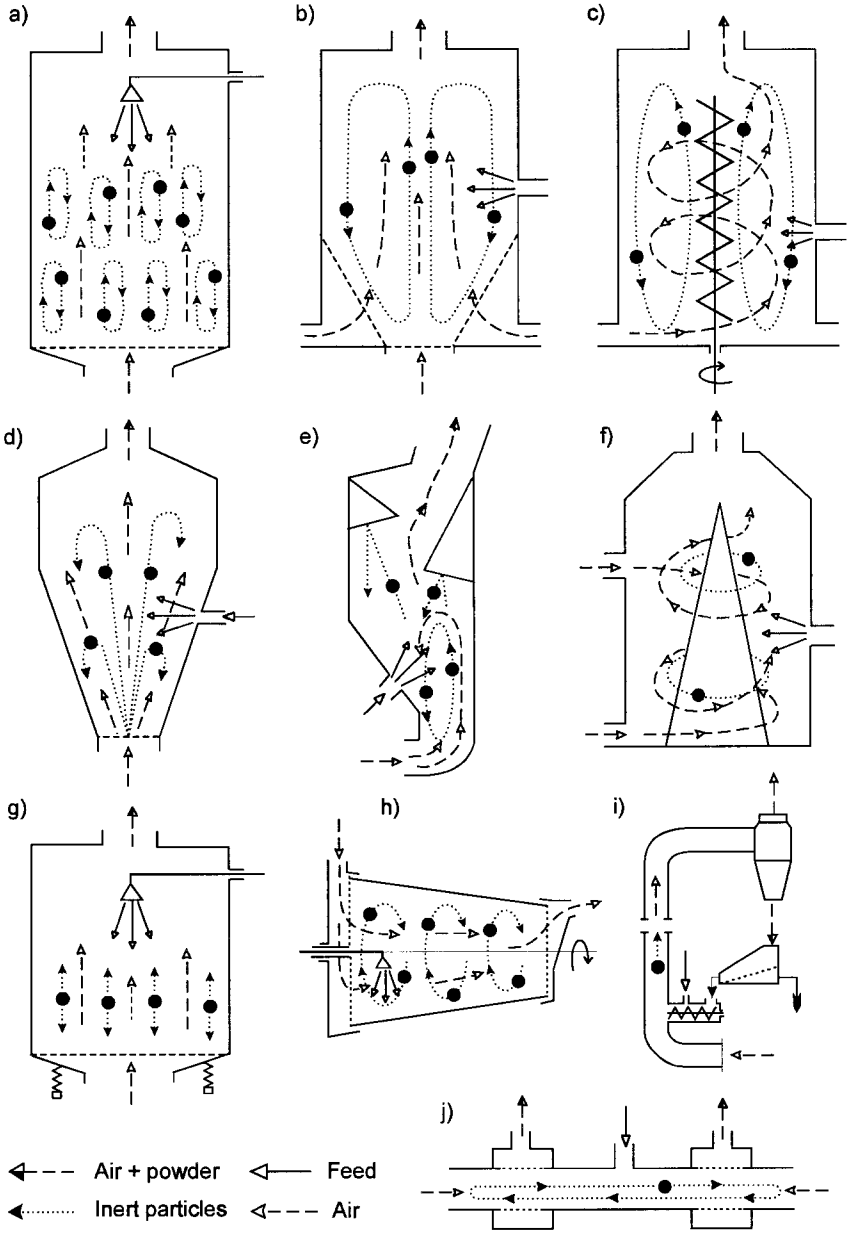

FIGURE 4.1 Basic configurations of dryers with inert carriers: a) fluid bed; b) spout-fluid bed; c) fluid bed with inner conveyor screw; d) spouted (jet-spouted) bed; e) vortex bed; f) swirling streams; g) vibrofluidized bed; h) rotary dryer; i) pneumatic dryer; j) impinging stream dryer.

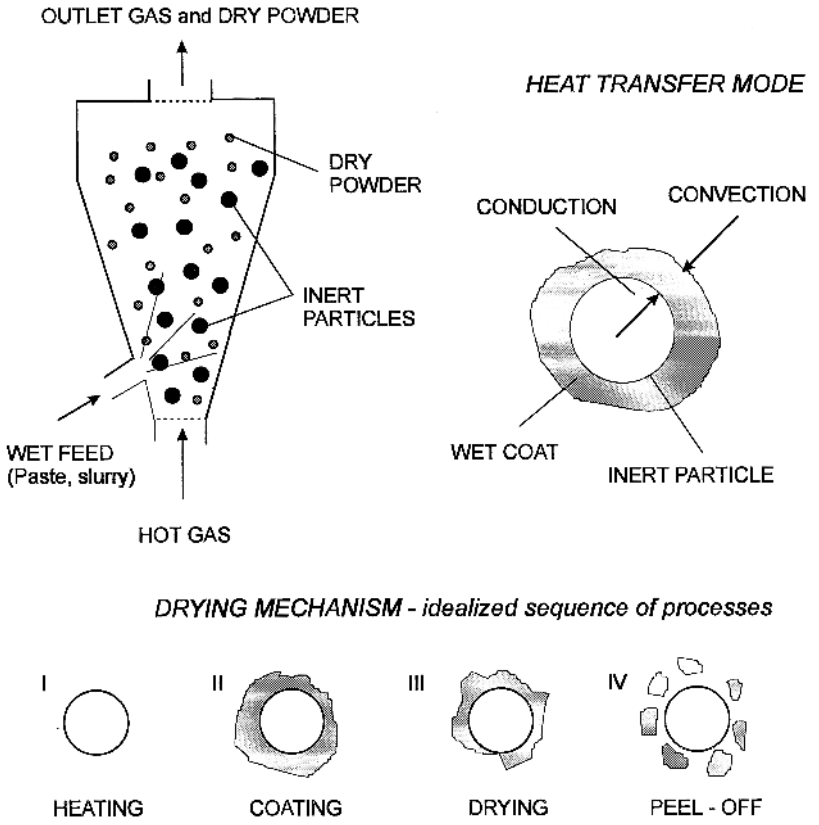

FIGURE 4.2 Process schematic and idealized mechanism for drying of liquids on inert particles.

ble operation of the dryer requires the combined rate of drying/peeling-off to be greater than the rate of coating. Otherwise, the wet coat would build up on the inert particles and the bed would collapse eventually. The bed would also collapse with excessive saturation of exhaust air (Schneider and Bridgwater, 1989).

Another condition for stable operation of the dryer with inert particles stems from the material properties—no elastic shell should be formed on the solid carrier at any stage of drying as impact due to particle collisions might not be sufficient to crack the shell. Here, the ''almond''-shaped inert particles formed of bimetallic canopies, which change their shape when subject to tem-

perature changes during drying could facilitate cracking of a dry shell (Dmitriev et al., 1989). Fibrous materials (e.g., pulp and paper sludge), which could bridge solid particles and therefore immobilize the bed, are also not good candidates for drying on inert particles. The bed can also collapse when drying sticky materials such as meat-rendering sludge with excessive fat content. In such a case, melted fat acts as a binder, which immobilizes particles and traps dry meat powder inside the dryer. This problem can be solved when altering the process by contact sorption drying (see Chapter 12). In this particular case, the meat-rendering sludge with fat content up to 30% w/w was successfully dried in the jet-spouted bed dryer when using either calcium carbonate or wheat bran in the mass ratio of 4.6% and 2.5%, respectively (Amazouz and Benali, 2000). An alternative solution to the problem of hydrodynamic stability is the use of a hydrocyclone to remove excess fat prior to thermal drying (Kudra, 2000).

Studies on drying of a single 8-mm ceramic particle coated with a 0.6–0.8-mm layer of the pasty pigment have shown that drying kinetics are typical for convective drying of capillary porous material (Leontieva et al., 2002). The clearly marked plateau of the material temperature corresponds well with the wet bulb temperature of the air stream during the first drying period (Figure 4.3). An analysis of literature data on drying in spouted and fluidized beds of

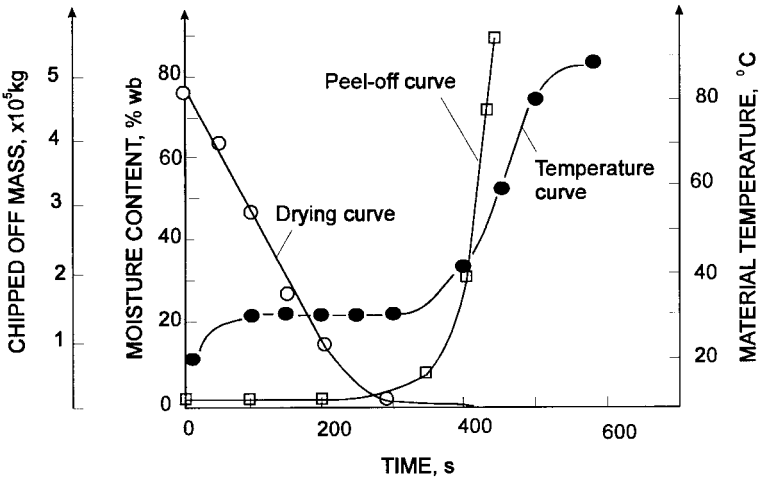

FIGURE 4.3 Drying, material temperature and peel-off curves for drying R-salt on inert particles. (Adapted from Leontieva et al., 2002.)

inert particles indicates, however, that the material temperature during drying is between the wet bulb temperature and the exhaust air temperature. This is because not all inert particles in the bed are always fully covered with the wet coat, so heat conduction supplements convective drying and thus the condition for the wet bulb temperature does not hold. Also, the material temperature at the moment of peel-off is higher than the wet bulb temperature because removal of a dry coat starts at a certain moisture content, which is close to the final one. This can be seen in Figure 4.3, in which we have extracted literature data (Leontieva et al., 2002) to combine the curve representing the kinetic of the peel-off process with the drying and temperature curves.

The same conclusion holds for other literature data as well. For example, Figure 4.4 presents the relationship between the equilibrium material (bed) temperature and inlet and outlet air temperature for drying of egg melange in a vortex bed dryer with forced pulsation of inert particles (Kutsakova and Utkin, 1989). Clearly, the material temperature is higher than the respective wet bulb temperature. At the same time, the material temperature is lower than the outlet air temperature, and this difference tends to be larger at lower inlet air temperatures. These data are consistent with measurements by Mar-

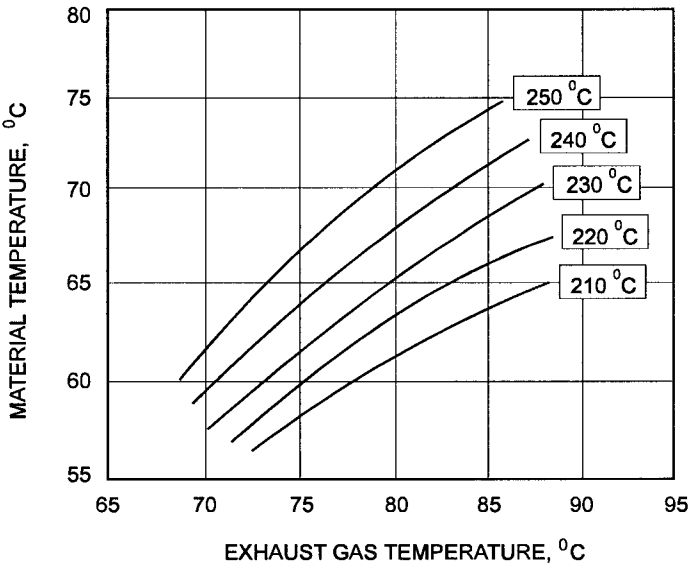

FIGURE 4.4 Material temperature versus exhaust and inlet air temperatures. (From Kutsakova and Utkin, 1989.)

kowski (1992), who found the difference between the particle surface temperature and the wet bulb temperature to be at least 20°C. Also Grbavcic and coworkers (Grbavcic et al., 1998) report on fluid bed temperatures lower by 15°C than the temperature of the outlet air.

Assuming that drying the relatively thin layer of the wet material on inert carriers is externally controlled, Kutsakova and Utkin (1987) proposed the following equation for the moisture evaporation rate:

$$\frac{dX}{dt} = \frac{\beta(1 + X_i)}{\varphi R(T_s + 273)}[P_s(T_p, X) - P_g] \tag{4.1}$$

where $R = 462$ J/(kgK) is the gas constant for water vapor, P_s and P_g are the water vapor pressure at the material surface and in the gas core, respectively, and φ is the parameter that quantifies distribution of the wet coat on the surface of inert particles given by the mass of wet material that adheres to the unit surface area of inert particles.

Integration of Equation 4.1 gives the following relationship for drying time:

$$t = \frac{\varphi R(T_s + 273)}{\beta(1 + X_i)} \int_{X_i}^{X_f} \frac{dX}{P_s(T_p, X) - P_g} \tag{4.2}$$

To calculate drying time, one should first identify the variation of the water vapor pressure at the material surface with the average temperature of inert particles and material moisture content. For drying in a vortex bed of inert particles, Kutsakova and Utkin (1987) developed the following experimental equation:

$$P_s(T_p, X) = \exp\left[A - BX^C - (5073 - DX^E)\left(\frac{1}{T_p + 273} - \frac{1}{T_0 + 273}\right)\right]F \tag{4.3}$$

where the parameters for Equation 4.3 for selected protein-based materials are given in Table 4.1.

The average temperature of the bed (T_p) can be determined experimentally or assumed to be lower than the exhaust gas temperature by 15° to 20°C. Also, the water vapor pressure in the bulk of drying gas can be calculated based on the exhaust gas humidity. The φ parameter should be determined experimentally, as it depends on dryer configuration, particle and material characteristics, and operating parameters. For the drying of materials listed in

TABLE 4.1 Parameters in Equation 4.3 (Kutsakova and Utkin, 1987)

Material	*A*	*B*	*C*	*D, K*	*E*	*F*	T_0, °C
Protein hydrolyzate	11.53	1.027	−0.8	4.605	−1.8	1.0	120
Skim milk	21.53	0.053	−1.0	0.313	−2.3	0.032(112-T_p)	100
Whey	11.53	0.00378	−1.7	6.620	−1.7	0.032(112-T_p)	100

Table 4.1, the following semi-empirical formula can be used (Kutsakova and Utkin, 1987):

$$\varphi = \frac{\Delta H \rho_p c(T_p - T_{eq})}{3\left[\dfrac{X_i - X_f}{1 + X_i}\Delta H + c(T_{g1} - T_{g2})\right]} \tag{4.4}$$

When drying the protein hydrolyzate from $X_i = 4$ kg/kg to $X_f = 0.05$ kg/kg at $T_{g1} = 300°C$, $T_p = 105°C$, and $T_{eq} = 100°C$, the parameter φ was found to be 0.7 kg/m^2 at dry coat thickness from 0.2 to 0.3 mm. The calculated drying time varied from 60 to 90 seconds, whereas the experimentally determined material residence time was in the order of 200 to 400 seconds. This indicates that several wet coats were dried in this case before dry material was cracked and peeled off from the inert carrier (Kutsakova and Utkin, 1987).

Despite extensive studies on drying on inert particles, there is practically no data on the material residence time except those cited here for a swirling bed of inert particles. Also, the material residence time from 30 to 85 seconds has been specified for drying of animal blood and egg products dried as a film of 60 to 200 μm on a fluidized bed of 3- to 5-mm Teflon cubes (Table 4.2). Such a substantial residence time as compared to the residence time of a drying air was claimed to be sufficient to suppress undesirable microorganisms when combined with the material temperature in the range from 70° to 90°C (Rysin et al., 1981).

From the other point of view, the residence time in the order of several minutes in combination with the relatively low material temperatures explains successful drying on inert carriers of some biomaterials such as Zn-bacitracine, animal blood, vegetable extracts, egg products, pea protein, starch, and meat

TABLE 4.2 Drying of Food Products on Inert Particles

Parameter	Egg melange	Egg white	Animal blood
Inlet air temperature,°C	110–112	120–130	110–135
Outlet air temperature,°C	63–68	67–80	63–75
Unit feed rate, kg product/kg bed/hr	1.35	1.35	1.4
Air consumption, kg/kg product	2.0	2.0	1.7
Layer thickness, mm	60–200	60–150	100–200
Material temperature,°C	69–77	77–90	73–85
Residence time, sec	50	30	85

Source: Rysin et al., 1981.

processing sludge (Re and Freire, 1989; Markowski, 1992; Pan et al., 1994, 1995; Amazouz et al., 2000; Amazouz and Benali, 2000). However, the drying of heat-sensitive products of biotechnology like enzymes or vitamins as well as living microorganisms (e.g., yeast and bacteria) is yet a challenging task because of product degradation. The positive or negative results depend on the following main factors that result from the drying mechanism (Kudra and Strumillo, 1998):

1. Mechanical effect of inert particles due to wall-to-bed and particle-to-particle impact, and attrition due to circulation of the bed. These two phenomena depend on air flow rate, mass and properties of inert particles, dryer geometry as well as dryer configuration (jet-spouted bed, pneumatic transport, mechanically spouted bed, etc.).
2. Thermal effect due to convective and contact heat transfer that depends mainly on heat transfer rate, bed hydrodynamics, properties of drying material, and dryer configuration.
3. The effect of material accumulation, which depends on rheological properties of the material being dried and bed loading, and therefore it can be important only for some materials.

The risk of product degradation can be quantified in terms of the quality loss risk (QLR)

$$QLR = 1 - \Delta_{HT}\Delta_M\Delta_A \tag{4.5}$$

where Δ_{HT}, Δ_M, and Δ_A are the heat transfer, mechanical, and accumulation effects, respectively. Detailed information and an example of the QLR analysis for drying in a jet spouted bed can be found in the reference literature (Markowski, 1992, 1993a, 1993b; Kudra and Strumillo, 1998).

From Equation 4.5 it follows that success in drying of living microorganisms can be achieved when reducing any of the components that contribute to quality losses. An interesting option to alleviate thermal effect appears to be heat pump drying (Alves-Filho et al., 1998). With reference to Figure 4.5, the bacterial suspension (*Streptococcus thermophilius* in a potassium phosphate buffer with and without trehalose protectant) was dried by spraying over the fluid bed of 3.5-mm polypropylene beads. The inlet air temperature was kept below 35°C by the use of a classical heat pump circuit (see Chapter 15). The powdery product, which was dried with the addition of 100 mM of trehalose, showed 86% viability at inlet air temperature of 10°C. Thus, it was concluded that this technique could be competitive to heat pump-assisted freeze drying in a fluidized bed that offers 100% viability but when drying at −20°C

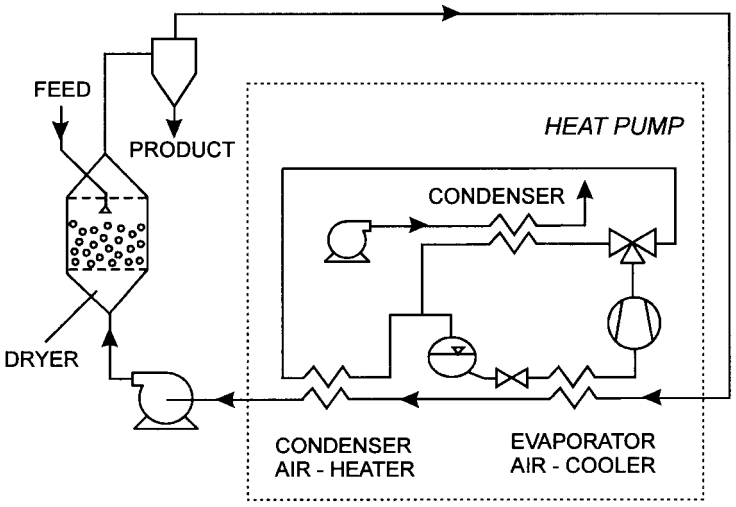

FIGURE 4.5 Heat pump dryer with a fluidized bed of inert particles.

for 15 h, then at −10°C for 2 h, at −5°C for 0.5 h, and finally, at 10°C for 0.3 h (Alves-Filho et al., 1998).

4.3 MODELING AND SCALE-UP

Despite numerous published papers on the subject of drying of suspensions on inert particles, there is insufficient data available in the open literature that can be used with confidence for process calculations and dryer design, with the possible exception of a vortex bed dryer with inert particles (Kutsakova and Bogatyriev, 1987). Drying on inert particulate carriers can be performed in diverse hydrodynamic configurations (see Figure 4.1), which have distinctly different characteristics with respect to bed structure, particle and gas flow patterns, circulation velocities and distributions, re-coating ratio, surface renewal rate, etc. Moreover, the drying mechanism—and hence the corresponding mathematical model for a particular dryer configuration—depends on material characteristics including adhesion, cohesion, possible case-hardening, and the value of the critical moisture content at which the elasto-plastic layer turns into an elasto-brittle coat (Strumillo et al., 1983).

Because the overall drying rate depends on the rate of the component subprocesses, that is, on the drying of the wet layer on the individual particles and removal of the dry coat, the mathematical model for this process must

adequately account for variables that affect both of these processes. It is generally recognized that drying on inert carriers is controlled by the external heat and mass transfer conditions. Even for materials with internal resistance to transfer processes, the operating conditions are chosen (thin layer and rapid evaporation at 100°C) so as to minimize this resistance (Kutsakova and Utkin, 1987). Hence, the rate of wet film drying is directly affected by the inlet air temperature and its flow rate and indirectly affected by the solids circulation rate. The rate of dried coat removal is affected by air velocity, mass of the inert bed, feed rate, and the solids circulation rate aside from the nature of the particle-dry film adhesion characteristics.

Since removal of dry material from the dryer is critical for the hydrodynamic stability of dryers with inert carriers, the preferential configuration is the conical spouted bed as it offers intense motion of the particulate phase, which promotes fracture of the dried coat by interparticle collisions and resulting attrition. Moreover, the conical drying chamber has been shown to result in better energy efficiency than the cylindrical one (Kutsakova et al., 1964). Consequently, most of studies aimed at process modeling have been carried out with conical spouted beds.

Pham (1983) has proposed a simple model for the classical spouted bed dryer with clearly separated spout and annulus zones. Though no interaction between these two zones was assumed, he obtained satisfactory agreement between his model predictions and experimental data. A more realistic approach, which accounts for interaction between gas and particles, was proposed by Barret and Fane (1989). No mathematical formulation for this qualitative mechanistic model was given, however. Other models for drying of suspensions on inert particles are of the lumped-parameter type where drying rates are given by equations obtained from multiple regression of experimental data or from heat/mass balances over the entire bed (Markowski, 1992; Oliveira et al., 1994; Reger et al., 1967; Csukas et al., 1976). Such models often have limited applicability only for the given material and given equipment operated over the range of parameters chosen by the authors.

Considering hydrodynamics of the spouted bed, the most logical description of the drying process appears to be provided by the three-region model (TRM) (Oliveira and Freire, 1996). This model is based on a generalized assumption that each distinct region of the bed (an annulus, a spout, and a fountain) contributes to water evaporation in a proportion determined by their respective heat and mass transfer coefficients, residence times within the zones, and the local temperature and humidity gradients.

Spitzner and Freire (1998) have critically reviewed various models for drying in spouted beds of inert particles and made a qualitative comparison

between the three-region model and the thermodynamic model using literature data for drying of animal blood and aluminum hydroxide in a conical spouted bed. They have shown that the three-region model predicts an outlet air temperature and drying rate with deviations from experiments of less than 15% in contrast to the thermodynamic equilibrium model where a 50% difference was obtained between model estimates and experimental data.

The three-region model is built on the assumption that the solids temperature (inert particle and drying material) is equal to the wet bulb temperature at the outlet from each region. In our opinion, better accuracy from the model could be expected when allowing for material temperature higher than the wet bulb temperature, as shown in several papers revieved in the previous paragraph.

Although spouted and fluidized bed dryers of inert particles are built in sizes from laboratory models to industrial units up to 10 m^3 of the dryer volume, the scale-up procedure is still based on know-how rather than on theoretical foundations except for attempts to define hydrodynamic stability of the spouted beds based on the mechanics of heterogeneous media (Menshutina et al., 2000). Aside from extensive but inaccessible works from the former USSR, the most complete scale-up procedure developed for the jet-spouted bed is due to Strumillo et al. (1980). Here, sizing of the dryer for required throughput boils down to maximizing the ratio of the most active zone (V_{act}) to the dryer volume (V) that comprises a cylindrical section and a conical one with the 35° cone angle. The volume of the most active zone is assumed to be a cylinder with a diameter equal to the inlet cone diameter and the height equal to the dynamic bed height:

$$V_{act} = \frac{\pi D_{in}^2}{4} H_d \tag{4.6}$$

For the cylindrical-conical dryer, the volume is given as

$$V = \frac{\pi}{12}(D_{in}^2 + D_{in}D_w + D_w^2)H_c + \frac{\pi}{4}D_w^2 H_w \tag{4.7}$$

The inlet diameter is calculated from the following equations:

$$D_{in} = \sqrt{\frac{4Qv}{\pi c_H (T_{in} - T_0)u}} \tag{4.8}$$

$$Q = \frac{Vw\Delta H}{k} \tag{4.9}$$

where w is the volumetric evaporation rate and k is the heat utilization factor defined by the ratio of the heat for moisture evaporation to the total heat input.

These equations are complemented by the following inequalities, which identify the conditions for stable operation:

$$\frac{D_w}{D_{in}} \geq 3; \qquad H_{st} \leq 2D_{in} \tag{4.10}$$

$$u_{mf} \leq u \leq 6_{mf}; \qquad u \leq 35\ m/s \tag{4.11}$$

The volumetric evaporation rate, heat utilization factor, and dynamic bed height need to be taken from experimentally obtained correlations. The static bed height (H_{st}) can be chosen assuming that for a particular drying material, its residence time in the small and large dryers is the same:

$$t = \frac{m}{W} \tag{4.12}$$

where m is the mass of the material in the bed and W is the material feed rate.

Since the material hold-up below the clogging point is related to the mass of inert particles, the static bed height can thus be determined.

The aforementioned scale-up procedure was used to design a series of jet-spouted bed dryers based on experiments performed on a 0.5 m^3 unit. Field trials on a 1.5-m^3 dryer filled with 30 kg of Teflon cubes 4 mm in equivalent diameter have shown that the volumetric evaporation ratio varied from 55.4 kg/(m^3h) to 120.6 kg/(m^3h) against 100 kg/(m^3h) taken for design calculations. Also, the heat utilization factor from 0.192 to 0.335 corresponded well to the assumed value of 0.25 (Strumillo et al., 1980).

4.4 SELECTED DRYERS WITH INERT PARTICLES

The principle of operation, basic design, and process characteristics for most common types of dryers with inert carriers are well described in easily accessible literature. These are the vibrated fluid bed dryer and the fluid bed dryer in its conventional and two-chamber configurations (Kudra and Mujumdar, 1995; Erdesz and Ormos, 1986), spouted bed dryer (Re and Freire, 1989), jet-spouted bed dryer (Markowski, 1992), pneumatic dryer (Blasco et al., 1996), rotary dryer (Limaverde et al., 2000), impinging stream dryer (Kudra and Mujumdar, 1989), dryer with a vertical inner conveyor screw (Pallai et al., 1995), etc. Therefore, here we present less common configurations that are interesting from research and applications points of view.

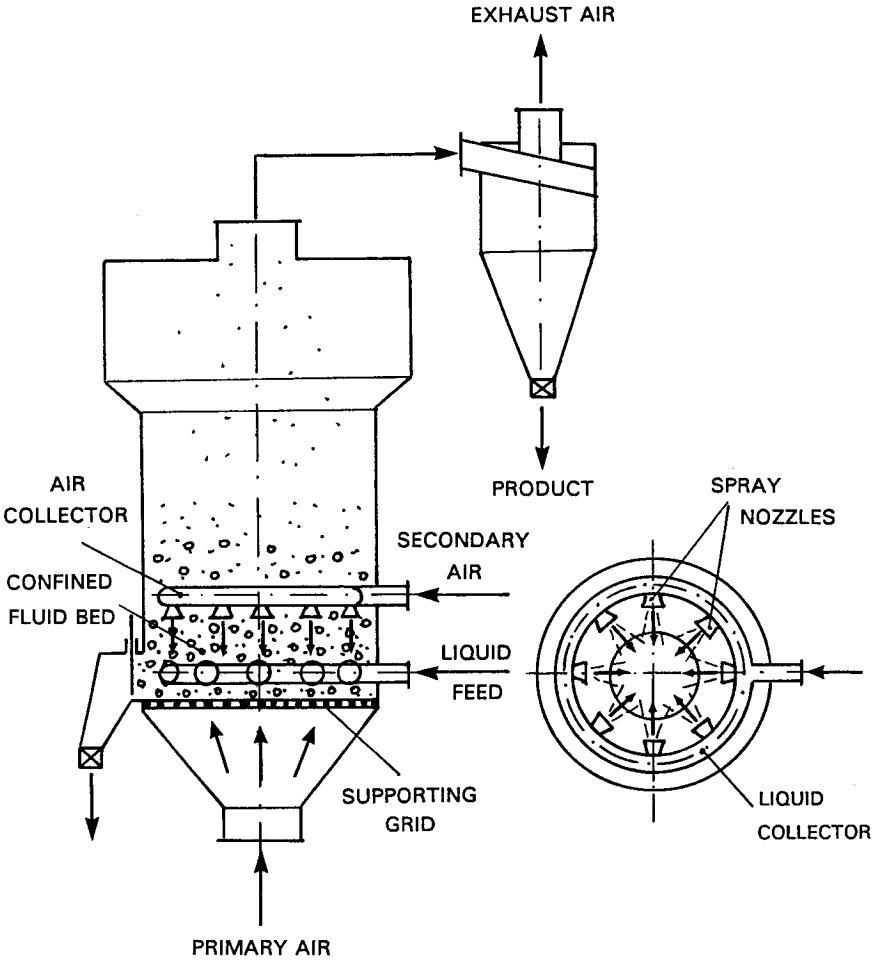

FIGURE 4.6 Confined fluid bed dryer.

Figure 4.6 displays the so-called confined fluid bed (Fedorovich et al., 1990). The toroidal (''doughnut'') collector for liquid feed is positioned in a drying chamber in the middle of a fluidized bed of particles. The collector is equipped with an even number of spray nozzles, which face each other so the liquid to be dried is dispersed in a countercurrent mode perpendicularly to the fluidizing air stream. An additional toroidal collector mounted above the

collector for liquid feed provides secondary air directed against the fluidizing air. The combined action of the liquid spray and air jets results in ''confinement'' of the fluid bed, thus reducing its dynamic bed height without losing advantages of a highly turbulent motion. Heating of liquid prior to spraying up to 70°C and heating the inert packing permit processing of heat-sensitive substances such as protein concentrates or saccharose solutions. Evaporation rates of up to 200 kg/h can be achieved at the inlet and outlet air temperatures in the range of 120° to 200°C and 40° to 50°C, respectively.

Figure 4.7 depicts a schematic of a fluid bed of inert particles with partial bed circulation (Pikus et al., 1975). Here, a cylindrical drying chamber is fitted with a twin set of oppositely directed stubs for tangential entry of the secondary air. A streamlined insert located in the center of the chamber creates velocity distribution with a maximum at the impingement plane from the two counterrotating streams of secondary air. A fraction of the inert particles (which are generally free of dry material entrained with the exhaust air) is picked up by a peripheral ring-type entry located just below the limiting grid and returned to the near-grid region where they are re-coated with a liquid feed. Such a design eliminates possible dead zones in the dryer and permits extension of the particle residence time.

An interesting modification of the classical spouted bed is the so-called swirl-jet spouted bed (SJSB) designed for drying of slurries and pastes on the surface of inert particles (Markowski et al., 1977). The dryer (Figure 4.8) consists of cylindrical and conical chambers equipped with standard feeding and product discharge devices. In contrast to the classical spouted or fluid bed dryers, no grid supports the inert particles, which are loaded to the dryer during the start-up period via an air lock. The gas inlet is formed of two jointly twisted ducts configuring a double spiral at the bottom of the cone which act as a swirl vane. These ducts are coupled to the cylindrical chamber by two short stubs attached tangentially to the cylinder wall. At each duct–stub junction an air nozzle is mounted so as to operate as an injector. A standard pneumatic nozzle is used to disperse the liquid or pasty material on the surface of the inert particles. This special design of the gas inlet produces an inlet gas swirl, which forces the particles to spout in a rotary motion. Relatively high gas-to-particle velocity and intense interparticle and wall-to-particle collisions enhance heat and mass transfer rates between the gas and the wet film on the inert particle surface and facilitate removal of the dry coating from the inert particles. Due to the injectors, a noticeably lower pressure exists in the near-wall region of the cylinder. Thus, a fraction of the inert particles is sucked off the chamber, accelerated with an air stream, and redirected to the dryer

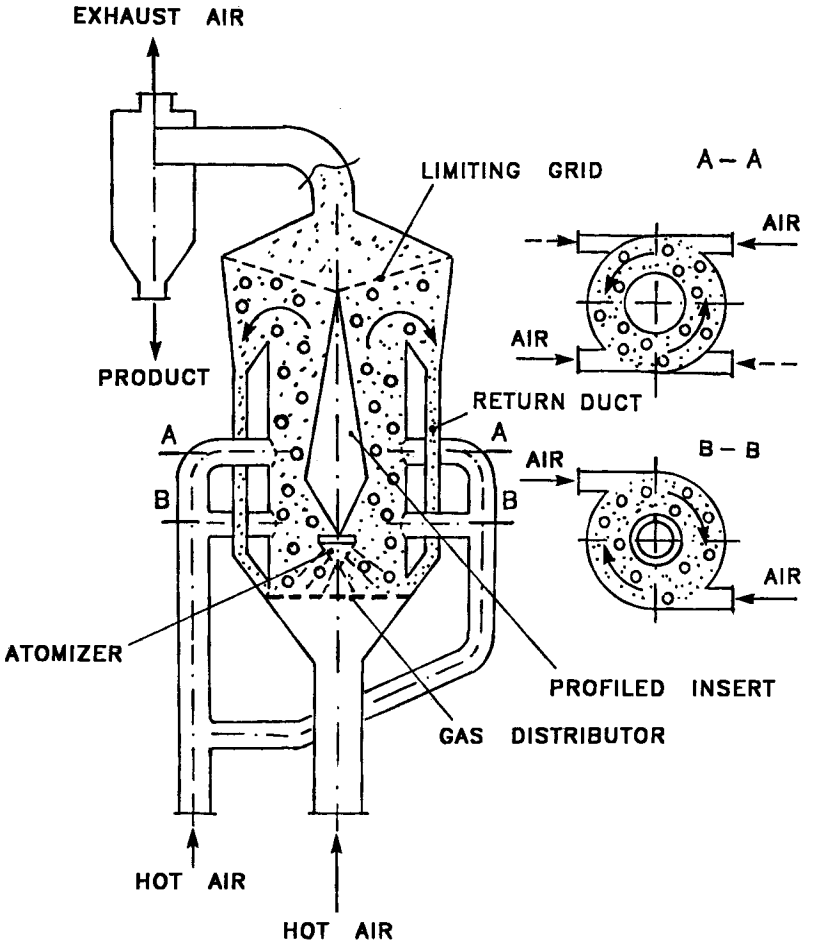

FIGURE 4.7 Fluid bed dryer with partial recirculation of inert particles.

inlet. During passage through the venturi tubes and air ducts, the inert particles are additionally heated by a hot-air stream so that the temperature of recycled inert particles is much higher than the bed temperature. Hence, evaporation of moisture from the wet coat is not only due to sensible heat of gas phase but also due to the sensible heat stored in the inert particles. The performance characteristics of a swirl-jet dryer for dye Red-K are given in Table 4.3.

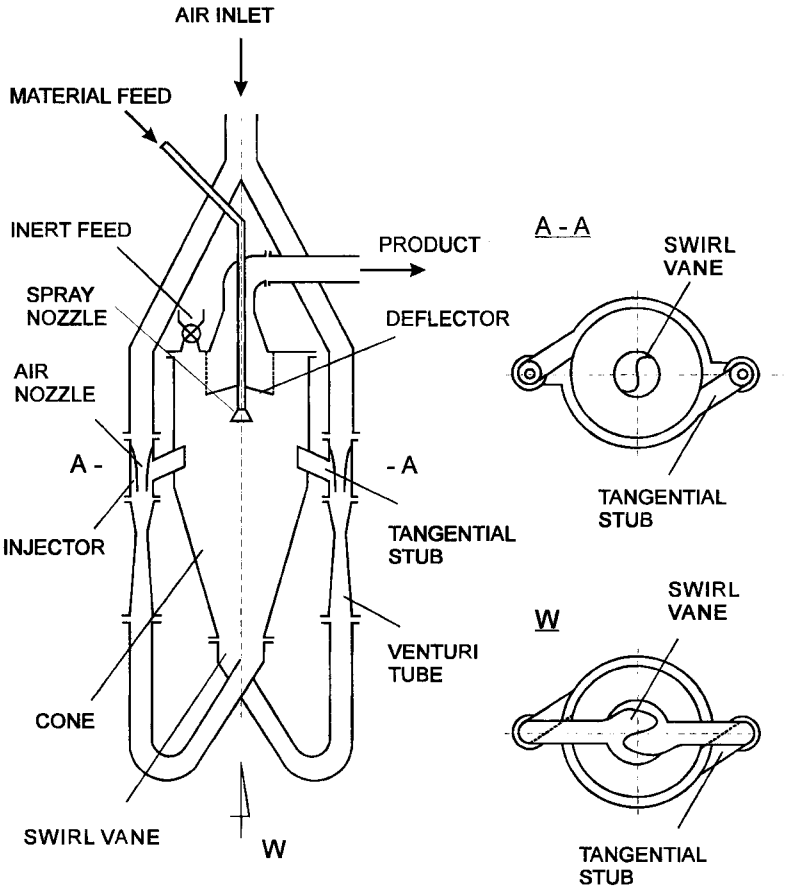

FIGURE 4.8 Swirl-jet-spouted bed dryer.

As compared to the jet-spouted bed dryer of inert particles used for drying of detergents and dyestuffs, backmixing of inert particles along with swirl-jet spouting allows for the following (Markowski et al., 1978):

Increase the volumetric evaporation rate by 25% to 30%
Decrease the final moisture content down to 0.03 to 0.05 kg/kg
Increase thermal efficiency to 0.45

Figure 4.9 presents the general principle of the so-called Ecal dryer (Moeller, 1974), which falls into the category of a dryer with an internal con-

TABLE 4.3 Performance Characteristics of the Swirling-Jet-Spouted Bed Dryer

Dryer volume, m^3	0.046
Feed rate, kg/h	4.5
Moisture content, % w.b.	
Initial	80
Final	7
Particle size, mm	0.01–0.025
Air flow rate, Nm^3/h	250
Air temperature, °C	
Inlet	180
Outlet	127
Inert particles (Teflon cubes)	
Equivalent diameter, m	0.0046
Mass of load, kg	2.5

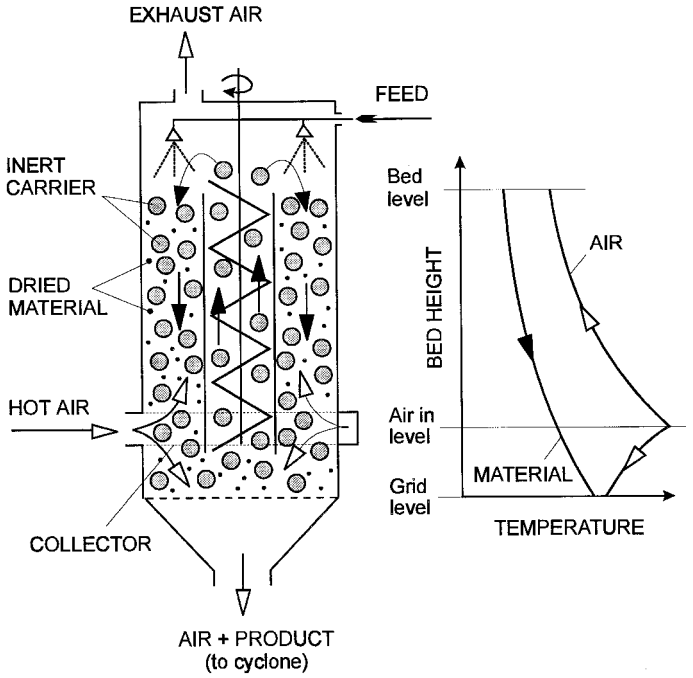

FIGURE 4.9 Schematic of the Ecal dryer and temperature distribution along the bed height. (Adapted from Moeller, 1974.)

veyor screw. The cylindrical drying chamber has a centrally located vertical screw conveyor. When rotated at 10 to 30 rev/min, this conveyor transports inert particles from a disengaging zone at the grid area to the top of the bed, where they are coated with the feed by rolling in the liquid on a collar. Then the coated particles descend slowly as a falling bed through the annular drying zone, which is about 0.8 m high. Drying air is supplied to the falling bed by radial air inlet ducts located above the bed bottom. Hence, the hot air is split into two fractions: the upward stream, which evaporates most of water and thus cools down almost to the dew point; and the downward one (about 10% of the total inlet air), which provides finish drying. The operating conditions are selected in such a way that the peeling-off starts below the air inlet so the powdery material is entrained only with the concurrent air stream. The flow of particles over the supporting grid along with the mechanical action of the screw conveyor facilitates abrasion of the dry coat so the particles transported by the screw conveyor are essentially free of the drying material.

Unlike spouted and fluidized bed dryers, which require relatively small-sized inert particles, relatively large balls (18 to 40 mm in diameter) made of plastics are used as inert carriers in Ecal dryers. When drying liquids such as whey or animal blood, the thickness of the coat ranges from 0.1 mm to 1 mm. Inlet and outlet air temperatures vary from 150° to 65°C and from 50° to 25°C, respectively. To dry highly labile bioproducts such as living yeast cells, a secondary cold air stream can be injected at the dryer bottom to bring the cyclone air temperature down. Drying times for the same unit are between 50 and 5000 seconds, depending on the drying material and operating conditions. The evaporation capacity of the Ecal dryer is up to 2000 kg H_2O/h for food products and up to 6000 kg H_2O/h for sludges, which are not heat-sensitive. Interestingly, quality products were obtained even when drying large size solid particles such as sliced parsley, onion, leeks, and apples.

5

Impinging Stream Drying

5.1 BASIC FEATURES

The term ''impinging stream dryer'' (ISD) refers to a class of flash dryers in which moisture evaporation from wet particles or liquid droplets occurs in the impingement zone that develops as a result of the ''collision'' of two oppositely directed high-velocity gas streams, at least one of which contains the dispersed material to be dried. At the outset a distinction should be made from the impingement dryers in which gas jets are directed onto the web, sheetform, or slablike materials (Mujumdar and Huang, 1995) or the ''jet-zone'' dryer in which a layer of particulates is ''pseudo-fluidized'' by a multiplicity of high-velocity airstreams exiting a number of perpendicularly oriented air nozzles (Kudra and Mujumdar, 1995).

If a solid or liquid particle starts to flow with one of the impinging streams, then it accelerates from zero velocity to a certain velocity resulting from the hydrodynamics of the gas–solid flow (Figure 5.1). After crossing the impingement plane, the particle penetrates into the opposite stream due to its inertia and decelerates to a full stop at some distance of penetration within the domain of the opposing jet flow. Thereafter the particle accelerates in the opposite direction and, after crossing the impingement plane again, penetrates

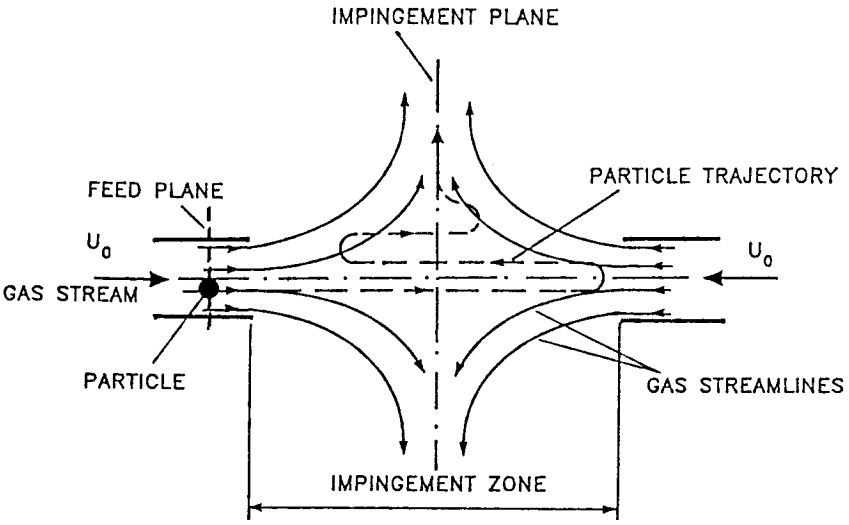

FIGURE 5.1 The principle of impinging stream dryers (ISDs).

the original gas stream up to the stagnation point. Thus, the process of deceleration and acceleration repeats itself. After several damped oscillations, the particle velocity in the impingement zone drops to the terminal velocity so that it is carried away with the outgoing gas stream.

Because of such an oscillatory motion with progressively decreasing amplitude, the residence time of a single particle (of large inertia) in the impingement zone is longer than that of the gas stream. This residence time may be reduced for a multiplicity of particles because of interparticle collisions that lead to enhanced energy dissipation. Although it is possible to feed solids to both gas streams, the rate of particle collision and the resulting loss of momentum are much higher than that for a single stream feed, because particles that do experience nonelastic collisions greatly lose their momentum and are driven out of the system. This might result in such a significant decrease of the residence time and penetration depth that the beneficial effects of impingement are dramatically reduced. The same effect of particle collisions exists in a single feed, as well, especially for high solids concentration. In our opinion, the problem could be alleviated by intermittent material feed with frequency proportional to the material residence time.

The constraint of reduced residence time is practically eliminated in impinging streams with a mobile impingement zone (Elperin and Meltser,

1978). In this arrangement, the impingement plane is made to move between the two locations (I and II in Figure 5.2) by alternate switching of the gas flows from left to right and then from right to left. The particles can be fed into the accelerating flow duct or into the central (reverse flow) duct that links both impingement chambers. In either case, particles accelerate with the original gas stream into one of the impingement chambers where they collide with the secondary gas stream, penetrate it up to the stagnation point, and then begin to accelerate in the opposite direction. At this moment, the gas outlet of the first impingement chamber is closed while the outlet of the second impingement chamber is open. This procedure results in the flow of a secondary gas stream with accelerating particles along the reverse-flow duct toward the second impingement chamber where the process of jet collision, penetration of particles into the original gas stream, and the following acceleration toward the first impingement zone is repeated. The period of oscillatory motion of the particles is self-controlled by decreasing the inertia force due to reduction of particle size in the course of processing and by reduction of particle mass due to moisture evaporation. Alternatively, a suitable limiting grid can be placed at the outlet ducts to restrict particle entrainment.

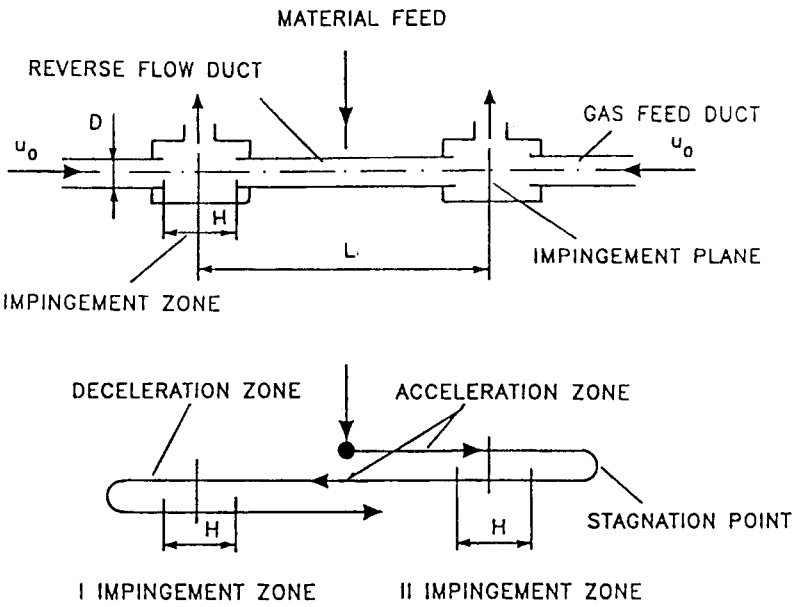

FIGURE 5.2 Coaxial ISD with a mobile impingement zone.

Another modification of the ISD with the mobile impingement zone contains inert spherical particles that oscillate continuously and throughout the operation of the dryer between the two impingement zones. This allows drying of slurries or suspensions that are sprayed on the surface of inert particles. Because the inert particles are heated by the hot air, drying of the liquid coat occurs by combined convective and conductive heat transfer. Also, drying with simultaneous grinding can be performed if metallic beads are used along with the material being dried.

Basically similar transport phenomena occur in other configurations of impinging streams (Figures 5.3 and 5.4). For example, in a system consisting of four mutually perpendicular ducts of the same diameter (the ''X'' configuration), the two primary gas streams mixed in an impingement zone are split into two secondary streams carrying the particles off the impingement zone.

Figure 5.5 shows the principle of semicircular impinging streams in which a primary gas stream is split equally into two secondary streams flowing inside two ducts bent to form semicircular channels. In this case, the flow of the drying material (and, to a smaller extent, the flow of the carrying gas) is affected by centrifugal forces, which might reduce the thickness of the boundary layer at the solid surface.

Another variant of the impinging-stream concept can be formed when one or two gas–solid suspensions are brought into collision inside a confined volume that forms a cyclone, for example (see Figure 5.3c). Because such a configuration was originally developed to carry out chemical reactions, it is commonly termed the ''impinging-stream reactor'' (Tamir and Grinholtz, 1987). Figure 5.6 presents some of these impinging-stream reactors that could be used for drying granular or liquid feeds (Tamir, 1994).

Depending on the geometry and flow direction (see Figures 5.3 and 5.4), the following basic variants of impinging streams can be identified according to:

Type of flow
- Rectilinear, where streamlines are parallel with either aligned axes of the gas jets (coaxial flow) or displaced axes of the gas jets (eccentric flow)
- Rotating (swirling), in which streamlines do follow a helix
- Curvilinear, in which streamlines are represented by circular arcs

Flow direction
- Countercurrent, in which gas (or solid suspension) streams flow in opposite directions

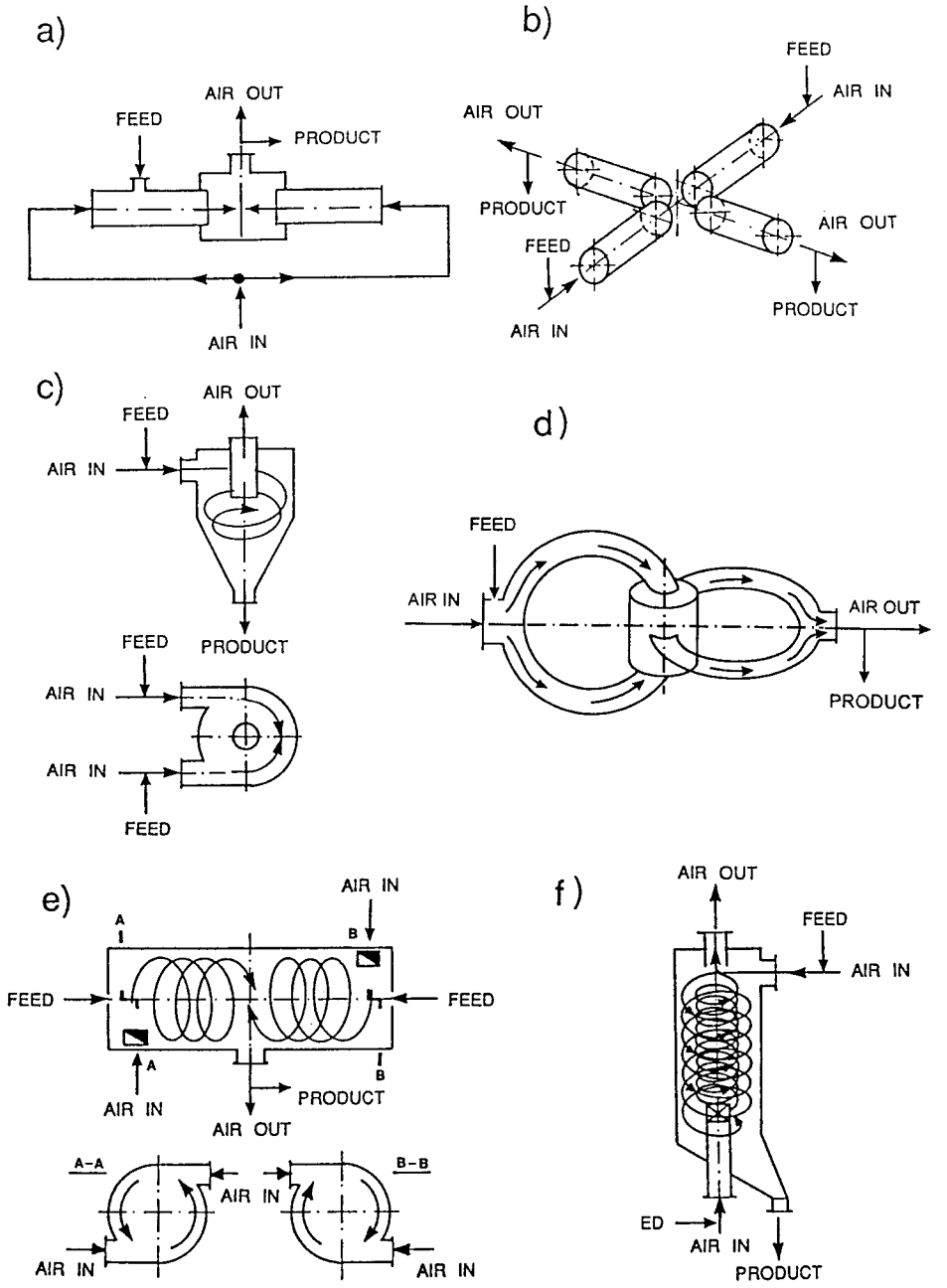

FIGURE 5.3 Basic types of impinging-stream flows: a) coaxial; b) mutually perpendicular X configuration; c) curvilinear countercurrent; d) semicircular impinging streams (''chain'' configuration;) e) counterrotating countercurrent; f) co-rotating countercurrent.

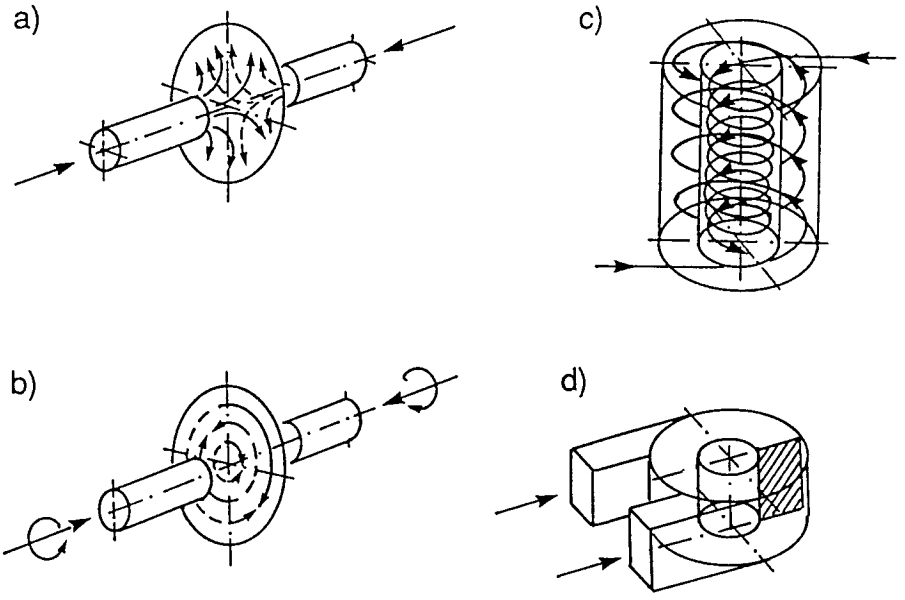

FIGURE 5.4 Impinging plane/zone geometries: a) planar with radial flow; b) planar with circumferential flow; c) tubular; d) annular.

Concurrent, in which gas (or solid suspension) streams flow in the same direction

Streamline direction

Counterrotating, in which gas (or solid suspension) streams rotate in opposite directions

Co-rotating, in which gas (or solid suspension) streams rotate in the same direction

Type of impingement zone

Stationary, in which the position of the impingement plane does not change in time

Mobile, in which the position of the impingement plane changes periodically or continuously

Geometry of impingement plane/zone

Planar with radial flow, in which streamlines diverge radially toward the impingement plane

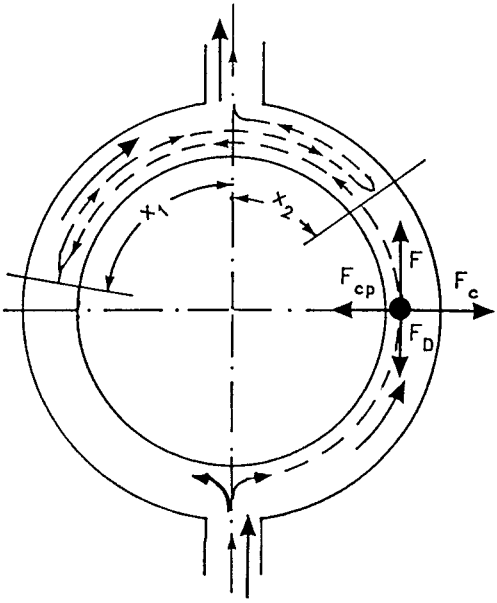

FIGURE 5.5 Particle trajectory for double penetration in a semicircular impinging streams (F_c = centrifugal force; F_{cp} = centripetal force; F_D = drag force; F = lift force).

Planar with circumferential flow, in which streamlines form concentric circles in the impingement plane
Tubular, in which impinging streams meet at the cylindrical surface
Annular, in which impinging streams meet in a sector of annulus

Single impinging stream units can be combined in series and/or in parallel to form a system allowing extension of the residence time and development of different hydrodynamic or temperature regimes. Also, hybrid configurations such as the coaxial impinging streams combined with the semicircular ones have found certain advantages over the simple systems (Dengying et al., 1999; Huai et al., 2000).

Besides the high intensity of turbulence in the impingement zone, a common feature of any impinging stream is the unsteady particle motion, acceleration, deceleration, and movement of the particles against the gas stream for

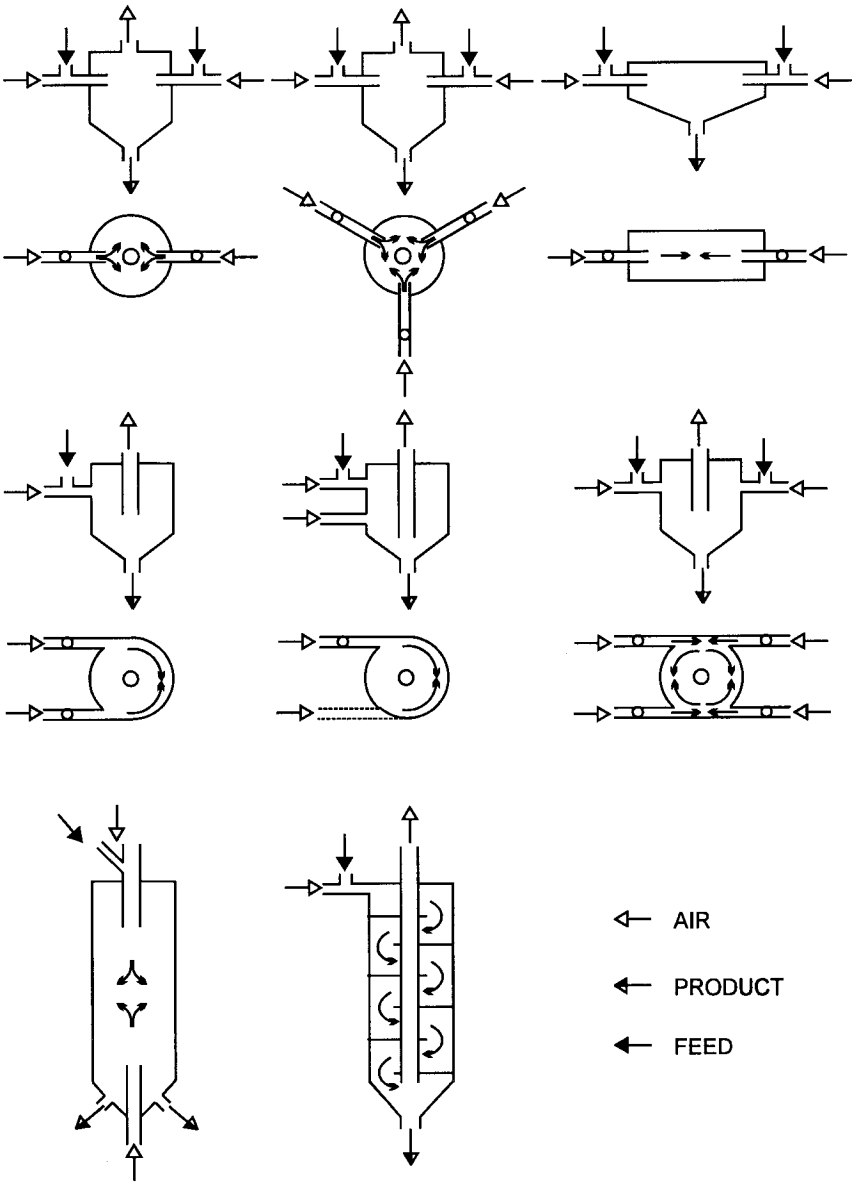

FIGURE 5.6 Some configurations of the impinging-stream reactors.

TABLE 5.1 Range of Operating Parameters for Coaxial Impinging Stream Dryers

Gas velocity, m/s	10–150
Particle diameter, mm	0.2–3
Volumetric concentration of solids, m^3/m^3	up to 0.0035
Particle residence time, s	0.5–15
Production rate, kg/h	
—of dry material	50–2000
—of water evaporated	up to 5000
Volumetric throughput, kg/(m^3 h) of wet material	1500–30,000
Evaporative capacity, kg/(m^3 h)	up to 1700
Pressure drop, kPa	1–10

half of its oscillatory flow. All these phenomena significantly enhance the heat and mass transfer processes and hence reduce drying times (see Table 5.1).

The unique characteristics of impinging streams also offer special advantages for thermal processing. An example is the intermittent drying that takes place when the opposing streams are supplied at different temperatures. Thus, particles are heated and cooled periodically when oscillating between hot and cold gas streams. Another example is puffing of grains (thermal micronizing), which occurs when wet grain is subject to high moisture and temperature gradients.

5.2 HYDRODYNAMICS AND HEAT TRANSFER

Detailed description of the fluid-particle dynamics in various configurations of impinging streams and resulting correlations allowing modeling of the hydrodynamics, and heat/mass transfer as well as scale-up and design recommendations can be found elsewhere (Kudra and Mujumdar, 1989; Kudra et al., 1990; Meltser et al., 1992; Tamir, 1994; Kudra et al., 1995; Strumillo et al., 1996). Here, only the information of a general nature and the correlations pertinent to coaxial impinging streams are provided to give the reader the background knowledge on impinging streams.

5.2.1 Penetration Depth and Oscillation Time

The maximum penetration depth (i.e., the distance the particle covers during first penetration into the opposing stream) and penetration time (i.e., the time

spent by a particle in the penetration distance) can be determined from the following relationships (Elperin et al., 1972):

Laminar region ($\mathrm{Re}_r \leq 1$)

$$x_{\max} = 0.016 \frac{u\, d_p^2\, \rho_p}{\nu\rho}; \qquad t_{\max} = 0.036 \frac{d_p^2\, \rho_p}{\nu\rho} \tag{5.1}$$

Transient region I ($1 < \mathrm{Re}_r < 13$)

$$x_{\max} = 0.01415 \frac{\rho_p\, u^{0.8}\, d_p^{1.8}}{\rho\nu^{0.8}}; \qquad t_{\max} = 0.328 \frac{\rho_p\, d_p^{1.8}}{\rho\nu^{0.8}\, u^{0.2}} \tag{5.2}$$

Transient region II ($13 \leq \mathrm{Re}_r \leq 800$)

$$x_{\max} = 0.02675 \frac{\rho_p\, u^{0.5}\, d_p^{1.5}}{\rho\nu^{0.5}}; \qquad t_{\max} = 0.0635 \frac{\rho_p\, d_p^{1.5}}{\rho\nu^{0.5}\, u^{0.5}} \tag{5.3}$$

Self-similar region ($\mathrm{Re}_r < 800$)

$$x_{\max} = 0.598 \frac{\rho_p\, d_p}{\rho}; \qquad t_{\max} = 1.54 \frac{\rho_p\, d_p}{\rho\, u} \tag{5.4}$$

where the Reynolds number for the accelerating/decelerating particle is defined in terms of the gas-particle relative velocity ($\mathrm{Re}_r = d_p(u \pm u_p)/\nu$).

The penetration depth and oscillation time for subsequent periods of oscillatory motion which are useful for process calculation and dryer design can be determined from the following empirical correlations valid over $2.5 \times 10^{-4} \leq d_p \leq 4 \times 10^{-3}$ m, $10 \leq u \leq 150$ m/s, $0.2 \leq x_0 \leq 4.8$ m, $3 \leq \mathrm{Re}_p \leq 80$, and $30 \leq T \leq 300$°C (Levental et al., 1981):

$$t^* = 1.42\, \mathrm{Re}_p^{0.28}\, \mathrm{L}^{-0.51}; \qquad x^* = 0.09\, \mathrm{Re}_p^{0.21}\, \mathrm{L}^{-0.44} \tag{5.5}$$

with

$$t^* = \frac{t_{\max}\, u}{x_0}; \qquad \mathrm{x}^* = \frac{x_{\max}}{x_0} \tag{5.6}$$

where

$$\mathrm{Re}_p = \frac{u\, d_p\, \rho}{\mu} \qquad \text{and} \qquad L = \frac{2\rho\, x_0}{\rho_p\, d_p} \tag{5.7}$$

The dimensionless time and distance are related to their maximum values, which appear in the first period of oscillation.

For $\mathrm{Re}_p > 800$, Eq. (5.5) can be simplified to the form

$$t^* = 9.23\ \mathrm{L}^{-0.51}; \qquad x^* = 0.37\ \mathrm{L}^{-0.44} \tag{5.8}$$

In a given impinging stream's configuration, the following inequalities should be satisfied for the oscillatory motion of a single particle about the impingement zone of length H (Soloviev, 1964):

$$\frac{8u}{H} \geq \frac{3\mu}{4d_p^2\rho_p}; \qquad H \leq \frac{9ud_p^2\,\rho_p}{4\nu\rho} \tag{5.9}$$

Thus, the minimum gas velocity in the flow ducts and the minimum particle diameter are respectively given by

$$u \geq \frac{4\nu\rho H}{9d_p^2\rho_p}; \qquad d_p = \sqrt{\frac{9\nu\rho H}{4\rho_p u}} \tag{5.10}$$

Since the particle velocity decreases during consecutive passage through the impingement plane, during some oscillation it approaches the gas velocity necessary to suspend the particle in a horizontally flowing gas stream. This critical gas velocity at which the particle is carried away from the impingement zone can be calculated from the following equation (Soloviev, 1964):

$$u_{\mathrm{cr}} = 0.9\left(\frac{D}{d_p}\right)^{1/7}\sqrt{\frac{\rho_p - \rho}{\rho}gd_p} \tag{5.11}$$

or

$$u_{\mathrm{cr}} = 5.6\,D^{0.34}\,d_p^{0.36}\left(\frac{\rho_p}{\rho}\right)^{0.5}\beta^{0.25} \tag{5.12}$$

where β is the volumetric concentration of the solid phase ($\mathrm{m}^3/\mathrm{m}^3$).

5.2.2 Pressure Drop

Because of the high gas velocities, solids' loading ratios, and momentum loss in the collision zone, the pressure loss in ISDs is much greater than that in pneumatic dryers, but it is comparable with that of fluidized and spouted bed dryers and varies from 1 to 10 kPa for the range of parameters that result in a stable operation (Kudra and Mujumdar, 1989; Tamir, 1994). The impinging

TABLE 5.2 Performance of Selected Dryers for Granules of Aluminium Alloy[a]

Parameter	Vibrofluidized bed	Fluidized bed	ISD
Drying time,[b] s	300–480	600	1–20
Unit gas consumption,[c] Nm^3/kg	8	13	1.2–2
Unit energy consumption,[c] kJ/kg	1380	3240	850
Product quality[d]	Decreased	Decreased	Unchanged

[a] Reference productivity, 250 kg/h; $d_p = 0.65–2$ mm; $X_1 = 0.17$ kg/kg.
[b] To reach $X_2 = 0.01$ kg/kg.
[c] Per kg of dry solids.
[d] Estimated from oxidation tests.

stream configurations can, however, compete in various aspects with the classical systems for drying of particulates and pastes (Table 5.2).

The pressure drop in the two-phase flow (ΔP_s) in the impingement zone can be calculated from

$$\Delta P_s = \Delta P + \zeta_s \frac{u^2 \rho}{2} \tag{5.13}$$

where ΔP is the pressure drop in the single phase flow, and ζ_s is the friction coefficient resulting from the solid phase present in a gas stream. This coefficient is related to the geometry of the impingement zone, gas velocity, and the solids' concentration and can be estimated using one of the following equations (Elperin et al., 1968):

$$\zeta_s = 3420\ \mathrm{Re}_t^{-0.18}\ \beta, \tag{5.14}$$

This equation is valid for an ISD with a cylindrical impingement zone for $45 \leq \mathrm{Re}_t \leq 1150$ and $\beta \leq 0.0006\ m^3/m^3$.

Note that the term ''geometry of the impingement zone'' refers only to the ''active'' fraction of the impingement chamber volume that contributes to the transfer processes. On the basis of numerous experiments, the limiting value of *H/D* below which the impingement zone can be considered to be active is 1.2 to 1.5.

The pressure drop for single phase flow [ΔP in Eq. (5.13)] can be calculated from the following correlations derived for impinging streams with cylindrical impingement zones for *H/D* varying from 0.25 to 1.125 (Elperin et al., 1968):

$$\mathrm{Eu} = 8.3 \left(\frac{H}{D}\right)^{-1.3} \mathrm{Re}^{-0.25} \tag{5.15}$$

for $1.2 \times 10^4 \leq \mathrm{Re} \leq 4 \times 10^4$, and

$$\mathrm{Eu} = 0.6 \left(\frac{H}{D}\right)^{-1.3} \tag{5.16}$$

for $\mathrm{Re} > 4 \times 10^4$.

5.2.3 Heat Transfer

Due to the inherent hydrodynamics of ISDs, the heat transfer rates from gas to particle depend on time as well as space. Reported data indicate, however, that the average heat transfer coefficient for ISDs differs by less than 10% from its local value, which gives acceptable accuracy for design calculations (Meltser and Pisarik, 1980).

In general, the average gas-to-particle heat transfer coefficients for ISDs are much higher than those in classical dryers that operate under similar hydrodynamic regimes. For example, when the heat transfer coefficient in a coaxial ISD is 850 W/(m^{2}K), the values for pneumatic dryers calculated for the same operating conditions from several available equations ranged from 300 to 520 W/(m^{2}K) (Strumillo and Kudra, 1986). For the TIS dryer with coaxial impinging streams, the heat transfer coefficient is 1.1 to 1.8 times higher than that for the geometrically similar spouted bed under the same operating conditions (Tamir, 1989). The volumetric heat transfer coefficients for ISDs are also higher, reaching 125,000 W/(m^{3}K) for coaxial, countercurrent configurations (Kudra and Mujumdar, 1989). Comparing the geometrically similar systems, one can find that the volumetric heat transfer coefficient for curvilinear, countercurrent configurations are 3 to 4 times higher than the values for spouted bed and cyclone dryers (Tamir, 1989) and about 20 times higher than those for spray dryers (Kudra and Mujumdar, 1989). Since the evaporation rate during the first drying period is proportional to the heat transfer rate, ISDs are much smaller than the spouted bed, fluid bed, and spray dryers.

The average heat transfer coefficient in an impingement zone can be calculated within $\pm 18\%$ from the following correlations (Meltser and Pisarik, 1980):

$$\mathrm{Nu} = 0.173\ \mathrm{Re}_r^{0.55}\ \beta^{-0.61} \tag{5.17}$$

for $300 < \mathrm{Re}_r < 3500$ and $\beta \leq 0.0009$ m^3/m^3, or

$$\mathrm{Nu} = 1.59\ \mathrm{Re}_r^{0.55} \tag{5.18}$$

for $300 < \mathrm{Re}_r < 3500$ and $0.0009 < \beta < 0.0021$ m^3/m^3, where the Reynolds

number is based on the relative gas-particle velocity averaged over the length of the impingement zone.

Interestingly, the heat transfer coefficient in impinging streams with mobile impingement zones can be calculated from the standard equation for gas flowing past a sphere with particle Reynolds number based on the gas velocity in an accelerating flow duct:

$$\mathrm{Nu} = 2 + 1.05\ \mathrm{Re}_p^{0.5}\mathrm{Pr}^{0.33}\mathrm{Gu}^{0.175} \tag{5.19}$$

For any impinging stream system, the heat transfer coefficient, both local and averaged over the total residence time of particles, increases as the gas velocity increases and decreases as the gas temperature increases. Such a temperature influence on heat transfer results not only from the variation in gas properties but also from an appreciable change in the hydrodynamic conditions; with an increase in the gas temperature, the penetration depth into opposing gas stream increases, which extends the period of unsteady particle motion, thus enhancing the total heat transfer.

5.3 DRYING

Because drying in impinging streams (without use of inert media) is purely convective, both constant and falling drying rate periods can be observed if the processing materials have both internal and external resistances to mass flow. The material temperature during the first drying period is equal to the wet bulb temperature or slightly higher when drying on inert particles because of supplementary conductive heat transfer. Generally, the period of constant drying rate is short because of the high heat and mass transfer rates and is measured in fractions of a second. The dryer ducts are usually insulated, but it may be possible to heat the ISD walls and provide additional heat by conduction to enhance both the drying capacity and thermal efficiency. No reports are available in the literature for this case, however.

Figure 5.7 shows the time variation of moisture content, temperature and location for 1-mm aluminum beads covered with a thin layer of surface water that is evaporated in an ISD with mobile impingement zones (Meltser et al., 1985). It can be seen that the heat transfer rate differs significantly in the period of particle deceleration and acceleration due to the different gas-particle relative velocities. Despite the stabilizing effect of oscillatory motion, this difference can be as high as 35% to 40%. Because of surface water evaporation, the drying rate is controlled by the rate of external heat transfer. Thus, it is higher in the deceleration period than in the acceleration period because of the larger difference between gas and particle velocities. The particles are completely dry within 0.6 second, that is, within less than one cycle of oscillation.

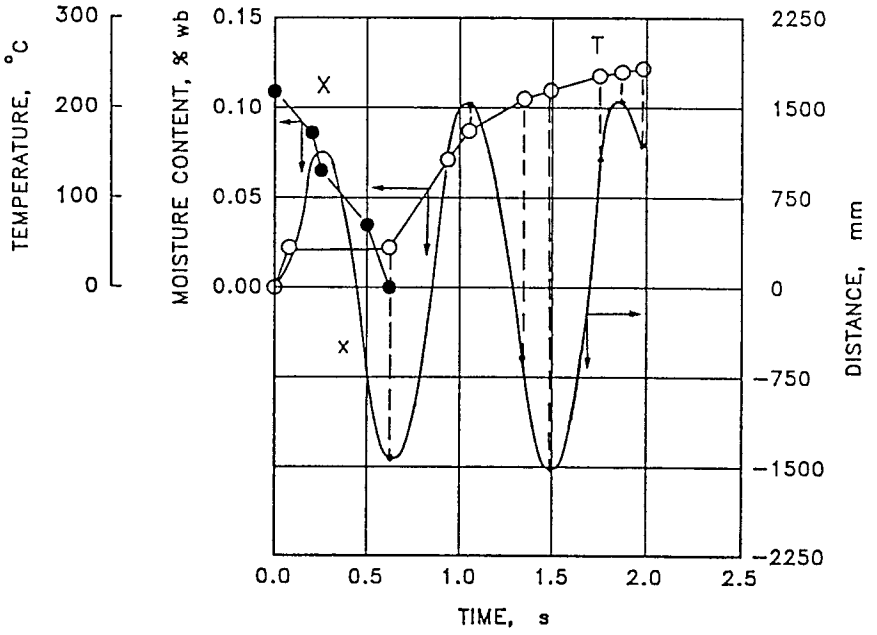

FIGURE 5.7 Temporal variation of axial position, moisture content, and particle temperature in an impinging-stream dryer with a mobile impingement zone ($T_{g1} = 250°C$, $u_0 = 30$ m/s, $X_1 = 0.11$ kg/kg).

Figure 5.8 presents the drying kinetics of crystalline lysine with initial moisture content of 15.2% in an ISD with mobile impingement zones. The air temperature was 120°C, flow velocity 20 to 23 m/s, and the frequency of reversing motion of about 1.0 to 1.2 Hz (Meltser and Tutova, 1986). Curve 1 represents drying of monodisperse crystals (0.4 mm mean diameter) at mass concentrations of 0.2 to 0.5 kg/kg of air. In this case the surface water is removed within one period of motion (2 to 3 s). The desired moisture content level of 1% can be achieved within 5 periods of oscillation. Curve 2 shows the drying kinetics for polydisperse lysine with a mean diameter ($d = \sum x_i d_i$) equal to 1 mm with simultaneous grinding due to the oscillatory motion of the inert material (mixture in 1 : 1 mass ratio of 2 mm steel and 3 mm aluminum beads) at a mass concentration of 1.0 to 1.5 kg of inert per kg of drying material. Compared with curve 1 the drying rate with simultaneous disintegration is appreciably higher in the first period of reverse motion mainly due to a reduction of the heat transfer resistance inside the material and increase of

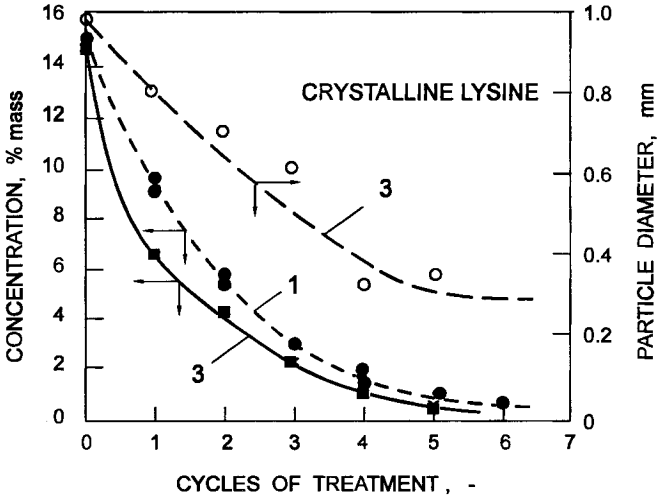

FIGURE 5.8 Drying and grinding characteristics for lysine: 1—drying kinetics for monodisperse crystals; 2—drying kinetics for polydisperse crystals; 3—grinding curve for polydisperse crystals.

the mass transfer area due to particle disintegration. After a certain number of oscillations the drying rate decreases and follows a similar decrease in the intensity of crystal disintegration (curve 3).

Figure 5.9 presents a schematic of the impinging streams dryer used to dry a crystalline lysine. The dryer consists of air conveying ducts with two impingement chambers situated at the ends of a central drying duct 1.5 m in length. Both chambers are connected via outlet ducts and cyclones to a flow-switching device. The outlet ducts are constrained by grids with a grid opening of 1.3 mm. A mixture of steel (2 mm) and aluminum (3 mm) beads in 1:1 mass ratio is used to disintegrate the crystals and brake lumps. The mass concentration of the inert beads in the drying duct is maintained at 1 to 1.5 kg/kg. The frequency of reverse motion between the impingement chambers is 1 to 1.2 cycles per second. Hot air at 135°C and 20 to 23 m/s enters both ends of the impingement chambers. A switching device moves the impingement zone periodically between the two impingement chambers. This results in an oscillatory motion both of the inert beads and the wet particles, which are continuously fed to one end of the duct only. After performing 4 to 5 oscillations, which are the equivalent of 10 to 15 seconds of drying time, the material is well ground and dry (see Figure 5.8) so it is carried away through

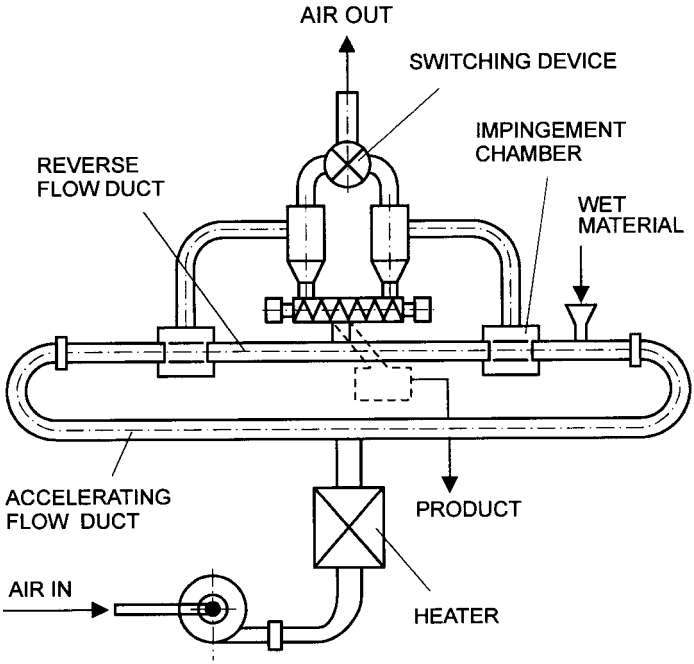

FIGURE 5.9 Impinging-stream dryer with mobile impingement zone for drying of crystalline lysine.

the constraining grids to the cyclones. The volumetric evaporative capacity of the dryer is about 1700 kg $H_2O/(m^3h)$, while air and heat consumption (without heat recovery) per kg of water evaporated are 200 to 250 Nm^3 and 3 to 3.6 MJ, respectively. These show that the performance of the ISD is superior to that of a fluidized bed dryer (Meltser and Tutova, 1986).

Interestingly, better drying performance (lower final moisture contents and higher volumetric evaporation rates) was found for ISD with a rectangular impingement chamber than for the cylindrical one that is commonly used in laboratory studies and industrial units (Cao and Liu, 2000). This effect can be attributed to a different flow pattern that results in improved heat and mass transfer.

More information on other types of industrial dryers with impinging streams can be found in open literature (Kudra et al., 1995, Tamir, 1994). These are the semicircular configuration developed for thermal processing of grains in superheated steam (e.g., drying, puffing, and carrying out certain

thermally induced biochemical reactions), the vortex spray dryer for suspensions and slurries that operates essentially as a countercurrent counterrotating impinging stream dryer, the hybrid system based on drying of a sewage sludge in a coaxial ISD followed by flash drying in the pneumatic duct and drying in a swirling stream during segregation in the centrifugal separator, the impinging-streams spray dryer for salt solutions and products of biotechnology, as well as the ISD with swirling streams for highly dispersed pharmaceuticals.

5.4 SOME RECENT STUDIES ON ISD

Mujumdar (1990) proposed a novel two-dimensional superheated steam ISD to minimize the problems of scale-up when using round ducts in ISD and to benefit from the advantages of superheated steam as a drying medium (discussed elsewhere in this book). Hosseinalipour and Mujumdar (1996) carried out a fundamental computational fluid dynamic analysis of the confined opposing jet system for the first time to explore the flow fields in both single-phase and two-phase particle-gas turbulent flows. A two-phase turbulence model was used to predict the turbulent two-phase flow. This study was extended to include drying of mono-sized particles entrained into one of the opposing jets with superheated steam as the drying medium. Further, the effects of all key parameters (e.g., geometry, flow rate, steam temperature) as well as operating pressure for various size particles entering the system at different locations within the jet were examined. It was shown that under certain conditions the particles penetrate deep into the opposite stream before being re-entrained into the impingement zone. This phenomenon may repeat itself several times, resulting in longer residence times for the larger particles. The smaller particles follow the streamlines and exit the chamber with shorter residence times.

There are several advantages to a mathematical simulation of the system when there are numerous parameters affecting the outcome. ISD provides a particularly challenging transport problem for CFD simulations. In view of the fact that no detailed turbulence measurements are available in the literature for a confined opposing jet system, the model of Hosseinalipour and Mujumdar remains to be validated with data. The results, however, are physically realistic. For numerical details, the reader is referred to the source work (Hosseinalipour, 1997).

Some of the basic conclusions of the simulation work are summarized as follows: Residence time of particles in the ISD decreases with increasing Reynolds number of the jet (stream) but increases with spacing between the opposing nozzles. Particles entering closer to the jet mid-plane tend to have

longer residence times. Increasing steam temperature yields better drying performance. The effect of operating pressure is quite complex due in part to the highly nonlinear behavior of the system and the effect of pressure on thermophysical properties of steam. The optimum operating pressure for superheated steam drying of particles in the surface water removal period in the simple opposing jet system modeled was found to be 202 kPa, which gave a higher heat transfer coefficient and longer residence time for the particles. The existence of optimum pressure is, however, very difficult to explain in simple physical terms due to the inherently highly nonlinear nature of the hydrodynamics involved as well as the nonlinearity of temperature-dependence of the thermal and physical properties of the carrier medium. This remains a challenging problem for both theoretical and experimental research.

More advanced mathematical models along with careful experimental data are needed to design and analyze ISD systems more reliably. There is a further complication associated with the fact that the entrained particles may agglomerate or disintegrate on collision with other particles. Also, little is known about the collision characteristics of wet particles, which must depend on their moisture content as well.

6

Drying in Pulsed Fluid Beds

Fluidization is one of the most commonly used techniques for drying particulate solids. The technique relies on a high-velocity hot gas stream that creates a ''fluid bed'' with special hydrodynamic and heat/mass transfer characteristics. Although well entrenched in industry, fluid bed dryers have the following disadvantages that limit their application:

A relatively high pressure drop that calls for high-pressure blowers
Particle shape restricted to those approaching sphere or cuboid
Bed height limited to between the minimum height that will ensure uniform fluidization and the maximum height allowed by the pressure drop
Restricted particle size and size distribution; polydisperse materials cause excessive entrainment, while both fine and coarse materials do not fluidize well
Susceptible to aggregative fluidization or channeling resulting in bed instability and reduced transfer characteristics

The negative effects from the last two constraints can be alleviated or even eliminated when applying periodic flow of the fluidizing gas which cre-

ates the so-called pulsed fluidized bed. Although simple shut-off and start-up of a fluidizing gas stream with frequency from 0.5 to 4 Hz is used in some dryers (e.g., Anon, 1990a), in most cases gas pulsation is generated by a butterfly valve installed in the gas inlet duct and rotated at a specified angular velocity. Thus, the instantaneous superficial gas velocity varies across the bed area from zero to the maximum. Better hydrodynamics of such a pulsated fluid bed are, however, offset by additional pressure drop due to the on–off operation of the valve as well as by the back-pressure developed that can create problems with direct gas firing. Vibration of the dryer body is also of important concern, although in a design patented by Sztabert et al. (1978), pulsation of a gas stream is used to vibrate the supporting grid in a special type of the vibrated fluid bed. Figure 6.1 presents the schematic of a pulsed fluidized bed dryer manufactured by Buhler-Miag GmbH (Germany) where pulsation of a fluidizing gas is obtained by rotation of a dual butterfly valve with wings displaced by 90°. Such a design greatly reduces the negative effects of a single pulsator as the gas shut-off phase is alternated between two longitudinal segments of the bed.

The pulsed fluidization can be further altered with some advantage if one uses periodic relocation of the gas stream; that is, when the fluidizing gas is supplied sequentially to different sections of the bed. In fact, the idea of ''relocation'' of a supplementary gas to eliminate channeling in a fluidized bed of fine particles originated over 40 years ago (Belik, 1960), but it was not followed up. A similar principle of the gas-jet relocation has been proposed to fluidize particulate material by sequential relocation of the ''spouting'' gas

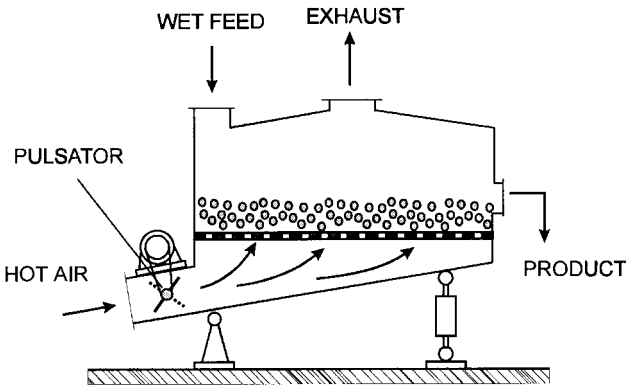

FIGURE 6.1 Pulsed fluid bed dryer with a dual butterfly valve.

jet (Gawrzynski, 1987; Elenkov et al., 1989). With reference to Figure 6.2, the so-called rotation-pulsed fluidized bed (RPFB) is formed when a continuous gas jet is injected into the bed via a rotating disk with one or several sector-shaped orifices. When the rotational speed of the disk is relatively low (several rpm), the bed behaves as the rotating jet-spouted bed with a distinct spout moving around an essentially fixed bed of particles (see Chapter 31). When the disk rotates with sufficient velocity, which depends on the number of orifices, the bed starts to be fully fluidized. It was found that for a frequency of gas jet relocation above 2 Hz, the transition from fixed to fluidized bed as

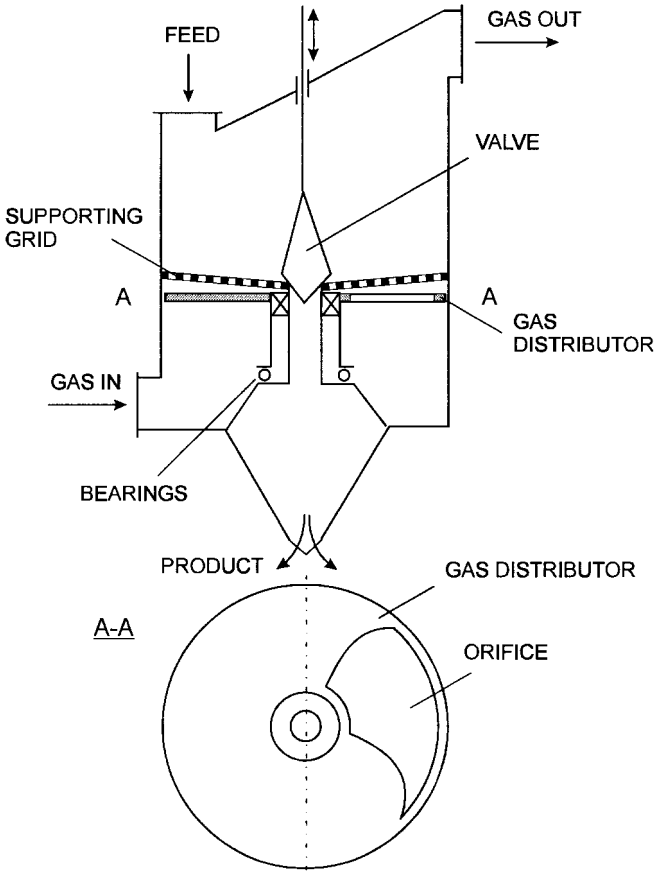

FIGURE 6.2 Rotation-pulsed fluid bed dryer. (From Gawrzynski, 1987).

well as the bed pressure drop do not depend on the shape or particle size. High fluidization ratio at lower volumetric flow rates as well as uniform but intensive particle mixing are claimed as additional benefits of the RPFBs (Elenkov and Djurkov, 1992).

Basic hydrodynamic parameters of the rotation-pulsed fluidized bed can be calculated from the following relationships (Elenkov and Djurkov, 1992; Djurkov, 1998):

$$\mathrm{Re}_{mf} = 0.013 Ar^{0.63} \tag{6.1}$$

$$\Delta P = 9.36 \frac{m}{F} - 160 \tag{6.2}$$

or

$$\Delta P = K[1 - 0.52\varphi(1 - 2.7 \cdot 10^{-4} K)] \tag{6.3}$$

where the parameter K (N/m^2) is defined as

$$K = \frac{mg}{F}\left(1 - \frac{\rho_g}{\rho_s}\right) \tag{6.4}$$

and Re_{mf} is the Reynolds number defined by the minimum fluidization velocity and equivalent particle diameter.

As reported by Djurkov (1998), Eq. (6.3) was used for the successful design of two industrial dryers: for sesame seeds and minerals with capacities of 100 kg/h and 3000 kg/h, respectively.

Another drying technology, which is based on relocation of the fluidizing gas stream is the so-called pulsed fluidized bed with relocated gas stream (for simplicity, to be referred to as the PFB), which combines features of pulsofluidization with gas stream relocation (Gawrzynski and Glaser, 1996; Gawrzynski et al., 1989). A PFB dryer is essentially similar in design to a conventional fluid bed dryer except that the plenum chamber below the supporting grid is divided into several sections by vertical partitions (Figure 6.3). The primary hot air enters the dryer through a rotary valve-distributor, which periodically interrupts the air stream and directs it in rapid succession to different gas chambers below the supporting grid. Air in the ''active'' chamber fluidizes that segment of the bed, which is located above the active chamber. This fluidized segment of the bed becomes almost stagnant when the air stream is directed to the next chamber. In practice, however, the entire bed is fairly fluidized because of gas compressibility and bed inertia as long as the frequency of gas relocation is high enough (typically from 6 to 12 Hz). Even a

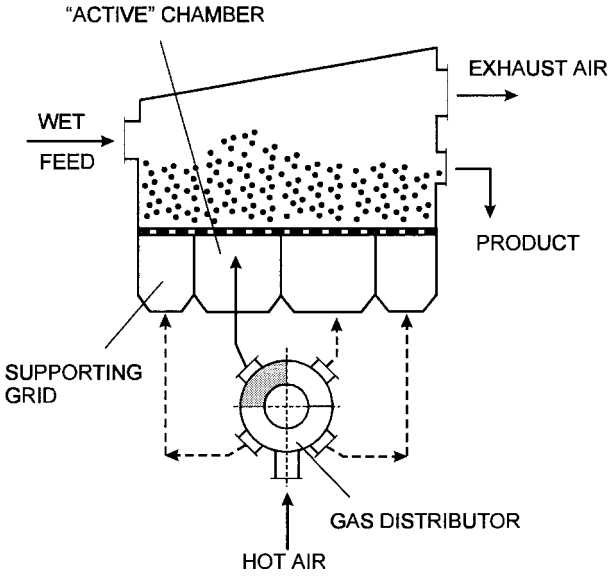

FIGURE 6.3 Principle of the pulsed fluid bed with relocated air stream.

simple on–off valve can be used to direct a gas stream to consecutive sections of the bed. The advantage of the rotary valves is, however, that the nearly sinusoidal variation of the gas flow makes relocation of the ''active'' bed smoother. In addition, a special design of a disk-type gas-distributor eliminates the back-pressure effect as well as facilitates fluidization by superposing constant and pulsed air streams (Kudra et al., 1999). A modification of the pulsed fluid bed with relocated gas stream is a spouted bed configuration where the gas stream from a rotary valve-distributor periodically activates the bed of particles in a tapered chamber with a rectangular cross-sectional area (Jezowska, 1993).

The hydrodynamic characteristics of a PFB are essentially the same as those of fluidized or spouted beds. However, there is no peak in the pressure–velocity curve; the pressure drop increases gradually with gas velocity, even with fully developed fluidization (Figure 6.4). Although the pressure drop in the PFB is of the same order as that in the classical fluid bed for the same gas velocity and the same free cross-sectional area of the supporting grid, the PFB technology offers a lower pressure drop because of the combined effects from the following:

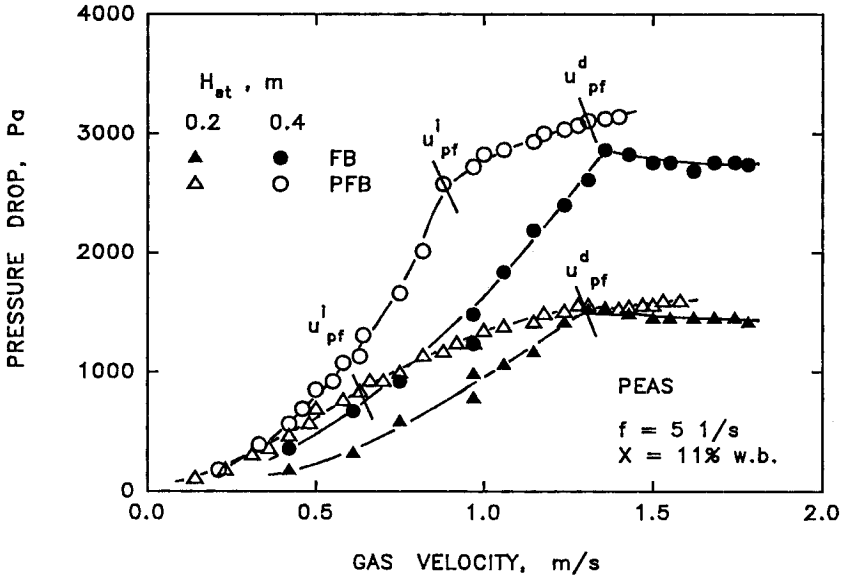

FIGURE 6.4 Pressure drop in a fluidized bed and a pulsed fluid bed dryer with relocated air stream. (Adapted from Zgorzalewicz and Glaser, 1989.)

1. Larger free cross-sectional area (up to 30%) of the supporting grid as compared to several percent in the case of conventional fluid beds
2. Lower operating velocity (on average by 8%–25%) because both the minimum and the maximum pulsed fluidization velocities are shifted toward lower values

Examples of correlations for pressure drop in a PFB are given in Table 6.1.

It should be noted that the term ''fluidization'' does not adequately reflect the bed behavior as particles in the PFB are vibrated rather than fluidized. Thus, at incipient pulsed fluidization (also called the lower pulsed fluidization velocity) and above, the bed performs as the vibrated or vibro-fluidized bed with frequency and amplitude depending on air velocity, static bed height, and frequency of the air stream relocation (Gawrzynski and Glaser, 1996; Blacha-Jurkiewicz, 1987). With increasing air velocity, more air bubbles and isolated spouts appear in the bed; this velocity is called the upper (developed) pulsed fluidization velocity. Above this velocity, the bed turns into a classical

TABLE 6.1 Pressure Drop in PFB for Selected Materials

Material	Correlation	Remarks
Recycled polypropylene (Gawrzynski et al., 1999)	$\Delta P = \rho g H_{st}$, Pa	$d_e = 0.00005–0.0011$ m $u = 0.18–0.25$ m/s $f = 5–15$ l/s $N = 3$
Acenol[a] Pentaerythritol *Calcium gluconicum* (Gawrzynski et al., 1989)	$\Delta P = 1.52\, u^2 \rho\, \mathrm{Re}^{-1.45}\, Ar^{0.68} \left(\frac{H_{st}}{d_e}\right)^{1.01}$, Pa	$H_{st} = 0.05–0.2$ m $f = 5–15$ l/s $d_e = 0.0006–0.0024$ m $N = 3$
Thiohexame[b] (Gawrzynski et al., 1989)	$\Delta P = 7242\, u^{0.409}\, H_{st}^{1.06}\, f^{0.08}$, Pa	$H_{st} = 0.055–0.2$ m $f = 5–15$ l/s $N = 3$ $d_e = 0.0015$ m
Peas, bean (Gawrzynski et al., 1989)	$\Delta P = 28.73\, u^2\, \rho \left(\frac{H_{st}}{d_e}\right)^{1.06} \left(\frac{u}{u_{mf}}\right)^{-0.86} \left(\frac{d_e f}{u_{mf}}\right)^{0.17} X^{0.15}$, Pa	$H_{st} = 0.05–0.4$ m $f = 2.9–10.7$ l/s $N = 6$
P&P primary sludge (Gawrzynski et al., 2002)	$\Delta P = 0.47 \Delta P_{st} H_{st}^{0.18} f^{0.19}$, Pa	$d_e = 0.0001–0.01$ m $f = 5–10$ l/s $H_{st} = 0.05–0.2$ m $N = 3$ $u = 0.1–1.4$ m/s

[a] $OHC_6H_4NHCOCH_3$
[b] $C_{13}H_{16}S_2N_2$

fluidized bed, and the effect of the pulsating air flow, and thus particle vibration, becomes relatively insignificant.

Review of published papers and our own experiments indicate that the PFBs can handle a variety of particulate materials ranging from fine powders of about 0.05 mm in diameter (recycled polypropylene) through large granules and crystals up to several millimeters (P&P primary sludge, potash), flakes (shredded polyethylene foil, sliced vegetables), and fiber (hog fuel), to large strips like wood strands. Therefore, the real advantage of the PFB over the classical fluid bed is its ability to process materials that are difficult to fluidize. The advantage over the vibro-fluidized bed is no vibration of the dryer body.

The typical operating parameters of a PFB dryer are

1. Bed height: from 0.1 to 0.4 m
2. Gas velocity: from 0.3 to 3.5 m/s (depending on the particle characteristics)
3. Pressure drop: from 300 to 1800 Pa
4. Frequency of gas pulsation: from 4 to 16 Hz

Table 6.2 provides, as an example, the set of design equations for drying of sliced vegetables in a PFB dryer with relocated gas stream. Another set of equations for a spouted bed configuration obtained from experiments with wheat, barley, beet, onion, rapeseed, and carrot seeds is given in Table 6.3. Detailed information as well as relationships for other products such as sugar or pharmaceuticals can be found in a comprehensive paper by Gawrzynski and Glaser (1996).

Drying kinetics in a pulsed fluidized bed (Figure 6.5) are similar to those for convective drying in a system with perfect gas–solid contact which conforms to the ''thin-layer drying'' conditions. The following equations are given as examples:

For sliced vegetables (beet, parsley, carrot, celery, potato, onion) dried in a rectangular PFB with relocated air stream (Gawrzynski, 1996)

$$\frac{X}{X_0} = e^{-\mathrm{kt}} \tag{6.5}$$

For wheat and beet seeds dried in the spouted bed configuration (Jezowska, 1993)

$$\frac{X - X_{eq}}{X_0 - X_{eq}} = \exp(-kt^n) \tag{6.6}$$

TABLE 6.2 Design Correlations for Drying of Sliced Vegetables[a] in a Pulsed Fluid Bed Dryer

Parameter	Equation
Incipient pulsed fluidization velocity, m/s	$u_{pf}^{i} = 0.486 \dfrac{\mu}{d_e \rho} \dfrac{\varepsilon_{st}^3 \, Ar^{0.442}}{\varphi(1 - \varepsilon_{st})}$
Incipient pulsed fluidization velocity, m/s (if φ and ε are not known)	$u_{pf}^{i} = 0.612 \dfrac{\mu}{d_e \rho} Ar^{0.386}$
Developed/incipient pulsed fluidization velocities ratio	
for raw material	$\dfrac{u_{pf}^{d}}{u_{pf}^{i}} = 1.91 \pm 15\%$
for product	$\dfrac{u_{pf}^{d}}{u_{pf}^{i}} = 1.88 \pm 20\%$
Pressure drop, Pa (bed of raw material)	
$u_{pf}^{i} \le u \le 0.7 \, u_{pf}^{d}$	$\dfrac{\Delta P}{u^2 \rho} = 2.75 \cdot 10^{-5} \, \mathrm{Re}^{-1.72} \, Ar^{1.33} \left(\dfrac{H_{st}}{d_e} \right)^{1.48}$
Pressure drop, Pa (bed of product, except onion)	
$u_{pf}^{i} \le u \le u_{pf}^{d}$	$\Delta \mathrm{P} = 1229_{u}{}^{0.76} \mathrm{H}_{st}^{1.09}$
Pressure drop, Pa (at $u = u_{pf}^{d}$)[b]	
bed of dry product	$\Delta P = H_{st} \rho_{bd} \, g$
bed of raw material	$\Delta P = H_{st} \rho_m (1 - \varepsilon_{st}) \, g = H_{st} \, \rho_{bw} \, g$
Pressure drop, Pa (temporal)	$\Delta P = \Delta P_0 \left(\dfrac{X}{X_0} \right)^{0.61}$
Bed height, m (temporal)	$H = H_0 \left(\dfrac{X}{X_0} \right)^{0.28}$

[a] Parsley, carrot, beet, celery, potato, onion.

[b] ρ_{bd} and ρ_{bw} are bulk densities of the product and raw material, respectively; ρ_m is solid (wet material) density; index 0 refers to the initial conditions.

Source: Glaser, 1991.

TABLE 6.3 Equations for Pulsed Spouted Bed Dryer for Grain and Vegetable Seeds

Parameter	Equation
Pressure drop at incipient spouting, Pa	$12.08\ H_{st}^{1.11}\ \rho_b^{0.99}$
Pressure drop at fully developed spouting, Pa	$8.63\ H_{st}^{0.97}\ \rho_b^{0.99}$
Incipient spouting velocity, m/s	$72.87\ H_{st}^{0.52}\ d_e^{0.62}\ \rho_b^{0.09}$
Fully developed spouting velocity, m/s	$190.56\ H_{st}^{0.56}\ d_e^{0.74}\ \rho_b^{0.08}$

Source: Jezowska, 1991.

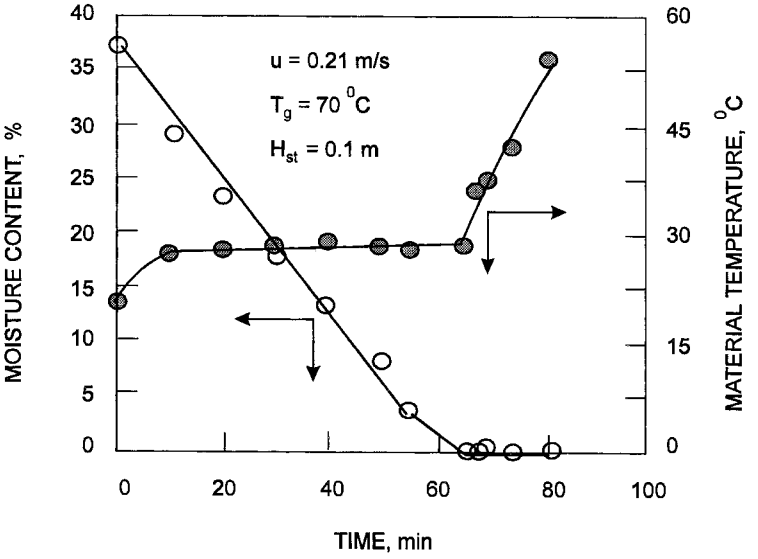

FIGURE 6.5 Drying and temperature curves for recycled polypropylene. (From Gawrzynski et al., 1999.)

TABLE 6.4 Comparison of the PFB with Band Dryers for Sliced Parsley and Celery Roots[a]

Index	PFB[b]	Band dryer SP-66 (Yugoslavia)	Band dryer 41A (Bulgaria)
Unit consumption of thermal and electrical energy	1.0	1.16	1.37
Floor area (dryer only)	1.0	4.7	6.25
Space volume (dryer only)	1.0	3.04	4.06

[a] Throughput 150 kg/h of dry product.
[b] The PFB dryer is taken as a basis.
Source: Glaser and Gawrzynski, 1990.

where

$$k = B(273 + T_g)^C \tag{6.7}$$

and

$B = -1.94 \cdot 10^{-12}$; $C = 3.66$; $n = 0.78$ (for beet seeds)
$B = -1.91 \cdot 10^{-21}$; $C = 7.28$; $n = 0.63$ (for wheat seeds)

A comparison of the PFB dryer with conventional band dryers for sliced vegetables operated under the same conditions (Table 6.4) clearly indicates better performance of the PFB dryer, which results in lower energy consumption and smaller dryer volume.

7

Superheated Steam Drying

7.1 INTRODUCTION

Although the concept was originally proposed over 100 years ago and the first industrial applications were reported some 60 years ago in Germany, superheated steam drying has emerged as a viable technology with immense potential only in the past decade or so. Essentially, superheated steam drying (SSD) involves the use of superheated steam in a direct (convective) dryer in place of hot air, combustion, or flue gases as the drying medium to supply heat for drying and to carry off the evaporated moisture. Any direct or direct/indirect (e.g., combined convection/conduction) dryer can be operated as a superheated steam dryer, in principle. However, the SSD technology is more complex and hence this conversion is not simple. Also, additional criteria must be considered when selecting a dryer for possible adaptation to SSD conditions.

Currently, fewer than 10 major dryer manufacturers around the world offer SSD technology on a commercial scale. Often, it is necessary to custom-design a superheated steam dryer for a new application, which may involve a new dryer type or an application to a new product. Mujumdar (1990) has presented an extensive review of principles, practice, industrial applications, potential new applications, market penetration potential, and R&D needs for

SSD technologies. Special consideration is given to potential applications for use of electricity and reuse of the exhaust steam from an SSD. Kumar and Mujumdar (1990) have provided an extensive bibliography and discussed the basic principles and applications of SSD.

One of the obvious advantages of SSD is that the dryer exhaust is also steam, albeit at lower specific enthalpy. In air drying, the latent heat in the exhausted stream is generally difficult and expensive to recover. Indeed, at current world prices of energy sources, it is often more expensive to recover energy in the exhaust stream than to waste it in the stack gases for most direct dryers with low- to medium-temperature exhausts.

If air infiltration is avoided (or minimized to an acceptable level), it is possible to recover all of the latent heat supplied in the SSD from the exhaust by condensing the exhaust stream or by mechanical- or thermo-compression to elevate its specific enthalpy for reuse in the dryer. Since the SSD produces steam equal in amount to the water evaporated in the dryer, it is necessary to have a useful application for this excess steam in the process plant. If this steam is used elsewhere, the latent heat recovered is not charged to the SSD, leading to a net energy consumption figure of the 1000 to 1500 kJ/kg water removed for the SSD compared with 4000 to 6000 kJ/kg water removed in a corresponding hot-air dryer. Thus, reduced net energy consumption is a clear advantage of the SSD. Other key advantages of superheated steam dryers are as follows:

No oxidative or combustion reactions are possible in SSDs. This means no fire or explosion hazards and often also a better quality product.

Higher drying rates are possible in both constant and falling rate periods, depending on the steam temperature. The higher thermal conductivity and heat capacity of superheated steam lead to higher drying rates for surface moisture above the so-called inversion temperature. Below the inversion temperature, drying in air is faster. The main reason for accelerated drying rate, the inversion temperature is the higher product temperature in SSD (over 100°C at 1 bar) and no resistance to diffusion of water vapor in superheated steam. Also, it is known that many products that exhibit the so-called case-hardening in rapid air drying do not form such water-impermeable shells when dried in superheated steam.

For products containing toxic or expensive organic liquids that must be recovered, steam drying avoids the danger of fire or explosions while allowing condensation of the off-streams in relatively smaller condensers.

Superheated steam drying permits pasteurization, sterilization, and/or deodorization of food products.

Accompanying the above advantages are several limitations:

The superheated steam system is more complex. No leaks can be allowed since noncondensables cause problems with energy recovery by compression or condensation. Feeding and discharge devices must protect the dryer from the infiltration of air. The product itself may bring in noncondensables. Start-up and shut-down are more complex operations for SSD than for an air dryer.

Since feed enters the dryer at ambient temperature, there is inevitable condensation in the SSD before evaporation begins. This adds about 10% to 15% to the residence time in the dryer. At 1 bar operating pressure, the drying begins at a product temperature of 100°C in the constant rate period when surface water is being removed. Alternatively, a preheater is needed for the feedstock.

Products that may melt, undergo glass transitions, or be otherwise damaged at the saturation temperature of steam at the dryer operating pressure cannot clearly be dried in superheated steam even if they contain only surface moisture. Operation at reduced pressure, however, is a feasible option that may also enhance the drying rate. Products that may require oxidation reactions (e.g., browning of foods) to develop desired quality parameters cannot be dried in superheated steam. However, it may be possible to consider a two-stage drying process (e.g., steam drying followed by air drying). For drying of silk cocoons, for example, such a process appears to yield a higher quality product, namely, brighter and stronger silk fiber.

If the steam produced in the dryer is not needed elsewhere in the process, the energy-related advantages of SSD do not exist. Also, steam cleaning may not always be a simple task. The chemical composition of the condensate must be carefully evaluated. The cost of the ancillaries (e.g., feeding systems, product collection systems, exhaust steam recovery systems, etc.) is typically much more significant than the cost of the steam dryer alone. In most cases, the SSD is a justifiable option only for continuously operated and very large tonnage systems because of the technoeconomics of the ancillary equipment needed.

There is currently limited field experience with SSD for a smaller range of products. This database is expected to increase significantly in the coming decade. In the meantime, more pilot testing is recommended for the SSD application since the quality aspects are generally unpre-

dictable although the drying rates are predictable with some confidence in some cases.

7.2 BASIC PRINCIPLES OF SUPERHEATED STEAM DRYING

Superheated steam has heat transfer properties superior to air at the same temperature. Since there is no resistance to diffusion of the evaporated water in its own vapor, the drying rate in the constant rate period is dependent only on the heat transfer rate. The convective heat transfer coefficient (h) between steam and the solid material surface can be estimated using standard correlations for interphase heat transfer. Neglecting sensible heat effects, heat losses, and other modes of heat transfer, the rate at which surface moisture evaporates into steam is given simply by

$$w_D = \frac{q}{\Delta H} = \frac{h(T_{ss} - T_s)}{\Delta H} \tag{7.1}$$

where w_D is the evaporation rate [kg water/(m^{2}s)], T_s is the drying surface temperature, which corresponds to the saturation temperature at the operating pressure, and T_{ss} is the temperature of the superheated steam.

In hot-air drying the surface temperature is equal to the wet bulb temperature ($T_s = T_{wb}$), and hence at the same gas temperature the temperature difference (ΔT) is higher in air drying but the heat transfer coefficient (h) is lower. It turns out that these counteracting effects lead to the phenomenon of ''inversion''—a temperature at which the superheated steam drying rate is greater than dry-air drying rate (Figure 7.1). This is confirmed experimentally and numerically for water as well as several organic solvent systems (superheated vapor drying). It is observed that the inversion temperature is in the order of 160 to 200°C for evaporation of water in superheated steam for various flow configurations and flow regimes, i.e., laminar/turbulent boundary layer flows, impinging jet flows, free convective flow over bodies of complex geometry, etc. Thus, superheated steam will yield high drying rates above the corresponding air drying rates for convective drying when surface moisture is being removed. The ''inversion temperature'' is thus defined only for surface moisture evaporation and not for internal moisture removal. Note that SSD may lower the critical moisture content as well (Shibata et al., 1998).

Often it is observed that drying rates in the falling rate period are also higher in superheated steam drying relative to air drying. The mechanisms responsible for this phenomenon are, however, quite different. In superheated

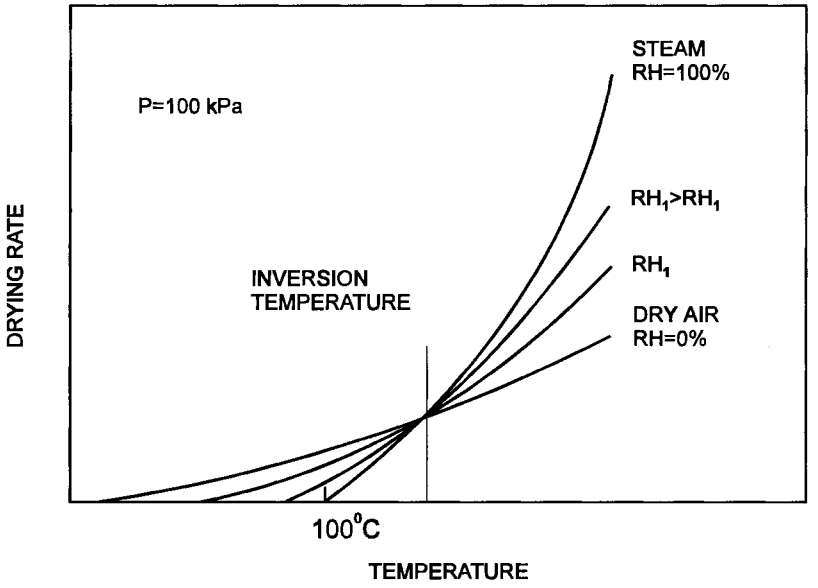

FIGURE 7.1 Drying rate vs. gas temperature for air and steam.

steam drying, the product temperature is higher and hence moisture mobility is greater. Note that in steam environment, case-hardening (or ''skinning'') may not occur, which eliminates a possible impediment to intensive drying. The product is likely to be more porous as well.

7.3 CLASSIFICATION AND SELECTION OF SUPERHEATED STEAM DRYERS

Figure 7.2 provides a classification of superheated steam dryers based on their operating pressure. The product temperature necessarily exceeds the saturation temperature of steam corresponding to the operating pressure. So for products that may undergo undesirable physical transformations (e.g., melting) or chemical transformations (e.g., hydrolysis) at elevated temperatures with steam or with the small quantities of oxygen that leaks usually into any drying system, a low-pressure operation is desirable. The vapor evolving from the product may be withdrawn from the chamber, condensed, and the latent heat recovered. Alternatively, the vapor is reheated within the chamber by tubular or plate heat exchangers and recirculated as a convective drying medium to

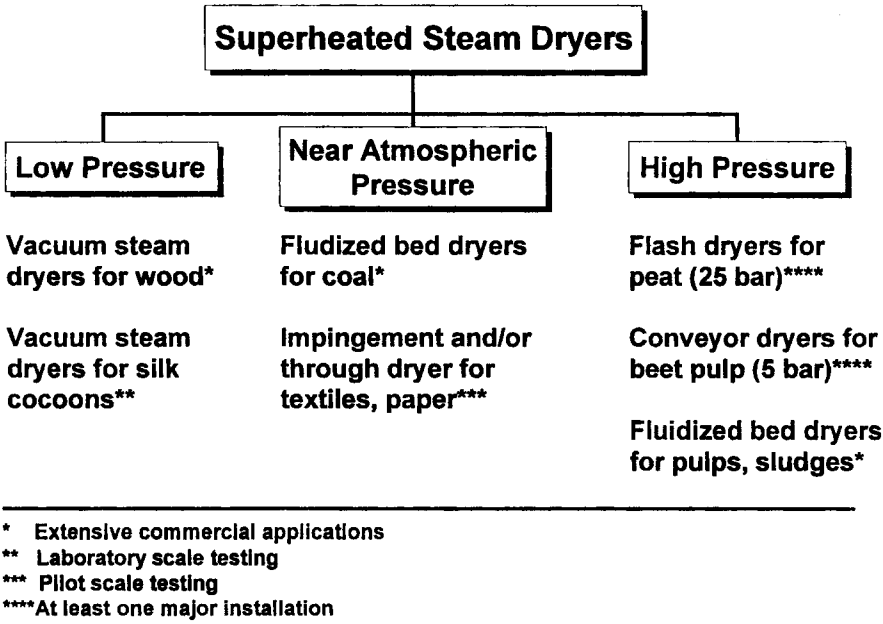

FIGURE 7.2 Classification of superheated steam dryers.

enhance the drying rate. Such systems are used commercially to dry timber with very attractive results; while the net energy consumption is reduced several-fold, the product quality is enhanced and the environmental problem of emission of the volatile organic compounds (VOCs) produced during drying is also eliminated (Mujumdar, 1990). The organic volatile components (boiling point ranging from room temperature to over 200°C) are condensed out with the steam; since these two are immiscible, simple decantation allows recovery of the condensables, which may be sold separately (e.g., terpenes, essential oils).

In general, superheated steam drying is worth considering as a viable option only if one or more of the following conditions apply:

Energy cost is very high; product value low or negligible (e.g., commodities like coal, peat, newsprint, tissue paper, waste sludges which must be dried to meet regulatory requirements).

Product quality is superior if dried in steam rather than in air (e.g., newsprint, which yields superior strength properties in steam and permits

lower chemical pulp content to attain the same strength and runability).

Risk of fire, explosion or other oxidative damage is very high (e.g., coal, peat, pulps, etc.). Lower insurance premiums may partially offset the higher investment cost of a steam dryer.

Quantity of water to be removed as well as production capacity required are high. This affords economy of scale. Clearly, such dryers are worth considering only for continuous operation because of the inherent problems associated with start-up and shut-down when water condensation on the product as well as presence of noncondensables (air) cause problems.

7.4 QUALITY CONSIDERATIONS

It is impossible to generalize the effect of steam drying on product quality. Table 7.1 gives a summary of tests carried out at McGill University on batch drying of hand sheets in a static apparatus in which the samples were dried under an impingement flow of superheated steam. Note that the effects are all positive relative to drying in air environment or, at most, comparable. Similar tests on paper dried on a dynamic pilot scale apparatus in Finland have yielded comparable results (Douglas, 1994).

TABLE 7.1 Summary of Tests Carried Out at McGill University

Property	Effect of steam drying (relative to air drying)
Bulk	Slight increase
Surface roughness	Marginal increase
Burst	20% Enhancement (typical)
Tensile index	20%–30% Improvement
Stretch	No significant effect
Folding endurance	No noticeable difference
Scott internal bond strength	10%–20% Higher
Wet strength	Little effect
Permeability	Little effect
Crystallinity	No measurable change
Brightness	Above 300°C, a little worse
Fiber strength (zero span)	Little change

TABLE 7.2 Factors Contributing to the Feasibility of Superheated Steam Drying

Factor	Impact
Product-related factors	
Low-temperature sensitivity	To avoid higher steam temperature, more expensive vacuum systems are required.
High moisture content	Since the latent heat of the moisture can be recovered with SSD, the bigger the portion it represents, the greater the efficiency improvement will be.
High thermal resistance	Higher surface temperature with SSD reduces heating and drying times.
High sensitivity to oxidation	Lack of oxygen with SSD improves product quality.
Undesirable taste or aroma	SSD strips more of the acids that contribute to bitter aromas.
High product values	Drying-time reductions provide biggest inventory cost savings with higher-value products.
Process-related factors	
Other uses of steam available	Marginal energy consumption for the process is small and the capital costs are minimized.
Environmental emissions from dryers	SSD provides easier recovery of solvents and particulates.
Combustion/explosion hazards	Lack of oxygen significantly reduces fire/explosion hazards.
Expensive source of thermal energy	Thermal energy savings with SSD will offset greater energy costs than with waste fuels (e.g., hogged wood waste).

Extensive results have been reported in the literature on the drying of wood as well. Again, all quality indicators are positive. Thus, the vacuum superheated steam drying systems have already been commercialized by several vendors worldwide. It is noteworthy that besides enhancement of the prod-

uct quality, the drying times are reduced two- to fivefold, which results in a significant reduction of inventory cost of the dryer.

For drying of silk cocoons, laboratory scale tests done in China had proven the enhanced quality parameters (e.g., brightness, strength of fiber, etc.) of the silk produced by steam drying at a temperature around 45°C. For certain food or vegetable products, the yielded porous structure of the product dried in superheated steam (due to evolution of steam within the product, which enhances porosity) is a desirable characteristic. This decreases the bulk density of the product while enhancing rehydration characteristics. The color and texture of the product may also become more desirable. Thus, the increased cost of steam drying may be offset by the additional credit received for the better quality of the dried product.

As noted above, any direct dryer, in principle, can be converted to superheated steam operation (e.g., flash, fluidized bed, spray, impinging jet, conveyor dryers, etc.). Thermal efficiencies can be improved and the unit size reduced by supplying a part of the heat indirectly (e.g., by conduction or radiation). Note that the inversion temperature is lowered in the presence of indirect heat supply, which is a further benefit. For example, in the presence of appropriate radiant heating, the ''inversion temperature'' can be reduced from 250°C to even 170°C.

It is not necessary to always operate the superheated steam dryer above the inversion temperature to benefit from the advantages of the SSD, however. Aspects other than higher drying rates or lower energy consumption, such as quality or safe operation, may dominate the selection procedure in most cases. For relatively low-value products (e.g., sludges, coal, peat, hog fuel, etc.) that are also readily combustible in hot air and dried in large tonnages, the reduced net energy consumption in SSD is particularly advantageous since this also reduces the environmental emissions of greenhouse gases (e.g., CO_2) as well as toxic gases (NO_x, SO_x, etc.). However, the excess steam produced must have a viable application in or near the process.

Table 7.2 summarizes the key factors contributing to the feasibility of superheated steam drying. Both product- and process-related factors must be considered. Laboratory testing is required before proceeding with any decision to consider superheated steam drying.

The following dryer types have been successfully tested at a pilot scale and/or commercialized for at least some products:

Flash dryers, with or without indirect heating of dryer walls, with high-pressure steam

Fluidized bed dryers, with or without immersed heat exchangers, operated at low, near-atmospheric, or high (up to 5 bar) pressures
Spray dryers (operated at near atmospheric pressures, for drying of whey; pilot scale only)
Impinging jets (for newsprint, tissue paper, etc., at small scale; for textiles at commercial scale)
Conveyor dryer, operated at near-atmospheric or high pressures
Agitated bed dryers, operated at near-atmospheric pressure
Packed bed/through circulation dryers
Impinging-streams (opposing jet) dryers
Vibrated fluid bed dryers with immersed heat exchangers

Because of space limitations, this chapter discusses steam dryers only for a selected range of products. However, the references cited provide detailed information. Also, other chapters in this book include discussion of some steam-based drying technologies such as airless drying or solvent drying.

7.5 SUPERHEATED STEAM DRYING OF SELECTED PRODUCTS

7.5.1 Drying of Sludges

Sludges can be dried continuously in large tonnages in flash, fluid bed, or agitated trough-type dryers using superheated steam. Hirose and Hazama (1983) have reported on a sewage sludge treatment plant that used a steam-fluidized bed dryer. The sludge, containing 400% water (dry basis), was mechanically dewatered and then evaporated to 75% before it was fed to the dryer to obtain a final moisture level of about 5%. The steam generated in the dryer was used as a heat source in the evaporator. Heat for the dryer was obtained by incinerating a fraction of the dry product as the calorific value of dry sludge was in the range 8.4 to 19 MJ/kg. In case of sludge with a calorific value of 12.6 MJ/kg, an auxiliary energy of 420 kJ per kg of sludge incinerated was required. The incineration process in a cyclone furnace vitrifies the sludge (by melting and solidification), thus reducing the volume of waste to be sent to a landfill. Further, the waste product is not leached into the soil.

An agitated multistage steam dryer with concurrent flow of steam and the product has been developed successfully in Japan to dry 15 tons per day of dewatered sludge. Steam at 360°C at flow rates up to 3600 kg/h enters the dryer and exits at 150°C, giving a volumetric heat transfer coefficient of up to about 100 W/(m^3K). Unlike a fluid bed, the low-steam velocities cause little entrainment in the exhaust stream, which is cleaned in a cyclone. To

avoid odor release, the dryer is held at a pressure of 10 to 100 mm water column below atmospheric. For start-up, hot air is circulated and then water is injected into the hot air until the system is full of steam. It should be noted that sludges come in various chemical/biochemical compositions as well as physical characteristics. To save energy, it is also important to dewater (nonthermally) as much of the water as possible before the sludge is fed to a thermal dryer. Not all sludges can be combusted to provide a part or all of the heat required for drying.

There are advantages as well as limitations to each dryer type, and a careful technoeconomic evaluation is necessary when a final selection is to be made. The well-known Carver–Greenfield process (discussed elsewhere in this book) utilizing the multiple-effect evaporation concept as well as several indirect dryers provides competing technologies for drying of sludges. It should be noted that the use of high-temperature air could lead to significant fire and explosion hazards in drying of sludges of all types. Atmospheric emissions of organic volatiles and fine particulates are problems of special concern as well. For very large cities in developed countries, steam-drying technologies, which utilize dried sludge as fuel and yield vitrified, easy-to-handle dry product for landfills, appear to be especially attractive. Vitrified sludge particles do not leach their undesirable chemicals into the soil, which is a major advantage of such a process.

Although no details are available, an impinging-streams dryer for sludges using superheated steam as the drying medium has been operated at pilot scale successfully in Russia. Additional information on these special types of dryers can be found elsewhere in this book and in the review papers by Kudra and Mujumdar (1989), Mujumdar (1990), and Kudra et al. (1990).

7.5.2 Drying of Coal

Coal is a raw material for many chemical syntheses as well as a fuel. Depending on its initial moisture content, coal is dried to increase its calorific value and simplify loading, unloading, transport, and improve boiler-combustion efficiency. Although not commonly required in North America, drying of low-grade coals containing high levels of moisture is necessary in many parts of the world. Coal is also dried for briquetting, coking, gasification, carbonization, liquid fuel synthesis, and so on. Coke-oven efficiency can increase 30% to 50% in preheating, and 10% to 15% in drying if coal is predried. Direct dryers (e.g., rotary, pneumatic, fluid bed, vibrating fluid bed, shaft dryers, etc.) are used commonly with hot air or combustion gas at 700 to 900°C before the dryer and 60 to 120°C after the dryer. Rotary dryers with indirect heating

are used for hard coals. These dryers have higher energy efficiencies, about 3100 kJ/kg water evaporated. For air fluidized bed dryers, the corresponding figure is 3100 to 4000 kJ/kg water evaporated. Frequently, fluid bed dryers are equipped with an internal heat exchanger (Figure 7.3). A commercial vibratory dryer for hard and brown coals (manufactured by Escher-Wyss of Switzerland) uses a vibrational frequency of 50 to 100 Hz and an amplitude of 0.5 to 3 mm, giving a conveying velocity of 0.01 to 0.3 m/s with an angle of inclination of 5° to the horizontal. Low gas velocities are needed since vibration suspends most of the pseudo-fluidized beds. The efficiency is better than in a conventional fluid bed employing high gas velocities. Attrition is reduced and gas cleaning requirements are minimized in a vibrated bed dryer.

In pilot trials, Potter et al. (1986) and Potter et al. (1988) have shown that extremely favorable heat transfer rates as well as drying efficiencies are obtained when drying brown coal in a steam-fluidized bed with internal heat exchanger tubes immersed within it. Typical processing conditions were reported as

Heating tube temperature: 140–170°C
Bed temperature: 110–127°C
Minimum fluidization velocities: 0.57 m/s (approximately)
Steam temperature: 130–150°C
Coal feed rate: 40–70 kg/h
Product: 16–28 kg/h

Using steam exhausted from one dryer stage as carrier steam for another stage, multiple-effect operation (similar to that common to evaporators) can be achieved yielding a steam economy of 1.9 for a triple-effect dryer. Potter et al. (1988) used a continuous fluid bed dryer for drying Victoria brown coal. The rectangular 0.3 × 0.3 m fluid bed dryer was 3 m high with four bubble caps to distribute steam. The disengaging region was 2.5 m. Both horizontal and vertical tube bundles were tried.

Faber et al. (1986) have compared drying rates in air and in steam-fluidized beds of pulverized coal. They found the inversion temperature of about 180°C above which the steam-drying rate in the constant-rate period in fluidized bed drying exceeds that in (dry) air drying. For a 2000-kg/h dryer for alumina, the capital cost was 20% lower for the steam dryer, while the total energy cost was lower by 15%. No credit was given to the steam produced in the steam dryer.

Faber et al. (1986) also reported on a successful industrial installation using a steam dryer for activated carbon pellets (2000 kg/h dry basis) from an initial moisture content of 50% to 2% (dry basis). The pellets were dried

to 8% dry basis prior to feeding an evacuated chamber in which the final moisture content of 2% was achieved. The steam entered the dryer at 300°C and left at 150°C. The steam discharged was used to preheat the feed. The authors reported smooth operation of the dryer since 1985. The installed cost of the steam-drying system was 40% lower than that for a conventional air dryer. Besides, the air dryer can operate at a maximum temperature of 125°C to avoid combustion in the dryer. The energy costs (1986 data) were estimated to be about $3.6 per ton of dry product in South Africa.

Woods et al. (1994) have reviewed steam-drying technologies for coal and presented interesting results on steam drying of 1.0 to 1.3 mm coal particles and the evolution of volatiles during drying. It is noted that, in steam drying, the drying time (actual residence time in the dryer) does not affect the volatiles' liberation, unlike air drying. Further, they found that under the

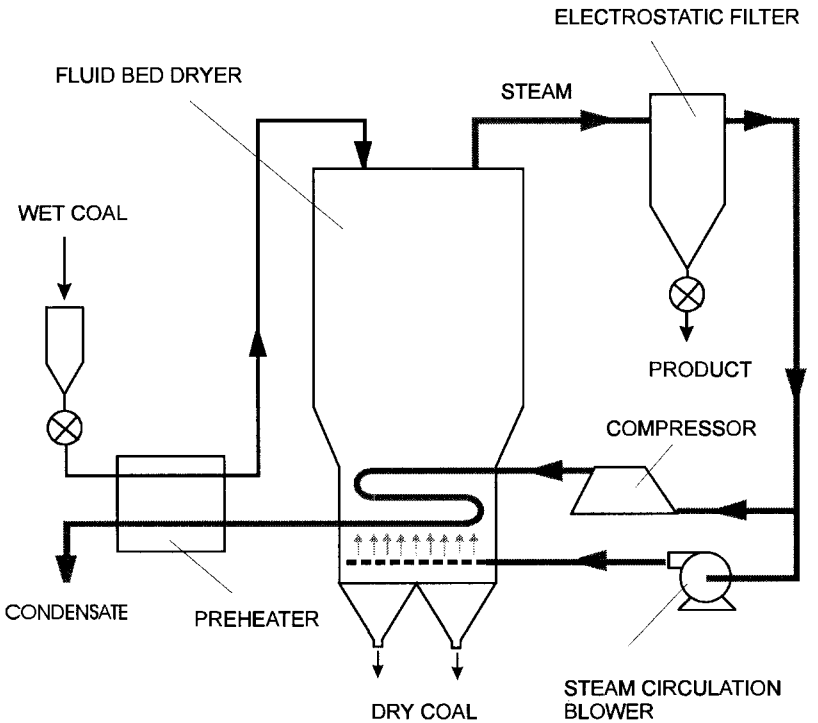

FIGURE 7.3 Schematic of a fluid bed dryer for pulverized coal with immersed heat exchangers (German design).

conditions of their experiment, the constant-rate drying period is 6 to 7 times longer in steam drying and the heat transfer rate is 1.7 to 2.0 times that in air. They also report favorable industrial experience with steam-fluidized bed drying of brown coal with an evaporative capacity of 25 tons/h. No details are given about the use of steam produced by the dryer.

Black coal generally has low water content, while brown coal may have 60% to 80% (wet basis) moisture. Regardless of whether brown coal is burned, gasified, coked, or liquefied, the wet raw coal should be dried to 5% to 10% moisture for economic utilization. For some gasifiers, the additional requirement of free flowability for a well-metered feed rate means that the pulverized coal must be low in moisture content. Coal drying in a steam-fluidized bed of coal containing 65% moisture (wb) is estimated to reduce energy wastage in the subsequent combustion step by two-thirds, resulting in some 15% increase in the overall powerplant efficiency, a similar level of reduction in CO_2 emission, and a 30% reduction in flue gas generation for the same thermal output.

Steam drying is claimed in some reports to reduce power consumption for milling since the grindability index is increased due to steam drying. At elevated degrees of superheat and prolonged exposure times, some studies have reported a reduction in the sulfur content of coal. This is not necessarily an advantage since the sulfur will then enter the dryer exhaust steam. Additional data are needed to evaluate this aspect in detail.

Following are some of the key advantages claimed for steam-fluidized bed drying of brown coal:

Better energy utilization by condensing steam generated in the dryer; an overall efficiency was increased from 36% (typical for a brown coal-fired powerplant) to 42%.
Ability to couple the dryer with powerplants to use latent heat of condensed low-pressure steam (co-generation potential).
Coal moisture discharged as liquid water rather than as dusty vapor. No biological or chemical treatment is needed for the condensate water.
Large-capacity dryers (up to 15 tons/h) are feasible.
The dryer is compact (e.g., heat transfer coefficients in the order of 200 $W/(m^2K)$ versus 20 to 50 $W/(m^2K)$ in steam tube rotary dryers).
The operation is safer (reduced insurance costs).
Product is dried to greater uniformity and better briquette strength.

The coal dryer itself is not the most expensive component of the drying system; coal grinding prior to drying, milling after drying, and cleaning the

effluents are by far the most expensive steps in the process. Commercial-scale dryers for this application are operational in Australia and Germany.

7.5.3 Drying of Beet Pulp

Drying of wet, pressed beet pulp after extraction of sugar in a conventional high-temperature dryer requires 9 kWh/100 kg beet, which amounts to over 33% of the energy consumption in a sugar factory. BMA AG of Germany have developed a high-pressure superheated steam dryer for beet pulp drying that consumes only 2900 kJ/kg water evaporated, compared with nearly 5000 kJ/kg in conventional air drying. The BMA dryer is a horizontal pressure vessel made of mild steel and is 6.5 m in diameter and 37 m long (Bosse and Valentin, 1988). Special airlocks are provided at entry and discharge ports. The feed pulp is preheated in a screw conveyor to 105°C and then deposited on the drying screen—this avoids condensation and corrosion problems. Three traveling screens of stainless steel have a total area of 240 m^2 for a throughput of 32 tons/h of pressed beet pulp with 30% solids to be dried to 90% solids. The pulp bed height is between 40 and 120 mm, which affects the dryer throughput. The steam is made to circulate through the bed of beet pulp, causing it to dry as the screen moves. Nine parallel fans capable of handling 200,000 m^3/h of steam circulate the steam in the dryer. Heat exchangers are used to reheat the recirculating steam. A mean residence time of up to 720 seconds is needed for a bed of 120 mm with effective evaporation capacity of 16 to 20 tons/h. The pulp is brighter than air-dried pulp. However, the dryer costs are high, with payback periods of up to 6 to 7 years.

Recently, Niro A/S of Denmark have successfully commercialized a pressurized steam–fluid bed dryer for particulate and sludgelike or pulpy materials (Jensen, 1992). The bed has a special ''cellular'' or multicompartment design and operates at 3 bar. The fluid bed is driven by a superheated steam flow that is recycled through a heat exchanger by a fan and blown up through the fluid bed (Figure 7.4). Capacities of 2 to 40 tons/h water evaporation are available. Initiated as pilot scale in 1982, the full industrial-scale dryer (6 m in diameter) for drying beet pulp came onstream in Denmark in 1985.

Compared with conventional rotary dryers, energy savings of up to 90% are feasible. The product quality is found to be better in steam drying (i.e., appearance and texture, as well as digestibility by cattle).

Although existing dryers using this concept are currently operational in Europe for drying of beet pulp, pilot tests indicate that this dryer can successfully dry the following products as well: spent grain from brewery, hay, alfalfa, fish to produce fish meal, peels and pulp from citrus fruits, apple pomace, bark, wood chips, bagasse from sugar cane, municipal sewage sludge.

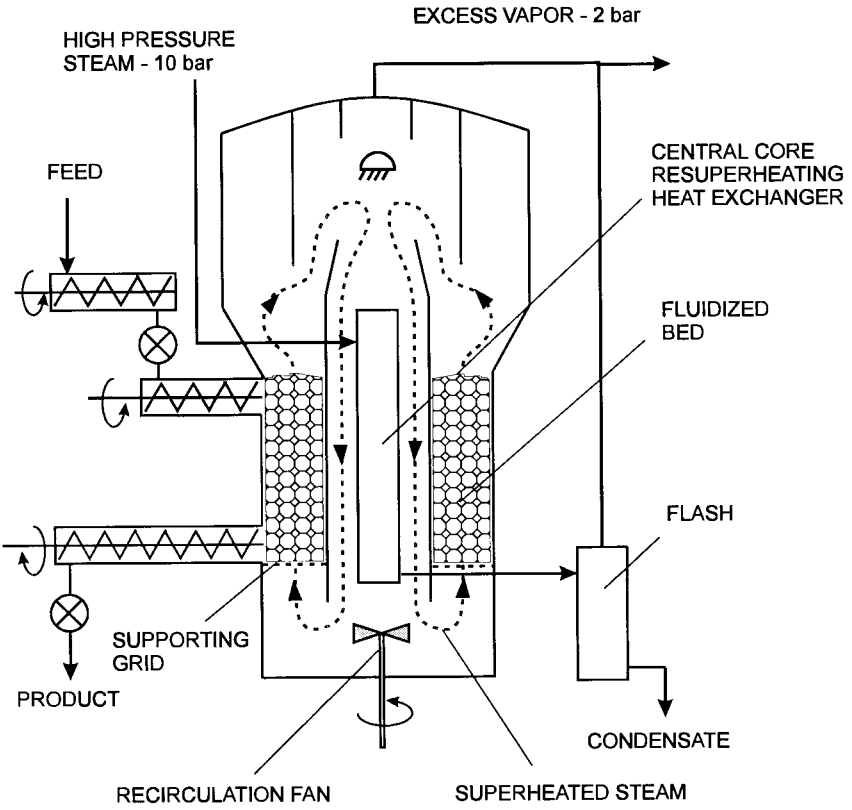

FIGURE 7.4 Pressurized superheated steam multicompartment fluidized bed dryer (Courtesy of Niro A/S, Denmark).

Among some of the specific advantages claimed of this dryer are as follows:

Closed system drying eliminates odor emission.
Automatic, reliable, and maintenance-free operation is feasible.
No danger of fire or explosion.
Lower or no contamination or oxidation of products as in conventional gas-fired dryers.
No environmental pollution.

It is interesting to compare the energy flows in the rotary dryer versus the pressurized steam dryer for 32 tons/h of water evaporation. If 16 bar-gauge steam is supplied to the steam dryer, it will generate 3 bar-gauge steam,

which could have produced 2 MW of thermal energy. Instead, it is available as low-pressure steam although the 2 MW is not used by the dryer. Rotary dryer will consume 26 MW of fuel energy, none of which can be recovered. Of course, all the advantages are gained at increased capital costs; as the cost of energy rises, the high-energy efficiency of steam drying becomes economically more attractive. The potential for significant energy savings exists only when the steam produced by the dryer can be used effectively elsewhere in the process or at a nearby location.

Specific energy consumption of the Niro pressurized fluid bed dryer is reported to be in the range of 130 to 190 kWh per ton water evaporated compared to 800 kWh per ton water evaporated for conventional air drying (Woods et al., 1994).

7.5.4 Drying of Lumber

Drying is an important step in processing lumber. Atmospheric steam dryers have been studied for drying green softwoods and hardwoods. Effects on resin exudation, surface discoloration, loosening of knots, and other quality parameters have been studied to varying extents for a variety of wood species. High-temperature drying of lumber (above 100°C) in air–steam mixtures causes greater defects, such as collapse, honeycomb, and checking in high-temperature-dried lumber than in lumber dried at lower temperatures. Rosen (1982) has given pilot-scale data on pressurized steam drying of lumber for 27-mm-thick green and yellow poplar and red oak. He also made a technoeconomic study based on a number of plausible assumptions. Essentially, he showed that the capital cost of the steam dryer was about the same as that of a conventional kiln, although the drying times were reduced. The electrical energy usage was only about 0.82 kWh/kg (2.95 MJ/kg) water evaporated for the electric heater. Since the steam flowrates used were higher than those in conventional kilns, the blower power was about 40% higher for steam dryers. However, since the dryer system is a closed one (in which dryer exhaust is recirculated after electrical heating), this energy is also available for evaporation. It is important to note that the electrical energy requirements for drying depend on the type of lumber and the moisture range. Rosen dried yellow poplar from 100% moisture content to 5% (dry basis) in 28 to 30 hours, while red oak was dried from 19% to 5% (dry basis) in 21 hours. About 40% of the dollar value of the lumber was lost due to degradation associated with drying. The total energy requirements for red oak were estimated to be triple those for yellow poplar.

In the past decade, a low-pressure steam dryer for timber has gained momentum in Southeast Asia and Europe. The so-called Moldrup process mar-

keted by Iwotech Limited of Denmark (1993) is carried out in an enclosed autoclave in which the sawed timber is stacked on trolleys for easy feeding and discharge. The drying process is initiated by evacuation of the autoclave with a low-power vacuum pump, which takes 1 to 2 hours. It is then filled with superheated steam, which is heated in the range of 50°C to 90°C. Heat for drying is supplied by recirculating the steam at velocities up to 20 m/s at 4 millibar pressure using a series of fans within the chamber. The drying steam is heated by steam or hot-water coils located in the autoclave to a temperature above the saturation temperature of steam. At the operating pressure (around 3 to 5 millibar) used, the boiling point of water is lowered to below 50°C. The process is controlled automatically. Figure 7.5 shows schematics of two vacuum superheated steam dryers for wood. The main difference is in the location of the condenser; in one design it is within the chamber and in the other it is placed outside.

Among the advantages claimed for the process are the following:

High drying rates (drying is by 2 to 5 times faster)
Better product quality
Simple process control
No risk of fire and explosion
Staining and mold attack are avoided
No oxidative discoloration (e.g., oak, beech, etc., do not discolor)
Minimal risk of corrosion
Minimal removal of extractables from wood
Reduced stresses, cracking, warpage, and the like
Low inventory costs due to several-fold faster drying

The autoclaves (drying chambers) come in diameters up to 4 m and lengths up to 24 m. The autoclave is equipped with a rubber air tube that is pressurized to hold against the top part of the timber stack with an overpressure of 10 kPa to reduce the risk of deformation. The moisture coming out of the timber is condensed. The drying time ranges from one to several days depending on the wood species and the thickness of the wood. At the end of the drying cycle, the vessel is filled with atmospheric air prior to unloading of the charge.

The higher drying rates result in energy savings of about 50% over conventional kilns. One of the limitations of the process is that the autoclaves are much smaller than the conventional hot-air kilns. However, since the drying cycles are several-fold shorter, this is not a major limitation. In fact, the shorter drying times offer the user more flexibility in drying different species or sizes of wood while reducing the cost of inventory, especially for wood species

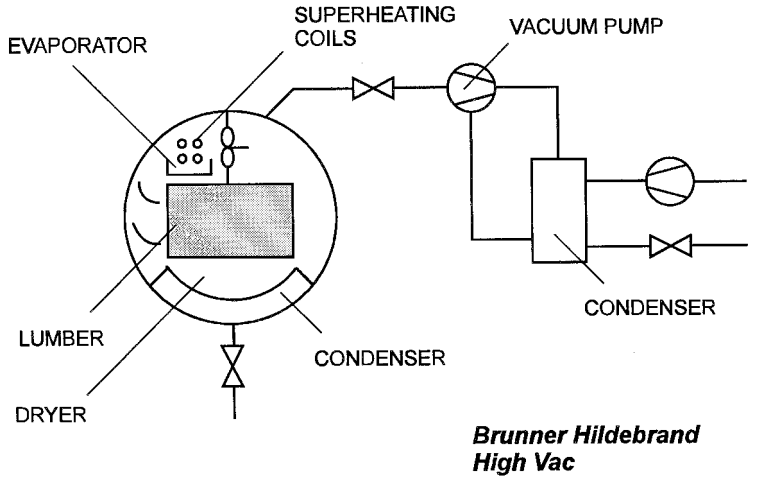

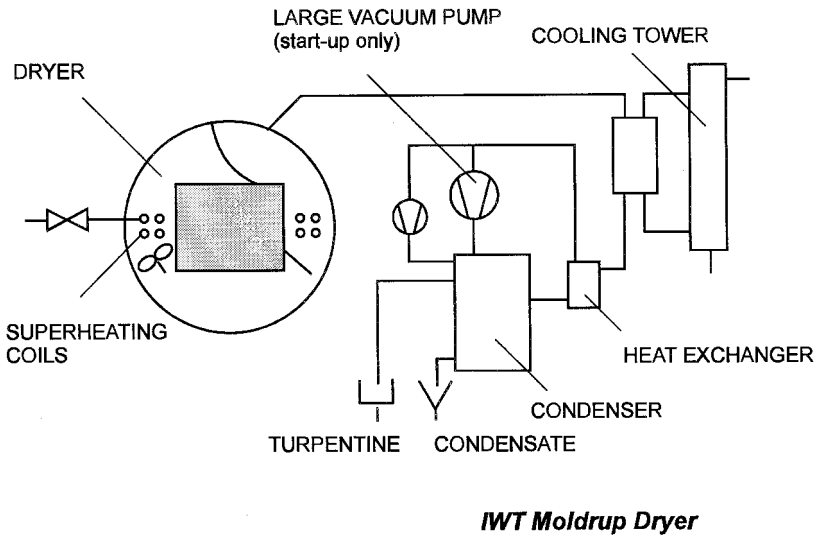

FIGURE 7.5 Schematics of two low-pressure superheated steam lumber drying systems.

requiring several weeks of air drying. No oxygen in the dryer may also help to kill microorganisms or insects in wood, although experimental verification is needed. Since the drying temperatures may be lower, thermal distribution may not be adequate in some instances. This process appears to be especially attractive for species and timber dimensions that take a very long time (several weeks) to dry in conventional kilns. This technology is likely to become a standard in wood-drying technology in many parts of the world in the next decade. It should be considered seriously when old kilns are ready to be replaced.

Table 7.3 compares two vacuum–superheated steam drying applications (for pine and oak) in terms of energy consumption and costs (Woods et al., 1994). Note the difference in initial moisture levels that is reflected in the

TABLE 7.3 Energy Consumption and Costs for Two Vacuum–Superheated Steam Drying Applications

Wood		
Type	Pine	Oak
Dimension	200 mm	50 mm
Charge capacity	45 m^3	37 m^3
Initial/final moisture content	80%/16%	35%/8%
Drying cycle		
Temperature	70°C	70°C
Drying time	105 hours	148 hours
Total charge time	120 hours	195 hours
Annual capacity	2875 m^3	1424 m^3
Energy consumption		
Thermal energy	762,650 kJ/m^3	464,310 kJ/m^3
Electrical energy	52.9 kWh/m^3	105.8 kWh/m^3
Energy costs		
Fuel oil price ($/liter)	0.344	0.344
Electricity price ($/kWh)	0.142	0.142
Heating costs ($/$m^3$)	7.38	4.49
Electricity costs ($/$m^3$)	7.50	14.99
Financial costs		
Price	$420,000	$420,000
Depreciation period	7 years	7 years
Scrap value	$70,358	$70,358
Interest rate	10%	10%
Financial costs/year	$7,066	$7,066
Financial costs/m^3	$24.57	$49.63
Total cost per cubic meter	$39.45	$69.12

significantly higher cost of drying oak for the case examined. These cost figures apply for the Canadian situation in 1995.

7.5.5 Drying of Pulp

The first industrial pulp dryer utilizing superheated steam as the carrier for conveying the pulp to be dried was installed in 1979 at the Rockhammars in Sweden. Drying is accomplished by indirect heating with steam extracted from a turbine at 10 bar. Steam formed by evaporation within the dryer ducts is circulated in the dryer, where it acts as a convective drying medium. A fraction of the steam generated is used elsewhere in the mill since the dryer operates at 5 bar. Even after allowing for the energy loss in the turbine, it is found that this dryer consumes less than one-half of the energy used in flue gas drying—the conventional technology. Drying times are in the order of 10 to 30 seconds. This type of the dryer has also been used successfully for drying of peat, sawdust, and forest biomass that, when pulverized, can be used as fuel in existing oil-fired thermal power plants. Figure 7.6 gives a schematic of the flash dryer for pulp and hog fuel.

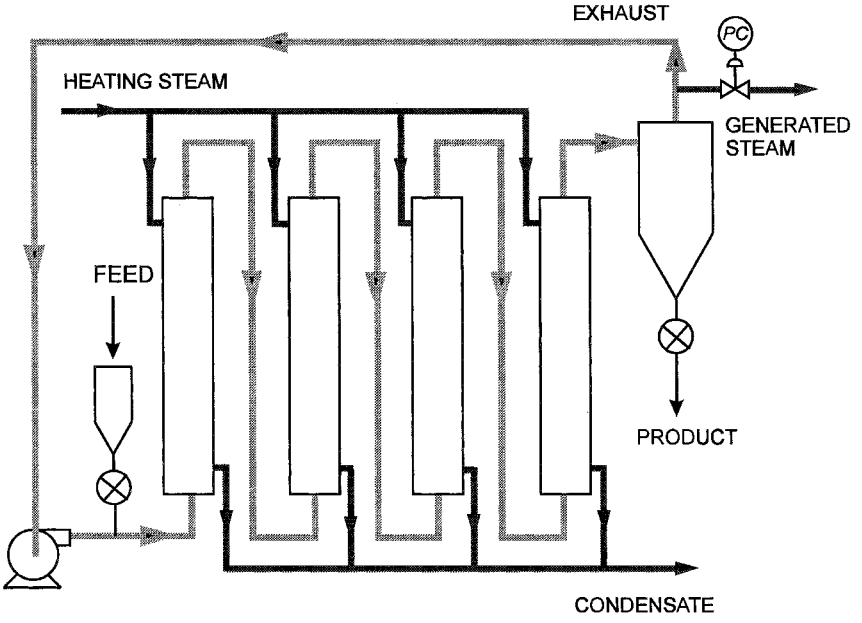

FIGURE 7.6 Steam flash drying system.

According to Munter (1989), flash dryers for pulp can be designed and operated economically at evaporation capacities of the order of 400 tons/day. If the steam produced is used elsewhere in the process, then the ''net'' energy consumption chargeable to the steam dryer can be very low. Currently, no full-scale industrial installation appears to exist that utilizes vapor recompression technology for the steam flash dryer similar to that commonly employed in multiple-effect evaporators. The higher capital costs associated with steam flash dryer units coupled with lower energy consumption result in the cost of drying pulp by air or steam about the same, that is, of the order of US$23 per ton water removed (in Quebec in 1989).

Possible operating problems for such dryers include deposit formation and erosion of the pneumatic tubes due to high-velocity transport of particles that may contain abrasive impurities such as sand. Erosion, particularly in bends, can be minimized or taken care of by using special materials or replaceable elbows. Deposits may form within the dryer walls if the transporting steam temperature falls to saturation level. Corrosion is also a problem to be considered, so stainless steel construction is often required. It is important to disintegrate the solids prior to feeding in the flash dryer since large lumps and the like will not be suspended by the transport steam.

7.5.6 Drying of Peat

Peat is usually dried at power plants and briquette factories with flue gases (300 to 600°C) from the boiler. More recently, steam flash dryers have been commissioned in Sweden using back-pressure steam.

Briquetting industries in Ireland and the former Soviet Union have used the so-called Peco dryer for peat for over seven decades (Fagernas and Wilen, 1988). The Peco dryer is a two-stage system where the latent heat of evaporated water from the second stage is used as the drying energy in the first stage. The dryer contains five columns, each containing about 500 pipes of about 70-mm diameter. The milled peat is carried by airflow or air–steam mixture in the pipes, while the energy for drying is supplied by hot water (first stage) and condensing steam outside the pipes (second stage). Peat is separated by cyclones after each stage. The energy consumption for the Peco dryer is 1.7 to 1.8 MJ/kg water evaporated, which is much lower than that for a flue gas dryer (3 to 4 MJ/kg water). However, electrical power demand for the compressors used for pneumatic conveying is relatively high.

Another dryer for peat (or lignite) is the tubular steam dryer, mostly used in Germany. It is a rotating inclined cylinder in which the material flows in 100-mm pipes, while steam flows in the shells at a pressure of 0.60 MPa.

Air is drawn through the pipes to remove evaporated water. The energy consumption is reported to be 2.9 to 3.2 MJ/kg water removed. The exhaust energy is generally not utilized. It is interesting to note that the flow properties of peat depend on the presence of wood and fiber content. If there is low content of fiber and wood with a bulk density of 400 kg/m^3, such dryers operate well.

The pressurized steam flash dryer originally developed at the Chalmers University of Technology (Gothenburg, Sweden) in the early 1970s is ideal for drying peat as well as pulp, bark, and so on. This dryer is a closed, pressurized system in which the peat is exposed to indirectly heated superheated steam. The dryer consists of transport ducts, heat exchangers, a cyclone, and fans. The superheated steam recirculates at a pressure of 2 to 6 bar. The primary heating steam is condensed (usually 8 to 15 bar) on the shell side.

Dry steam and material are separated in a cyclone, and the basic stream of steam is recirculated while the excess steam is bled off. If the material is dried from 45% to 50% dryness to 85% to 90% dryness, about one ton of steam is generated per ton of material processed. This steam is available as process steam at 2 to 6 bar. Typical drying time is 10 to 30 seconds. The transport velocities are 20 to 40 m/s. If the excess steam is used (e.g., for district heating), then the net dryer energy consumption is only 0.5 to 0.7 MJ/kg water removed, which may be compared with 3.5 to 4.8 MJ/kg, which is typical for hot-air flash dryers. Dust and explosion hazards are eliminated in steam drying, thus reducing the insurance costs as well.

A recent installation in Sweden uses peat (replacing coal) as the fuel in a 440 MW thermal powerplant. The peat is dried, briquetted (3 million tons/year) at source about 400 km from the power plant, and then milled for combustion. Peat is dried from 60% to 10% (db) moisture for briquetting at an output level of 20 tons/h per drying unit. Two dryers are used in parallel. The total tubular heat exchanger area is 5500 m^2. The electricity demand of the compressors and blowers is 10 MW. About 3.6 MW district heat is produced, giving a net energy demand of the dryer of about 0.5 MJ/kg water, which is only about one-sixth to one-seventh the energy consumption of typical flue gas drying systems.

At Helsinki University of Technology, successful demonstration of fluidized bed drying of peat has been reported at the pilot plant level (100 kg/h of water evaporated). A tubular heat exchanger immersed in the bed provides indirect heat for drying. It uses condensing steam at 0.8 MPa. Steam evaporated from peat is used as the fluidizing medium. Wet peat is fed into the lower zone of the fluid bed while dry peat is withdrawn from the upper zone by a screw conveyor. The miffed peat is about 1 mm in average size. The

bed-to-tube heat transfer coefficient is rather low at 100 W/(m^{2}K) (i.e., of the same order as that in a flash dryer but much lower than that for a fluidized bed due to the poor thermal properties of peat). Sand may be used as a bed material to increase the drying rate, but separation of peat from sand is not very effective. If a fluidized bed combustor with sand is used, then sand separation is not a problem. Fine-size magnetite as a bed material increases the bed-to-tube heat transfer coefficient to 350 W/(m^{2}K) while allowing easy magnetic separation from dry peat (Jahkola et al., 1989). This dryer is claimed to be economically justified for use on new, large powerplants. The investment costs are high and a demonstration plant is necessary to study the reliability and technoeconomics of the process. The fluid bed installation is likely to be more compact than the flash dryer but with net energy consumption of the same order.

Aside from differences in the flow characteristics, similar conclusions should apply for drying of lignite, biomass, and similar organic materials in steam flash or steam–fluid bed dryers. The cost and net energy consumption should be of the same order for the same production capacity (i.e., in the order of 0.5 to 0.7 MJ/kg water evaporated), provided the steam generated by the dryer is used elsewhere.

One important consideration in drying of peat is the evolution of organic compounds when flue gases are discharged into the stack or if the energy is recovered and the condensate sent as a waste stream. Indeed, such a problem exists whenever the material being dried can result in evolution of organic compounds due to heating or due to interaction with steam at elevated temperatures. The quality of the condensate is affected by drying conditions (e.g., time, residence time in dryer, etc.) and by the amount of moisture removed, type of peat, and so on. Acetic acid, formic acid, and furfurals are the main organic compounds in the condensate. The average biochemical oxygen demand (BOD) is 140 to 150 mg/kg dry peat, chemical oxygen demand (COD) is 500 to 850 mg/kg dry peat, and the total organic carbon (TOC) is 90 to 300 mg/kg dry peat in different dryers. Table 7.4 provides a summary of the effluents from steam peat dryers based on the Fagernas and Wilen (1988) data. Note that drying of bark in steam-fluidized beds yields higher solids content ($\approx$400 mg/l), higher COD ($\approx$2600 mg/l), and higher TOC ($\approx$450 mg/l) than corresponding figures for peat; other effluent levels are comparable.

In general, increased bed temperature leads to increased load of organics in the condensates. Increasing bed temperature from 110°C to 120 to 130°C can increase BOD, COD, and TOC values nearly threefold. Finally, a novel high-pressure steam flash dryer (25 bar) has been operated successfully in Finland for drying of mined peat, which is then fed continuously to a high-

TABLE 7.4 Effluents from Steam Peat Dryers

Parameter	Fluid bed steam dryer	Pilot fluid bed dryer	Industrial peat dryer
Temperature, °C	100–140	140–170	170
Pressure, bar	—	2–8	5.7
pH of condensate	4.1	5.7	3.8
Solids, mg/l	80	220–400	70–170
NH_3—N, mg/l	1.2	28.0	11.0
Phosphorous, mg/l	0.04	1.60	0.07
BOD, mg/l	520	130–190	—
COD, mg/l	880	470–630	440–1300
TOC, mg/l	310	90	310–450

BOD: biological oxygen demand; COD: chemical oxygen demand; TOC: total organic carbon.

pressure gasifier. Clearly, such a sophisticated dryer is not warranted for a drying application.

7.5.7 Drying of Paper and Tissue

No commercial dryers exist for direct drying of paper webs with superheated steam. Mujumdar (1981) proposed, for the first time, a variety of possible configurations for direct and direct/indirect drying of paper using superheated steam. These include

Pure impingement with steam jets with web supported on a heated roll
Impingement and through drying (so-called Papridryer configuration) but using steam rather than combustion gases (which pose a serious fire hazard)
Pure through drying with steam drawn under suction with web (assumed permeable at reasonable pressure drop) supported on a perforated roll or honeycomb roll

All of the above processes have been tested at pilot scale or are already in commercial operation using hot air or combustion gases. All of these are highly energy-intensive processes requiring 4800 to 5700 kJ/kg water evaporated. Also, the electrical power consumption is high for the fan power needed for gas jets, through flow, as well as the high recirculation ratios (up to 90% in some high-performance impingement dryers). Such dryers are in use for the drying of highly permeable grades such as tissue and toweling. The Papridryer process has been tested at pilot scale for newsprint (Burgess et al., 1972a, b;

Crotogino and Allenger, 1979). Mujumdar (1992) has discussed the superheated steam drying of paper in some detail including its history, current status, and potential.

Aside from the higher drying rates and lower net energy consumption in a superheated steam dryer, two additional major advantages of interest to the papermaker are elimination of fire hazard and improvement in product quality as measured by its strength and optical properties. Cui et al. (1986) and later David (1987) confirmed this in laboratory-scale static drying tests. Cui and Mujumdar (1984) and Loo and Mujumdar (1984) employed simple models to calculate the drying rates (under several assumptions later validated experimentally) and energy consumption for different steam-drying configurations. They concluded that if the steam produced in dryers is fully utilized elsewhere (without vapor recompression), the net energy consumption for paper drying can be as low as 1500 kJ/kg water evaporated. This energy requirement is mainly to account for leakage, sensible heating of the web, other losses, and energy for steam recycle. Pilot and mill tests are needed before these preferential results can be confirmed.

Bond (1991) and Poirier (1991) have presented valuable data and analyses of steam drying of handsheets in static laboratory test rigs. Limited pilot-scale data exist at this time on steam drying of paper or tissue. Application to tissue drying (impingement and/or through drying) appears to be the more imminent industrial-scale operation. Another potential near-term application is as a booster dryer to increase the productivity of a dryer-limited mill. Douglas (1994) has summarized various studies on steam drying of paper. Despite the obvious and demonstrated advantages of steam drying of lignin-containing paper, many engineering problems remain to be tackled.

7.5.8 Drying of Wood Particles and Wood Wafers

Salin (1986, 1988) has reported a significant study on steam drying of small wood particles for particleboard to very low moisture levels (2% to 3% water). The conventional process uses direct contact flue gas drying or indirectly heated air drying; both processes do not permit economic energy recovery from dryer exhaust. Wood particles were dried in a pressurized steam dryer in which the particle–steam mixture is conveyed through a series of vertical heat exchangers where the mixture is heated to maintain a required degree of superheating. Upon exhaust, the particles are separated from steam in cyclones and recirculated except for an amount equivalent to that produced by the dryer. A 13-m long single-tube dryer was used in the pilot tests, giving a residence

time of 12 to 15 seconds; a second pass was needed to achieve the required dryness in 25 to 30 seconds. The desired dryness of 2% was achieved for both softwood and hardwood (birch) particles. About 40°C superheat was found to be adequate in the dryer. Fouling of heat exchanger surfaces was minimal, although this should be examined closely for industrial-scale operations. For bark drying in a similar dryer, no problems have been reported on heat exchanger surface encrustation even after six years of operation in Sweden.

Salin (1988) compared the quality of particleboard manufactured from steam-dried versus air-dried wood particles; the bending and tensile strength as well as water absorption properties of the former were found to be superior. This results in a 9% reduction in glue consumption in particleboard making. Optimal selection of dryer temperature and heat treatment can further enhance the board quality. No industrial-scale steam dryers appear to be in operation anywhere at this time for this application.

7.5.9 Miscellaneous Applications

Akao et al. (1982) reported on a commercial steam-drying/deodorization plant to process soy sauce cakes as feedstock. An agitated trough steam dryer (1.5 tons/h dry product capacity) was used. Deodorization commenced at moisture levels below 4% db and a temperature of 135°C. The oils and fats distilling from the cake resulted in deodorization of the product. Indeed, the fats and oils were used as auxiliary fuels for the process. Concurrent steam drying and deodorization of rice bran, fish meal, and silk cocoons were also reported by Akao (1983). In these products, the odor is due to oxidation of lipids. He also showed that the quality of green tea and vegetables dried in steam (e.g., color, smell, etc.) was acceptable.

Among other applications of steam drying developed in Japan, one may cite drying of potato slices in which color and vitamin C are preserved due to no contact with oxygen. Lack of formation of a case-hardened skin on the product in solvent drying was applied to advantage in dry spinning of synthetic fibers in superheated solvent vapor. Yoshida and Hoydo (1963) reported that stronger and finer fibers without surface wrinkles were obtained in this process.

7.6 UTILIZATION OF EXHAUST STEAM

Assuming no losses, the evaporated moisture in steam dryers becomes excess superheated steam at lower specific enthalpy. Economic use of this steam generally holds the key to the success of the steam-drying process. This steam is

typically at near-atmospheric pressure and is likely to be contaminated with solid impurities as it is in the case of paper drying where steam picks up fibers and dust. This is not a major concern in high-temperature drying of tissue paper, for example, in which the fibrous debris picked up by the drying gases are incinerated prior to recycling. However, in SSD, the steam must be cleaned for reuse. The degree of cleaning required (using bag filters, cyclones, or electrostatic precipitators, etc.) depends on how the steam is recycled or utilized in the process. It is important to ensure that no condensation occurs in the vapor cleaning systems.

Figure 7.7 shows schematics of three possible ways to utilize the excess steam produced by a steam dryer. Following is a brief discussion of potential systems for steam utilization for dryer exhausts as a detailed discussion is beyond the scope of this chapter. The significance of this aspect, however, cannot be overemphasized.

Vapor recompression technology is widely used in continuous evaporators. Billet (1989) has discussed this subject in considerable detail. In the pulp and paper industry, there are currently two major application areas in which mechanical vapor compressors are employed to achieve significant energy savings. One is the use of compressors in conjunction with the black liquor evaporators, which results either in a decrease in the number of evaporators or in increased evaporator efficiency. The compressor is used to compress the vapor leaving the evaporator and, under appropriate conditions, the mechanical energy (or electrical power) required by the compressor is significantly lower than the recoverable heat value in the vapor. The second major application area is in the thermo-mechanical pulp (TMP) plants in which a compressor can be used to recover heat from the TMP vapor normally vented to atmosphere. In this system, heat exchangers are needed to generate low-pressure steam using the latent heat of the TMP vapor. The steam compressor boosts the clean low-pressure steam to the pressure required in the paper mill. According to van Gogh (1985), either screw or centrifugal compressors can be used. Table 7.5 summarizes key features of these two types of compressors for vapor (steam) compression.

Note that other types of compressors can also be used for steam (e.g., lobe, reciprocating, axial, turbo blowers, etc.). Benstead (1982) has reported on some preliminary studies at the Electricity Council Research Center (Capenhurst-Chester, England) on a pilot steam-spray dryer for ceramics. The dryer exhaust steam was split off and compressed; the high-pressure steam gave up its latent heat to the incoming steam. He modeled two designs for comparison. One used a standard compressor that withstood the superheat. The other considered a compressor with water injection into the suction vapor

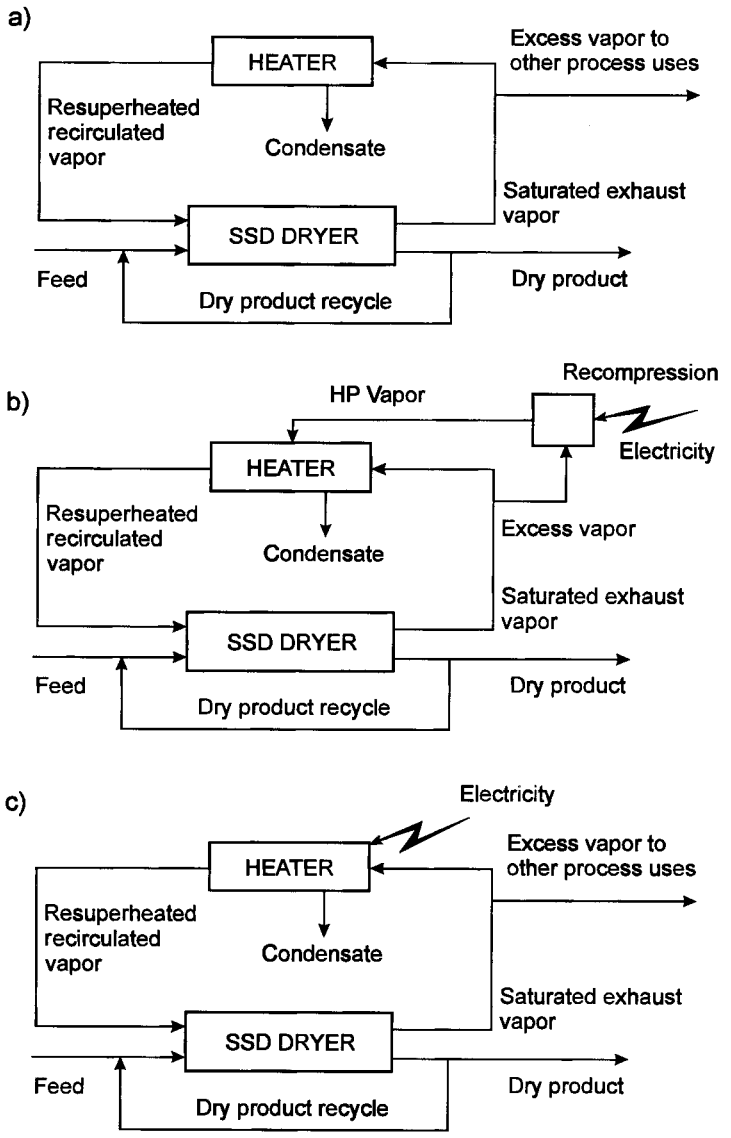

FIGURE 7.7 Simplified process flow diagram of superheated steam dryer configuration to recover energy from dryer exhaust: a) excess steam with recuperation by high-pressure steam; b) excess steam recompressed to superheat; c) excess steam with recuperating by electricity.

TABLE 7.5 Characteristics of Screw Versus Centrifugal Compressors

Feature	Screw	Centrifugal
Suction capacity	500–25,000 m^3/h	2,000–100,000 m^3/h
Maximum pressure ratio	6:1	2:1
Temperature difference	≈60 K	≈20 K
Other	Water droplets, dust may cause damage. No surge line.	Dry steam needed to avoid impeller erosion. Bypass control to avoid compressor surge.

to cool the steam during compression. The latter is about 10% more efficient due to reduction in steam volume at lower temperature.

Anthony (1989) has summarized the virtues of vapor-compression evaporation (VCE) followed by crystallization to treat waste brines from chemical process plants. He compared VCE followed by a crystallizer with other options, such as reverse osmosis/crystallizer, crystallizer plus centrifuge plus air flash dryer, steam-heated crystallizer, etc. Anthony also compared the process performance, utility requirements, as well as investment and utility costs of treating cooling tower blowdown at utility plants for five different methods utilizing VCE. It is interesting to note that the capital costs of all combinations are within 10% of each other although the operating utility costs of steam, electricity, and fossil fuel (natural gas/oil) can vary by a factor as high as five. A reverse osmosis/VCE/crystallizer/solar pond combination consumes only one-fifth the electrical power consumed by a VCE/spray dryer combination. The selection among different systems is thus dictated by the relative costs of fossil fuel versus electricity.

It is impossible to arrive at generalized guidelines at the present time regarding the technoeconomics of steam compression by thermo-compression (e.g., steam jet ejectors) versus mechanical recompression for steam-drying plants. The costs of installation of such systems are such that they should be considered only for large-scale continuous steam dryers, that is, those with evaporation capacities of 100 tons/day or higher. The steam compressors for such service are expected to cost over $500,000 (1990 estimate for North America). To this, one must add the costs of spares and maintenance.

It is important to note that existing steam compressor technologies may not meet the requirements of some of the steam-drying systems, especially if very high degrees of superheat are needed. Often, two centrifugal compressors will be needed to boost the steam pressure to a level that is useful (e.g., 3 bar

absolute from nearly atmospheric pressure). Increasing the discharge pressure typically involves increasing the rotational speed of the impeller. In some cases, this may exceed the design speeds of commercially available compressors. Thus, some new design problems may arise to obtain discharge steam pressures desired.

Detailed design and technoeconomic calculations in close association with manufacturers of compressors, steam jet ejectors, and steam dryers and with utility companies are required to make confident conclusions regarding the optimal steam reuse/recycle systems for steam dryers.

7.7 CLOSING REMARKS

Although touted as the drying technology of the future some two decades ago, the continuing low-to-moderate cost of energy has kept this technology from developing faster since low net energy consumption is one of the key advantages of this technology aside from quality enhancement and safe operation due to lack of fire and explosion hazards. Further, there are both product and process limitations to be overcome.

The cost of electricity as well as fossil fuels clearly drives the choice of the system chosen. There are significant capital costs involved in superheated steam operation as well as energy recovery. Development in newer and more efficient compressors for steam will give a boost to vapor recompression technology for steam dryers. Cleaning of the steam is another obstacle to be overcome. Overall, it appears that there are some niche markets for superheated steam drying but much laboratory, pilot-scale, as well as engineering design studies are needed before the technology becomes widespread.

This chapter summarizes the essential features of current steam-drying technologies. Improved energy efficiency, enhanced quality, reduced emissions, safer operation, and the like are some of the key advantages of such drying systems. Much R&D is still needed before some of the technological problems are resolved. For the drying of sludges, pulps, timber, brewer's spent grains, coal, peat, biomass, and so on, the current steam-drying technologies are already cost-effective and deserve to be considered very seriously despite their limited commercial experience to date.

8

Airless Drying

''Airless drying'' appears to be a technique for energy conservation in drying as it enables the energy lost to atmosphere with the water vapor in the exhaust gases in conventional air dryers to be recycled. Because about 85% of the thermal energy in the water vapor produced by drying is the latent one, only the remaining 15% can be potentially recovered, as the dew point at which the latent energy could be recovered from the vapor–air mixture at the typical dryer exhaust is around 40°C and therefore not industrially useful. Hence, replacing hot air in convective drying by water vapor as it is in airless drying would offer substantial energy savings, typically from 40% to 90% depending on process conditions (Anon., 1994a; Stubbing, 1993; Stubbing, 1994a–c; Stubbing, 1999). An example of an energy audit for a conventional and an airless dryer is given in Table 8.1.

The concept of airless drying (Stubbing, 1987) relies on evaporating the moisture from the wet product to form an atmosphere of almost pure steam. Since steam is slightly superheated, this leads to energy savings through avoiding the requirement to heat large quantities of air. In addition, the water evaporated in the dryer can be used as a source of heat for other processes. This concept is similar to that of superheated steam drying (see Chapter 7),

TABLE 8.1 Energy Audit for Conventional and Airless Drying of Ceramic Materials in a Tray Dryer

Energy use with an efficient conventional dryer	kJ/kg	%
Evaporation energy (from assumed 20°C ambient temperature)	2594	75
Energy for dry material heating (50% moisture content; from assumed 20°C to 60°C; at 1.25 kJ/(kgK))	50	2
Structural energy losses (from well-insulated dryer)	100	3
Air heating losses (to heat air through-flow from 20°C to 80°C exhaust temperature)	700	20
Total:	3444	100
Energy use with an airless dryer	**kJ/kg**	**%[a]**
Evaporation energy (from assumed 20°C ambient temperature)	2594	74
Energy for dry material heating (50% moisture content; from assumed 20°C to 100°C; at 1.25 kJ/(kgK))	100	4
Structural energy losses (from well-insulated dryer)	150	4
Air heating losses (to heat air through-flow from 20°C to 80°C exhaust temperature)	nil	nil
Total:	2844	83
	−2170	−63
Equals:	674	20

[a] Percent of the conventional dryer's thermal energy.
Source: Courtesy of Heat-Win Ltd., Bitterley, UK.

however at the lower degree of superheating, and steam being generated by evaporation of water from the wet material.

In batch mode of operation, airless drying has three distinct stages. These are described next.

1. *Warm-up phase*. During this stage, the drying chamber initially contains wet solid and air at ambient temperature and at atmospheric pressure. At the start of the process, the recirculation fan is turned on and the air is circulated through the drying chamber and the heat exchanger as it is in conventional convective drying. No air is allowed to enter the dryer, but a fraction of air equal to its expansion volume is vented to atmosphere. As evaporation progresses, a fraction of humid air is vented to atmosphere before the remainder passes again through the heat exchanger and the recirculation fan. Now the drying medium is a mixture of air and water vapor. As the sequence of

venting, heating, and drying continues, the composition of the drying medium becomes richer in water vapor and poorer in air until finally it consists of almost pure water vapor. Because of heating in an internal heater, this water vapor is at a temperature of about 120 to 150°C on entering the drying chamber and at about 100°C at exit. Its pressure is slightly above atmospheric. Therefore, the vapor at any point of the dryer is superheated (although the degree of superheating drops along the dryer) and thus is capable of transferring heat to the moisture in the solid and carrying away the vapor without any water condensing out.

2. *Airless drying phase*. This phase begins as soon as the last portion of air has been vented from the system and the drying medium consists essentially of superheated water vapor. The superheated vapor continues to circulate around the system while a continuous stream of excess vapor is vented so as to maintain the required pressure in the system. The vented steam has a pressure of 1 atmosphere and is only slightly above saturation. Therefore, it can be used as a source of heat in a number of ways. It can be condensed by mixing with cold water to produce a supply of hot water at slightly less than 100°C, or it can be mechanically compressed to increase its temperature before being used as a source of heat for the dryer itself.

3. *Cool-down phase*. When all liquid in the wet solid has been evaporated, a cool-down phase is initiated in which air is readmitted to the drying chamber to drive out the superheated vapor.

Figure 8.1 presents a schematic diagram of an airless batch dryer with vapor recompression. By compressing the vented steam and then condensing it in an internal heater of the airless dryer, most of the latent heat can be repeatedly recycled within the drying process. Since energy savings remain at around 80% (see Table 8.1), the energy-cost savings are lower because of the electrical energy needed for driving the compressor. Alternatively, the vented steam can be either condensed and used as hot process water or reused as a heating medium in another convective dryer. Net external thermal energy requirements to remove 1 kg of water in three possible configurations of airless dryer (see, Stubbing 1994b) and conventional hot air dryer are compared in Table 8.2.

The main problem to be solved when evolving from the batch process to the continuous one is conveying the material through the dryer within the superheated atmosphere without allowing ambient air to enter the drying chamber. Since mechanical seals around the conveyor would be impractical, a nonmechanical sealing method has been developed (Stubbing, 1998). With reference to Figure 8.2, this method utilizes the horizontal thermal and density differential stratification layer. This layer is located at a certain level across

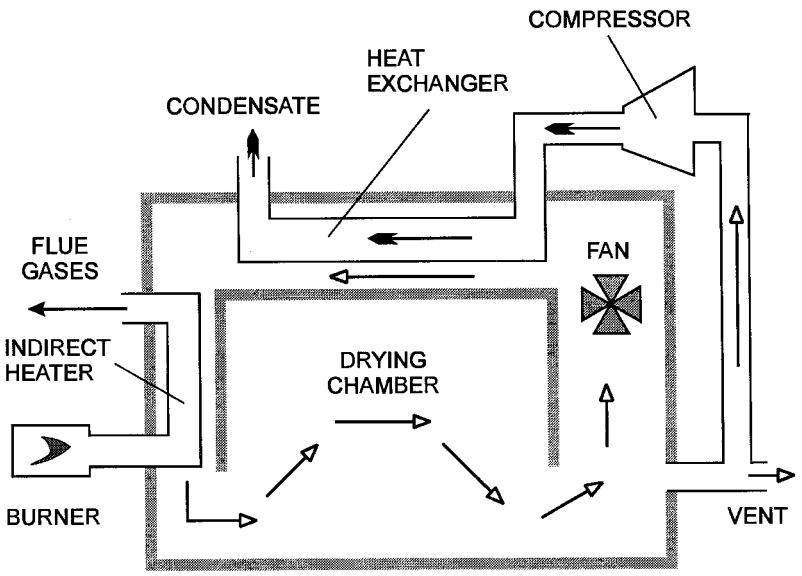

FIGURE 8.1 Airless batch dryer with vapor recompression.

the ducts that extend from the drying chamber and form the entry and exit ports for the conveyor with the material to be dried. According to Stubbing (1994b), the substantial (55%) difference in density between air and steam at 100°C combined with the temperature difference itself give rise to the stability of the layer. As proven in pilot tests, conveyed materials can move up and down through the stratification layer with no apparent disturbance—this was confirmed by the fact that no vented air was detected through the dryer's condenser (Anon., 1994a).

TABLE 8.2 Comparison of Energy Consumption

Type of dryer	
An airless dryer producing hot process water	626 kJ/kg
An airless dryer with vented steam compression to recycle energy	400 kJ/kg
An airless double-dryer reusing energy from its airless section in its air section	1900 kJ/kg
A typical efficient conventional hot-air dryer	3500 kJ/kg

Source: Courtesy of Heat-Win Ltd., Bitterley, UK.

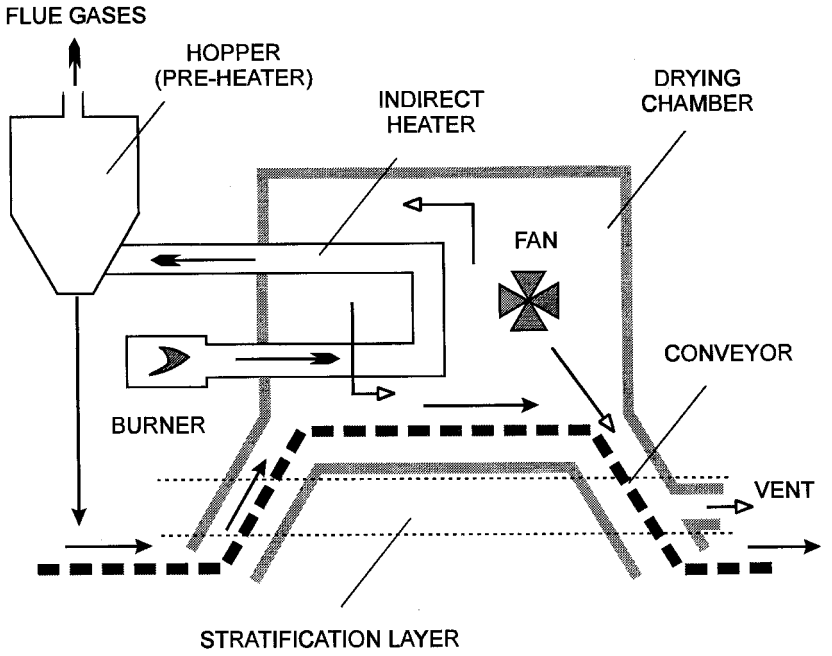

FIGURE 8.2 Continuous airless dryer.

Once a part of the wet material is inside the drying chamber, air heating, circulation, and progressive replacement with water vapor takes place as in a batchwise operation until the process temperature reaches 100°C. At this stage, the stratification layer is formed at a certain level across the product inlet and outlet ducts. From that point on, the wet material can be conveyed through the drying chamber while evaporated water is continuously heated and recirculated at atmospheric pressure. To avoid possible oxidation of the product by the air contained in the drying chamber during the warm-up period, water may first be sprayed in the chamber until the target temperature is attained.

Besides the typical advantages of drying in a steam/superheated steam atmosphere such as no oxidation, reduced fire and explosion hazard, higher drying rates due to preferential properties of steam against air such as viscosity and specific heat capacity, the main advantage of airless drying appears to be energy savings and thus lower processing costs and reduced CO_2 emissions. For example, the energy savings in high-humidity paper drying with exhaust heat recovery in comparison with the conventional paper drying are claimed

to be up to 7.75 TOE (tons of oil equivalent) per 100 t of paper produced. This approximates to 10 t of fossil fuel savings and reduction of CO_2 emissions by up to 30 t/100 t of dry paper produced. The cost of thermal and compression energy inputs has been estimated at £456 for airless dryer as compared to £1094 for conventional paper dryer (Stubbing, 1990). More information about energy consumptions and cost estimates can be found in literature for this chapter.

9

Drying in Mobilized Bed

Fluidized bed dryers have found widespread applications for drying of particulate or granular materials in the chemical, food, ceramic, pharmaceutical, polymer, and similar industries. More recently, they also found special applications in drying of suspensions, sludges, and soft pastes which are atomized into a fluidized bed of already dry material (back-mixing) or the bed of inert particles (Mujumdar, 1995; Devahastin, 2000). Among the advantages of the fluidized bed dryers, one may cite

- High drying rates due to excellent gas–particle contact
- Higher thermal efficiency, especially if part of the thermal energy for drying is supplied by internal heat exchangers
- Lower capital and maintenance costs compared to a rotary dryer of a similar drying capacity
- Easy to control

The main limitations of the fluidized bed dryers are as follows:

- Depending on density, the particle size is limited to 2 to 5 mm to maintain technically reasonable superficial velocity of fluidizing air.

Size distribution should be as narrow as possible to avoid excessive carryover.
Particle should be isometric as flakes, strips, and fibers cannot be fluidized.
High power consumption due to the need to suspend the entire bed in a gas stream leading to high pressure drop.
Low flexibility and potential of defluidization if the feed is too wet.

Several techniques evolved from the fluid bed principle in order to overcome some of these limitations. The centrifugal fluidized bed was developed to intensify heat and mass transfer rates for rapid drying of surface wet particles as well as to deal with the nonconventional properties of certain materials. Because larger airflow may be used in such a dryer, it was successfully applied to dry materials with relatively low bulk density such as pieces of potato, apple, and carrot (Lazar and Farkas, 1971), bell pepper, beet (Hanni et al., 1976), and quick-cooking rice (Roberts et al., 1980). For materials that are difficult to fluidize because of their odd shapes, the pulse fluid bed described elsewhere in this book can be recommended (Gawrzynski and Glaser, 1996). Mechanical vibration applied to the particulate material has lead to the vibro-fluidized bed drying (Erdesz, 1990; Rysin and Ginzburg, 1992; Pakowski et al., 1984) and vibro-spouted bed drying (Finzer and Kieckbusch, 1992). This makes possible the pseudo-fluidization of large and nonuniform particles such as tea leaves (Shah and Goyel, 1980). Another approach is the spouted bed technique in a variety of modifications which allows processing of Geldart's Type D particles that are too coarse or too dense to fluidize well without channeling (Kalwar et al., 1990; Passos et al., 1987).

Aside from numerous techniques for drying of particulates, the fluidization of fibrous entangled materials such as cut lamina tobacco particles is of great technical interest. One solution to this problem is a novel technique termed the ''mobilized bed'' which relies solely on its hydrodynamics to achieve bed mobilization. Although this chapter is based on data from a single source (Legros, 1986), the technique and results appear to be of sufficient significance as to warrant further development.

The idea of a mobilized bed is derived from the spout-fluid bed concept, which combines some characteristics of both fluidization and spouting techniques. The main part of the mobilized bed apparatus is the gas-distributor shown schematically in Figure 9.1. Since the drying chamber used in these experiments was square in cross-section, the distributor has a square configuration with the four walls inclined at 30° to the vertical. The lower section is

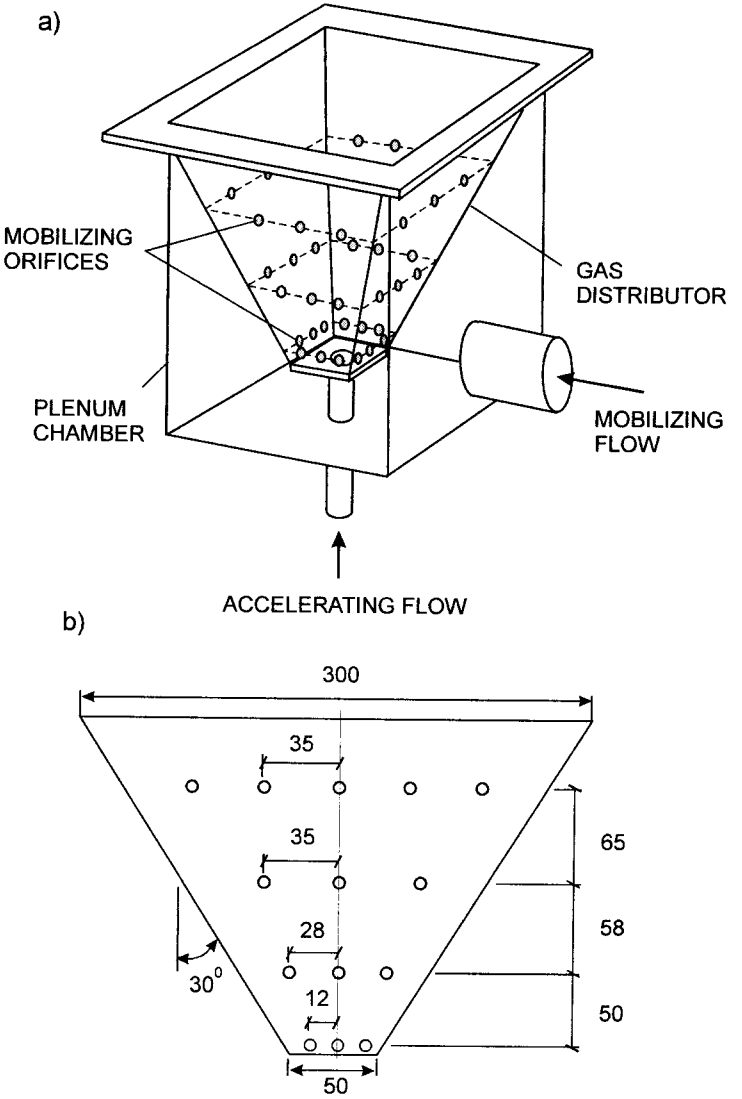

FIGURE 9.1 Mobilized bed distributor: a) design; b) spacing of the orifices (large distributor).

5 cm square, while the upper section is 15 × 15 cm (small distributor) or 30 × 30 cm (large distributor). The inclined surfaces have a number of orifices positioned in three horizontal rows, the lowest row being at the junction of the base and the inclined wall. Each row contains a series of orifices 4 mm in diameter as illustrated in Figure 9.1, which also shows details of the spacing of the orifices on one wall of the larger distributor. The base of the mobilizer contains a single orifice (7 or 10 mm in diameter) positioned on the central vertical axis. The fluidizing air is introduced to the dryer as two independently controlled and metered streams. The fluidization flow provided by the high-velocity jets from the wall nozzles which loosen and partially disentangle the bed material and force the tobacco particles toward the central upward moving region was termed by Legros (1986) the ''mobilizing flow.'' The spouting flow, provided by the central gas jet, was named the ''accelerating flow'' as its purpose is to promote overall circulation of the bed material by accelerating the particles in the upward direction.

When the mobilizing flow is started with no accelerating flow, the bed moves away from the inclined walls of the distributor. The material is compressed and a cavity appears in the lower region adjacent to the lower orifices. As the flow is increased, the upper bed surface becomes domed and the bed lifts. At a certain instant, the surface of the bed breaks and motion is apparent from the central vertical axis toward the walls. At this point, the entire bed becomes mobile, with a rolling circulating pattern. Gas and solids together move upward in the central core near the bed axis, while solids move outward in the freeboard and then downward along the inclined walls. With increasing gas flow, the motion becomes more turbulent until eventually the rolling mobilization is disrupted and the charge is transported out of the column. Once mobilization is established, it is possible to reduce the gas flow below the incipient level required to induce the initial motion without losing circulation. Observation of particle motion indicated that the fibers are largely disentangled under these conditions.

The mechanisms involved during the onset of bed mobilization can be better described with the help of a plot of the bed pressure drop as a function of mobilizing gas flow rate (Figure 9.2). The following sequence of events was reported as the mobilizing flow rate is increased (Legros, 1986):

1. For small mobilizing flow rates, the bed of cut tobacco behaves as a standard fixed bed of particulate material with the pressure drop steadily increasing with airflow.
2. At a certain airflow, the lower region of the bed starts to move away

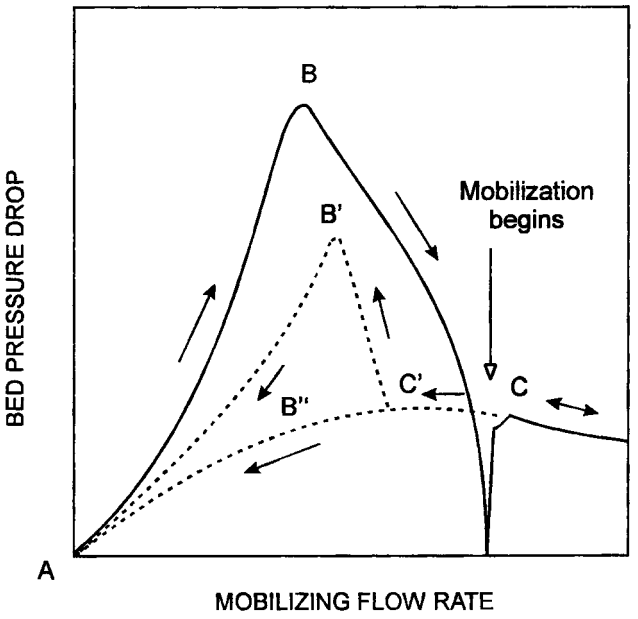

FIGURE 9.2 Pressure drop versus mobilizing flow rate.

from the walls and a cavity appears. The slightly compressed bed has reduced voidage so the pressure drop continues to rise along the line AB.

3. At point B, the bed is fully suspended by the hydrodynamic action of the gas flow and the pressure drop reaches maximum. With further increase of the gas flow rate, the bed starts to expand, causing the pressure drop to fall.
4. Beyond point B, the relationship between pressure drop and mobilizing flow is dependent on the fiber length of the tobacco, which is in relation to self-cohesion of the bed. It was observed that for short-fiber tobacco, the mobilizing gas jets push the particles away and start behaving like free jets, thereby diminishing the interaction between the gas and solids. With long-fiber tobacco, the particles are entangled and the jets only penetrate short distances before losing their identity.
5. At a certain mobilizing flow rate, corresponding to point C in Figure

9.2, the pressure drop falls sharply and the bed becomes mobile. The value of the mobilizing flow rate is very dependent on the bed history and is not fully reproducible.

6. Once the bed is mobilized, the pressure drop remains substantially constant with a further increase of mobilizing flow. The excess flow results in a more turbulent bed and higher bed expansion, without significant effect on the pressure drop.
7. When the mobilizing flow is decreased, the bed remains mobilized until point C′, which corresponds to a lower value of mobilizing flow than at point C. This value is called the minimum mobilizing flow rate. The bed pressure drop curve beyond this point depends on the manner in which the mobilization stops. The bed may collapse and turn into a packed bed with no channel. In this case, the bed pressure drop increases sharply as mobilization is lost and then decreases smoothly with reducing mobilizing flow (path C′B′A). More frequently, the bed may collapse in such a way that a preferential channel still exists. The pressure drop then remains at a low value, since most of the airflow passes through the channel and decreases slowly with decreasing mobilizing flow (path C′B′A).

Although it is possible to fluidize particles with the mobilizing flow only, stable fluidization is possible over a wide range of flows when mobilizing and accelerating flows are used in combination. The behavior of the bed is the same as that observed without accelerating flow (Figure 9.3). The mobilizing flow needed to initiate motion is dependent on the accelerating flow rate. The relationship between mobilizing and accelerating flow rates at minimum incipient mobilization is also dependent on the orifice size of the accelerating nozzle. As the orifice size is reduced (from 10 to 7 mm in diameter), the dependence on the magnitude of the accelerating flow becomes more important. Figure 9.4 shows the range of stable mobilization for a bed of tobacco particles. Start-up represents the conditions where the rolling motion of the bed starts, as distinct from minimum mobilization conditions, which correspond to the minimum flow conditions to maintain motion. The fast mobilization regime corresponds to excessive carryover of the bed material.

According to Legros (1986), the behavior of cut lamina tobacco in a larger mobilizer is similar to that observed in the smaller one. However, the accelerating flow has a noticeably smaller effect upon the mobilizing flow rate necessary to initiate mobilization. In general, the operation remains stable on the larger-scale apparatus.

Following Legros (1986), the mobilizing flow rate (V) necessary to sup-

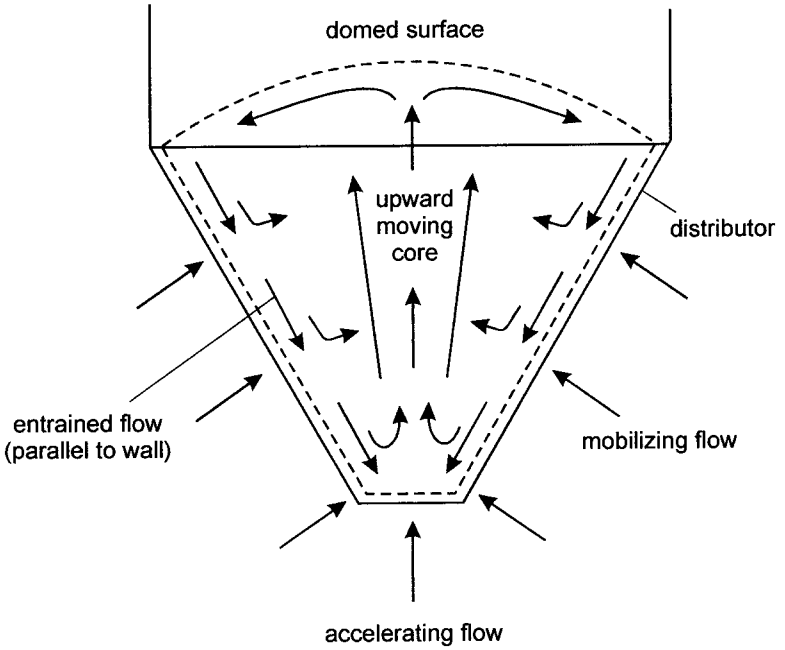

FIGURE 9.3 Flow pattern in a mobilized bed.

port a bed of cut lamina tobacco at the peak pressure drop (point B in Figure 9.2) can be calculated from the following equations:

$$F_y(V) = \frac{4\rho V^2 \sin \alpha}{C_m n \pi d_m^2} - \frac{\rho V^2}{D^2} + F_p(V) \tag{9.1}$$

and

$$F_y(V) = \text{mg} \tag{9.2}$$

where $F_p(V) = \sum F_{pi}(V)$ is the total pressure force calculated by adding the contributions from individual pressure forces for each zone of the mobilizer that are identified by the position of mobilizing orifices along the mobilizer height (y):

$$F_{pi}(V) = AQ_i(y_i - y_{i-1}) + \frac{BQ_i}{2 \tan \alpha}\left[\frac{1}{d_m + 2y_{i-1} \tan \alpha} + \frac{1}{d_m + 2y_i \tan \alpha}\right] \tag{9.3}$$

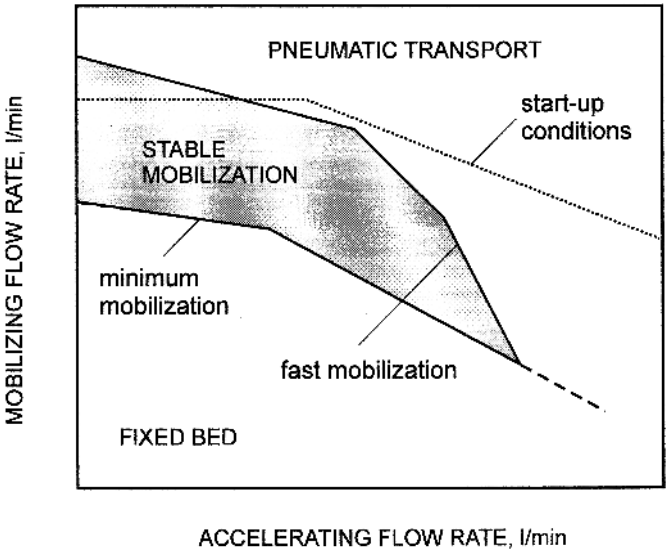

FIGURE 9.4 Phase diagram for mobilization.

Based on the packed bed experiments, the coefficients A and B were found to be

$$A = 25{,}440\,\frac{(1-\varepsilon)^2}{\varepsilon^3} \qquad \text{and} \qquad B = 12{,}740\,\frac{(1-\varepsilon)}{\varepsilon^3} \tag{9.4}$$

for the range of $\varepsilon > 0.8$.

The bed voidage was determined from the measured bulk density (ρ_b) at a given moisture content (X) as

$$\rho_b = 665\,(1+X)(1-\varepsilon) \tag{9.5}$$

To estimate the point of the peak pressure drop of a bed of cut lamina tobacco of bulk density (ρ_b) and moisture content (X), Legros (1986) proposed the following procedure:

1. Calculate the bed voidage from Eq. (9.5).
2. Calculate the coefficients A and B from Eq. (9.4).
3. Plot the ratio $F_y(V)/mg$ as a function of V with $F_y(V)$ calculated from Eq. (9.1).
4. Determine the value of V for which the ratio of $F_y(V)/mg = 1$.

5. Calculate the pressure drop from the following equation:

$$\Delta P = \sum \Delta P_i = \sum \left\{ \frac{AQ_i}{2 \tan \alpha} \left[\frac{1}{d_m + 2y_{i-1} \tan \alpha} - \frac{1}{d_m + 2y_i \tan \alpha} \right] + \frac{BQ_i^2}{6 \tan \alpha} \left[\frac{1}{(d_m + 2y_{i-1} \tan \alpha)^3} - \frac{1}{(d_m + 2y_i \tan \alpha)^3} \right] \right\} \quad (9.6)$$

It should be noted that the gas flow rate [Eqs. (9.3) and (9.6)] in each zone (Q_i) is considered to be the sum of the total gas flow entering below the zone's lower boundary while V represents the mobilizing flow rate.

Figure 9.5 shows a comparison between the predictions of the bed pressure drop calculated from Eq. (9.6) and experimental results obtained in the

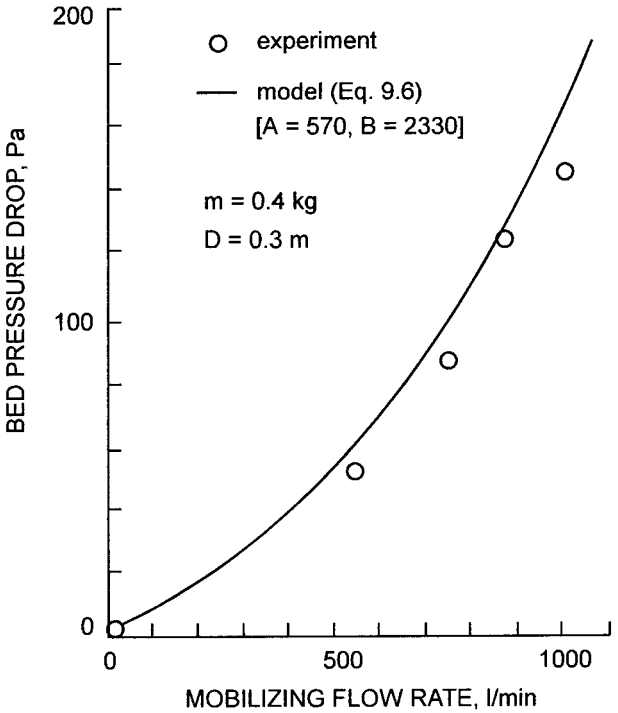

FIGURE 9.5 Comparison between model predictions and experimental data. (From Legros, 1986.)

30-cm square mobilizer. The coefficients A and B for $\rho_b = 95$ kg/m^3 and $X = 0.16$ kg/kg were equal to 570 kg/(m^{3}s) and 2330 kg/m^4, respectively.

Heat transfer experiments (Legros, 1986) performed at various hydrodynamic conditions showed that the mobilized bed may be regarded as being perfectly mixed for both gas and solid phases. The heat transfer rates were high enough to achieve thermal equilibrium in both phases. In the case of drying, a falling rate period was observed for the entire drying curve of cut lamina tobacco; for air superficial velocities above 0.8 m/s the drying rate was found to be controlled by internal mass transfer rate. Further, a drying model was proposed that is based on liquid diffusion mechanism. Because cut tobacco particles had a width of 1.0 mm, it was assumed that the moisture migration occurs only in one direction, that is, through the cut faces of the lamina. For such a unidirectional flow, the solution of the diffusion equation

$$\frac{\partial X}{\partial t} = \frac{\partial\left(D_e \dfrac{\partial X}{\partial x}\right)}{\partial x} \tag{9.7}$$

for a constant effective diffusion coefficient and particle surface reaching instantaneously the hygroscopic moisture content in equilibrium with the gas phase has the following form derived for an infinite slab:

$$\frac{X - X_e}{X_0 - X_e} = \frac{8}{\pi^2} \Sigma \frac{1}{(2n + 1)^2} \exp\left[- (2n + 1)^2 D_e \left(\frac{\pi}{2l}\right)^2 t \right] \tag{9.8}$$

where $2l$ is the thickness of the tobacco lamina, X_0 is the initial moisture content, and X_e is the equilibrium moisture content.

The experimental moisture content data were then plotted according to Eq. (9.8) and the effective diffusion coefficient was determined from the slope of the plot. The logarithm of the effective diffusion coefficient as a function of the bed temperature is shown in Figure 9.6. It is clear that the effective diffusion coefficient varied with the solid's temperature according to the Arrhenius relationship

$$D_e = 0.00102 \exp \frac{-E_a}{RT} = 0.00102 \exp \frac{-39500}{RT} \tag{9.9}$$

To reflect the experimental drying curves, Legros (1986) proposed to simplify Eq. (9.8) to the following form:

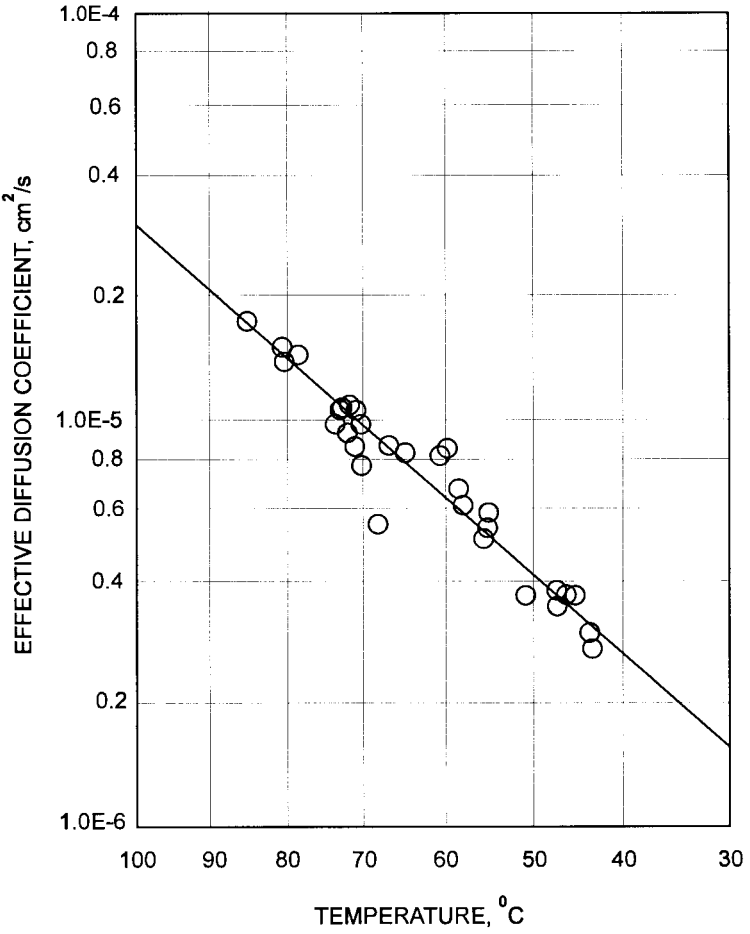

FIGURE 9.6 Effect of temperature on the effective diffusion coefficient. (From Legros, 1986.)

$$\frac{X - X_e}{X_0 - X_e} = \exp\left[-\left(\frac{\pi}{2l}\right)^2 D_e t\right] \tag{9.10}$$

Comparison of the actual drying results with predictions from the models given by Eqs. (9.8) and (9.10) is shown in Figure 9.7. Clearly, the model based on moisture diffusion can be used to predict adequately drying kinetics of tobacco fibers in the mobilized bed dryer.

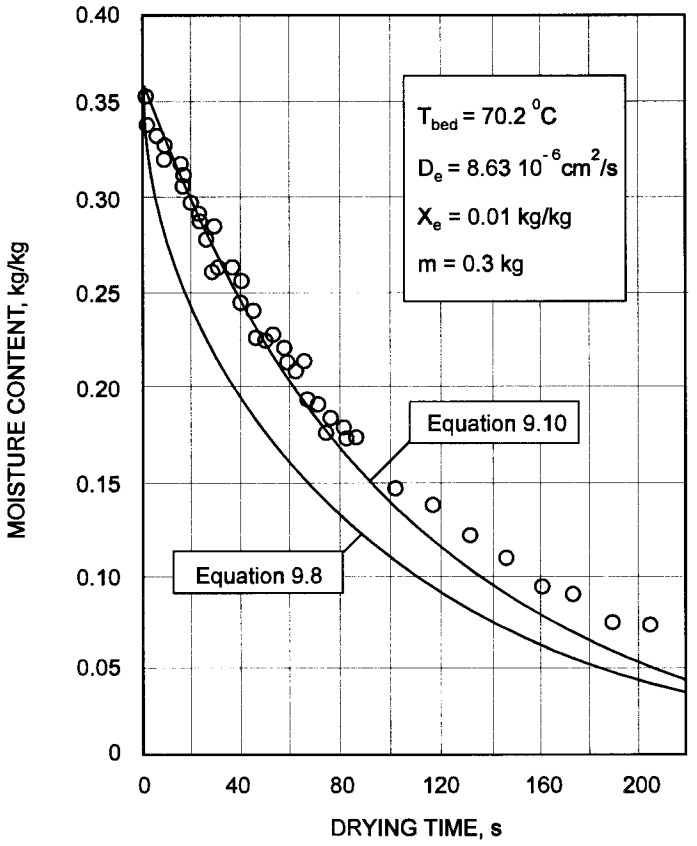

FIGURE 9.7 Prediction of drying curves for cut tobacco lamina. (From Legros, 1986.)

Detailed derivation of the equations cited in this chapter as well as other correlations describing a mobilization technique for drying fibrous materials, heat transfer and drying results can be found in the thesis by Legros (1986) and papers by Legros et al. (1994, 1995).

10

Drying with Shock Waves

One of the innovative technologies for atomizing viscous liquids and thin pasty materials in a gas is the use of shock waves. This method could be used in spray drying to disperse the liquid feed (see Chapter 14) and thus eliminate the conventional atomizer from the system. This will avoid problems with erosion in disk atomizers and clogging of single- or two-stream spray nozzles. Potential applications of this idea in other types of dryers for dispersed materials include pneumatic, ring, spin-flash, and vortex dryers, in which the momentum of shock waves can enhance the hydrodynamic impact of a conventional gas-carrier.

It should be noted that the term ''shock waves'' refers to a pressure wave of large amplitude that arises from sharp and violent disturbances when the velocity of wave propagation exceeds the velocity of sound propagation. Characteristically, an abrupt change of the medium properties (e.g., pressure, stress, density, particle velocity, temperature, etc.) takes place in a limited space across the shock wave (Schetz and Fuhs, 1996; Shapiro, 1953; Anderson, 1982; Saad, 1992). In the case described in this chapter, the physical phenomenon of shock wave is restricted to one-dimensional plane wave propagation, in which properties of air in the resonant tube of the wave generator

vary with respect to only one spatial coordinate and time. Although it is technically feasible to generate a true shock wave by moving a piston into a compressible medium, the velocity of wave propagation in the system presented here is lower than the sonic velocity. However, the almost flat pressure profile at the front of the wave exiting the generator is similar to a nearly discontinuous shock front propagating at a supersonic velocity. Because there is no adequate definition for the pressure wave of such characteristics, the term ''shock wave'' will be used throughout this chapter.

Atomization and drying in shock waves is still at the development stage, e.g., laboratory- and pilot-scale experiments. Figure 10.1 presents schematically the experimental shock-wave generator used by Lyulin (1998) to disperse pasty materials in a spray dyer. The generator consists of a stainless steel tube 0.04 m in diameter, which propagates the pressure waves and serves as a quarter-wave (Helmholtz) resonator (see Chapter 14). One end of the resonance tube is open to the atmosphere while the other is connected to a pulse generator through a truncated cone 0.2 m long. The generator comprises a cylindrical chamber 0.08 m in internal diameter and a crankshaft-connecting rod assembly, which moves the piston in a reciprocating manner. The stroke of the piston is 0.082 m. The pulse generator is driven by a 7-kW DC motor with controllable rotational speed allowing variable frequency of the strokes from 7 to 28 Hz.

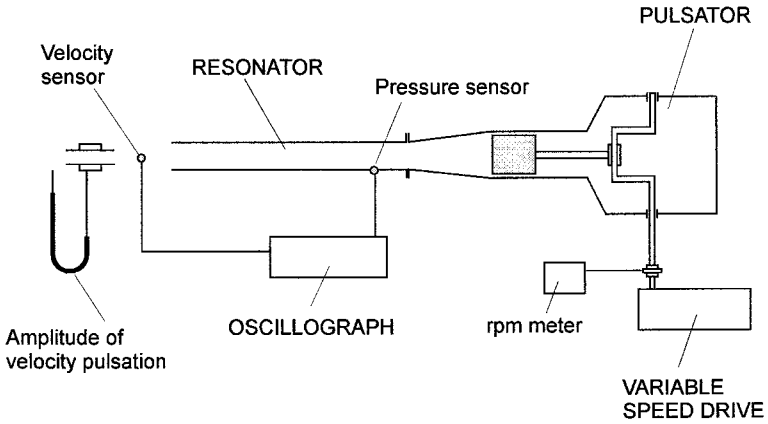

FIGURE 10.1 Schematic of the experimental shock-wave generator. (From Lyulin, 1998.)

The instantaneous pressure and velocity distributions along the resonance tube are monitored by piezoelectric transducers and hot-wire thermal anemometer that are connected to the oscilloscope and photo film recorder. These make possible the tuning of the generator to the acoustic resonance by varying the rotational speed of the crankshaft. Also, there is a provision to attach resonance tubes of various lengths and diameters to obtain required amplitudes of pressure and velocity pulsations.

Figure 10.2 presents a typical temporal pressure oscillation at various points along the resonance tube. It is clear that the profile of pressure oscillation near the piston is sinusoidal because of the reciprocating movement of the piston. As the pressure wave travels along the resonant tube, its descending part (the front of the wave) becomes shorter while the ascending one (the tail of the wave) levels off gradually, giving finally a steep pressure front characteristic of a shock wave. The extremely high gradients of pressure at the front of the plane wave not only initiate mechanical effects such as liquid dispersion but also can alter drying rates due to enhanced evaporation and capillary flow of liquid and vapor moisture.

Unlike pressure, the profile of the velocity pulsation remains practically unchanged along the resonant tube and distortion of the sinusoidal velocity pulsation occurs only at the tube outlet. As shown in Figure 10.3, the amplitude of velocity pulsation decreases sharply with the distance of wave propagation in open air. To take full advantage of the momentum of shock waves, liquid to be dispersed should be fed close to the outlet from the resonant tube, in this case up to about 20 cm. Also, the strongest impact of shock wave due to air velocity might be expected over a distance up to 1 m from the resonance tube.

Figure 10.4 presents amplitude-frequency characteristics of two different resonant tubes, where the first and second resonance frequencies are clearly identified by the consecutive maxima on the respective curves.

For a given tube length, the resonance frequency is calculated as

$$f_r = (2n - 1)\frac{v}{4L_t} \tag{10.1}$$

where v is the velocity of sound propagation, L_t is the tube length, and n is the order of the harmonic frequency.

From Eq. (10.1) it follows that the product $f_r L_t$ does not depend on the tube diameter but is a constant characteristic of the gaseous environment. Hence, at the sound velocity in air equal to 330 m/s, the first resonance is obtained at $f_r L_t = 82.5$ m/s.

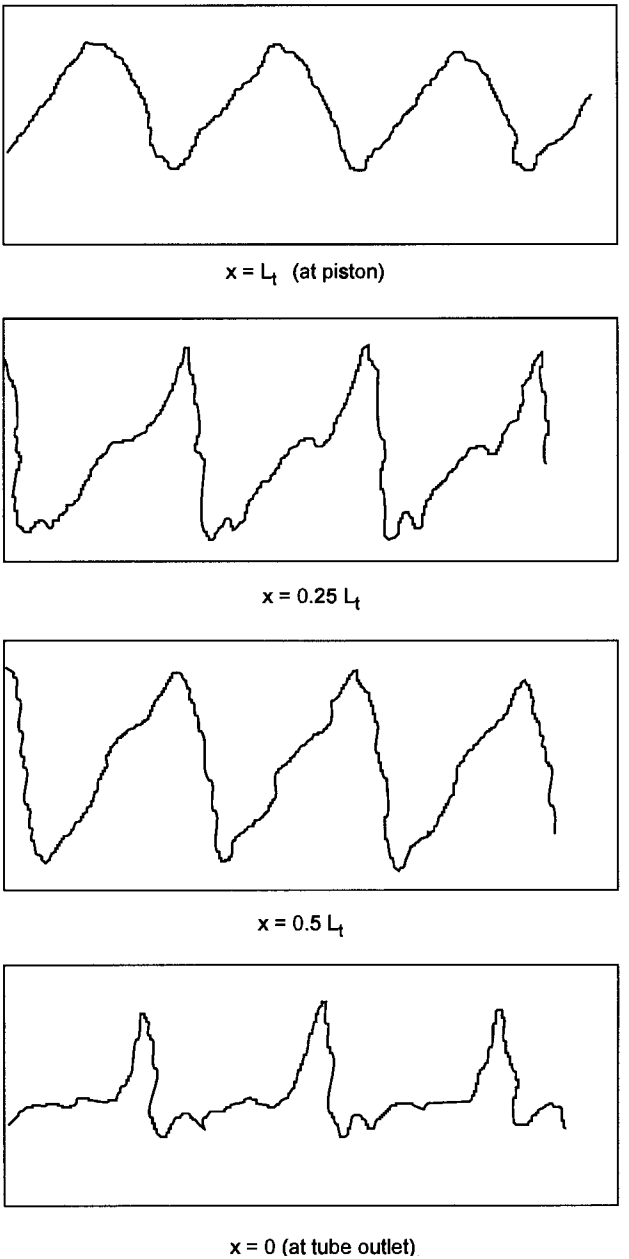

FIGURE 10.2 Characteristic of pressure oscillation in the resonance tube.

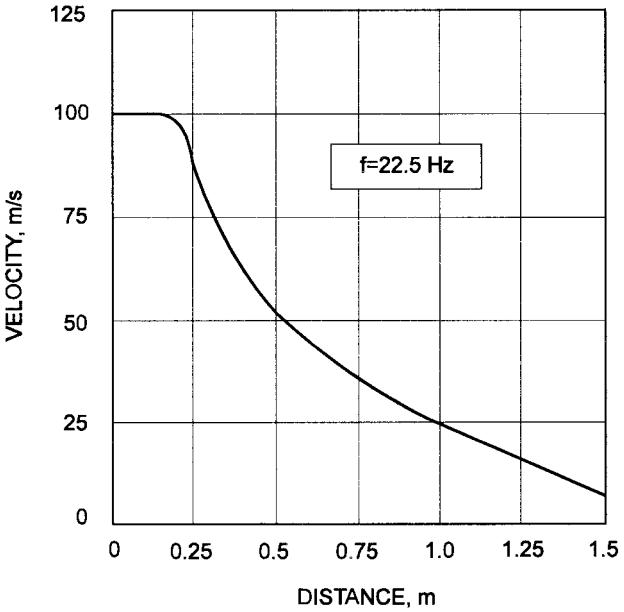

FIGURE 10.3 Variation of the amplitude of the pulsating velocity with distance from the outlet of the resonance tube.

The maximum amplitude of the velocity pulsation appears at $n = 1$ (Figure 10.4). It is quite reasonable to assume that the amplitude of air pulsation at the tube outlet is proportional to the amplitude of the velocity of piston movement

$$u = Ku_c \tag{10.2}$$

Accounting for the different diameters of the resonant tube (d_t) and substituting u_c by (πfs), the following equation (valid for $u < 140$ m/s) was derived by Lyulin (1998):

$$u = Z\pi fs \frac{d_c}{d_t} \tag{10.3}$$

where s is the piston stroke length, d_c is the piston diameter, and Z is a constant equal to 11.0 for $0.044 < d_t < 0.005$ m and equal to 9.1 for $0.033 < d_t \leq 0.044$ m. These values were determined experimentally.

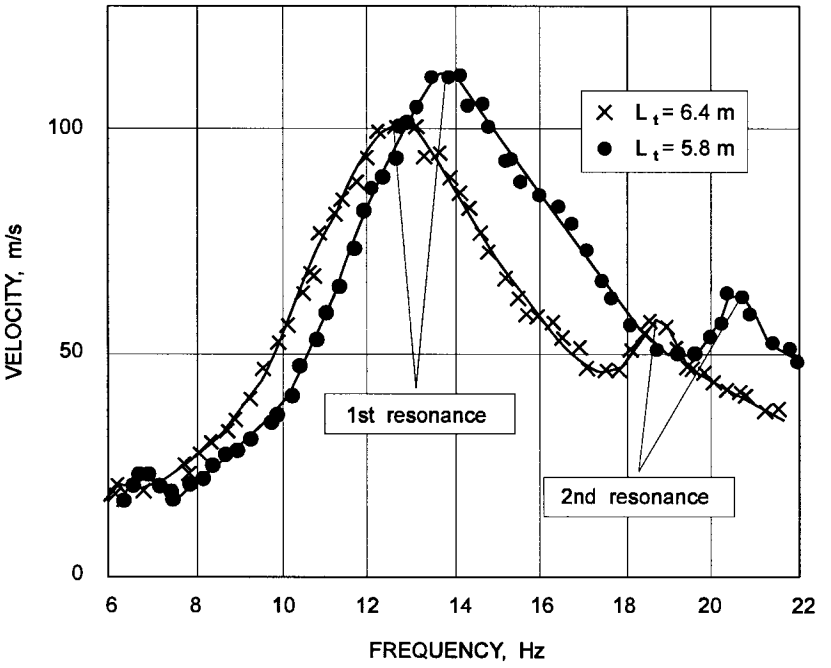

FIGURE 10.4 Typical resonance characteristics of the shock-wave generator. (From Lyulin, 1998.)

Expressing the frequency in terms of the crankshaft rpm, the following experimental correlation can be used to calculate the length of the resonant tube and the amplitude of air velocity at the tube outlet:

$$u = 0.0523ZsN\left(\frac{d_c}{d_t}\right), \text{ m/s} \qquad \text{and} \qquad L_t = \frac{15v}{N}, \text{ m} \tag{10.4}$$

The shock wave acts as a liquid atomizer up to the point at which the momentum of the shock wave is able to disperse the liquid stream. By analogy with two-phase flow in packed columns, such hydrodynamic conditions can be construed as ''flooding.'' Hence, the region of stable atomization is mapped in terms of a flooding coefficient, defined as the mass flow ratio of undispersed liquid to the total liquid subject to the shock-wave field

$$\beta = \frac{W - W_d}{W} \tag{10.5}$$

Lyulin (1998) provided the following empirical correlation for the flooding coefficient:

$$\beta = \left[\left(1 - A\,\frac{u_g}{u_l}\right)\left(\frac{d_t}{d_l}\right)\right]^2 \tag{10.6}$$

where A is the constant, d_l is the diameter of the liquid jet subject to atomization, and u_l and u_g are the liquid jet velocity and the amplitude of the gas velocity pulsation, respectively.

Thus, the generalized correlation for the flooding velocity shown in Figure 10.5 is

$$u_l = 0.00161\, f^{1.31}\,\frac{(u_g - 37.3)^{1/3}}{d_l^{0.25}} \tag{10.7}$$

where the liquid jet diameter d_l is in mm, frequency f is in Hz, and the gas velocity u_g is in m/s.

The dispersion of pasty pigments with shock waves was studied experimentally using the shock-wave generator with a resonance tube of 0.033 m. This allows achieving air velocity equal to 163 m/s at 19.8 Hz of the reciprocating movement of the piston. The pasty feed was located 0.05 m from the resonance tube outlet at its axis. Such a distance was found to be optimal over the range from 1.5 to 5 times the tube diameter.

The following procedure was used to obtain a droplet size distribution (Muranov et al., 1997). Dispersed pigments were trapped in a filter paper placed perpendicularly to the tube axis 1 m from the pasty feed. Segments of the filter paper with spots of droplets were then analyzed under a microscope, and about 2000 droplets were counted for the size distribution. Knowing the dry mass of the dispersed pigment (m) and total surface area of the spots (S_S), the volume of the droplet having (X, % wb) moisture content that leaves the spot with diameter (d_S) can be calculated from

$$V_p = \frac{\pi d_S^2}{4\rho_m}\,\frac{m}{S_S}\,\frac{100}{100 - X} \tag{10.8}$$

where ρ_m is a density of the wet material.

Thus, the droplet diameter is

$$d_p = \left(\frac{6V_p}{\pi}\right)^{1/3} = \left(\frac{150 d_S^2 m}{S_S(100 - X)\rho_m}\right)^{1/3} \tag{10.9}$$

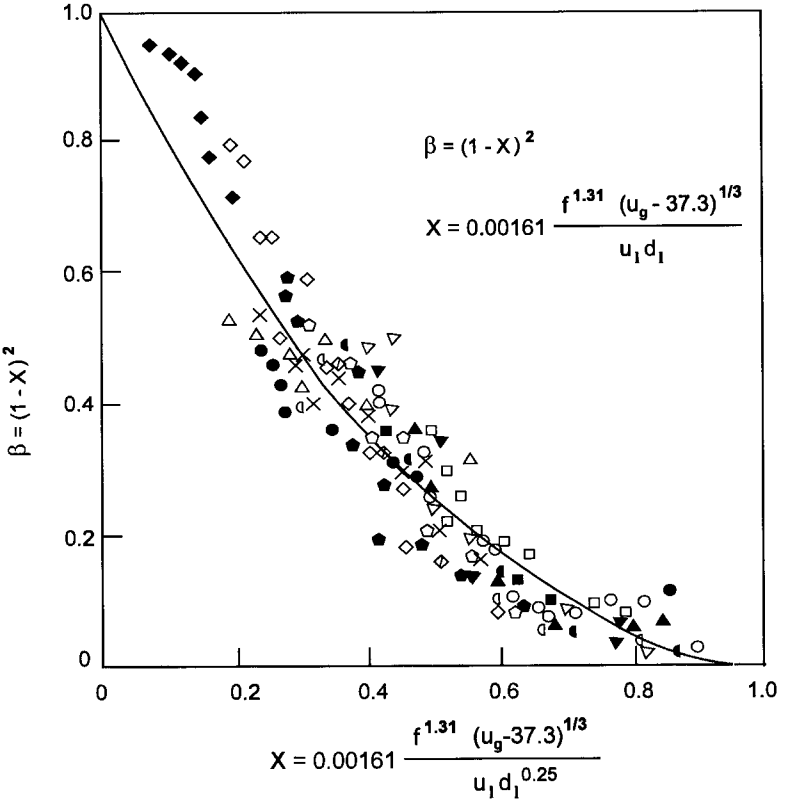

	×	○	●	△	▲	□	■	◇
d_l, mm	5.7	7.8	4.2	3.7	8.1	7.8	7.8	7.8
f, Hz	19	19	19.2	19.2	19.1	19.2	19.2	19.2
u_g, m/s	113	113	113	113	113	97	84	37.6
u_l^{max}, m/s	4.7	2.4	5.77	8.37	2.33	7.2	7.28	2.51
u_l^{min}, m/s	1.96	1.16	1.44	1.86	1.26	1.36	1.36	0.84

	◆	⬟	⬠	◈	◖	◐	▽	▼
d_l, mm	7.8	7.8	7.8	7.8	7.8	7.8	7.8	7.8
f, Hz	19.2	19.2	19.2	15	16.8	17.8	20	22
u_g, m/s	55.5	67.2	83	83	83	83	83	83
u_l^{max}, m/s	1.78	2.51	7.28	7.28	7.28	7.28	7.28	7.28
u_l^{min}, m/s	0.42	1.05	1.15	0.73	0.94	0.94	1.15	1.36

FIGURE 10.5 Flooding curve for atomizing liquids with shock waves. (From Lyulin, 1998.)

whereas the total surface area of dispersed liquid trapped in the filter paper is

$$S = \sum_{i=1}^{n} S_{d,i} = \sum_{i=1}^{n} \pi(d_p^2)_i \tag{10.10}$$

Typical distribution of droplet size for anticorrosive paint based on zinc phosphate is shown in Figure 10.6. The symbol d_M identifies here the median diameter (midpoint of the size distribution) and d_{sV} is the surface volume diameter, i.e., diameter of the sphere having the same ratio of surface area-to-volume as the droplet, and calculated as

$$d_{sV} = \frac{\sum d_i^3 n_i}{\sum d_i^2 n_i} \tag{10.11}$$

Figure 10.6 indicates that droplets generated by the shock wave are nearly monodispersed since the mass fraction of droplets larger than 27 μm is negligible compared to the mass fraction of fine droplets. Because the surface-volume diameter falls into the range of large droplets (106 μm), the median diameter appears to be more appropriate for evaluation of the atomizing capability of shock waves. The experiments also proved that the size distribution depends on air velocity, and the median diameter decreases with decreasing velocity to reach the range from 40.5 to 54 μm at 36.7 m/s (Lyulin, 1998). The best dispersion was found for air velocities above 100 m/s.

The pilot plant experiments were carried out with various pigments (Table 10.1) dried in a spray dryer with the shock-wave atomizer designed according to the aforementioned procedure (Figure 10.7). Each test was run for 8 hours to obtain a representative sample of about 2000 kg of dry product. The filter cake at an initial moisture content from 50% to 60% wb was dried under optimum conditions determined from laboratory tests, that is, at an inlet air temperature of 170°C and a feed rate of about 120 kg/h. An average evaporation rate for all tests was about 28 kg $H_2O/(m^3h)$, which is markedly higher than for currently used spray dryers for which the volumetric evaporation capacity is about 10 $kg/(m^3h)$.

Table 10.2 presents as an example the basic characteristics of zinc phosphate dried in a pilot spray dryer with reference to industrial standards (Lyulin, 1998). It is evident that pigments dried in a spray dryer with the shock-wave atomizer satisfy all requirements for the commercial product. In addition, pigments obtained with the shock-wave atomizer have a narrower size distribution so the throughput of the ball mills used in a downstream process of standardizing is increased by about 20% to 30%.

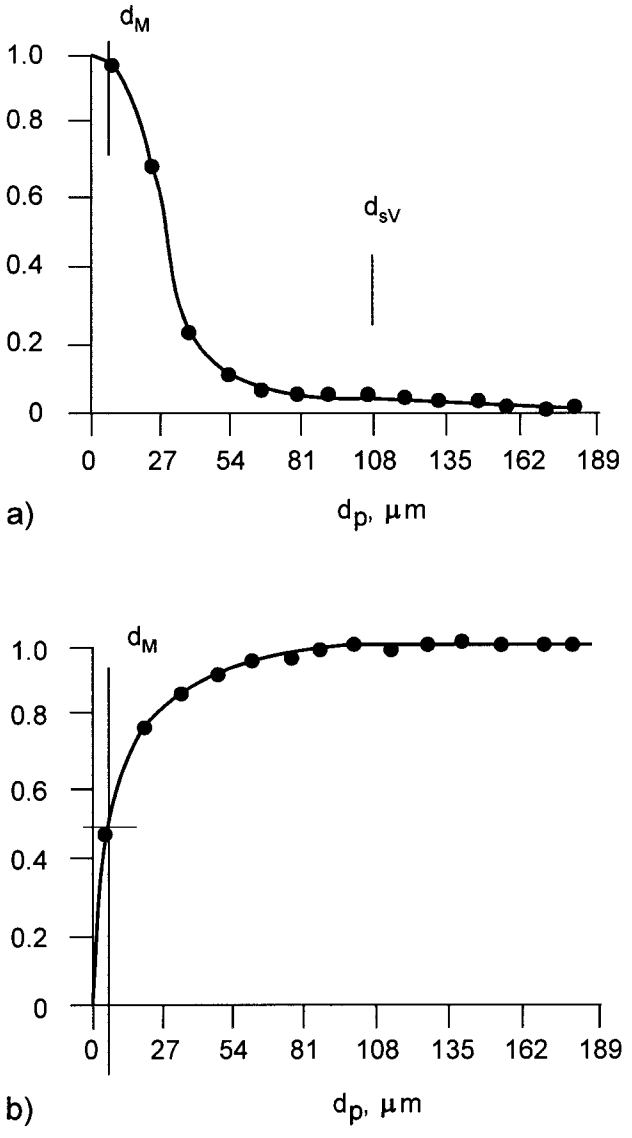

FIGURE 10.6 Droplet size distribution for zinc phosphate-based anticorrosive paint at 163 m/s; a) frequency distribution (histogram), b) cumulative distribution. (From Lyulin, 1988.)

TABLE 10.1 Comparison of Selected Pigments Dried in a Spray Dryer with Shock-Wave Atomizer with a Reference Pigment

Pigment	Inlet air temperature, °C	Covering power, g/m^2		Grindability,[a] μm	
		Standard	Product	Standard	Product
Titanium dioxide					
R-02	170	40	35	15	10
A-01	180	45	40	15	12
Lithopone	250	140	130	15	10
Chrome yellow					
KL-1	200	60	60	15	10
K2H-1	200	50	45	15	10
OS	200	20	17	20	15
Zinc phosphate	170	—	—	50	30

[a] After 30 min of grinding.
Source: Lyulin, 1998.

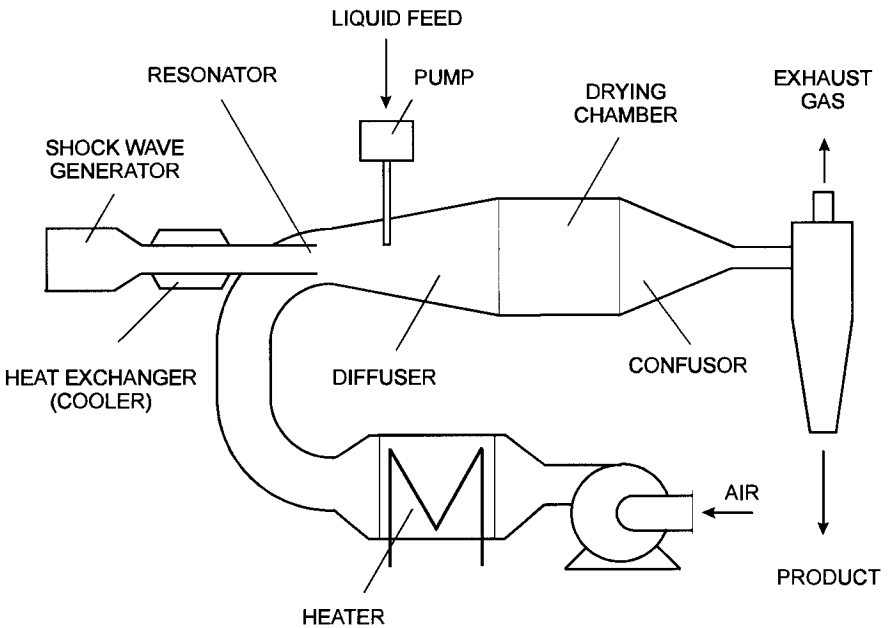

FIGURE 10.7 Schematic of the experimental set-up for spray drying with shock waves.

TABLE 10.2 Quality Indices for Zinc Phosphate for Anticorrosive Paint[a]

Index	Standard	Pilot dryer
Density, kg/m^3	3,000	3,000
Mass fraction of phosphorous compounds in terms of ZnO, %	45.0–55.0	50.0
Mass fraction of phosphorous compounds in terms of P_2O_5, %	30–40	33
Mass fraction of water-soluble components, %	<0.3	<0.1
Mass fraction of volatiles, %	<0.3	<0.5
pH of aqueous suspension	6.0–8.0	6.7
Oversize solids on sieve 0.063 mm, %	<0.5	<0.05
Mass capacity, g/100 g pigment	<50	<50
Whiteness, arbitrary units	>92	>93
Degree of dispersion, μm	<30	<15

[a] White loose powder with no tendency to agglomerate.
Source: Lyulin, 1998.

Although results of this pioneering Russian study have documented advantages of drying with shock waves, extension of this novel drying technology to other products will require additional studies, both theoretical and experimental. To our knowledge Lyulin's thesis is the only study of this novel concept. It is therefore difficult to make definitive recommendations about its potential without extensive independent tests.

APPENDIX: PROCESS CALCULATIONS AND EQUIPMENT DESIGN

The design criteria for a spray dryer with the shock-wave atomizer used by Lyulin (1998) are as follows:

Dryer type: horizontal, concurrent, material fed to the zone of shock wave
Drying agent: ambient air at 20°C and 70% RH
Material dried:
  Pasty filter cake (viscosity of about 200 Poise) fed by the metering pump
  Initial material temperature 20°C, final material temperature 80°C
  Initial moisture content >50% wb, final moisture content <0.5% wb

Shock-wave generator:
Piston 0.08 m in diameter, stroke length 0.072 m
Motor 4 kW
Frequency 22.5 Hz
Spray angle 30°

Because the spray angle generated by the shock-wave atomizer is 30°, and the feeding point is at the outlet from the resonance tube, it is clear that the optimal drying chamber should be made as a truncated cone of included angle 30°. In such a configuration the liquid droplets atomized at the outlet from the resonance tube located at the cone tip will decelerate while traveling along the cone axis until their terminal velocity will reach the velocity of a drying air stream. At this point, the unsteady flow turns into a steady one, and the drying chamber can be shaped as a cylinder.

The following assumptions can be made for design calculations (Lyulin, 1998):

1. Droplets are spherical and do not collide during drying.
2. Droplet size and mass do not change during drying; heat and mass transfer area is equal to the total surface area of dry particles.
3. The velocity field of a droplet spray follows the velocity field of the shock wave in the plane of propagation.
4. The flow pattern in the dryer is a plug flow.
5. Distribution of a dispersed material and a drying agent is uniform throughout the dryer volume.
6. Heat transfer coefficient can be calculated using $Nu = 2$.

All these assumptions except the third one are usual in engineering calculations for spray dryers. Assumption 3 might appear to be too general, but considering the novelty of the shock-wave drying, it can be accepted as the first approximation to more accurate calculations.

Experiments on atomization of various pasty materials showed that 100 m/s is the minimum amplitude velocity required for the narrow droplet size distribution. Based on assumption 3, the maximum (i.e., initial) velocity of liquid droplets is thus equal to 100 m/s. Furthermore, the spatial variation of droplet velocity will be the same as for the amplitude velocity of shock wave shown in Figure 10.3 and defined by the following equation:

$$u = u_p = -14.11e^L + 73.26 \tag{10.12}$$

Solving Eq. (10.12) for $u_p = 0$ gives $L = 1.65$ m, which identifies the unsteady region of the dryer and hence determines the maximum length of

the conical drying chamber. In a conventional spray dryer, however, droplets evaporate in an air stream flowing at a superficial velocity from 0.2 to 0.5 m/s. It is therefore reasonable to accept that the terminal velocity of droplets will be equal to the air velocity. Hence, for air velocity in a cylindrical part of the drying chamber (stationary region of the air-droplet flow) equal to 0.5 m/s, the real length of the conical drying chamber is 1.64 m.

Substituting the droplet velocity in Eq. (10.12) for *dL/dT*, the following equation is obtained for the residence time distribution:

$$t = \int_0^L \frac{dL}{-14.11e^L + 73.26} \tag{10.13}$$

The length of the resonance tube for the first (maximum) resonance is given by

$$L_t = \frac{v}{4f_r} = \frac{330}{4 \cdot 22.5} = 3.66 \text{ m}$$

where the velocity of sound propagation in air at 20°C is 330 m/s.

Taking $Z = 11.0$, the maximum diameter of the resonance tube securing the amplitude velocity at least 100 m/s should be larger than

$$d_t = \pi Z \frac{d_c f_r s}{u} = \pi \cdot 11.0 \frac{0.08 \cdot 22.5 \cdot 0.072}{100} = 0.045 \text{ m}$$

To obtain a uniform velocity profile in a drying chamber, the resonance tube and the drying air inlet should be concentric. Hence, the drying chamber is formed as a truncated cone with the inlet diameter (D) and the outlet diameter equal to the diameter of the cylindrical drying chamber (D_{ch}). For an inlet diameter of 0.2 m, the chamber diameter is thus

$$D_{ch} = D + 2Ltg\frac{\gamma}{2} = 0.2 + 2 \cdot 1.64tg\frac{30}{2} = 1.08 \text{ m}$$

Hence, the volumetric flow rate of the drying air is

$$V = \frac{\pi D_{ch}^2}{4} u_{g,ch} = \frac{\pi 1.08^2}{4} 0.5 = 0.458 \text{ m}^3/\text{s}$$

Assuming the diameter of the material feeding tube is 8 mm, the flow velocity of the pasty feed can be calculated from Eq. (10.7) as

$$u_l = 0.00161 f^{1.31} \frac{(u_g - 37.3)^{1/3}}{d_l^{0.25}}$$

$$= 0.00161 \cdot 22.5^{1.31} \frac{(100 - 37.3)^{1/3}}{0.008^{0.25}} = 1.26 \text{ m/s}$$

The maximum volumetric flow rate of the feed is

$$V_l = u_l \frac{\pi d_l^2}{4} = 1.26 \frac{\pi 0.008^2}{4} 3600 = 0.228 \text{ m}^3/\text{h}$$

Because the density of the pasty pigments from the filter press is in the order of 1600 to 1700 kg/m^3, the maximum capacity of the shock-wave atomizer of these characteristics is in the order of 370 to 390 kg/h.

From the drying kinetics it is clear that drying of pasty pigments which belong to the class of capillary-porous materials takes place mainly in the constant drying rate period. Hence, the drying time can be calculated from the heat transfer equation

$$t = \frac{Q}{hF\Delta T_e} \tag{10.14}$$

where F is the heat transfer area, which is equal to the total surface area of droplets and h is the heat transfer coefficient calculated from $Nu = 2$ as

$$h = \frac{k\,Nu}{d_p} = \frac{0.0285 \cdot 2}{2 \cdot 10^{-5}} = 2850 \text{ W/(m}^2\text{K)}$$

where the droplet diameter is taken from Figure 10.6.

The evaporation rate of water is

$$W_w = G_m \frac{X_i - X_f}{100 - X_f} = G_m \frac{50 - 0.5}{100 - 0.5} = 0.497 G_m$$

Because the dryer throughput is limited by the capacity of the shock-wave atomizer (airflow rate equal to 0.458 m^3/s), the maximum feed rate is

$$G_m = \frac{V_g \rho_g (Y_f - Y_i)}{0.497} = \frac{0.458 \cdot 1.2(0.088 - 0.011)}{0.497}$$
$$= 0.0826 \text{ kg/s} = 297 \text{ kg/h}$$

which is less than the 390 kg/h found as the maximum capacity of the shock-wave atomizer.

Density of drying air was calculated from the humid volume v_H as

$$\rho_g = \frac{1 + Y_l}{v_H} = \frac{1 + 0.011}{0.8436} = 1.2 \text{ kg/m}^3$$

where

$$v_H = 22.4\left(\frac{1}{29} - \frac{Y_i}{18}\right)\frac{T_{g,i}}{273.15} = 22.4\left(\frac{1}{29} + \frac{0.011}{18}\right)\frac{293.15}{273.15}$$
$$= 0.8436 \text{ m}^3/\text{kg}$$

The humidity of the exhaust air equal to 0.088 kg/kg was taken as the maximum, yielding a dew point of the exhaust air of 50°C which is the value needed to avoid condensation of water vapor in cyclones and bag filters.

Heat transferred to the dispersed material is used for sensible heating of the material and for moisture evaporation. Thus,

$$Q = W_w\,\Delta H + G_m c_m(T_{wb} - T_{m,i}) + G_m(1 - W_w)c_s(T_{m,f} - T_{wb})$$
$$= 0.0826 \cdot 0.497 \cdot 2377 + 0.0826 \cdot 0.504(53 - 20)$$
$$+ 0.0826(1 - 0.0826)0.18(80–53) = 99.8 \text{ kW}$$

The heat transfer area per unit time can be calculated as

$$F = \frac{6(G_m - W_w)}{\rho_s\, d_p} = \frac{6(0.0826 - 0.497 \cdot 0.0826)}{600 \cdot 2 \cdot 10^{-5}} = 2.08 \text{ m}^2/\text{s}$$

Hence, the drying time is

$$t = \frac{Q}{h\,F\,\Delta T_e} = \frac{97580}{2850 \cdot 2.08 \cdot 70.2} = 0.235 \text{ s}$$

where the temperature difference is calculated as a logarithmic mean temperature from the inlet and outlet temperatures of air and material in a concurrent flow

$$\Delta T_e = \frac{(T_{g,i} - T_{m,i}) - (T_{g,f} - T_{m,f})}{\ln\dfrac{T_{g,i} - T_{m,i}}{T_{g,f} - T_{m,f}}}$$
$$= \frac{(250 - 20) - (90 - 80)}{\ln\dfrac{250 - 20}{90 - 80}} = 70.2°\text{C}$$

Thus, the minimum length of the cylindrical drying chamber is

$$L_{ch} = u_g t = 0.5 \cdot 0.235 = 0.12 \text{ m}$$

Considering 110°C as the lowest possible inlet air temperature, a similar sequence of calculations gives $L_{ch} = 1.1$ m. Thus, the total dryer length (excluding the confusor) should equal 2.74 m.

The minimum heater duty is calculated from the enthalpy of air stream assuming 10% of heat losses:

$$Q_h = V_g \rho_g (I_{g,i} - I_{g,0}) \phi = 0.458 \cdot 1.2(290 - 48)1.1 = 142 \text{ kW}$$

11

Vacu Jet Drying System

One of the major problems with classical vacuum drying is the relatively long retention time required, which sometimes may be as long as 100 hours. Since thermal degradation is a time-temperature-related process that doubles for every 10°C increment, a long residence time may result in product deterioration, even at low processing temperatures. The Vacu Jet Drying (VJD) system designed for continuous processing of liquid materials at relatively high temperatures with a short residence time appears to be advantageous over the vacuum-tray, vacuum-drum, or freeze dryers. The system uses indirect heating of the liquid feed, sudden adiabatic expansion, and vacuum drying with mixing in series to evaporate solvents from the liquid feed and get a powdery product.

The Vacu Jet Drying system (known in Japan as the Crux Vacuum Drying System) represents a continuous, closed, single-stage vacuum drying process. It appears to be suitable for drying pumpable feeds and sludges that are composed of nonvolatile components or solid, and water and/or organic solvents. The system is particularly suitable for materials, which are difficult to dry in a single step. It has proven to be versatile for such applications as the production of ultrafine particles with minimal secondary agglomeration

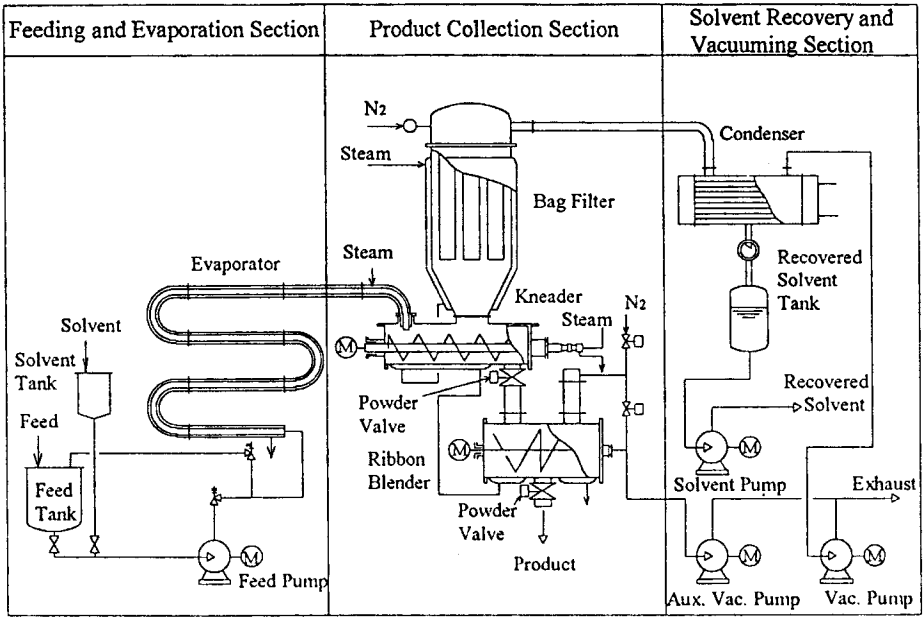

FIGURE 11.1 Schematic of the Vacu Jet Drying system for tarlike materials. (Reprinted with permission of Hosokawa Micron Corporation, Japan.)

and for the direct drying of polymers and other substances in solvent solutions with solvent recovery (Maekawa, 1994a).

Figure 11.1 presents the basic configuration of the VJD system used to dry tarlike residues and polymer solutions. Other possible configurations, shown schematically in Figure 11.2, differ in the method of vaporized solvent-dry material separation, which depends greatly on the physical properties of the solid and vapor phases. Independently of the particular configuration, each system consists of three integral sections. The function of the first section is material feeding and moisture evaporation. The second section operated under vacuum performs drying and product blending as well as fines collection and product discharge. The third section generates vacuum and accomplishes solvent recovery.

An integral part of the system is a Vacu Jet Dryer—a serpentine tube-type evaporator, which is typically 8 to 80 m long with a diameter of 8 to 50 millimeters. The inlet of the evaporator is connected to the feeding system, which supplies the liquid material diluted with a solvent if necessary. In the

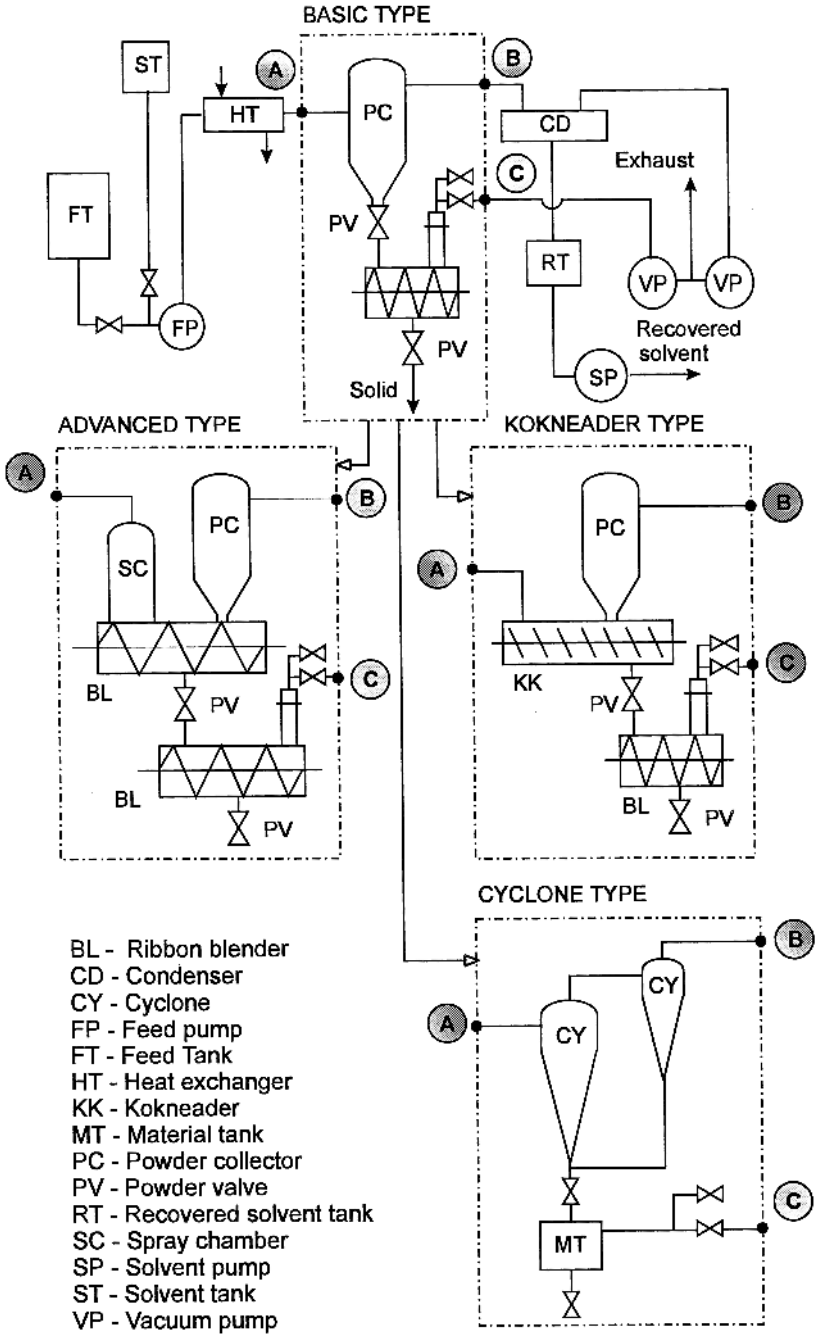

FIGURE 11.2 Typical configurations of the Vacu Jet Drying System. (Reprinted with permission of Hosokawa Micron Corporation, Japan.)

kneader-type configuration, the outlet of the evaporator is connected to the double-screw kneader fitted with a heating jacket where porous and/or rigid products are crushed before being discharged to the jacketed ribbon blender. The kneader and the ribbon blender form a postdrying stage where the residual solvent is removed from the product. The auxiliary vacuum pump and powder valves installed at the kneader and blender outlets allow intermittent product discharge without leakage. Prior to condensing in the solvent recovery section, the evaporated solvent passes through a bag filter of special design for complete recovery of fines. Since only two points of the VJD system (product discharge and exhaust from the vacuum pump) are open to atmosphere, the system is pollution-free as the efficiency of solvent and solids collection reaches 99.99% (Anon., 1994b).

The majority of liquid heating and solvent evaporation takes place inside the evaporator, which is heated indirectly by steam or hot oil. Typically, the wall temperature is kept 20 to 30°C higher than the solvent boiling point. A significant portion of the remaining solvent is evaporated when the material expands adiabatically in the product collection section, which is held under reduced pressure.

The liquid feed diluted (if necessary) with an additional amount of solvent is metered by a feed pump into the evaporator where the solvent starts to evaporate after a short heating period. Because of vapor generation, the volume of the feed expands, which causes a rapid increase in the velocity of the liquid–vapor mixture (Figure 11.3a). As vaporization progresses along the evaporator, the flow pattern evolves from an initial bubble flow through a plug flow, a turbulent flow, a ring flow, to a spray flow in most cases (Figure 11.3b). Finally, the slightly superheated vapor–liquid mixture is discharged from the evaporator to the product collection section (kneader, bag filter, spray chamber, or cyclone depending on the system configuration) at the velocity ranging from 100 m/s to the near-sound velocity. Such conditions, superposed with a reduced pressure in the product collection section, result in a rapid evaporation of the liquid spray, thus producing a finely dispersed material. Figure 11.4 presents a particle-size distribution of titanium oxide before and after drying in the VJD system. Solid particles in the 25% w/w water slurry had a mean diameter of 1.19 μm with a maximum diameter of 10 μm. After drying the mean diameter was reduced to 0.41 μm and no particle was larger than 1 μm.

A powdery product is obtained in cases where solid particles in a slurry feed do not dissolve even at the solvent boiling point. In the case of viscous liquids, which contain only a small amount of the solvent and therefore do

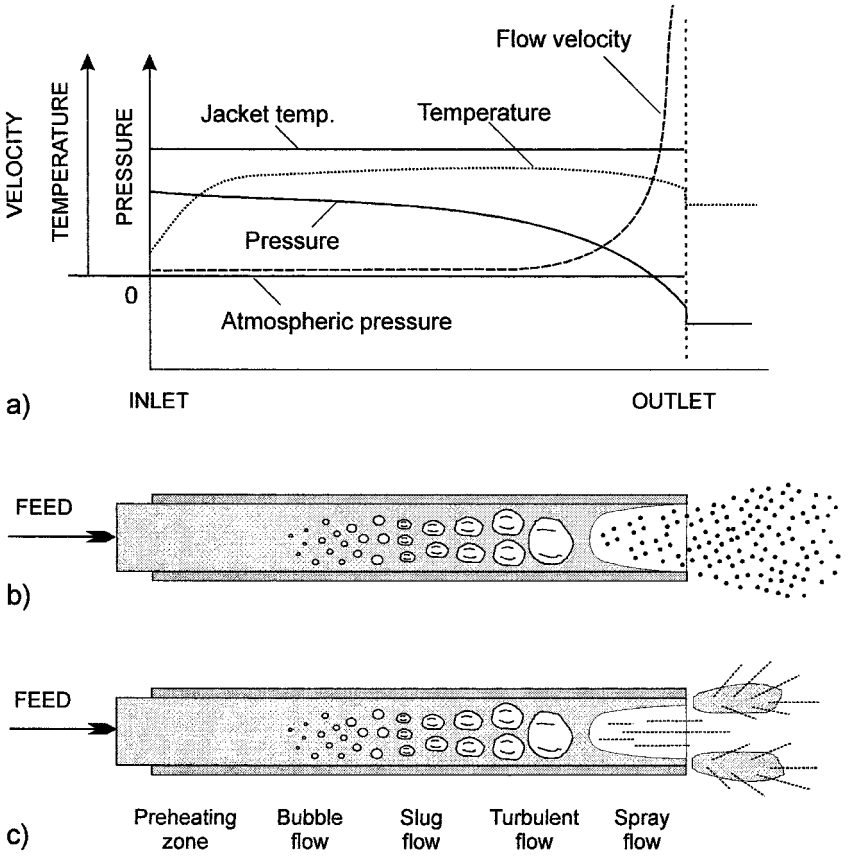

FIGURE 11.3 Flow characteristics in the Vacu Jet Dryer: a) distribution of temperature, pressure, and flow velocity along the evaporator; b) ''spray'' flow mechanism; c) ''pocket'' flow mechanism. (Reprinted with permission of Hosokawa Micron Corporation, Japan.)

not vaporize so intensely, the liquid feed is forced to the exit of the evaporator by the feeding pump and vaporized solvent. Here, the ''pockets'' of superheated liquid evaporate rapidly (''explode'') as a result of an abrupt pressure drop (Figure 11.3c). At the same time, the product temperature decreases due to the Joule–Thompson effect and latent heat of vaporization. Such drying

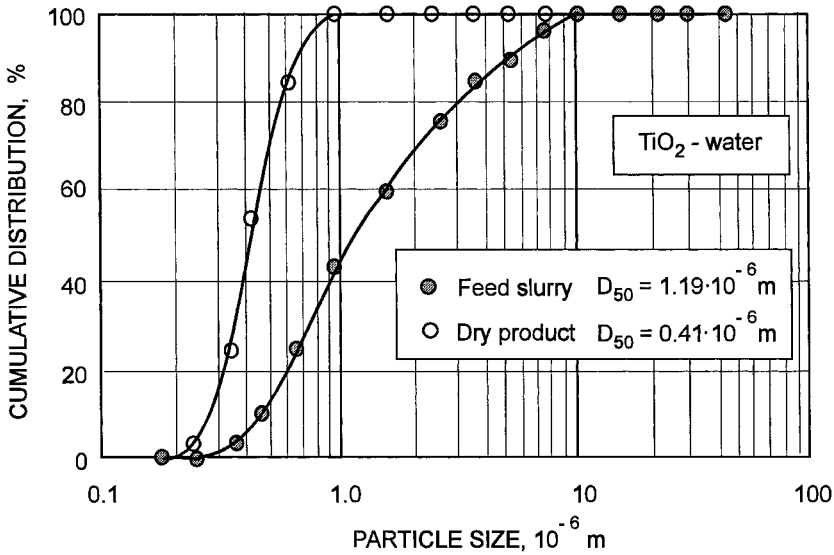

FIGURE 11.4 Particle-size distribution for titanium dioxide dried in the Vacuu Jet Drying system. (Reprinted with permission of Hosokawa Micron Corporation, Japan.)

conditions allow producing highly porous or submicron powders depending on the feed characteristics.

It should be noted that the vapor–liquid mixture flowing through the last part of the evaporator as well as the residual vapor in the kneader and the blender are superheated. This accelerates removal of the solvent as superheated steam has preferential thermal properties (see Chapter 7). In addition, the high velocity of the liquid–vapor mixture in the tube results in self-cleaning that prevents fouling of the inner wall of the evaporator. The high liquid–vapor velocity in the evaporator compensates its length so the residence time of the feed in the Vacu Jet Dryer varies from one to several minutes for small systems and from several to 20 minutes for larger ones. The distribution of this time is also small due to piston-flow of the feed. Therefore, thermal degradation of the product dried at 120°C in the VJD is lower than during conventional processing at 80°C for 6 hours.

One of the preferable applications of the Vacu Jet Drying system is the separation of solids from solvent slurry or solution with simultaneous recovery

of solvent for recycling. In conventional methods such as hybrid drying technologies that involve mechanical separation followed by thermal drying (see Chapter 29), the filter cake is filled with residual solvent. Since organic solvents are usually flammable, the selection of a dryer is troublesome for safety reasons and the recovery of organic solvent is difficult. Additionally, a pulverizing process for the dried solid is required because of caking of the product, which occurs during drying. In the case of solutions or diluted slurries, a spray dryer could be used but it incurs high operation costs resulting from a special design and low solvent recovery ratio. Similarly, a rotary vacuum dryer has a relatively low productivity due to the long processing time and the need for postprocessing pulverization. In comparison with the above-mentioned methods, the Vacu Jet Drying system provides the following merits (Maekawa, 1994a):

Hazardous solvents are claimed to be safely removed with superior recovery.

In most cases, the final product is a fine or very fine powder and thus does not need subsequent pulverizing or milling.

The solids are continuously dried from the slurry or solution in a single process.

The system is remarkably smaller as compared with the spray dryer, which translates into lower capital, installed, and maintenance costs.

According to Maekawa (1994b), the materials that are generally easily processed are slurries in which an organic solvent (or water) contains insoluble solids even at the boiling point. Solid components of ceramics, organic/inorganic materials, metal powders, etc., can be listed as examples. Organic and thermoplastic resins and similar materials that are dissolved in organic solvents may be processed under certain conditions. The products obtained from such a solution would be in the form of powder, porous solid matter, or paste so the proper configuration of the system as shown in Figure 11.2 is required. In general, it is difficult to obtain a powder or porous solid matter if the softening point of the solid component is not 50°C higher than the boiling point of the solvent, but sometimes a form of paste can be obtained. If the paste can be easily solidified by cooling, the kneader-type system is recommended to continuously extract the solidified lumps. Alternatively, the paste can be pumped out of the system and solidified separately in a flaker, for example. Aqueous solutions and water slurry of inorganic/organic materials are not recommended unless the desired product quality cannot be obtained in other ways due to strong coagulation of fine particles, etc. These are, for example, salts

TABLE 11.1 Typical Operating Parameters of the VJD System for Drying Applications

Product	Solvent (boiling point)	Feed	Temperature in evaporator	Solvent content	
				Feed	Product
Organic chemicals[a]	Hexane + water 69°C, 100°C	Slurry	140°C	80%	1%
Agricultural materials[b]	Benzene + water 80.1°C, 100°C	Slurry	130°C	62%	0.5%
Polymer intermediates[c]	Various solvents 160°C	Solution	200°C	60%	0.5%
Dye intermediates[d]	Benzene 80.1°C	Jelly	135°C	70%	0.2%
Dyes[e]	Aniline 184.7°C	Viscous tar	210°C	55%	1%
Organic pigments[f]	Trichlorobenzene 212.8°C	Slurry	210°C	70%	2%
Dyes[g]	Water 100°C	Slurry	158°C	85%	1%

[a] Impossible to dry by any other method.
[b] Instant drying including water of crystallization is possible. Improved quality.
[c] Significant decrease in utilities as compared with conventional steam distillation.
[d] Better solvent recovery ratio.
[e] Remarkable rationalization of the process. No pollution.
[f] Same as above.
[g] Simplified process.
Source: Reprinted with permission of Hosokawa Micron Corporation, Japan. (From Anon., 1995a.)

of organic acids, solutions of thermosetting resin, and emulsions of polymer, rubber, and similar materials.

Typical operating parameters of the Vacu Jet Dryer for representative materials are given in Table 11.1. More information about industrial applications of the VJD system can be found elsewhere (Maekawa, 1994a).

12

Contact–Sorption Drying

12.1 GENERAL CHARACTERISTICS

Contact–sorption drying integrates two drying techniques: (a) classical contact drying, where the moisture is evaporated using heat conducted from a heated solid surface; and (b) sorption drying (also termed ''desiccant drying'' or ''adsorption drying''), where moisture transfer is driven by a mass concentration gradient between the material being dried and the adsorbent material it is contacted with.

A very general scheme of contact–sorption drying comprises mixing a solid sorbent with the material being dried followed by separation of these two media once the desired mass transfer has taken place. The solid sorbent is then regenerated and returned to the process. Clearly, the technical justification for the contact–sorption drying depends on whether the sorbent can be easily regenerated and recycled.

The sorbent may be passive (inert) or active depending on whether it is used only for moisture removal and then separated from the dried material or it becomes an integral part of the dry product. Typical inert sorbents are molecular sieves, zeolite, chabazite, activated carbon, bentonite, or silica gel.

The group of active sorbents comprises starch, peat, bran, straw, cellulose, wheat bran, corn meal, potato starch, sugar beet pulp, fruits and oil plants, cut green parts of plants such as hay, and many others. Often the already dry product is regarded as an active sorbent since it can be mixed with the wet feed prior to drying. An example of such a process is simultaneous drying and granulation of biomaterials in a fluidized bed (Dencs and Ormos, 1989). The alternative term for active sorbent is a ''carrier'' or a ''filler'' as the materials being dried are usually solutions or suspensions that are either spread over the surface of inert particles or absorbed within the porous structure of the solid material (Kudra and Strumillo, 1998; Tutova and Kuts, 1987).

In contrast with drying on inert sorbents, which has found application in drying leather and agricultural products (Piper and Alimpic, 1993; Lapczynska and Zaremba, 1988; Kudra and Mujumdar, 1996; Ciborowski and Kopec, 1979; Anon., 1980; Ghate and Chhinnan, 1983; Alikhani, 1990; Sotocinal et. al., 1997), contact–sorption drying on active sorbents has been proven to be especially suitable for drying biomaterials and products of biosynthesis as it turns the process of drying of liquid droplets into drying of capillary-porous materials wetted with the same liquid. This makes it possible to take certain advantages of convective drying of solids such as drying at the wet bulb temperature. In such a case, it is possible to maintain biological activity of heat-sensitive products at a much higher level than with most other drying techniques (Kudra and Strumillo, 1998; Tutova and Kuts, 1987; Adamiec et al., 1990; Pan et al., 1994; Pan et al., 1995). Also, the end product can be a ready-to-use mixture of a sorbent-carrier with other additives such as vitamins, antibiotics, amino acids, flavor enhancers, pesticides, bacteria concentrates, etc. This eliminates otherwise necessary downstream operations as grinding, sieving, or blending. Because the majority of applied research was done using a sorbent carrier, the commonly used term ''contact–sorption drying'' is synonymous with drying on active sorbents.

A typical fermentation culture is an aqueous mixture of microorganisms or biopolymers, unreacted residues of nutrients, byproducts, process-controlling additives, and other components, with solid content amounting to only several percent. Thus, the solid sorbent used in contact–sorption drying performs two basic functions:

It absorbs a great fraction of moisture from the highly diluted suspension of biomaterials subject to drying. This alters the heat and mass transfer characteristics as the moisture is to be evaporated from a capillary-porous solid instead of from a liquid spray.

It changes the physical structure of the material fed to the dryer from a diluted suspension to the multicomponent mixture of a particulate material.

Although both functions are inseparable, the first one dominates when the suspension to be dried is contacted with the solid sorbent simultaneously with the process of moisture sorption and partial evaporation. A typical example is drying the fermentation broth that is sprayed onto a fluidized bed of the sorbent particles or atomized within the spray cone of a dispersed sorbent as it is in the spray dryer with a solid–liquid feed. The second function of the sorbent-filler plays the key role when the suspension and the sorbent get into contact prior to the drying in a separate device installed outside the drying chamber. This is the case of drying a preformed feed in a rotary, band, tunnel, and compartment dryer as well as in a classical fluid-bed dryer which accept particulate materials of high moisture content. Mixing of the suspension to be dried with a sorbent-filler in the mixer with subsequent granulation that precedes drying is an example of such a variant of the contact–sorption drying (Kudra and Strumillo, 1998; Tutova and Kuts, 1987).

12.2 MECHANISM OF CONTACT–SORPTION DRYING

The mechanism of contact–sorption drying is very complex because moisture transfer takes place in heterogeneous and multicomponent systems and is accompanied by thermal effects. The idealized scheme of contact–sorption drying shown in Figure 12.1 reflects phenomena taking place in a dynamic system (e.g., mixing or fluidization), where interaction between the sorbent–material, material–material, and sorbent–sorbent is likely to occur.

When the wet material is brought into contact with a capillary-porous dry sorbent, the surface layer of the sorbent starts to adsorb liquid moisture by ordinary capillary flow so the rate of mass transfer depends greatly on the contact area. Because the amount of liquid moisture at the material surface decreases gradually, the suction potential at the material surface equals, at a certain point, the suction potential at the sorbent surface. This stops the moisture transfer through the interface between both media. However, the concentration gradient that developed in the sorbent and material particles causes moisture from the surface to diffuse throughout the sorbent volume as well as the moisture from the material core to migrate to the contact surface. When contact time is sufficiently long, equilibrium between moisture content in the

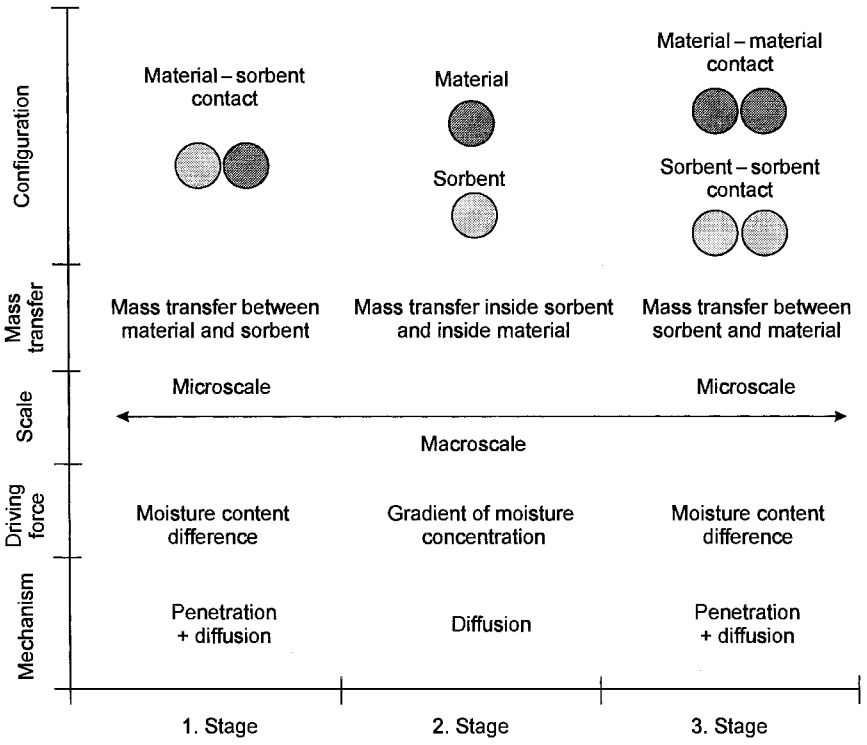

FIGURE 12.1 General mechanism of contact–sorption drying in a dynamic particulate system.

sorbent and the material particle can be expected. Because at this moment the mass exchange is maximal, the sorbent could be separated and regenerated while the material being dried could be contacted again with a dry (or regenerated) sorbent for deeper drying. In practice, the contact time is much shorter than that required to attain equilibrium conditions so diffusion of moisture proceeds when sorbent and material particles are no longer in contact. In case of random motion that is characteristic of fluid beds, vibrated fluid beds, or spouted beds, there is a possibility of sorbent–sorbent and material–material contact, which may lead to further moisture transfer at the microscopic level. Then the sorbent particle can again contact temporarily more wet material and, as the process continues, a dynamic equilibrium between the material

being dried and the wet–dry sorbent mixture is attained at the lower level as the previous one.

Though contact–sorption drying was a subject of numerous studies, mostly in Russia, the mechanism of the process and the respective mathematical models are not well established. According to Tutova (1988), mass transfer during contact–sorption drying is determined by a dynamic nature of the sorption process. Therefore, to analyze the process of mass transfer she proposed a model configuration in which a semi-infinite plate of a bone dry sorbent is suddenly contacted with a semi-infinite slab of the wet material of uniform moisture distribution. Prior to physical contact, the initial moisture concentration in the material being dried (material moisture content) is C_i^m, and initial concentration of moisture in dry sorbent is $C_i^s = 0$. At the contact time ($t = 0$), moisture from the material surface is assumed to be transferred instantly to the sorbent surface. Thus, the sorption front with the moisture content being in equilibrium with the material moisture content is established at the sorbent surface. At the same instant, moisture from the sorbent surface begins to diffuse into the sorbent core. Assuming definite velocity of a progressing sorption front u, the time needed for the sorption front to travel a distance x is given by

$$t^d = \frac{x}{u} \tag{12.1}$$

and it quantifies the time delay (relaxation time) after which the process of moisture sorption starts at the kth layer of a sorbent located at the distance x. The net time of sorption (t_k) in a kth layer is then equal to

$$t_k = t - t_k^d = t - \frac{x_k}{u} \tag{12.2}$$

Because of time delay, a certain moisture concentration profile is established in the sorbent volume. In due time, the moisture concentration at any point of a sorbent attains the equilibrium value C_f^s that is considered as the final moisture content of the sorbent.

Accounting for the time-delay effect, the equation for moisture concentration in the sorbent can be written as

$$C^s(t, x) = HC^m(t - t_k, x) \qquad \text{for} \quad t \geq t_k \tag{12.3}$$

and

$$C^s = 0 \qquad \text{for} \quad t < t_k \tag{12.4}$$

where H is the Henry's constant $H = C_f^s/C_i^m$. The function $C^m(t - t_k, x)$ can be expanded into a Taylor series with the argument t:

$$C^m(t - t_k, x) = C(t, x) - \left(\frac{\partial C^m}{\partial t}\right)_{t=0} t + \ldots \tag{12.5}$$

Then, at $t_k = 0$

$$\frac{dC^s}{dt} = H\frac{dC^m}{dt} \tag{12.6}$$

and

$$\frac{dC^s}{dt} = \frac{1}{t_k}(HC^m - C^s) \tag{12.7}$$

When the delay time is very short ($t \gg t_k$), the general equation simplifies to the ordinary equation of a sorption kinetics

$$C^s(t, x) = HC^m(t, x) \tag{12.8}$$

Analyzing the above mathematical model for the dynamics of the contact–sorption drying, one can conclude that:

An increase in the velocity of a sorption front and a decrease in the delay time accelerate moisture transfer rate.

Larger contact areas create favorable conditions for adsorption rather than for much slower sorption, which is limited by diffusion in the sorbent volume.

Because of opposite processes of mass transfer in the sorbent and the material being dried, the maximum transfer rate can be attained at optimum contact time.

Figure 12.2 illustrates the variation of a reduced drying efficiency with time, and the variation of a dimensionless sorption capacity with time in contact–sorption freeze-drying of water-saturated ceramics by a granulated zeolite type CaA (Tutova, 1988). The reduced drying efficiency η is defined here as the ratio of the moisture content drop during freeze-drying with the assistance of a sorbent to that in pure freeze-drying taken as a reference process:

$$\eta = \frac{\Delta X}{\Delta X_0} \tag{12.9}$$

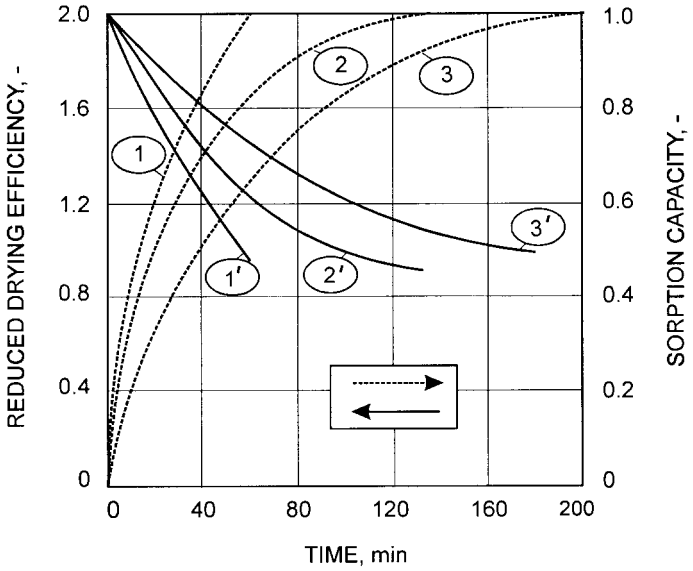

FIGURE 12.2 Drying and sorption curves for contact–sorption freeze-drying for different thicknesses of the zeolite layer: 1, 1′—10 mm; 2, 2′—20 mm; 3, 3′—30 mm.

while the dimensionless sorption capacity a^* relates the current sorption capacity of the sorbent to its initial sorption capacity:

$$a^* = \frac{a}{a_i} \tag{12.10}$$

It is clear that the efficiency of contact–sorption drying attains its maximum at the moment of contact with solid sorbent and drops with time reaching $\eta = 1$ when the sorption capacity approaches zero. Because the sorption capacity is maximum at the beginning of the process when the sorbent is dry, and reduces dramatically when the sorbent is close to saturation, it is reasonable to interrupt the contact of the material with the sorbent after a certain time. Based on numerous experiments the following relationship was proposed for determination of the optimum contact time (Tutova, 1988; Tutova and Kuts, 1987):

$$t_c = (0.3 - 0.5)t_s \tag{12.11}$$

where t_s is the time for sorbent saturation according to the kinetic sorption curve.

Once the contact time is chosen, the partially saturated sorbent may be removed and replaced with the new charge of a dry sorbent; renewal of the sorbent can then increase the rate of contact–sorption drying even by several-fold (Tutova and Kuts, 1987). Having the contact time established, the rate of sorbent renewal can be expressed by the number of renewals per batch (run) and determined from the ratio of the total amount of moisture to be removed to the amount of moisture absorbed during a contact time:

$$n = \frac{m_{H_2O}}{m_{H_2O,t_c}} \tag{12.12}$$

In practice, renewal of the partially wet sorbent can be accomplished either by complete separation of the sorbent from the material being dried, by a counterflow of sorbent–material layers, or by continuous replacement of a fraction of the sorbent as it is in contact–sorption drying in a fluidized bed. These methods are briefly described in Section 12.4 of this chapter. Details of various technologies can be found elsewhere (Kudra and Strumillo, 1998; Tutova and Kuts, 1987; Tutova, 1988).

Another approach to mathematical modeling of contact–sorption drying that was used to simulate drying of corn by mixing with zeolite particles (Alighani, 1990) is based on the following simplified system of Luikov's differential equations for heat and mass transfer (Luikov, 1966; Luikov and Mikhailov, 1961):

$$\frac{\partial C}{\partial t} = D\nabla^2 C + \alpha\delta\nabla^2 T \tag{12.13}$$

$$\frac{\partial T}{\partial t} = \alpha\nabla^2 T + \frac{\varepsilon\Delta H}{c}\frac{\partial C}{\partial T} \tag{12.14}$$

Considering grain as a spherical particle surrounded by a layer of powdery sorbent (Figure 12.3) and neglecting the second term in Eq. (12.13) as insignificant, Eqs. (12.13) and (12.14) turn into the following set of particular equations for corn and sorbent, respectively:

$$\frac{\partial C_C}{\partial t} = D_C\left(\frac{2}{R}\frac{\partial C_C}{\partial R} + \frac{\partial^2 C_C}{\partial R^2}\right) \tag{12.15}$$

$$\frac{\partial T_C}{\partial t} = \alpha_C\left(\frac{2}{R}\frac{\partial T_C}{\partial R} + \frac{\partial^2 T_C}{\partial R^2}\right) + \frac{0.5\Delta H_C}{c_C}\frac{\partial C_C}{\partial t} \tag{12.16}$$

for $t > 0$ and $0 \le R \le R_1$, and

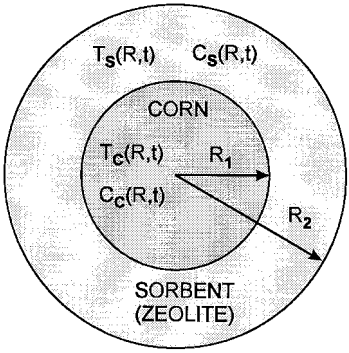

FIGURE 12.3 Nomenclature for the mathematical model of contact–sorption drying.

$$\frac{\partial C_S}{\partial t} = D_S\left(\frac{2}{R}\frac{\partial C_S}{\partial R} + \frac{\partial^2 C_S}{\partial R^2}\right) \tag{12.17}$$

$$\frac{\partial T_S}{\partial t} = \alpha_S\left(\frac{2}{R}\frac{\partial T_S}{\partial R} + \frac{\partial^2 T_S}{\partial R^2}\right) + \frac{1.0\Delta H_S}{c_S}\frac{\partial C_S}{\partial t} \tag{12.18}$$

for $t > 0$ and $R_1 \leq R \leq R_2$.

The parameter R in Eqs. (12.15) through (12.18) is the radial coordinate, ΔH is the heat of sorption, and the subscripts C and S refer to corn and sorbent, respectively. The values of the phase change coefficient were assumed a priori to be 0.5 for corn and 1.0 for the zeolite, and these were then confirmed during process simulation (Alighani, 1990).

The initial conditions at $t = 0$ for the system shown in Figure 12.3 are as follows:

$$C_C = C_{Ci} \quad \text{and} \quad T_C = T_{Ci} \quad \text{for} \quad 0 \leq R \leq R_1 \tag{12.19a}$$

$$C_S = C_{Si} \quad \text{and} \quad T_S = T_{Si} \quad \text{for} \quad R_1 \leq R \leq R_2 \tag{12.19b}$$

The boundary conditions for an adiabatic process are defined by the following equations:

$$R = 0 \qquad \frac{\partial C_C}{\partial R} = 0 \qquad \frac{\partial T_C}{\partial R} = 0 \tag{12.20a}$$

$$R = R_2 \qquad \frac{\partial C_S}{\partial R} = 0 \qquad \frac{\partial T_S}{\partial R} = 0 \tag{12.20b}$$

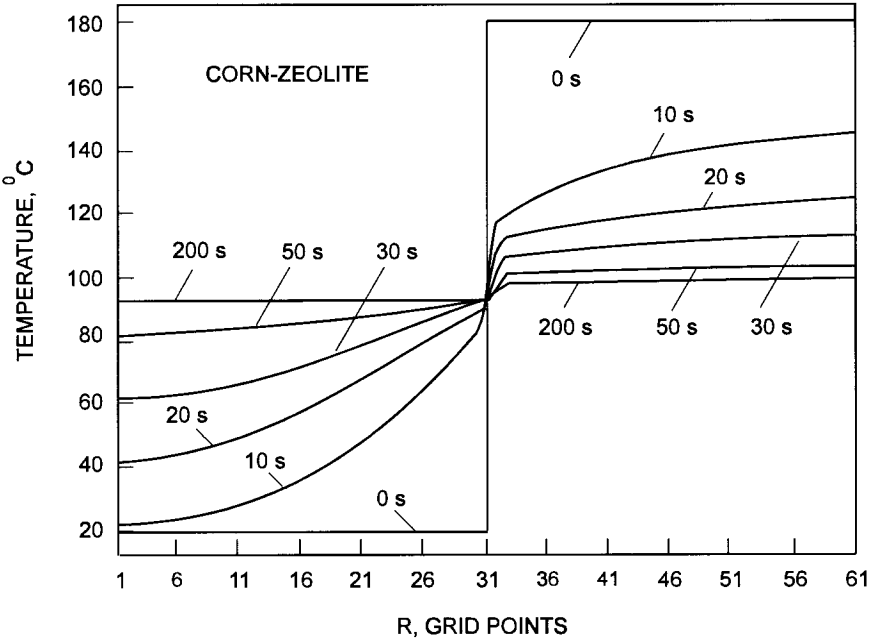

FIGURE 12.4 Temperature profile in the corn–zeolite mixture. (From Alighani, 1990.)

$$R = R_1 \qquad C_C = C_S \qquad -k_C \frac{\partial T_C}{\partial R} = h(T_C - T_S) \tag{12.20c}$$

where h is the heat transfer coefficient between a granular material and a particulate sorbent.

Equations (12.15) through (12.18) together with the initial and boundary conditions were solved numerically using differential systems simulator DSS/2 and source code for the computer programs written in FORTRAN 77 (Alikhani, 1990). Figures 12.4 and 12.5 present typical variations in temperature and moisture content of a corn–zeolite mixture as a function of time and the spatial coordinate. Figure 12.6 shows the temporal variation of an experimentally determined average moisture content of corn kernels and the one calculated from the mathematical model. The relatively small difference between experimental and simulated data confirms the adequacy of the mathematical model for the contact–sorption drying of corn kernels. Details of the experi-

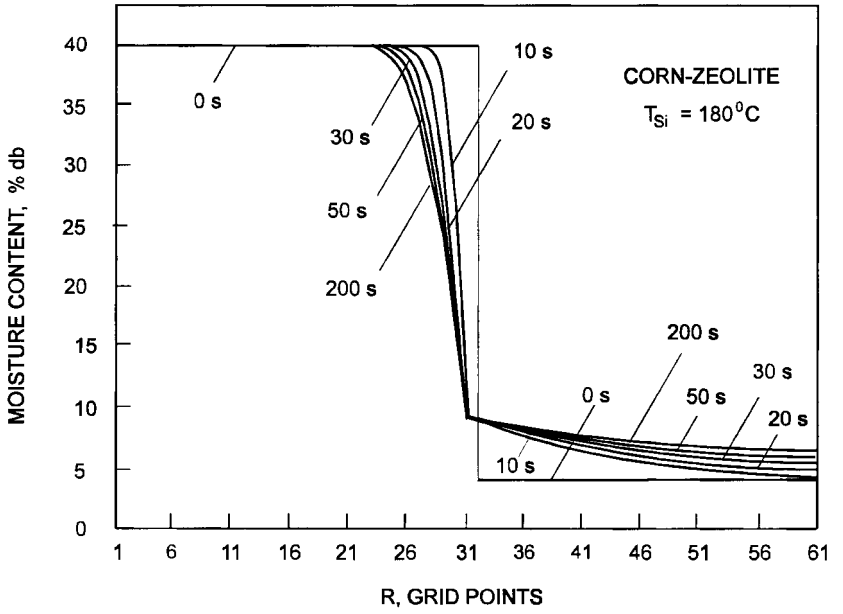

FIGURE 12.5 Moisture profile in the corn–zeolite mixture. (From Alighani, 1990.)

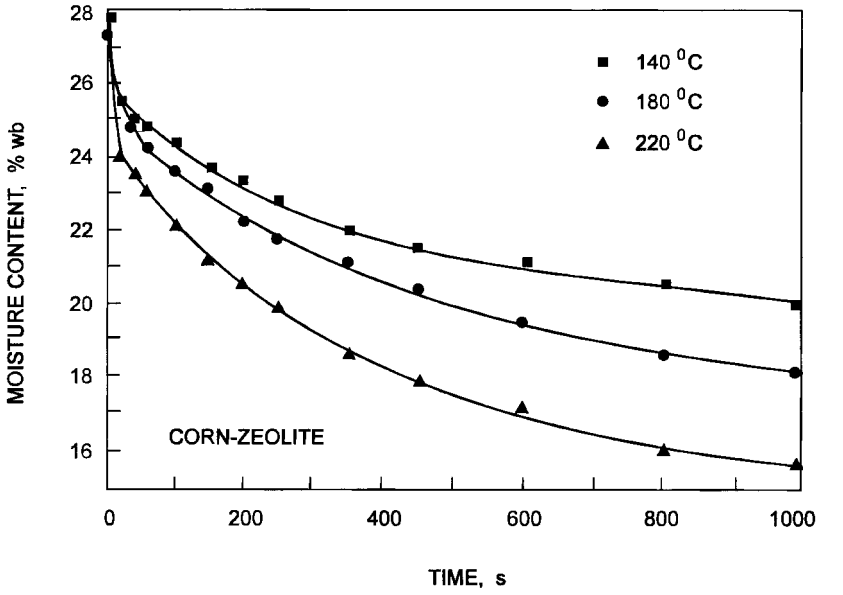

FIGURE 12.6 Temporal variation of an average corn moisture content. (From Alighani, 1990.)

ments, model solution, and validation can be found in the source literature (Alikhani, 1990; Alikhani and Raghavan, 1991; Alikhani et al., 1992).

12.3 CHARACTERISTICS OF SORBENTS/CARRIERS

When selecting a sorbent for contact–sorption drying, the following aspects should be taken into account:

- Type of dry product and its end-use
- Physical and biochemical affinity of the sorbent/carrier and the material being dried
- Sorption characteristics of the sorbent
- Commercial availability of the sorbent and economic aspects
- Possibility to perform upstream and downstream processes

Type of a dry product and its end-use is one of the main criteria for selection of a sorbent. Because of separation, the end-use of a product is usually not critical in contact–sorption drying on inert sorbents unless contamination of the product by traces of sorbent is undesirable, as in the case of products for human consumption. From the other side, the presence of residual sorbent in a product may even be an additional feature of contact–sorption drying. This is the case of drying grains for animal feed using natural zeolite where certain minerals or salt should otherwise be added. The main feature of contact–sorption drying on active sorbents is, however, an option of sorbent to be an integral part of the final product. Thus, the sorbent/carrier not only cannot pose any limitations in further use of the product but also should improve its quality, extend shelf-life, or broaden the range of application. For example, a dried product that is to be used as an additive to animal feed (e.g., vitamins, antibiotics, protein concentrates, etc.) should incorporate such a sorbent/carrier that not only is easily digestible by animals but also can enhance the taste and flavor of the end product. If dry product is to be used as an additive to fertilizers, then the properly prepared calcium or other industrial byproducts, which contain components that improve soil structure or composition such as peat, chaff, silicon, and magnesium compounds, are best as the sorbent/carrier. In the case of pesticides, such sorbents as kaolin, silicones, and activated carbon with aromatic compounds that have adhesive properties are recommended as they allow the pesticide to stick to the plant or compose the soil.

Physical or biochemical affinity of the sorbent/carrier to a material being dried means no negative effect of the sorbent on the product quality. For example, activated carbon, despite its high sorption activity, may not be used in dewatering of bacterial biomass as it kills microorganisms. The use of wheat flour or corn meal is also not recommended because these otherwise good sorbents are substrates for the growth of lactic acid bacteria and other microorganisms.

Sorption characteristics, which comprise sorption kinetics, sorption isotherms, and sorption capacity, determine the efficiency of contact–sorption drying and selection of the drying method and dryer design.

Figure 12.7 shows a set of isotherms for sorption of water vapor on the most frequently used sorbents. A variety of sorption isotherms, which frequently change the slope at certain moisture concentrations, complicate direct comparison of different sorbents. Specifically, an average sorption capacity over the entire range of moisture concentrations might not be representative of that over the narrow range of moisture concentrations to be used in a partic-

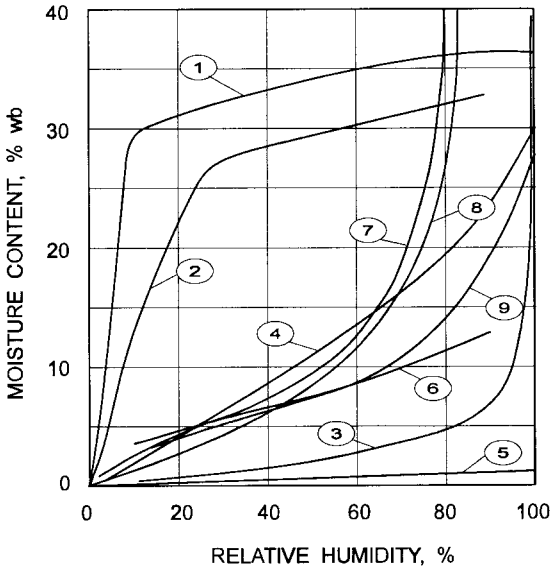

FIGURE 12.7 Sorption isotherms for selected sorbents: 1—zeolite CaA; 2—activated carbon; 3—peat; 4—sawdust; 5—kaolin; 6—potato starch; 7—silica gel; 8—wheat bran; 9—filter paper. (Adapted from Tutova, 1988.)

ular case. In order to evaluate the sorption capacity of various sorbents under comparable conditions, Tutova (1988) defined a property called the *relative sorption capacity*, which relates the specific sorption capacity of the sorbent to that of the reference material:

$$K = \frac{a}{a_r} = \frac{X}{X_r} = \frac{X}{0.01X_{r,\max}} \tag{12.21}$$

Because the specific sorption capacity is defined as the mass of water adsorbed by the unit mass of a sorbent at given relative air humidity, the relative sorption capacity can also be given in terms of the moisture content. A filter paper, which features constant sorption capacity over the whole range of air humidities, was taken as a reference material. Hence, the parameter X_r in Eq. (12.21) is replaced with $0.01X_{r,\max}$, where $X_{r,\max}$ is the maximum moisture content of the filter paper at 25°C. The constant 0.01 results from the definition of the mass transfer potential, where the specific sorption capacity of the reference material was assumed to be equal to 100 degrees of mass.

Figure 12.8 shows a variation in the relative sorption capacity of several sorbents with the relative humidity of the environment, which represents the contribution of the partial pressure of absorbed moisture (sorbate) in the sorbent–air system. Using absolute values of the relative sorption capacity and

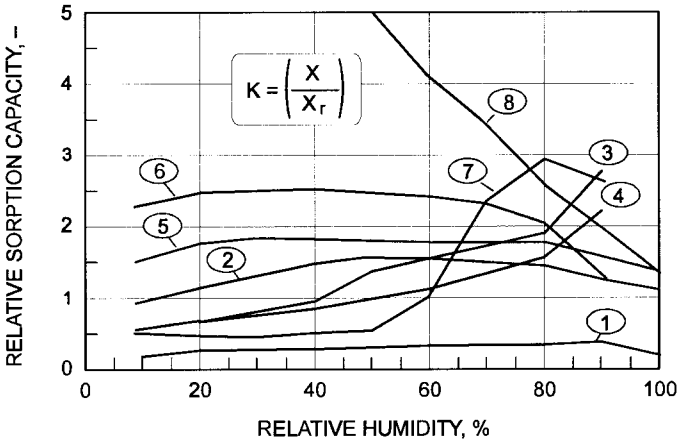

FIGURE 12.8 Relative sorption capacity for some sorbents: 1—peat; 2—sawdust; 3—wheat bran; 4—ground rapeseed; 5—potato starch; 6—silica gel; 7—activated carbon; 8—zeolite. (Calculated from data by Nikitina, 1968.)

comparing the shape of curves in Figure 12.8, it is possible to rank and further select the best sorbent for a specified application. Tutova (1988) proposed to regard materials with $K < 1.0$ as low-capacity sorbents in contrast to high-capacity sorbents for which $K > 3.0$. However, such classification is not explicit because only certain materials (e.g., kaolin or potato starch) exhibit no or little variation of the relative sorption capacity with sorbate concentration. Most sorbents are characterized by a significant change of the sorption capacity that may either fall (e.g., zeolite) or rise (e.g., silica gel) with relative humidity of the ambient. Therefore, it is advisable to categorize sorbents into low, moderate, and high capacity over specified ranges of sorbent concentration (Kudra and Strumillo, 1998). Thus, wheat bran, silica gel, and ground rapeseed could be categorized as the high-capacity sorbents for air humidity above 80% (Figure 12.8).

Obviously, the best option is to use a sorbent with maximum sorption capacity over the required range of moisture concentration unless other selection criteria prevail. Zeolites and activated carbon, for example, should be used in processes where a low water–vapor pressure exists such as freeze- and vacuum drying. Wheat bran or ground rapeseed are recommended for spray drying or drying in a fluidized bed as they are characterized by high sorption capacity at ambient air humidity ranging from 80% to 90%. The amount of sorbent to be used to extract a given mass of moisture can be calculated from the mass balance over the material–sorbent system being in equilibrium. The final moisture content of the sorbent necessary to solve the balance equation can be determined from sorption isotherms, as shown in Figure 12.9.

Commercial availability and cost of a sorbent/carrier have a basic practical importance, specifically for technologies with high mass yield. Sorbent should also be easily available irrespective of season. If it is produced seasonally, it should be possible to store it for a long time without special storage conditions. The cost of a sorbent/carrier is particularly important when drying materials of relatively low market value, such as animal blood, pulp and paper secondary sludge, or meat processing sludge.

Possibility to perform upstream and downstream processes is important when considering the operations accompanying contact–sorption drying such as screening, sterilization of sorbents, disintegration of agglomerates, cleaning of the exhaust air, packaging, transportation, and storage of the final product. In return, contact–sorption drying on active sorbents does not require certain operations such as homogenization and mixing because all components of the product may be integrated either before or during contact–sorption drying. Of prime importance are the upstream operations such as disintegration, screen-

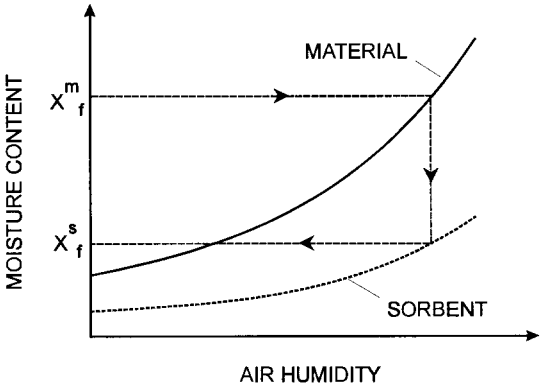

FIGURE 12.9 Determination of the final moisture content of the sorbent from sorption isotherms.

ing, and sterilization. It is important that during sterilization, the physical and structural-mechanical properties of sorbents should be preserved. For example, sterilization of flour or bran with hot air brings about a risk of self-ignition and explosion. In the case of many agricultural and food products it is not possible to carry out direct sterilization with superheated steam because this might change the material structure and reduce sorption capability. Therefore, a suitable method for sterilization of such materials is indirect heating of the sorbent (Tutova and Slizhuk, 1990). Cold sterilization or gamma-irradiation of sorbents as well as the addition of antibiotics may also be used where appropriate and permitted (Tutova and Kuts, 1987).

12.4 TECHNOLOGY OF CONTACT–SORPTION DRYING

12.4.1 Drying of Particulate Materials on Inert Sorbent

A continuous-process apparatus for drying of particulate materials by contact with sorbent particles is depicted schematically in Figure 12.10 (Raghavan and Pannu, 1986). Although originally developed for drying corn with sand as the heat transfer medium, it can be used also for contact–sorption drying as it integrates three operations in one unit: contact drying, sorption drying, and sorbent regeneration. The unit consists of three coaxially located conical

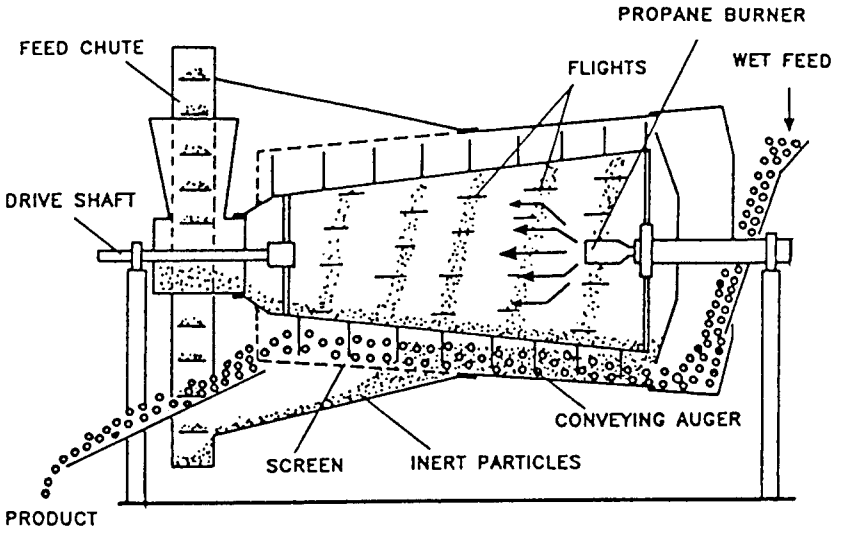

FIGURE 12.10 Continuous contact–sorption dryer for particulate materials.

chambers with a central heating chamber in the form of a conical drum supported axially by drive and stationary shafts. The stationary shaft is made as a hollow cylinder, thus permitting fuel feed to the burner situated on the longitudinal axis of the heating chamber. The gas burner, fed additionally by compressed air for complete combustion, generates a flame that extends into the heating chamber and directly evaporates water from the sorbent particles while they traverse the heating chamber. To accelerate heating and moisture evaporation, the sorbent particles are showered by scopelike flights staggered at the chamber wall.

Wet particulates fed into the dryer are mixed with hot sorbent particles discharged from the outlet end of the heating chamber and conveyed continuously by the auger disposed between the heating chamber and the outer conical drum. This auger is thus rotated with the heating chamber at 100 to 160 rpm, which causes the material–sorbent mixture to be thoroughly mixed and transported along the drying section. As the granular mixture is conveyed, the moisture is removed by contact–sorption drying, which is enhanced by evaporation due to sensible heat stored in the hot sorbent particles. The tail end of the outer drum is screened to permit the sorbent particles to pass through and to be collected in an annular cone-shaped collector. The end of the collector is

a peripheral annular chute equipped with buckets to transport the particles back to the feeding chute.

Although the residence times of the sorbent particles in the heating chamber are relatively short (in the order of 15 to 20 seconds), direct contact with a flame and flue gases allows for increase of particle temperature by approximately 100 to 200°C (Raghavan and Pannu, 1986; Sotocinal, 1998). This is sufficient not only to regenerate sorbent by moisture evaporation, but also to heat the sorbent to the required temperature. The sorbent renewal rate can be controlled by the sorbent-to-particulates mass ratio, which (aside from the geometry of the dryer) depends on the wet feed rate, mass of the sorbent in the system, and rotational speed of the dryer.

12.4.2 Drying in a Fluid Bed of Inert Sorbent

A novel technique for contact–sorption processing of large sheet-type solids such as textiles, leather, or veneer is drying in an *active fluidized bed* (Ciborowski and Kopec, 1979; Anon., 1980). In this technique, the material to be dried is immersed in a fluidized bed of highly hygroscopic particles, which extract moisture from the wet material and release it to the fluidizing air (Figure 12.11).

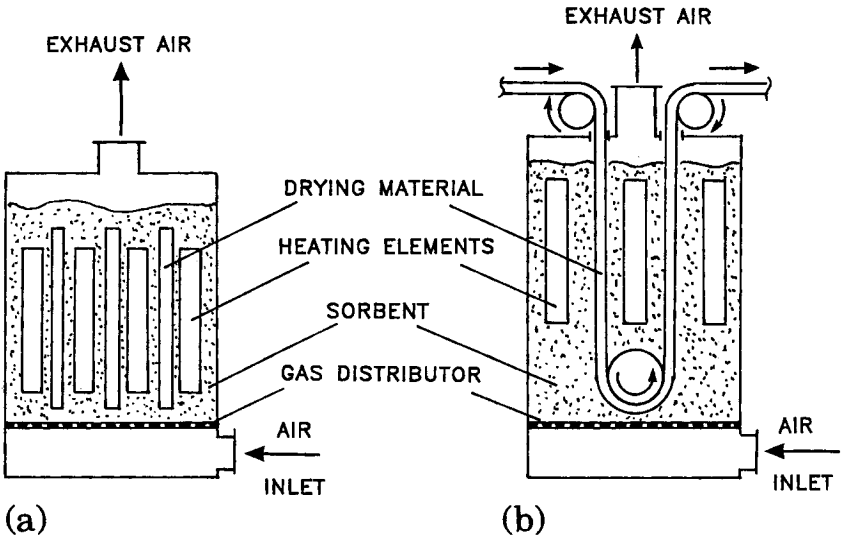

FIGURE 12.11 Contact–sorption drying in a fluid bed: (a) batch and (b) continuous.

In a continuous system, the band of drying material is transported in a serpentine fashion through the fluidized bed of sorbent particles. Heat required for moisture release from the sorbent to fluidizing air is supplied by immersed heaters. The use of fluidized beds of active particles enhances not only the convective but also material–sorbent, sorbent–sorbent, and sorbent–heater contact heat/mass transfer rates. Comparison of the fluid bed dryer with inert sorbent with the cylinder dryer is given in Table 12.1.

As compared to convective drying, the application of fluidized silica gel for drying 1.5- to 2.5-mm-thick cowhides from 60% to 20% at 60°C allows reduction of the drying time from 7 h to 15 to 20 min, reduction of the steam consumption by 30%, and lowering of the capital cost by a factor of three. The dryer is of modular type with up to 20 modules, which form a compact assembly 2.1 m long, 2.2 m wide, and 2.0 m high (Anon., 1980).

A fluidized bed of sorbent particles can also be used for drying-granulation of highly adhesive materials. Fine particles of a suitable sorbent are fluidized by hot air in the upper chamber of a two-stage dryer-granulator (Figure 12.12). Wet granules formed in a disk-type granulator are coated by the hot, pulverized sorbent as it falls through the fluid bed. Due to the high rates of contact heat and mass transfer, the surface layers of the granules are desiccated rapidly. The resulting porous (and thus permeable to vapor) dry coating facilitates further moisture diffusion and does not allow the lumps and granules to aggregate. Drying of the coated loose granules to the final moisture content is then carried out in a standard fluid bed, which is formed in the lower chamber of the dryer (Tutova et al., 1979; Tutova, 1988). The same principle of reducing surface moisture content by coating wet granules with dry powder recovered from an exhaust gas was applied in a fluid bed dryer for casein (Marchevski, 1998).

TABLE 12.1 Comparison of Fluid Bed Dryer with Inert Sorbent with Cylinder Dryer

Parameter	Fluid bed dryer	Cylinder dryer
Drying medium	Air	Steam
Temperature, °C	100	160
Drying time, min	10	37
Specific heat consumption, kJ/kg H_2O	4200	22,300
Path length, m	12	56

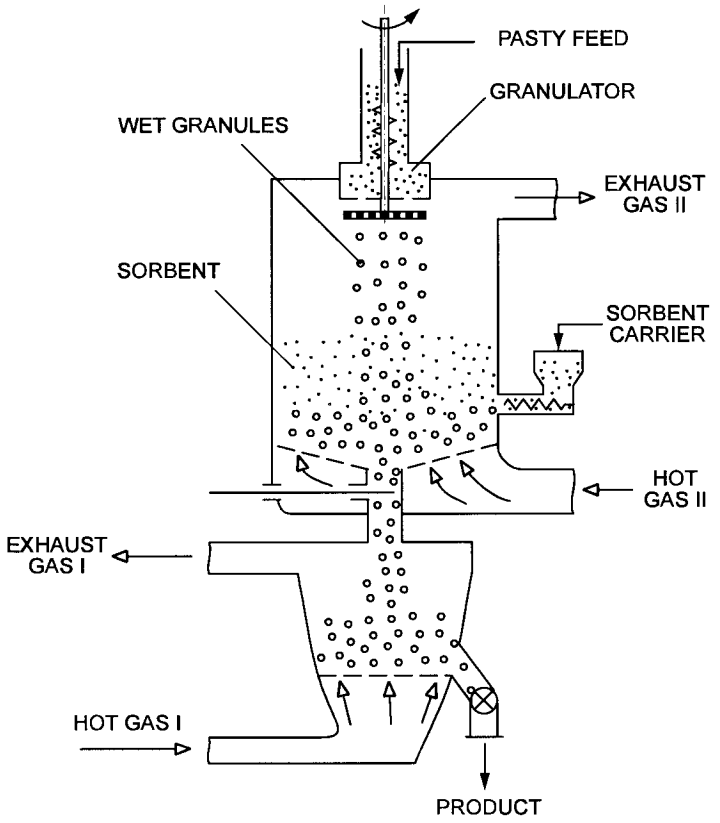

FIGURE 12.12 Contact–sorption fluid bed dryer for pasty materials. (From Tutova, 1988.)

12.4.3 Sorption Drying Using Filler Materials

With respect to the product, the solid sorbent can be neutral (placebo) or active. In the first case the sorbent is used only as a carrier for heat-sensitive and otherwise hard-to-dry materials. Typical examples here are liquid bioproducts such as antibiotics, enzymes, yeast, amino acids, etc., which when conventionally dried, can lose up to 70% of their biological activity. Sawdust, activated carbon, ground straw, or hay are typical solid carriers. After drying, the solid sorbent is either separated from the product or left as is for further utilization as is in the case of fodder antibiotics. Figure 12.13 shows the concurrent and

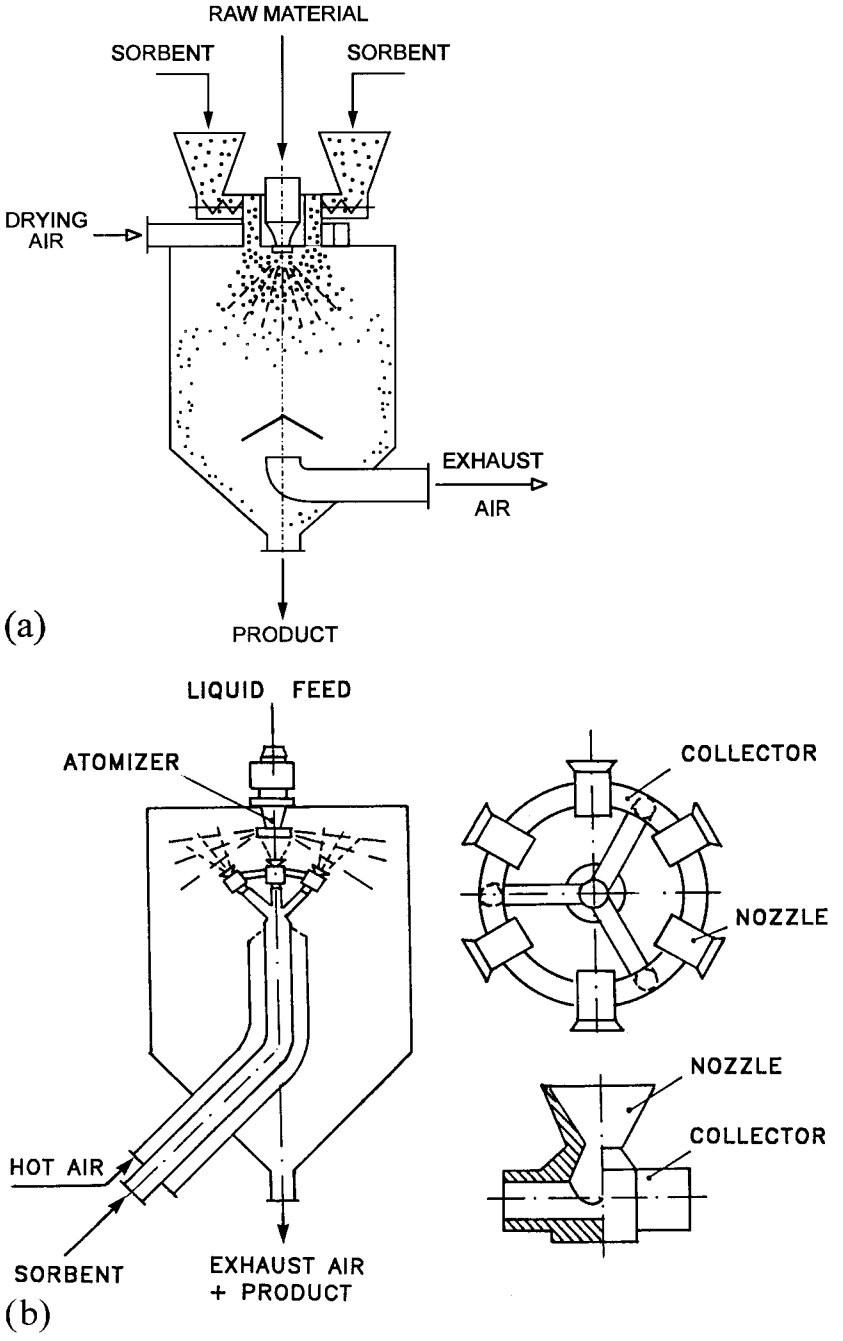

FIGURE 12.13 Contact–sorption spray drying: (a) concurrent and (b) countercurrent.

countercurrent modes of contacting solid carriers with liquid biomaterials in a spray dryer configuration (Tutova and Kuts, 1987).

An interesting option for contact–sorption drying is the use of a sorbent, which can be incorporated into the drying material, as an integral part of the final product. Wheat bran, starch, powdered skim milk, casein, peat, corn flour, etc., are reported to be good fillers for drying liquid bioproducts in fodder, fermentation, pharmaceutical, and similar industries (Adamiec et al., 1990; Tutova and Kuts, 1987; Tutova et al., 1979; Tutova et al., 1985). As applied to drying of lysine, for example, the use of wheat bran as active filler gives the following advantages:

- Reduces by two the relative hygroscopicity of the product and thus lowers three- to fourfold the rate of moisture sorption during storage
- Shifts the equilibrium humidity from 50% up to 70% in the temperature range from 20 to 50°C
- Eliminates otherwise necessary downstream operations such as mixing or tempering
- Stabilizes moisture evaporation during drying, which in fact takes place from a porous material instead of from a highly viscous droplet
- Eliminates product build-up on dryer walls
- Lowers material temperature during drying, thus preserving up to 98% of its biological activity in the liquid state

Figure 12.14 presents a schematic of the spray-drying system for contact–sorption drying of bacterial preparations, while the design of a three-stream nozzle used to disperse solid sorbent within the spray of these preparations is shown in Figure 12.15. Performance data of this nozzle are given in Table 12.2, and characteristics of contact–sorption drying for selected bacterial cultures are specified in Table 12.3.

An example of an industrial spray-drying system where the combined sorption–spray drying is applied for manufacturing of forage lysine-based concentrates is shown in Figure 12.16. As reported by Tutova and Kuts (1987), introduction of wheat bran directly into the spray cone of dispersed lysine (with the mass ratio of 0.7 to 1.0 kg of bran/kg of dry lysine) markedly improved the product quality. In particular, the following features were claimed:

- Significant reduction of the water vapor sorption rate; the sorption rate for pure lysine at 80% relative humidity is 10.5% per day, whereas that of lysine with wheat bran is about 2.5% to 4% per day.

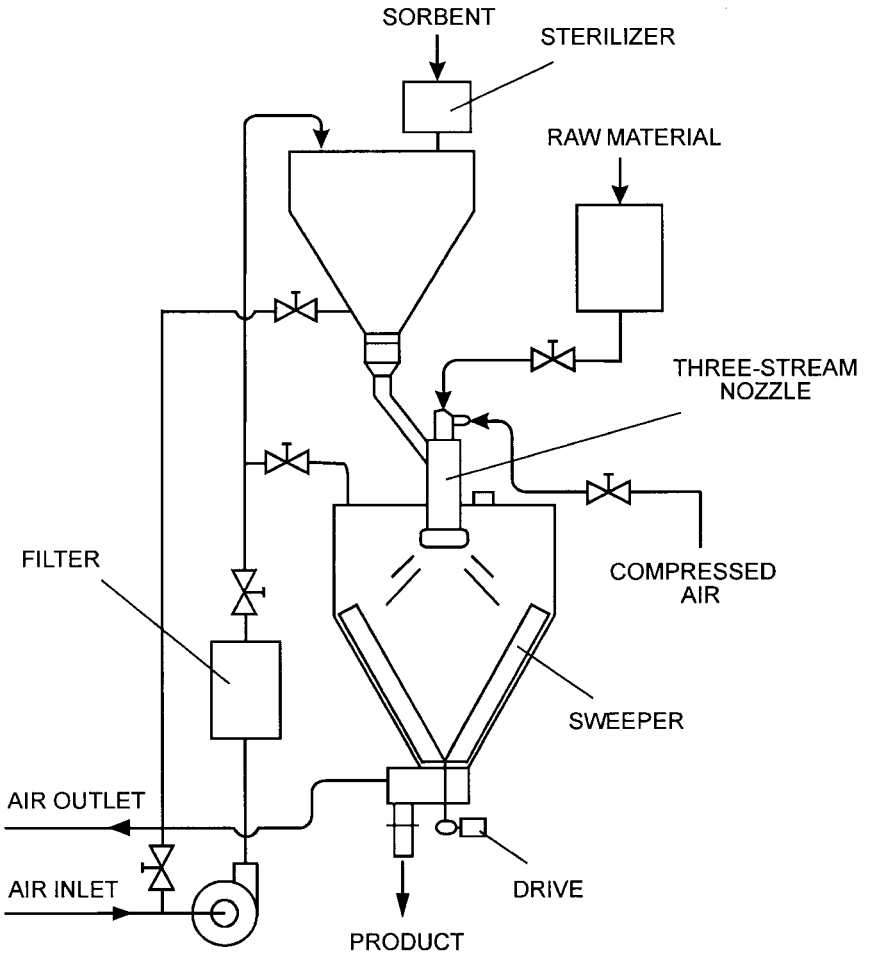

FIGURE 12.14 Contact–sorption spray dryer for bacterial preparations. (From Tutova and Slizhuk, 1990.)

Lowering of the relative hygroscopicity by 50% to 300% as compared to lysine without sorbent.

Stabilizing of the liquid moisture content; for pure lysine an increase in air humidity from 50% to 60% increases by 1.5 times the equilibrium moisture content. If the relative humidity approaches 80%, the equi-

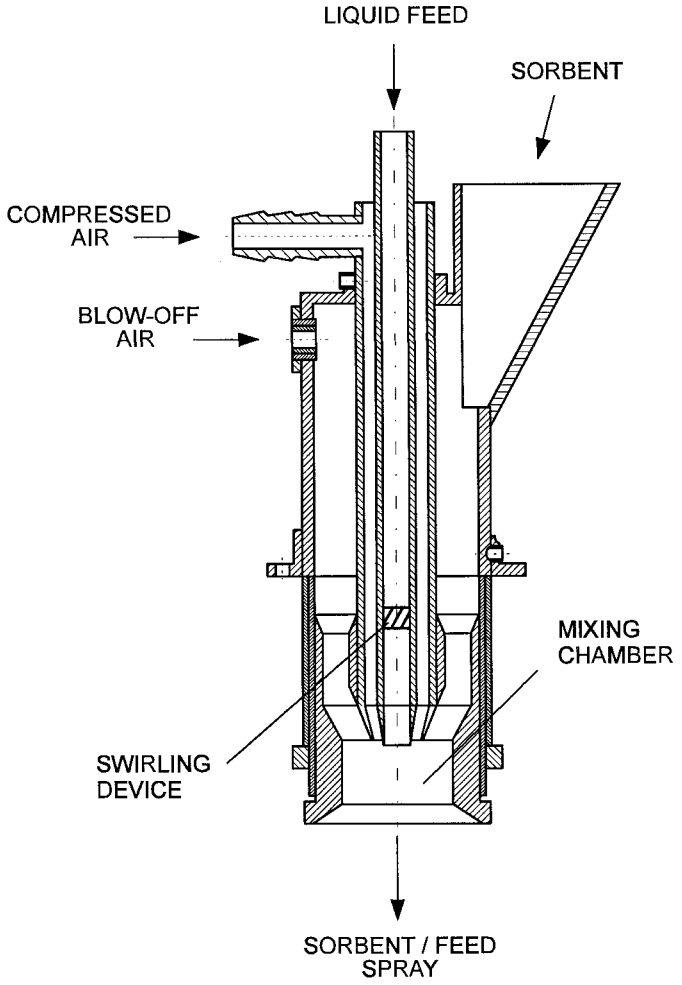

FIGURE 12.15 Three-stream nozzle for dispersing particulate sorbent within the liquid spray. (From Anon., 1990.)

librium moisture content is increased by 4 to 4.5 times. Moreover, for lysine with sorbent, the equilibrium moisture content does not depend practically on temperature and relative humidity of the ambient air.

TABLE 12.2 Characteristics of a Three-Stream Pneumatic Nozzle

Parameter	Type			
	AF-1	AF-2	AF-8	AF-10
Throughput, kg/h				
Sorbent	400	800	1000	800
Liquid	700	1500	2000	1500
Air consumption, kg/h	700	1500	2000	1500
Air pressure, MPa	0.3	0.3	0.3	0.3
Swirling device	Spiral	Spiral	Tangential	Tangential
Solids concentration in sprayed liquid, % mass	<40	<40	<40	<40
Spray angle, degree	60–180	60–180	60–180	60–180
Dimensions, m				
Length	0.9	1.0	1.1	1.0
Width	0.12	0.16	0.16	0.15
Height	0.16	0.21	0.21	0.17
Mass, kg	13	14	14	13

Source: From Anon., 1990b.

It may be noted that the sorption capacity of organic sorbents can be improved significantly (up to 40%) when in relatively small (5% to 10% w/w) mixture with salt or lactose (Tutova and Kuts, 1987). Another method of improving sorption capacity is drying with internal steam generation. Figure 12.17 depicts a sterilizer for granular peat in which the sterilization process takes place by water vapor evaporated from the peat and superheated due to heat supplied by indirect steam. In addition to the steam-heated jacket of a

TABLE 12.3 Contact-Sorption Drying of Bacterial Preparations on Wheat Bran

Culture	Moisture content of biomass, % wb		Final moisture content of sorbent, % w.b.	Sorbent-to-biomass, mass ratio, kg/kg
	Initial	Optimum		
Lactobacterium plantarum	95.0	40.0	35.9	1.66
Lactobacterium pentoaceticum	94.0	47.6	21.8	3.50
Streptococcus lactis diastaticus	96.0	35.0	18.7	4.30

Source: From Tutova and Slizhuk, 1990.

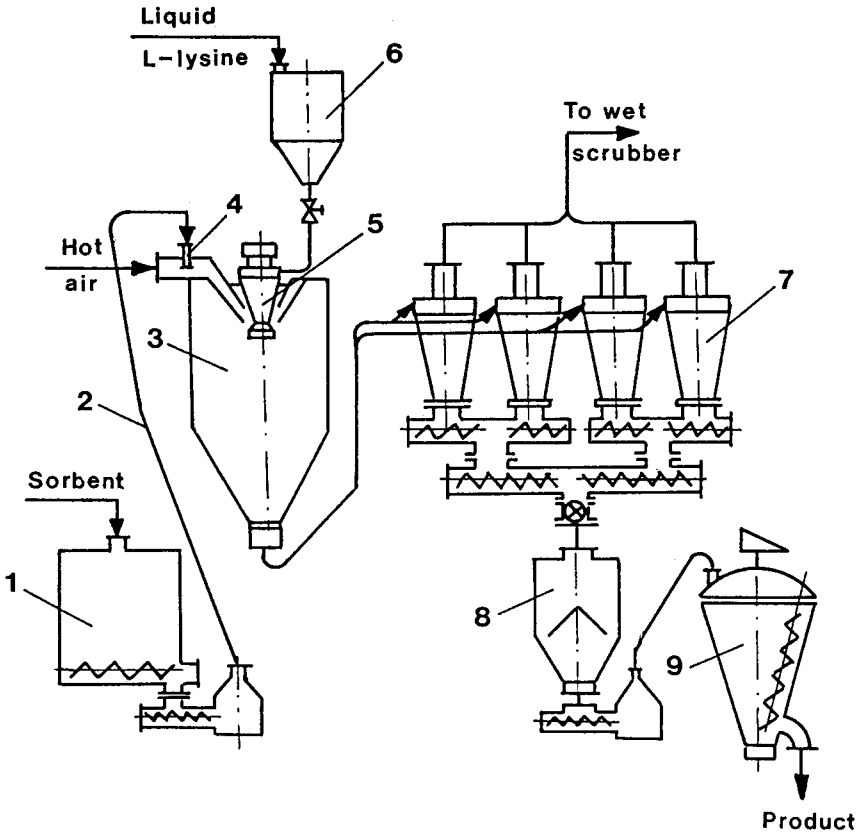

FIGURE 12.16 Contact–sorption spray drying of lysine: 1—wheat bran tank; 2—pneumatic duct; 3—spray dryer; 4—sorbent feed; 5—atomizer; 6—lysine tank; 7—cyclone; 8—activator; 9—blender. (From Tutova and Kuts, 1987.)

cylindrical sterilizer, a system of vertical steam tubes supplies heat to the moving bed of peat that is vibrated to facilitate flow of the particulate material and eliminate channeling. In case of granular peat with initial moisture content from 35% to 55%, the temperature of about 50 to 160°C maintained for 90 to 60 min was found to be optimum. Such conditions guarantee not only the required moisture content but also greater porosity of dry peat due to internal generation of superheated steam (Tutova and Slizhuk, 1990).

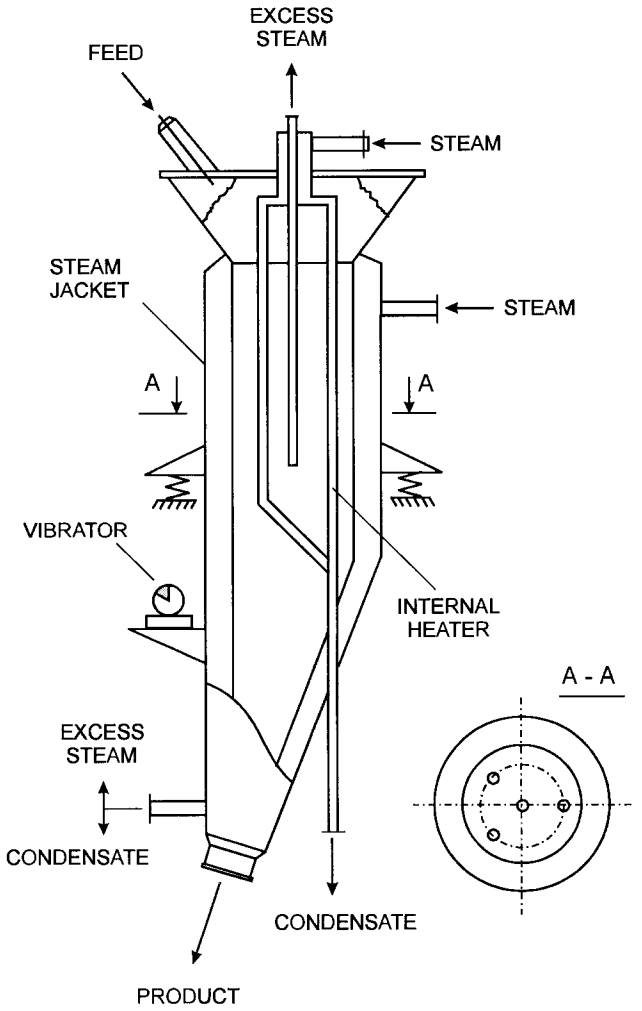

FIGURE 12.17 Sterilizer for particulate materials. (From Tutova and Slizhuk, 1990.)

12.4.4 Contact–Sorption Freeze-Drying

The principle of contact–sorption drying on inert sorbents can also be applied under conditions of reduced pressure. Since the evaporation rate in freeze-

drying depends, among other factors, on the partial pressure of water vapor at the material surface and at the condenser surface, one of the possible methods to reduce mass transfer resistance is to shorten the distance between the sublimation zone and the region of vapor condensation. This can be done when using an inert sorbent in direct contact with the material surface, which not only minimizes the diffusion path for water vapor but also increases the heat and mass transfer area-to-volume ratio. In this case, zeolites of group A are preferable over other sorbents as they possess high sorption capacity at reduced pressures (see Figure 12.8) that practically does not vary with temperature.

The intensity of freeze-drying depends greatly on the partial pressure of water vapor in the vapor–air mixture at the material surface and on the intensity of vapor removal. One of the methods to reduce the partial pressure of water vapor is to shorten a distance between the sublimation zone and the

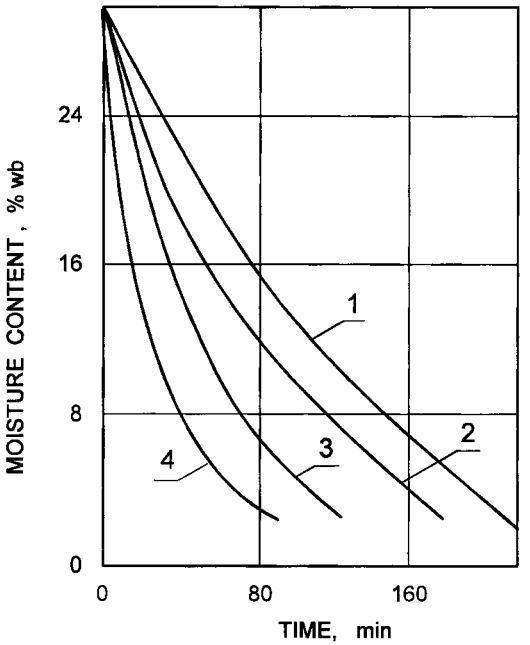

FIGURE 12.18 Drying curves for freeze-drying in layered sorbent–material configurations: 1—sublimation from free material surface; 2—two-layer structure of material–sorbent; 3—three-layer structure of sorbent–material–sorbent; 4—multilayer structure. (From Tutova, 1988.)

region of vapor condensation. Solid sorbents being in direct contact with the surface of freeze-dried material could play the role of a desublimator. Figure 12.18 illustrates the effect of a sorbent layer on freeze-drying curves. It is clear that the layered structure allows freeze-drying to be enhanced up to fourfold.

In general, release of heat of sorption has a negative effect on the process kinetics as the thermal resistance of the sorbent increases and its sorption capacity decreases. Even in the case of zeolite CaA, an increase of sorbent temperature from 20 to 80°C at a pressure of 133.3 Pa causes a decrease in sorption capacity by about 35% to 40%. The heat of sorption can, however, be used to intensify the process of contact–sorption freeze-drying with no additional energy consumption. For this purpose, a method has been devised at first to accumulate the heat of sorption released during the period of moisture absorption, and next to transfer it to a wet material directly during freeze-drying with moisture sorption (Tutova et al., 1985). This method is based on a comblike structure made of high thermal conductivity metals such as copper or aluminum that is placed between the material to be dried and the sorbent layers (Figure 12.19). Experimental verification of this method for freeze-drying of granulated baker's yeast confirmed that at double-sided contact of the material and the sorbent (zeolite), the sorption capacity of zeolite increased by 9%, heat demand decreased by 7.9 to 8.5 kJ per kg of evaporated water, and dewatering rate increased by almost 50% as compared to contact–sorption dewatering under vacuum when no elements for accumulation and transfer of the heat of sorption were applied (Tutova and Kuts, 1987).

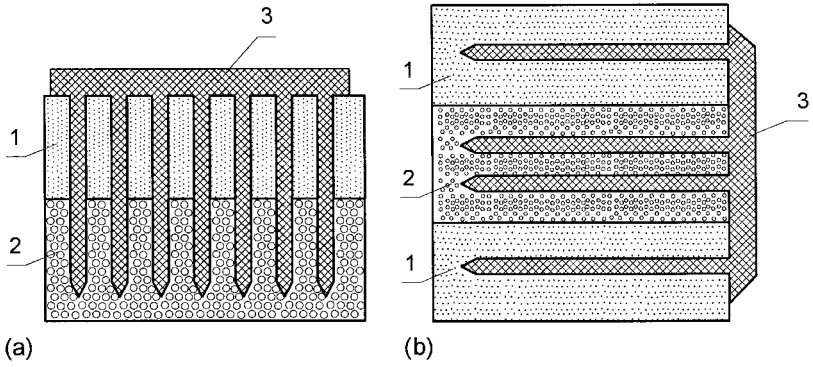

FIGURE 12.19 Basic structures for contact–sorption drying with heat-transferring elements in vertical (a) and horizontal (b) configurations: 1—sorbent; 2—material; 3—solid (metal) structure. (From Tutova et al., 1985.)

13

Sonic Drying

13.1 BASIC CHARACTERISTICS OF SOUND

Although known for many decades, sound- and ultrasound-assisted drying has recently found renewed interest mostly because of the significant progress in nonthermal dewatering (Mujumdar, 1991; Muralidhara and Lockhart, 1988). Sound is a special form of energy transmitted via pressure fluctuations in air, water, or other elastic media. Any displacement of a particle of this elastic medium from its mean position results in an instantaneous increase in pressure. When leveling, this pressure peak restores the particle to its original position, but also passes on the disturbance to the next particle. The cycles of pressure increase (compression) and decrease (rarefaction) propagate through the medium as a sound wave.

On a microscale, sound is characterized by pressure and particle velocity. The product of these two parameters is called *sound intensity*—a vector quantity that describes the rate of energy flow through a unit surface area normal to the direction of sound propagation

$$\text{Sound intensity} = \text{Pressure} \times \text{Particle velocity} = \frac{\text{Force}}{\text{Area}} \times \frac{\text{Distance}}{\text{Time}} = \frac{\text{Energy}}{\text{Area} \times \text{Time}} = \frac{\text{Power}}{\text{Area}} \quad (13.1)$$

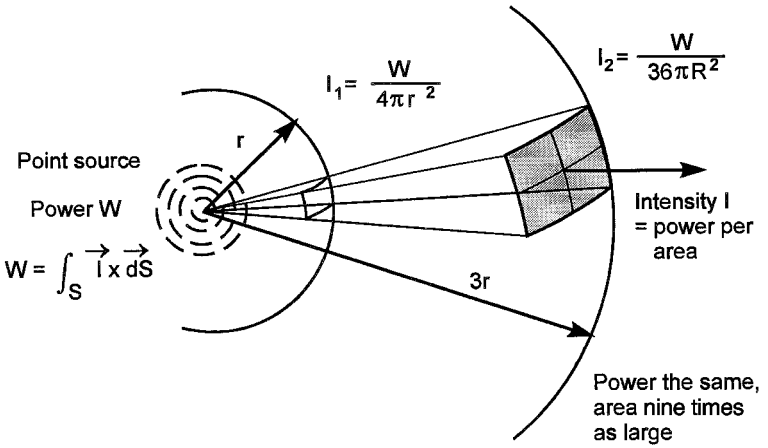

FIGURE 13.1 Sound intensity around the point source of acoustic energy.

As seen from Figure 13.1, sound generated by a point source with power W propagates as a spherical wave so the sound intensity is inversely proportional to the square of a distance from the sound source.

The variations of both pressure and velocity follow a sinusoid; if they are in phase the peak pressure occurs at the same time as a peak in the particle velocity, and the product of these two gives the intensity, which is not only the maximum instantaneous intensity but also the maximum time-averaged intensity (Figure 13.2). At the other extreme, when pressure and velocity are out of phase, the time-averaged intensity is zero. Phase compatibility is extremely important in drying since processes, which affect drying rate (e.g., cavitation), depend on the sound intensity.

On a macroscale, sound is primarily characterized by the frequency (f), which relates the speed of wave propagation (u) (sound velocity) to the wavelength (λ):

$$f = \frac{u}{\lambda} \tag{13.2}$$

The second main quantity used to characterize sound on a macroscale is the amplitude of the pressure fluctuations expressed as the sound pressure level (SPL) on the decibel (dB) scale with 20 Pa as reference level. Because the sound pressure depends on the distance from the source generating given sound power (energy per unit time) and on the acoustic environment (sound

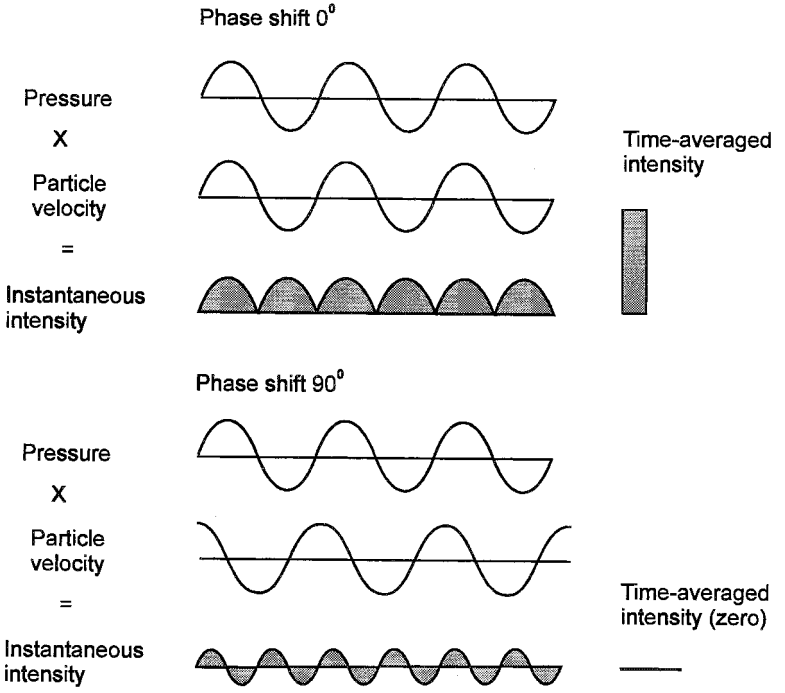

FIGURE 13.2 Time-averaged sound intensity versus phase shift.

field), it is then frequently quantified in terms of the sound intensity. Because of the large range of sound intensity, it is also given on a decibel scale but with 1 pW/m^2 as the reference level. The relations between sound power, sound intensity, and sound pressure are presented in Figure 13.3. The decibel scale is given in Table 13.1.

In a free acoustic field such as that in an open air or anechoic chamber, the pressure and intensity levels in the direction of propagation are numerically the same. In a diffuse field in which sound is reflected so many times that it travels in all directions with equal magnitude and probability (reverberation chamber), the pressure and intensity levels are different and this difference is known as the pressure-intensity index (phase index or reactivity index).

Aside from the frequency and sound intensity, the key point in the design of sound-assisted dryers is the mode of energy propagation. Sound energy can be propagated as longitudinal waves (also called compression waves) or transverse waves for which vibration of the particle in the material occurs

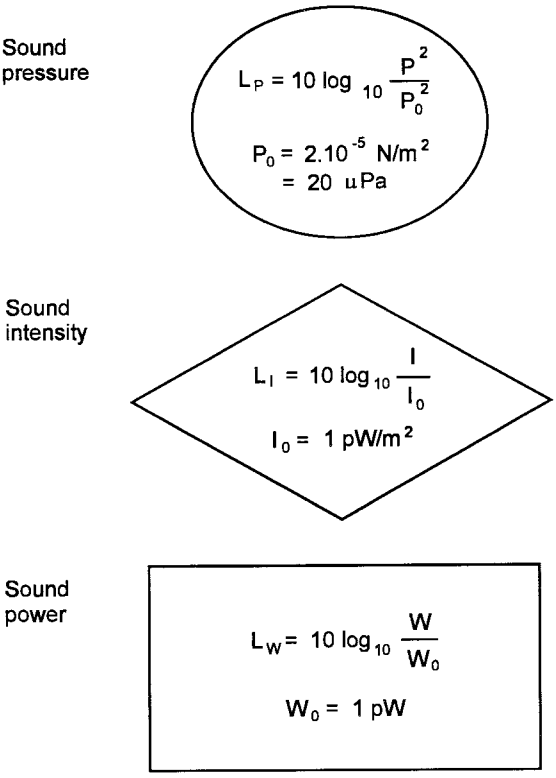

FIGURE 13.3 Decibel scale and the relation between the Sound Power Level (L_W), Sound Intensity Level (L_I), and Sound Pressure Level (L_P).

TABLE 13.1 Decibel Scale

Units	Pressure, N/m^2	Decibels	Sound source
1	0.00002	0	Threshold of hearing
10	0.0002	20	Forest
100	0.002	40	Library
1,000	0.02	60	Normal conversation
10,000	0.2	80	Workshop
100,000	2	100	Pneumatic chipper
1,000,000	20	120	Jet takeoff
10,000,000	200	140	Threshold of pain

perpendicularly to the direction of wave motion. Since the latter cannot be propagated in gases and liquids except for highly viscous liquids over very short distances (fraction of a millimeter), the sound-assisted dryers are designed to accommodate longitudinal waves.

In a free space, the sound source can be considered as a point source (see Figure 13.1). In practical industrial applications, however, sound is either radiated from the source of definite size (e.g., loudspeaker membrane) or, more frequently, reflected from the point source by surfaces of different shapes such as horn, paraboloid, ellipsoid, etc. In both cases such sound radiation can be regarded as coming from a plane source. This results in a specific pattern of sound intensity; in the zone near the sound source, the sound intensity is constant (Fresnel zone), whereas outside this zone (the Fraunhofer zone) the sound intensity decreases inversely with the square of the distance from the plane source, i.e., in the same way as for a point source (Figure 13.4).

In some configurations of dryers the length of zones and thus the sound intensity distribution may become important. For example, the Fresnel zone for the plane source 10 cm in diameter is negligible (couple of millimeters) for sound at 100 Hz (cf. frequency of pulse combustion) but extends for 15.6 cm in the range of ultrasound at 20 kHz and 31.2 cm at 40 kHz.

According to the frequency of pressure pulsation, sound can be classified as infrasound ($f < 20$ Hz), sound (audible) (20 Hz $< f <$ 20 kHz), and ultra-

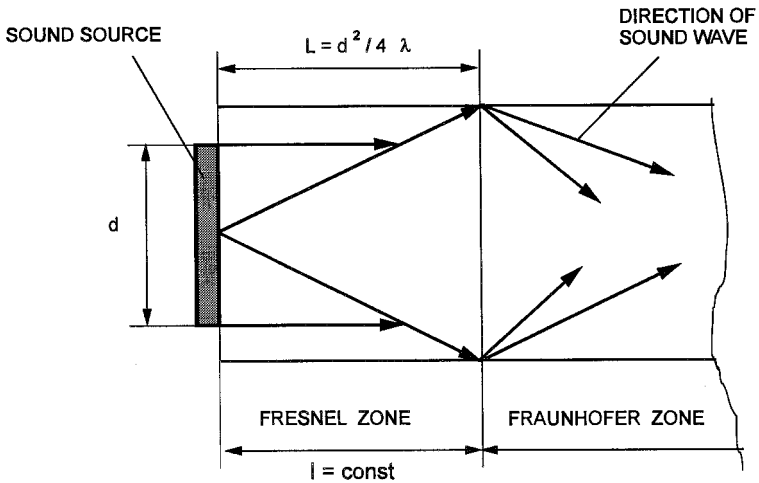

FIGURE 13.4 Propagation pattern from a plane sound source.

sound ($f < 20$ kHz). In the past, the R&D were targeted at frequencies over 15 kHz. The newly developed pulse combustion technique has, however, shifted the frequency range toward lower frequency (Kudra and Mujumdar, 1995), in the order of 50 to 200 Hz (see Chapter 14). Also, interesting laboratory results were reported in the range of infrasound (Kudra, 1998; Woods, 1991; Woods, 1992) (see Chapter 26).

Ultrasonic applications are rigidly classified into low and high intensity. Low-intensity applications are made typically in the mega-Hertz frequencies and acoustic power up to tens of milliwatts, and usually do not alter material properties under operation. In contrast, the high-intensity ultrasound is generally used for changing the properties of the material through which it is passed or altering the physical–chemical processes. High-intensity applications are made at low frequencies, about 20 to 40 kHz, and these are used in drying and dewatering.

13.2 SOUND GENERATION

In industrial applications sound waves are generated by a transducer, which converts the original form of energy to the energy of oscillatory motion. Such transducers are classified into six main groups:

1. Piezoelectric, in which periodic changes in physical size of certain crystals (such as quartz, tourmaline, and zinc oxide) due to applied electric potential generates mechanical vibrations, which are propagated as sound waves. Used in the range from 20 kHz to 10 GHz.
2. Magnetostrictive, in which mechanical vibrations are caused by changes in the physical size of certain metals such as nickel, cobalt, or iron, or certain nonmetals known as ferrites due to external magnetic field. Used in the range of 40 to 100 kHz.
3. Electromagnetic, in which the vibration of a solid armature (e.g., membrane in loudspeakers and microphones) is due to coupled electric and magnetic fields. Used at $f < 50$ kHz.
4. Electrostatic, in which the periodic variation of charges in an electrical capacitor of a special design induces mechanical vibration. Used at $f < 100$ kHz.
5. Mechanical, in which sound waves are generated due to the action of a truly mechanical device such as rotating counterbalanced weights or a mechanical device energized by the kinetic energy of the working fluid (sirens and whistles). Used at $f < 50$ kHz.
6. Miscellaneous, in which thermal, chemical, optical, and other phenomena are exploited.

For high-intensity generation and propagation of sound in gases at frequencies up to about 25 kHz, mechanical generators are used almost exclusively because of their design and operational simplicity, energy capability, and low cost as compared to the other types of transducers. These generators, which produce the so-called airborne sound, are used in sound and sound-assisted convective drying. Figure 13.5 presents the most frequently used types of mechanical generators from the group of cavity resonators (Galton and Hartman whistles), wedge resonators, and sirens. Usually, in a modified Hartman whistle a rod is centrally positioned along the axis of the gas jet. Such a design allows for a more compact generator of increased efficiency. In the Branson pneumatic sound generator the exhaust air jet is separated from the sound field, which not only results in higher sound intensity (no air turbulence effect) but also permits the generator to be used in processing material for which the contact with air is not acceptable. One of the possible designs of industrial sound generators is shown in Figure 13.6.

In processing of liquid systems, such as dewatering of slurries and pasty materials, piezoelectric or magnetostrictive generators are used. The active part of such a generator (called a driver) generates and transmits mechanical vibrations via a solid rod (a booster) to the metal profile (a horn). This horn serves as an amplitude transformer to amplify the displacement of the driver and to match the transducer impedance with the impedance of the material to be processed (Figure 13.7). The mechanical vibrations from the horn are further coupled to the material processed either directly (the horn is inserted into a liquid or pasty material) or indirectly via a membrane.

13.3 MECHANISM OF SONIC DRYING

Since only exploratory studies have been reported so far on sonic drying, the following discussion of the drying mechanism focuses on the ultrasonic applications, which have been of research interest for years. Definitely, some of these mechanisms may also contribute to sound and infrasound drying. In these cases, postulation of a particular mechanism requires, however, further studies.

An analysis of available literature data indicates the following possible mechanisms of heat and mass transfer alteration in an ultrasonic field:

Alternating compression and expansion due to high-frequency pressure pulsation create surface cavitation that breaks the boundary layer and allows liquid to evaporate under partial vacuum (Boucher, 1959).

Intensive circulation flows (induced by sound pressure) on the drying

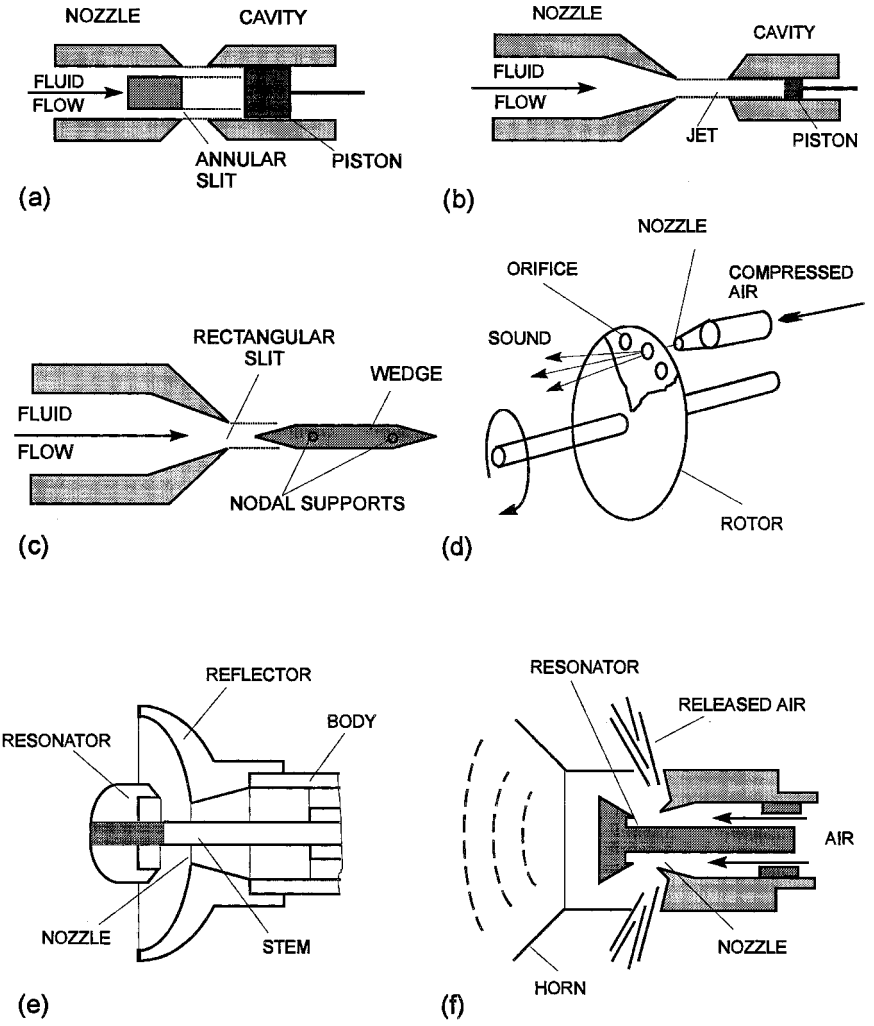

FIGURE 13.5 Principles of sound generation in mechanical sound generators: (a) Galton whistle, (b) Hartman whistle, (c) wedge resonator, (d) dynamic siren, (e) modified Hartman whistle, and (f) Branson sound generator.

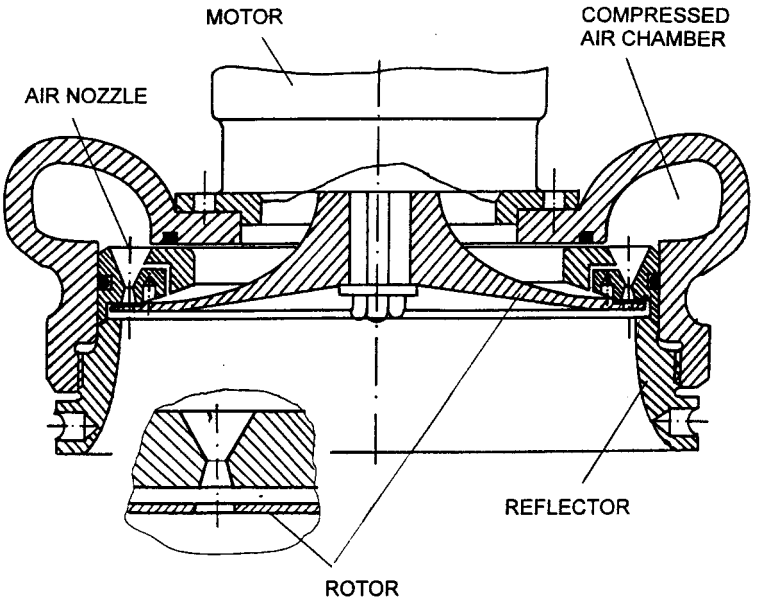

FIGURE 13.6 Design of a pneumatic sound generator.

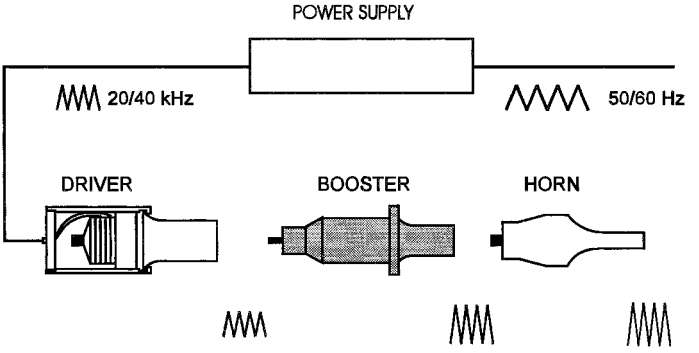

FIGURE 13.7 Schematics of the ultrasonic generator for operation in liquid and pasty materials.

surface thus promotes surface evaporation (Borisov and Gynkina, 1962).

Pressure pulses from the sound waves increase the turbulence of the gas stream flowing over (or through) drying material, which reduces the thickness of the laminar sublayer (Zayas and Pento, 1975).

An increase in moisture diffusivity and decrease in viscosity (Bartolome et al., 1969; Greguss, 1961).

Pulsating partial vacuum transmitted into the material affects water vapor transport, possibly by decreasing or overcoming the attraction forces between water and solid molecules (Muralidhara and Ensminger, 1986).

Expansion of the vapor bubbles inside capillaries yields a migration of the water filament (sonic diffusion current) (Greguss, 1961; Greguss, 1963).

Shear reduction in boundary film surrounding the material (Muralidhara and Ensminger, 1986).

Plug flow of liquid through the capillaries toward the material surface (Otsuka et al., 1977).

Rectified diffusion due to alternating compression and rarefaction (Muralidhara and Ensminger, 1986; Muralidhara et al., 1986).

The review of literature data indicates that cavitation, enhanced turbulence of the gas phase at the solid (or liquid droplet) surface, and mechanical effects due to internal stresses appear to be the major contributors to enhanced moisture removal during drying. It is also reasonable to expect that the liquid viscosity be lowered in ultrasonic fields which promotes diffusion of moisture toward the evaporation surface.

The term *cavitation* refers, in general, to the formation and subsequent dynamic behavior of vapor bubbles in liquids. Acoustic cavitation occurs when high-intensity sound waves are coupled to the liquid surface, which results in propagation of alternating regions of compression and expansion—thus formation—of micron-size vapor bubbles. If the bubbles are of a critical size (determined by the frequency of the sound wave), they may implode violently, releasing energy in the form of impulses ($t < 0.1$ s) with local point temperatures and pressures in the order of 5000 K and 1000 atm, respectively (Suslick, 1988). Since the effective temperature zone is confined to about 0.2 m from the surface of the collapsing bubble, the bulk of the liquid remains practically at the same temperature. However, as the bubbles at or near the surface implode, micron-size liquid droplets can be released into the surrounding air and evaporated instantaneously. Because of the cavitation threshold, larger

acoustic pressure amplitudes at a given frequency are required for highly viscous liquids.

It is reasonable to assume that pressure fluctuation caused by sound waves disrupt the boundary layer at the solid or liquid surface, so they should affect the interphase transfer rates and therefore accelerate drying rates. In fact, a substantial decrease (up to 15%) in the boundary layer thickness has been found when conventional spray-drying of blood plasma was complemented by the high-intensity sound at $f = 15$ kHz and $I = 155$ dB (Zayas and Pento, 1975).

Aside from cavitation, the enhanced mass transfer rates in acoustic fields can be attributed to plug flow of capillary liquid as well as to enhanced dispersion of the liquid and vapor moisture due to alternating compression and expansion cycles, which result in reduced viscosity of the liquid–vapor mixture. In fact, a substantial increase in the amount of liquid diffusing through porous solids has been noted in the presence of ultrasound (Fairbanks and Chen, 1969; Woodford and Morrison, 1969; Kuznetsov and Subbotina, 1965). The enhanced diffusion appears to be of the directional type since mass transfer was hindered when ultrasound irradiation was opposed to the direction of diffusive flow (Kuznetsov and Subbotina, 1965).

According to Kardashev (1990), the mechanism of acoustic drying of capillary-porous materials depends on the moisture content level. When the material is very wet ($X' = 200\%$ to 500% w.b.), the effect of an ultrasound field is truly mechanical and moisture is removed due to better dispersion of liquid water, especially at the antinodes of a standing wave. When the material moisture content is much lower (10% to 70% w.b.), but drying takes place during the constant-rate period, the sound waves reduce the thickness of the boundary layer, which alters moisture evaporation. In the falling rate period, the sound waves enhance only the moisture diffusivity due to temperature rise as the sonic energy is dissipated as heat. In the case of dispersed materials, the positive effect of sound waves on a drying rate appears for sound pressure levels above a certain threshold value. For spherical particles with a diameter smaller than the wavelength, the critical pressure level can be determined from the following equation:

$$P_{cr} = v\rho\sqrt{\frac{2.5gd(C_s - C_g)}{\rho}} \tag{13.3}$$

where ρ is the gas density, v is the sound velocity in a gas phase, d is the particle diameter, C_s and C_g are the water vapor concentration at the particle surface and in the gas core, respectively.

Because this sound pressure level is proportional to the square root of the particle diameter, the best result of sonic irradiation can be expected in fluid bed drying of powdery materials. The same conclusion can be drawn when considering evaporation of free water from a spherical particle. Relating the mass transfer rate due to air stream velocity resulting from a sound wave flowing past a sphere to the convective mass transfer due to the same air velocity, the enhancement ratio can be expressed as (Kardashev, 1990)

$$E = 2\sqrt{\frac{A}{d}} \tag{13.4}$$

where A is the amplitude of the sound wave and d is the particle diameter.

Directional diffusion as well as the acoustic resonance that appears only under specific conditions may explain, in our opinion, some contradictory experimental results and controversial conclusions on the effect of sound energy on the drying rate (Bartolome et al., 1969; Carlson et al., 1972). In most cases, however, sound energy appears to have a positive effect on the mass transfer, which translates into shorter drying times. For example, application of 160 dB of sound energy in the frequency range from 5 to 15 kHz to the fluid bed of a highly heat-sensitive, sticky product such as lactic sugar dried from 17% to 0.25% d.b., by air at 50°C and 1.4 m/s reduced the drying time from 80 to 30 min (Makarov et al., 1972).

The above phenomena, which contribute to the overall mechanism of drying in a sound field, do not include thermal effects as it is generally accepted that the increase in the bulk temperature due to energy dissipation is too small for moisture evaporation (Muralidhara and Lockhart, 1988; Zayas and Pento, 1975; Strumillo and Kudra, 1986; Borisov and Gynkina, 1973). In the case of a plane progressive wave penetrating the material being dried, the sound energy is attenuated due to various mechanisms including relaxation processes, viscous shearing effects, and molecular absorption. Neglecting scattering of the sound energy, the amplitude of acoustic pressure at a distance x from the material surface at which the incident sound pressure is P_0 may be expressed as

$$P(x) = P_0 \exp(-\alpha x) \tag{13.5}$$

where $\alpha(1/s)$ is the absorption coefficient being a function of material properties and sound frequency (in most cases α should be determined experimentally).

Equation (13.5) can be written conveniently in terms of sound intensity, which reflects the energy flux per unit surface area

$$I = \frac{P^2}{v\rho} \tag{13.6}$$

where ρ is the material density, and v is the sound velocity. Hence,

$$I(x) = I_0 \exp(-2\alpha x) \tag{13.7}$$

Equation (13.7) indicates that the energy lost by absorption from the sound of intensity I crossing a unit distance ($x = 1$) is equal to the product ($2\alpha I$). Assuming no heat loss from the absorbing volume, the rate of temperature rise is given by

$$\frac{dT}{dt} = \frac{2\alpha I}{\rho c} \tag{13.8}$$

where c is the material specific heat.

Under real drying conditions heat generated within the material volume is transported away by conduction and convection so the final temperature tends to equilibrium determined by the heat balance. The equilibrium temperature for the bulk of the material is the order of few degrees (Zayas and Pento, 1975; Strumillo and Kudra, 1989; Brun and Boucher, 1957), which justifies moisture evaporation due to thermal effects of sound irradiation to be neglected. This obviously favors sonic drying as a method for processing heat-sensitive materials.

Considering heat generation on the microscale, thermal effects may become important as localized temperature increases are likely to affect fluid properties and solid–fluid interactions (e.g., lower surface tension or viscosity). According to Moy and DiMarco (1970), for example, 7% of the sound-enhanced freeze-drying rate of liquid food can be attributed to the thermally induced mechanical effects on the gas phase resulting in friction and adiabatic compression.

Detailed discussion of these and other phenomena activated by the sound energy can be found elsewhere (Muralidhara et al., 1986; Suslick, 1988; Rosenberg, 1973; Ensminger, 1986; Ensminger, 1988).

13.4 DRYING KINETICS

An analysis of the literature data indicates that drying by airborne sound, which in many cases becomes in fact sound-assisted convective drying, is essentially similar in drying kinetics to conventional convective drying, i.e., there are initial, first, and second drying periods. However, there are several singularities noted for a given class of the material. For example, sound-

assisted drying of capillary-porous materials is characterized by an extended constant drying rate period toward the lower moisture contents. In contrast, the constant-rate period in sound-assisted convective drying of colloidal solutions such as blood plasma or protein hydrolysate is shorter by 25% to 30% (Zayas and Pento, 1975). Moreover, evaporation rate in the first drying period is proportional to the sum of the local sound velocity and the air velocity vectors (Marziniak, 1972).

Acoustic drying of colloidal, capillary-porous materials such as potato starch (370 kHz, 147 dB) with the maximum hygroscopic moisture content of 68% takes place at a much lower constant drying rate, and two periods of the falling drying rate are usually observed. In contrast, the drying kinetics of swollen bentonite, which also falls into the category of colloidal-capillary-porous material, is characterized by the presence of two constant-rate periods (Stadnik and Kazanskii, 1966). Shifting of the critical moisture content can be attributed to the fact that the acoustic vibrations intensify moisture evaporation, which increases the critical moisture content, but also alters the process of diffusion, which reduces the critical value. Thus, the balance between the moisture transported to and removed from the material surface determines the relative length of the constant-to-falling rate period (Borisov and Gynkina, 1973).

The drying rate depends on the sound wave pattern in a drying chamber, which may be attributed both to the Fraunhofer zone and to the resonance phenomenon, which results in nodes and antinodes in the sound pressure/intensity. A significant difference (up to 250%) was observed in the first drying period for potato samples placed in nodes and antinodes of sound pressure waves. In the falling drying rate period, these differences were insignificant (Figure 13.8).

From a truly practical point of view, the infrasound field appears to have advantages over audible sound or ultrasound fields. Provided the effect of accelerated transfer processes occurs at the velocity node (pressure antinode), the wavelength of infrasound is long enough for most materials to be exposed to the useful region of the standing wave. Also, infrasound is less attenuated within the material being dried. Moreover, infrasound is not audible, and therefore at similar pressure levels it is less of a nuisance in a plant environment than audible sound. The drawbacks of infrasound are the difficulty of acoustic isolation, if required, and the possibility for large-amplitude vibrations of the mechanical parts of the equipment if not off the resonance.

Although there is no clear picture to explain the effect of frequency and sound intensity on the moisture transfer rate, the enhancement of the drying rate becomes significant at sound intensity in excess of 150 dB with little effect of the frequency unless the sound wave attenuation is critical.

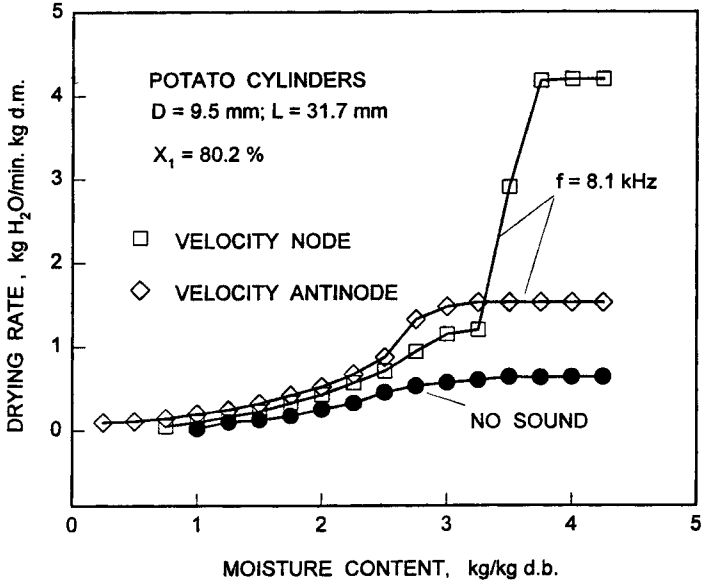

FIGURE 13.8 Drying rate for potato cubes placed in nodes and antinodes. (From Bartolome et al., 1969.)

The effect of acoustic energy on enhanced drying rates is especially advantageous at low temperatures. For example, in combined acoustic-convective drying, the effective increase in drying rate due to acoustic energy decreases with temperature, and under certain conditions the contribution of the sound energy is as significant as the effect of temperature and air velocity (Fairbanks, 1970).

Aside from low-temperature drying, the sound energy may also be advantageous in high-temperature drying. The experiments on drying several albumin-based biomaterials in a conventional spray dryer equipped with air-driven whistles located at the disc atomizer level have shown reduced material temperature in the dryer by 10 to 22°C (Figure 13.9), which results in a better product quality. In particular, sound-assisted spray-drying of blood plasma carried out at inlet and outlet air temperatures from 115 to 145°C and from 65 to 80°C, respectively, resulted in lower final moisture contents by 0.3% to 0.5%, increased concentration of soluble protein by 2% to 3%, and reduced concentration of (—SH) groups by 5% to 20% as compared to the control sample dried without the sound energy (Zayas and Pento, 1975).

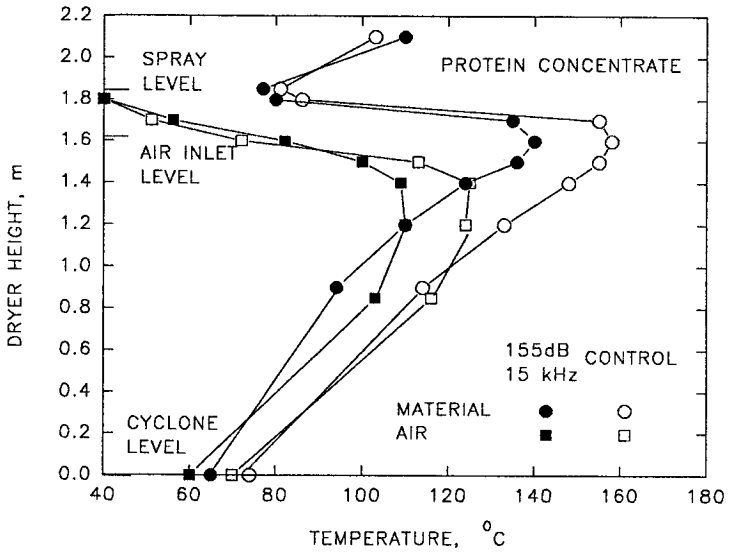

FIGURE 13.9 Temperature profile in a sound-assisted spray dryer. (From Zayas and Pento, 1975.)

Especially attractive is the synergistic effect on drying rate when combining sound energy with other mass transfer driving forces produced by other energy fields such as magnetic, electric, or electromagnetic. An example of such an effect is shown in Figure 13.10, which compiles the results of acoustic drying, microwave drying, and acoustic-microwave drying of silica gel taken as a model material (Shatalov, 1976). In these studies, microwave energy at 2450 MHz was applied in a pulsed mode to maintain the material temperature at 80°C. It was found that addition of ultrasound increases the rate of microwave drying in the first drying period by 30% to 35%. Our detailed analysis of the original data indicates, however, that the experimental points for sound-assisted microwave drying are located above the curve obtained by superposition of the isolated acoustic and microwave drying data. This synergistic effect is more pronounced during the initial and the falling rate periods, which implies alteration of the internal mass transfer mechanism rather than evaporation from the free water surface. The same conclusion can be drawn from the experimental data on vacuum drying with the assistance of electric and ultrasonic fields (Figure 13.11).

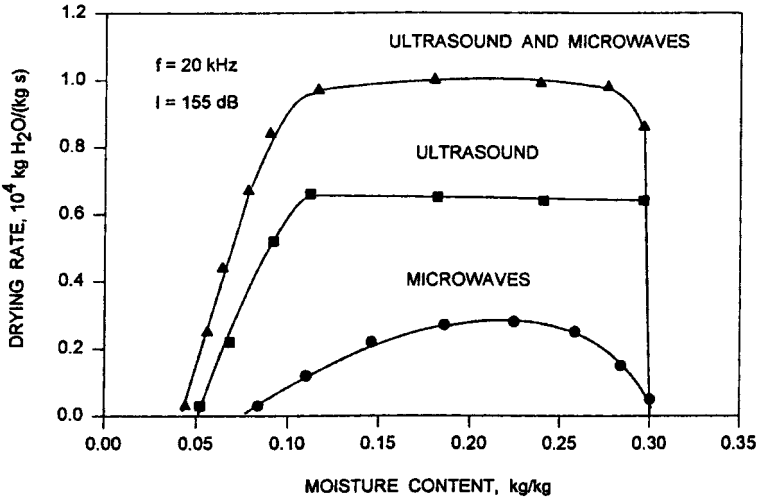

FIGURE 13.10 Drying rates for sound-assisted microwave drying. (From Shatalov, 1976.)

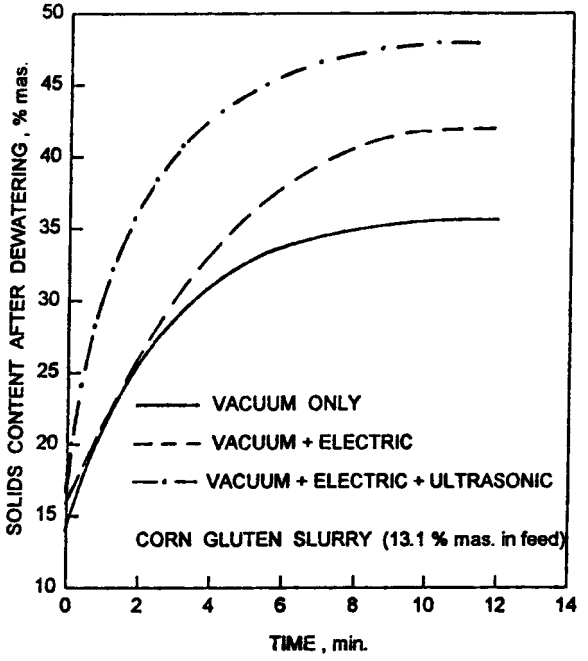

FIGURE 13.11 Effect of the sound and electric field on vacuum drying rates. (From Muralidhara et al., 1988.)

13.5 SOUND-ASSISTED DRYERS

The basic constraint in sound-assisted drying is the maximum penetration depth, which restricts the material thickness to about 30 to 50 mm. The material thickness could be higher in the case of infrasound; however, no data on infrasound drying have been reported to date although a positive effect on heat transfer has been documented (Woods, 1991; Woods, 1992).

In the case of acoustic dryers, sound propagates in confined volumes (tubes or chambers) so the resulting standing waves cause Rayleigh acoustic streaming. This streaming has a closed vortex character, and the vortex scale in the direction of the radiation is equal to a quarter-wavelength (Borisov and Gynkina, 1973). At acoustic pressure levels above 145 to 150 dB, the streaming velocity can be in the order of several meters per second (Borisov and Statnikov, 1965). Such a high velocity not only alters the heat and mass transfer processes but also can have a definite hydrodynamic effect on a particulate material. It was found, for example, that sound waves of frequency from 50 to 500 Hz and intensity above 111 dB can sustain stable fluidization of particles with diameters ranging from 2 to 1000 μm if density is within the range from 1200 to 2700 kg/m^3.

The effect of sonic irradiation on drying of particulate materials in a fluidized bed was analyzed by Kardashev and coworkers (1972). Considering a quasi-stationary model of a fluidized bed in which the voids are assumed to be cylinders of radius r and length L, the following equations were developed for drying rate in a classical fluid bed of particulate material:

$$w_D = k_1\left(1 + k_2\sqrt{\frac{r^3\Delta P}{4\nu^2\rho L}}\right) \tag{13.9}$$

and in the fluidized bed with acoustic irradiation:

$$w_{D,a} = k_1\left(1 + k_2\sqrt{\frac{\pi r\Delta P_a}{\nu}}\left(\frac{4L^2\nu\rho^2\omega}{r^2} + \frac{16\rho^2\omega^2L^2}{9}\right)^{-0.25}\right) \tag{13.10}$$

where ΔP and ΔP_a is the pressure drop in a classical (hydrodynamic) fluidized bed and in a fluidized bed with sonic irradiation, respectively.

The experimental coefficients k_1 and k_2 depend on material properties and bed characteristics such as particle diameter, diffusion coefficient, water concentration gradient, etc. For example, for the bed of silica gel with equivalent diameter $d_e = 0.22$ mm, $k_1 = 5.72 \cdot 10^7$, and $k_2 = 0.23$ g/(cm^{2}s), while

$k_1 = 1.1 \cdot 10^3$ and $k_2 = 0.23$ g/(cm^{2}s) in the case of the styrene/α-methylstyrene copolymer with $d_e = 0.12$ mm.

Accounting for the penetration depth, surface phenomena, and hydrodynamic effects, the industrial sonic dryers are therefore mainly of the dispersed-flow type, e.g., spray, throughflow, rotary, or fluid bed dryers (Kudra, 1998; Zayas and Pento, 1975; Kardashev, 1990; Borisov and Gynkina, 1973; Soloff, 1964; Huxsoll and Hall, 1970; Borisov and Gynkina, 1967; Borisov and Ginin, 1967; Tutova and Kuts, 1987; Mashkova, 1960; Bezzubov et al., 1966; Simonyan, 1965).

Figure 13.12 presents the design principle of a sound-assisted rotary dryer, which was a subject of studies by Soloff (1964), Huxsoll and Hall (1970), Borisov and Gynkina (1967), and Borisov and Ginin (1967). The drum of the dryer used by Soloff (other dryers were similar in design and operation) was 0.2 m in diameter and 1.2 m in length. The drum had eight lifting baffles to tumble the particulate material. A variable-speed motor controlled the drum rotation up to 80 rpm. The maximum feed rate was 45 kg/h at the inlet air temperature up to 150°C. A pneumatic sound generator (Branson Ultrasonic Corporation) was mounted at the discharge end of the drum. The sound was propagated along the drum, and a standing wave was established because of reflection from the feed end of the drum. A sound pressure level of 169 dB

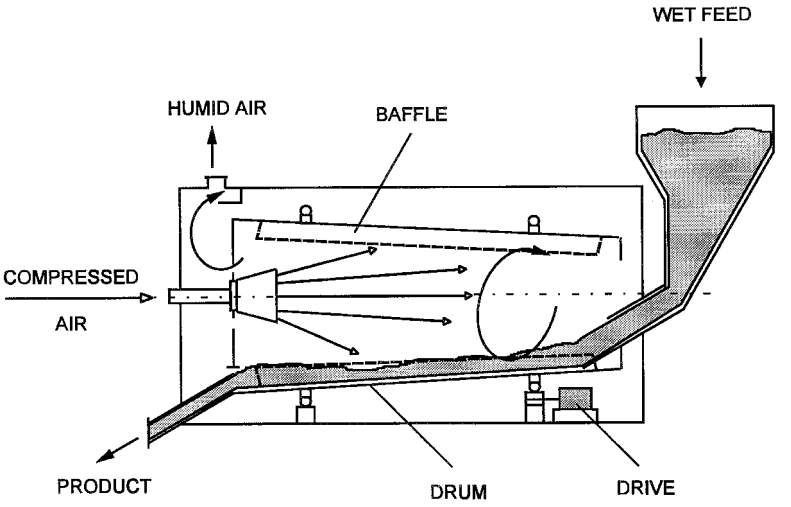

FIGURE 13.12 Sound-assisted rotary dryer.

at 10.9 kHz was attained at the pressure antinodes in the drum. The results of several drying tests are given in Table 13.2.

The major limitation of rotary dryers is the relatively low volumetric load ratio of the drum, which typically ranges from 3% to 16%. Because sound energy is absorbed in the bulk of particulates, it is difficult to secure the efficient use of high-intensity sound energy in large rotary dryers. Much better energy utilization is in the case of spray dryers since sonic irradiation intensifies heat and mass transfer but also enhances liquid atomization (see Figure 13.9).

An interesting design of the industrial sound-assisted spray dryer in which the sound energy is used to homogenize the mixture of the liquid biomaterial and the solid sorbent-carrier is shown in Figure 13.13. A standard spray dryer with a tangential air inlet is equipped with two sirens situated at the spray cone level. The combined action of the sound energy and the air streams from the sirens activated by compressed air not only improves dispersion of the solid–liquid spray but also enhances heat and mass transfer rates, which finally allows for product of required quality (Tutova and Kuts, 1987). Unfortunately, no technical information about the dryer and operating parameters is given in the source literature.

Figure 13.14 presents the design of a fluid bed dryer equipped with three pneumatic sirens (Mashkova, 1960; Bezzubov, 1966). Fluidization of

TABLE 13.2 Drying of Selected Materials in Sonic Rotary Dryer

Material	Moisture content, % w.b.		Residence time, min	Throughput, kg/h	
	Initial	Final		With sound	Without sound
Wood flour	5.5	1.53	3.0	40.8	16.8
Grated cheese	16.8	5.9	16.2	15.9	11.3
Antacid powder	15.1	6.0	15.0	12.2	6.8
Gelatin beads	12.9	3.7	20.0	10.0	5.4
Enzyme crystals	9.8	6.4	120.0	2.3	0.9
Carbon black	48.7	1.0	25.0	8.2	5.4
Rubber crumbs	44.0	6.0	90.0	3.2	1.8
Polystyrene powder	0.5	0.1	30.0	6.4	2.7
Aluminum oxide	0.5	0.2	5.0	25.4	14.5
Rice grains	27.6	14.5	11.0	18.1	8.2

Source: Adapted from Soloff, 1964.

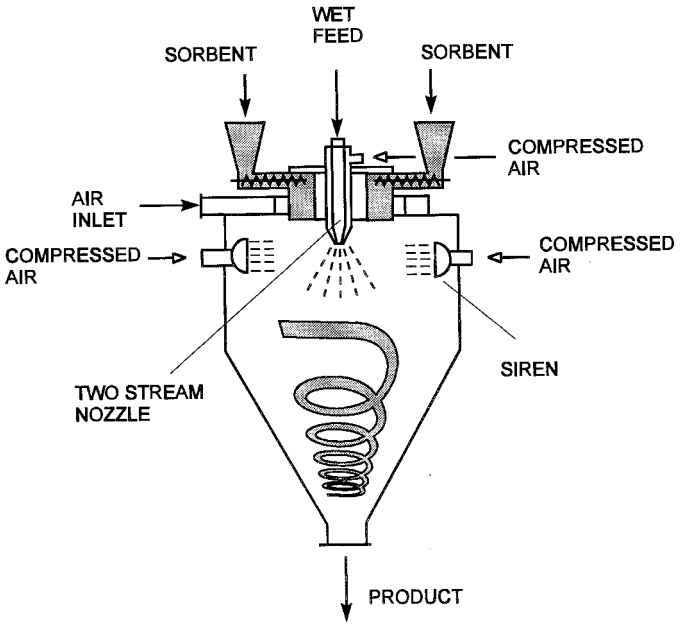

FIGURE 13.13 Sound-assisted spray dryer for drying liquid biomaterials on active sorbents. (From Tutova and Kuts, 1987.)

particulate material takes place due to combined action of sound energy from the static siren located below the supporting grid, and the air stream that excites the siren. An interesting feature of this design is the use of two additional sirens located at the sidewall and at the top of a drying chamber to reduce carryover of fines by acoustic coagulation of aerosols. In order to prevent spent compressed air from affecting bed hydrodynamics, the side siren is covered with a membrane. Because the membrane and the supporting grid absorbs about 50% of incident sound energy, this dryer has found only a limited application.

More energy efficient appears to be the design by All-Union Scientific-Research Institute of New Structural Materials (VNIINSM) (Simonyan, 1965) in which the conventional fluid bed dryer is equipped with the gas-jet sound generator (Galton or Hartman whistle) located in the axis of the upper part of a drying chamber (Figure 13.15). Because at 1.5 kW of acoustic power the air consumption is about 160 m^3/h (Fridman, 1967), this additional air stream exiting the sound generator facilitates transportation of fine particles to the

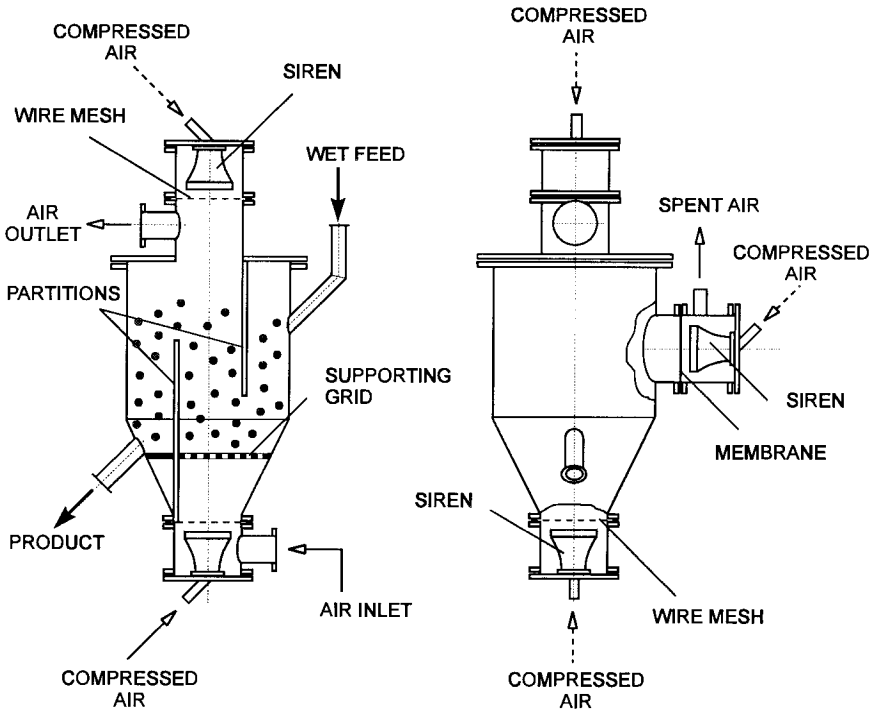

FIGURE 13.14 Sound-assisted fluid bed dryer. (From Mashkova, 1960.)

cyclone. In case of larger particles, the dryer can be equipped with an overflow discharge. Table 13.3 compares the performance of the dryer with and without sonic irradiation.

The review of available literature indicates that acoustic drying has unquestionable advantages over other drying technologies as far as drying rate (drying time) is concerned. An analysis of energy requirements done by Borisov and Gynkina (1973) has proved, however, that consumption of sonic energy per kg of water removed is roughly the same as in convective drying, assuming that the efficiency of sound generators is 100%. Since the energy efficiency of dynamic sirens is about 30% to 35% and gas-jet generators about 25%, the cost of acoustic drying is higher than that of convective drying. This limits sonic drying to expensive and otherwise hard-to-dry materials and to products for which quality issues or safety aspects offset the higher drying cost.

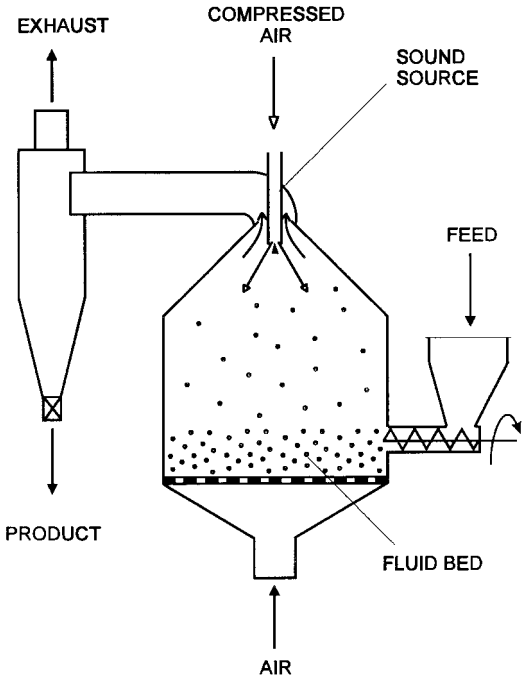

FIGURE 13.15 Design principle of sound-assisted fluid bed dryer. (From Simonyan, 1965.)

TABLE 13.3 Performance of Low-Temperature Drying in an Acoustic Fluid Bed Dryer Designed by VNIINSM

	Moisture content, kg/kg			
Material	Initial	Final	Temperature, °C	Throughput, kg/h
Quartz sand	0.037	0.0080	23	11.5
Potassium chloride	0.033	0.0032	23	7.5
Potassium chloride	0.030	0.0033	30[a]	21.0
Potassium chloride	0.019	0.0030	23	25.0
Potassium chloride	0.003	0	23	24.0

[a] With hot air stream.

Source: Adapted from Simonyan, 1965.

14

Pulse Combustion Drying

14.1 PRINCIPLE OF PULSE COMBUSTION

Pulse combustion is an emerging technology of significant potential since it is claimed to increase productivity, maximize utilization of the input fuel, and reduce pollutant emissions (Mujumdar, 1991; Maralidhara and Lokhard, 1985; Kudra and Mujumdar, 1995).

The term ''pulse combustion'' originates from intermittent (pulse) combustion of solid, liquid, or gaseous fuel in contrast to continuous combustion in conventional burners. Such periodic combustion generates intensive pressure, velocity, and to a certain extent, temperature waves propagated from the combustion chamber via a tailpipe (a diffuser) to the process volume (an applicator) such as a dryer, calciner, or incinerator. Because of the oscillatory nature of the momentum transfer, pulse combustion intensifies the rates of heat and mass transfer.

The mechanism behind the operation of a pulse combustor is a complex interaction between an oscillatory combustion process and acoustic waves that are propagated from the combustor (Figure 14.1). The process of pulse combustion is initiated when air required for combustion and fuel in the form of a gas jet or a liquid spray are drawn into the combustion chamber, mixed to

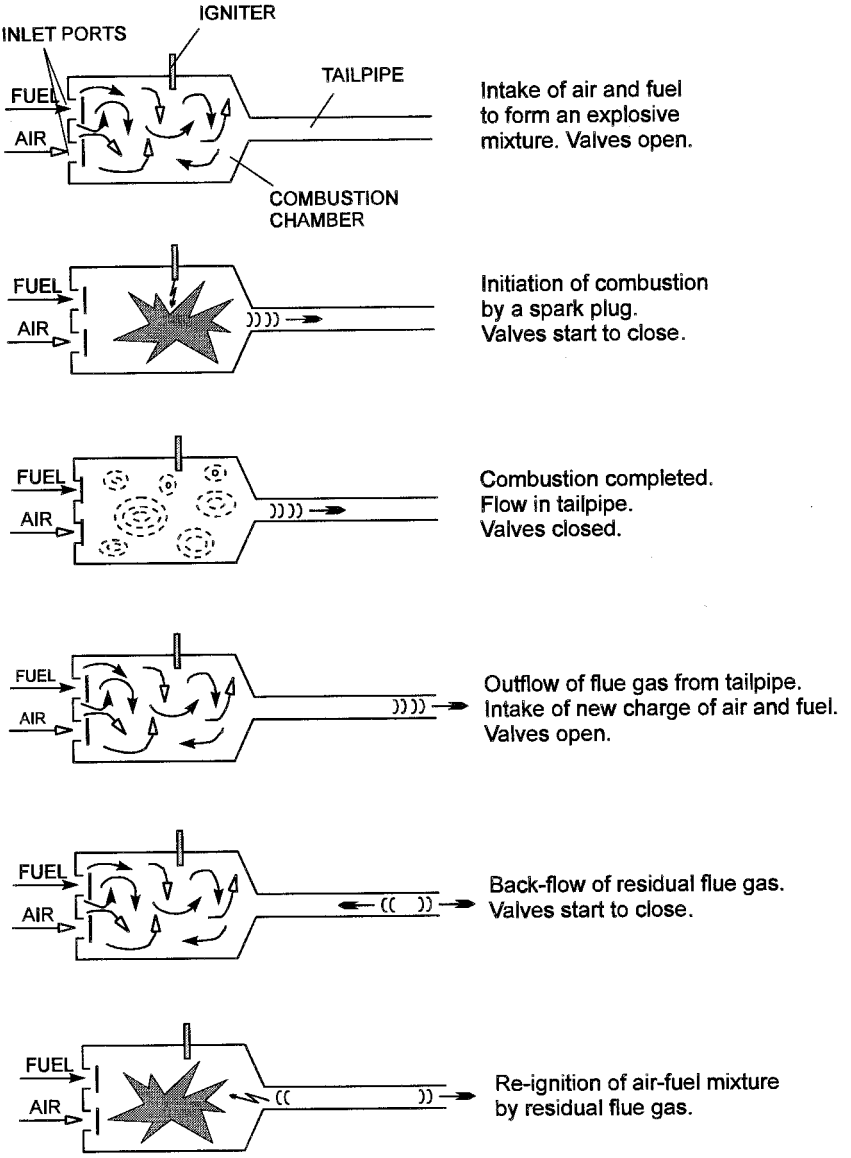

FIGURE 14.1 Principle of pulse combustion.

form an explosive mixture, ignited by a spark plug, and combust instantly in an explosionlike manner. At this moment, the air and fuel inlet ports are closed either by a valve-operating mechanism or due to the hydrodynamic action of the rapidly rising pressure. The combustion-generated pressure forces the combustion products to flow out through the tailpipe to the process volume. The exhaust of flue gases continues as long as the pressure rise in the combustion chamber is larger than the pressure drop due to the outflow of combustion products. As the hot flue gases discharge, the resulting outward momentum causes the pressure in a combustion chamber to decrease (Figure 14.2). When the pressure reaches its minimum, the inlet ports open and admit fresh fuel and air into the combustion chamber. This new charge ignites itself due to contact with remnants of hot flue gases left in the tailpipe from the preceding cycle, which reenter the combustion chamber during the minimum pressure period. These combustion cycles repeat themselves at a definite frequency, which depends on the design of the pulse combustor and characteristics of the tailpipe. Ignition of the air–fuel mixture by a spark plug is needed only during the start-up cycle as under a stable operation the mixture is reignited automatically. In addition, the start-up fan is normally shut off once self-aspiration is established.

It should be noted that thorough mixing of the combustion air with fuel is not a *sine qua non* condition for the efficient operation of a pulse combustor. In the design of the Novadyne pulse combustor, for example, a fuel distributor in the combustion chamber injects the fuel in streaks in the combustion air stream, forming a striated charge (Kitchen, 1987). For liquid fuels, striated charges have been shown to be more efficient than thoroughly mixed charges in that they improve the combustion during the start-up period. Furthermore, striated charges produce pressure and sound waves that are of larger amplitude, which is beneficial in some applications but may also have the drawback of producing excessive noise.

Typically, pulse combustors operate at frequencies from 20 to 250 Hz. Pressure oscillation in the combustion chamber of ± 10 kPa produces velocity oscillation in the tailpipe of about ± 100 m/s, so the instantaneous velocity of a gas jet at the tailpipe exit varies from 0 to 100 m/s (Keller et al., 1992). Although pulse combustors deliver flue gases at a higher pressure than the inlet air pressure, the resulting increase in stagnation pressure is relatively small. This restricts practical applications of pulse combustors to the systems where pressure drop is not critical. The amplitude of the pressure rise may vary from 10% (domestic heating applications) to 100% as for heavy-duty pulse combustors for industrial use (Kentfield, 1993). The output power for commercially available pulse combustors ranges from 70 to 1000 kW.

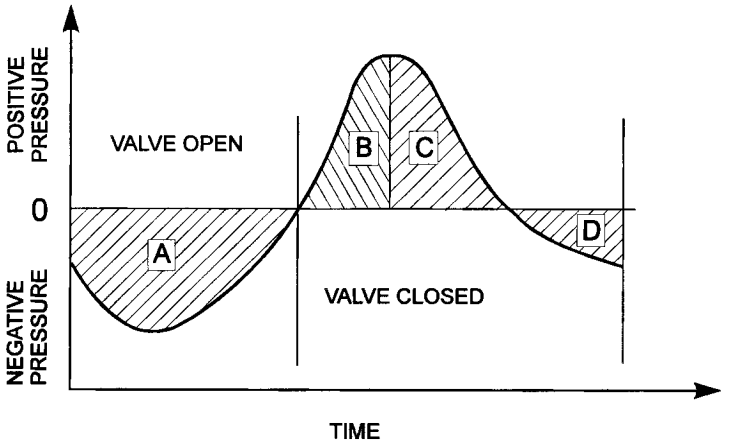

(a)

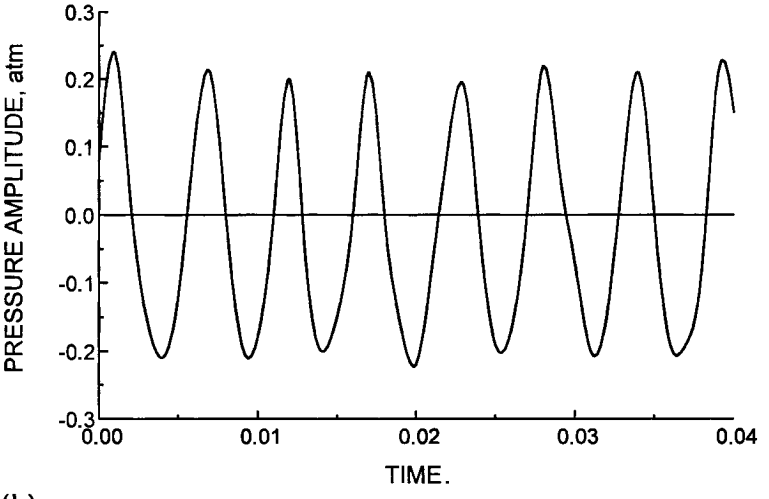

(b)

FIGURE 14.2 (a) Theoretical and (b) experimental pressure trace in a pulse combustor: A. Air and fuel enter the combustion chamber. B. Fresh charge ignited, pressure rises as combustion gases heat up, stop of air and fuel inflow. C. Combustion complete, pressure decreases as flue gases are vented. D. Momentum of exhausting gases creates negative pressure in the combustion chamber.

Numerous studies on a variety of pulse combustor designs have demonstrated that pulse combustion can offer the following advantages over conventional (i.e., continuous) combustion (Keller et al., 1992; Ozer, 1993; Stewart et al., 1991):

Increased heat and mass transfer rates (by a factor of 2 to 5)
Increased combustion intensity (by a factor of up to 10)
Higher combustion efficiency with low excess air values
Reduced pollutant emissions (especially NO_x, CO, and soot) by a factor of up to 3
Improved thermal efficiency by up to 40%
Reduced space requirements for the combustion equipment

The major disadvantage of pulse combustion systems is noise generated in normal operation, which may be a deterrent to wide industrial applications. The sound pressure level (SPL) emitted by the burner that resonates in the applicator depends on the operating pressure and frequency; the higher the operating pressure, the higher the SPL. From a technical viewpoint, large pressure amplitudes are desirable in processes such as drying, since they tend to increase the rate of heat and mass transfer and thus reduce the size of the burner required to generate a given amount of heat. However, from a practical point of view, noise emission may be a much more important design criterion than minimizing the burner size. Resonant frequency may also be critical in the design of pulse combustion systems because high-frequency noise can be far more easily attenuated than low-frequency sound.

14.2 PULSE COMBUSTORS: DESIGN AND OPERATION

14.2.1 Basic Types of Pulse Combustors

Pulse combustors may be categorized into three distinct classes according to the specific acoustic system on which their operation depends. These are the Quarter-Wave (or Schmidt) combustor, the Helmholtz combustor, and the Rijke-type combustor.

Quarter-Wave (Schmidt) Pulse Combustor

The operation of the Schmidt pulse combustor is based upon the principle of the quarter-wave sound resonator formed of a tube closed at one end. The acoustic pressure oscillations excited within this tube experience their maximum value at the closed end (at the lid) and their minimum value (which is

approximately zero) at the open end. In the Schmidt combustor, a mechanical or an aerodynamic valve replaces the lid that closes the quarter-wave resonator. Thus, the combustor may be divided into three distinct sections: the inlet, the combustion chamber, and the tailpipe. Basically, the combustion process takes place in the vicinity of the mechanical valves where the pressure oscillations are maximized and the fresh charges of fuel and air are admitted into the combustor when the pressure has reached its minimum value. Therefore, to sustain pulsation it is essential to balance correctly the duration of the mixing and firing phases so a greater portion of the combustion heat is released when the combustor pressure is near its maximum. This implies that both the mixing and firing processes must be completed within half a period of pulsation. The combustor will cease to function if the duration of either the pulsation or the mixing/firing processes is too short.

Helmholtz Pulse Combustor

The Helmholtz pulse combustor operates under the principle of the standard acoustic Helmholtz resonator in which a short, small-diameter stub (tailpipe) is attached to one of the walls of a large cavity (combustion chamber) and valves are placed at the wall opposite the tailpipe. A Helmholtz resonator operates at a frequency determined by both the volume of the combustion chamber and the length and cross-sectional area of the tailpipe. It is important to note that the pressure within the Helmholtz combustion chamber is considered to be uniform in space while the pressure oscillations become space-dependent once within the tailpipe.

Rijke-Type Pulse Combustor

This class of pulse combustors has its design based on the operating principle of the Rijke tube. The Rijke tube consists of an open channel where air and fuel are supplied through one open end and products of combustion exit the system through the other. To ensure stable operation it is necessary to complete the firing phase within the first half of the combustor length. Even more specifically, the process should occur at a distance $L/4$ from the entrance plane of the combustor, where L represents the length of the tube. Further, it has been shown that the length of the tube equals half the wavelength of the oscillation.

14.2.2 Valve and Valveless Pulse Combustors

The oscillatory pressure variation inside the combustion chamber allows us to use mechanical valves actuated by the over- and underpressure, which is especially advantageous when the low output power or high turndown ratios

are required (Buchkowski and Kitchen, 1995). An alternative design of a pulse combustor is the so-called valveless combustor in which mechanical valves are replaced with an aerodynamic ''diode'' in the form of a profiled orifice in the inlet pipe, contoured diffuser, or a shrouding duct. This aerodynamic diode admits inflow of air and fuel to the combustion chamber but prevents the backflow of flue gasses out of the combustor through the inlet section.

Based on the manner in which fuel and air charge the combustion chamber, pulse combustors are divided into two general categories: those with mechanical valves and those with aerodynamic valves (also called valveless combustors). Mechanical valves can be further divided into three types: flapper valves, reed valves, and rotary valves.

Since mechanical valves provide a physical barrier to the flow of combustion products out of the pulse combustor through the combustor inlet during the positive pressure phase of the pulse combustion cycle, the unidirectional flow is the fundamental feature of valved pulse combustors. There are, however, some problems associated with the design of mechanical inlet valves. Due to the high frequencies attained in pulse combustors, it becomes necessary to have valve inertia minimized. Another design consideration is the need to protect the valves from thermal stress that may be incurred due to the combustion process as well as from corrosion when in contact with hot flue gases. These specific design problems are amplified when considering heavy-duty pulse combustors operated at large pressure amplitude (Kentfield, 1993).

Flapper and Reed-Type Valves

In general, the types of valves incorporated in heavy-duty pulse combustors are reed valves made from thin-sheet spring-steel (Figure 14.3a). The spring action of reed valves is such that the valves normally shut are sprung lightly. In order to ensure vigorous mixing of fuel and air, the fully open flow area of the inlet reed valves is considerably less than the cross-sectional area of the combustion zone. At present, one major problem often encountered with reed-type mechanical valves is fatigue failure.

Valves that are not controlled through spring action but instead move freely are called flapper valves (Figure 14.3b). The basic design considerations are that the flappers must move rapidly enough to open and close the flow passages at the burner operating frequency. In addition, the valve must be able to withstand the maximum pressure differences imposed and yet open with only a small pressure difference. By opening in response to pressure differentials, flapper valves, in effect, control the amount of air flowing into the combustor during each cycle and do so in such a manner that the air flow is sufficient to meet the air/fuel ratio required to burn the charge.

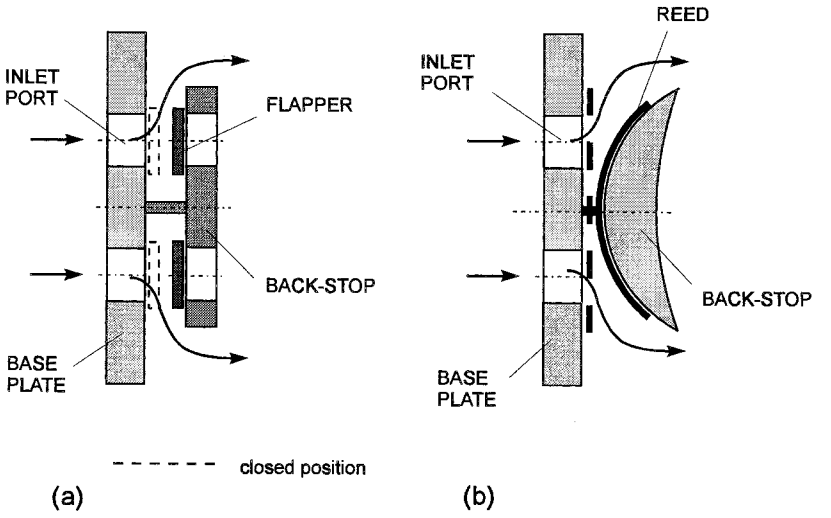

FIGURE 14.3 Mechanical valves: (a) flapper type and (b) reed type.

Generally, in gas-fueled pulse combustors separate gas and air valves are situated in their respective inlet pipes thus set back from the combustion chamber. In the case of pulse combustors that burn liquid fuels, fuel valves are generally not present; the liquid fuel is admitted downstream of the air valve. In some systems, however, the fuel is premixed with air and in such instances a thermal-protection device is required between the valve and the combustion chamber.

Rotary Valves

Rotary valves are closely related to flapper valves in that they are both designed to seal the inlet section during the part of the combustor cycle when the pressure within the chamber is greater than atmospheric pressure (i.e., during the positive pressure phase). The rotation of the valve determines the running frequency of the pulse combustor and, therefore, an adequate ''feedback system'' is required to synchronize the rotation of the valve with the resonant frequency of the burner. The speed of the valve, which influences the resonant frequency, is determined through the sensing and processing of pressure pulses occurring within the burner.

There are many advantages offered by rotary valves. Since the design of these robust valves is independent of the combustor design, one rotary valve

is able to accommodate a wide range of combustor frequencies and firing rates. Other important features of rotary valves include durability, flexibility of use, and resistance to oil and dirt accumulation.

The general design of a rotary valve is composed of two plates: a motor-driven ''butterfly-shaped'' rotating plate and a stationary plate possessing two slots that are 180° apart from each other. The air for combustion passes through the valve, perpendicular to the direction of rotation, and enters the burner. The height and width of the two slots on the stationary plate determine the area for airflow through the rotary valve. The other design of the rotary valve is based on three coaxially disposed sleeves with a plurality of slots in their lateral surface (Figure 14.4). When rotated by a motor with controllable speed, the slots periodically admit the intake air at the rate required for optimum combustion.

While discussing the types of valves used in pulse combustors, a distinction should be made between the words ''pulsed'' and ''pulse,'' which are often used synonymously to describe combustors operated in a pulse mode.

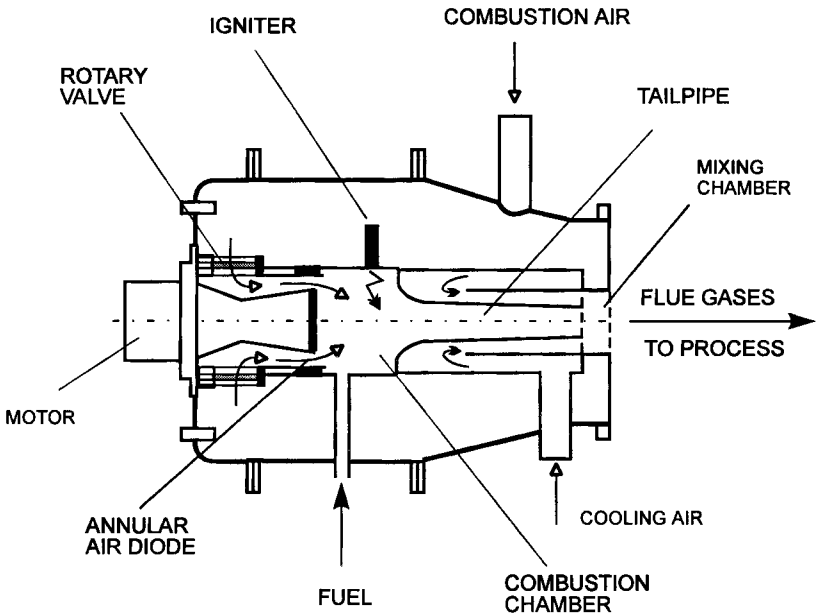

FIGURE 14.4 Design principle of pulse combustor with rotary valve. (From Lockwood, 1987.)

According to Kentfield (1993), a pulse combustor is a combustion-driven device with self-aspirating feature, and this effect is achieved as a consequence of the internal unsteady flow events. In contrast, a pulsed combustor is a device with cyclic but nonresonant combustion as dictated by wave events. Pulsed combustors usually operate at a much lower than natural frequency, often controlled by an ignition, fuel injection, or a valve sequence. Therefore, valveless or flapper valve combustors fall into category of pulse combustors while mechanically driven valves (e.g., rotary valve) used to control either air or fuel inflow, flue gas outflow, or both should be categorized as pulsed combustors, unless the operation of a mechanical valve is controlled by resonant phenomena in a feedback mode. Such a design is known as a frequency-tunable pulse combustor.

One of the possible designs of a frequency-tunable pulse combustor takes advantage of the natural nonlongitudinal acoustic modes of the processing chamber to which the combustor is coupled (Zinn, 1983). In order to obtain the maximum benefit from the acoustic oscillations of the process chamber, the pulse combustor is tuned to one (or more) of these acoustic modes by modulating the flow of fuel to the combustion chamber. This modulation of fuel flow may be accomplished by exciting acoustic resonance within the fuel line or by periodic interruption of the fuel flow by use of a rotary valve. Placement of a valve in the exhaust flow to regulate the exciting combustion gases from the process chamber also assists in tuning the combustor.

The frequency-tunable pulse combustor consists of a tube comprised of a combustion zone and an exhaust zone. It is within the combustion zone that the reaction between fuel and air occurs, causing heat to be released and thereby exciting an acoustic wave in the combustor. Separate air and fuel inlets are present to supply the combustion zone with the necessary reactants. Rotary valves are used in the Sonotech system to control fuel and airflows into the combustion chamber (Lockwood, 1987). The resulting hot combustion gases are freely exhausted from the combustor.

The acoustics of the combustor may be altered in such a manner as to provide a selectively variable (or frequency-tunable) pulsating combustion. There exist several methods by which the acoustic characteristics of the combustor may be altered in order to match the optimum frequency of the processing chamber. An axially translatable interfitting sleeve is present, and by moving it, the length of the combustor tube can be increased or decreased. Thus, the length of the wave within the combustor may be changed, thereby allowing for tuning. The length of the combustor can also be changed by means of the axially translatable back wall of the combustor. The location of the fuel injector may be adjusted in order to reposition the combustion zone to a more preferred location within the pulse combustor.

Aerodynamic Valves

Aerodynamic valves employ the fluid mechanical properties of specially designed inlets to act as a physical barrier to the backflow of combustion products out of the combustor through the inlet section. The main advantage of aerodynamic configurations is lack of valves and moving parts so the risk of mechanical breakdown or failure is eliminated. This is a key consideration for heavy-duty pulse combustion burners where the inlet section undergoes severe operating conditions.

The most common design concept allows the lowest possible resistance to inflow while simultaneously maintaining the greatest possible resistance to outflow. An inlet arrangement such as this is often referred to as a fluid diode. Fluid diodes are, of course, inferior in performance when compared to mechanical one-way valves due to the fact that backflow cannot be completely prevented. One mechanism known to limit the amount of backflow is the presence of a nonuniform cross-sectional area. A tapered inlet that diverges gradually toward the combustion chamber initially accelerates the entering stream of air and subsequently diffuses it before it enters the combustion chamber; in such a manner, minimum losses are incurred. Such a tapered inlet acts effectively as a nozzle during backflow and thus may serve to minimize it. Figure 14.5 presents, as an example, the schematic of a reverse-flow, pressure-gain, valveless pulse combustor designed at the University of Calgary. Details of the design of valves and pulse combustors can be found elsewhere (Kentfield, 1993; Speirs, 1989; Olorunmaie and Kentfield, 1989).

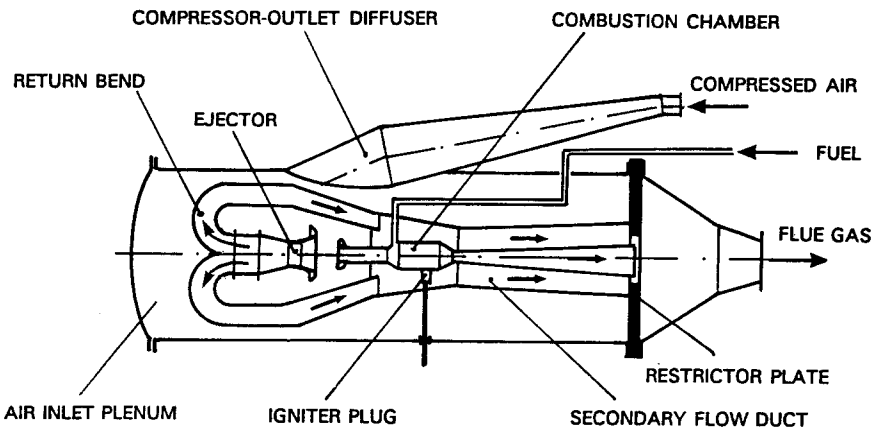

FIGURE 14.5 Configuration of University of Calgary pressure-gain valveless pulse combustor. (Courtesy of Kentfield, J. A. C.)

14.3 PULSE COMBUSTION IN DRYING

In general, pulse combustion drying can be performed either within the gas jet exiting the combustion chamber or in a separate cavity (also called an applicator or a processing volume) that serves as a sound resonator. In the later configuration, the typical pulse combustion dryer consists of a combustor and a drying chamber where the hydrodynamic action of pressure and velocity waves enhances drying rates (Buchkowski and Kitchen, 1993; Kudra et al., 1994). Under certain conditions, these pressure waves can be favorably amplified by an acoustic resonance. Because the primary function of a pulse combustor in this configuration is to excite large-amplitude velocity/pressure fluctuations, the pulse combustor may supply only a fraction (10% to 30%) of heat required for evaporation, which opens retrofit applications to existing rotary, band, spray, and other dryers. To excite enhanced pulsation in a drying chamber, the operating frequency of the pulse combustor must match the frequency of one of the natural acoustic modes of the process volume. When this condition is satisfied, both pulsations are in resonance, and the process is called ''resonance-driven'' (Zinn et al., 1991; Bramlette and Keller, 1989). The energy input from the pulse combustor in the resonance-driven processes could be relatively low. It should, however, exceed a certain threshold value because of energy dissipation.

In practice, the downstream volumes do not affect the acoustic frequency of the pulse combustor provided that the tailpipe is long enough to secure backflow of combustion products. Conversely, the natural acoustic frequencies of the applicator depend on the chamber geometry and material load and may vary in time and space with the operating conditions (e.g., temperature, moisture content, or air humidity). Excluding a trial-and-error method in a pilot-scale apparatus, the best method to achieve resonance-driven processing is to use a frequency-tunable burner, which can actively follow the variations in the amplitude of pressure pulsation in the applicator (Technical Bulletin, 1992; Zinn, 1988). Such a process known as a Sonotech's pulse combustion technology based on the frequency-tunable pulse combustor has been retrofitted to the rotary kilns and spray dryers, and pilot-tested for water evaporation, limestone calcination, and waste incineration (Figure 14.6) (Ozer, 1993; Richards, 1994).

An alternative mode of pulse combustion drying is to disperse liquid material within a pulsating jet of flue gases, which is especially advantageous when drying biomaterials. Figure 14.7 presents a block diagram of the Unison™ Pulse Combustion Dryer where the sound energy generated in a pulse combustor is used primarily for atomization of the liquid feed, which finally accelerates convective drying due to the extended surface area of the liquid

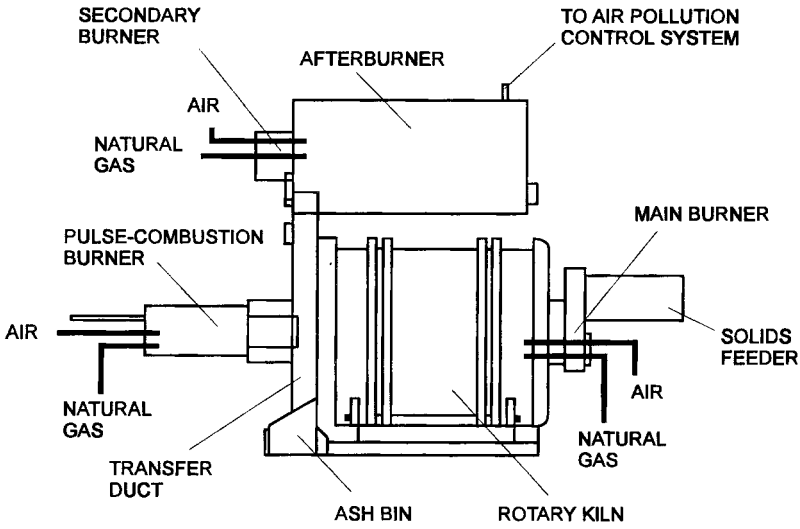

FIGURE 14.6 Rotary kiln with frequency-tunable pulse combustor. (From Richards, 1994.)

spray (Keller et al., 1992; Ozer, 1993; Stewart et al., 1991; Ozer et al., 1993; Zbicinski et al., 1999). The liquid or pasty feed material is introduced into a gas stream from a pulse combustor in the feed chamber situated at the top of the drying chamber. The dryer and product collection system is held under a slight negative pressure by an exhaust fan to eliminate possible leakage. Gas temperature at the dryer inlet is controlled by the fuel feed rate to the combustor while the outlet temperature is adjusted by varying the material feed, which generally floats according to the evaporative load. Normal operating temperatures for the pulse combustor are in the range from 810 to 1470 K. The frequency range extends from 60 to 200 Hz (typically 125 to 150 Hz), and the sound pressure level is up to 180 dB. The maximum power output of one of the current units is 235 kW, which allows evaporation of up to 300 kg H_2O/h with drying air supplied at 600 kg/h (Keller et al., 1992; Ozer, 1993). The dryer can handle slurries (with solids up to 2 mm in diameter and up to 10 mm in length) with viscosity up to 1600 cP as well as solutions with viscosity up to 300 cP. If desired, nozzles can be built-in to preatomize highly viscous liquids. The particle-size distribution is finer than that normally obtained in a spray dryer using conventional nozzles and varies from 30 to 60 μm. The residence time of dispersed material in the ''hot zone'' of flue gases is less

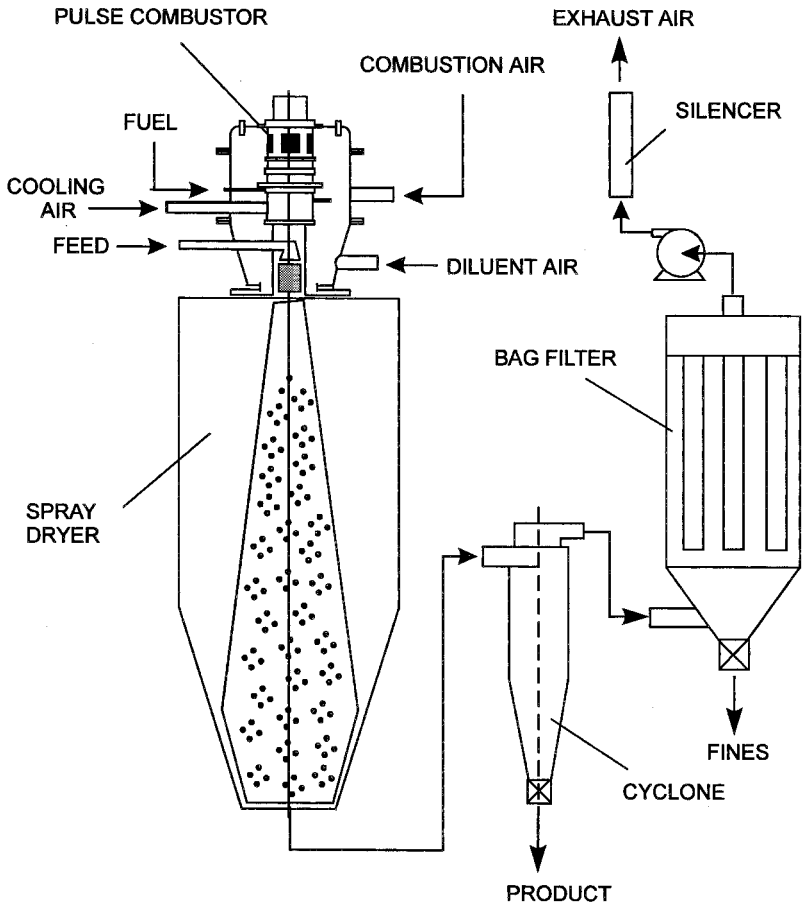

FIGURE 14.7 Pulse combustion spray-drying system. (From Ozer et al., 1993.)

than 5 milliseconds, which allows the drying of even thermally-labile products. Some materials dried in the Unison™ pilot-scale pulse combustion dryer that compare well in the products from a spray dryer on the product quality and unit cost bases include animal antibiotics, vitamins, yeast, spices, vegetable protein, fibers, whole eggs, food colorings, caramel, biopesticides, acrylic latex, flame retardants, etc. (Keller et al., 1992; Kentfield, 1993). Performance data of the pulse combustor spray dryer for selected products are given in Table 14.1.

TABLE 14.1 Comparison of Unison Pulse Combustion Dryer with Conventional Spray Dryer for Selected Materials

Material	Conditions	Spray dryer	Unison™ dryer
Antibiotics	Inlet temperature, °C	400	704
	Outlet temperature, °C	127	104
	Product moisture content	Base	Same
	Atomization	Rotary	By pulse
	Air consumption	Base	20% Less
	Throughput	Base	Up to 11% higher
Vegetables	Inlet temperature, °C	232	704
	Outlet temperature, °C	82	88
	Product moisture content	Base	Same
	Atomization	Nozzle	By pulse
	Air consumption	Base	30% Less
	Flavor	Base	2–3× More flavorful
Protein	Inlet temperature, °C	300	840
	Outlet temperature, °C	82	90
	Product moisture content	Base	Same
	Atomization	Nozzle	Nozzle
	Air consumption	Base	25% less
	Protein level	Base	Same
Acrylic latex	Inlet temperature, °C	204	760
	Outlet temperature, °C	71	77
	Product moisture content	Base	Same
	Atomization	Nozzle	By pulse
	Air consumption	Base	33% Less
Whole eggs	Inlet air temperature, °C	260	871
	Outlet air temperature, °C	79	82
	Product moisture content	Base	Same
	Atomization	Nozzle	By pulse
	Air consumption	Base	40% Less
	Protein level	Base	Same

Source: Courtesy of J. O. Keller.

The advantage of a strong oscillating hot gas jet from a tailpipe can also be taken to promote the dispersion of pasty and particulate materials (Buchkowski and Kitchen, 1995; Buchkowski, 1996; Buchkowski, 1999; Gray, 1987; Technical Bulletin, 1999). Figure 14.8 shows flow diagrams of two prototype pulse combustion dryers designed by Novadyne Ltd. (Canada). In a flash dryer configuration, the unit consists of a pulse combustor, a pneumatic

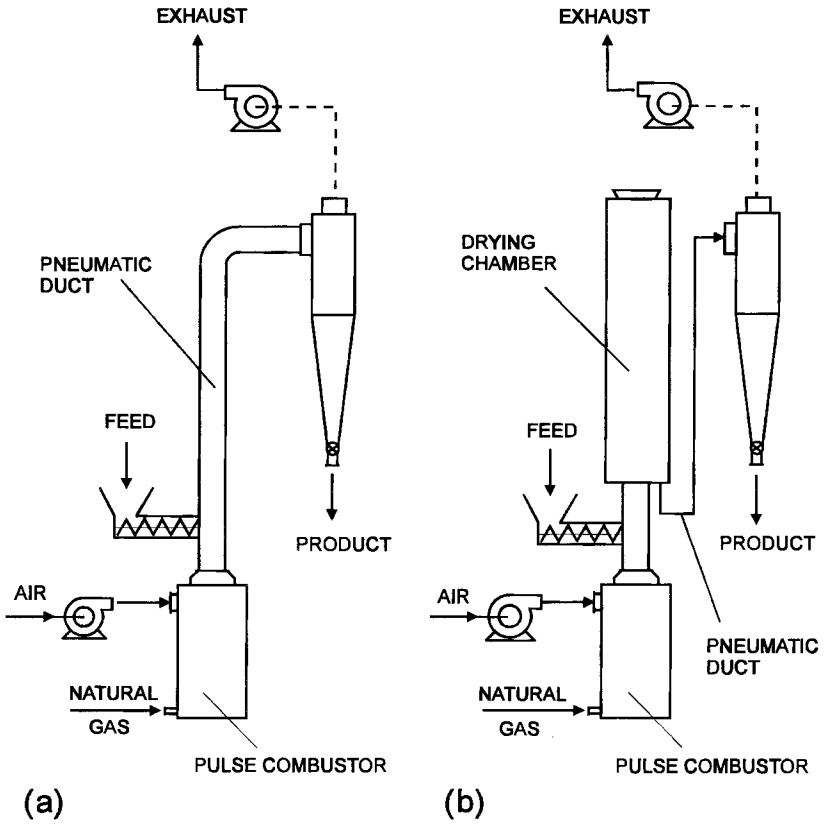

FIGURE 14.8 Flowsheets of (a) the pulse combustion flash dryer and (b) pulse combustion dryer. (Courtesy of Novadyne Ltd., Hastings, Ontario.)

duct that extends from the tailpipe of the pulse combustor, and devices for material feed and discharge. The pulse combustor uses a self-actuated flapper valve and its operating frequency is about 70 Hz. The rated capacity of the combustor equal to 300 kW with turndown ratio 3:1 offers an evaporative capacity of about 275 kg/h of water. Wet particulate material such as sawdust, hog fuel, corn fibers, or spent coffee grounds is injected directly into the tailpipe of the pulse combustor where it is finely dispersed and dried intensively due to high turbulence of the hot combustion gases and large temperature difference. Finish drying is accomplished in a pneumatic duct. A series of drying tests proved that the thermal efficiency of a pulse combustion flash

dryer is similar to that of conventional flash dryers but electrical power requirements are lower by 40% to 50% since motors tended to be smaller and some material handling equipment (e.g., slinger) was eliminated (Buchkowski, 1999). Table 14.2 provides a sample characteristic of a pulse combustion dryer for green hardwood sawdust and pulverized hog fuel.

As some materials require longer residence times, the flash dryer was further modified by replacing the pneumatic duct with a pressurized drying chamber connected directly to the tailpipe of the pulse combustor (Figure 14.8b). In this configuration, the material is forced vertically by the thrust of the pulse combustor into the drying chamber where most of the water evaporates. This makes it possible to take advantage of the most beneficial aspects of the pulse combustor; that is, a high momentum of the exhaust thrust and extreme turbulence and gas pulsation in the exhaust zone, which intensify heat and mass transfer processes. The gas–solid suspension from the drying chamber is then drawn to the cyclone through a conveying duct where water evaporation to the final moisture content takes place. In case of drying sludge or extremely wet particulates, a fraction of the dry product collected in a cyclone can be backmixed with a feed to reduce initial moisture content and improve flowability of the material entering the dryer. For a higher degree of drying, the product from the cyclone can be returned to the drying column.

The dryer has provisions to recuperate heat by redirecting exhaust gases from the cyclone to the pulse combustor for cooling the tailpipe; to preheat

TABLE 14.2 Test Data for Wood Waste Dried in a Pulse Combustion Flash Dryer

Throughput (per wet material)	590 kg/h
Initial moisture content	45–55% w.b.
Final moisture content	10–20% w.b.
Temperature in the tailpipe	1040°C
Exhaust gas temperature	104°C
Combustion airflow rate	306 m^3/h
Flue gases airflow rate	1,275 m^3/h
Heat input	237 kW
Evaporation rate	204 kg/h
Unit heat consumption	4,187 kJ/kg H_2O
Electrical energy consumption	0.019 kW/kg H_2O
Backmixing fraction	40%

Source: Courtesy of Novadyne, Ltd., Hastings, Ontario.

the combustion air; and to quench the primary flue gases to reduce drying gas temperature.

The pulse combustion dryer is flexible enough to handle not only homogeneous feeds but also mixtures of fine and coarse particles (Table 14.3). For example, the 25-mm clay fiber lumps that are difficult to break apart by hand were largely disintegrated by the pulsating action of flue gases. In the case of sawmill residues, larger pieces of wood and bark (up to 50 mm in length) were carried through the dryer along with fine sawdust. The dryer can also handle sticky materials such as primary sludge #2, but mixing with sawdust or backmixing with dry product may be required for smooth operation. As seen from Figure 14.9, the unit heat consumption of the pulse combustion dryer is in the same order as flash dryers, which are similar in operation. The

TABLE 14.3 Characteristics of Selected Feed Materials Tested in Novadyne Pulse Combustion Dryer

Material	Moisture content, % w.b.	Max. size, mm	Description
1. Paper mill primary wood sludge #1	80	3	Fine, nonsticky granules
2. Paper mill primary wood sludge #2	68	20–25	Fine sticky particles forming clumps easily
3. Mixture of:			
Paper mill secondary sludge, and	85	0.5	Liquid sludge mixed with sawdust in a ratio 1:0.36 by weight
Sawdust	60	5	Appearance is that of very wet sawdust
4. P&P de-inking sludge #1	52	25	Mixture of clay and fine fibers dewatered by a screw press. Forms clumps difficult to break apart by hand
5. P&P de-inking sludge #2	42	25	Similar to No. 4 above
6. Sawdust	44	5	Coarse mill sawdust with pieces of wood and bark up to 50 mm in length of
7. Spent coffee grounds	60	0.05	Fine, nonsticky particles

Source: Buchkowski, 1999.

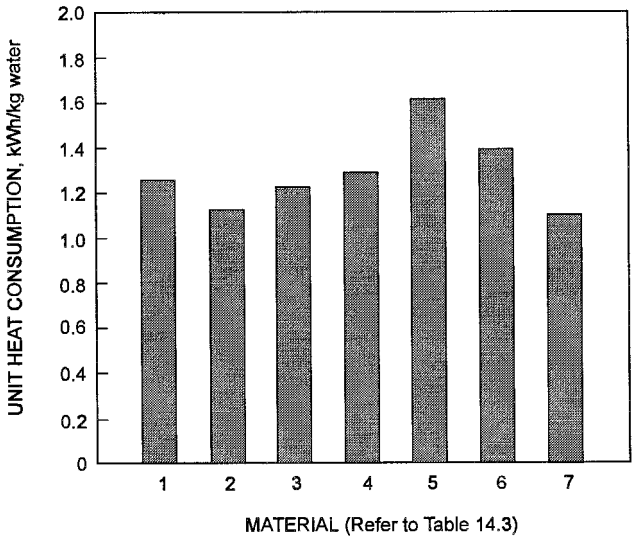

FIGURE 14.9 Unit heat consumption by a pulse combustion dryer (Fig. 14.8b). (From Buchkowski, 1999.)

heat consumption may be reduced by about 10% as up to half of the fresh air could be replaced with hot recycled gases.

Figure 14.10 presents another design of a pulse combustion dryer (Pulse-Dryer®), which combines dispersion/drying in a tailpipe of the combustor and finish drying/separation in a primary cyclone. Air for combustion (and optionally quenching flue gases) is introduced into the system through an air column and is drawn into the combustor room and around the pulse combustor. The room can accommodate either one or more valveless pulse combustors operated at 250 Hz. Raw material is fed directly to the drying cone formed from a Venturi-shaped tailpipe of the combustor. Dry product and water vapor are blown from the drying cone into the primary collector, where the heavier particles are separated by gravity. Vapor and fine particles continue through the system to the cyclone. Dry product falls out of the system through airlock valves while vapors are drawn through the spray tower before being vented to the atmosphere. The required moisture content is maintained by the air vent temperature, which controls the material feed rate. The Pulse-Dryer can handle products as diverse as fishmeal, brewer's yeast, whey, various manure, sewage sludge, fruit and vegetable waste, kaolin clay, and plating wastes. Particle size may vary from submicron to about 6 mm, and moisture content may be as

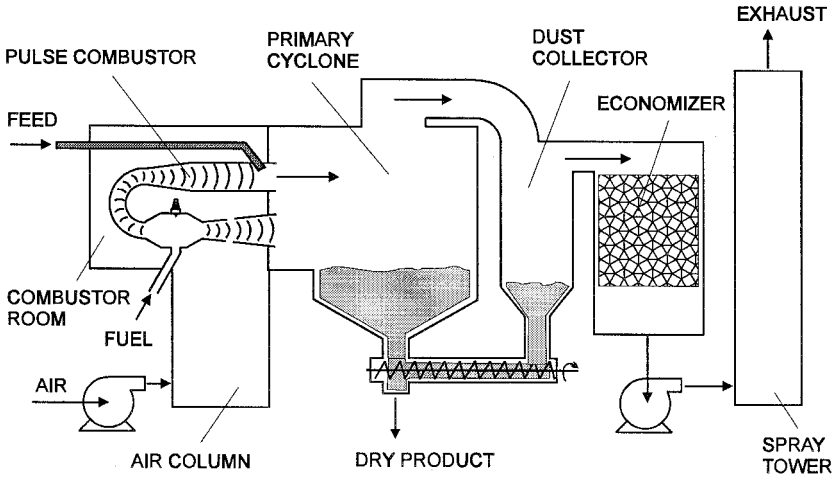

FIGURE 14.10 Basic configuration of the Pulse-Dryer. (Courtesy of Pulse Drying Systems, Inc., Portland, Oregon.)

high as 99% w.b. Regardless of the feed rate of the raw material, the system removes a nearly constant amount of water per hour from the feedstock, equal to approximately 1225 kg/h per combustor. A single module dryer shown in Figure 14.10 can accommodate up to two pulse combustors. The number of dryer modules can be increased as necessary to configure a drying system with required capacity. Table 14.4 shows typical operating characteristics of the Pulse-Dryer when used for industrial plating waste treatment.

The advantageous drying rates result from the impact of the sound pressure waves, which separates the surface moisture from the feed material by breaking the cohesion between the water molecules and solid particles. This greatly increases the surface area of disaggregated particles as well as causes rapid evaporation of water that was scrapped from the solid surface and atomized into many fine droplets. The average energy consumption is claimed to be about 3370 kJ/kg of water evaporated, but it may be as low as 2950 kJ/kg for finely dispersed materials having mostly surface water such as kaolin clay, metal oxides, or calcium carbonate (Technical Bulletin, 1999). Depending on the material to be dried, gas temperatures in the primary cyclone are maintained around 80 to 110 degrees Centigrade, or just above the dew point of the gas–vapor mixture passing out of the dryer. This thermal energy can be recovered from exhaust gases in a gas-to-gas heat exchanger or in a direct gas-to-water heat exchanger (scrubber) providing hot water for wash-

TABLE 14.4 Characteristics of Pulse-Dryer for Industrial Plating Waste

Parameter	Description
Composition:	
Aluminum hydroxide	23%
Iron hydroxide	19%
Calcium hydroxide	25%
Calcium ferrite	12%
Other[a]	21%
Raw material feed	13,600 kg/day to 32,000 kg/day at 10% solids to 15% solids as delivered to the dryer from two belt presses
Dry product	1,640 kg/day to 3,900 kg/day at 10% moisture
Water removed	12,000 kg/day to 28,800 kg/day
Unit heat consumption	3,373 kJ/kg
System size	2 pulse combustion dryers
Operators required	1 man per shift
Fuel required	Natural gas
Heat consumption	7,380,000 kJ/h
Operating hours	12 hours/day to 24 hours/day
Sound level	70 db when the complete system is housed in a sound enclosure
Space requirements	4.8 m wide, 11 m long, 5.5 m high
Materials of construction	6.5 to 25 mm mild steel plate
Electrical requirements	440 V, 3-phase, 60 Hz power at 50 kW
Material temperature (in primary cyclone)	52°C
Product temperature (mixture of material from primary cyclone and dust collector)	38°C
Temperature of exhaust gases	74°C

[a] Nickel, copper, chromium, selenium and zinc hydroxides plus insolubles made up of silicates, aluminates, and phosphates of iron and calcium.
Source: Courtesy of Pulse Drying Systems, Inc., Portland, Oregon.

down or for uses in other parts of the plant. The high temperatures on the exterior of the combustor chamber offer an optional radiant heat recovery. When the pulse combustor is equipped with a steam jacket, the unit is capable of producing live steam at around 130 kg per hour.

Because the residence time in the drying cone is measured in thousandths of a second and the exit temperature of most products averages 52°C,

the risk of thermal degradation is practically eliminated. At the same time, however, much longer residence time in combination with relatively high temperatures in the primary cyclone ranging from 80 to 120°C creates conditions to reduce the content of pathogen microorganisms (Table 14.5). Also, the oxygen concentration in the dryer is less than 1%, which practically eliminates the explosion and fire hazard and minimizes product oxidation.

The only design of the pulse combustion fluid bed dryer appears to be the one patented by Lockwood (1983). To avoid attenuation of the pulsating gas stream by a perforated gas distributor, the flue gases from a pulse combustor enter the bed of particulate material just above the solid floor, which rotates under a plurality of ducting blades adjacent to the floor. The radially spaced blades are fixed to the central hub at one end and to the inner annular baffle at the other one (Figure 14.11). The space between the baffle and dryer wall forms a gas manifold connected to the tailpipe of a pulse combustor. Each

TABLE 14.5 Characteristics of Pulse Dryer for Sewage Sludge Processing

	Sludge A		Sludge B	
Parameter	Before drying	After drying	Before drying	After drying
Solids content, % mass	12.4	90.6	3.3	88.8
Volatile solids, % mass	41.4	53.4	47.1	55.9
TKN, mg/kg	32,540	29,540	57,060	29,260
NH_3—N	8,559	2,117	21,100	2,530
T—PO_4—P	53,760	34,450	53,650	27,760
Pathogens:				
Salmonella	Negative	Negative	Negative	Negative
Shigella	Negative	Negative	Negative	Negative
Pseudomonas spp., #/ml	24,000	750	240	1,100
Total coliforms, #/ml	>240,000	>30	9300	36
(*E. coli*), #/ml	>240,000	>30	930	36
Unit heat consumption, kJ/kg of dry solids	19,000		66,500	
Design capacity:				
Feed rate	160 tons/day digested sludge dewatered by belt press to 20% solids			
Throughput	40 tons/day at 80% mass solids			
Plant size	302,000 m^3/day of activated sludge			

TKN: total Kjeldahl nitrogen; NH_3—N: ammonia nitrogen; T—PO_4—P: total phosphate phosphorous.

Source: Courtesy of Pulse Drying System, Inc., Portland, Oregon.

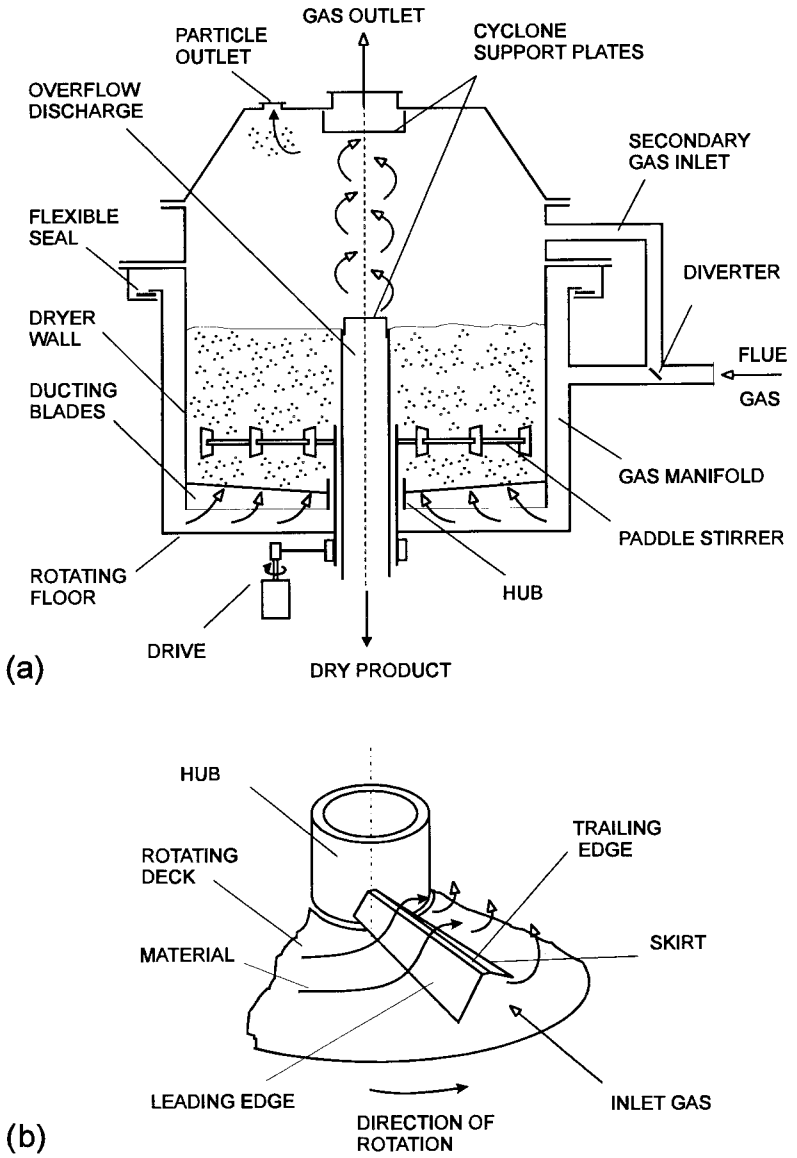

FIGURE 14.11 Pulse combustion fluid bed dryer: (a) design principle, (b) partial perspective of the ducting blade. (From Lockwood, 1983.)

ducting blade is inclined in the direction of floor rotation to provide a leading edge and a raised trailing edge located further above the floor that is the leading edge. The leading edge is sufficiently close to the floor to sweep the material off the rotating floor and pass it along the top of the blades over the trailing edge. Streams of pulsating flue gases that flow upward from under the trailing edge fluidize the bed of particles. To improve the gas distribution through the fluidized bed, each ducting blade includes a tapered skirt depending from the trailing edge at an angle toward the floor. The skirt is widest near the baffle, tapers along the blade, and narrows to a point at the hub. The skirt restricts dissipation of flue gases near the baffle and thus provides a more even distribution along the blade in the radial direction.

Although the incoming flue gases flow essentially from the periphery of the floor toward its center, they also swirl concurrently with the floor rotation due to the sloping of the blades and tangential connection of the tailpipe with the gas manifold. Hence, the gas streams passing through the bed have both radial and tangential velocity components. This results in a waving and spiraling of the bed, which greatly reduces channeling and dead zones. To enhance swirling motion, an auxiliary gas inlet is tangentially located at the dryer wall above the fluidized bed. An adjustable bypass diverts the flow of gas from the auxiliary inlet to the gas manifold for controlling the strength of the swirl. In addition, a pair of cyclone support discs located above the overflow discharge and below the gas outlet enhances the swirling motion of gases in the drying chamber.

Wet material is fed into the dryer through an inlet in the sidewall so the wet particles drop into an outer portion of the bed. Several stirring arms with inclined paddles spread the material uniformly around the bed and facilitate fluidization by mechanical mixing. Dry product is removed from an overflow discharge through the floor. Swirling exhaust gases carry fine particles through an outlet in the top of the dryer. To our knowledge, the design presented here is not yet commercialized.

An analysis of the reported data shows that the productivity of industrial dryers is increased if the drying is performed in a pulsating flow. This is true since the drying time depends on the rates at which heat and moisture are transferred to and from the wet material, respectively. Since pulsation of flue gases tends to increase these rates of heat and mass (moisture) transfer, the application of pulse combustion in drying increases the productivity of such dryers by decreasing the required residence time in a drying chamber and thus allowing for more material to be dried in a given time. Aside from decreased drying time, there are a few other advantages offered by pulse combustion dryer systems. Such dryers are thermally efficient and seem to be effective in

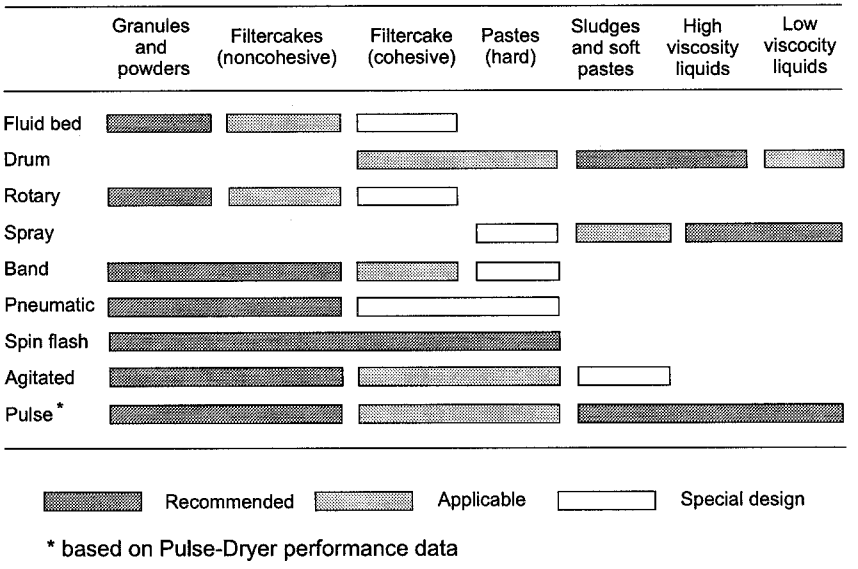

FIGURE 14.12 Application chart for selected dryers.

the drying of a wide range of materials including low- and high-viscosity liquids and pastes (Figure 14.12). Since the residence time of the product in the drying section is extremely short, little chemical alteration of the product may be expected and this fact enables drying of biomaterials and temperature-sensitive chemicals. Aside from enhanced heat and mass transfer rates due to velocity pulsation, the larger fraction of input energy is transferred to the wet particles from flue gases in pulse combustion drying due to higher heat transfer rates. This results in an increased thermal efficiency, which translates into lower fuel consumption. An overview of the available data indicates that as compared to classical (continuous) drying, pulse combustion drying enables one to:

Increase the drying rate by a factor of 2 to 3
Reduce unit air consumption by 3% to 40%
Eliminate property (e.g., temperature, concentration, moisture content) distribution within the dryer, which improves the product quality
Lower gas and product temperatures during processing
Handle sticky materials that form lumps or aggregates without mechanical mixing or disintegration

Disperse liquids, slurries, and suspensions without the need for a disk atomizer or high-pressure nozzle
Lower air volumes discharged to the atmosphere
Eliminate the air blower from the system

Besides the above advantages, an added benefit of pulse combustion drying is its contribution to environmental protection. The rapid combustion allowing very little time for the formation of nitrogen oxides, and lower peak temperatures as compared to alternative methods of combustion, result in extremely low NO_x emissions from the pulse combustors (Figure 14.13). This is especially advantageous in drying foods and bioproducts provided the pulse combustor is fed with no sulfur-containing fuels such as propane or natural gas (Kudra, 1998; Kudra, 1999).

Recent studies on pulse combustion indicate that design of the combustion chamber and the geometry of a combustor-dryer system may affect the level of noxious emission. Noticeably lower concentrations of CO, NO, and NO_x were obtained for those combinations of the combustor volume and lengths of the tailpipe that provide smoother and sinusoidal pressure fluctuations (Zbicinski et al., 1999).

Concerning other gaseous emissions, the high temperatures of combustion gases when in contact with the wet material fed into the tailpipe may

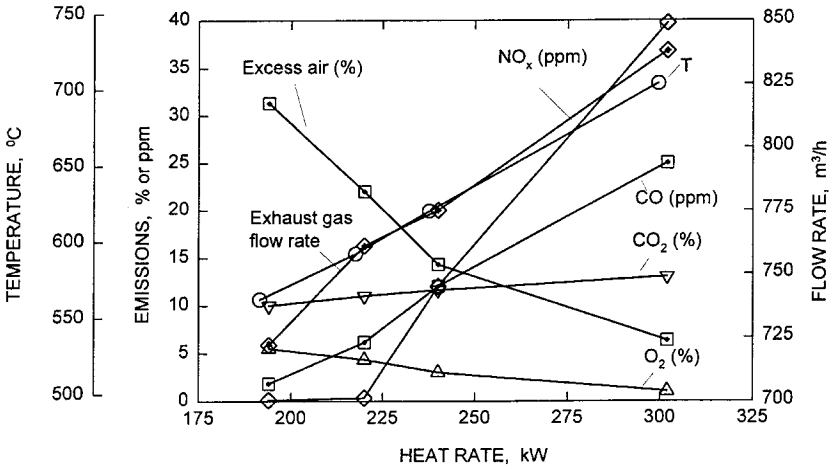

FIGURE 14.13 Typical emissions from pulse combustor. (Courtesy of Novadyne Ltd., Hastings, Ontario.)

result in destruction of odor, toxic contaminants, and other volatile organic compounds (VOC) by thermal dissociation or free radical oxidation reaction (Rafson, 1998; Guy et al., 1997). From the other point of view, odor concerns are lessened in pulse combustion dryers where wet material is injected directly into the tailpipe. This is because of extremely short residence time (fractions of a second) as well as the effect of evaporative cooling, which keeps the product temperatures sufficiently low not to release volatile substances.

15

Heat-Pump Drying

15.1 INTRODUCTION

For years heat pumps have been known as an efficient method of energy recovery. Their ability to convert the latent heat of vapor condensation into the sensible heat of an air stream passing through the condenser makes them attractive in drying applications especially when combined with the ability to produce well-controlled drying conditions. For these reasons heat-pump drying has been used for decades in wood kilns to dehumidify air and control lumber quality (Rosen, 1995). Following the general trend to improve product quality and reduce energy consumption, many researchers have acknowledged the specific features of heat pumps, which has resulted in the rapid growth of both theoretical and applied research on heat-pump drying (Table 15.1).

15.2 THE PRINCIPLE OF HEAT-PUMP OPERATION

The principle of the heat pump is based on the same thermodynamic cycle as that used in the refrigeration technique. The term ''heat pump'' originates from the operation of a standard heat pump, where the low-temperature heat

TABLE 15.1 Recent Studies in Heat-Pump Drying

Source	Location	Application(s)
Chou et al. (1998); Chua et al. (1998)	Singapore	Agricultural and marine products (mushrooms, fruits, sea-cucumber, and oysters)
Carrington et al. (1996a; 1996b); Sun et al. (1996)	New Zealand	Timber and wood drying
Prasertsan et al. (1997); Prasertsan and Saen-saby (1998)	Thailand	Agricultural food drying (bananas)
Mason and Blarcom (1993)	Australia	Macadamia nuts
Meyer and Greyvenstein (1992)	South Africa	Grains
Rossi et al. (1992)	Brazil	Vegetable (onion)
Nassikas et al. (1992)	Greece	Paper
Strommen and Krammer (1994)	Norway	Marine products (fish)

from the heat source is upgraded by bringing it (''pumping'') to the higher temperature in a heat sink. Such energy valorization is done at the cost of input energy used to compress and drive the working fluid in a closed loop of the thermodynamic cycle. An alternative design to the compressor-driven heat pump is the absorption heat pump, in which the function of the mechanical compressor is performed by the so-called chemical compressor driven by the sorption phenomenon (Furutera et al., 1996; Labidi et al., 1996). Hybrid technologies such as radio-frequency-assisted heat pumps are presented elsewhere in this book.

Another variant of the classical heat pump is the chemical heat pump (CHP), where upgrading of the thermal energy is due to heat of a chemical reaction. This special type of heat-pump drying technology will be presented later in this chapter. The general configuration of a heat-pump comprises four major components: a compressor, a condenser, an evaporator, and an expansion (throttle) valve. These elements form a closed cycle for the process fluid (e.g., freon), which evaporates in the evaporator and condenses in the condenser, thus bringing heat that passes through the evaporator and condenser to a higher temperature level. In the open-cycle heat pump, the process fluid such as water vapor from a dryer forms a part of the heat recovery system. Following mechanical compression, this vapor is condensed in a heat exchanger giving up heat for further evaporation of water while the condensate is taken out of the heat-pump system.

The operation of the heat pump is illustrated in Figure 15.1 (a), which presents a schematic diagram of the heat-pump dryer-dehumidifier used to

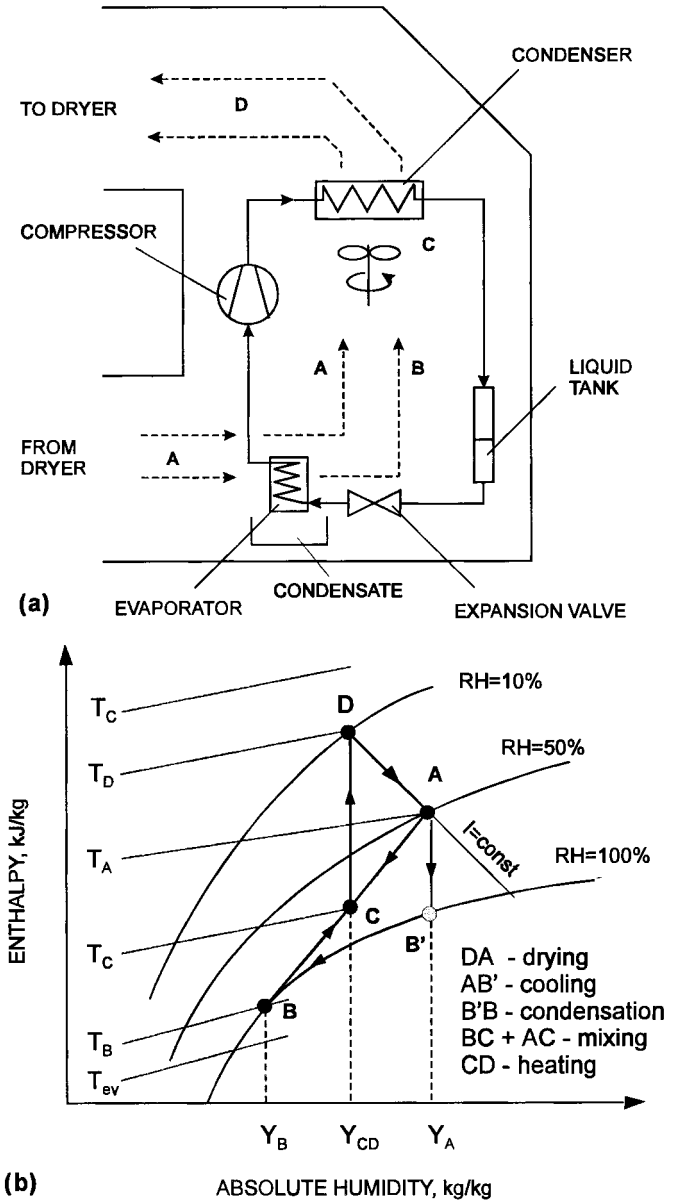

FIGURE 15.1 (a) Schematic of the heat-pump dryer–dehumidifier and (b) air cycle on the Mollier chart.

recover the latent heat from dryer exhaust air. Here, the fraction of humid air (A) leaving the dryer is cooled in an evaporator to a temperature T_B (B) close to T_{ev}, which is below the dew point. Consequently, part of the moisture from this air stream is condensed, and heat recovered in this way causes the working fluid to boil in the evaporator. The cooled and moisture-reduced air is mixed with the remaining fraction of humid air from the dryer (C). With the addition of the external work provided by the compressor, the vaporized working fluid increases its pressure and temperature. It is then condensed in the condenser, thus transferring heat to the air mixture (C) and raising its temperature to T_D (D), which is below the condensation temperature T_C. Finally, the heated and dehumidified air is directed to the drying chamber. The thermodynamic cycle for the air stream in a Mollier chart is shown in Figure 15.1(b).

The efficiency of a heat pump is defined by the coefficient of performance (COP):

$$\text{COP} = \frac{\text{Useful heat output}}{\text{Power input}} \tag{15.1}$$

The maximum theoretical heat-pump efficiency is determined by the Carnot efficiency:

$$\text{COP}'_{\text{Carnot}} = \frac{T_{\text{condenser}}}{T_{\text{condenser}} - T_{\text{evaporator}}} \tag{15.2}$$

If the condenser temperature is 350 K and the evaporator temperature is 300 K, for example, then the COP is 7. This means that the input of 1 kW of mechanical energy to the heat pump recovers 7 kW of thermal energy. Heat-pump efficiency in the range of 40% to 50% of the theoretical Carnot efficiency can be achieved in practice.

For drying, a more appropriate efficiency parameter is the specific moisture evaporation (extraction) rate (SMER) defined by

$$\text{SMER} = \frac{\text{Amount of water evaporated}}{\text{Energy used}}, \quad \text{kg/kWh} \tag{15.3}$$

Alternatively, the reciprocal of the SMER is reported as the heat-pump dryer efficiency, which is the energy required to remove one kg of water.

The SMER depends on the maximum air temperature in the dryer, the air's relative humidity, the evaporation and condensation temperatures, and the efficiency of a refrigeration system. Figure 15.2 presents some SMER values for a typical range of temperature differences in the heat-pump dryers plotted against the air inlet temperature (Song, 1990; Strømmen and Kramer,

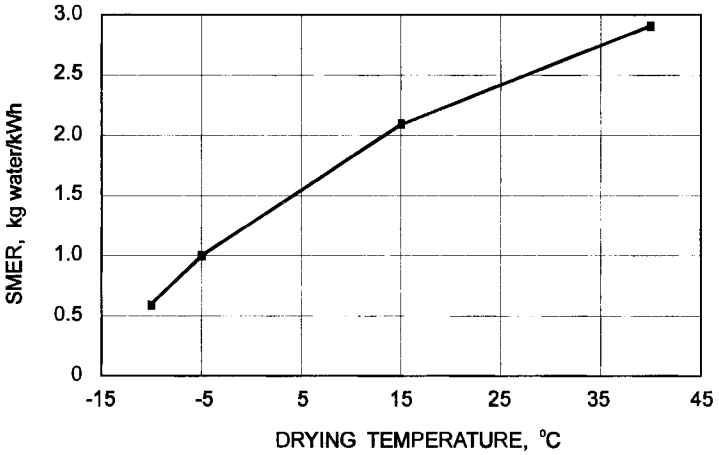

FIGURE 15.2 Specific moisture extraction rate (SMER) versus inlet air temperature.

1994). Characteristically, the relatively high amount of removed water per unit of input energy at elevated temperatures decreases dramatically with temperature drop, mostly because of the low COP of the refrigerator. Therefore, higher drying temperatures should be used unless temperatures below the freezing point are required for quality reasons.

The energy consumed by fans (E_F) used to force air through the drying system is not included in the classical definition of the SMER. In low-temperature drying, however, the energy for driving fans can be a significant fraction of the total energy consumption. In such a case, the following definition of the coefficient of performance is recommended (Kudra and Strumillo, 1998):

$$\text{COP}^* = \frac{Q_0}{E + E_F} \tag{15.4}$$

Thus, energy required to remove the unit mass of water is given by the heat-pump dryer efficiency (HPDE) defined as

$$\text{HPDE} = \frac{(\Delta H/\Delta Y)}{\text{COP}^*} = \frac{1}{\text{SMER}^*} \tag{15.5}$$

The theoretical maximum SMER for conventional thermal drying is 1.55 kg/kWh (based on the latent heat of water vaporization at 100°C). A typical SMER value achieved by a heat pump is 3 kg/kWh, which compares very favorably with conventional convective drying for which values ranging from

0.5 to 1 kg/kWh are standard. A summary of moisture removal efficiency for selected dryers is shown in Figure 15.3. It is clear that heat-pump dryers are approximately 10 times as effective as traditional drying systems, e.g., vapor recompression dryers and hot-air dryers.

To further improve energy efficiency and refine temperature and humidity control in the heat-pump dryer, a more advanced heat-pump system can be incorporated for drying. Figure 15.4 shows an example of a two-stage heat pump in parallel configuration where the evaporator of the first heat pump operates at a higher pressure level than that of the second heat pump. In terms of energy efficiency, the two-stage heat pump allows recovery of much more of the latent energy from the humid air than the single-stage heat pump allows (Figure 15.5).

One of the unique features of the heat-pump dryer is its ability to operate in a closed cycle with precise control over the thermal environment of the system. With advanced PID controllers it is possible to regulate the air temperatures at different stages of the drying process to follow the optimum operating conditions. In the case of a two-stage heat-pump dryer, two control circuits have been proposed (Chua et al., 1998). The first one uses the air-bypass through the evaporators to control the degree of dehumidification, while the second one regulates the mean coil surface temperature of the high-pressure evaporator for optimal recovery of both the sensible and latent heats. With respect to the ambient air, heat-pump dryers are able to produce both cold

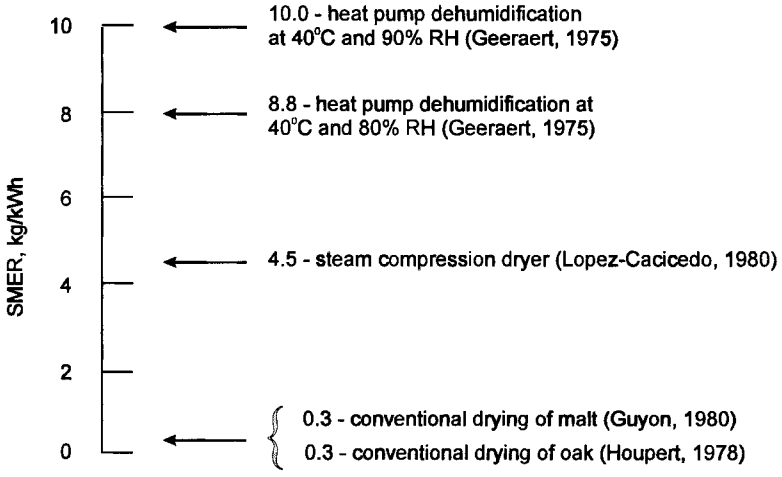

FIGURE 15.3 Effectiveness of various drying systems.

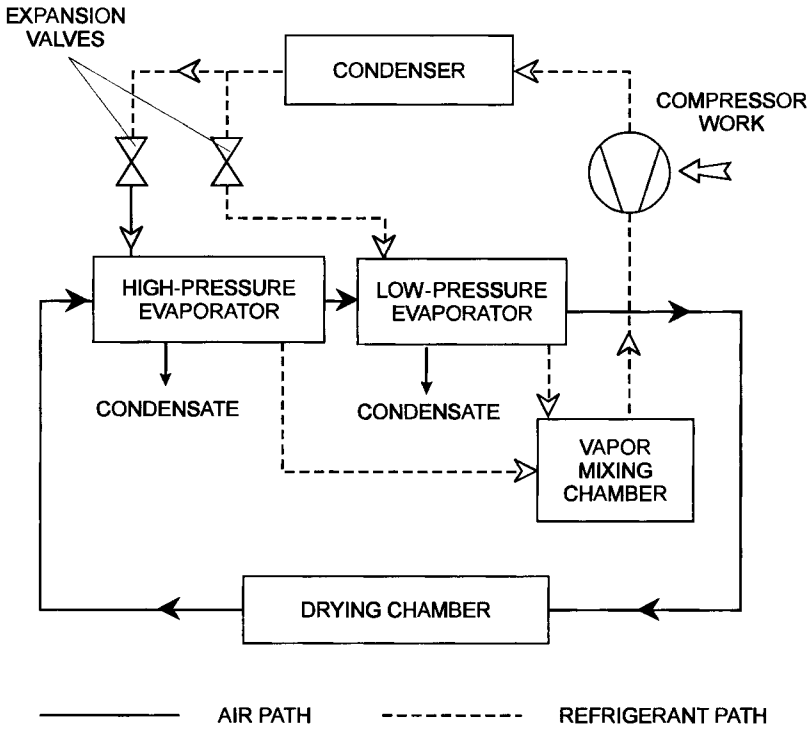

FIGURE 15.4 Schematic of a closed-loop, two-stage heat-pump dryer.

and hot drying conditions with specified humidity at different stages of the drying process. Thus, it is possible to set different combinations of drying conditions in order to maximize the performance of the system and improve product quality. Figure 15.6 shows some of the temperature profiles that can be set in a two-stage heat-pump dryer (Chua et al., 1998).

It should be noted that the mechanical work to run the compressor is the only energy supplied to the heat pump. Therefore, the thermal efficiency of the HP system defined by the coefficient of performance is higher than 100%. However, the cost of the electric energy needed to drive the heat pump might be higher than the value of the heat recovered. Therefore, the profitability of the device depends largely on the relative costs of electricity and thermal energy. The economics of the heat-pump systems can be improved when combined with other heat sources such as natural gas or fuel oil. Figure 15.7 shows a coupled heat-pump–gas engine used for heating a malt house and for drying

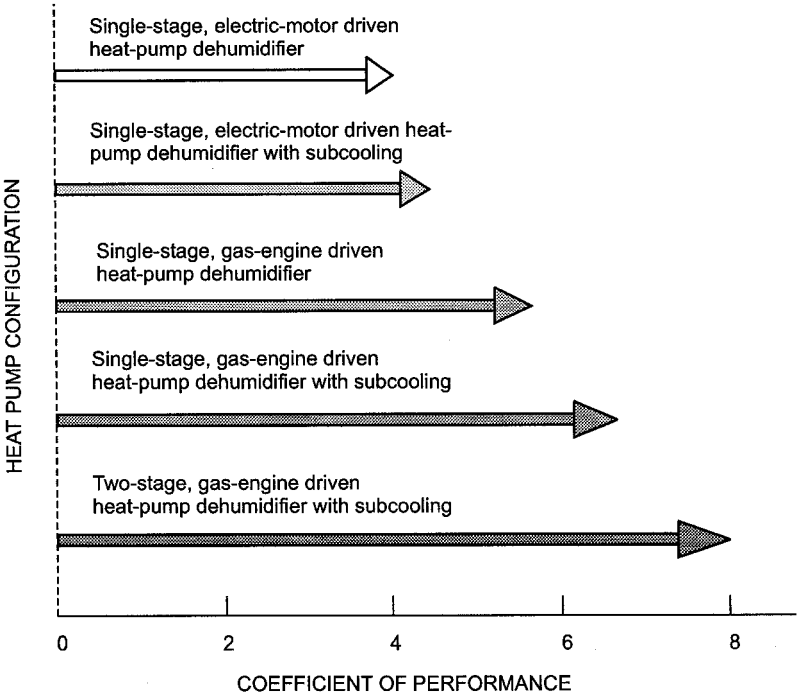

FIGURE 15.5 Feasibility study of heat-pump drying of barley at 66°C and 5% RH. (Adapted from Perry, 1981.)

of malt (Newbert, 1985). The application of this system reduced energy consumption by 40%. In general, the premium value of a higher-quality product that a heat pump may produce should also be taken into consideration when evaluating the economics and payback times for a heat-pump dryer.

Because of economic and technical limitations, heat pumps have so far been used in special applications only, e.g., in drying timber and ceramics that are easily damaged if subjected to high drying rates and for which the more gentle drying obtained at a lower temperature with dehumidified air is advantageous. Recently, however, growing interest is noted for the heat-pump drying of foods and biomaterials where low-temperature heat and well-controlled drying conditions are required to stabilize or enhance product quality. The higher cost of heat-pump drying may be more than offset by the premium price the consumer is willing to pay for the higher quality. The key advantages and limitations of heat pump dryers are as follows:

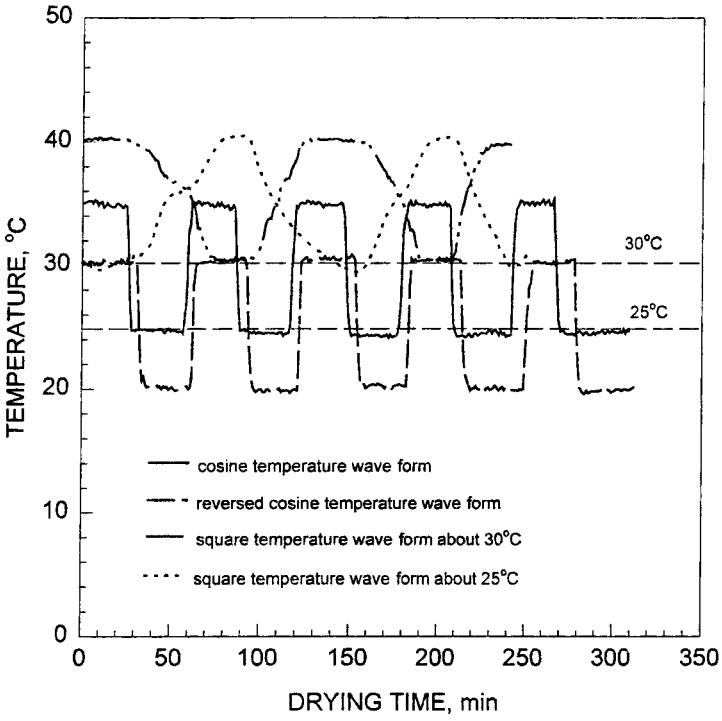

FIGURE 15.6 Temperature profiles in a two-stage heat-pump dryer.

Advantages:

Higher energy efficiency with improved heat recovery method resulting in lower energy consumed for each unit of water removed.

Better product quality with controlled temperature profile to meet product requirements.

A wide range of drying conditions typically from −20°C to 100°C (with auxiliary heating) is feasible.

Consistent output of the product.

Excellent control of the environment for high-value products and reduced electrical consumption for low-valued products.

Suitable for both high-value and low-value products.

Aseptic processing is possible.

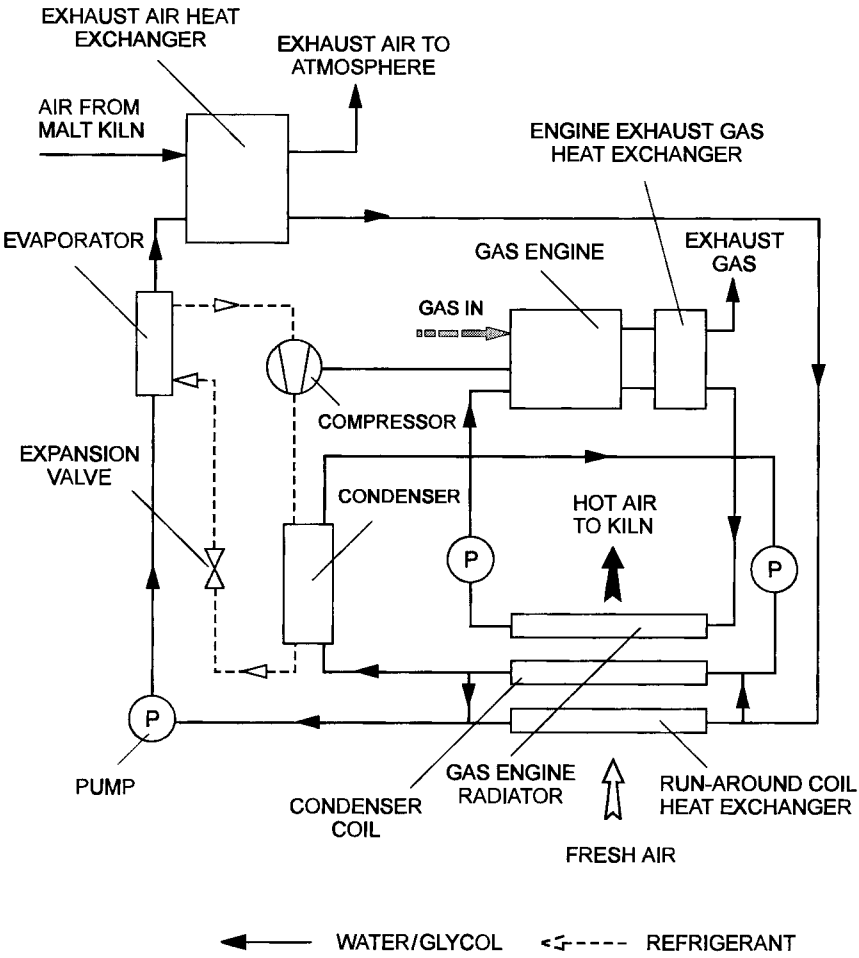

FIGURE 15.7 Schematics of the coupled heat-pump–gas engine system.

Limitations:

CFCs are used in the refrigerant cycle.

Auxiliary heating may be required for high-temperature drying due to the critical pressure level of some refrigerants. Example: R22—approximately 99.6°C.

Initial capital cost may be high due to many refrigerating components.

Requires a steady-state period for system to attain desired drying conditions.

Requires regular maintenance of components (compressor, refrigerant filters, etc.). Regular charging of refrigerant is also required.

Leakage of refrigerant to the environment if cracking of pipes occurs due to pressurized system.

Three-phase power supply may be required for higher refrigerating systems.

15.3 LOW-TEMPERATURE HEAT-PUMP DRYING

Figure 15.8 shows a tunnel dryer for heat-sensitive products fitted with a heat pump and the corresponding processes on a Mollier chart. Drying temperatures are typically in the range from 0°C to 70°C. However, for special purposes the lower temperature limit can be shifted down to −10°C. Inlet relative air humidities are usually kept around 30% to 40% (Magnussen and Strømmen, 1981; Strømmen, 1980).

For some products the aroma compounds or other volatiles might be released from the material being dried. Since all drying air is recirculated, the partial pressure of these components increases until either saturation or a dynamic equilibrium between evaporation and condensation/sorption processes in the evaporator is reached. In general, the problem of deodorizing or degassing in a heat-pump dryer is much easier to handle because only a liquid phase exits from the drying system. Further recovery of the aroma components or removal of absorbed pollutants from a relatively small amount of water is not as difficult as it is from a large volume of the exhaust air.

The closed system of a heat-pump tunnel dryer makes it possible to use N_2, CO_2, or other inert gases as drying agents to reduce fire and explosion hazards and also to eliminate degradation of products sensitive to oxygen. In this case, however, a special design of the feed and product discharge is required to prevent leakage of the drying agent and infiltration of the ambient air.

Efficient heat and mass transfer in dispersed systems and low temperatures required for drying heat-sensitive materials justify the application of a heat-pump system in conjunction with pneumatic, fluid bed, vibrated bed, conveyor, spin-flash, and similar convection dryers. A simplified layout of a heat-pump fluid bed dryer developed at the Norwegian Institute of Technology (NTNU) and thoroughly tested for various products (Jonassen et al., 1994; Strømmen and Jonasen, 1996; Alves-Filho and Strømmen, 1996) is shown in

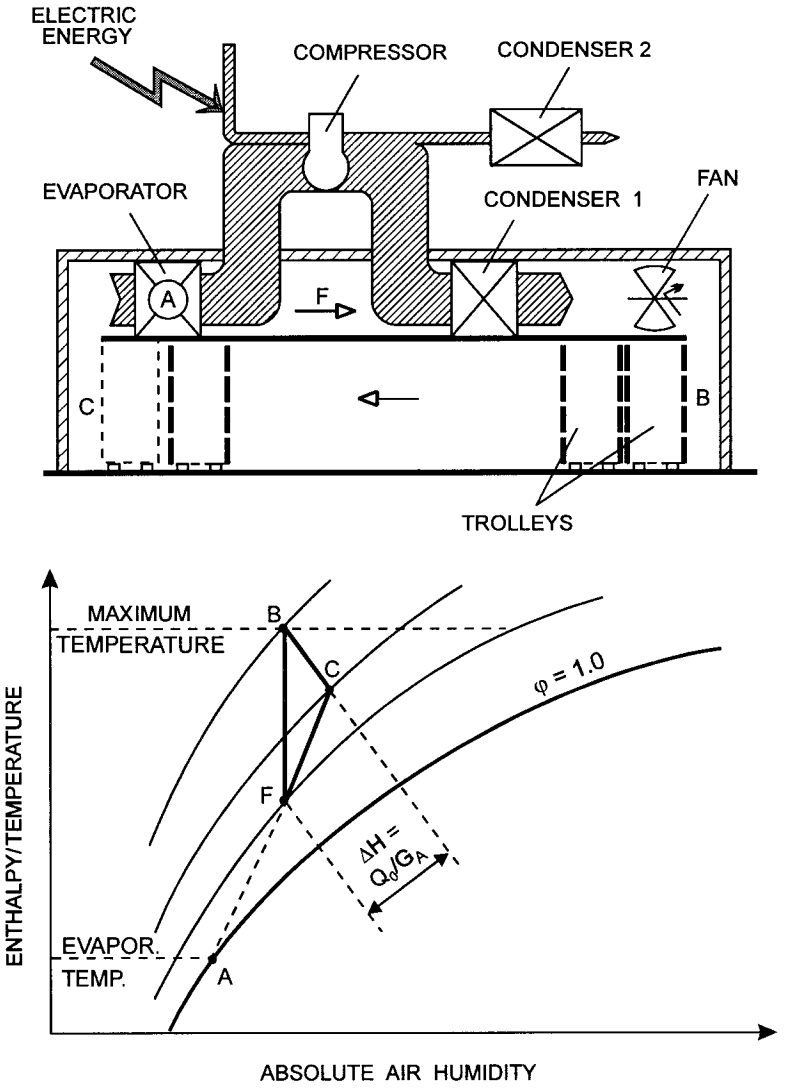

FIGURE 15.8 Tunnel dryer with a heat pump and representation of the drying process on a Mollier diagram. (From Strømmen, 1980.)

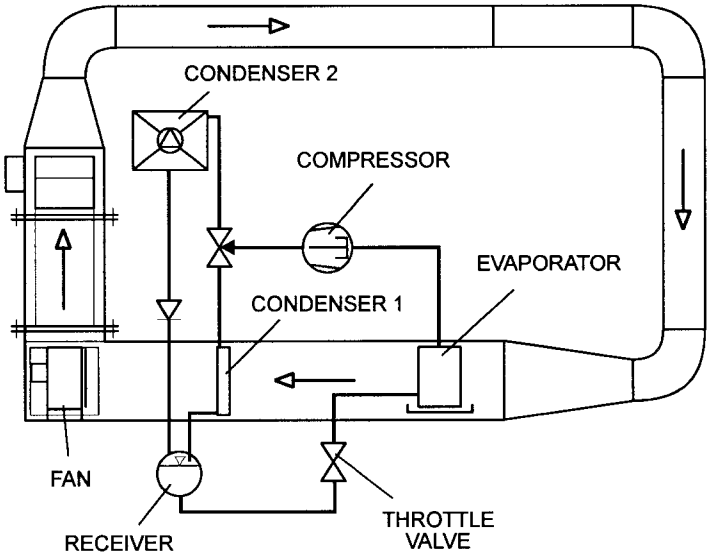

FIGURE 15.9 The laboratory heat-pump fluid bed dryer. (From Strømmen and Kramer, 1994.)

Figure 15.9. The operating temperature in the dryer is set at the desired level by adjusting the condenser capacity, and the required air humidity is maintained by varying the compressor capacity via frequency control of the motor speed. This set-up permits drying at temperatures from −20°C to 60°C and air humidities from 20% to 90%. The flow rate of the drying agent (air) permitting a superficial velocity from 0.3 to 5.0 m/s is adjusted by controlling the fan rpm.

With these features, heat-sensitive materials can be dried under conventional or freeze-drying conditions using either air or inert gases (CO_2 or N_2) as the drying medium. A possibility to sequence these two operations is especially advantageous when drying food and bioproducts because drying under frozen conditions causes minimal shrinkage although at lower drying rates. Furthermore, splitting of the drying process into freeze-drying at temperatures around −5°C, for example, followed by much faster finish drying at 20° to 30°C makes it possible to control such quality parameters as porosity, rehydration rates, strength, texture, color, taste, etc. Tests performed at NTNU on various heat-sensitive materials of biological origin as well as pharmaceuticals, medicinal and biotech products, bacteria, fruits and vegetables, spices,

etc., have proved that without exception heat-pump fluid bed drying offers a much higher-quality product albeit at a higher cost of drying. This technology is thus recommended for premium-grade products (Alves-Filho and Strømmen, 1996).

Figure 15.10 shows a multistage fluid bed heat-pump dryer consisting of two fluidized bed dryers arranged in series and two heat pumps connected in parallel to each other that provide conditioned air to the drying chambers. Each heat pump can run at completely different conditions with different refrigerants and secondary fluids. The wet product fed to the first dryer is fluidized by an air stream at a temperature always kept below the product's freezing point. The drying conditions are controlled by adjusting the heat-pump's components according to the specific enthalpy curves (Alves-Filho, 1996). The residence time in the first dryer is such as to attain the critical moisture content. Then the semidry product is transferred to the second dryer, where it is fluidized at higher temperatures for finish drying. The advantage of the multistage dryer is the same as that of the single-stage unit but with sequential drying conditions, i.e., reducing moisture content at a low temperature to maintain product quality and finish drying at an elevated temperature to increase the overall heat-pump efficiency (Alves-Filho et al., 1998).

Figure 15.11 presents an adiabatic fluid bed dryer designed to operate at temperatures from 60° to 110°C (Jonassen et al., 1994; Strømmen and Jonassen, 1996). This dryer has the following features:

Increased drying temperature; a new heat pump with ammonia as refrigerant and with a new compressor designed for pressures of 6 to 7 MPa allows condensing temperatures above 100°C.

If an isothermal drying process can be achieved by supplying extra heat to the fluidized bed of a dried material, a substantial increase in water content can be reached. Because of the large drying potential, an isothermal process provides several-fold larger water uptake compared to the adiabatic process in the humidity range from 30% to 90%.

The use of a multistage fluid bed where air and product to be dried flow in a countercurrent direction. A superheat exchanger between the two beds in the experimental dryer is used as shown schematically in Figure 15.11. The reheating system in the drying beds has two purposes: (i) to reheat the air from the ''dry bed'' in order to increase a drying potential in the ''wet bed,'' and (ii) to allow for higher drying temperatures; the products in the upper bed are wet, and even higher temperatures than those in the lower bed can be used without spoiling the product.

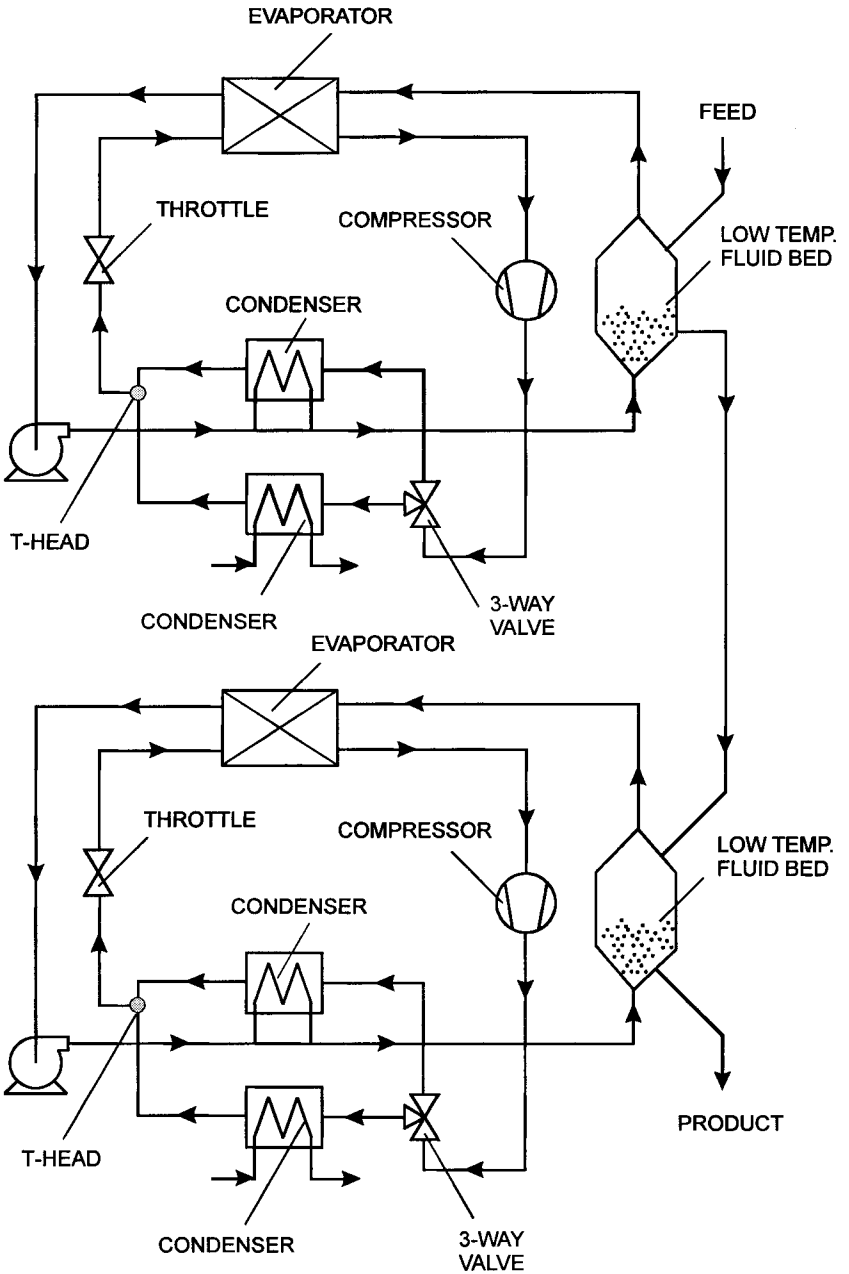

FIGURE 15.10 A multistage fluid bed dryer. (From Alves-Filho et al., 1998.)

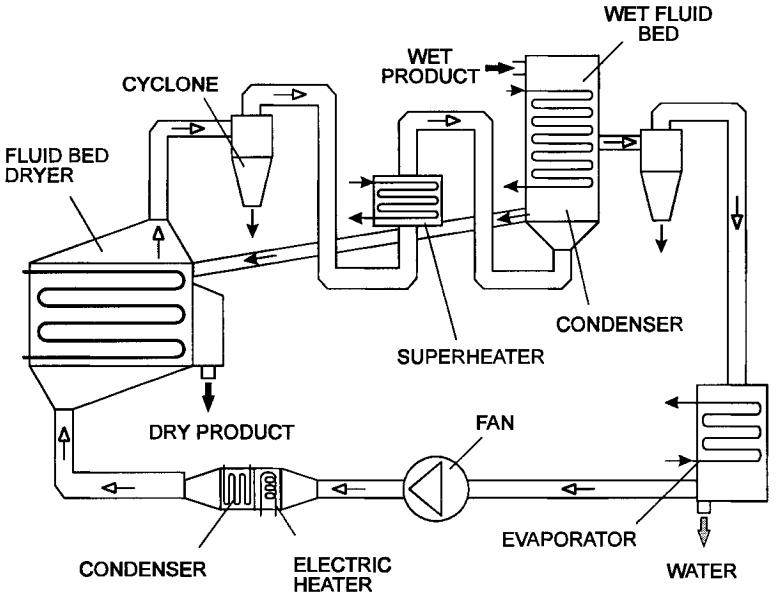

FIGURE 15.11 A schematic of the nonadiabatic heat-pump fluidized bed dryer. (From Strømmen and Jonassen, 1996.)

Electrically driven heat pumps are potentially attractive as most of the main components were directly transferred from refrigeration technology. However, this limited the early applications to the temperature range of 60° to 65°C. By choosing working fluids other than R-12, R-22, it was possible to extend the range of heat pumps to temperatures up to 120°C, thereby reducing energy consumption and allowing the use of this drying method for a wider range of materials. Tests on batch timber drying comparing modern conventional kilns and a heat-pump system using R-114 showed that, with the high-temperature heat pump, an energy cost saving of 40% for drying hardwoods and 65% for softwoods could be achieved with U.K. energy price ratios (Lopez-Cacicedo, 1986). The actual savings depend on the relative costs of electricity and fossil fuels as well as the operating conditions in the dryer.

The wider application of the vapor-compression heat pump in the future may be jeopardized by the increasing concern on the ozone-depleting potential of the working fluids (freons) that were developed for high-temperature heat pumps (e.g., R-114). Extension of the heat-pump technology to large-scale continuous operations and temperatures above 120°C points to possible use

of water vapor as a working fluid, provided steam compression could be accomplished efficiently. In such a system, water evaporated from the material being dried is compressed and used for heating the incoming material. The principle of operation is similar to the well-known mechanical vapor recompression systems (see Chapter 16). Efficiency of the process will fall, however, if noncondensable gases such as air are present within the system.

15.4 CHEMICAL HEAT-PUMP DRYING

Interesting alternatives to compression heat pumps with ozone-depleting fluids are the so-called chemical heat pumps. A chemical heat pump (CHP) can store thermal energy in the form of chemical energy via an endothermic reaction in a suitably designed reactor. This energy is then released at various temperature levels during the heat demand period by exo/endothermic reactions (Ogura et al., 1991; Ogura et al., 1997; Mbaye et al., 1997, Goetz et al., 1991). The CHPs operate using only thermal energy and do not release any contaminant gases, which is a distinct feature from the mechanical heat pumps. From numerous possible chemical reactions, the $CaO/Ca(OH)_2$ hydration/dehydration reaction for heat storage and cold/hot heat generation has been validated as a good candidate reaction for CHP by experiments and simulations carried out at Kyushu Institute Technology and Nagoya University in Japan (Ogura et al., 1991; Ogura et al., 1997). Based on these promising results, an original concept of the chemical heat-pump dryer (CHPD) with heat recovery/generation for ecologically friendly and effective utilization of energy in thermal drying has been proposed (Ogura and Mujumdar, 2000). The following description is based on their proposal.

Figure 15.12 shows a typical gas–solid chemical heat-pump configuration. The CHP is a closed system of coupled low- and high-temperature reactors operated according to the reactions given by Eqs. (15.6) and (15.7):

$$A(s) + \mathrm{C}(g) \leftrightarrow AC(s) + Q_H \tag{15.6}$$

$$B(s) + \mathrm{C}(g) \leftrightarrow BC(s) + Q_L \tag{15.7}$$

The heat-storage and heat-release reactions occur at different pressure levels. The low-temperature side has a higher reaction equilibrium pressure. The CHP, as studied earlier, operates as a batch system with a heat-storing step followed by a heat-releasing step. For example, hydration and carbonation reactions can be used on the high-temperature (600 to 1200 K) side reactor. Evaporation and condensation of the reactant media are often used on the low-temperature (273 to 523 K) side reactor.

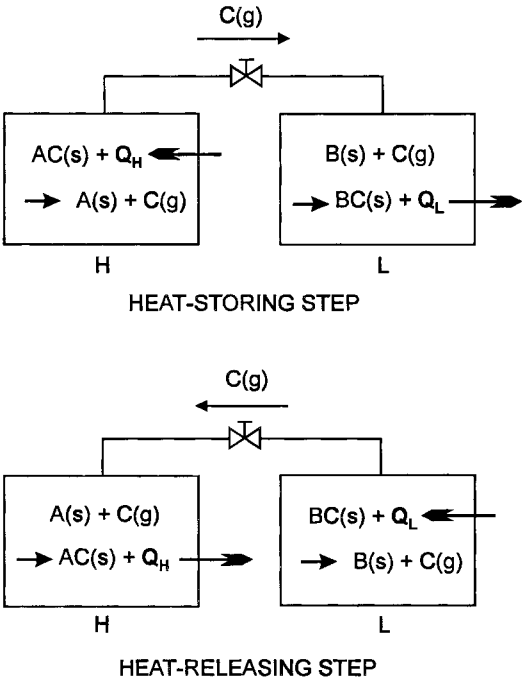

FIGURE 15.12 Operation principle of the chemical heat pump (H—high-temperature side reactor, L—low-temperature side reactor).

In the heat-storing step, the heat Q_H is stored in the form of thermochemical energy by decomposition of the reactant $AC(s)$ in the high-temperature side reactor. The released gas $C(g)$ flows into the low-temperature side reactor due to a pressure difference maintained between the two reactors. The gas $C(g)$ reacts with the reactant $B(s)$, releasing low-temperature heat Q_L. As long as the reactant $A(s)$ is separated from the gas $C(g)$, the reaction heat can be stored for any period in the form of chemical energy.

In the heat-releasing step, the gas $C(g)$ flows from the low-temperature side reactor to the high-temperature side reactor by opening a valve (Figure 15.12) due to the pressure difference between the reactors. The exothermic reaction of the reactant $A(s)$ at a high-temperature level with the gas $C(g)$ takes place in the high-temperature side reactor. The low-temperature side reactor stores the low-temperature heat Q_L or is cooled down by releasing its decomposition heat when it is insulated.

The CHP has four possible operating modes according to the operating pressure levels: heat-storage mode, heat-enhancement mode, refrigeration mode, and temperature upgrade mode. Figure 15.13 shows the relationships between the reaction equilibrium pressure and temperature for each mode. The actual operating pressure and temperature of CHPs depend on the reaction equilibrium values—they are governed by the thermodynamics of the system chosen.

In the heat-storage mode, heat Q_M is stored at T_M in the heat-storing step, and this heat is released at the same temperature in the heat-releasing step. In the heat-enhancement mode, the low-temperature heat (e.g., room-temperature heat) is used as Q_L in the heat-releasing step. So it is possible to use Q_M two times by storing unit Q_H as a result of the CHP operation. The principle of the chemical heat pump operated in the refrigeration mode is similar to that operated in the heat-enhancement mode. Here, the medium-temperature heat Q_M and cold heat Q_L are obtained simultaneously in the same heat-releasing step. The cold heat Q_L is generated by releasing its decomposition heat under adiabatic conditions. In the temperature upgrade mode, heat Q_H at the higher-temperature level can be obtained by using Q_M two times.

Figure 15.14 presents a schematic diagram of the essential concept of the proposed CHPD. In order to apply CHPs to dryers, thermal energy from some source should first be stored in the CHP. In this particular configuration, the thermal energy in exhaust air from the dryer is stored in the CHP1. If the exhaust heat is not sufficient to complete the heat-storing reaction taking place in the CHP1, additional heat might be required. If the exhaust air needs to be dehumidified, the CHP1 can operate as a cooling dehumidifier in the refrigeration mode of operation. The stored energy in the CHP1 is released from the CHP2 as ''hot'' heat for drying. These two steps run simultaneously as a batch cycle, and the continuous supply of heat to the dryer is secured by altering the heat-storing/releasing steps. An air stream changes its flow direction according to the current mode of operation.

When the CHPs work in the heat-enhancement mode (Ogura and Mujumdar, 2000), the released energy from the CHP2 can be above 200% of the stored heat in the CHP1 depending on the chemical system selected. On the other hand, when the temperature of the released heat from the CHP2 is required to be much higher than that of the stored heat in the CHP1, the temperature upgrade mode is especially effective.

In addition to the choice of CHP modes, one must select the candidate reactions considering the reaction temperature, the pressure level, reactivity, reaction reversibility, safety, corrosion, costs, etc. This means that the features of the reaction system determine the features of the CHPD system. Some

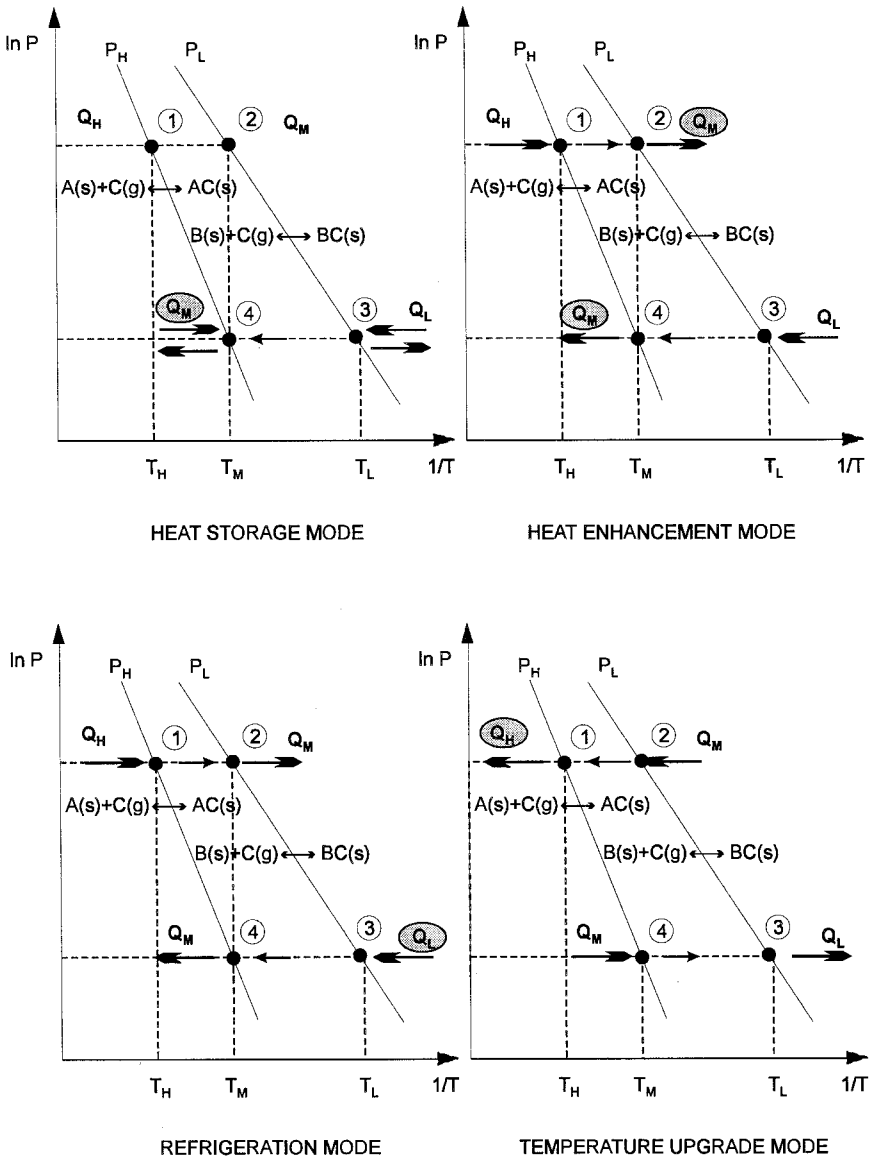

FIGURE 15.13 Basic operating modes of chemical heat pumps.

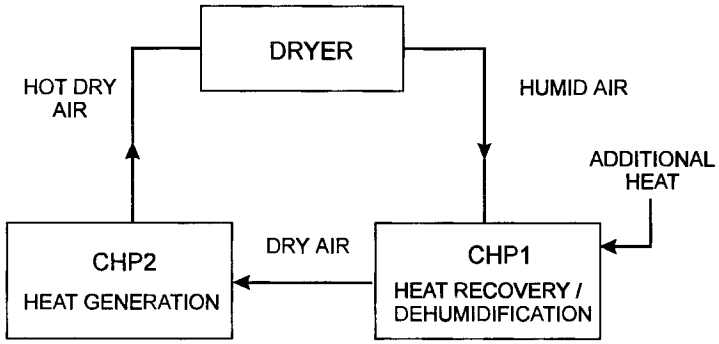

FIGURE 15.14 Concept of a chemical heat-pump dryer.

feasible reaction systems for the CHPD can be found in the study by Ogura and Mujumdar (2000).

From the above considerations, more than two CHPs need to be used for continuous operation of a CHPD. The reaction system and the operation mode need to be arranged for the special purpose of energy savings in drying.

Ogura and Mujumdar (2000) illustrated the CHPD idea by selecting the calcium oxide/calcium hydroxide reaction from the viewpoints of their safety, reactivity, reaction enthalpy, and reaction equilibrium temperature–pressure level and material cost. The $CaO/H_2O/Ca(OH)_2$ reaction system is expressed by the following reactions:

$$CaO(s) + H_2O(g) \leftrightarrow Ca(OH_2)(s) + 104.2\ kJ/mol \tag{15.8}$$

$$H_2O(g) \leftrightarrow H_2O(l) + 41.7kJ/mol \tag{15.9}$$

Figure 15.15(a) shows the operating line for this CHPD showing the relationships between reaction equilibrium pressure and temperature. This system works in the heat enhancement mode, and both CHPs operate concurrently. In the configuration shown in Figure 15.15, the CHP1 is in the heat-storing step and the CHP2 is in the heat-releasing step. These CHPs switch steps with each other every hour or so; the switching time is decided during previous experiments such as those reported in studies by Ogura and co-workers (Ogura et al., 1991; Ogura et al., 1997; Ogura et al., 1999).

Figure 15.15(b) shows a flowsheet of the corresponding CHPD. In CHP1, high-temperature heat Q_{HS} supplied by a gas burner or a heater with Q_{in} at $T_{HS} > 594°C$ is stored in the CaO reactor. Water vapor in the reactor is released from the reactor and condensed in the condenser. The condenser

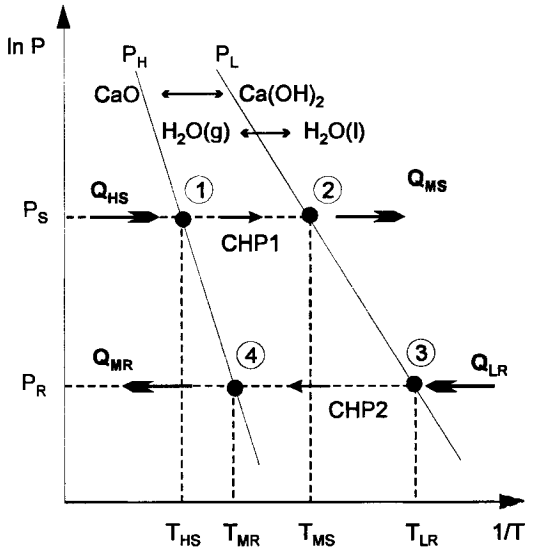

(a) OPERATING LINE

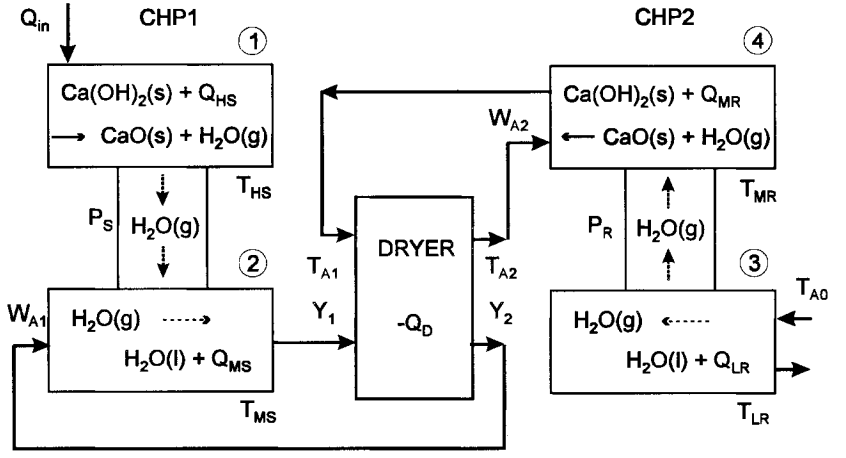

(b) FLOWSHEET

FIGURE 15.15 Principle of the CHPD with $CaO/H_2O/Ca(OH)_2$ operated in the heat-enhanced mode: (a) operating line and (b) flowsheet.

releases medium-temperature heat Q_{MS} around $T_{MS} = 150°C$ by controlling the heat transfer rate. On the other hand, CHP2 also releases medium-temperature heat Q_{MR} around $T_{MR} = 360°C$ in the CaO reactor by controlling the evaporator temperature around $T_{LR} = 20°C$ with room-temperature heat. In summary, the CHP system stores the 600°C heat and continuously releases heat at 150°C and 360°C by flipping the CHP steps.

In order to supply dry hot air at $T_{A1} = 130°C$, the mass of 100 kg of dry air per hour is recirculated, as shown in Figure 15.15. The amounts of heat Q_{MS} and Q_{MR} needed to heat the exhaust air at $T_{A2} = 100°C$ to the dryer inlet temperature $T_{A1} = 130°C$ can be calculated using Eq. (15.10):

$$Q_{MS} + Q_{MR} = W_A c_A (T_{A1} - T_{A2}) \tag{15.10}$$

From the reactions expressed by Eqs. (15.6) and (15.7), the heats of reaction are produced in the following ratio:

$$Q_{MS} : Q_{MR} = 41.7 : 104.2 = 1 : 2.5 \tag{15.11}$$

From Eqs. (15.10) and (15.11), the following results are obtained: $Q_{HS} = Q_{MR} = 595$ W $= 2.14$ MJ/h, $Q_{MS} = Q_{LR} = 238$ W $= 0.86$ MJ/h. The mass flow rates are calculated to be $W_{A1} = 38.6$ kg and dry air/h $W_{A2} = 71.4$ kg and dry air/h. The amounts of reactants needed are CaO $= 1.15$ kg and H_2O $= 0.37$ kg.

In the dryer, heat calculated from Eq. (15.10) ($Q_D = Q_{MS} + Q_{MR}$) is used for heating the material and evaporating the moisture. Hence,

$$Q_D = W_B c_B \Delta T_B + W_A \Delta H \Delta Y \tag{15.12}$$

where ΔY is the mass transfer driving force equal to $Y_2 - Y_1$.

From the above, the rate of moisture evaporation can be calculated. Neglecting the sensible heat of the solid material, the evaporation rate is $Y_2 - Y_1 = 0.0125$ kg water vapor/kg dry air or $W_{ev} = 1.25$ kg water vapor/h. In this case, the consumed energy in this CHPD for evaporation is calculated from Eq. (15.13):

$$Q_{ev} = \frac{Q_{HS}}{W_{ev}} \tag{15.13}$$

The calculated value of Q_{ev} as 1.71 MJ/kg of water evaporated is much lower than the evaporation heat of water, which is about 2.4 MJ/kg. If the material's sensible heat is assumed to be 30% of the drying energy Q_D, the evaporation rate W_{ev} is 0.875 kg water/h, and $Q_{ev} = 2.45$ MJ/kg. Although

the rate of evaporation is not high, this amount of consumed energy is a good value for industrial drying.

In the chemical heat-pump system, the circulating air gains humidity in the course of drying. In the case under analysis, the relationship between absolute air humidity and the number of cycles can be written as

$$Y_{(1,n)} = Y_{(1,10)} + (n + 1)\Delta Y = 0.01 + (n - 1)0.0125 \tag{15.14}$$

Hence, the absolute air humidity $Y_{(1,10)} = 0.135$ kg water vapor/kg dry air is attained after 10 cycles. The relative humidity is, however, lower than 2% because air circulating in the system is kept over 100°C. The above analysis was done under the assumption that the drying rate does not change over the period of operation, which might not always be true.

In the case of a convective dryer of the same performance as the CHP dryer, the air should be heated to $T_{A1} = 130$°C from room temperature of $T_{A0} = 25$°C. The consumed heat calculated as

$$Q_{in,c} = W_A c_A (T_{A1} - T_{A0}) \tag{15.15}$$

is then equal to 2.92 kW or 10.5 MJ/h. The energy consumption ratio R_Q defined as

$$R_Q = \frac{Q_{in}}{Q_{in,c}} \times 100 \tag{15.16}$$

is 20.4%. This means that this particular chemical heat pump consumes only about 20% of the energy needed with a conventional convective dryer of the same capacity.

The energy efficiency of the CHPD was estimated by Ogura and Mujumdar (2000) to be much greater than that of the conventional convective dryer. The features of the CHPD depend on the chemical reaction system chosen as well as on the mode of operation. Further detailed studies, both theoretical and experimental, are needed to examine the potential of CHPDs. Cost and reliability studies are also needed in view of the increased complexity of the new conceptual designs suggested. New reactor designs of CHP may be needed for continuous operation at the right temperature levels. Note that the results given here are based on a highly simplified analysis and are subject to refinement.

15.5 NEW DEVELOPMENTS AND TRENDS IN HEAT-PUMP DRYING

The most important considerations concerning heat pumps are summarized below (Strumillo et al., 1995):

Compressors of heat pump dryers should be able to operate continuously for extended periods without maintenance.

The heat capacity and working temperature of the heat pump should suit the drying process.

The heat pump should not be the only heating device for the dryer; it should be treated as a moisture-extracting device.

For optimum performance, the heat pump should operate at the same heat load (i.e., with the same amount of moisture condensed and at a constant temperature). Compensation for any changes in dryer operating conditions should be by other methods.

The temperature difference between an evaporator and a condenser for a single-stage vapor-compression heat pump should not exceed 40°C. This gives practically the COP in the range from 3 to 4.

Recent studies in heat-pump drying focus on process control as well as on the individual refrigerating component, in particular on compressors. The latest developments in scroll compressors in terms of energy efficiency and the size of the compressor have made them technically attractive to be integrated into a heat-pump drying system. Also, advanced heat exchangers with the internal tube's ribbed surface and external wavy fins promote better heat transfer and reduce the size of heat exchangers (Matsuo et al., 1984). These features make heat-pump dryers more compact and more energy-efficient through better heat recovery and also allow the implementation of better air-control strategies.

As many processes require both hot and cold drying, frost on the evaporator surface builds up rapidly in low-temperature applications. Once frosting occurs, heat transfer between the evaporator and drying air decreases dramatically due to the additional resistance to conductive heat transfer. Some research has been initiated to study the ice build-up process and its influence on air dehumidification with the objective of eventually coming up with better mechanisms to reduce the build-up rates (Sanders, 1985).

The basic concept of coupling a chemical heat pump to dryers is new and hence not explored in any depth. It appears that chemical heat pumps will need to be designed for continuous (rather than batch) operation if they are to find wide application in industrial drying. In fact, new reaction systems and new reactor designs may be required for drying applications. It is too early to predict the potential of this novel idea.

Part III

Selected Techniques for Drying and Dewatering

This part describes some new drying techniques that have been demonstrated at laboratory scale but need considerable further development efforts. It is expected that they will attract the attention of academic researchers and industry so that more R&D efforts can be devoted to testing their eventual viability. In some cases, these ideas could be coupled with some of the conventional drying concepts to increase their chances of commercial success.

16

The Carver–Greenfield Process

The Carver–Greenfield Process® (C–G) is an innovative dehydration technique involving the use of a nonvolatile liquid medium as a carrier for dispersed wet solids to be dried in multiple-effect evaporators (Pluenneke and Crumm, 1986). The technology of multiple-effect evaporation is well established in the distillery, sugar, corn, pulp and paper, and other industries dealing with the progressive concentration of aqueous solutions. Apparently high thermal efficiency of the multiple-effect evaporation results from a process configuration where steam from an external source is supplied only to the heating element of the last unit from a series of effect evaporators. If steam temperature is above the boiling point of the solution to be concentrated, then 1 kg of delivered steam will evaporate almost 1 kg of water. Because the final evaporator operates at the highest boiling temperature, the water vapor from the final evaporator can serve as a heating medium in the preceding evaporator. Here almost another kilogram of water is evaporated, so the water vapor may be further used as a heating medium in another evaporator or condensed, if the system features a double-effect evaporation (Perry et al., 1998). Such a reuse of vapor from adjacent evaporators is repeated through any number of effects, so the theoretical steam economy is proportional to the number of effects. In practice, the unit heat consumption is higher than the theoretical

one but still impressive. For example, the energy consumption in a five-stage Carver–Greenfield unit averages 163 kJ/kg of water evaporated, including steam and electricity (Pluenneke and Crumm, 1986).

The economic advantages of a multiple-effect evaporation resulting from better steam utilization are reduced to a certain extent by additional costs due to (a) pressure gradient over the series of evaporators, which is necessary to maintain the reasonable temperature difference between steam and boiling solution in a sequence of evaporators, and (b) larger heat transfer surface area necessary to maintain a technically justified evaporation rate. Therefore, the design of a particular evaporation system should be based on economic-balance calculations.

So far the major constraint in the application of multiple-effect evaporation to industrial drying has been the decreasing fluidity of the processed material in the course of water evaporation. The use of oil as a carrier medium, which is the essence of the Carver–Greenfield process, solved this problem, allowing this energy-efficient method to be used to dewater solids in the process stream to virtually zero moisture content.

The early Carver–Greenfield process commercialized in 1961 utilized the indigenous carrier oil concept developed for vitamin oil recovery. In this case, tallow obtained from slaughterhouse waste was used as the oil carrier for processing meat sludge. In the C–G rendering system, the meat waste was first ground into a rough meal and mixed with tallow to ''liquefy'' the solid granules. The slurry was then boiled in a two-stage, multiple-effect evaporation system. The mixture of tallow and dry solids discharged from the second evaporator was separated by centrifuging. High-pressure presses were used to further reduce the tallow content in the meal to about 15% mass. A fraction of tallow from the separator and presses was recycled to the process in order to maintain the oil-to-product mass ratio of about 8:1. Excess tallow was drawn off, filtered, and sold as a commercial product. Dry solids were used for animal feed. Some 60 plants of this type still operate in the United States.

The critical point of the C–G rendering process was the mechanical separation of the tallow rendered from the centrifuge. The cost of carrier oil lost with dry product greatly reduced the economic advantages of an energy-efficient system. Therefore, the original ''heavy oil'' process was further modified to use a more volatile carrier oil (Table 16.1), which can be recovered by evaporation rather than by mechanical pressing (Pluenneke and Crumm, 1986). Besides minimizing carrier oil losses, light oils also extract indigenous oils present in the feed material, such as greases and fats from sewage sludge, oils from peat and lignite drying, or corn oil from the spent mash in whiskey manufacture. One disadvantage of the ''light oil'' process is evaporation of some of the oil along with the water. The presence of oil in the water vapor

TABLE 16.1 Physical Characteristics of Light Carrier Oils

	Amsco® 140	Isopar L
Initial boiling point, °C	185	185 min
Dry point, °C	204–210	204–211
Flash point, °C	64	60 min
Density @ 15.6, °C, kg/m^3	784	767

used as a heating medium reduces the overall heat transfer coefficient by 25% to 30% as compared to pure water vapor. Another concern when using more volatile oil is its lower flash point, which requires a more stringent electrical code classification.

An advanced modification to the Carver–Greenfield process allowing better energy utilization includes the mechanical vapor recompression (MVR). Here, the exhaust water/oil vapor is mechanically compressed to the higher pressure and temperature and used as a heating medium in the same evaporator. This makes it possible to reduce energy consumption to about 50 kJ/kg of water evaporated. Figure 16.1 presents the basic configuration of the Carver–Greenfield process utilizing mechanical vapor recompression to concentrate

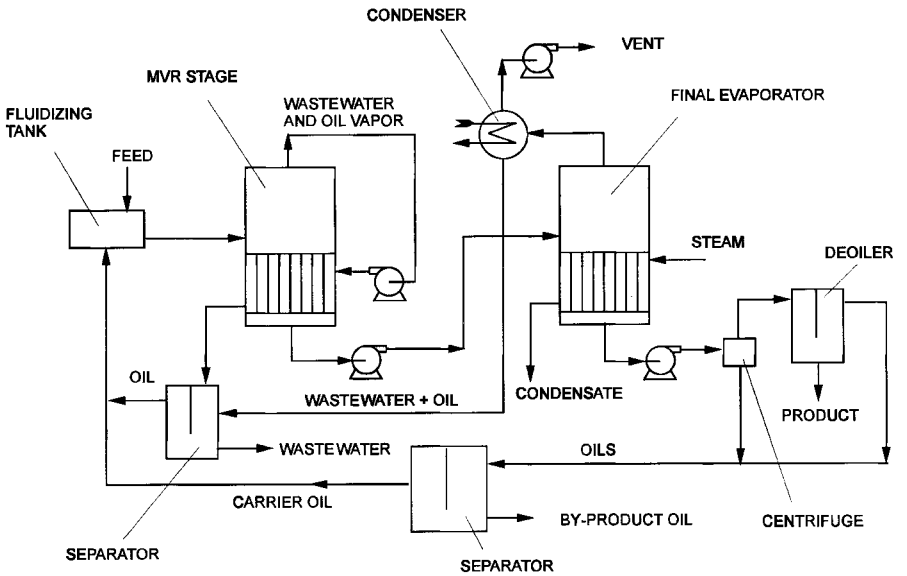

FIGURE 16.1 Carver–Greenfield process with mechanical vapor recompression.

feeds from solids' content ranging from 2% to 50% mass. Because the particle size must not exceed 7.5 mm along any axis, some feed material may require grinding prior to mixing with carrier oil. Drying of such sludge is accomplished in a two-effect system comprising the MVR and conventional steam-heated evaporators. The evaporators in all drying stages are typically equipped with forced-circulation heat exchangers. Alternatively, heat exchangers can be of the falling-film tubular type except the final evaporator in which forced convection is required because of increased solids' content and a higher boiling point.

In case of the light oil system, the press-type deoiler is replaced with a devolatizer. The unit resembles a screw-feeder in which both the flights and the through are steam-heated. The system is operated under vacuum, so that the carrier oil is rapidly drawn off the solids as the process stream moves down the flight. To further enhance vaporization, steam may be injected directly into the solids.

Process condensate from the evaporators is treated in a two-stage system to remove most of the oil. The first stage consists of the baffled unit that relies on residence time and low velocity to separate the oil by flotation. The second stage is a contact-type unit that ''polishes'' the water by forcing it through a barrier system, where the oil coalesces.

The system to separate the carrier oil from the indigenous oils that have been extracted from the feed material usually consists of a falling-film vaporizer followed by a ''cook-pot,'' both of which are steam-heated. The concentrated sludge from the centrifuge is fed to the falling-film evaporator, where about 90% of the light oil is vaporized. This hot vapor is used instead of steam in the final evaporator of the multiple-effect system, to reduce energy consumption. The concentrate that has not been vaporized is transferred into the pot, which is equipped with a mixer. Vapor from the pot flows directly to the first multiple-effect evaporator. The nonvaporized indigenous oil is removed from the pot continuously and pumped to the storage.

Current applications of the C–G process include the drying of activated sludge from wood pulp plant, wool-processing waste from textile manufacturing facility, instant-coffee processing waste, dairy product waste, and sewage sludge. Products like lignite and peat have been dried successfully at the pilot level with energy consumption in the order of 135 kJ/kg water evaporated. The process is particularly attractive for drying peat. One may expect that this process and its variants will find new and major applications around the world as engineers and managers concerned with decision-making become familiar with the technology and as experience with its industrial operations accumulates. Several major installations that use the C–G process for drying municipal waste sludge exist in Japan.

17

Drying in a Plasma Torch

The term ''plasma'' refers to a partially ionized gas, composed essentially of photons, ions, and free electrons as well as atoms and molecules in their fundamental or excited states. Because of the presence of free charges, plasma is electrically conductive and follows the law of electromagnetism. Thus, a static electric field, for example, will tend to separate and accelerate plasma charges. Overall, however, plasma is neutral since the number of negative-charge carriers is equal to the number of the positive ones.

Because of its unique properties, plasma is often called the fourth state of matter according to the following scheme expressing an increase in energy level:

solid $\rightarrow$ liquid $\rightarrow$ gas $\rightarrow$ plasma

Plasmas can exist within solids as well as liquids, but the most common are gas plasmas. In view of thermal conditions, the following basic types of plasma are distinguished:

Fusion plasmas: millions of degrees (10^5–10^9K)
Thermal (hot) plasmas: thousands of degrees (10^3–10^4K)
Cold plasmas: tens of degrees (near ambient)

Cold plasma exists only under reduced pressure, whereas hot and fusion plasmas are formed at atmospheric or elevated pressures. Therefore, the vast majority of thermal processing is based on thermal gas plasmas, which provide technically acceptable heat input. Although artificial plasmas can be originated by various energy sources, one of the most popular methods of plasma generation involves electrical excitation by the external electromagnetic, DC or AC field. Here, the areas of greatest interest to hot-plasma technologies are the glow discharge and arcs. Considering electric arcs, the plasma generators can be broadly classified into electrode and electrodeless devices. Electrode-type generators always have cathode and anode, though these may alternate. In either configuration, plasma becomes part of the electric circuit. Further, such generators can be subclassified into transferred and nontransferred jet plasma arcs (Figure 17.1)

Electrodeless devices are used to generate cold plasma, typically within a quartz tube by a high-frequency electromagnetic energy. A surface-wave applicator with longitudinal propagation of microwave energy is especially

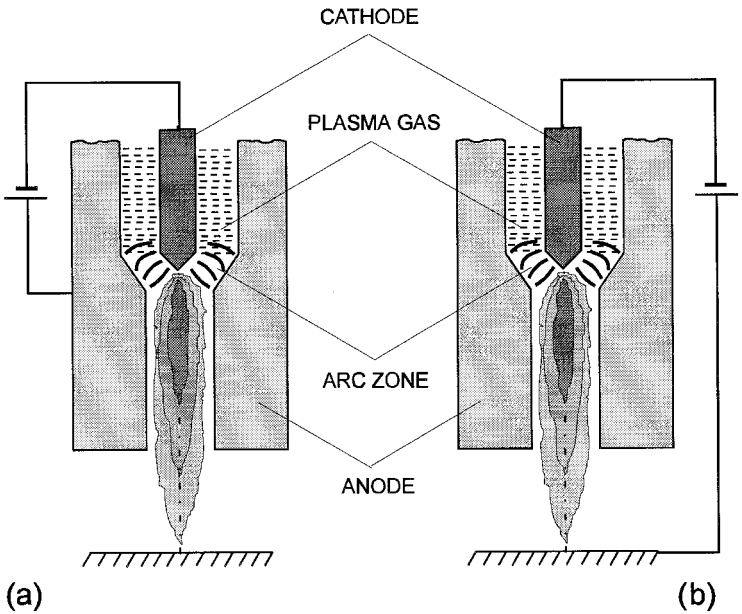

FIGURE 17.1 Modes of operating a plasma torch: (a) transferred arc and (b) nontransferred arc.

suitable for coupling electromagnetic energy to the plasma (Bosisio et al., 1972; Bosisio et al., 1973). Because it has no electrodes, this type of plasma generator can handle corrosive gases and reactive substances.

The industrial potential of the hot-plasma technology results from high specific enthalpy and power capacity of the plasma jet; technically feasible power ranges from 20 kW to 100 MW. A truly broad array of hot-plasma applications can be classified into three main categories:

Mechanical processes (e.g., welding, cutting, spraying of coatings, dust treatment)
Metallurgical processes (e.g., metal extraction, alloy production)
Chemical/physical processes (e.g., chemical synthesis, pigment production, toxic waste destruction, vitrification of nuclear wastes, utilization of by-products)

In general, plasma technologies are well suited to handle small particles, whereas these particles must be agglomerated or pelletized for many conventional techniques. The thermal and kinetic energies of the plasma jet offer some special advantages for drying, especially when combined with other processes such as coating polymers (Bosisio et al., 1980). The configuration of electrodes and the torch-form of the plasma jet designate, however, dispersion dryers such as fluidized bed, spouted bed, stream, or spray dryers to be the most appropriate technologies. The earliest information on fluidized bed sys-

TABLE 17.1 Plasma Torch Specification and Operating Parameters

Parameter	Range
Power, kW	10–20
Voltage, V	30–50
Current, A	300–400
Cooling water flow rate, m^3/h	0.42
Gas flow rate, m^3/h	
Nitrogen	1.8–2.4
Argon	3.0
Gas pressure, kPa	690
Particle size, μm	
Initial	10–150
Final	40–850
Flame temperature, °C	470–970
Bed temperature, °C	215–700

tems in which a plasma serves as a fluidizing agent appears to be given in a patent describing the process of solids coating by condensing a high-temperature plasma onto a bed of particulate material (Goldberger and Baroch, 1963). Since then, the plasma fluid beds evolved into plasma reactors rather than dryers (see Manohar and Gleit, 1971). Similarly, early research into plasma spouted beds was related to the plasma reactor in a gas–solid system (Bal et al., 1971; Szuba et al., 1996). Furthermore, Jurewicz et al. (1985) reported on a plasma spouted bed reactor operated with alumina powder as a test material

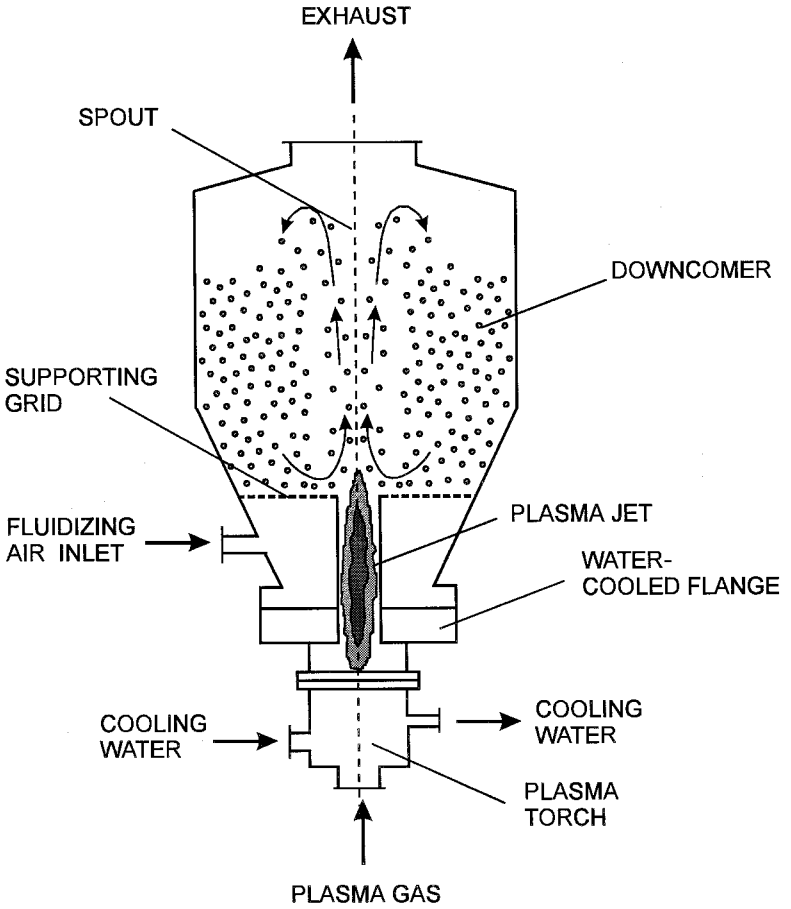

FIGURE 17.2 Spouted dryer with a plasma torch.

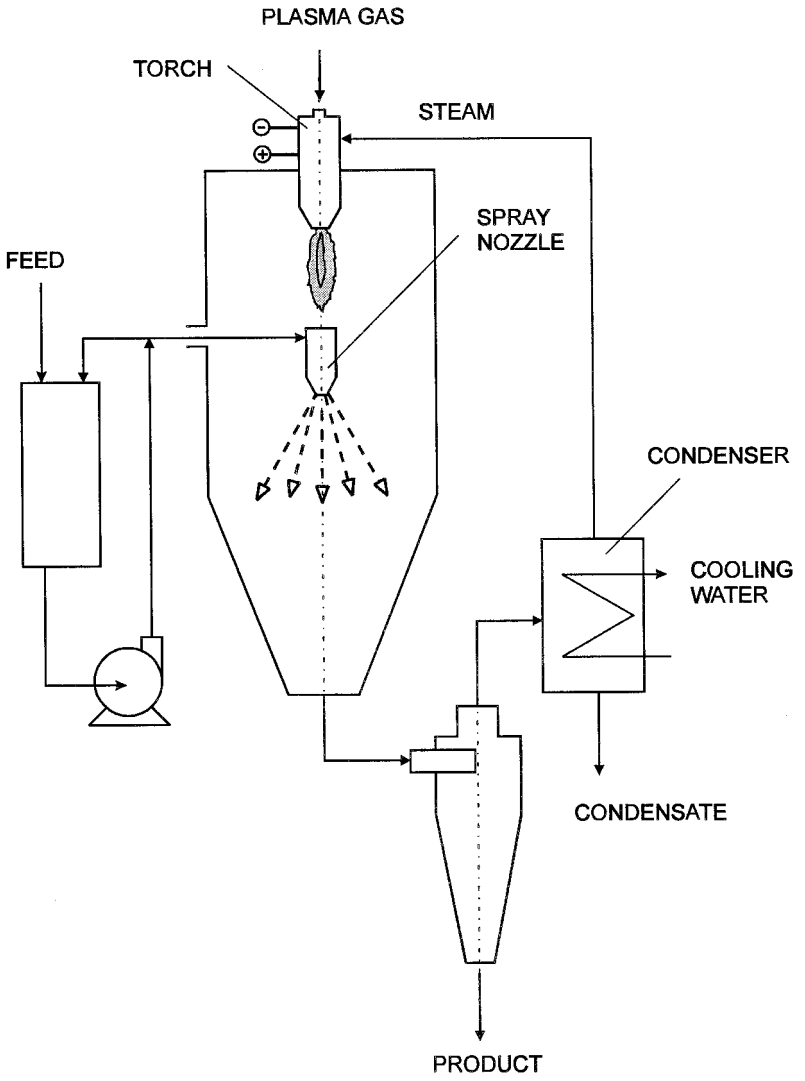

FIGURE 17.3 Basic configuration of the plasma spray-drying system.

and argon or an argon–nitrogen mixture as the plasma gas. Also, the plasma spouted bed with a suitable plasma torch has been used to study spouting of V_2O_5 in mixture with various sodium salts in order to produce the sodium vanadate (Kreibaum, 1986; Munz and Mersereau, 1990) and for treatment of solid waste and biomass gasification (Hamid and Jurewicz, 1997; Lemoine and Jurewicz, 1999). Characteristics of the plasma spouted bed are given in Table 17.1. Although stable and uniform spouting at substantial conversion of the vanadium oxide was obtained, the major problem encountered was fusing of small particles in the near-wall region due to poor solids circulation, especially at temperatures above 700°C. This disadvantage was eliminated by the use of a spout–fluid bed, which combines the advantages of the fluid and spouted beds (see, Passos et al., 1987). In the configuration shown in Figure 17.2, the conventional spouted bed is fitted with a supporting grid located above the gas-jet inlet. Thus, the plasma jet entering the bed core moves the particles in the spout while an additional air stream passing through the supporting grid fluidizes particles, which normally would move downward as a falling bed.

A novel approach to plasma application has been presented by Gauvin and co-workers (Gauvin, 1981; Amelot, 1983; Amelot and Gauvin, 1986), who used thermal plasma of a water vapor or nitrogen–water vapor mixture in spray drying. In these experiments, pure water and a solution of sodium nitrate with mass concentration of 10% to 30% were atomized by a pressure nozzle in a drying chamber 0.305 m in diameter and 1.78 m in height. The plasma torch was fed with a relatively small amount of steam so the plasma jet exited the torch nozzle at about 3600 K. This high-enthalpy jet of the plasma–superheated steam mixture was diluted and rapidly cooled by the steam generated during evaporation of water from the finely dispersed feed. Therefore, the finish drying was performed in a gaseous mixture consisting

TABLE 17.2 Spray Drying in Thermal Plasma

Material	Feed rate, kg/h	Pressure, MPa	Power, kW	Temperature, K	Drying rate, kg H_2O/h
Water	14.80	1.03	12.80	553	14.80
	14.50	1.34	12.80	558	14.50
	12.75	1.20	13.00	838	12.75
$NaNO_3$(10%)	15.50	0.85	12.90	583	14.00
$NaNO_3$(30%)	18.20	2.07	12.65	588	12.75

Source: Amelot, 1983.

of about 6% nitrogen and 94% steam by volume. Following separation of the dry particles entrained by the exhaust stream, the effluent steam was partially condensed to produce clean steam for plant use (Figure 17.3). The use of water vapor from the drying process, which is similar to the airless drying technique (see Chapter 8), resulted in a considerable reduction in dryer size and a large decrease in energy consumption; the unit evaporation rate was about 24.5 kg/m^{3}h, and the thermal efficiency was in the range of 79% to 86%. The representative set of data obtained is presented in Table 17.2.

As a result of these extensive studies, the feasibility of using plasma and

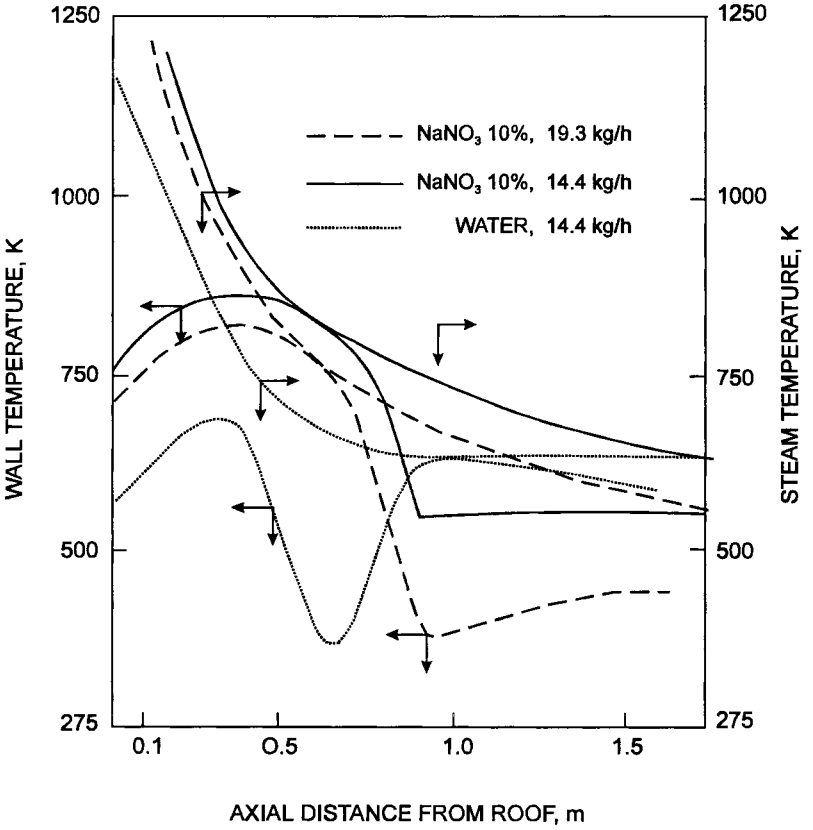

FIGURE 17.4 Temperature profiles in the plasma spray dryer. (Adapted from Amelot, 1983.)

superheated water vapor as a heat source for spray drying was demonstrated. Although the plasma temperature is relatively high (in the order of 3500 K), the operating temperature of a drying medium can be much lower, approaching 500 to 650 K. It can even drop to 370 K in the lower section of the dryer if the material feeding rate is high enough (Figure 17.4). This makes it possible to use plasmas for drying even for heat-sensitive materials, provided a very short residence time is used, to prevent overheating of the dried product.

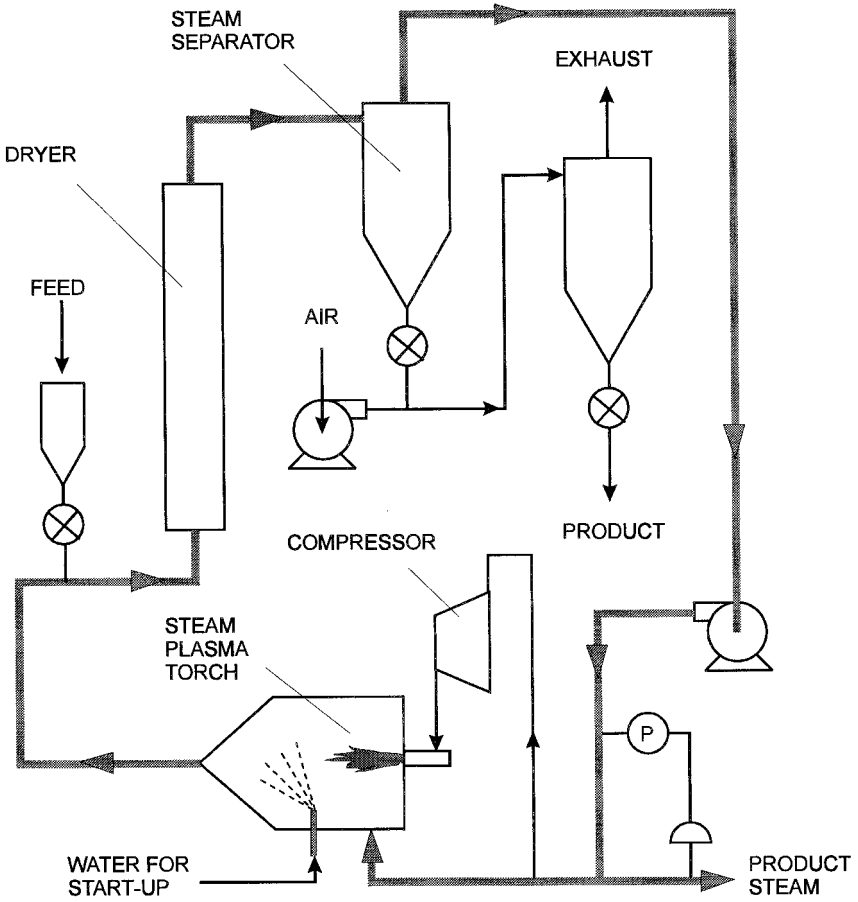

FIGURE 17.5 Experimental plasma flash dryer.

Another potential application of plasmas to the drying process is superheated steam drying where plasma torches can provide high-temperature gas streams at an efficiency of about 85% (Drouet, 1984). The technical viability of the plasma–superheated steam drying was tested in an experimental flash dryer shown schematically in Figure 17.5 The plasma torch designed at Research Laboratories of Hydro Quebec (IREQ) provides thermal energy for direct heating of the drying medium and water evaporation. During the start-up period, water is sprayed into the system to generate a sufficient amount of steam. At steady-state operation, steam circulates in a closed system, and steam generated in excess because of drying is bled off for other process needs. A fraction of the steam is recompressed for use in the plasma torch. To examine the effect of operating parameters and dryer design, Meunier and Munz (1986) developed a simple one-dimensional model based on mass and energy

TABLE 17.3 Standard Simulation Conditions of Plasma Superheated Steam Drying

Parameter	Range
Particles	
Product flow rate	200 tons/day
Initial moisture content	1 kg/kg
Final moisture content	0.1 kg/kg
Heat capacity	1.38 kJ/(kg K)
Apparent density	500 kg/m^3
Void fraction	0.5
Particle diameter	0.05–2.0 mm
Dryer	
Diameter	0.8–2.0 m
Length	2–50 m
Cone angle	0°–10°
Pressure	1–5 bar
Energy consumption	0.79 kWh/kg water
Steam	
Initial velocity	2–20 m/s
Initial temperature	550–1400 K
Final temperature[a]	T_b + (20–30 K)
Input power	6000 kW
Initial steam-to-solid ratio	1.2–11 mas.

[a] T_b is the boiling point (K) of water at a given pressure.

balances along the dryer assuming constant-rate period. For standard simulation conditions given in Table 17.3, the effect of inlet steam temperature, particle size and particle size distribution, and operating pressure was examined for both cylindrical and conical geometries of the drying chamber. It was found that a great reduction in dryer size might be expected at very high-temperature steam obtained by superheating a portion of the steam in a plasma torch. The use of a conical, rather than cylindrical, dryer offers shorter dryer height and more uniform processing of particles with a broad size distribution. The use of higher pressure reduces the residence time required for drying and thus the dryer height. However, the higher operating pressure will increase the duty of the superheater as well as increase the particle temperature, which might limit drying of heat-sensitive materials.

It appears that the results of experimental studies presented in this chapter have amply demonstrated the technical feasibility of plasma-assisted drying. The most promising is the use of a plasma and/or superheated water vapor as the heat source and drying carrier. In addition to the advantages inherent to superheated steam drying (see Chapter 7), the use of steam plasmas may offer the following benefits:

Gas–solid separation and latent heat recovery are easily achieved by condensation.
The pressure necessary for operation is developed by the steam boiler, which is an inexpensive way of pressurizing the whole drying system.
The steam recycled to the system can easily be compressed at low cost.
The high evaporative capacity and enhanced thermal efficiency allow major savings in both capital and operating costs.

18

Displacement Drying

One of the nonthermal methods of drying and dewatering is displacement drying, where water–immiscible solvent having a higher density than water is used to ''displace'' liquid moisture from the wet material (Brandreth and Johnson, 1980; Devine, 1980). Such a displacement results from the combined action of buoyancy and surface forces when the wet material is immersed in a drying solvent. The mixture of both liquids is then separated by gravity, centrifugal forces, or evaporation and recycled to the drying system. The process depends greatly on the ability of the displacement liquid to detach water droplets from the solid surface. Since the surface tension at the water–solvent and water–solid interfaces is a key factor in water release, the process can be intensified by addition of the surface-active agents. Advantages of displacement drying include

Reduced energy consumption compared to hot-air drying
Higher drying rates and therefore shorter drying times
Lower investment and operating costs
Capability of handling heavier water loads (up to 10% by volume) with no loss in drying efficiency

Additionally, this is a spot-free drying technique that leaves no trace of moisture on the material surface, which is especially important when drying films, plastics, polished metals, ceramics, and so forth. So far, displacement drying has found application in the field of electronics (printed circuit boards, relays, semiconductors, TV tubs), optics (eyeglass frames and lenses, films, cameras), electromechanics (copiers, electric motors), and mechanics (tools, cutlery, medical instruments). According to Devine (1980), in 1980 there were over 600 drying systems in operation in Europe, ranging in capacity from 40 liters to several cubic meters.

Two alternative mechanisms have been proposed to explain displacement drying (Brandreth and Johnson, 1980):

1. ''Roll-up'' mechanism [Figure 18.1(a)]—when the surface-active agent dispersed in a displacement liquid adsorbs at the solid–water interface, the wettability of the solid surface for water decreases and the area of contact becomes so small that buoyant forces overbalance the adhesion forces and finally cause water droplets to be released.

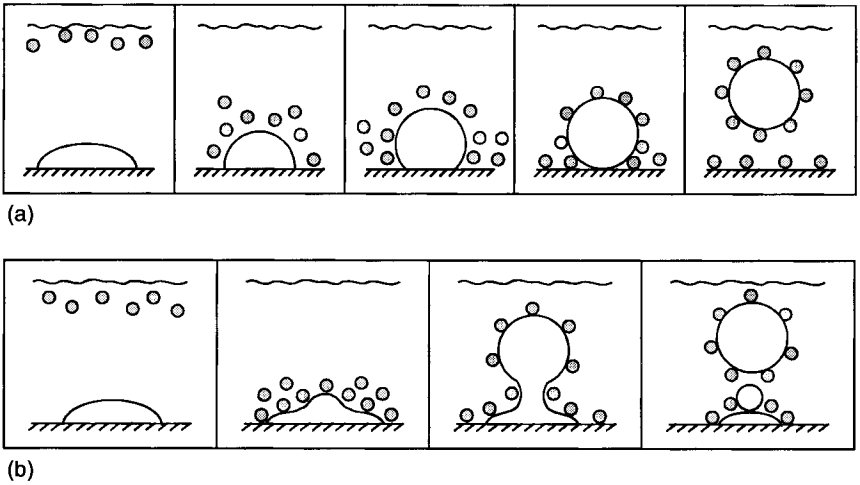

FIGURE 18.1 Mechanism of displacement drying: (a) roll-up of water droplet; (b) water–solvent interfacial tension lowering. (a) Water contact angle increases due to adsorption of a hydrophobic surfactant. (b) Water break-up by lowering interfacial tension between liquid phases.

2. Water–solvent interfacial tension lowering [Figure 18.1(b)]—when the adsorption of a proper surfactant at the liquid–solvent interface results in a marked reduction of the water-displacement liquid tension. In effect, the ''skin'' on the water droplet is weakened, the droplet necks down in the presence of agitation, and a significant fraction of primary water droplets is broken away and floated to the surface of the solvent batch due to buoyant forces.

In most cases, both mechanisms contribute to the overall displacement effect although to different extents. Because displacement drying is based on the surface phenomena, it is clear that internally bound water at molecular level, osmotically bound water or crystal water cannot be removed by this technique. It is possible, however, to remove water held in small pores.

In a typical configuration of a drying system, small solids (e.g., fine metal or plastic parts) are sunk into displacement fluid (Figure 18.2). Larger parts may be sprayed with a solvent, whereas solid structures like textile fibers or particulate materials can be washed with a drying fluid forced through the solid matrix.

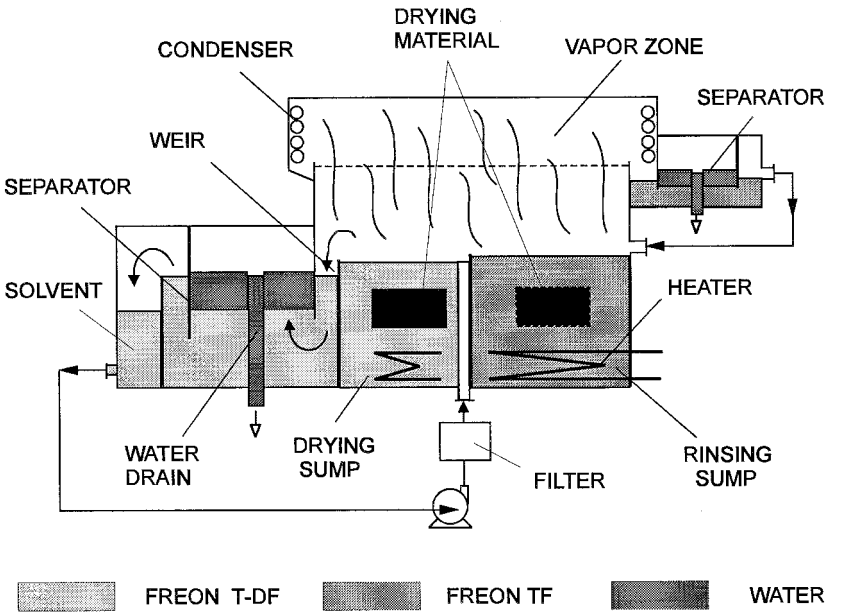

FIGURE 18.2 Typical displacement drying system.

A perfect solvent to displace water should have the high density and low interfacial tension for water. It should also be nontoxic, inflammable, immiscible with water, and chemically inert. As a displacement liquid, a variety of organic solvents can be used. Of these, freon F-113 is the most frequently selected because it is nontoxic (T.V.A.—1000 ppm), its density is 50% greater than the density of water, its boiling point is only 48°C, and the latent heat of evaporation at the boiling point is 146.5 kJ/kg. Unfortunately, freons are not environment-friendly, so their use is restricted in various countries. In either case, the system should be perfectly tight to avoid gas release.

The theoretical energy requirements in displacement drying are very small compared to thermal drying because the external energy is used only for breaking the adhesion and sorption forces. Figure 18.3 presents energy consumption against water loading for hot-air drying and displacement drying in a system used to dry small metal parts such as that shown in Figure 18.2. At the no-load condition, the fluorocarbon system consumes a certain amount

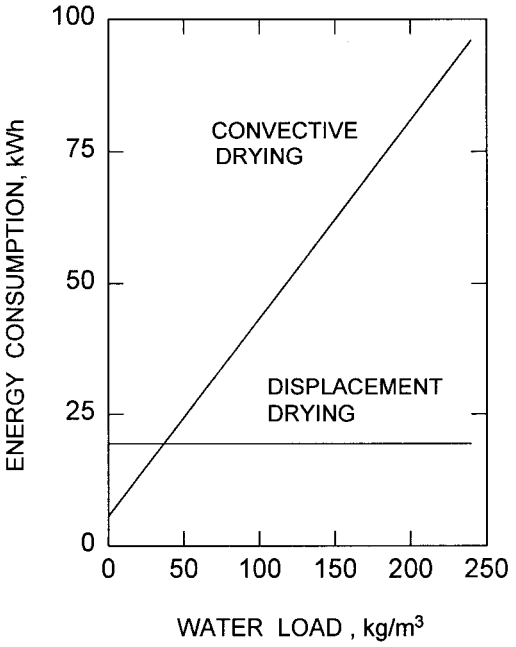

FIGURE 18.3 Comparisons of energy consumption for hot-air and displacement drying.

of energy because the solvent is being evaporated even under idle conditions. Under operation, energy consumption remains at the same level regardless of water load because there is no water evaporation. To the contrary, energy consumption for hot-air drying is lower at no water load (although not equal to zero because energy is used to heat dry solids) but rises sharply with moisture content. Starting from a water load of about 37.5 kg per cubic meter of drying parts for which the energy consumed in each process is equal, displacement drying always offers energy savings.

Another variant of displacement drying is solvent drying, where the solid material to be dried is immersed in a miscible organic solvent that is heated to its boiling point. During this extraction phase, water contained in the porous wet material is displaced by the solvent because of binary diffusion. Thus, the water concentration in the water–solvent mixture decreases gradually inside the material (solid phase) while it increases in the surrounding liquid until equilibrium is established with an equal concentration in both phases (Salin, 1991). Then, the material wetted with the solvent–reach mixture is dried thermally to remove the residual solvent. The evaporated solvent is recovered from the gas phase in a condenser while the solvent from the solvent–lean postprocessing mixture is regenerated by simple distillation. As in the case of displacement drying in water–immiscible liquids, drying in an organic solvent is an energy-saving technology since the latent heat of evaporation of volatile solvents is much lower than that of water. Thus, the energy consumption may be reduced considerably though thermal energy is needed for finish drying and solvent regeneration.

This method of drying was recently studied at the Forest Products Laboratory of the Technical Research Center of Finland (Pajunen et al., 1988; Salin, 1991). The small-scale laboratory tests were carried out with pine sapwood and heartwood (*Pinus silvestris*) as well as with birch (*Betula verrucosa*) and spruce (*Picea abies*) veneer. The wood samples were $25 \times 25 \times 80$ mm, and the veneer samples were $1.5 \times 90 \times 95$ mm. The solvents used were methanol, ethanol, and 2-propanol at their boiling points. The tests were performed with green wood using various combinations of treatment time from 0.5 to 12 hours and solvent-to-wood mass ratios ranging from 4 to 12.

The experimental data were interpreted in terms of the equilibrium between the water content in the water–solvent mixture held in the wood pores and that in the surrounding solvent at the end of the extraction phase. A comparison of these two concentrations based on a simple mass balance indicates how far the displacement process has proceeded during the treatment time used. Figure 18.4 presents representative data for veneer samples treated for different periods from 0.5 to 2 hours at a solvent-to-wood mass ratio of 4. It

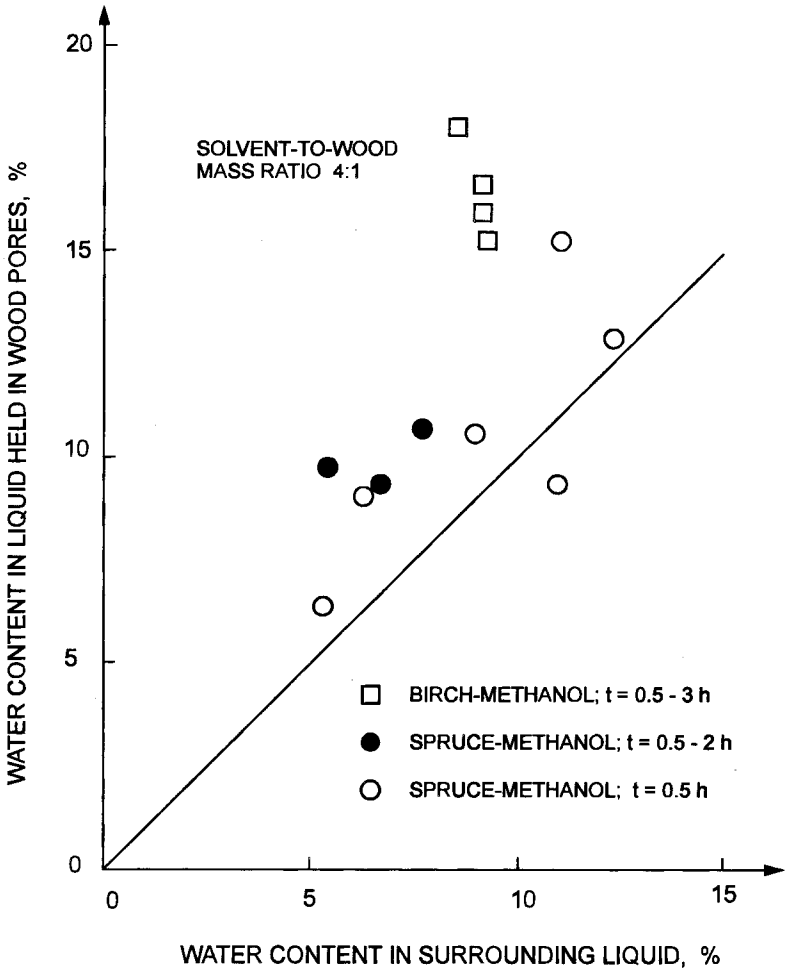

FIGURE 18.4 Concentration of water in the water–solvent mixture at the end of the extraction phase of green veneer. (From Pajunen et al., 1988.)

was found that equilibrium between two phases was attained during the shortest extraction time (30 min) and that further treatment did not have a substantial effect on water concentration. Such a relatively short time to reach equilibrium can likely be attributed to the relatively small sample thickness (1.5 mm), as for the much thicker wood samples (25 mm), these time periods were much

longer. For example, when solid pine sapwood was treated with methanol for different time periods from 2 to 12 hours, the concentrations of water close to equilibrium were attained in about 2 hours; thus, the concentration did not substantially change when longer times were used. The final water content in the wood was within the range 8% to 17% w.b. When propanol was used instead of methanol, the approach to equilibrium was reached in about 6 hours. Because the processing temperature in the case of propanol was higher, the lower displacement rates must be due to a slower diffusion of propanol compared with methanol. Thus, diffusion of methanol was estimated to be from 3 to 6 times faster than that for propanol, probably due to the lower molecular mass.

In the case of solid pine heartwood treated with methanol for periods of 1 to 5 hours, the final water concentrations were far from equilibrium even after 5 hours of extraction. The smaller displacement rates (by one order of magnitude than those in sapwood) seem to result from the less porous structure of heartwood, although other factors might contribute to the major difference in the observed displacement rates (Salin, 1991).

To quantify the effect of wood anisotropy on displacement rates, some experiments were performed with solid pine sapwood where the sample ends were sealed to permit mass transfer only in the tangential and radial directions. These tests proved that after two hours of treatment the water concentrations were very far from equilibrium, thus showing that the displacement rate is much faster in the longitudinal direction. The difference in these rates is about two orders of magnitude.

Concerning quality issues, no checking or other drying defects were noticed, but sample dimensions used were small. The surface of the wood samples was light-colored compared with that in conventional drying. The amount of extractives in the solvent phase after treatment was about 0.2% to 0.3% of the wood's dry weight for birch veneer and 0.4% to 0.7% for spruce veneer.

From the equilibrium data, it is clear that single-stage extraction requires low water concentrations in the solvent phase and high solvent flow rates. Thus, to reduce energy consumption, the process has to be realized in a multistage, countercurrent configuration where residual moisture is extracted with almost pure solvent.

To evaluate the potential application of solvent drying to the wood industry, Salin made the following process design for veneer and ethanol as the most suitable solvent (Salin, 1991). He assumed that water concentration in the liquid absorbed by the veneer is 20% higher than in the surrounding liquid after each extraction stage. Thus, for a given number of extraction stages, it

was possible to calculate the moisture displacement in the veneer samples for different veneer–ethanol flow ratios and different initial water contents in the extraction liquid. The ethanol regeneration stage was assumed to be a normal distillation unit in which the energy consumption is primarily fixed by initial and final concentrations and by the total flow of liquid. For each combination of the process variables in the extraction stage, the corresponding energy consumption in the regeneration stage was then calculated. Finally, the energy consumption in the thermal drying stages was estimated from the mass of ethanol and water held in the veneer after the extraction stage. The heat of evaporation for ethanol is only 29% of the corresponding value for water if the comparison is based on equal liquid volumes. In Salin's calculations, the theoretical heat consumption was increased by 25% to account for heat losses.

Taking the minimum energy consumption as the design criterion, which translates into a minimum in operating costs, the following results were obtained:

There is an optimal ethanol concentration level of about 90% in the regenerated liquid, which is almost independent of other conditions.

As the number of extraction stages increases, the optimal amount of moisture displaced also increases.

The total energy consumption decreases as the number of extraction stages increases (Table 18.1).

TABLE 18.1 Energy Consumption Versus the Number of Extraction Stages for Displacement Drying of Veneer in Ethanol

Number of extraction stages	Energy consumption (MJ/m^3 of veneer)
0[a]	1200
1	1110
3	910
5	820
10	730

[a] Conventional drying.
Source: Salin (1991).

This preliminary process design for solvent drying of veneer with ethanol indicates that an energy consumption about one-third lower than that for a conventional process may be achieved when using 5 to 10 extraction stages to displace about 70% to 90% of the water in the wet material. Such substantial energy savings could make displacement drying of wood products technically attractive, especially if other issues such as product quality or recovery of extractives can offset more complex equipment, handling inflammable solvents, and so on.

19

Vapor Drying

The term ‘‘vapor drying’’ refers to a process of convective drying where the vapor of an organic solvent is used as the medium for heating the material to be dried and removal of evaporated moisture. Because condensation of vapors offers much higher heat transfer coefficients than forced convection of air, the process heat is transferred to the drying material more rapidly and uniformly, so drying times are considerably reduced. Moreover, the use of partial vacuum in the system increases the rate of moisture removal. A distinction should be made at this point from superheated steam drying (Chapter 7) and airless drying (Chapter 8), where steam is used as the convective drying medium. Also, vapor drying differs from solvent (displacement) drying (Chapter 18), where moisture is displaced by the solvent in the liquid phase due to surface tension forces or diffusion in the water–solvent mixture, and evaporation is used only to regenerate the spent solvent.

Credit for the early research on vapor drying belongs to Besemfelder (Besemfelder, 1910) and Hudson (Hudson, 1942, 1948, 1950), who proved that predrying large-section lumber for subsequent pressure preservation by the use of solvent vapor is advantageous over conventional kiln drying. In addition to a considerable reduction in drying time, higher final strength, and

less drying degradation, Hudson found much better penetration of the preservatives into vapor-dried wood stocks. Such effects were attributed to the greater number of small internal checks that were formed in the outer layers of impervious wood species during vapor drying, compared with a smaller number of much bigger checks in air drying. This promising drying technology was further explored at CSIRO, Division of Forest Products, by Ellwood and coworkers (Ellwood et al., 1953) to determine whether the process of vapor drying could have commercial application to Australian native timber. The research was performed with the impervious, collapse-susceptible species such as ''ash'' eucalyptus and myrtle beech, previous timbers such as various pines, and miscellaneous impervious and moderately pervious timbers, including subtropical rain-forest species. Drying was carried out from the ''green'' and partly air-dried conditions down to moisture contents characteristic of seasoned lumber as well as the ones that required treatment with preservatives. The following solvents were examined: Stanvac K9 with an average boiling point of 196°C; mineral turpentine (160°C); perchlorethylene (121°C); and commercial toluene (110°C). The working pressure was varied from a vacuum of about 7 kPa through atmospheric to an overpressure of about 55 kPa. The wood temperature was kept within the range of 55° to 82°C. In general, the usefulness of each of these fluids was found to depend on its boiling point. The fluids of lower volatility gave higher drying rates at a given working pressure but became inefficient at low pressures and temperatures. The most volatile solvent, toluene was found difficult to condense at low working pressures, which led to considerable losses. Perchlorethylene was useful over the widest range of drying conditions and, as a fluid with a relatively low boiling point, was ranked as the best for the vapor drying process. Overall, these studies demonstrated a reduction in drying time with equivalent or better product quality by about 30% in the drying of refractory species and by about 5% to 10% in drying pervious timbers as that required for kiln drying.

Despite attractive features, some engineering and process difficulties need to be solved for successful industrial application of the vapor drying technique. These are as follows:

Arrange for an even vapor distribution within the drying chamber in order to ensure uniform temperature and drying conditions throughout the drying load.

Prevent working fluid retention by pervious or moderately pervious timbers when high vacuum is used in the process.

Identify an inexpensive, nonflammable, and nontoxic working fluid.

Vapor phase heating has found another application in the drying of coils and insulation for shell-form and core-form power transformers prior to oil impregnation (Westinghouse Engineering Transformers, 1965; Feather, 1965; Strumillo et al., 1971). These two processes in sequence greatly affect the cost, processing time, and reliability of air and moisture removal from the paper and paperboard insulation of oil-filled transformers. The conventional procedure for drying consists of hot-air heating of the insulation followed by vacuum drying. Since residual moisture in a transformer winding can cause failure, the drying conditions are very stringent on temperature uniformity and vacuum control. Aside from nonuniform drying, the major drawback of convective drying is the temperature constraint; at higher temperatures used to improve drying effectiveness, the surface layer of insulation might be overheated, resulting in discoloration and embrittlement of some or all of the insulation in windings because of oxidation by the hot air. Also, oxidation of the oil held on the surface of the insulation is a problem if reprocessing of a transformer is required when part of its insulation has already been oil-impregnated.

A simplified flow diagram for vapor drying is shown in Figure 19.1 (Feather, 1965). The entire process of heating, drying, and oil impregnation is carried out in the same drying chamber and consists of the following stages:

1. Preliminary evacuation of air from the chamber
2. Heating of the windings under partial vacuum using vapor of a boiling organic liquid
3. Final drying under high vacuum
4. Vacuum impregnation with oil

The vapor for heating windings is generated by boiling a shallow pool of the organic liquid in the bottom of the drying chamber. The heat input is sufficient to produce excess vapor. This ensures good circulation of the vapor in the drying chamber and allows water vapor released from the insulation to be taken away from the chamber with excess vapor of the organic solvent. The mixture of both vapors is directed to the condenser and, after separation, the solvent is reclaimed for reuse. Once the desired temperature of the windings is reached, the liquid solvent is removed from the boiling pan and the pressure in a drying chamber is further reduced. Such a vacuum operation removes residual water and condensed solvent from the insulation. Wall heaters provide additional heat for evaporation, if needed. At the completion of the vacuum drying, the chamber is filled with transformer oil to impregnate the windings. Figure 19.2 compares the heating and drying characteristics for

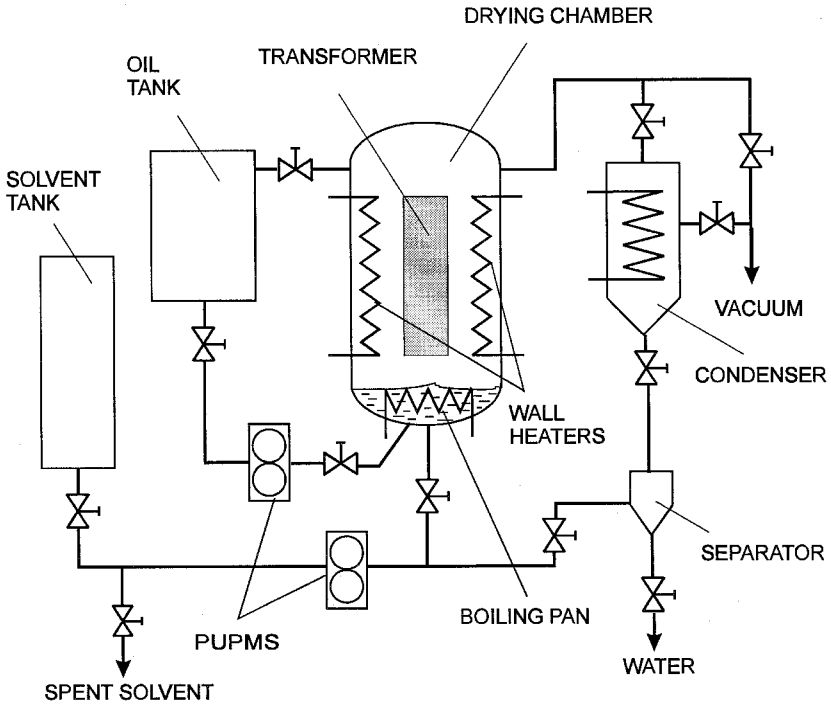

FIGURE 19.1 Schematic diagram of the vapor drying of power transformers.

vapor heating followed by vacuum drying, forced convective drying, and vacuum drying of the insulation of power transformers (Feather, 1965). Much faster drying and more complete moisture removal during vapor drying than for the other processes can be attributed to higher heat transfer rates and more uniform heating of the entire structure of the windings.

To take advantage of the high condensing heat transfer coefficients, the operating temperature and pressure in the drying chamber are such that the organic vapor is saturated or only slightly superheated. The solvent to be used in vapor drying should have the following characteristics:

Its boiling temperature should match the desired operating temperature at an absolute pressure that is well below the water vapor pressure at that temperature.

The vapor pressure should be high enough to completely remove the solvent that is trapped in the insulation at the end of the drying stage.

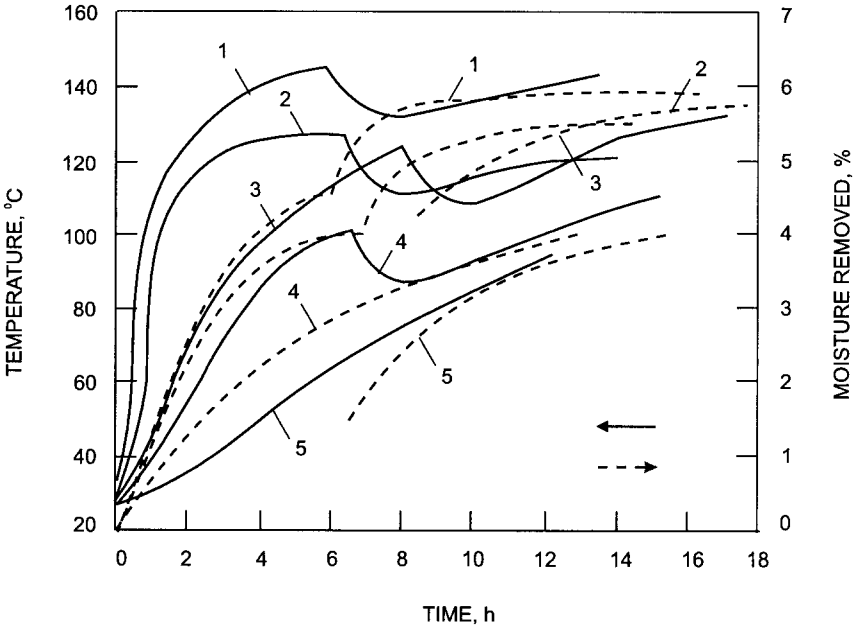

FIGURE 19.2 Heating and drying characteristics of the insulation structure of power transformers. 1—vapor drying: 150°C, 6 h; vacuum drying: 150°C. 2—vapor drying: 130°C, 6 h; vacuum drying: 130°C. 3—convective drying: 150°C, 8 h; vacuum drying: 150°C. 4—convective drying: 130°C, 8 h; vacuum drying: 130°C. 5—vacuum drying: 130°C. (Adapted from Feathers, 1965.)

It should be compatible with the insulating oil, both electrically and chemically, so that traces of solvent will not damage the windings and the insulating oils.

The organic liquid that meets all these criteria and was used in vapor drying of power transformers is the petroleum solvent.

The key benefits of the vapor drying of power transformer insulation are as follows:

Because the heat of condensation combines with the sensible heat of the vapor, the heating rate is much higher, particularly within the insulation structure, where it is difficult to maintain an adequate flow of hot-air stream during convective heating.

Higher temperatures can be used without deterioration of the insulation because no oxygen is present in the vapor of organic liquid.

All subsequent stages can be performed in a single unit.

The presence of oil-impregnated insulation during reprocessing creates no problems since oil oxidation during the heating stage is essentially eliminated. Because the organic liquid is compatible with the impregnating oil, cross-contamination of the two liquids is eliminated.

In view of its evident advantages, this old but unpopular drying method is worth further exploration.

20

Slush Drying

Fresh fruit juices are complex aqueous slurries (80% to 90% by weight of water) containing numerous organic compounds. Most juices are very heat-sensitive because of the potential for enzymatic reactions and the volatilization of flavor and aroma components.

Conventional air-drying techniques such as spray drying, for example, require low-temperature operation, which prolongs the drying time and may even lead to undesirable microbiological reactions. Vacuum drying and microwave-vacuum drying reduces the temperature of evaporation, but the loss of volatile flavor species can still be significant. Freeze-drying, on the other hand, allows product quality to be maintained, but the process is difficult to carry out at a rate fast enough to be economically justified for most fruit juices.

To handle dehydration of fruit juices, a technology called slush drying was proposed and tested with apple juice for the potential loss of volatile flavor and aroma substances (Chandrasekaran and King; 1971; Lowe and King, 1974). The principle of this method stems from the dependence of the freezing point on the concentration of dissolved solids (Figure 20.1). It boils down to the fact that drying takes place from an ice–liquid mixture (slush) in which 20% to 70% of the water present in the fruit juice is frozen (the

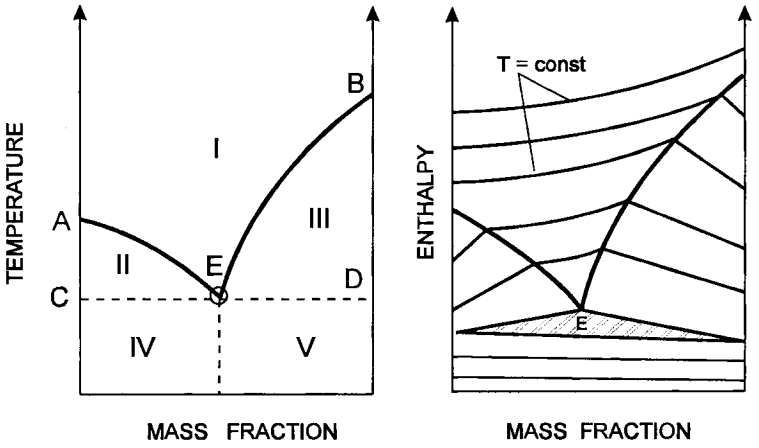

FIGURE 20.1 Phase equilibrium of a binary system: I—unsaturated solution, II—saturated solution, III—saturated solution + solute, IV—eutectic mixture + solidified solvent, V—eutectic mixture + solute. AEB—saturated solution, CED—three phases.

remainder is still liquid). The higher the dissolved solids' content in the unfrozen liquid juice, the greater the retention of the volatiles. At the same time, there is no need for maintaining the ultra-low temperatures required in freeze-drying, which allows favorable drying rates to be achieved.

Slush drying is somewhat analogous to freeze concentration (Kudra and Strumillo, 1998) except that the stage of separating the ice from the supernatant liquid in slush drying is accomplished by sublimation of the ice along with evaporation of some of the water from the liquid concentrate. Similarly to conventional thermal drying, slush drying is limited by the phase equilibrium (Figure 20.2), which indicates the maximum (equilibrium) percent ice present at a given temperature and dissolved solids' concentration. For any concentration–temperature conditions in the area below the equilibrium curve, the percent of water present as ice can be calculated from the lever-rule mass balance.

Essentially, slush drying is a batch process, which starts with cooling the liquid to be concentrated to a temperature intermediate between the freezing point and the eutectic point of the slurry (see Figure 20.1). The semisolid material is then placed in a vacuum chamber and air is evacuated to reduce the pressure to around 1 mm Hg. The ice crystals are sublimated by heat supplied by an internal heater. The water vapor and volatile compounds are sucked away by a vacuum pump and condensed in a vapor trap (Figure 20.3).

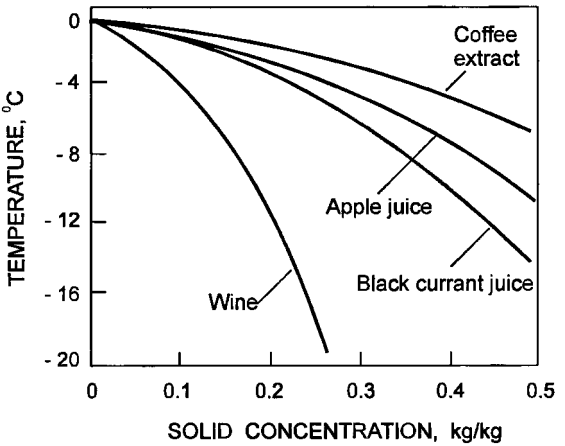

FIGURE 20.2 Freezing equilibrium for selected liquids.

As reported by Chandrasekaran and King (1971), the slush drying of apple juice takes place at a nearly constant drying rate with respect to time and solids' content, especially if an allowance is made for the lower amount of water contained in a given volume of juice at higher solids' concentrations.

Figure 20.4 indicates that the surface temperature during slush drying (and also during freeze-drying) is well below 0°C. In contrast to freeze-drying, where the surface temperature at the end of drying is always below the estimated eutectic temperature of −23°C, in slush drying the surface temperature does not drop below −18°C. Experiments on liquid pool drying performed

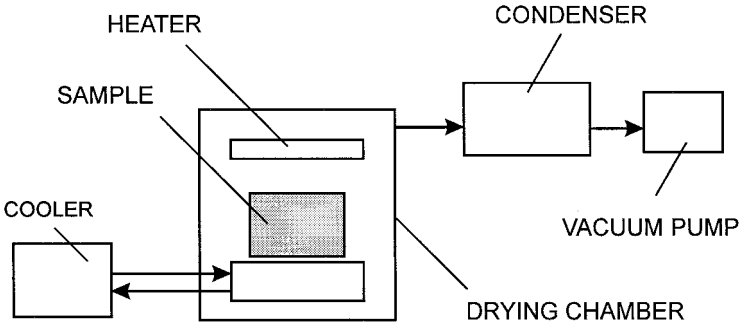

FIGURE 20.3 Block diagram for slush drying.

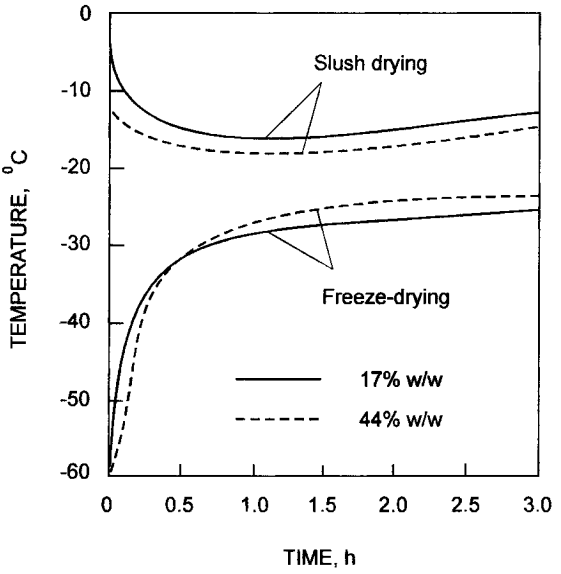

FIGURE 20.4 History of the surface temperature for slush drying and freeze-drying of apple juice.

at the chamber pressure of 1 atm have proved that the surface temperature in pool drying should be 50° to 60°C to maintain the same order of a drying rate as the combined evaporation and sublimation rates in slush drying (Chandrasekaran and King, 1971).

An interesting phenomenon observed in the slush drying of apple juices was the formation of a stable and coarse foam over the surface of the slush bed. The amount and durability of the foam increased with increasing initial content of dissolved solids. This foam formation did not occur in drying from a free liquid and occurred in freeze-drying only to a minor extent near the end of drying when traces of liquid began to appear on the surface. The formation of sugar-rich foam may explain the selective retention of aroma in slush drying, as sugars are known to lock in volatile flavors. In fact, slush evaporation was found advantageous in aroma retention over air or vacuum drying from the liquid state because of the beneficial effects of solute concentration and temperature. Under evaporation or drying conditions leading to substantial aroma retention, the loss of volatiles is governed by a diffusion mechanism. It is generally accepted (see Chandrasekaran and King, 1972a, b) that aroma retention increases markedly in most drying processes with increasing initial

dissolved solids' concentration. This is a result of diffusion coefficients for volatile solutes decreasing much more rapidly than those for water as the dissolved solids' content increases. In slush evaporation, the separation of some of the water as ice leaves a liquid concentrate of higher dissolved solids' content. Evaporation from this liquid should then occur with improved volatile retention. Furthermore, any water removed by sublimation should not entail much volatile loss. Volatile compounds can be expected to remain with the concentrate upon partial freezing rather than being incorporated into the ice crystals, a behavior that accounts for the high degree of volatile retention that is found in freeze concentration. At the temperatures prevailing for slush evaporation, diffusion within the concentrate should keep volatiles from accumulating ice crystal–concentrate interfaces, unless the solubility limit is passed for formation of a volatiles-rich oil phase. The low temperatures of slush evaporation should also help aroma retention, since diffusivities of volatile solutes decrease more rapidly with decreasing temperature than does that of water (Chandrasekaran and King, 1972b; Thijssen, 1971).

Although slush drying has apparently yet to be commercialized, there are several benefits over freeze-drying. In contrast to the relatively high drying rates in slush drying, the freeze-drying rates for fruit juices and other sugar-containing substances are lower because of the need for holding very low frozen-zone temperatures to achieve adequate solidification during drying (Bellows and King, 1972). At the much higher temperatures of slush evaporation, the mass transfer driving forces are higher because of the much higher vapor pressure of water at the operating temperature, and hence the drying rates are much higher. Another advantage in comparison to freeze-drying is the lower refrigeration cost because of a higher condenser temperature. In comparison to freeze concentration, slush evaporation has the same benefits resulting from lower operating temperatures (e.g., reduced product degradation and loss of aroma). In addition, there is no loss of the concentrate entrained with the ice during a solid–liquid separation as it is in freeze concentration.

21

Atmospheric Freeze-Drying

Vacuum freeze-drying is an expensive operation—up to an order of magnitude more expensive than the next-expensive drying operation (spray drying). The high capital and energy costs stem from the need to generate and maintain very low temperatures and very high levels of vacuum. Therefore, this technique is justified mainly for very high-value materials and high-quality/special properties products such as pharmaceuticals, nutraceuticals, enzymes, and certain products of biotechnology.

Among ways tested to reduce the cost of freeze-drying are avoiding the need for a condenser for the sublimated vapor (which must be held at temperatures well below 0°C), to enhance contact between the heat- and mass-transferring phases, and to operate the process at near-atmospheric pressures. If the frozen product is in contact with a suitable solid adsorbent, the sublimated vapor is adsorbed by the solid, which performs the role of the external condenser in the conventional vacuum freeze-drying process. Both fixed packed beds and fluidized beds of adsorbent particles have been used with partial success. King and Clark (1969), for example, proposed alternating fixed beds of frozen material with beds of adsorbents. As low-pressure gas flows through the successive layers, the adsorbent captures the water vapor. The heat of

sorption transferred to the gas stream is then used for subsequent sublimation. Since the solid–solid contact is poor, the heat and mass transfer rates are low and hence the drying times are very long. The fluidized bed configuration is more efficient, however, because the adsorbent acts as both heat transfer medium and water vapor vehicle due to random collisions of the product with absorbing particles (Wolff and Gibert, 1991). If the heat required for sublimation is nearly balanced by the exothermic heat of adsorption of water vapor, then the adsorbent doubles as a heat carrier and mass transfer agent as well. Because the fluidized bed is well mixed, the bulk of solid adsorbent is far from saturation as mass transfer takes place also between the adsorbent particles of different saturation. Moreover, a continuous freeze-drying process can be more readily developed with atmospheric rather than the conventional high-vacuum process. The main limitation of such a system is the relatively long processing time. In addition, it is difficult to separate the adsorbent from a freeze-dried product so the adsorbents compatible with the materials dried are necessary. The flow diagram for the continuous atmospheric freeze-drying is depicted in Figure 21.1.

As reported by Wolff and Gibert (1991), drying kinetics of atmospheric freeze-drying depends not only on the bed temperature and material thickness but also on the operating pressure. Experiments were performed in a fluidized bed freeze-drying column fitted with a double jacket for cooling liquid (6 kW at −25°C). The column was filled with pre-gelatinized corn starch 0.16 mm in diameter that was found compatible with frozen at −25°C potato parallelopipeds 10 mm square base and thickness 2, 3, and 5 mm. In the course of drying, a potato sample of 0.3 kg was immersed into a 5-kg bed of corn starch fluidized by air flowing with superficial velocity equal to 0.04 m/s. The regeneration temperature was kept at 50°, 57°, 65°, 72°, and 85°C, and the bed temperature was maintained at −5°, −10°, and −15°C to avoid melting the product. As expected, an increase in bed temperature and a decrease in potato thickness resulted in higher drying rates. The regeneration temperature of the starch studied over the range from 50° to 85°C did not affect drying kinetics for the material/adsorbent mass ratio used in these experiments and in the study by Wolff and Gibert (1990a). The regeneration temperature of 65°C for starch was found to be sufficient to permit its recycling.

Figure 21.2 presents the effect of the overall pressure on drying kinetics. Because the shape of drying curves indicates that internal resistance to mass transfer is the limiting factor in atmospheric freeze-drying, the higher drying rates were obtained at lower levels of operating pressure. According to Wolff and Gibert (1991), a pressure reduction by 500 hPa shortens by a factor of 2

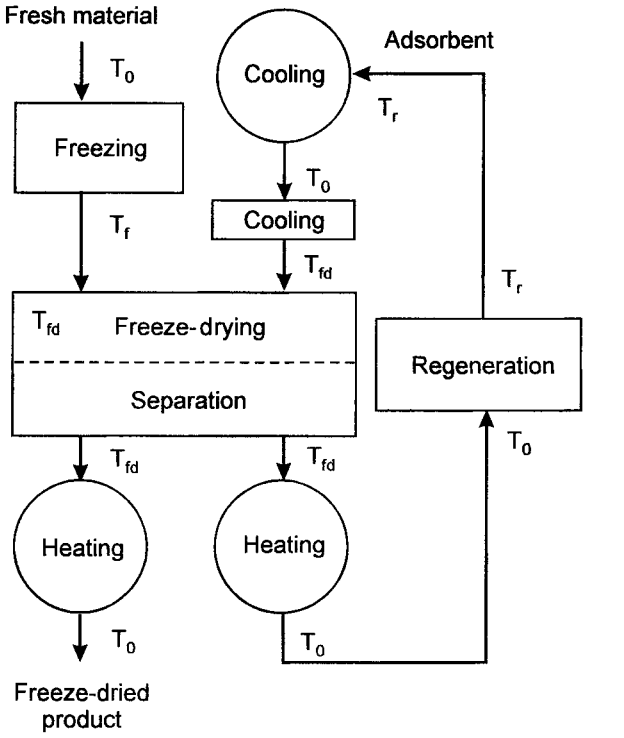

FIGURE 21.1 Process configuration for continuous atmospheric freeze-drying. (From Wolff and Gibert, 1990a.)

the total freeze-drying time needed to decrease the moisture content of potato samples from 4 kg/kg to 2 kg/kg (Figure 21.3). Optimum pressure was found to be around 100 hPa.

Assuming uniformly retreating ice front and using sorption isotherms for the solid adsorbent, Wolff and Gibert (1990b) proposed the following model for atmospheric freeze-drying in a fluidized bed of particulate adsorbent:

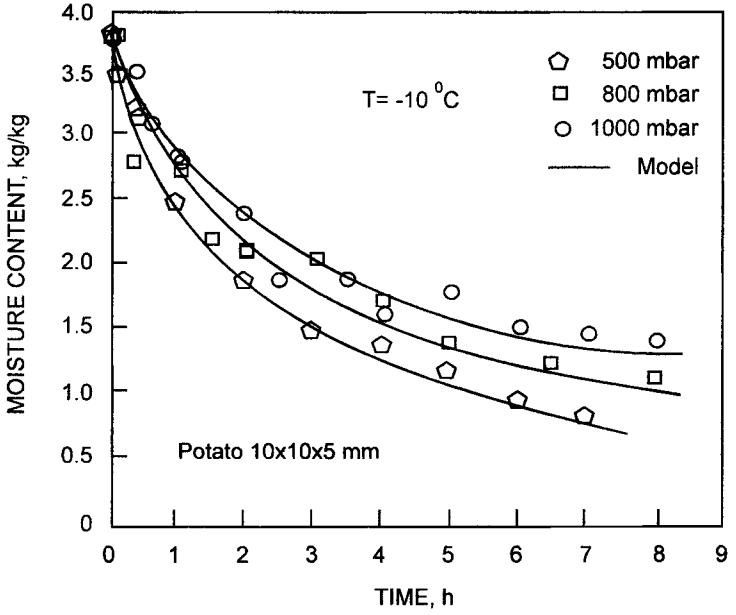

FIGURE 21.2 The effect of operating pressure on freeze-drying kinetics for potato particles 10 × 10 × 5 mm in a fluidized bed of corn starch (Wolff and Gibert, 1991).

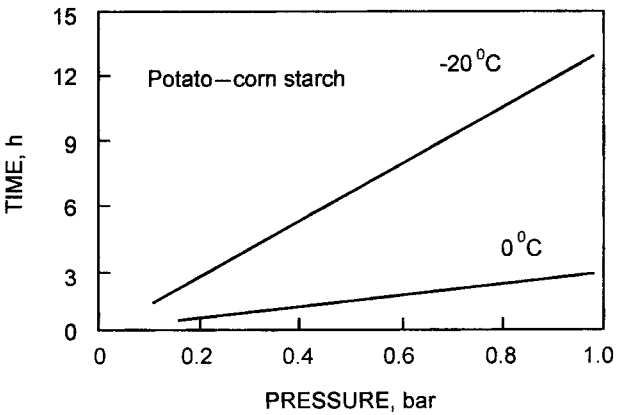

FIGURE 21.3 The effect of operating pressure on total freeze-drying time in the fluidized bed of solid adsorbent. (From Wolff and Gibert, 1991.)

$$\frac{A(p - p_c)}{R_e + bR_i} + \frac{M_a}{P\left(\frac{1}{a_w} \cdot \frac{da_w}{dX_a} - B_r \log \frac{a_{wa}}{a_w}\right)} \cdot \frac{dp_c}{dt} - \frac{M_a A_r \exp(-B_r X_a) + \frac{\Delta H_v M}{R}}{T^2\left(\frac{1}{a_w} \cdot \frac{da_w}{dX_a} - B_r \log \frac{a_{wa}}{a_w}\right)} \cdot \frac{dT}{dt} = 0 \tag{21.1}$$

where R_e and R_i are the external and internal resistances to combined heat and mass transfer, respectively, defined as

$$R_e = \frac{1}{k_e} + \frac{1}{h_e} \cdot \frac{\Delta H_s^2 pM}{RT^2} \tag{21.2}$$

and

$$R_i = \frac{RT}{MD_w} + \frac{1}{\lambda} \cdot \frac{\Delta H_s^2 pM}{RT^2} \tag{21.3}$$

Derivation of Eqs. (21.1) through (21.3) along with simulation results for different process conditions are given by Wolff and Gibert (1990b).

To compare atmospheric freeze-drying with conventional freeze-drying, a series of experiments was conducted with potato particles spread in a monolayer in a conventional freeze-dryer (Wolff and Gibert, 1990a). The heating plate temperature was set at 25°C, while the condensing plate temperature was set at −65°C. Drying kinetics were obtained at the operating pressure of 1 Pa, which is equivalent to the product core temperature of about −50°C, as well as at 300 Pa, which corresponds to a core temperature of −8°C, which is close to the bed temperature in atmospheric freeze-drying. As seen from Figure 21.4, drying kinetics for atmospheric freeze-drying do not exhibit a constant-rate period as they do in vacuum freeze-drying. The average drying rate in atmospheric freeze-drying was estimated at 0.09 kg of water per kg of fresh product and per hour against 0.15 kg/(kg h) and 0.42 kg/(kg h) for vacuum freeze-drying at 1 Pa and 300 Pa, respectively.

Because of the internally controlled mass transfer, drying times for atmospheric freeze-drying are longer than for the vacuum freeze-drying. The difference in drying time increases with particle size (thickness). Thus, for 5-mm-thick particles, about 2 hours are needed to reduce the moisture content from 4 kg/kg to 2 kg/kg in the vacuum process, whereas 6 hours are required

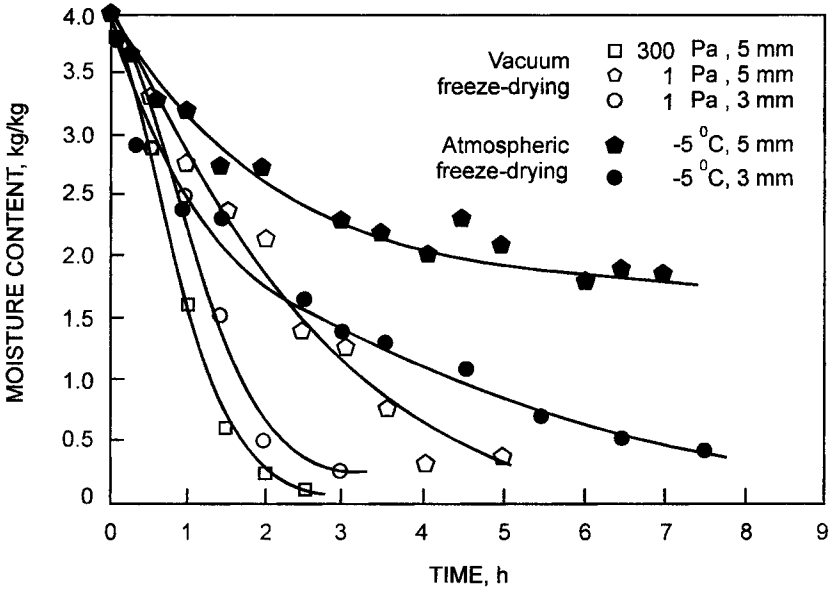

FIGURE 21.4 Comparison between freeze-drying and atmospheric freeze-drying for potato particles. (From Wolff and Gibert, 1990a.)

for atmospheric freeze-drying. For 3-mm-thick particles, these drying times are shortened to 1.5 and 2 hours, respectively.

Although the color and taste of potato dried with these two methods were not different, the edges and corners of the potato particles were found to be rounded after atmospheric freeze-drying because of erosion due to fluidization (Wolff and Gibert, 1990a). An average thickness of the product from atmospheric freeze-drying was 12% smaller as compared to 5% from the vacuum process. Also, up to 2% w/w of corn starch remained at the surface of the product from atmospheric freeze-drying, which should be taken into account when selecting adsorbent for the particular product.

Considering process economics, Wolff and Gibert (1990a) compared energy consumption to remove 1 kg of water contained in the product at 3 kg/kg of the initial moisture content. They calculated the cooling and heating energy requirements for vacuum freeze-drying as 3550 kJ and 3780 kJ, respectively. In atmospheric freeze-drying, the energy requirement for cooling was calculated as 2250 kJ, while that for heating (regeneration and blower) was 3440 kJ. These authors point out that these theoretical energy requirements

are underestimated since they did not account for energy losses and savings due to batch (vacuum) and continuous (atmospheric) processing. After the calculation procedure was adjusted for real process conditions, the energy costs were estimated to be lower by 38% on cold requirements and 34% on heat requirements as compared to the vacuum freeze-drying.

Recently, Donsi et al. (2000) demonstrated the feasibility of atmospheric freeze-drying for shrimp and showed that the drying time is indeed an order of magnitude longer than in the vacuum process. To shorten the drying time, part of the water was removed via an osmotic dehydration process. Freeze-drying was carried out in a fluidized bed apparatus using mineral adsorbents (zeolite particles 88 μm mean diameter) or organic adsorbents (wheat bran). The dried shrimp has rehydration properties that are similar to those obtained in conventional freeze-drying. The economics of the process were not reported, however.

Alves-Filho et al. (1998) also used a fluidized bed as the first-stage freeze-dryer at atmospheric pressure in a two-stage heat-pump system but with no adsorbent (see Chapter 15). Drying conditions at the first-stage fluid bed dryer were controlled by adjusting the heat-pump dryer components to keep the air temperature below the drying product's freezing point. This control is based on the specific enthalpy curves developed by Alves-Filho (1996). The product residence time in the first-stage dryer is selected to reduce moisture content to the critical value. Afterward, the semidry product is transferred to the second-stage fluid bed to be dried at higher temperatures. The advantages of the two-stage system are that the low-temperature drying reduces the moisture content while maintaining product quality and the higher-temperature drying increases the overall heat-pump dryer capacity. The authors reported excellent quality of dried shrimp, apple pieces, carrot slices, etc., albeit at a relatively high cost.

Part IV

Hybrid Drying Technologies

The term ''hybrid drying technologies'' is used in a rather general way in our discussion. As can be seen from the following schematic, it includes drying techniques that use multiple modes of heat transfer as well as those that use two or more stages of dryers of the same or different type. A broad range of successful new drying technologies fall in this category since they are based on intelligent combinations of well-known conventional know-how.

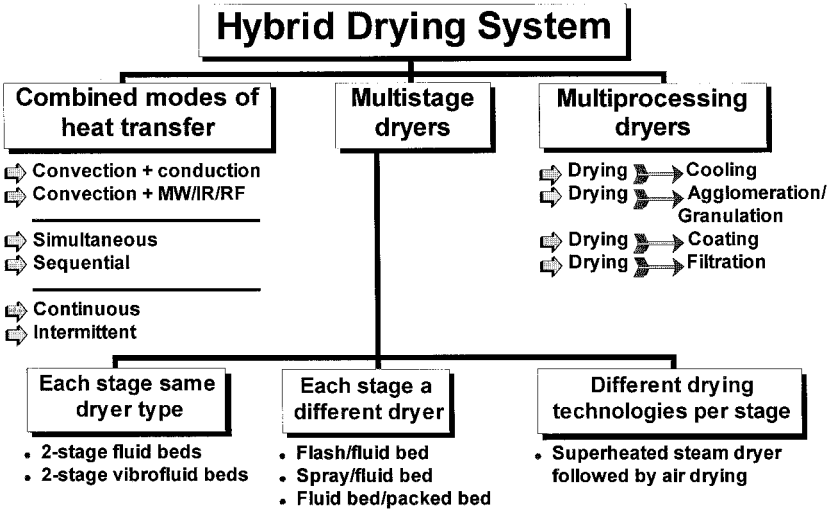

22

Radio-Frequency Drying with 50-Ohm Technology

In contrast to conventional thermal processes that rely on surface heating by convection, conduction, and/or radiation with subsequent diffusion of heat into the material interior, dielectric heating is based on volumetric heat generation where high-frequency electromagnetic energy is transformed into heat practically throughout the whole volume of the material. This heating method is particularly advantageous in thermal drying because favorable dielectric properties of water and other polar liquids cause heat to be generated in the wet parts of the drying material. This greatly eliminates thermal lag due to heat diffusion and provides some unique features such as (Strumillo and Kudra, 1986; Metaxas and Meredith, 1983; Metaxas, 1996; Sanga et al., 2000)

Enhanced diffusion of liquid and vapor moisture
Coincidental temperature and mass concentration gradients
Internal pressure gradient as an additional mass transfer driving force
Stabilized material temperature at or below the liquid boiling point

Electromagnetic energy is one of the forms of energy that is stored and transmitted by alternating electric and magnetic fields. It is propagated in space

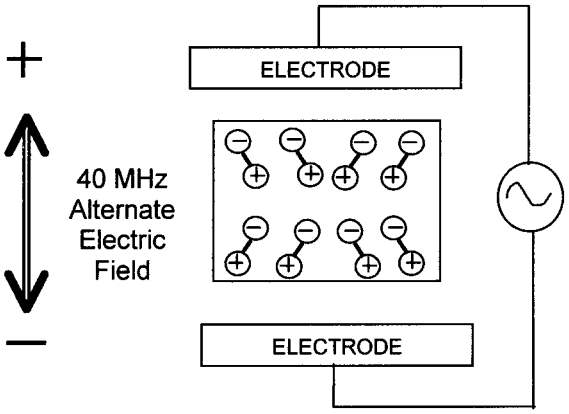

FIGURE 22.1 Heat generation in alternating electric field.

as an electromagnetic wave that is characterized by the wavelength λ, frequency *f*, magnetic field strength *H*, and electric field strength *E*. When an alternating electromagnetic field is applied to the special category of materials (called ''lossy'' dielectrics), the energy is transformed to heat (dielectric heating) due to ionic conduction and/or dipole oscillations, which attempt to follow the rapid changes in the electric field orientation. Materials with no dipolar electric charge do not heat because the electric field affects only asymmetrically charged molecules, of which water is by far the most common (Figure 22.1).

The power *P* absorbed in a unit volume of a dielectric material and dissipated as heat depends on dielectric properties of the material (mainly the loss factor ε'') and the electromagnetic field parameters, i.e., the frequency *f* and the electric field strength *E* within the drying material

$$P = 2\pi f \varepsilon_0 \varepsilon'' E^2 \tag{22.1}$$

where ε_0 is the permittivity of free space equal to $8.854 \cdot 10^{-12}$ F/m.

The effective loss factor ε'' is a frequency-dependent parameter determined by the material properties that characterizes the ability of the material to absorb electromagnetic energy. It is defined as a product of the dielectric constant ε' and the loss tangent tan δ (δ = phase angle between circuit currents)

$$\varepsilon'' = \varepsilon' \tau \delta \tag{22.2}$$

Dielectric heating in applications involving drying, pasteurizing, sterilizing, and similar thermal processes is carried out in two frequency regimes: radio frequency (RF) and microwave (MW). The radio-frequency range extends from about 1 to 300 MHz, while the microwaves cover the frequency range from 300 to 3000 MHz. Specific frequencies have been designated within the RF and MW bands for industrial, medical, and scientific applications. These are 13.56, 27.12, and 40 MHz in the RF region and 915 (896 MHz in Europe) and 2450 MHz in the MW region.

Because both the electromagnetic field and the processed material are allocated in a three-dimensional space, the field–material interaction can be quite complex, even for homogeneous materials and apparently simple geometries. For example, in the radio-frequency range, the processed objects are usually much smaller than the wavelength and a spatial power distribution can be made by using the low-frequency approach, such as an impedance analysis. Such an analysis indicates that a block of dielectric material placed between plate electrodes (see Figure 22.2) will distort an originally uniform electric field, causing higher field strength at the block corners, thus producing nonuniform heating rates. At microwave frequencies, the processed objects are generally larger than a wavelength, and the reflection and refraction phenomena at the material–air interface are more useful in determining the field distribution. Nonetheless, the electric and magnetic fields obey a few fundamental rules that allow us to present dielectric heating and drying within the limits defined by the scope of this book. An in-depth analysis of various problems concerned with processing in electromagnetic fields may be found in specialized literature (Jones, 1981; Metaxas and Meredith, 1983; Schiffmann, 1996; Strumillo and Kudra, 1986; Stuchly and Stuchly, 1983).

Radio-frequency power for industrial applications is normally generated by a standard oscillator circuit using triode valves, usually with ceramic envelopes and air- or water-cooled anodes. The applicator consists of an electrode system that together with the processed material (load), constitutes a tuned circuit coupled inductively to the generator output. The three most commonly used electrode configurations are shown in Figure 22.2.

The *through-field plate electrode* system is configured as two flat metal plates between which the processed material is located. The electrodes can be in contact with the load (sometimes under pressure or vacuum), or an air gap exists, which is the case in a conveyor-type apparatus.

The *staggered through-field electrode* system is also arranged as an array of electrodes but located alternately below and above the pro-

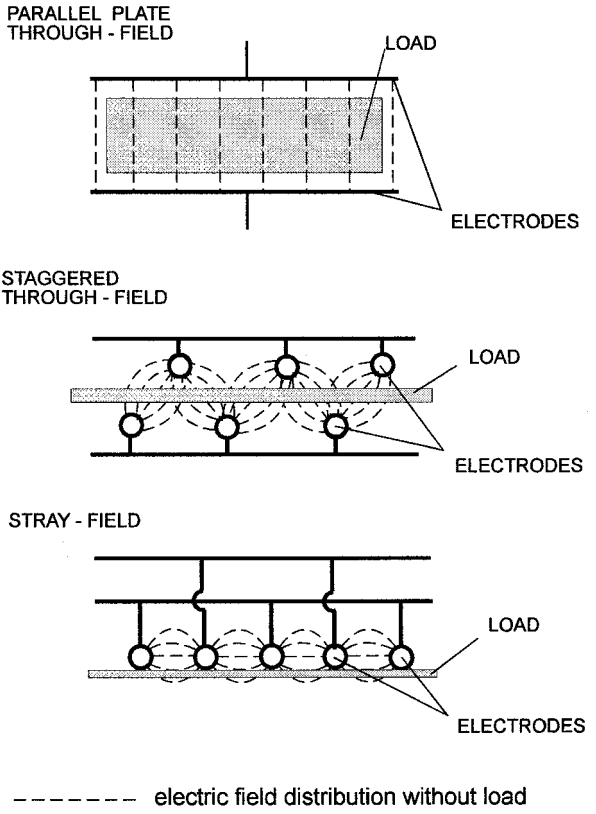

FIGURE 22.2 Typical RF applicators.

cessed material. Such a configuration is suitable for sheet-type materials.

The *stray-field electrode* system is arranged as an array of electrodes, usually in the form of rods, strips, or tubes situated in the same plane as the material to be processed. Such a configuration of electrodes produces a planar but nonuniform field through the material, and it is used to process plate-type materials.

When a wet material is dried, a variation in the loss factor due to water removal and temperature elevation produces a respective variation in the absorbed power. To compensate for this effect, graduated field configurations or pulsed field systems can be used (Strumillo and Kudra, 1986).

Radio-frequency drying, especially in combination with convective heating, is well established in industry for drying paper, paper board, wood, and plywood, as well as for combined drying and curing and gluing. The main limitations of the conventional systems are a difficulty in carrying out adjustments, inability to control the system during the process, and RF leaks. A conventional radio-frequency system includes the self-oscillating generator linked with the applicator (dryer) via a matching circuit. Often, the operating frequency determined by a resonant circuit varies with the permissible frequency band. The matching of the impedance is done for the entire system by adjusting the characteristics of the RF to fit a particular characteristic of a dryer. Such a system does not tolerate variations in the local characteristics of the load, which are typical for a drying process. Furthermore, all modifications to the process will need a readjustment of the matching done by an RF specialist.

An advanced technique in the RF region, which provides continuous tuning of the generator to the load, is the so-called 50Ω technology (Anon., 1997; Anon., 1998). In contrast to conventional RF generators with variable impedance, the output impedance of the quartz-driven RF generator used in a 50-ohm technology is fixed at 50 Ω. It permits the use of flexible coaxial cables (50 Ω) so the dryer is not physically constrained to the location of the power source. In addition, precise control over the incident and reflected power is possible since the impedance of the load can easily be measured using a spectrum analyzer, for example. The exact impedance then permits the calculation of a fitted matching unit with variable vacuum capacitors. In addition, the use of a phase and amplitude discriminator allows the system to be automated. Quartz-driven generators guarantee frequency stability and hence conform to the authorized frequency-band regulations.

A typical RF system operated with the 50-ohm technology consists of an RF generator with 50Ω output impedance, the matching unit, and the applicator (a dryer), all linked with 50Ω coaxial cables (Figure 22.3). Power specifications for the RF generator are defined according to the product being heated and permissible frequency of 13.56 MHz or 27.12 MHz. The output power of the generator can be adjusted automatically or manually by a potentiometer with the incident and reflected power displayed on the front panel of the generator. Because the reflected energy can destroy the RF generator, the system is equipped with a limiter, which adjusts the incident power in order to restrict the reflected power at 10% of the maximum power.

The matching unit permits the maximum of the RF energy from the generator to be transferred to the product. Such an optimum power transfer (reflected power is zero) is possible only when the input impedance of the

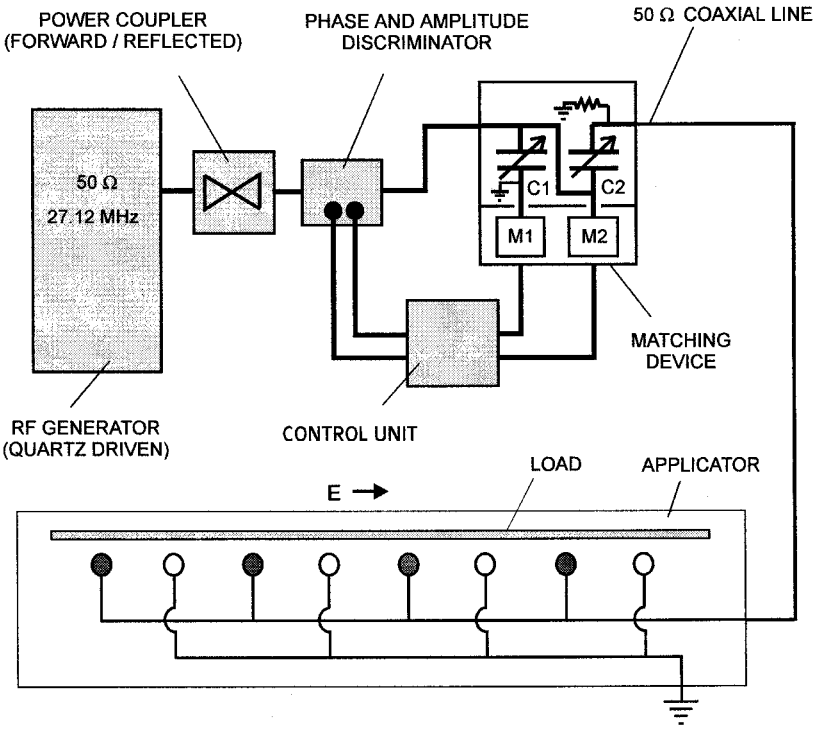

FIGURE 22.3 Basic configuration of the RF 50Ω technology for paper drying. (Courtesy of SAIREM, France.)

applicator is equal to the output impedance of the generator. To match the impedance, two parameters have to be adjusted: one to adjust the phase and one to adjust the amplitude. The matching unit can be automatic or operated manually. In most of the cases, the characteristics of the material change during the process. This requires continuous adjustments on the matching device; in such a case, the manual mode is not advised. In order to have an automatic matching unit, it is necessary to measure the phase and the amplitude of the system by means of a discriminator. The matching unit has to be as close as possible to the applicator to minimize the losses.

The applicator is defined according to the material to be treated (particulate materials, sheets or bands, bulk solids), the process to be used (e.g., drying, gluing), the treatment to be made (curing, surface heating, hardening), the

complementary energy source (hot air, infrared, heating plates), or special applications such as vapor extraction.

Essentially, the drying characteristics of the RF 50-ohm technology are the same as those for conventional RF drying. The main feature, however, is better utilization of the electromagnetic energy, which alters the drying rate and allows more uniform drying to be obtained.

The energy and drying performance of the 50-ohm technology were tested with a 190 × 190 × 14.3-mm board made of mineral and cellulose components that form the structure of foamed particles stuck in a fibrous network with pore size ranging from 1 to 100 μm (Dostie and Navarri, 1994). The board, whose initial moisture content was about 1.6 kg/kg, was placed between two vertical 200 × 200-mm electrodes spaced 40 (or 60) mm apart, in a 477 × 350 × 340-mm drying cavity. The electromagnetic energy from the 1.2-kW RF solid-state generator operated at 27.12 MHz was transmitted to the applicator by an automatic matching device yielding a constant 50-ohm impedance load. Drying experiments were performed for five levels of electrode voltage (0.8, 1.2, 1.6, 2.0, and 2.4 kV). Approximately 0.05 m^3/s of ambient air was blown through the cavity to remove the evaporated water.

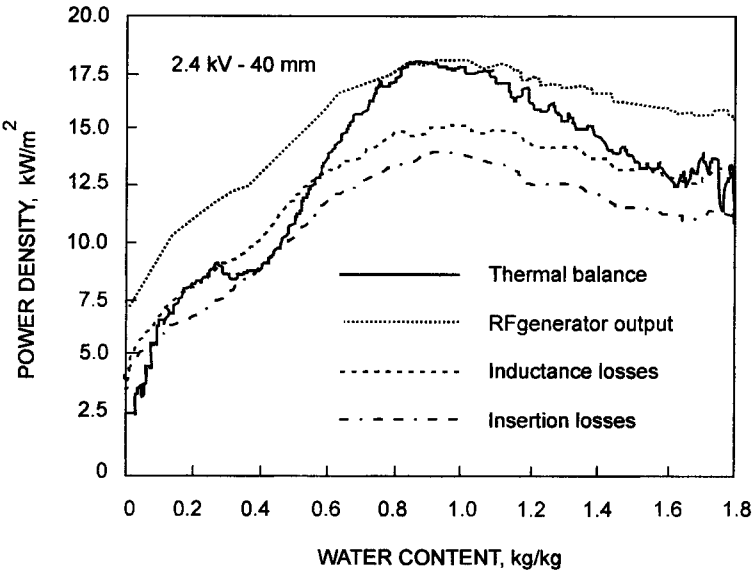

FIGURE 22.4 RF heating as a function of the moisture content. (From Dostie and Navarri, 1994.)

Three different methods were used to quantify the RF energy dissipated in the product: thermal energy balance based on the product mass and temperature measurements; electrical losses in the matching device (insertion losses); and inductance losses calculated from the flow rate and temperature rise of the cooling water.

Figure 22.4 presents a comparison of the energy transferred to the product determined with these three methods (for the case of worst discrepancy). These estimates all have about the same shape, which indicates that any one of these methods can be used for determination of the transmitted power. Figures 22.5 and 22.6 present the normalized RF power and drying rate plotted against the product moisture content for several values of the electrode voltage. The normalized values here are the ratios of the actual value to the maximum value obtained in the experiment. Characteristically, these curves are of the same shape, which indicates a close relation between the RF power and the drying rate and therefore confirms the favorable energy performance of the 50-ohm technology, as far as transmission and matching issues are concerned.

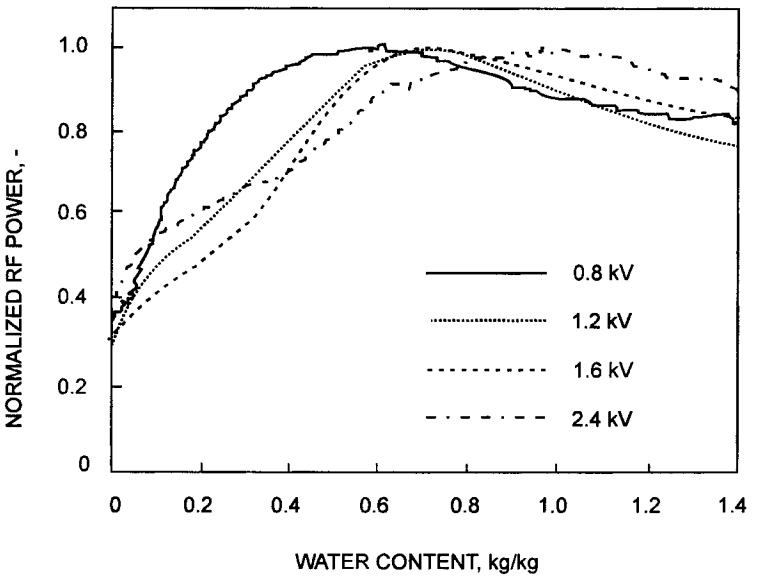

FIGURE 22.5 Normalized RF power as a function of the moisture content. (From Dostie and Navarri, 1994.)

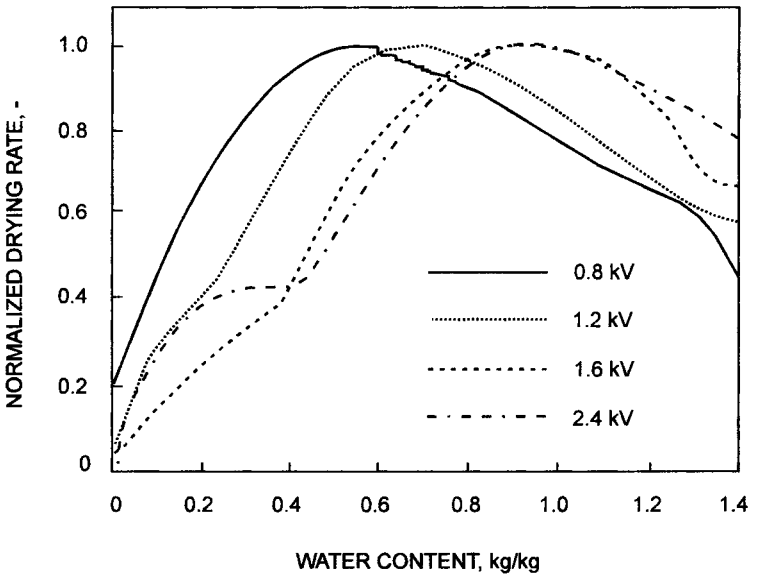

FIGURE 22.6 Normalized drying rate as a function of the moisture content. (From Dostie and Navarri, 1994.)

The main advantages of this technology are claimed to be as follows (Anon., 1998):

The use of the quartz-driven generators yields high-frequency stability
Reduction of RF radiation emitted by the applicator due to permanent tuning
Limitation of flash risk
Reduced power consumption as compared to the traditional RF equipment
Improved operation (simplified control, reduced adjusting time, complete automation, versatile and remote command of the system, etc.)

The RF technology appears to be well suited as a heating source for industrial applications that require high power and short process times, such as paper drying. Flexibility of the 50-ohm technology enables one generator to be used in sequential mode with two or three applicators. In terms of the costs of the RF drying systems, the investments are clearly very high, but the payback is relatively short.

23

Radio-Frequency-Assisted Heat-Pump Drying

The limitation of relatively low-heat transfer rates in conventional drying with hot air, particularly toward the falling rate period, can be overcome by taking advantage of volumetric heat generation during dielectric (microwave and radio-frequency) heating. This can be done by combing radio-frequency (RF) heating with conventional heat-pump drying (Marshall and Metaxas, 1998). Similarly to microwave drying, the RF field generates heat volumetrically within the material wetted with polar molecules such as water by the combined mechanisms of dipole rotation and ionic conduction. Such internal heat generation speeds up the drying process mainly because of unidirectional temperature and moisture concentration gradients, internal pressure build-up, and short time delay. Nonpolar materials, such as fat or oil, and dry solids, which usually form a skeleton of the material being dried, do not react essentially to the electromagnetic field, therefore, they are not directly heated by RF energy (Clark, 1997).

Figure 23.1 presents the electrical equivalent of a radio-frequency dryer where the applicator is in fact a drying chamber and the load is the material being dried. The electromagnetic power is generated at a frequency determined by the capacitance and inductance of the tank circuit. This power is fed to the

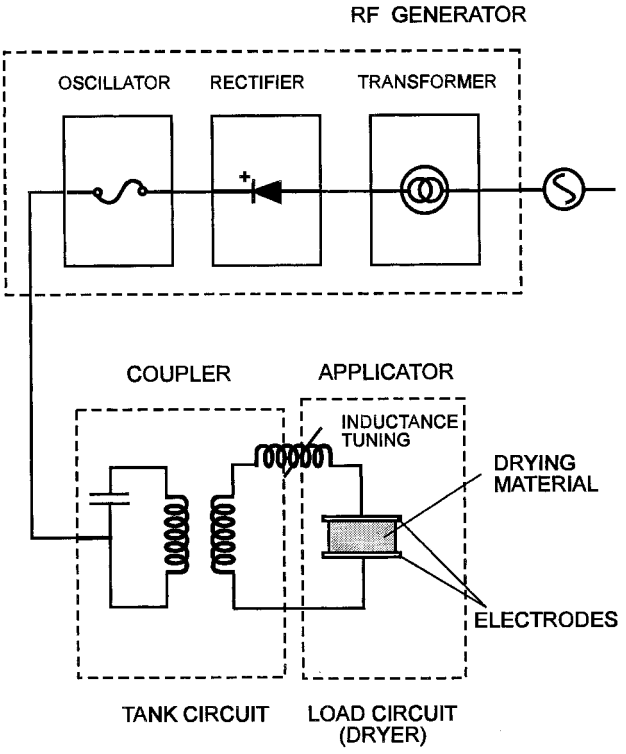

FIGURE 23.1 Layout of the radio-frequency system.

applicator circuit via inductive coupling and an electrical transmission line. The applicator circuit basically comprises an inductance and a capacitor, which induces the electric field in the material to be dried. The combination of the generator and applicator circuits forms a resonant system. To generate power and transfer it efficiently to the wet material, the resonant frequency of the applicator must be the same as that of the tank circuit. In addition, the inductive coupling between the circuits should be at some critical value determined by the characteristics of the generator and dielectric properties of the drying material. To avoid cumbersome power transfer and tuning of the system, the 50-ohm technology, which is becoming more popular in drying applications, could be used. Details about internal heat generation and drying in electromagnetic fields can be found in reference literature (Strumillo and Kudra, 1986; Kudra and Strumillo, 1998; Kudra, 1990; Kudra et al., 1990;

Metaxas, and Meredith, 1983; Metaxas, 1996), and basic information on heat-pump drying can be found in Chapter 15 of this text.

The radio-frequency-assisted heat-pump dryer comprises a vapor compression heat-pump system retrofitted with an RF generating system that is capable of imparting radio-frequency energy to the drying material at various stages of the drying process. In the configuration shown in Figure 23.2, the radio-frequency energy generated in the tank circuit of a self-excited power source is coupled via a matching circuit to the parallel-plate-type applicator located in the drying chamber (Marshall and Metaxas, 1999). The bottom electrode is made from a perforated metallic plate, while the upper electrode is a solid plate but of a smaller size to allow flow of air circulating in the dryer–heat pump system. The bottom electrode is the negative one and is connected to the casing of the drying chamber. The material to be dried and the electrodes form the load circuit of the RF system.

Materials that are difficult to dry with convection heating are likely to be good candidates for RF-assisted drying. Materials with poor heat transfer characteristics, such as ceramics and glass fibers, have traditionally been prob-

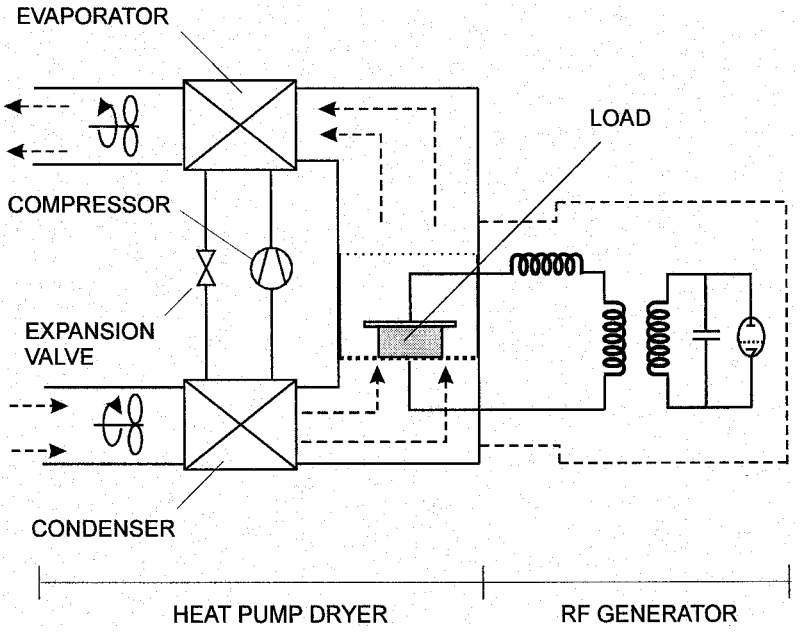

FIGURE 23.2 Radio-frequency-assisted heat-pump dryer.

lem materials when it comes to heating and drying. Radio frequency makes it possible to heat all parts of the product mass simultaneously and evaporates the water *in situ* at relatively low temperatures usually not exceeding 82°C (Thomas, 1996). Since water moves through the product in the form of vapor rather than by capillary liquid flow, migration of solids is avoided. The warping, surface discoloration, and cracking associated with conventional drying methods are also avoided (Thomas, 1996).

The most important advantages and disadvantages of the RF-assisted heat-pump drying from both the system and drying technology points of view are compared in Table 23.1.

Since the RF-assisted heat-pump drying is a relatively new technology, there is not much published data concerning energy, performance, quality issues, etc. Table 23.2 compares, for example, the dryer performance for crushed brick and clay agglomerates. It is clear that the combined use of pulsed RF heating with heat-pump drying improves the specific moisture extraction rate (SMER) of the system due to reduced electric energy because of RF heating (Marshall and Metaxas, 1998). The pulsed drying configuration has shown a slight reduction in the coefficient of performance (COP) for the R12 RF-assisted heat-pump dryer. This effect was probably due to the pulsed mode of RF application, which forces pulsed mode of material heating. Interestingly, the pulsed supply of the RF energy generally increases the COP. In the case of clay drying, the improvement in both COP and SMER can be attained with pulsed RF heating.

With respect to product quality, it appears that the RF-assisted heat-pump drying reduces discoloring of dried products, especially those that are highly susceptible to surface color change. This results from an inherent feature of RF drying, i.e., volumetric heat dissipation, which boils down to the higher temperature's being in the material core that at the surface. When combined with the outward mass flux, this feature minimizes overheating of the material surface. Also, cracking, caused by the stresses due to uneven shrinkage during drying, can be eliminated by RF-assisted drying. This is achieved by the dryer's heating evenly throughout the product, maintaining moisture uniformity from the center to the surface during the drying process.

The potential for RF-assisted heat-pump drying can be summarized as follows:

Simultaneous external and internal drying significantly reduces the drying time to reach the desired moisture content. The potential for improving the throughput of a product is good. For example, in the bak-

TABLE 23.1 Advantages and Limitations of RF-Assisted Heat-Pump Drying System

Advantages	Limitations
Accelerated drying due to volumetric heat generation by the combined mechanisms of dipole rotation and ionic conduction effects.	Radio frequency may not be as effective for drying materials that have poor dielectric properties.
Even drying throughout the material volume and thus more precise control of the moisture content and product temperature.	An additional power source is required for the radio-frequency-generating system.
Easy incorporation into a heat-pump drying system.	Additional capital cost should be added to the cost of the heat-pump drying system.
Can operate as a standalone RF dryer when heat-pump cycle is temporarily off.	Regular maintenance of RF-generating components besides heat-pump dryer is needed.
RF-assisted heat pump with pulsed RF heating improves the SMER of the dryer and the COP of the heat-pump system (Marshall and Metaxas, 1999).	Additional control of the RF power density to obtain quality product at desired moisture content is needed.
Enhanced drying rate with no need for an auxiliary heating system for the heat-pump dryer.	RF measurements are difficult to perform due to the stray capacitance between the various parts of the applicator and earth and between the applicator and the measuring equipment (Neophytou and Metaxas, 1997).
The RF-assisted drying system can operate in both continuous and pulsed heating modes, resulting in versatility of a drying operation.	For larger RF heat pump-assisted system, an additional system to cool the RF generator is required.
Due to instantaneous heat generation throughout the product, the dwell time in an RF dryer is far less than in a conventional dryer. This translates into significant savings in floor space.	Precautions are required to confine the high voltage and electromagnetic fields inside the dryer and to eliminate electric discharge and material breakthrough.

TABLE 23.2 Drying Performance for Crushed Brick and Clay Agglomerates

Crushed Brick	COP R12	COP R22	SMER kg/kWh
Heat pump only	2.8	2.9	1.16
Heat pump with RF (0.8A)	2.8	3.7	0.89
Heat pump with RF (1A)	2.9	3.7	0.98
Heat pump and pulsed RF (0.8A)	2.5	3.5	1.69
Clay Agglomerates	**COP R12**	**COP R22**	**SMER kg/kWh**
Heat pump only	2.7	2.9	1.16
Heat pump with RF (1A)	2.7	2.9	0.76
Heat pump (R12) and pulsed RF (1A)	3.9	—	1.69

Reprinted from the Journal of Microwave Energy and Electromagnetic Energy, with permission of the International Microwave Power Institute.
Source: Marshall and Metaxas, (1998).

ery industry, the throughput for crackers and cookies can improve by as much as 30% and 40%, respectively (Clark, 1997).

By greatly reducing the moisture variation throughout the thickness of the product, differential shrinkage can be minimized. This promotes using an RF-assisted heat-pump dryer for drying materials with high shrinkage properties.

Closer tolerance of the dielectric heating frequency—(1) 13.56 MHz ± 0.05%, (2) 27.12MHz ± 0.60%, and (3) 40.68 MHz ± 0.05% (Clark, 1997)—significantly improves the level of control for internal drying and thus has potential in industries with products that require precision moisture removal.

The moisture-leveling phenomenon of RF drying ensures a uniform level of dryness throughout the product. Industries with products requiring uniform drying, such as ceramics, can consider RF drying as a good alternative.

24

Radio-Frequency–Vacuum Drying

Conventional methods of lumber drying such as dehumidification drying or hot-air drying are energy-intensive and time-consuming mostly because of the low permeability of solid wood. High-temperature drying can shorten drying time, but it may result in drying defects such as discoloration, degradation, or checking. Aside from a pretreatment prior to drying such as ponding (Unligil, 1972) or explosion (Hayashi et al., 1994), one of the methods to accelerate drying is dielectric (radio-frequency) drying in combination with hot-air drying (Miller, 1971; Kobayashi et al., 1999).

Although the early reports on RF drying of wood were published over 50 years ago (Miller, 1948), this technology was not widely used until recent progress in process control and RF technology. In particular, a variable capacitor and other electrical components allow tuning of the RF generator to the varying load of the applicator to compensate for dielectric characteristics of wood that change substantially in the course of drying. This makes it possible to take full advantage of the internal pressure that builds up in the wood log due to volumetric heat generation. The pressure gradient drives both liquid and vapor moisture toward the wood surface, which alters evaporation rates. Therefore, the combination of RF heating and hot-air drying shortens the dry-

ing time (Figure 24.1) and thus could reduce energy consumption and drying costs, depending on the process characteristics and energy prices.

Another option for drying solid wood is the combination of the radio-frequency and vacuum drying (Saito and Sulaiman, 1999; Rasev, 1999; Rozsa, 1994; Smith et al., 1994). At lower drying temperatures, resulting from a reduced boiling point, wood retains its mechanical strength so it is less susceptible to drying defects such as checking. Because moisture is usually removed from the kiln as vapor, there is a potential for increased energy efficiency as heat is not lost with the vented hot and humid air. An added feature of RF heating for the vacuum drying of wood is the possibility to stack lumber in a solid pile (without stickers). This not only reduces the load volume but also allows the use of the load-restraining system (Anon., 1999), which prevents wood from any movement during drying and thus greatly reduces twist, bow, cap, crook, warp, and other defects.

Figure 24.2 presents typical characteristics for RF–vacuum drying of freshly cut northern oak (*Quercus* sp.) in 57-mm squares, solid packed in bundles and placed between three 2.4 × 7.5-m aluminum electrodes. The center electrode was positive, connected directly to the 3-MHz RF generator, while the top and bottom plates were negative and grounded to the drying chamber. The schedule of drying began with 120 kW of RF energy and a vacuum of 20 mm Hg. The power was then increased at about 3 kW per hour, up to 240 kW. As the wood reaches the fiber saturation point at about 30%

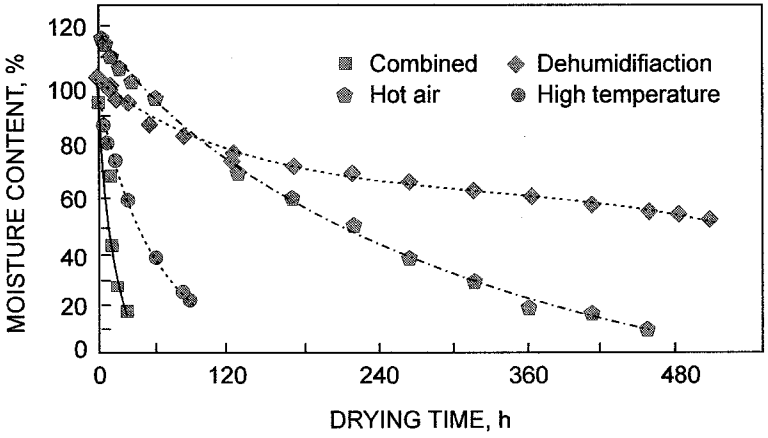

FIGURE 24.1 Comparison of drying curves for sugi (*Cryptomeria japonica*) lumber 120 × 120 × 1000 mm (Kobayashi et al., 1999).

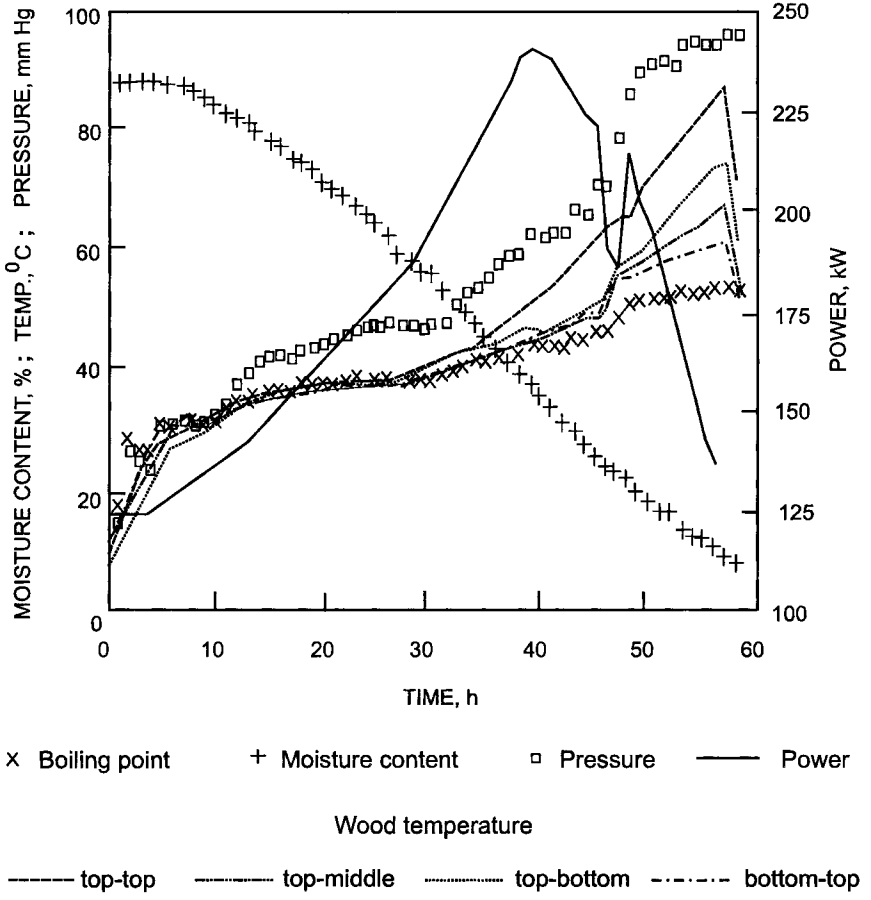

FIGURE 24.2 Radio-frequency–vacuum drying characteristics for 8/4″ in red oak squares (Smith et al., 1994).

to 35% w.b., its ability to absorb electromagnetic energy decreases, so the chamber pressure was increased to about 90 mm Hg to prevent arcing. The end drying point was indicated by a slower water flow rate from the vacuum condenser. At this point, the RF generator was turned off and the vacuum pump was run for an extra hour to complete drying. As seen from the drying curve in Figure 24.2, the drying of wood from about 90% w.b. takes place at the constant rate (excluding an initial warming-up period) down to about

6% w.b. Wood temperature measured by fiber optic probes inserted into four specimens located on the top, middle, and bottom rows of the upper packs, and at the top row of the lower packs, indicates the boiling point for the first 35 hours of the drying run. This period coincides with the fiber saturation point and the ''power reversal'' of the kiln, where the capability of the wood load to absorb electromagnetic power drops dramatically. From then on, the wood's temperature can be raised to maintain a reasonable drying rate without risk of wood damage (Smith et al., 1994).

Similar drying characteristics were obtained in a laboratory microwave-vacuum oven for drying of eucalyptus with the core temperature maintained at 30° and 40°C (Rozsa, 1994). After initial drying above 100%, the drying curve was near linear with the drying rate about 5% and 7.5% moisture content loss per hour at 30° and 40°C, respectively. During conventional predrying at 35°C and 85% RH, it took about 8 weeks to reach the fiber saturation point, which gives a moisture removal rate of about 1% to 2% per day.

Because penetration of electromagnetic waves at radio frequencies into the wood stack is much deeper than that of microwaves, the RF heating yields much more even drying of the entire cross-section of the wood load than microwave heating and obviously much more than conventional hot-air drying. Even penetration of the RF field throughout the lumber stack ensures that the entire cross-sectional area of the wood load is dried at the same rate, which results in much more uniform drying compared to conventional drying.

The end-point detection system integrated in the control circuit allows the average moisture content and the time to complete drying to be monitored over the entire drying cycle. Provided with an access to the Internet or an Intranet, the control system secures remote supervising of kiln operation. Once the target moisture content is reached, the kiln automatically stops and unloads the kiln charge.

As applied to the drying of solid wood, the RFV technology has the following production advantages (Anon., 1999):

The drying rate is up to 20 times higher than that in a conventional kiln. An added benefit is no stickering of the lumber packages.

Accelerated drying for smaller kiln charges. The ability to dry different species and dimensions at the same time allows for greater production and scheduling flexibility. The RFV kilns can also be used for pasteurization and fixation of preservatives.

Improved product quality; the RFV dried wood retains its natural color with the appearance of freshly sawn wood. In addition, there is no

heat discoloration or brown staining during drying. Chemical oxidation due to contact with drying air is practically eliminated.

Stress-free drying at low temperatures substantially reduces shrinkage, and this allows a reduction in green target sizes and improved lumber yields.

Table 24.1 compares drying time and electricity consumption for several wood species dried in the radio-frequency–vacuum wood kiln (Anon., 1999).

TABLE 24.1 Performance Characteristics of the Kiln

RFV kiln performance	Conventional kiln re-dries 22%–12%	2″ Hemfir 55%–10%	4″ × 4″ White pine 40%–10%	1″ and 2″ birch 50%–8%
Drying time, h	5	36	36	60
Total electricity, kWh/Mfbm	64	546	356	863

Source: Courtesy of HeatWave Drying Systems, Ltd.

25

Microwave–Convective Drying

Microwave (MW) and radio-frequency (RF) heating are highly intensive but also cost-incurred methods of thermal treatment (Sanio, 1989; Sanio and Schmidt, 1989). For these reasons, hybrid technologies involving combinations of various driving forces for heat and mass transfer are preferable. Typical examples are radio-frequency and microwave-assisted convective drying, where the high-frequency electromagnetic energy may be applied at different drying stages to supplement thermal energy supplied with drying air. By adjusting the balance among component technologies, it is possible to optimize the hybrid systems in terms of the process effectiveness and cost. Of various hybrid systems based on microwave irradiation, microwave–vacuum drying and microwave–freeze-drying have found the widest application in dehydrating fruits, foods, and thermolabile biomaterials such as microbial strains, plasmas, serums, enzymes, and others (Kudra, 1990, 1999; Kudra and Strumillo, 1998). Therefore, this chapter focuses on two prospective but less common microwave-assisted drying technologies.

Although drying kinetics for convective and dielectric (MW and RF) drying are similar except the period of internal pressure generation, several advantages of microwave drying stem from volumetric rather than surface

heating and from different temperature profiles due to power penetration. The main advantage is an enhanced drying rate resulting from such phenomena as a relatively large temperature gradient that coincides with the gradient of moisture concentration, or mass flow of vapor and liquid water that add to capillary and molecular flows. The most dramatic improvement in drying rates can be observed for materials having poor thermal conductivity since the energy is dissipated directly in the wet regions of the material being dried. The other advantage of dielectric heating is that it yields much more uniform drying and improved product quality. Because of the exponential dependence of the diffusivity on temperature, the molecular flow rate for a given moisture gradient will be higher in the material core than in the surface region. As a result, the moisture profile levels off to compensate for increased diffusion, and this makes it possible to eliminate such disadvantages of convective drying as case-hardening, surface cracking, or local overheating.

Since the electromagnetic energy is dissipated directly in the dried material, heat losses are considerably reduced. Thus, the performance of microwave drying is better than that of convective drying (Figure 25.1). The capital and operating costs of dielectric drying are higher so microwave heating may not be economical as the sole energy source, especially for drying high-moisture-content materials with long constant-rate periods. However, it is well suited for drying low-moisture-content products where the convective heat transfer is less efficient.

To overcome the economical constraints, the microwave and radio-frequency drying technique is frequently combined with convective drying. In such a combination, the air stream carries away moisture evaporated in during microwave irradiation. Figure 25.2 presents two basic modes of combining convective and microwave drying. In ''booster drying,'' electromagnetic energy is added to convective drying when the moisture content reaches its critical value and the evaporation front starts to recede into the solid. The drying rate is increased sharply with a leverage of up to 8 to 1 in terms of increased drying capacity for each unit of electromagnetic energy added (Schiffmann, 1996). In ''finish drying,'' electromagnetic energy is supplied to the material when its moisture content is so low that convective drying is inefficient. The third possible mode of combined drying uses microwave energy to preheat material prior to drying. It is rarely used due to the high capital costs of the microwave equipment, which might be difficult to offset.

One of the drying technologies that take advantage of combined microwave and convective drying is *microGas*™ drying (Anon., 1992b). This technology involves cogeneration, defined as the combined production of thermal and electric energy from a single fuel source. Cogeneration is recognized as

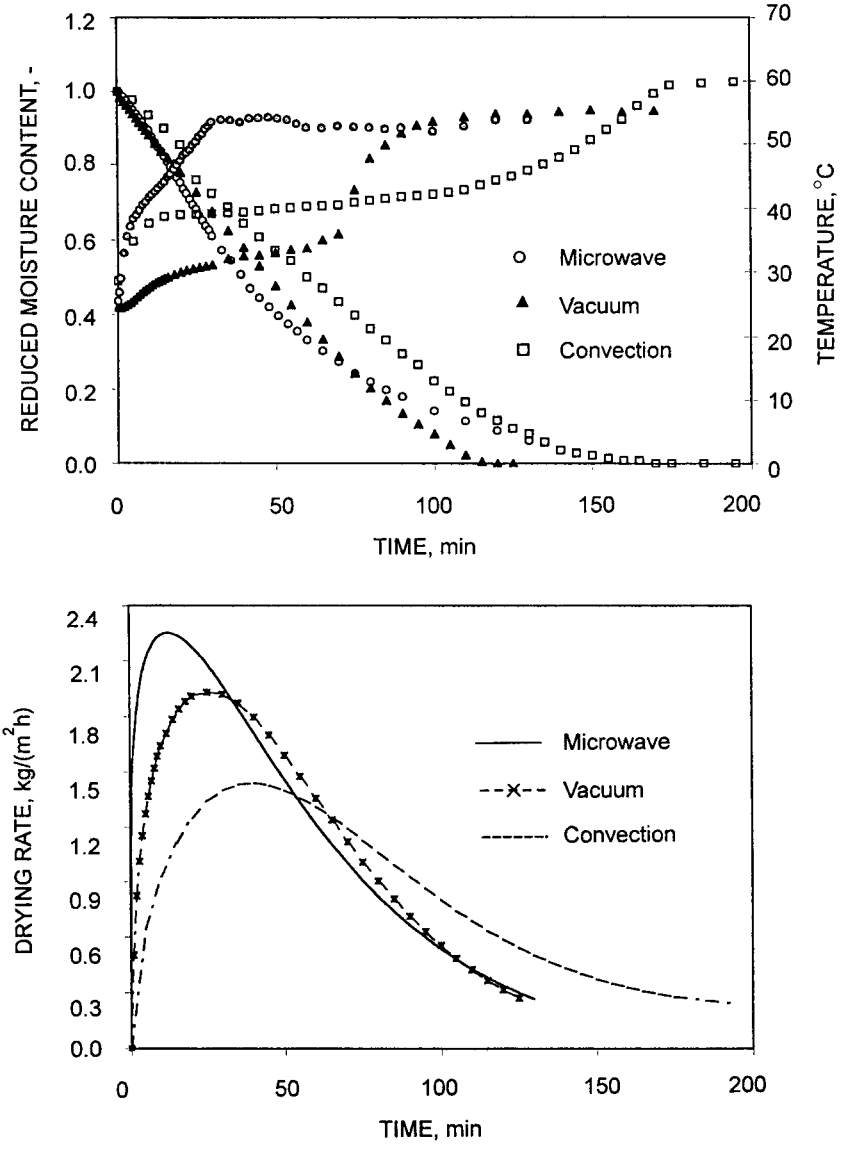

FIGURE 25.1 Convective, vacuum, and microwave drying of chlorpropamide: T = 60°C, P = 0.1 atm, u = 5.4 m/s, P' = 385 W/kg. (From Kardum et al., 2001.)

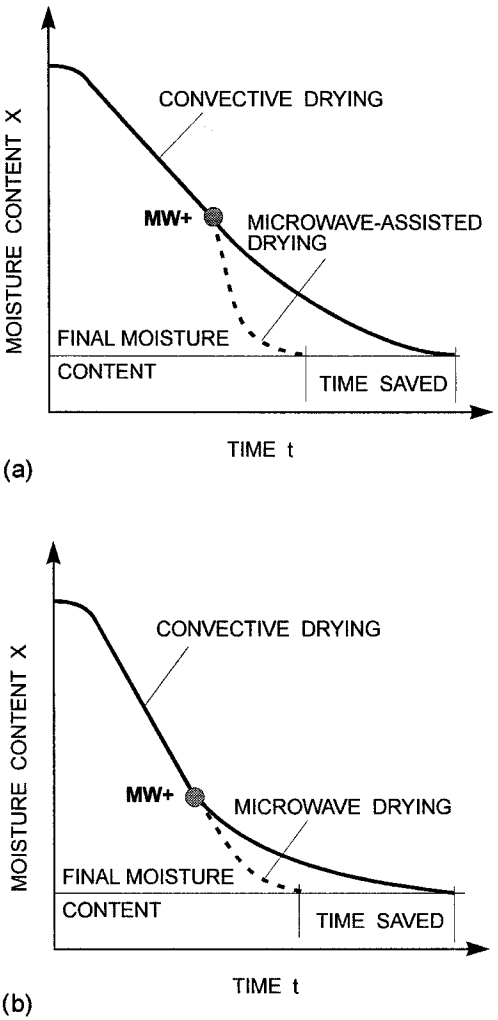

FIGURE 25.2 Typical applications of microwave energy: (a) booster drying and (b) finish drying.

one of the most efficient methods in energy transformation that provides a cost-effective alternative to traditional methods of generating electricity and heat alone. Aside from producing electricity, cogeneration provides an option to utilize thermal energy, which is otherwise wasted mostly with exhaust gases, engine coolant, and the lubrication oil-cooling system. The ''waste'' heat recovered as hot water or steam, for example, can be further used in low-temperature installations such as central heating or air conditioning or for process heating including industrial drying. Because of such heat recovery, the resulting efficiency of fuel utilization in a typical cogeneration system approaches 80% versus 35% to 40% for the utility power plant. The key components of a typical cogeneration plant are

- A prime mover (a steam turbine, a combustion gas turbine, or an internal combustion engine)—that, through fuel combustion, produces mechanical energy
- A generator—that converts the mechanical energy to electrical energy
- A heat recovery system (usually heat exchanger)—where waste heat is converted to a useful form

As applied to drying, heat from a cogeneration system can be taken from an engine cooling liquid and/or engine exhaust gases. Direct use of the exhaust gases (specifically those from gas turbines) as a heat and momentum carrier in convective dryers such as fluid bed, pneumatic, spin-flash, and others is technically feasible. However, the relatively constant energy output from the engine exhaust cannot usually match the hydrodynamic and thermal requirements of drying systems unless exhaust gases are used as a secondary heat transfer medium. The latter option is preferred since the temperature of the exhaust gases at turbine outlet is around 500°C, and for a majority of drying applications it must be lowered by mixing with ambient air. Indirect use of the gas engine exhaust is also possible. However, it may not be fully justified because contact drying is usually carried out at lower temperatures while the low gas-to-gas overall heat transfer coefficients (in the order of 30 to 60 W/(m^2K)) demand heat exchangers with extended heat transfer areas. The relatively low temperature of the engine coolant (typically 90° to 95°C) limits industrial applications to low-temperature drying because drying air temperature in a typical heat exchanger heated by the engine coolant may be raised only up to 80° to 85°C. As a general rule, each case of a cogeneration-driven drying system will need to be assessed individually.

Essentially, the microGas technology combines microwave and convective heating in an integrated drying system powered by natural gas. In its

basic configuration (Figures 25.3 and 25.4), the gas-fired prime mover drives a generator that provides electricity to power the microwave generator and all ancillary equipment such as feeders, conveyor belts, blowers, and pumps. Waste heat from the engine exhaust and cooling jacket is recovered as hot water at approximately 93°C and used to preheat air entering a convective dryer. If higher convective heat loads are required, an auxiliary burner may be used to raise the drying air temperature. For solid materials, the dryer is typically a staged, conveyor type with a continuous feed and product discharge. Specially designed inlet and outlet ports prevent leakage of microwave radiation that is routed through a waveguide to the convective/microwave stages of the microGas dryer. Of the natural gas energy fed to the prime mover, approximately 30% is converted to electricity, and 50% is recovered and utilized as convective heat. The resulting efficiency of the microGas system is claimed to be over 80%. This seems to be justified for processes where the

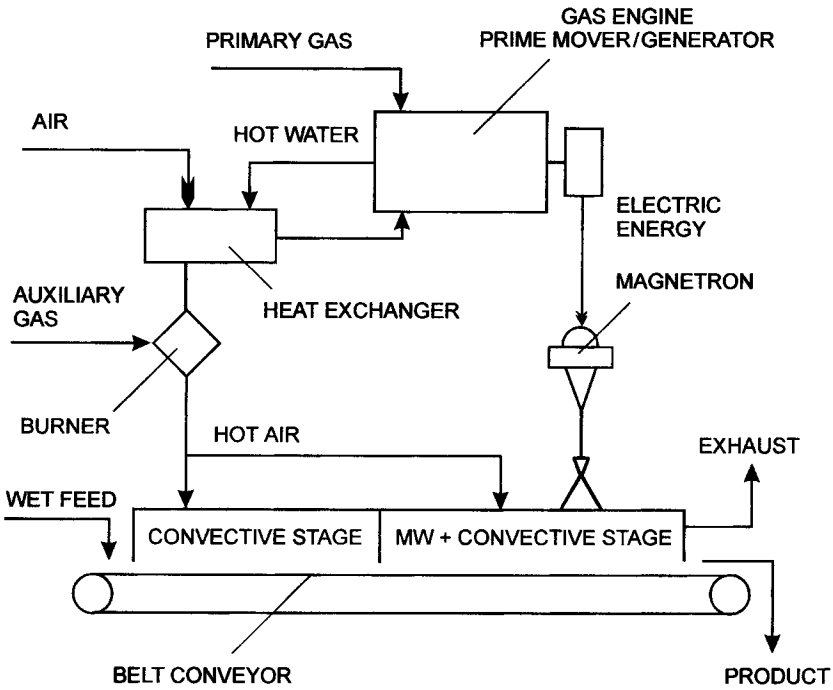

FIGURE 25.3 Schematic of the microGas dryer for solid materials. (From Anon, 1992b.)

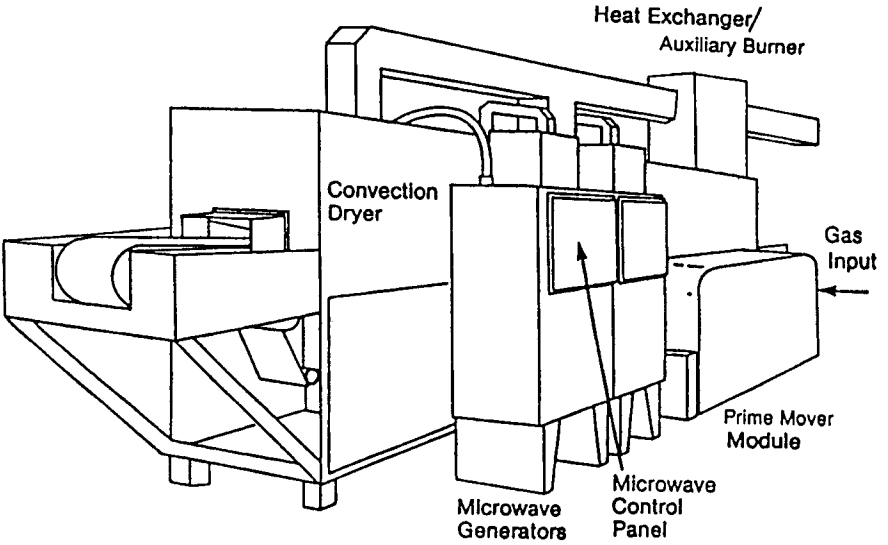

FIGURE 25.4 A conceptual design of the microGas dryer. (From Anon, 1995b.)

contribution of microwave heat is relatively small (finish drying) since the efficiency of electricity-to-microwave conversion is typically only about 50%. Even so, the microGas technology appears to be competitive to conventional drying systems (Tables 25.1 and 25.2). Moreover, the microGas technology offers the process advantages of volumetric heating at a lower expense than

TABLE 25.1 MicroGas Versus Conventional Dryer for Vegetables (throughput 13,500 kg/h)

	microGas	Conventional
Heating system	NG prime mover, auxiliary gas-fired burner	Direct gas-fired burners
Energy source	Natural gas	Natural gas + electricity
Conveyor length	23 m	68 m
Drying time	15 min	45 min
Energy consumption		
natural gas	2.6 MJ/kg	4.2 MJ/kg
electricity	0	270 kW

Courtesy of Energy International Inc., Chicago.
Source: Anon., 1994c.

TABLE 25.2 microGas Versus Conventional Dryer: Processing Time and Energy Comparison

Product	Process	Time reduction (%)	Energy savings (%)	Other results
Onions	Drying	55	38	Matched existing quality
Frozen french fried potatoes	Drying	83	36	
Pepperoni	Drying	25	6	
No-fat potato chips	Cooking/ texturing/ drying	—	—	Unique product
Spices	Sterilizing/drying	—	—	Eliminates use of ethylene oxide
Ceramic insulators	Drying	90	45	

Source: Adapted from Bernstein et al., 1993.

an all-electric system. In effect, the form value of natural gas is raised, making gas the energy source of choice in more industrial processes.

The principal benefits of *microGas* drying are claimed to be as follows:

1. Shorter drying time—volumetric heat generation results in accelerated transfer processes, which allow drying times to be in the order of one-fourth the time required for convective drying.
2. Product quality improvement—faster and uniform drying reduces the possibility of surface overheating, case-hardening, and stress cracking. It also allows better retention of color and flavor in processed foods. The shorter drying time also gives bacteria less time to grow, potentially eliminating the need for fumigation or chemical treatment.
3. Equipment size reduction—an integrated system is more compact and thus requires less floor area. In a typical configuration, a microGas system occupying 42 m^2 of floor space can replace the 400 m^2 floor space of the conventional dryer for an equivalent production rate.
4. Reduced operating costs—the microwave energy is generated within a gas-fired cogeneration system, and all recoverable waste

heat is utilized for the convective drying section. Both reduced dryer size and shorter processing time make the system easier to stop and restart for shift adjustment, product changes, cleaning, and maintenance, which finally reduces the labor costs.

The microGas technology has been laboratory- and field-tested for drying fruits and vegetables (apples, grapes, carrots, onions, potatoes), cereals (rice, breakfast foods, pet foods), pasta, candies, and ceramics (Anon., 1995b). Table 25.3 highlights the basic features of the microGas dryer for sliced vegetables.

The microGas versus conventional dryer performance comparison for production of 1800 kg/h of short cut pasta is as follows (Anon., 1992b): the conventional conveyor dryer heated by steam coils supplied by an oil- or gas-fired boiler is about 33 to 48 m long and 1.8 m wide. The total processing time is about 8 hours, and the unit requires 24 man-hours of labor for each cleaning cycle. A microGas dryer of the same width is only 7.5 m long, and processing time is reduced to about 75 min. Due to its smaller size, such a dryer requires only about 6 man-hours of labor for cleaning. The prime mover and auxiliary burner of the microGas system consume natural gas in the energy equivalent of 0.21 kWh per kilogram of product and require no external elec-

TABLE 25.3 Results of Field Experiments on Drying Sliced Vegetables

Maximum product throughput	330 kg/hr sliced vegetables
Moisture content	
Initial	80% w.b.
Final	5% w.b.
Drying temperature	60°C
Maximum belt speed	0.15 m/min
Residence time	2 hr 5 min
Rated gas input to prime mover	116.2 kW
Generator power	30 kW
Electric generating efficiency	25.7%
Recovered waste heat	64.1 kW
Rated gas burner output	468 kW (40:1 turndown)
Unit energy consumption (53% from gas burners, 44% from recovered engine heat, 3% from microwaves)	2.25 MJ
Energy cost of dry product (based on gas cost of 0.33 ¢ MJ)	8.8 ¢ kg

Courtesy of Energy International Inc., Chicago.
Source: Anon., 1995b.

tricity, while the conventional dryer consumes 0.36 kWh of gas equivalent and 0.03 kWh of electricity per kilogram of product. Based on an estimated installed cost of $4,300 per square meter of conveyor area, the conventional dryer costs between $300,000 and $400,000, while the microGas system costs about $225,000 (including $70,000 for the dryer component, $35,000 for the prime mover/generator combination, and $120,000 for the microwave equipment).

According to Bernstein et al. (1993), the use of microGas drying for ceramics is projected to yield the following results:

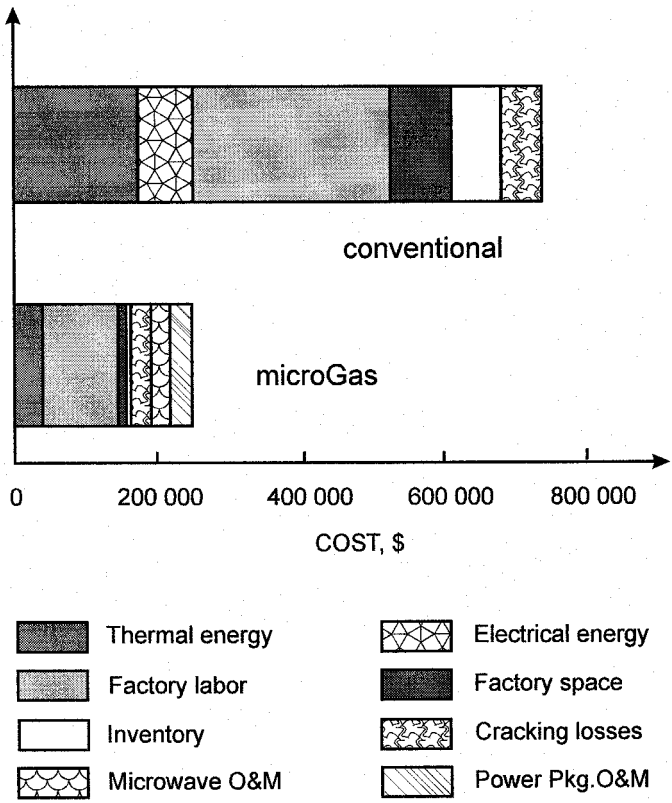

FIGURE 25.5 Cost-benefit analysis for ceramic products. (Courtesy of Energy International Inc., Chicago.)

Thermal and electrical energy costs are reduced by over 90% by the efficient use of natural gas and the production of a small amount of electricity used elsewhere in the plant.

Automating the drying process reduces labor costs associated with drying by approximately 50%.

The 90% reduction in drying time translates almost directly into a 90% reduction in factory space requirements.

The simple payback on a turnkey installation for this ceramic drying application is estimated at approximately 2.2 years.

These results are shown in graphic form in Figure 25.5.

Considering economic advantages and substantial productivity and quality benefits, the microGas system is recommended in the following applications (Bernstein et al., 1993):

Where there is appreciable value in significantly decreasing the process time.

Where a 20% to 50% reduction in energy consumption is needed to obtain cost savings.

Where product unit value is high.

Where a large decrease in equipment size is crucial.

Where the transformation of a batch process into a continuous process results in significant productivity increases, or noncontact heat transfer via microwave radiation can offer the product unique properties.

26

Microwave-Vacuum Drying

Microwave-vacuum drying (MVD) offers an attractive, cost-effective alternative to freeze-drying in the production of high-quality heat-sensitive products. In most freeze-dryers, heat is transferred to the surface of the frozen material by conduction from heating plates. In the course of drying, heat is transferred from the material surface to the sublimation front by conduction through the layer of already dry material. To perform the process at reasonably high drying rates, the sufficient temperature difference should be maintained between the material surface and its core. Thus, the surface layers can easily be overheated, especially for low-conduction materials. A solution to this problem could be microwave heating, where the material core is usually at a higher temperature because of internal heat generation. In fact, microwave freeze-drying has been extensively studied in the past 20 years and a number of laboratory and pilot tests have documented the technical feasibility and substantial advantages over conventional freeze-drying (Kudra and Strumillo, 1998). Microwave freeze-drying is, however, difficult to control because of a much higher loss factor for liquid water than that for ice. Thus, any localized melting would result in ''runaway'' overheating (Liapis and Bruttini, 1995). Microwave drying under vacuum appears to be the solution of choice as it offers all advantages of

dielectric heating but at a reduced processing temperature being the function of operating pressure (Figure 26.1). In addition, a volumetric heat transfer mechanism coupled with drying in the absence of oxygen (vacuum) provides an ideal low-temperature drying technique.

Figure 26.2 presents drying curves for 3-mm-thick carrot slices dried by hot air, freeze-drying, and microwave-vacuum drying (details of the material and procedure can be found in Lin et al., 1998, and Durance, 1999). Characteristically, the microwave-vacuum drying curves are relatively linear down to the moisture content of about 9% w.b.; that allows ambient temperature storage of the product. In this experiment, freeze-drying required approximately three days to reach the required moisture content (9% w.b.), air drying lasted 8 hours, while microwave-vacuum drying took only 33 minutes. For shrimp dried from 88% w.b. to 20% w.b., the respective drying times were 72 hours for freeze-drying, 4 hours for air drying, and 15 minutes for microwave-vacuum drying at operating pressure of 100 mm Hg (Lin et al., 1999).

Much higher drying rates than in air drying and freeze-drying were obtained for particulate foodstuffs such a meat balls, champignons, and valerian plants dried in a pilot combined microwave-vacuum-convective dryer. In this novel configuration a conditioned drying agent circulates through the drying chamber kept under pressure reduced to the level of 100 to 400 mbar (Figure 26.3). A standard system comprising the 2450-MHz generator with nominal

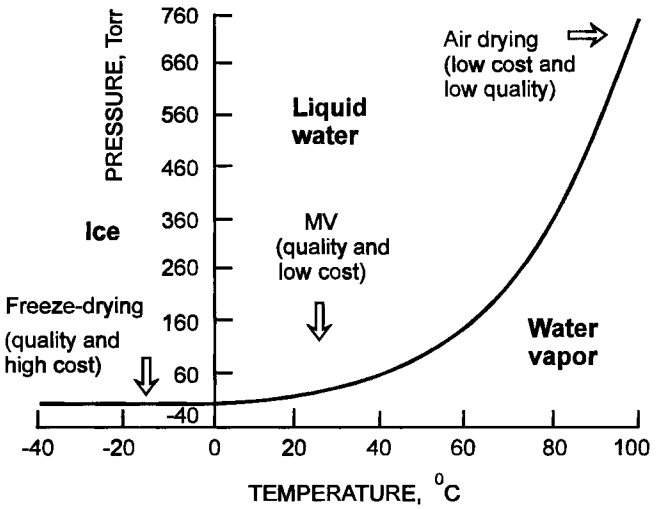

FIGURE 26.1 Microwave-vacuum drying versus air and freeze-drying. (From Durance, 1999.)

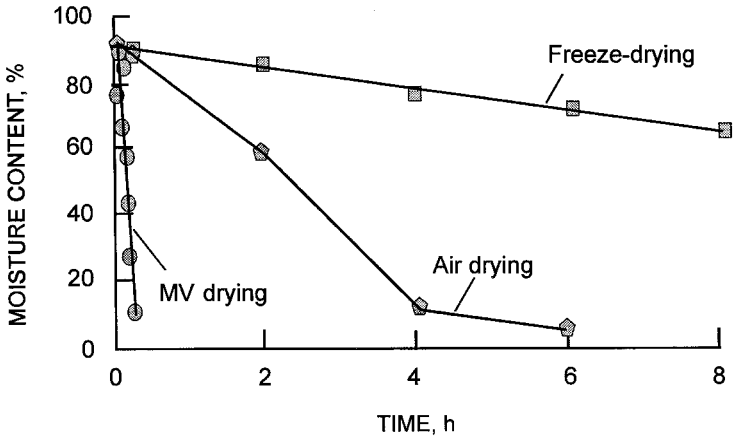

FIGURE 26.2 Drying rates for carrot slices dehydrated by hot air at 70°C, freeze-drying, and microwave-vacuum drying. (From Durance, 1999.)

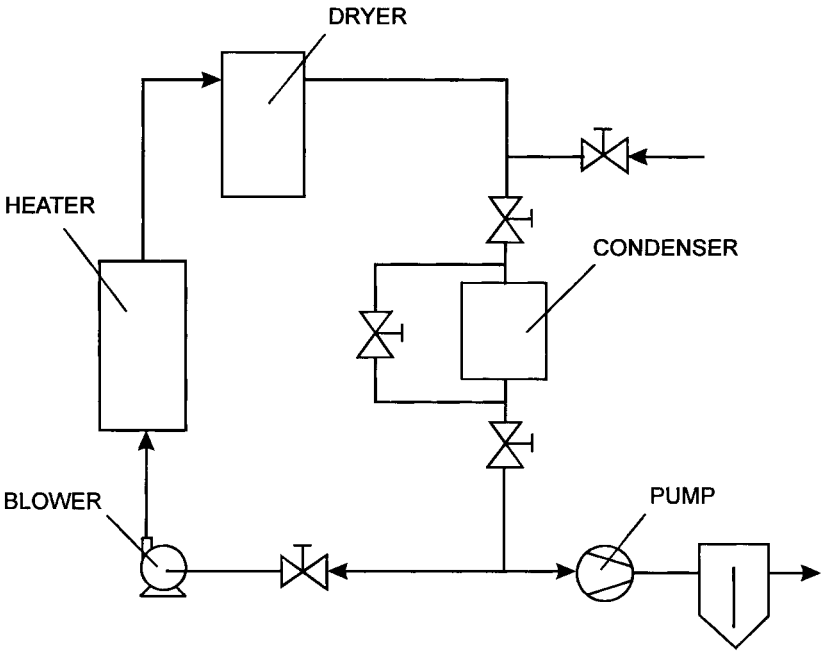

FIGURE 26.3 Schematic of microwave-vacuum-convection drying. (From Heindl, 1993.)

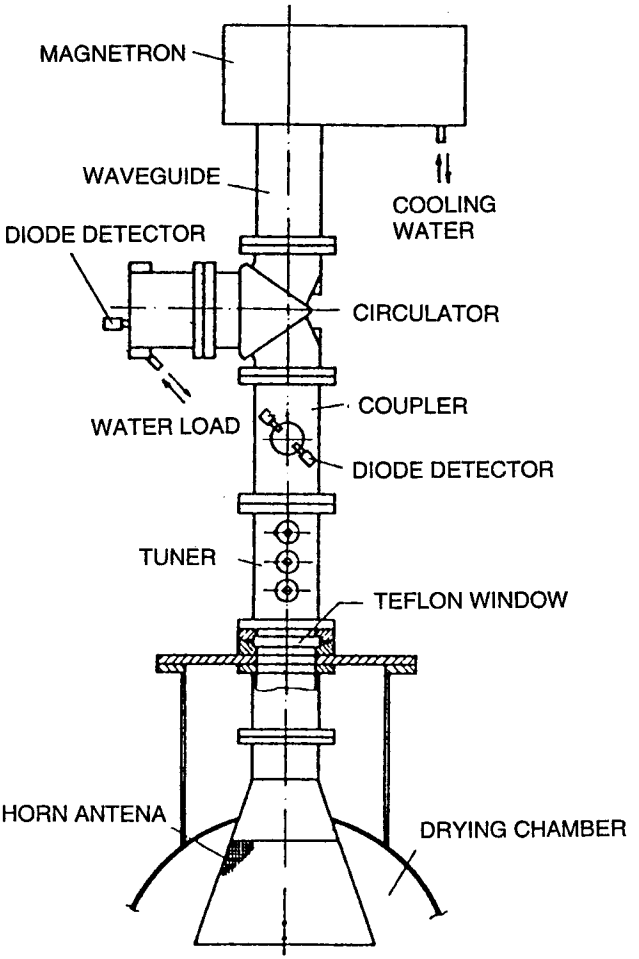

FIGURE 26.4 Microwave assembly for microwave-vacuum-convection dryer. (From Anon., 1990c.)

power of 1.2 kW, the circulator, the coupler, the tuner, and the horn antenna is used to feed microwave energy to the drying chamber (Figure 26.4). It was found that such a unique combination of these three drying techniques offers products with a quality equal to or superior than the quality of freeze-dried products as well as allows optimized and economic energy use (Heindl et. al., 1993; Heindl, 1993).

Besides giving drying rates in the order of minutes rather than hours, MVD provides quality parameters that compare favorably with those of conventional drying techniques. As expected, color, nutrient content, texture, rehydration characteristics, and so on are found to be superior to those found by air drying and comparable to those obtained by freeze-drying for products like cranberries (Yongsawatdiguul and Gunasekaran, 1996), grapes (Petrucci and Clary, 1989), carrots (Lin et al., 1998), and herbs (Yousif et al., 1999). Lin et al. (1998) compared the density, rehydration potential, texture, color, flavor, carotene content, vitamin C content, as well as sensory properties of carrot slices that were freeze-dried, air dried, and microwave-vacuum dried. Table 26.1 compares selected quality indices for microwave-vacuum drying with air drying and freeze-drying. It is clear that retention of active ingredients in materials dried in MVD is comparable with the freeze-dried products and much better than hot-air drying.

Although MVD provides all the advantages for a commercially viable system, few commercial units are in operation at this time. Figure 26.5 presents the schematic of the microwave-vacuum dryer with revolving trays (Anon., 1995c). The system comprises a horizontal vacuum chamber (2 m in diameter and 2.3 m long), a revolving rack with 12 trays, a microwave power supply, a vacuum pump, and a control panel. To secure uniform distribution of MW energy within the chamber, 16 symmetrically spaced microwave feed ports are connected through waveguides to separate 1.5-kW, 2450-MHz magnetrons. The material to be dried is held on trays made of glass fiber reinforced teflon. The rack with trays is rotated at 4 rpm. The evaporation rate is about 23 kg/h when moisture content is reduced from 90 to 20% w.b.

One limitation of this technique is that it uses electricity, which is generally expensive. The cost of magnetrons has declined significantly over the past decade. Change of operation pressure may permit changes in the quality of

TABLE 26.1 Quality Indices for Selected Products

Quality index	Freeze-dry	Air dry	MV dry
Vitamins in dry carrots, μg/g db			
α-Carotene	0.41	0.33	0.40
β-Carotene	1.15	0.93	1.11
Vitamin C	0.46	0.17	0.36
Biochemicals in herbs, mg/g db			
Alkamides in echinacea roots	3.3	2.8	3.1
Hypericin in St. John's wort	0.48	0.35	0.45

Source: From Durance, 1999.

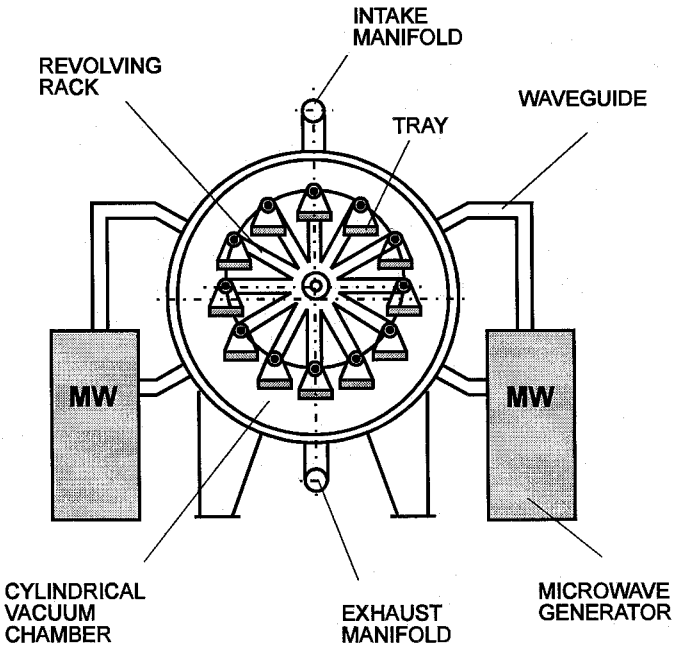

FIGURE 26.5 Cross-view of the microwave-vacuum dryer with revolving rack. (From Anon., 1995c.)

TABLE 26.2 Energy Cost Estimates for Microwave-Vacuum Drying and Air Drying

Method	Unit cost (per kg of water removed)[a]
100% air	$0.29/kg water
95% air/5% finish VM	$0.24/kg water
85%/15% finish VM	$0.20/kg water
70%/30% finish VM	$0.17/kg water
100% VM	$0.17/kg water

[a] Natural gas: $4.71/GJ; electricity: $18.03/GJ (6.5c/kWh).
Source: From Durane and Wang, 1999.

the product such as its density and porosity to some extent. Hybrid systems using hot-air convection for removal of the easily removed moisture, followed by MVD for the harder-to-remove moisture toward the end of the drying cycle, may be more cost-effective than pure MVD. More detailed technoeconomic studies for various products and local costs of energy sources are needed as these may affect selection of the drying method (Table 26.2). The final selection of the right system will depend on the quality of the desired product and the premium a high-quality product will fetch in the marketplace.

27

Filtermat Drying

Filtermat is the trade name for a multistage dryer that combines two well-established drying technologies: nozzle spray drying and continuous flow–through belt drying (Rheinlander, 1982; Anon., 2000a). In the first stage of drying, the high-moisture feed is atomized into a spray chamber of a unique design (Figure 27.1) dryer and contacted with air at a high inlet temperature. This provides for rapid evaporation of water, short contact time, and low material temperature, which translates into a favorable quality product and better process economics. The Filtermat spray dryer is designed to operate with two inlet air temperatures. High-temperature air enters the spray chamber around each spray nozzle, while low-temperature air enters the dryer through the out-of-the-nozzle area. Such a system of air supply ensures better mixing of the drying and atomizing air with the wet feed. Even when predrying feed conditions are not optimum, the manufacturer claims that product quality and process efficiency can be maintained by controlling process variables.

The belt dryer used as the second-stage dryer offers longer exposure time to much lower air temperatures needed to complete the drying process. In this primary drying chamber, the semidried product with internal moisture collects on a continuously moving belt made of a woven polyester filament and

situated at the bottom of the primary spray chamber. Because low-temperature drying air is continuously drawn through the powdery material as it deposits on the belt, the product forms a porous, agglomerated mat. Although the product from a spray dryer is still wet and thus sticky and difficult to dry on a conventional belt dryer, the inherent porosity of the bed on the moving belt facilitates further drying. Thus, by controlling the residence time and drying air temperatures, it is possible to successfully dry the product through its falling rate period.

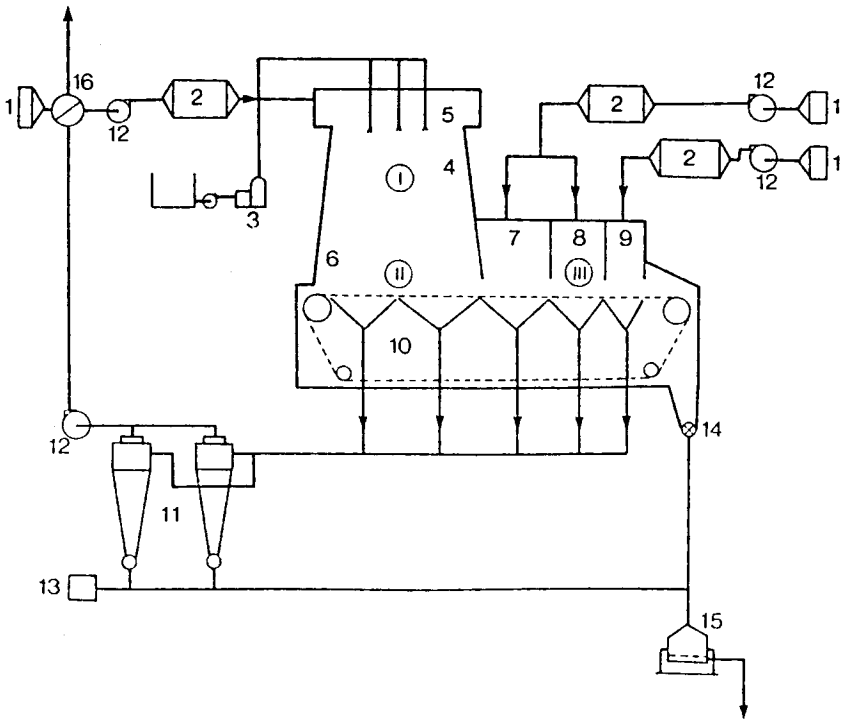

FIGURE 27.1 A three-stage spray-drying system (Filtermat): 1—air filter, 2—heater-cooler, 3—high-pressure pump, 4—nozzle system, 5—air distributor, 6—primary drying chamber, 7—retention zone, 8—finish drying zone, 9—cooling zone, 10—belt conveyor, 11—cyclones, 12—fan, 13—fines recovery system, 14—discharge, 15—screening system, 16—heat recovery system. I—first drying stage, II—second drying stage, III—third drying stage.

The gas plenum in the belt dryer can be segmented to arrange for different temperature regimes. Thus, special powder characteristics can be obtained in the so-called retention zone (Figure 27.1). Minimal flow of drying air, for example, permits crystallization or other desirable transformations to occur. For products that require additional drying, warm air can be ducted into the retention zone.

In the third drying stage, the final moisture content is achieved with warm air. When the essentially dry product reaches the final stage of processing, cold and low-humidity air can be blown through to lower the product's temperature in preparation for postdrying treatment such as milling, product sizing, classification, and final packaging.

The dryer is optionally equipped with the powder injection system around the spray nozzles. The cloud of fine particles provides for close and controlled contact between the powder and the liquid spray that facilitates formulation of stable agglomerates. This results in a new wet surface and builds larger particles before contact with the hot drying air. Thus, by controlling the agglomeration process, the Filtermat dryer can produce free-flowing, easily dispersible products with high bulk densities. It is claimed to be especially suited for drying of sticky materials, e.g., orange and other fruit juices, which tend to agglomerate and adhere to the dryer wall due to their sugar content.

Commercial Filtermat dryers are available for evaporation capacities from 230 kg/h to 5500 kg/h. Approximate building dimensions (length/width/height) to accommodate such units range from 12 $\times$ 7.5 $\times$ 14 m to 27 $\times$ 16.5 $\times$ 18 m (Anon., 2000a).

28

Spray–Fluid Bed–Vibrated Fluid Bed Drying

Figure 28.1 presents the schematic of a hybrid dryer where a spray dryer is integrated with a fluidized bed dryer and such a unit is combined with a vibrated fluid bed dryer/cooler (Tang et al., 1999). Filtered ambient air heated to 150°C in a finned heat exchanger is drawn to the air distributor of a concurrent spray dryer. The homogenized dairy feed with 50% solid content is pumped at 15 MPa into the pressure nozzle located axially at the top of a drying chamber. The semidry product of about 8% moisture content falls onto the dryer bottom while spent air at 80°C is filtered off in a bag filter surrounding the drying chamber and discharged to atmosphere. To this point, such a classical spray dryer with the volumetric evaporation rate about 5.5 kg/(m^3h) is considered as the first drying stage. To arrange for fluidized bed drying (the second stage of the process), the perforated conical grid is attached to the conical bottom of the spray dryer. Here, the semidry granules are dried by 120°C air supplied to the gas plenum formed by the perforated grid and the dryer cone. The product at about 4% moisture content falls through the central overflow to the vibrated fluid bed to agglomerate and complete drying at 90°C. Cooling of the product prior to packaging is performed at the last section of the vibrated

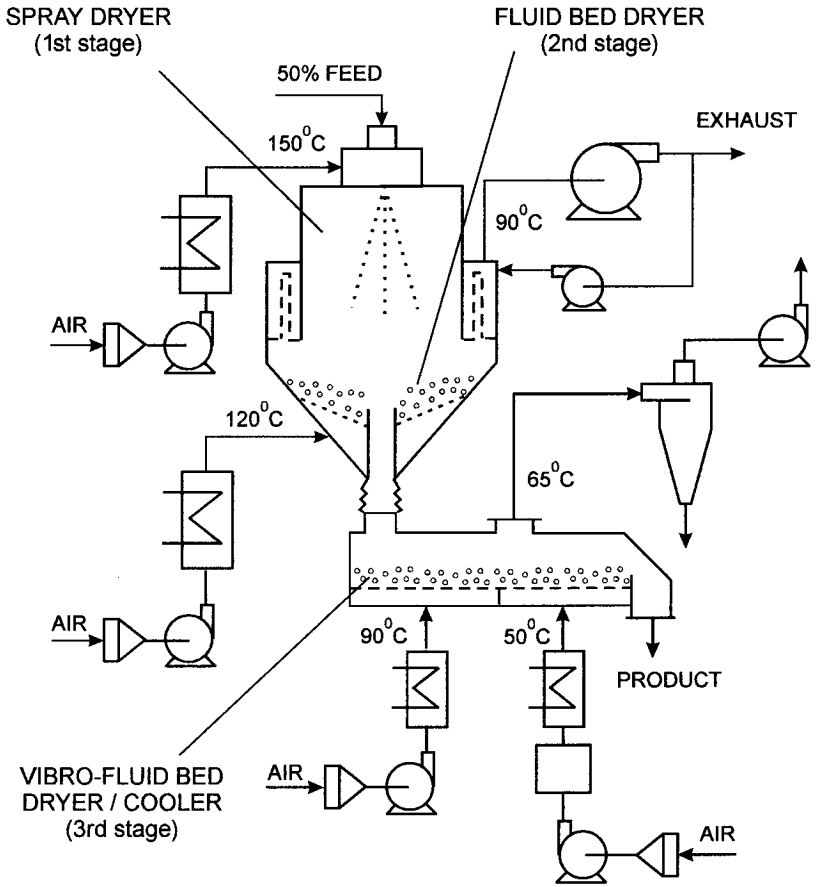

FIGURE 28.1 Three-stage drying system for dairy products.

TABLE 28.1 Energy Savings in a Three-Stage Drying System

Stage	Energy consumption, W	Energy savings, %
First stage	1447.5	0
Second stage	1233.2	15.4
Third stage	1103.5	24.3

Source: Tang et al., 1999.

fluid bed by blowing dehumidified air at 50°C. Drying and cooling in the VFB at the bed height from 200 to 300 mm takes about 2 to 3 min.

The capital cost of a three-stage system is higher than that of a one-stage spray dryer, but operating costs are lower because of energy savings (Table 28.1). Also, the quality of product from a three-stage dryer is much better because of a lower drying temperature. In addition, granules obtained in the vibrated fluid bed dissolve faster than powder obtained in a classical spray dryer.

29

Combined Filtration and Drying

29.1 INTRODUCTION

The energy consumption in conventional filters and centrifuges ranges typically from 0.5 to 10 kWh/m^3 of the suspension to be separated (Rippenger, 1998). The lower values apply to coarse particles and incompressible cakes where water is removed by bulk and film drainage. The higher values are expected for fine particles and pasty materials such as biosolids that form compressible cakes where water is removed by compaction and expression. Comparing latent heat of water evaporation, mechanical solid–liquid separation is 100 to 1000 times less energy-intensive than thermal drying. Thus, an intelligent combination of mechanical dewatering and finish drying could reduce thermal load on dryers and therefore lower production costs.

The key parameter for an optimum process configuration is not only the choice of an appropriate separator according to material characteristics (see, Figure 29.1) but also selection of the residual moisture content after mechanical separation. As pointed out by Rippenger (1998), the often-mentioned rule, ''The lower residual moisture content, the lower the operating costs'' is not always valid. Each case should be considered individually because for some materials the total cost can be lower when selecting a process configuration

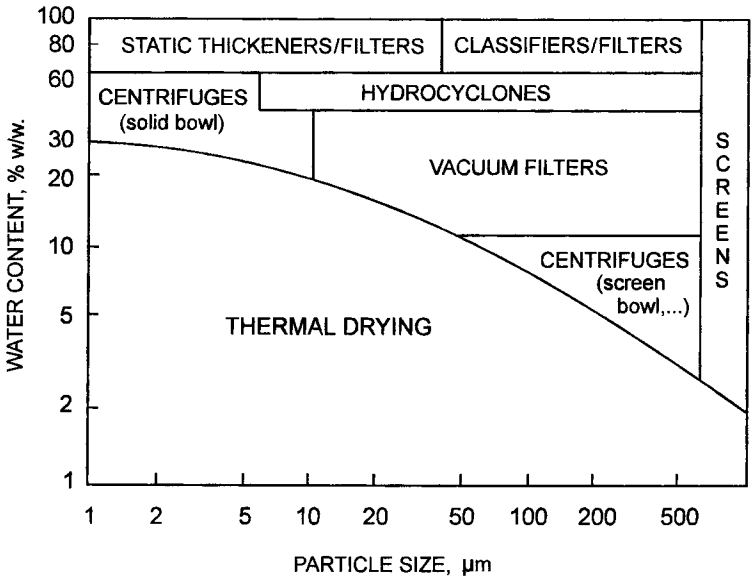

FIGURE 29.1 Liquid–solid separation of wettable minerals. (Adapted from Shafick, 1981.)

with a higher residual moisture content and thus a higher energy consumption. A case has been cited for cross-flow filtration of pigments followed by spray drying which offered a lower total cost than a press filter and a paddle dryer (Rippenger, 1998).

Further reduction of costs can be obtained when combining mechanical dewatering with thermal drying in a single-process vessel than performing these two operations in separate units (Figure 29.2). In addition, pressure filtration (or centrifugation) integrated with thermal drying can offer the following benefits:

- Improved product quality due to combination of various operations in one apparatus (high purity, no product contamination)
- Improved economics and production efficiency (no wet material transport, no product loss, lower consumption of wash liquid, shorter batch time)
- Increased process flexibility and control (normal, countercurrent, or reslurry washing; operating under vacuum or overpressure)

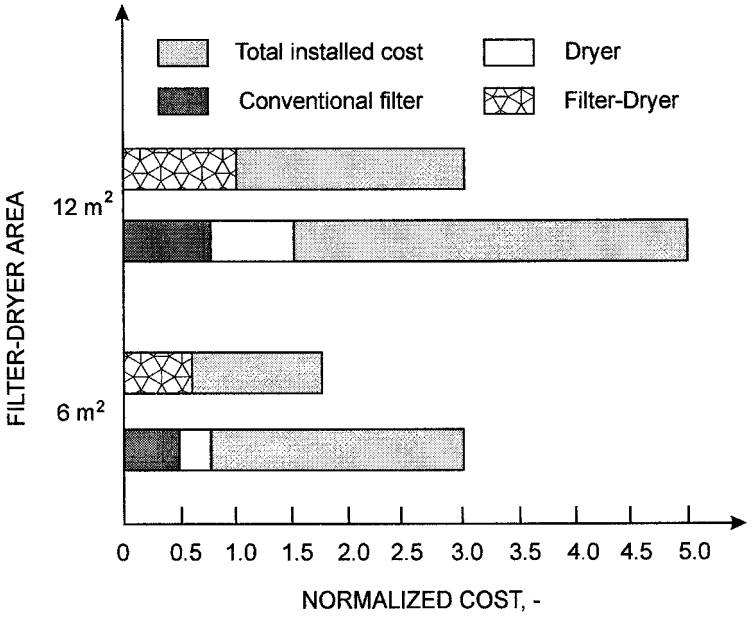

FIGURE 29.2 Capital and total installed costs: filter-dryer unit versus conventional filter and dryer. (Courtesy of Rosenmund Inc., Charlotte, North Carolina.)

Reduced environmental pollution and minimized personnel exposure to hazardous media (closed system also allows for operation with toxic products and organic solvents)

Reduced investment/running costs (no separate filter, centrifuge, wash tank, etc.)

Compact design (reduced space requirement, easy integration into existing building, lower installation and construction costs)

Flexibility (cold- or hot-air blowing, pressure or vacuum drying, drying in inert atmosphere)

Filter-dryers are especially appropriate for sterile batch processes where solids have to be separated from the mother liquor mechanically and thermally in an enclosed system. They are particularly suitable for process plants in which frequent product changes are made, for example, when producing pharmaceuticals, dyes and pigments, fine chemicals, agrochemicals, food stuffs, and so on.

29.2 PRESSURE FILTRATION AND DRYING

There are two basic configurations in industrial use for the combined filtering and drying: a vertical filter with a heated agitator, and a horizontal filter with a revolving housing.

29.2.1 The Vertical Filter-Dryer

The key to the vertical filter-dryer developed by Rosenmund Inc., Charlotte, North Carolina, is a heated paddle agitator (Figure 29.3) designed as a rotating three-arm structure with aerofoil blades that provide for increased stability at high torque levels and extended heat transfer area. This unique arrangement promotes axial and radial mixing as well as uniform drying by continuous

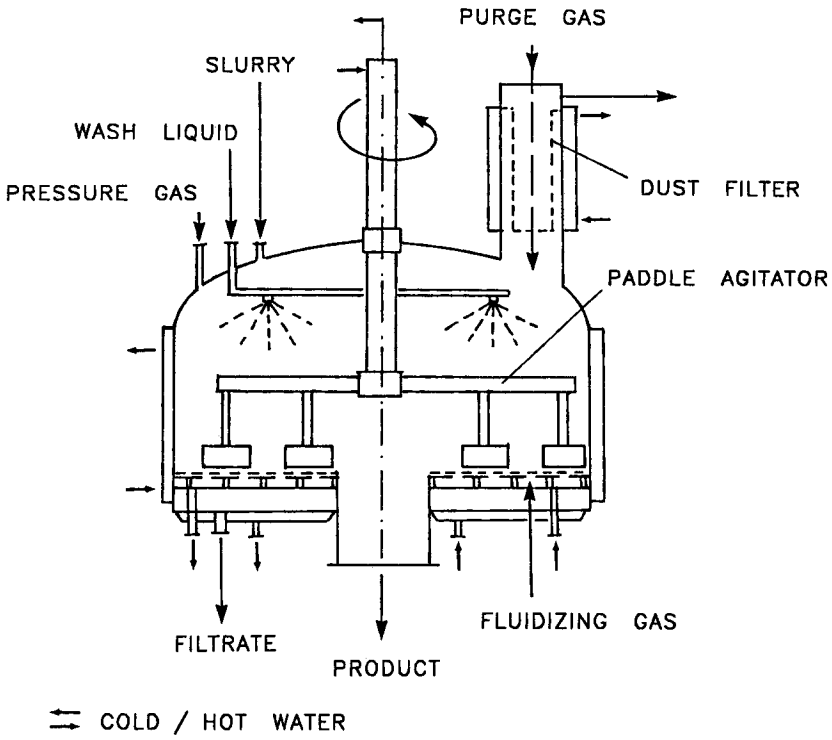

FIGURE 29.3 Vertical filter-dryer. (From Kudra and Mujumdar, 1995.)

exposure of each particle to the heated surface of the interior vessel walls, filter plate, paddle agitator, and the individual particles themselves.

Generally, after filtration and washing, most drying processes begin with a cold blow-through step to reduce the initial moisture content by liquid entrainment. Convective drying with hot gas supplies thermal energy to the cake for evaporation and continues the mechanical liquid entrainment. Finally, vacuum applied from both above and below the filter cake with intense agitation combined with contact heating from the agitator, vessel walls, and filter plate brings the product moisture to its required value, frequently below 0.5%. The representative results for a 8 m^2 filter-dryer are (Anon, 1990d)

1. The use of a heated agitator increases the heating rate by up to 70% over that provided by a filter-dryer with no agitator.
2. The heat transfer coefficient from the heated paddles is 3 to 4 times larger than that from the filter plate and up to 1.5 times larger than that from the vessel walls.
3. The estimated heat input contributions by component for the heated paddle agitator, vessel walls, and filter plate are 45%, 30%, and 25%, respectively.

Typical throughput of a 8 m^2 vertical filter-dryer is 1250 kg/batch at a cake depth of about 0.4 m and an agitator speed of 6.5 rpm. Clearly, these depend on the feed stock.

Figure 29.4 presents a schematic of a vertical filter-dryer with a helix-shaped filter element. During the filtration and cake-washing stages, the unit operates as a conventional filter with a filter cake formed on the upper surface of the hollow helix that serves as the filter grid. Then, steam or heated gas is introduced into the vessel in which it passes through the cake into the helix interior. Alternatively, a heating medium can be introduced into the internal tubing of the helix while a vacuum is applied to the vessel. The discharge solids are loosened from the filter element by spinning the helix, which further acts as a screw conveyor to transport dry and loose cake to the bottom of a pressure vessel. A scraper attached to the helix then discharges the cake through the outlet into a closed receptacle. The helix filter-dryer finds applications in pharmaceutical and fine chemical manufacturing processes—from coarse salts to fine antibiotics. Typical fed slurries may have solids' concentrations of less than 1% by weight. Due to the ease of automatic discharge, these filters have practical applications with solids' concentrations up to 10% or more. A choice of sintered metal or cloth filter media allows for particle cap-

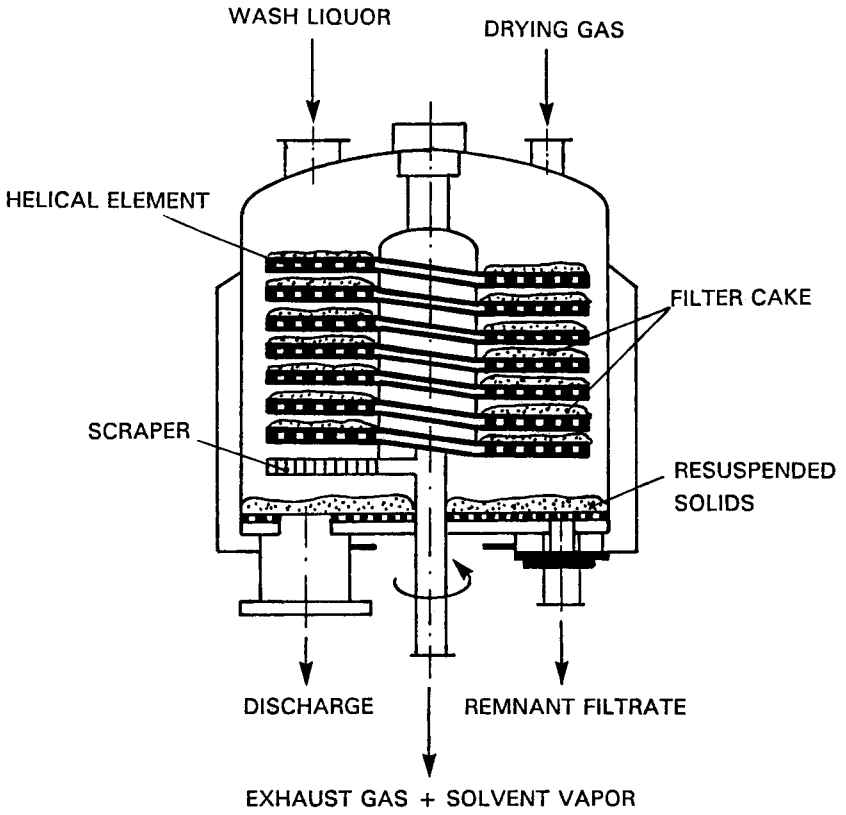

FIGURE 29.4 Filtroba helical filter-dryer. (From Kudra and Mujumdar, 1995.)

ture down to 0.5 μm. The ability to agitate rapidly settling slurries by rotating the helix makes it possible also to process coarse particles (Anon., 1992c).

29.2.2 The Horizontal Filter-Dryer

The horizontal filter-dryer (Figure 29.5) developed by Krauss-Maffei Corporation, Florence, Kentucky (Anon., 1991), and known as the Titus-Nutsch-Dryer (TNT), consists of a horizontal cylindrical housing designed for pressure and vacuum operation. The filter elements, strengthened by a perforated plate, are situated on the lower section of the housing. A hollow profile is welded onto the perforated plate, which allows heating of the filter elements. The upper

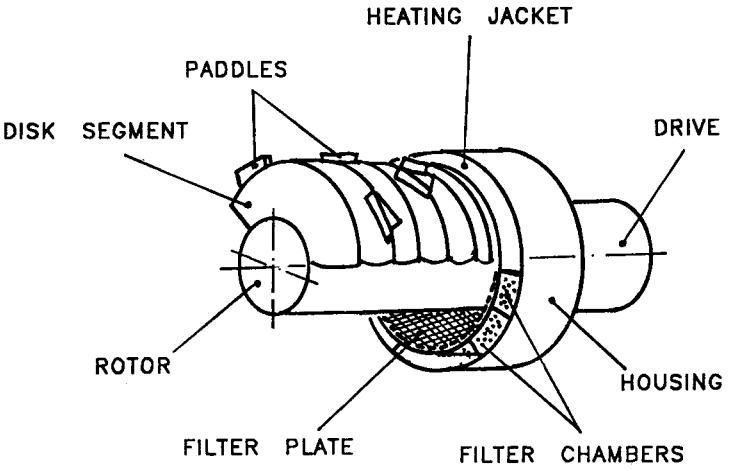

FIGURE 29.5 Cross-view of the Titus-Nutsch-Dryer. (From Kudra and Mujumdar, 1995.)

section of the housing may be heated by means of a heating jacket. The rotor, comprised of disc segments with paddles, is cantilever-mounted and also may be heated. Due to the cantilever rotor design, it is possible to withdraw the housing, thus allowing a visual check to avoid cross-contamination when changing products. The complete filter-drying operation consists of the following steps (Figure 29.6):

1. *Filling and filtration*. In a filtering position (filter area facing downward), the suspension enters from above until the filter area is fully covered. After opening the filter chamber valves, the mother liquor is removed by applying either pressure or vacuum.
2. *Normal washing*. The ring-shaped solid cake is flooded from above with wash liquid. A retention time of some minutes permits penetration into the cake, thus allowing saturation of the wash liquid with impurities. Then, pressure or vacuum is applied to remove the wash liquid from the cake.
3. *Countercurrent washing*. If the surface of the filter cake is not permeable, the cake can be rapidly washed via counterflowing wash liquid.
4. *Reslurry washing*. By rotating the housing into the drying position (filter area facing upward) and operating the rotor, the filter cake

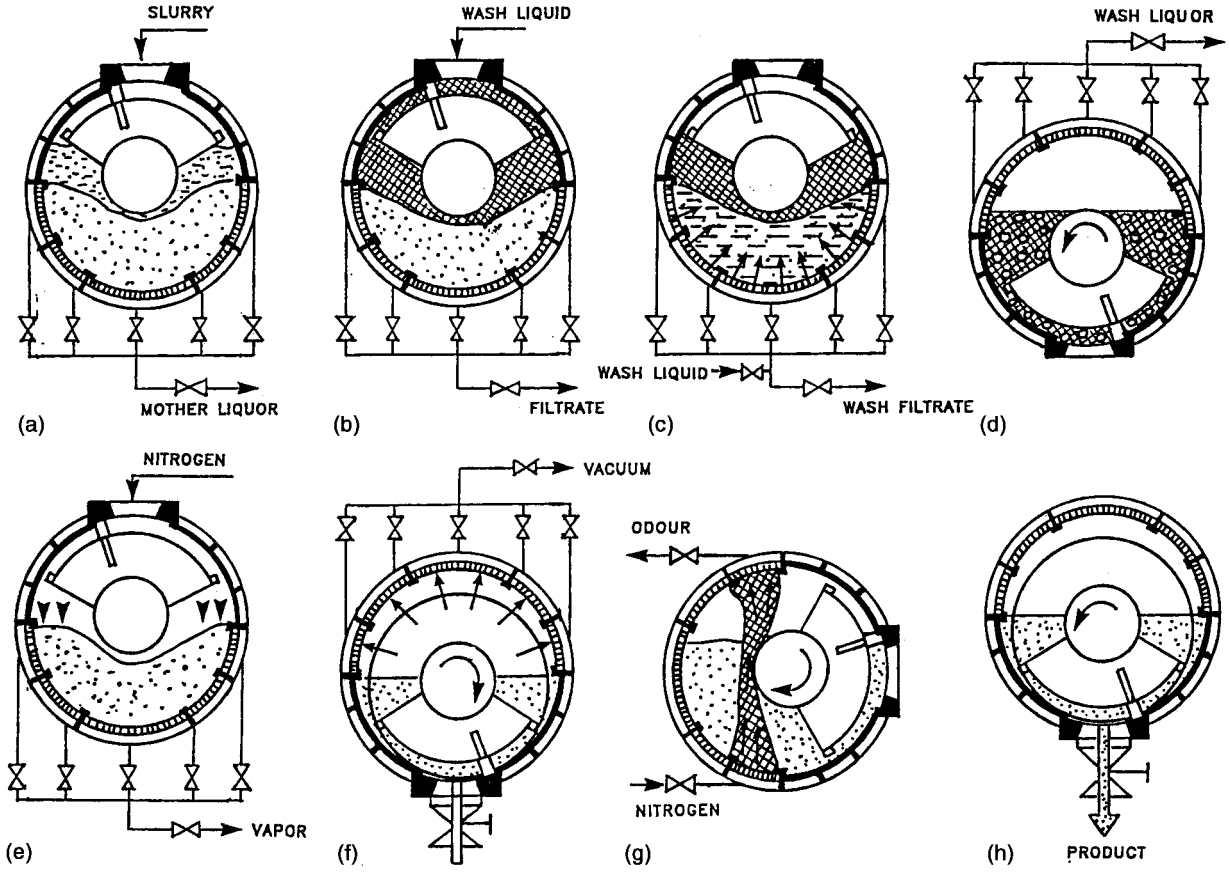

FIGURE 29.6 Process steps in the Titus-Nutsch-Dryer: (a) filling and filtration, (b) normal washing, (c) countercurrent washing, (d) reslurry washing, (e) Nutsch drying, (f) thermal drying, (g) deodorization, (h) discharging. (From Kudra and Mujumdar, 1995.)

is effectively broken-through, which results in an even reslurring. Further, the housing is rotated to the filtering position and the wash liquid removed.

5. *Nutsch-drying*. The effective pressure difference results in a reduction of the capillary height and with it a reduction in residual moisture. When the pressure difference is greater than the capillary pressure, nitrogen is drawn through the cake and the residual moisture is reduced by vaporizing.
6. *Thermal drying*. After housing rotation by 180°, the solid cake falls from the filter surface using gas pressure behind the filter plate, if necessary. The product is dried in the lower part of the vessel by contact with the housing and heated rotor. Since dry particles are trapped on the filter surface, the exhaust gas is dust-free.
7. *Deodorization*. The housing is rotated by 90°; thus, the outer side filters are situated one above the other. The gas flows through the product during rotation of the rotor and blows out the residual solvent down to 50 ppm.
8. *Discharging*. In the housing in drying position, the product valve is opened and the rotation of the rotor is reversed. The product is conveyed to the centrally situated opening and then completely discharged due to the eccentric arrangement of the rotor and the small clearance between the rotor blades and the housing. In the upper part of the vessel, the filter surface is unaffected as the clearance is larger.

A typical Titus-Nutsch-Dryer with a filter area of 3.6 m^2 and drying area of 14.6 m^2 allows batch processing of 1.7 m^3 of the liquor feed, which may contain up to 60% by volume of the dispersed solids.

29.3 VAPOR PRESSURE DEWATERING

The methods discussed earlier represent sequential filtering and drying, that is, drying starts when filtering is completed. Another combined filtration–thermal drying technique where drying is performed during filtration is the so-called vapor pressure dewatering (VPD) developed at the Technical University of Karlsruhe, Germany. Here, the differential pressure needed to displace bulk liquid comes first from saturated and then from superheated steam due to intense contact heating of one side of a water-saturated filter cake. On this side, the bulk liquid heats up and evaporates rapidly, causing a pressure build-up, which drives the bulk filtrate progressively through the filter cake and the filter

medium (filter cloth, membrane, etc.). Since differential steam pressure needs to be built up to displace the liquid, total saturation of the filter cake is necessary for successful dewatering. Subsequent drying of the filter cake is due to convective heat transfer from superheated steam and conductive heat transfer from the heating plate (Ruf et al., 1996; Ruf and Stahl, 1997). The mechanism of the VPD technique is illustrated in Figure 29.7, in which the white circles represent the solid particles and the filled areas of different grayness indicate zones with various saturation levels.

The cake is enclosed in a casing with the heating plate at the bottom and a perforated plate over the filter cloth at the top. At the beginning of dewatering, the voids in a filter cake are completely filled with liquid. As soon as the temperature of the cake layer adjacent to the heating plate passes the boiling point with respect to the capillary pressure, water starts to evaporate rapidly. This causes the pressure to build up, which starts to displace the bulk of liquid toward the filter medium. Thus, a dewatering front that separates the liquid zone (dark gray area in Figure 29.7) from the saturated steam zone (light gray area in Figure 29.7) detaches from the heating plate and moves to

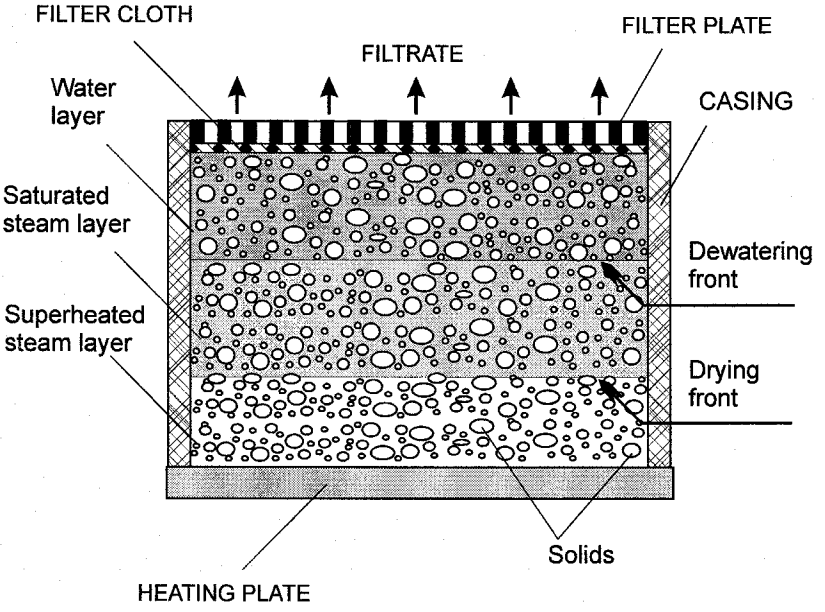

FIGURE 29.7 Mechanism of vapor pressure dewatering.

the filtering surface as water evaporation continues. Further on, a second front (the drying front) appears due to the continuous heat supply to the saturated steam zone so the zone with superheated steam develops. Figure 29.7 shows the instant when the drying front has detached from the heating plate but the dewatering front did not reach the filter cloth. The solid particles in the superheated steam zone are dried by convection from superheated steam and by conduction from the heating plate. When the dewatering front reaches the filter medium, a vapor breakthrough and thus the internal pressure is leveled to ambient conditions.

Contrary to dewatering by differential gas pressure, vapor pressure dewatering does not produce the ''fingering'' effect caused by the different capillary radii. If the steam saturation pressure precedes the dewatering front as a result of lower capillary pressure in larger capillaries, the vapor reaches colder layers of the filter cake and condenses (Ruf and Stahl, 1996). Thus, the dewatering front levels off and a premature vapor breakthrough is avoided. However, this effect fails if a fracture forms in the filter cake. To eliminate this drawback, the hot-filter press technique was further developed to suppress the development of cracks by compressing the cake during dewatering. A schematic diagram of a hot-filter press built based on the conventional membrane filter is shown in Figure 29.8. The press feed is designed as a corner inlet,

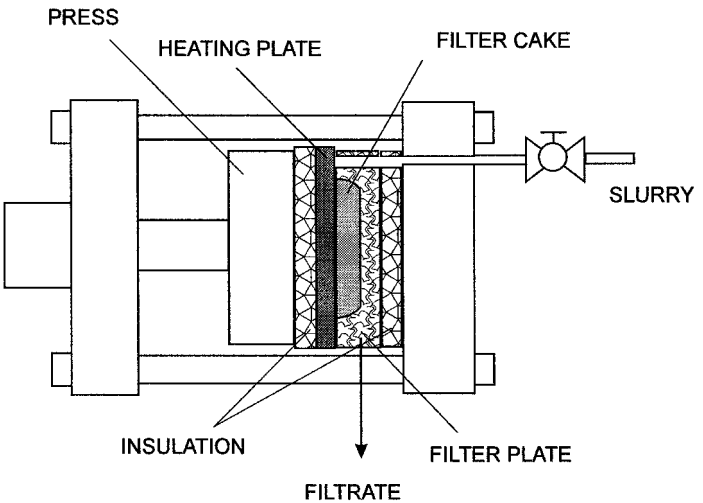

FIGURE 29.8 Schematic of the hot-filter press. (Courtesy of the Institute fur Mechanische Vervahrenstechnik und Mechanik, University of Karlsruhe, Germany.)

and drainage of the filtrate occurs locally at the membrane filter plate. The press is charged while the heating plate is unheated. When a cake of sufficient thickness is formed, the slurry inlet is closed and the membrane is exposed to pressure for prefiltering to achieve the desired consolidation of the filter cake. Then the heating plate starts to be heated with electricity, thermal oil, or other means, and the vapor pressure-induced dewatering begins.

As reported by Ruf and Stahl (1997), the theoretical minimum energy needed to displace all capillary liquid can be determined on the basis of the void volume, and an energy reduction of as much as 95% as compared with thermal drying is feasible. Experiments with model materials performed by these authors have shown that up to 80% of the liquid held in large capillaries can be displaced mechanically, i.e., through differential pressure dewatering. This translates into an actual reduction in energy consumption of 80% as compared to thermal drying for the same level of residual moisture.

29.4 STEAM PRESSURE FILTRATION

A modification to vapor pressure dewatering is the so-called Hi-Bar® Steam Pressure Filtration (Bokela GmbH, Karlsruhe, Germany), where pure steam

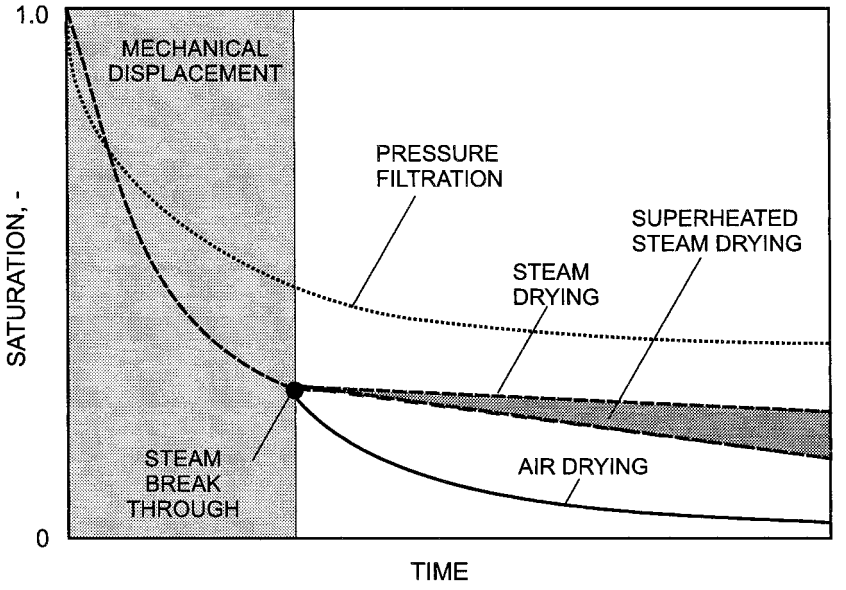

FIGURE 29.9 Steam pressure filtration. (From Stahl, 1998.)

for dewatering of the filter cake coming from an external source allows continuous operation (Bott, 2000). Moreover, after steam breakthrough, the heated cake becomes dewatered by compressed air flowing through the cake, which accelerates drying and reduces steam consumption (Figure 29.9). The steam pressure filtration is carried out in a rotary filter (disc or drum) where all sequential operations occur during one rotation of the filtering element. As seen from Figure 29.10, the steam area of the rotary filter is covered and sealed by a steam cabin separating the steam room from the interior of the pressure vessel, which is filled with compressed air. Generally, the steam cabin covers the cake up to the point of steam breakthrough (see Figure 29.9), and the cake is washed, dewatered, and heated in this first stage with minimum steam consumption. After leaving the steam cabin, the cake is dried to its final moisture content by compressed air.

The steam pressure filtration can lead to significant cost savings because of integrated filtration and drying. Table 29.1 presents a comparison of energy

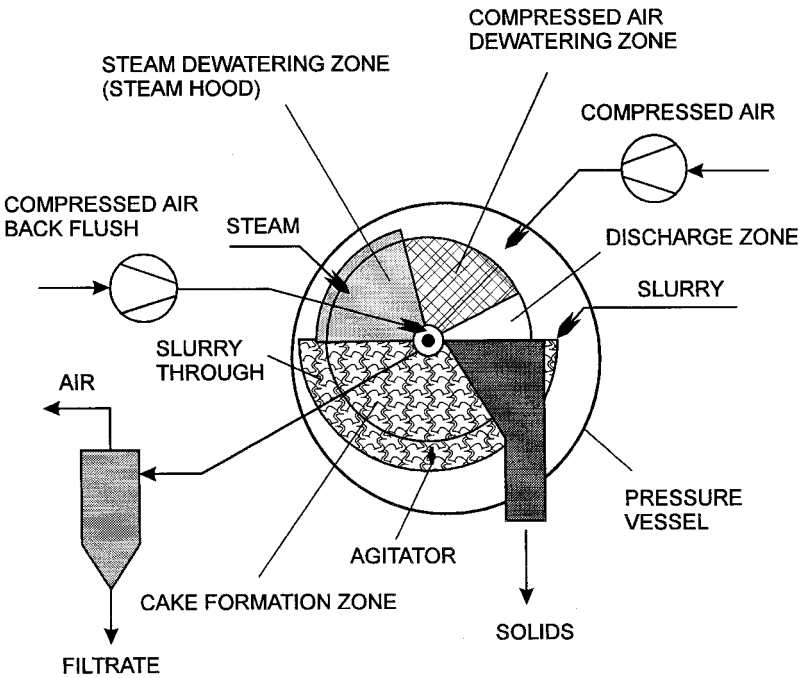

FIGURE 29.10 Process phases in Hi-Bar® disc filter. (Courtesy of Bokela GmbH, Karlsruhe, Germany.)

TABLE 29.1 Comparison of Dewatering Technologies for Coal Fines (< 63 μm)

Parameter	Coal concentrate 1		Coal concentrate 2	
	Pressure filter	Hi-Bar SPF	Pressure filter	Hi-Bar SPF
Technical characteristics				
Filter area, m^2	120	146	120	85
Pressure difference, bar	2.5	2.5	2.0	2.5
Final moisture content, % w.b.	19.5[a]	8.5	18.0[a]	9.5
Solids' throughput, t/h	100	100	70	70
Air throughput, m^3/h	4500	1600	3500	2100
Steam consumption, t/h	0	9.2	0	7.0
Steam/kg water removed, kg/kg	—	0.62	—	0.67
Energy costs				
Air compression, DM/a[b]	208,000	81,000	139,000	101,000
Steam production, DM/a	0	966,000	0	735,000
Thermal dryer, DM/a	2,327,000	0	1,228,000	0
Total energy costs, DM/a	2,535,000	1,047,000	1,367,000	836,00
Energy costs ratio	1.0	0.41	1.0	0.61

[a] Because target moisture content is 10% w.b., the filter cake must be thermally dried.
[b] DM—Deutch mark.
Source: Bott, 2000.

costs for compressed air filtration with thermal drying and for steam pressure filtration for two coal concentrates.

29.5 JET-STREAM CENTRIFUGATION

An alternative technique to steam pressure filtration is the jet-stream centrifugation concept developed by Heinkel AG, Germany (Anon., 2000b). Here, the filter centrifuge is fitted with a gas-tight drum. Thus, compressed gas (e.g., nitrogen) is heated and fed into the drum to expel liquid and evaporate residual moisture to much lower moisture levels than in a conventional centrifuge (Figure 29.11 and Table 29.2). When organic solvents are to be removed, the drying gas circulates in a closed system as shown in Figure 29.12. During the filling, washing, and discharge phases of a standard centrifugation process, the gas recirculation system is disconnected from the centrifuge. During the drying step, the gas leaving the centrifuge at normal pressure through a small

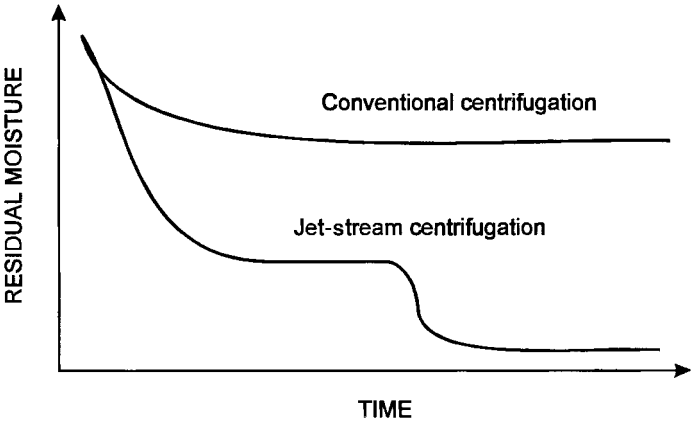

FIGURE 29.11 Comparison of classical centrifugation with jet-stream centrifugation. (Courtesy of Heinkel AG, Bietigheim-Bissingen, Germany.)

buffer is recompressed in a liquid-piston compressor, cooled in a tubular heat exchanger and washing tower, reheated, and recycled to the centrifuge. The compression heat is transferred to the circulation sealing liquid and released in a tubular heat exchanger with cooling water. Gas cooling and condensation of vaporized solvent are carried out in a brine-cooled heat exchanger and in

TABLE 29.2 Residual Moisture Content in Conventional and Jet-Stream Centrifugation

	Residual moisture content, % w.b.	
Product	Conventional centrifugation	Jet-stream centrifugation
Sodium ascorbate	4.5	<0.01
Mebhdrolin salt	15.0	<0.1
Acetylsalicylsalicylic acid	7.0	<0.02
Food coloring agent	7.8	0.2
Surfactants	39.4	<0.4
Penicillin	13.7	<0.5
Vitamins	5.0	0.1

Source: Courtesy of Heinkel AG, Bietigheim-Bissingen, Germany.

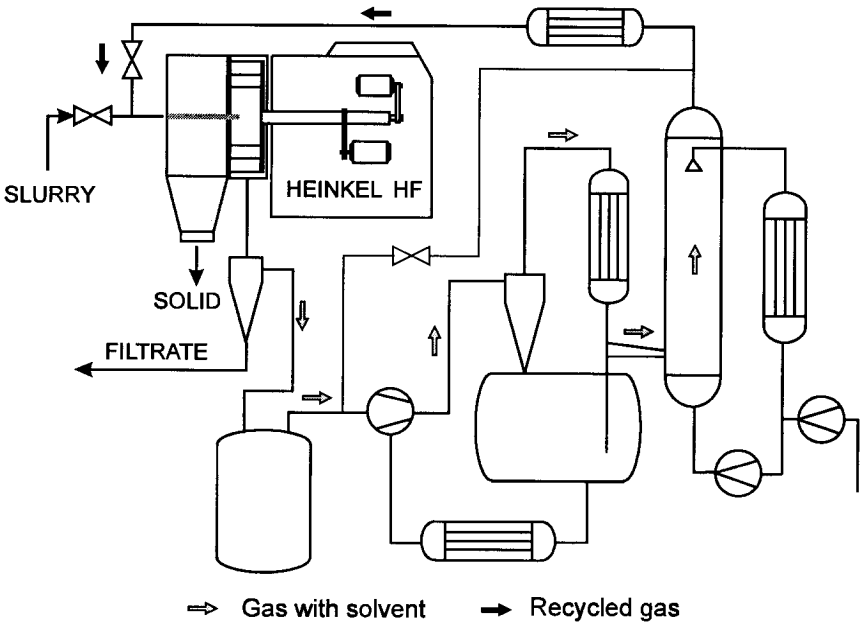

FIGURE 29.12 Gas recirculation for jet-stream centrifugation. (Courtesy of Heinkel AG, Bietigheim-Bissingen, Germany.)

a washing column fed with the recirculating brine-cooled washing liquid. The main benefits of combining jet-stream centrifugation with the gas recirculation system are a reduction in the amount of fresh gas use of 90% to 95% and a substantial reduction of environmental pollution.

29.6 MICROWAVE-ASSISTED PRESSURE FILTER DRYING

McConvey and Shering (2000) have recently presented results on drying pharmaceutical compounds in a pressure filter into which a microwave field is supplied. Based on their results with microwave-assisted pressure filter dryers of filtration areas of 0.05 m^2 and 0.5 m^2, they have shown that the drying period could be reduced by at least 50% when compared with drying with heated nitrogen in the same pressure filter. The average microwave power input was in the range of 2 to 4 kW per m^2 of filter area. They used acetone as the solvent to be removed. The initial moisture level was 20%, and the final

100 ppm. They found that intermittent agitation of the filter cake improved the drying performance, while continuous agitation had a negative effect. Indeed continuous agitation formed large balls instead of a free-flowing powder, which is obtained by intermittent agitation. In terms of cost, these authors report that microwave-assisted drying was 2.5 times more effective than the installation of an additional pressure filter to double the production rate. Nitrogen was used as the drying gas. It was found that microwave-assisted nitrogen drying was as effective as microwave-assisted vacuum drying. The latter is, of course, more expensive because of the need for a vacuum system. If the solvent is predominantly water and the material is not very heat-sensitive, then it is preferable not to use the vacuum system.

Interestingly, the authors could reproduce laboratory-scale results on a pilot scale with a scale-up factor of 150. The optimum operating parameters for drying of a bulk drug wetted with acetone were found to be 2 kW microwave power/m^2, intermittent agitation, and vacuum.

30

Other Hybrid Technologies

30.1 COMBINED MICROWAVE AND SUPERHEATED STEAM DRYING

Microwave (MW) and superheated steam (SHS) are both well-known and well-established, if not commonly used, drying technologies. Each has some unique advantages and some disadvantages described elsewhere in this book. In general, both are more expensive than the traditional dryers and hence are justified only for some niche applications. Recently Shibata et al. (2000) made perhaps the first systematic study of a combined MW and SHS drying technique using a model material, i.e., a thin bed of sintered glass. Their experiments as well as a mathematical model show that the combined MW/SHS drying system yields higher drying rates than either one acting alone. Further, they also showed that MW/SHS drying was faster than MW–nitrogen drying under otherwise similar conditions. Interestingly, they also found that the critical moisture content was lower for the hybrid system, which implies considerably shorter drying times for the MW/SHS system.

Caution must be exercised when extrapolating these results to real systems that may deform, shrink, puff, or undergo thermally driven physical or chemical changes. Such a system is likely to produce lower apparent density

products due to puffing, which may or may not be a desirable product attribute. Finally, it certainly will be a more expensive process applicable in special cases only for reasons already discussed in earlier parts of this book.

A further variant of this technique could be the use of MW energy supplied periodically rather than continuously—this will save electrical energy costs but not the initial investment cost, however.

30.2 COMBINED INFRARED AND CONVECTION DRYING

Paakkone et al. (1998) reported on an extensive study of combined convection and infrared (IR) drying of herbs such as peppermint, parsley, and garden angelica. They dried beds of the leaves of these herbs in a conveyer dryer with three zones through which air was blown. Infrared lamp panels were installed in each zone. The infrared wavelength ranged from 2 to 5 microns. An interesting feature of this study is that infrared radiation was applied intermittently with periods of tempering with pure convection to keep the product temperature from reaching values that were too high. The cooling effect of convection allows use of higher IR power to speed drying without thermal degradation. As expected, at the highest drying temperature (peppermint), the drying time was shortest and the energy consumption lowest. Interestingly, the quality of an IR-dried product was assessed to be better than that dried in an electric oven. The total oil content of IR-dried angelica leaves, for example, was higher than in electric oven-dried samples. This means the product retains more aromas. In a related study, the authors report no change in the microbial quality when using IR drying with intermittent convection.

30.3 INFRARED HEAT-PUMP DRYING

Chua et al. (2000) have demonstrated the benefit of drying products like banana, guava, and potato under cyclically varying air-temperature conditions in a batch heat-pump dryer; they show that this process minimizes degradation of the original color of the feed. This is especially important for sugar-rich fruits, which tend to suffer significant color degradation in conventional air drying. The layer of water on the drying surface that is maintained in lower-temperature cyclical drying seems to protect the surface from undesirable browning reactions—both enzymatic and nonenzymatic. The intermittent heat supply allows one to maintain moderate drying rates without decreasing product quality.

A highly sophisticated multistage heat pump with PID control was used by Chua et al. (2000) to achieve sinusoidal and square-wave-type temperature variations of the drying air. However, it may be possible to achieve similar benefits in a batch dryer by an intermittent supply of energy using infrared lamps that go on and off at a desired frequency and amplitude of heat flux. Because of thermal inertia of IR sources, this method of energy supply is limited to low-frequency variations of heat supply. Alternative options for intermittent heating is volumetric heat generation by using microwave or RF (radio-frequency) irradiation. This mode of heating allows higher frequencies of intermittent energy supply to be attained. However, capital costs of the microwave and RF equipment are generally higher than that for infrared, so this technique may be justified only for high-value products for the high-end market.

To improve productivity with a simpler heat-pump dryer operating in the batch mode, it should be feasible to alternate the drying air supply to two or more shelf dryers. This will increase the dryer output (at the cost of some increase in batch processing time) without increasing the complexity of the heat-pump system. No prior work has been reported on this idea, however.

Part V

Other Techniques

This part includes some of the new dryer types and drying concepts that have appeared in the literature in recent years. Most are in their infancy, and so no definite evaluation is feasible at this time. Also, the techniques presented here are not categorized according to any rigid classification scheme or criteria. Nevertheless, the reader will find the ideas interesting and innovative at least for some special applications. They will be of special interest to readers who wish to identify new ideas for basic R&D.

31

Special Drying Technologies

31.1 DRYING BY ALTERNATING HIGH- AND LOW-PRESSURE OPERATIONS

Very recently Rakotozafy et al. (2000) proposed and successfully evaluated a novel concept for drying heat-sensitive materials (such as yeast, biotech products, enzymes, etc.) based on a succession of compression and decompression cycles. In this process, the material is subjected to pressures of 2 to 10 bar for a certain duration followed by evacuation to low pressures of the order of 100 mbar (Figure 31.1). The product is maintained at the low-pressure level for a certain time interval. This pressure–vacuum cycling may continue over a period of time that is much shorter than that needed for freeze-drying the same material. Their studies focused on the effects of the various relevant parameters including the pressure levels, cycle duration, vacuum level, etc. Examination of the quality of baker's yeast dried using this method compared with that freeze-dried showed a better performance of the pressure cycling process. Clearly, freeze-drying is a much more expensive and slower process. It is worth noting that the quality of the product (measured in terms of the viability of the yeast) is reported to be better in this process. This is likely due to the shortened duration of the total dehydration process. The cell survival

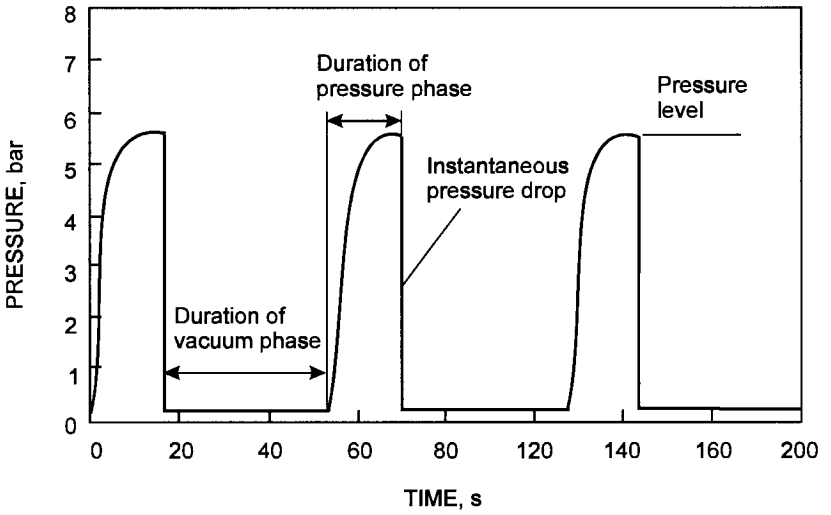

FIGURE 31.1 Pressure variation during dehydration by successive pressure drop cycles. (From Rakotozafy et al., 2000.)

rate for this process was found to be 10 times better than that in freeze-drying. However, this number is a function of the operating parameters tested and so should not be generalized. In addition, further optimization of the process is needed to enhance its performance even better, e.g., use of variable pressure ranges and variable cycle frequency, which is easy to achieve in a fully automated system. This process does seem to have potential for applications involving highly heat-sensitive materials.

31.2 THROUGH-AIR ROTARY DRYER

Rotary dryers belong to the group of the most common dryers for particulate solids mainly because of their simple design, versatility, flexibility, large throughput, and the ability to handle a variety of feeds ranging from crushed minerals to cut plants such as alfalfa. The convective heat and mass transfer between the drying gas and the wet solids take place mostly during ''showering'' of the lifted particles as the contribution of the rolling bed (''dead'' zone) to transfer processes is only in the order of 5%. In addition, the material hold-up is relatively small and varies from 10% to 20%. Therefore, conventional axial gas-flow rotary dryers are usually large, heavy, relatively expen-

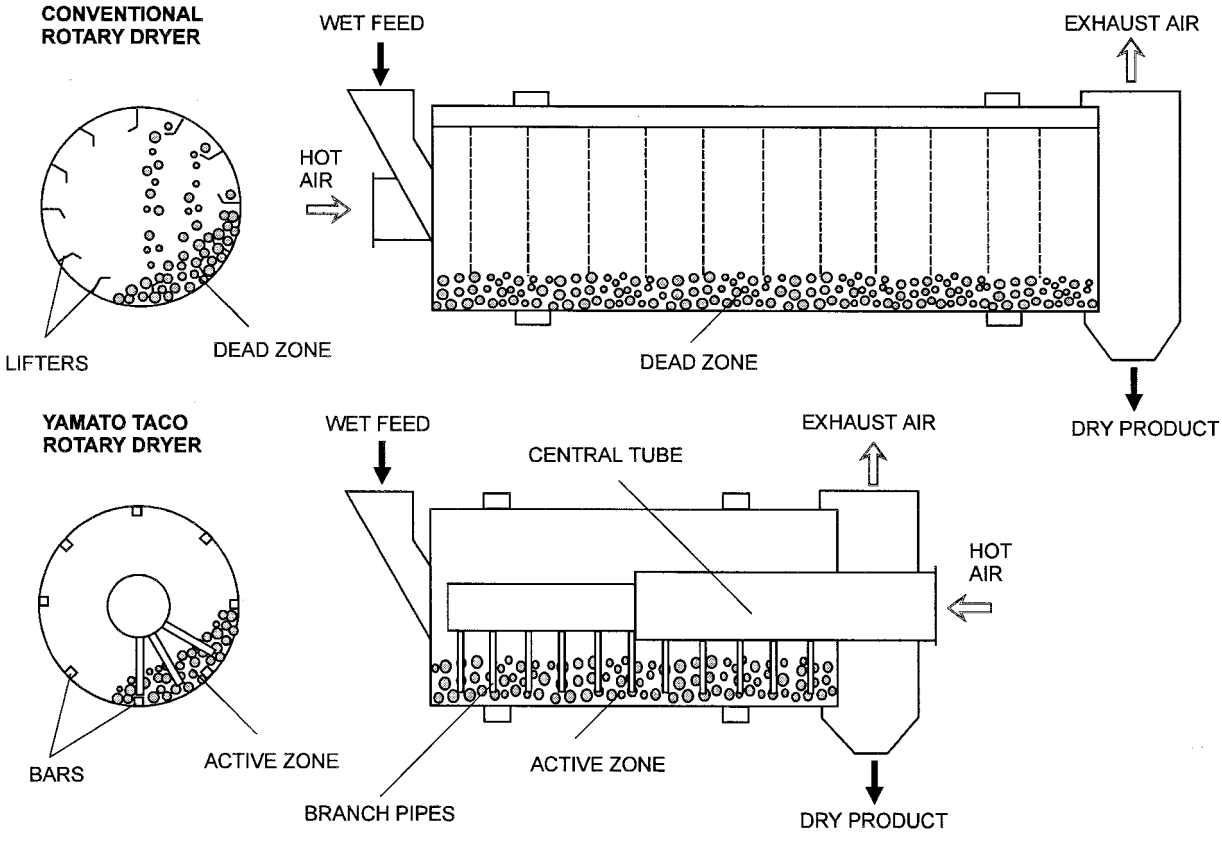

FIGURE 31.2 Comparison of the conventional rotary dryer with the Yamato TACO rotary dryer for the same capacity to same scale. (From Yamato, 1998. Courtesy of Yamato Sanko Mfg. Co. Ltd., Japan.)

sive, and energy-consuming. Rotary dryers of special design such as the louvre-type where drying gas flows through the rolling bed of particulate material (see Perry and Green, 1997) have better drying performance, but the capital and maintenance costs for such dryers are significantly higher.

To offset some of the basic disadvantages of conventional rotary dryers, such as large size for a given throughput, short residence time, heavy attrition, and particle carryover, a novel rotary dryer with drying air blown through the rolling bed of wet particles was developed and termed the Yamato Rotary Dryer or Yamato TACO (through air combination rotary dryer) (Yamato, 1987, 1996). With reference to Figure 31.2, the drying air in the TACO dryer is injected into the bed of the material being carried in a rotating cylindrical shell, through a multiplicity of pipes branching off from a central tube. The intensive particle motion created by the air jets issuing out of the branching pipes at velocities ranging from 20 to 25 m/s (max 45 m/s) secures intimate gas-to-particle contact and provides favorable conditions for heat and mass transfer (Table 31.1). Consequently, the drying rates are nearly doubled com-

TABLE 31.1 Sample Data for Yamato TACO and Conventional Rotary Dryers

Material	Moisture content, % w.b.		Inlet air temperature °C	Drying rate kg/(m^{3}h)	Heat transfer coefficient kW/(m^{3}K)
	In	Out			
Yamato TACO					
Coal (crushed)	12	1	200–300	50–60	160–190
Ores	40	10	300–400	70–90	210–270
Sand	15	0	300–400	50–80	175–325
Stone (crushed)	6	0	300–400	30–40	175–290
Silica gel	70	1	250–500	50–90	210–270
Clay	30	0	300–400	50–65	175–210
Asphalt	16	2	60–80	30–70	270–325
Wet ash	30	1	300–400	50–80	160–210
Fish meal	60	20	200–250	50–60	115–175
Conventional					
Coal (crushed)	13	1	300–500	20–30	95–115
Coal (pebbles)	20	10	300–400	20–30	95–115
Ores	23	13	350–500	25–30	115–140
Fertilizer	13	1	100–400	5–20	60–70

Source: Yamato (1998).
Courtesy of Yamato Sanko Mfg. Co. Ltd., Japan.

pared to the conventional rotary dryers; also, particle attrition is greatly reduced. Higher drying rates translate not only into a smaller shell volume (Figure 31.2) but also into more compact ancillary equipment such as dust collectors and fans. A comparison between conventional and through-air rotary dryers is presented in Table 31.2.

The basic design as well as the system configuration for the through-air rotary dryer used as a dryer, predryer, or cooler are similar to these for the conventional rotary dryers. Figure 31.3 presents a typical configuration for drying of particulate materials with partial heat recovery via recycling of exhaust air. When flue gases are used as a drying agent as in the case of drying and incineration, there is no need for the burner or the heater. Because of particle mixing by air jets, it is not essential to have internal flights as material lifters. If needed, small bars may be attached to the shell to enhance agitation of the bed. Since no showering of particles is required for proper drying, the rotational speed of the shell can be reduced by half, which simplifies the dryer design and reduces costs of the trunnions and gears.

Another industrially tested application of the Yamato TACO design is successive drying and incineration of semisolid sludges that contain organic matter (Figure 31.4). By using flue gases from the incinerator as a heat carrier for drying, much better fuel economy can be achieved as compared to direct incineration of the wet sludge. When processing sludge with an initial moisture

TABLE 31.2 Characteristics of the Yamato TACO and Conventional Rotary Dryers

Parameter	Conventional	Yamato TACO
Air flow	Parallel to the bed	Through the bed
Material hold-up	10%–20%	15%–25%
Drying time	Reference	Reduced
Drying ratio	Reference (1)	2
Volumetric heat transfer coefficient	175–230 kW/(m^3K)	350–1750 kW/(m^3K)
Shell rotation ratio	Reference (1)	1/2
Shell volume ratio (for the same capacity)	Reference (1)	1/2
Capacity ratio (for the same shell size)	Reference (1)	2
Attrition	Reference	Reduced
Dusting	Reference	Reduced
Bed zone in the shell	Passive (''dead'')	Active

Courtesy of Yamato Sanko Mfg. Co. Ltd. Japan.

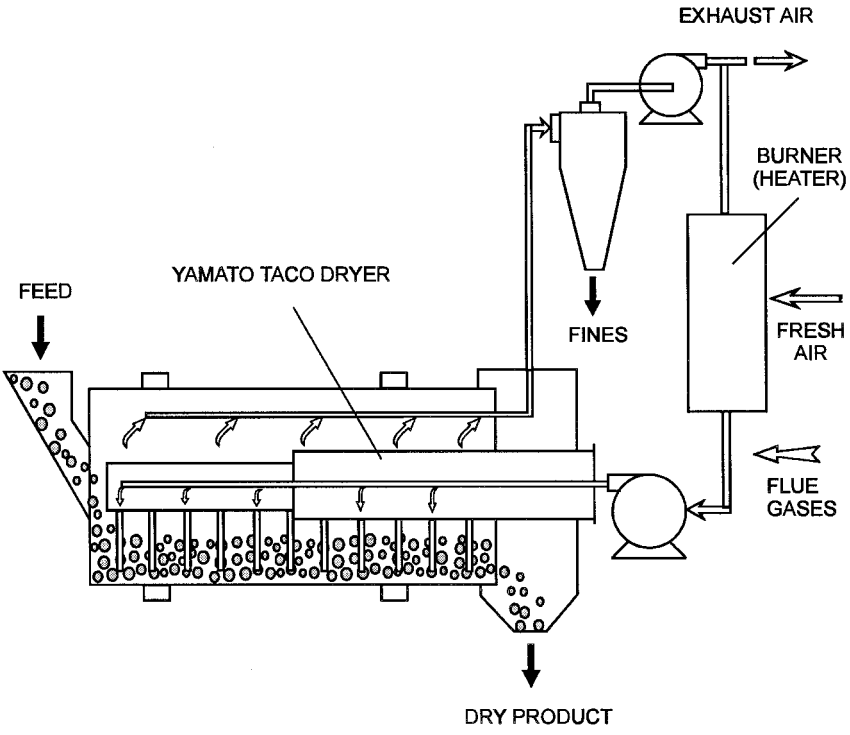

FIGURE 31.3 General flow diagram for Yamato TACO rotary dryer.

content of about 80% w.b., which does not require deodorizing equipment, the combined system based on the TACO dryer and the vortex incinerator is claimed to be operated with no additional fuel (Yamato, 1998). Besides the calorific value of the organic matter in the sludge, reduced fuel consumption results from much better combustion in the incinerator when burning sludge predried from 80% to 20% w.b. In such a case, only 25 kg of water per 100 kg of dry combustible matter has to be evaporated in a combined system instead of 400 kg of water to be evaporated in the case of wet-sludge incineration.

The vortex incinerator used in a preferred combined system with the Yamato TACO dryer can also be used as a standalone dryer-incinerator (Figure 31.5). The wet material is fed to the periphery of the incinerator equipped with a tangentially oriented gas burner mounted on the sidewall opposite the feed point. Due to the combined action of blades and nozzles attached to the

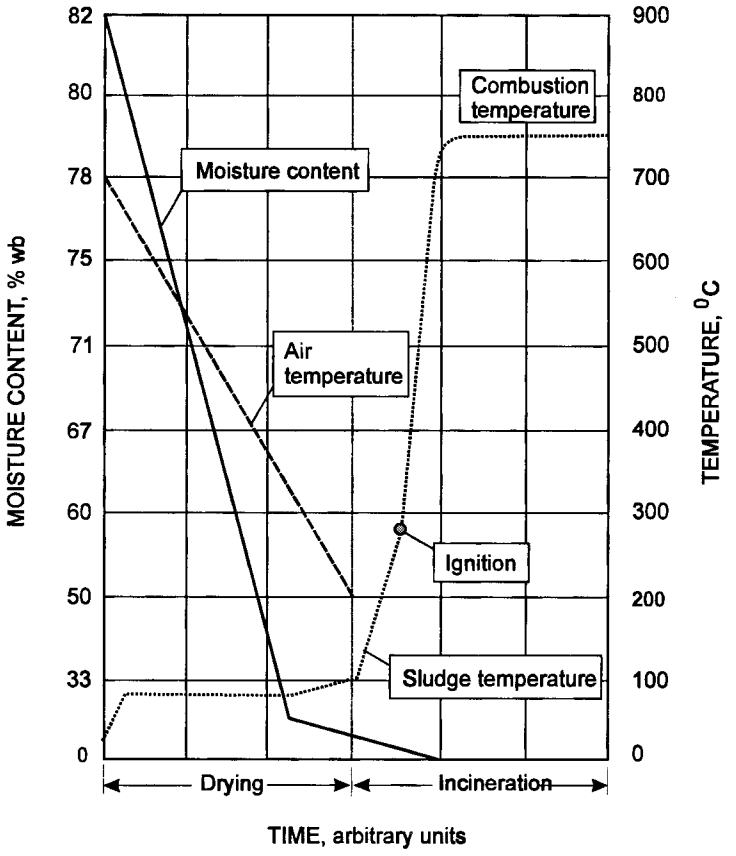

FIGURE 31.4 Principle of combined drying and incineration. (From Yamato, 1998.)

rotating branch pipes which supply combustion/drying air, the wet material is raked and transported along a spiral path toward the chamber center (Yamato et al., 1974). On this path, the water is first evaporated to the critical moisture content. Soon after, the material temperature reaches the ignition point and a violent combustion takes place with the help of fresh air supplied through the nozzles. The dry material or ash is discharged from the central port through a chute to the take-up device.

The TACO dryer is a simple but innovative dryer design. Pilot testing is recommended, as it may not be suited for the whole range of products the conventional rotary dryer can handle.

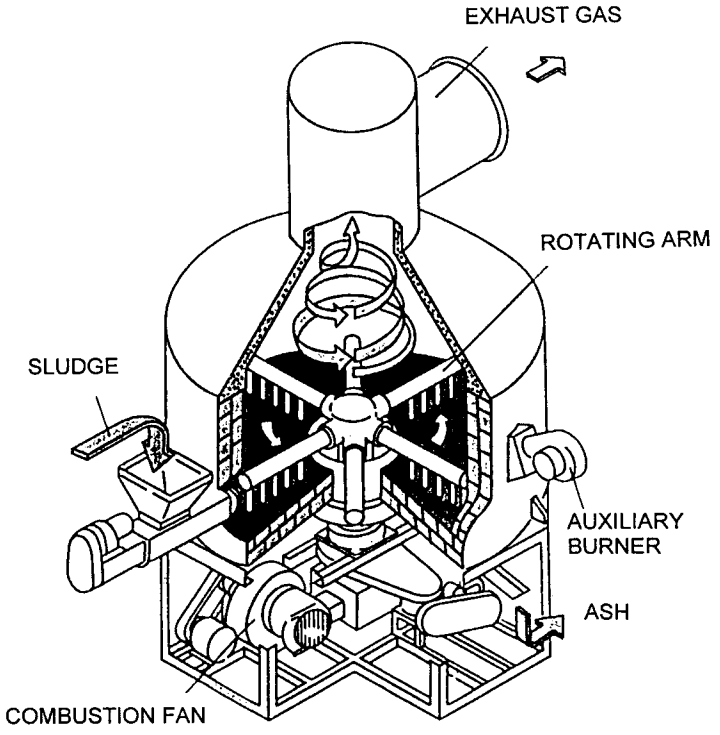

FIGURE 31.5 Vortex incinerator. (Courtesy of Yamato Sanko Mfg. Co. Ltd., Japan.)

31.3 DRYING WITH BED MIXING

A rather unique drying application involving bubbling or circulating fluidized bed combustor using peat, brown coal, wood biomass, and waste sludges has been reported by Imatran Voima Oy, Finland (Hulkkonen et al., 1995; Hulkkonen, 1997). The term ''bed mixing'' originates from the fact that the hot solid particles (the ''bed'') taken out of the fluid bed combustor are mixed with the wet fuel to extract a sensible heat of solid particles and take advantage of more effective contact heat transfer. In addition, the use of a steam atmosphere makes it relatively easy to recover the latent heat of evaporation back to the process at a higher temperature level. Thus, the thermal efficiency of the power plant is enhanced especially in combined heat and power (CHP) applications. This concept has been tested successfully in peat- and wood-fired power plants producing 6 MW electricity and 20 MW district heat. This type of drying

appears suitable for sawdust, wood bark, and possibly paper mill sludges as well.

Figures 31.6 and 31.7 show a schematic and general view of the ''bed-mixing dryer,'' respectively, while Figure 31.8 presents a flow diagram of a peat- and wood-fired power plant utilizing this novel drying concept. The dryer can be any type, but the simple flash dryer was used in the trials reported since only a few seconds are needed for drying the fuel due to

(1) The high temperature at the dryer inlet
(2) Direct contact between the bed material from the combustor and the wet fuel (40% to 60% w.b.)
(3) The injection of high-velocity superheated steam into the bottom section of the flash dryer

The superheated steam at atmospheric pressure carries the dried fuel together with the hot bed material to a cyclone where the solids are separated

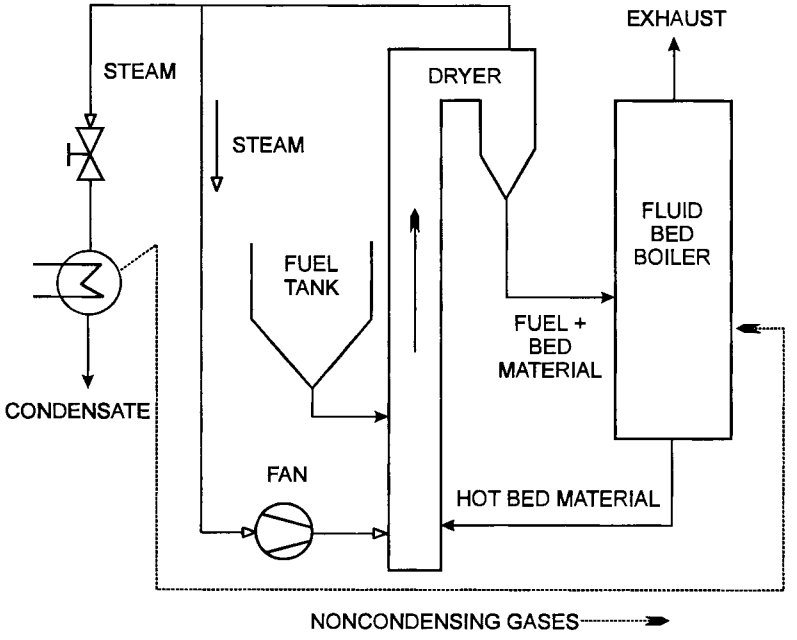

FIGURE 31.6 Drying with bed mixing. (Courtesy of IVO Technology Centre, Vantaa, Finland.)

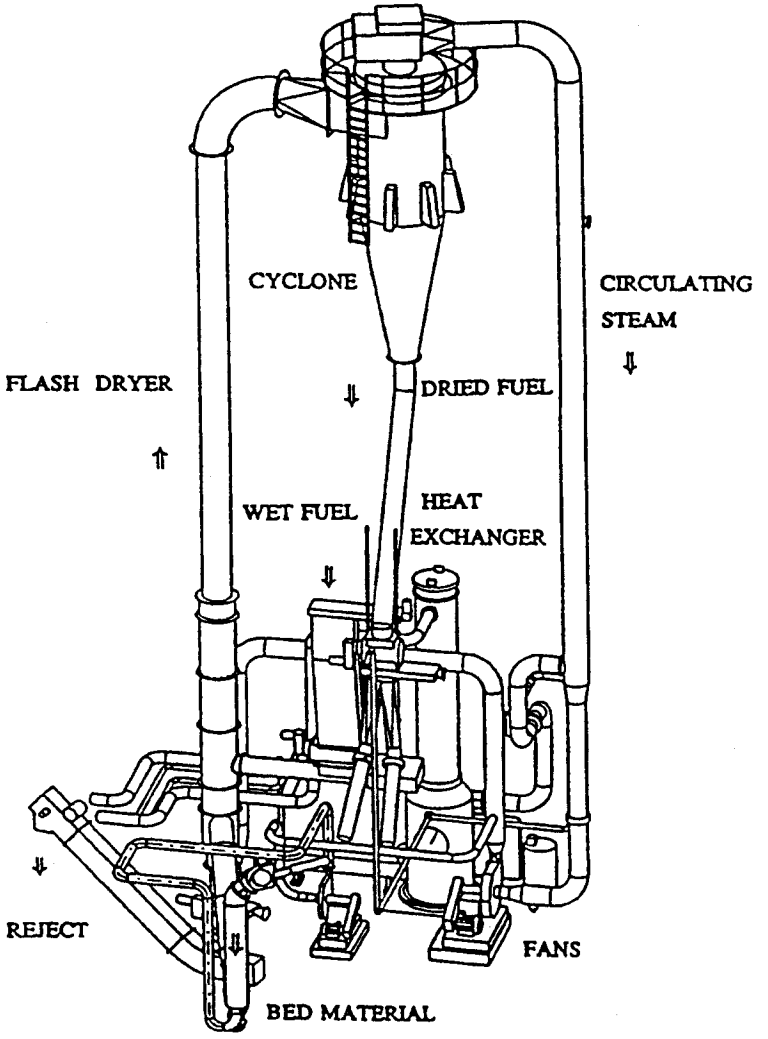

FIGURE 31.7 The bed-mixing dryer. (Courtesy of IVO Technology Centre, Vantaa, Finland.)

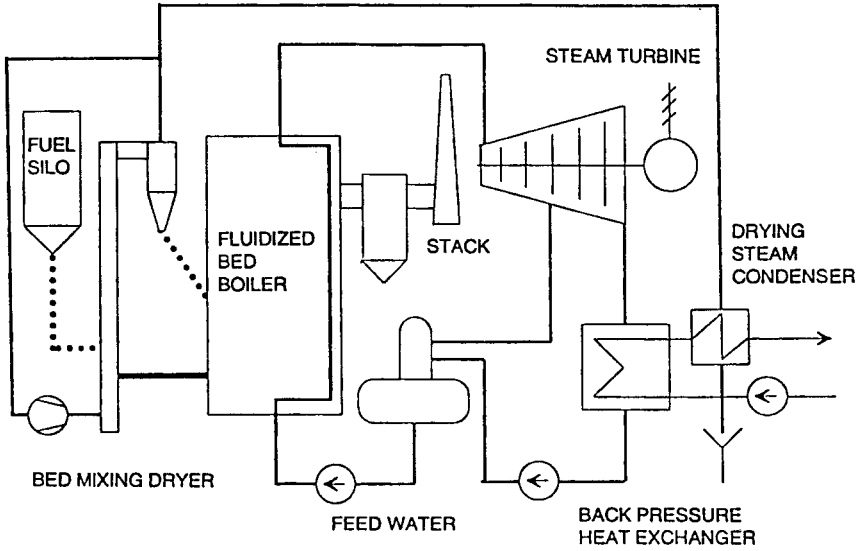

FIGURE 31.8 Flow diagram of the bed-mixing dryer in the peat- and wood-fired power plant. (Courtesy of IVO Technology Centre, Vantaa, Finland.)

from the steam and fed into the combustor (fluidized bed boiler). The pressure in the dryer is kept slightly above the boiler pressure. The main parameter to control, however, is the steam temperature after the cyclone, which is maintained at the set value by controlling the feed rate of the bed material to the dryer. A part of the steam from a cyclone is recycled to the dryer. The excess steam can be condensed and used to produce district heat as the initial Finnish application does or used for any other purpose. If the wet fuel comes in at 50% w.b., Hulkkonen (1997) reports a 10% to 15% improvement in the thermal efficiency of the power plant. Moreover, the flue gas channels can be smaller than usual because the moisture from the fuel does not go through the boiler. This reduces the size and investment costs of the new boiler or increases the capacity of the plant already in operation. The process characteristics for the power plant shown in Figure 31.8 are given in Table 31.3. The case study, which illustrates the possible capacity increase due to the bed mixing, is depicted in Table 31.4.

Among other advantages claimed for this process are simple construction, no odor emission, no fire or explosion hazard, and ease of control.

TABLE 31.3 Some Characteristics of a Power Plant with a Bed-Mixing Dryer

Fuel: peat, wood biomass
Boiler: bubbling fluidized bed (8 kg/s of steam at 61 bar pressure and 510°C)
Steam turbine: back pressure steam cycle with district heat produced at one pressure level

	Dryer off	Dryer on
Fuel input	26.3 MW	26.0 MW
Fuel moisture content	55%	~15%
Power output	6.1 MW	6.1 MW
District heating output	17.6 MW	21.2 MW
Thermal efficiency	90% (LHV)	105% (LHV)
	73% (HHV)	84% (HHV)

Courtesy of IVO Technology Centre, Vantaa, Finland.
LHV = lower heating value, HHV = higher heating value.

It should be noted that bed-mixing drying is somewhat similar to the so-called particulate immersion drying technique studied extensively by Raghavan and coworkers at McGill University (Pannu and Raghavan, 1987; Tessier and Raghavan, 1984). Using various heated solids such as sand, salt, molecular sieves, and natural zeolite particles as the heat transfer medium, they developed a rotary processor for drying grains and other granular materials of biological origin. The dryer essentially mixes the heated particulate media

TABLE 31.4 Capacity Increase in Power and Steam Output due to the Bed-Mixing Dryer[a]

Parameter	Without dryer	With dryer	Change
Fuel	Biomass	Biomass	
Fuel input, MW	92.1	110.8	+20%
Fuel moisture, % w.b.	55	~20	
Live steam, kg/s	32.7	40.8	+25%
Flue gas flow, Nm^3/s	51	51	
Stack gas temperature,°C	130	118	
Power output, MW	20.5	26.3	+28%
Process steam, MW	61	90.5	+48%
Thermal efficiency, %	88.5	105	+19%

Courtesy of IVO Technology Centre, Vantaa, Finland.
[a] For the same flue gas volume.

with wet grain, then allows a certain residence time for the necessary heat and mass transfer to occur, and finally separates the dried grains from the heat transfer medium. Natural zeolites as the capillary-porous drying medium have advantages over sand or other nonhygroscopic particles since such materials also enhance the potential for mass transfer by adsorbing the evolved vapor. Because mineral ingredients are required for animal feed, some retention of zeolite in the dried product is permissible. The fact that particle-to-particle heat transfer rates are much higher than these for the gas-particle systems helps accelerate the drying rate. Interested readers can find additional information on the particulate immersion drying technique as well as on contact-sorption drying in Chapter 12.

31.4 DRYING AT AMBIENT AIR TEMPERATURE

Because drying is the simultaneous heat and mass transfer process, one of the options for low-cost drying of waste materials is drying at ambient air temperature, where the moisture concentration gradient is the major driving force. Following this concept, the DRY-REX system was developed in which drying takes place when unsaturated ambient air is drawn through the moving bed of the wet particulate material or preformed pasty sludges such as these from pulp and paper mills (Barre, 1997; Barre and Masini, 2000). With reference to Figure 31.9, drying is carried out in two stages. In the first stage the solid material such as bark, wood chips, sugar cane, etc., is disintegrated to enlarge the heat and mass transfer area and reduce internal resistance to moisture diffusion. Pasty or semisolid feeds are mechanically pressed to form pellets (4 to 6 mm in diameter and 5 to 15 mm long) in order to increase the interfacial area and agglomerate the sludge to prevent the formation of dust during drying. In the second stage, drying occurs via passing ambient air through the bed of preformed material fed to the multideck perforated belt conveyor.

The ambient air dryer appears to be competitive to other dryer types because

- Its simple design reduces investment and operation costs
- No thermal energy is required for drying
- Drying at low temperatures (e.g., 5°C) prevents the formation of bed odor
- Pelletizing of the sludge prevents dust formation
- The risk of explosion is practically eliminated (no dust and low temperature)

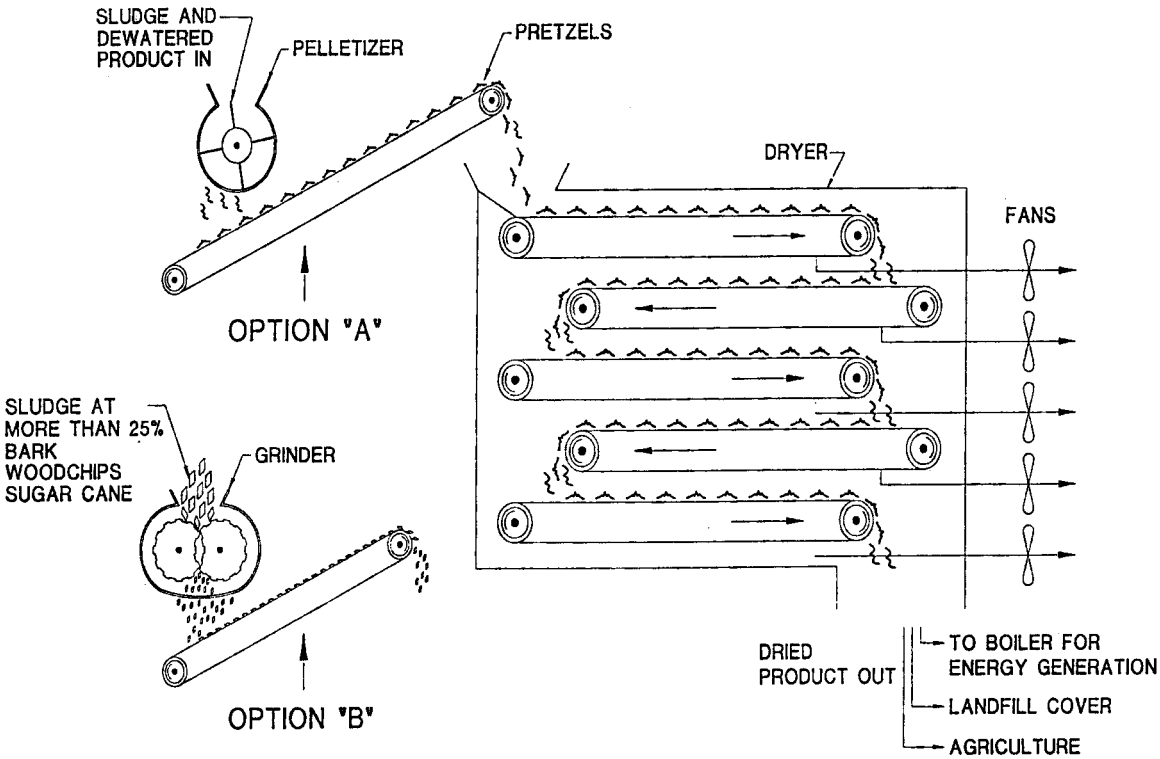

FIGURE 31.9 Basic configuration of DRY-REX dryer. (Courtesy of Solutions Mabarex, St. Laurent, Canada.)

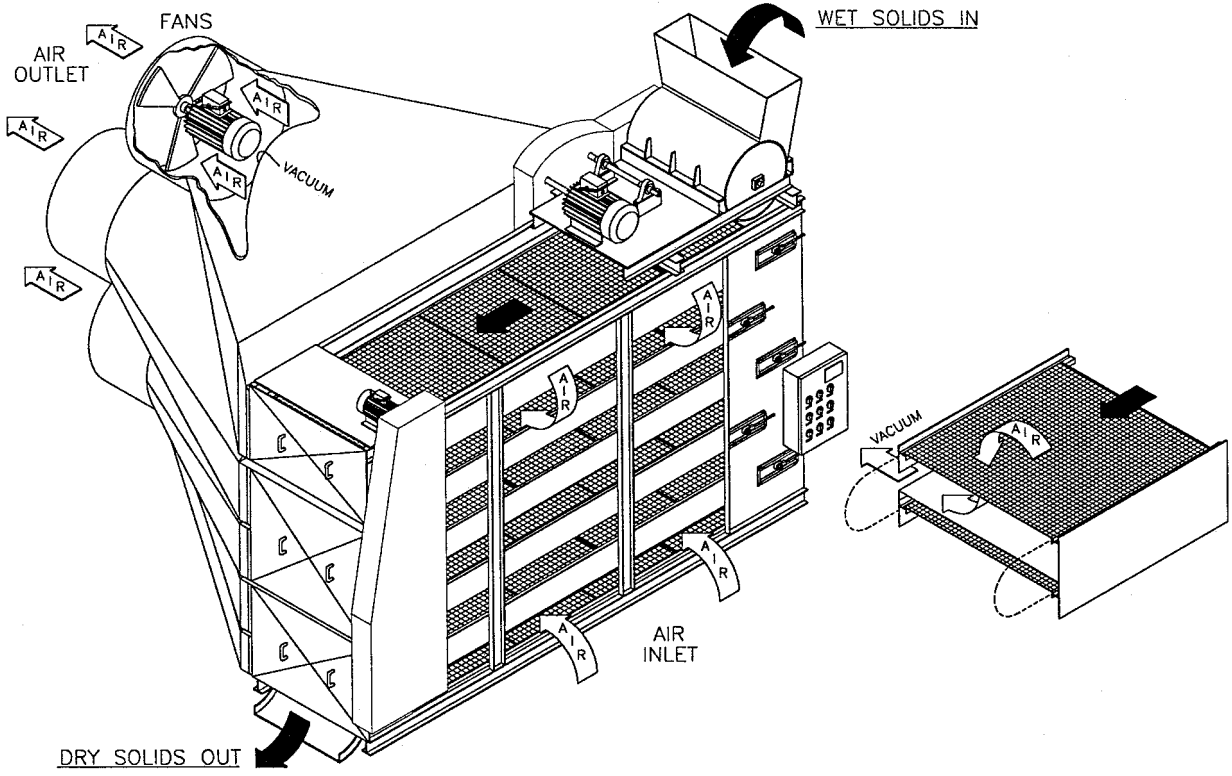

FIGURE 31.10 General view of the DRY-REX dryer. (Courtesy of Solutions Mabarex, St. Laurent, Canada.)

TABLE 31.5 Ambient Air Drying of Residues from Paper Mills

Material	Air temperature, °C	Air relative humidity, %	Moisture content, % w.b.	
			Initial	Final
Primary–secondary sludge (% mass)				
10–90	17	60	87.4	30.7[a]
66–33	17	60	85.4	32.0[a]
64–36	5.5	30	70.2	26.8[a]
35–65	18	62	84.4	22.0[a]
30–70	15	40	76.0	17.1
60–40	17	62	81.0	22.0[a]
De-inking sludge–50% clay	16	92	61.7	7.9
Frozen bark	20	62	60.0	30.0[a]
Bark–sludge (50%–50%)	20	29	60.0	20.5[a]

Courtesy of Solutions Mabarex, St. Laurent, Canada.

[a] Lower values could have been obtained, but these were determined by the end-users as sufficient for firing in the boiler.

These advantages are slightly offset by the need for more powerful fans to be installed to provide air velocity high enough to compensate for reduced drying rates when using low air temperatures. The ambient air dryer shown in Figure 31.10 was tested for a variety of waste materials including water-saturated bark and wood chips, wood pulp, ash and fly ash, sugar-cane residues, de-inking sludge, and the mixture of primary and secondary (biological) sludge in any mass ratio. Table 31.5 presents representative data on ambient air drying of various wastes from paper mills. Clearly, air consumption is higher and the process is slower than hot-air drying. The air should be sufficiently dry for this method to be efficient.

31.5 VACUUM–SUPERHEATED STEAM DRYING AND GRANULATION

Unlike the particle-size enlargement by agglomeration when mixing the key components with binders, surfactants, lubricants, fillers, and other end-use aids, the granulation of pasty materials is based on progressive concentration during drying under carefully selected hydrodynamic conditions to obtain

granules of required size and size distribution. Following the common terminology (Perry and Green, 1997), agglomeration by any means of agitation (e.g., tumbling, fluidization, spouting) is referred to as granulation in contrast to pressure agglomeration (compaction) known as extrusion, tableting, briquetting, or pelletizing. This relatively new and unconventional technology, which allows granules to be obtained in a single processor directly from a pasty feed, is called the vacuum hot steam process (VHSP) (Dürr, 1996, 1998). Simultaneous drying and granulation are carried out in a vacuum-tight mixer having a rotating mixing pan that is slightly inclined against the vertical line. Rotation of the mixing pan conveys the processing material into the zone of an eccentric high-speed rotor. Because both the rotor and the pan are rotated in opposite directions by independent drives with controllable speed, the material streams are characterized by high differential velocities and shear forces. A pseudo-fluidized circulating bed is also created mechanically due to the rotary movement of the rotor and the structural design of the knifelike mixing blades. A stationary deflector plate on the tank wall combined with the inclined arrangement of the mixing processor aids fluidization as it generates strong vertical currents, resulting in an intensive three-dimensional flow pattern of the material inside the processor (Figure 31.11). The deflector plate also prevents material from sticking to the pan wall. Material to be processed is fed to the processor from above and discharged through the central bottom port.

Granulation of the kneadable raw materials such as a filter cake, slime, or soft paste in a VHSP (Figure 31.12) is based on progressive moisture evaporation from the pseudo-fluidized bed of wet clumps. Drying takes place in

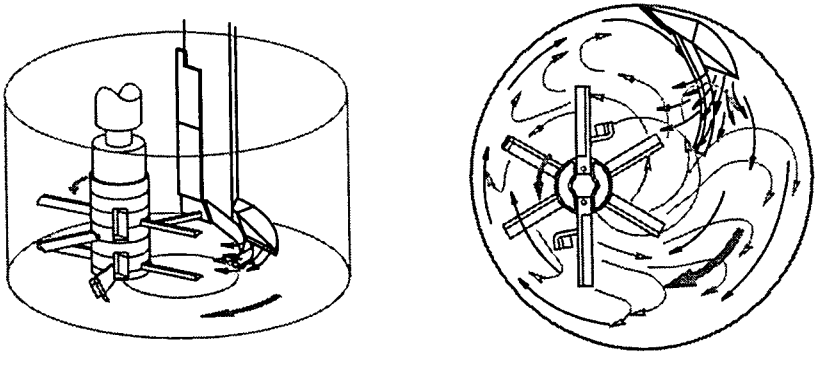

FIGURE 31.11 Flow pattern in the EVACTHERM® processor. (Courtesy of EIRICH, Hardheim, Germany.)

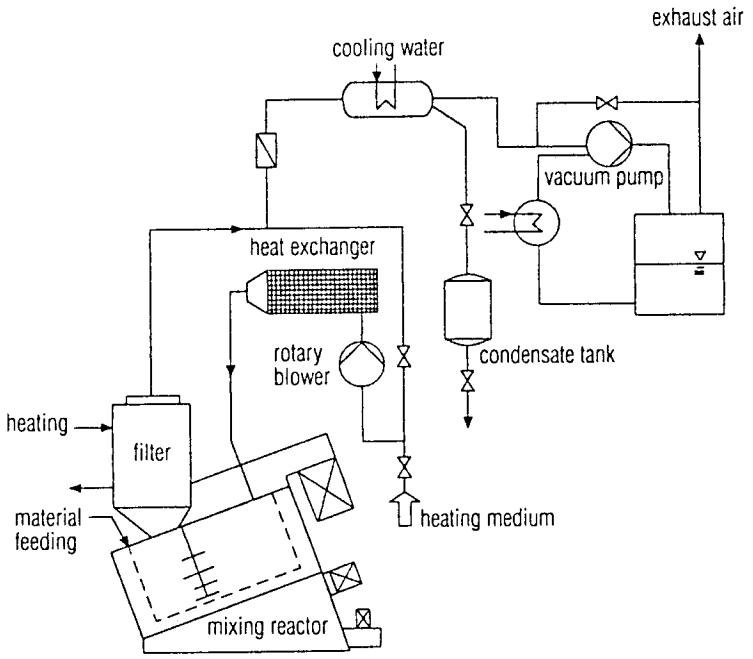

FIGURE 31.12 Flow diagram for superheated steam vacuum drying and granulation. (Courtesy of EIRICH, Hardheim, Germany.)

superheated steam that circulates in a closed system maintained under reduced pressure to lower the material temperature, even down to 40°C (Dürr, 1996). When granulating dry and multicomponent materials such as these in the production of ferrite granules (Dürr, 1997), the powders are thoroughly mixed and wetted to obtain a homogeneous pasty feed. Once homogenization of the feed material is completed, the system is set at the desired level of vacuum so practically all air inside the processor is removed and replaced by steam. A closed-circuit blower conveys the process steam through a heat exchanger (a superheater) to the mixing pan via a specially designed steam distributor arranged laterally to the deflector plate to enhance pseudo-fluidization. At the beginning of the drying cycle, the material is rapidly heated to the drying temperature by complete condensation of the steam (''shock heating''). As soon as the steady-state bed temperature is reached, the exhaust steam leaves the processor volume through the heated vapor filter and is redirected by the closed-circuit blower to the steam superheater and then back to the process volume. The energy for drying is supplied to the system via a heat exchanger

as well as by the circulation blower in the vapor compression arrangement. The excess steam due to moisture evaporation is condensed and bled out of the superheated steam loop. As drying proceeds, the cutting effect of the projecting star-shaped mixing blades of the rotor disintegrates the tough, crust-forming cake into smaller pieces that gradually lose their tendency to stick together because of surface moisture evaporation. The granulation process begins as the removal of liquid from disintegrated pieces advances. The pseudo-fluidization along with rolling movement of the material in a circulating bed as shown in Figure 31.11 promotes the formation of rounded granules.

Although the EVACTHERM® dryer is essentially a batch processor, it is possible to perform the so-called more or less continuous drying. It is normal that for high-moisture feeds the load of the dryer decreases as liquid vaporizes. Consequently, at the end of drying the smaller load of the dryer would diminish the process economics aside from the fact that hydrodynamics and thus the heat and mass transfer conditions could be heavily impaired. Industrial practice has shown, however, that the fresh material can be continuously added into the fluidized bed in the EVACTHERM® dryer at the rate equivalent to water evaporation (Dürr, 1998). In this way, the drying process is continued for a longer period under optimum conditions until the material hold-up has reached its maximum, when the processor must be discharged.

During the drying process, the material has a constant temperature according to the preset pressure of the system. A gradual increase of the material temperature along with a reduction in the amount of condensate collected indicates the end of drying. At this point, it is recommended that the supply of external energy be cut off and only vacuum applied to remove the residual moisture using the sensible heat of the load. Besides cooling the material, the use of vacuum allows any toxic volatiles to be collected in the condensate.

A distinct feature of the superheated steam drying–granulation process is that larger granules are generated first and smaller granules are produced by further drying and by impact of the rotor. Unlike conventional granulation where either one shell envelops another or several smaller particles consolidate around the nucleation center, the granules from the superheated steam processing are uniform and thus have higher density and mechanical strength (Table 31.6). Because the process of granulation takes place during a drying cycle, the granulate has the final moisture content as required so no finish drying is needed. Moreover, superheated steam drying–granulation provides such a uniform distribution of the residual moisture that downstream ‘‘maturing’’ can be eliminated from the process flow.

Depending on the system configuration and operating parameters, the mixing processor with the rotating mixing pan can also be used for other drying processes such as vacuum drying, superheated steam drying, vacuum

TABLE 31.6 Properties of Granulated Ferrites

Parameter	VHSP	Conventional
Bulk density of raw material, kg/m^3	800	800
Bulk density of granules, kg/m^3	2000	1500
Solid density of granules, kg/m^3	3000–3500	2600
Moisture content of granules, % w.b.	<10	16

Courtesy of EIRICH, Hardheim, Germany.

superheated steam drying, or superheated steam–granulation aside from other operations such as mixing, blending, and homogenizing. The evaporation capacity of the 3 m^3 and 7 m^7 of the mixing processor is about 1000 and 2200 kg of water per hour, respectively. The system appears to be scaled up easily since the design criteria for a 3-m^3 processor can be accurately derived from the experiments with a 0.075-m^3 trial processor (Dürr, 1996).

31.6 DRYING IN ROTATING JET SPOUTED BED

Conventional spouted bed (CSB) designs have some important constraints that limit commercial use of spouted beds compared to fluidized beds (Mathur and Epstein, 1974; Passos et al., 1987). Among these constraints one may cite high-pressure drop prior to onset of spouting, low aeration of the falling bed in the annulus, slow solids turnover, low capacity per unit floor space, and difficulty of scale-up. To overcome some of the limitations of CSBs, numerous modified configurations have been developed (Passos et al., 1987; Devahastin et al., 1996; Mujumdar, 1984, 1998). These modifications are concerned with the chamber geometry, spouting origin, air supply, operational mode, etc. (Devahastin et al., 1996). Not all designs have potential industrial significance. Some of the spouted bed configurations have, however, found an industrial application and are described elsewhere in this book (e.g., spouted bed of inert particles). The others have not been commercialized yet. One of these original modifications of the conventional spouted bed is the rotating jet spouted bed (RJSB) suitable for drying of Geldart type D particles (Geldart, 1973). Here the gas jet causing spouting of the particulate material does not enter the bed in a fixed position but turns around the bed center.

The RJSB dryer is built as a vertical cylindrical chamber with the flat perforated grid (Figure 31.13). Below the grid, a slowly rotating air distributor

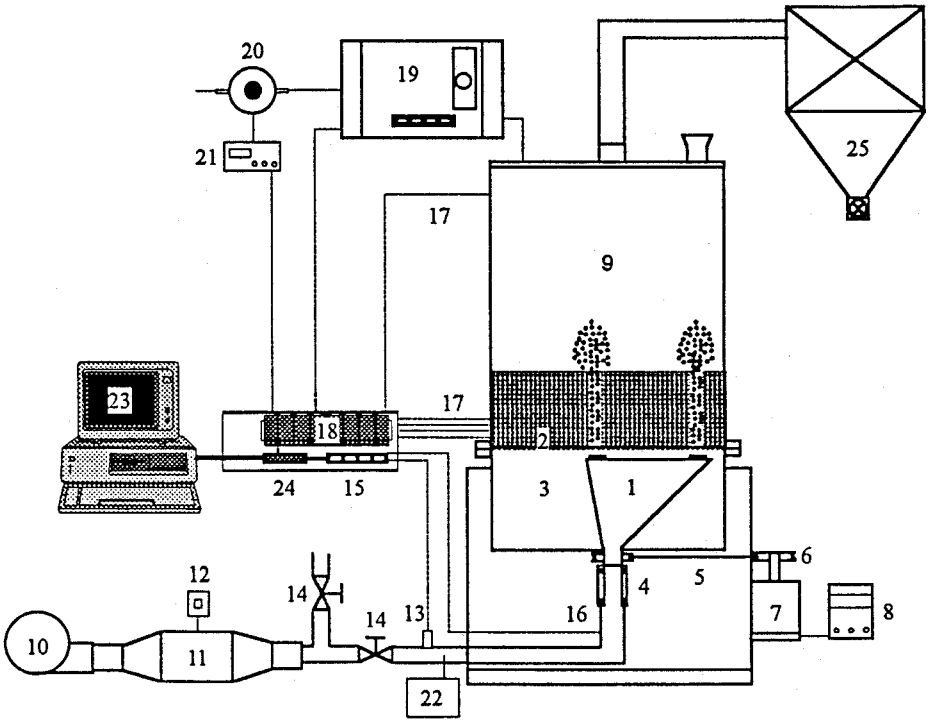

FIGURE 31.13 Experimental rotating jet spouted bed with central and peripheral air jets: 1—air distributor, 2—screen, 3—distributor cover, 4—ball bearings, 5—v-belt, 6—pulley, 7—drive, 8—motor controller, 9—glass vessel, 10—bir blower, 11—electric heater, 12—PID controller, 13—Pitot tube, 14—gate valve, 15—pressure transducers, 16—pressure taps, 17—thermocouples, 18—multiplexer, 19—IR hygrometer, 20—dew-point sensor, 21—dew-point hygrometer, 22—humidity meter, 23—computer, 24—terminal panel, 25—filter. (From Jumah, 1995.)

with one or several radially located spouting air nozzles is located in a small clearance from the grid. The rotating jet spouted bed is formed when the air jet (or jets) moves circumferentially in the annular region between the chamber wall and the central spout. Spouting characteristics of the rotating jet are essentially similar to these in conventional spouted beds. However, sequential relocation of the air jet greatly affects the onset of spouting—the peak pressure drop is lower by about 30% compared to the stationary spouting case. This can be explained by the pulsating action of the rotating gas stream, which

loosens the packed structure and hence facilitates spout evolution (Jumah, 1995). The same phenomenon is observed in pulsed fluid beds with relocated air stream (see Chapter 6) where not only the pressure drop is lowered at the onset of fluidization but also the peak pressure drop does not appear. For higher rotational speeds of the gas jet, the value of air flow rate required to maintain minimum spouting conditions is increased. It is likely caused by the higher-velocity component in the angular direction and hence larger deviation from vertical flow of the jet. As a result, more kinetic energy is required to maintain the spouting state.

As seen from Figure 31.13, the RJSB has the central air jet, which does not relocate as the peripheral one and thus does not provide intermittent drying. Another design for drying material in the falling rate period that is also based on relocation of the spout is the rotating jet annular spouted bed (RJASB) (Devahastin, 1997). The RJASB consists of a single rotating jet in the annular region between the dryer wall and a central tube, which does not allow air and material flow, so an on–off operation is possible over the entire area of the bed annular region (Figure 31.14). A particular portion of the bed is thus spouted only periodically, and in one rotation of the nozzle the bed is spouted once, which allows better control of the drying/tempering time. The RJASB also requires less air flow rate for onset of spouting at a fixed value of distributor rotational speed (since the higher value of jet velocity is achieved at the same air mass flow rate), thus allowing a deeper bed of the material to be processed. The slight reduction in bed capacity due to the centrally located tube estimated as about 20% at the same bed height can be compensated by an 8% increase of the chamber diameter.

One clear advantage of such a ''rotating jet'' configuration is intermittent spouting due to continuous relocation of the gas jet. This periodic spouting, which boils down to intermittent drying due to periodic heat supply, results in energy savings when drying materials in the falling rate period. For such materials, the tempering period without spouting and therefore without heating permits moisture to diffuse from the material core to its surface, which further intensifies evaporation during the spouting period. This particular advantage occurs only if the rotational speed of the air jet is relatively low (in the order of several rpm) as well as if the jet area is only a small fraction of the bed's cross-sectional area. Otherwise, the entire bed would turn into a special type of a pulsed fluid bed as described in Chapter 6.

The other feature of both the RJSB and RJASB is a precise control over the tempering-to-spouting periods ratio, simply by varying the rotational speed of the air nozzle. In conventional spouted beds and spouted beds with a draft

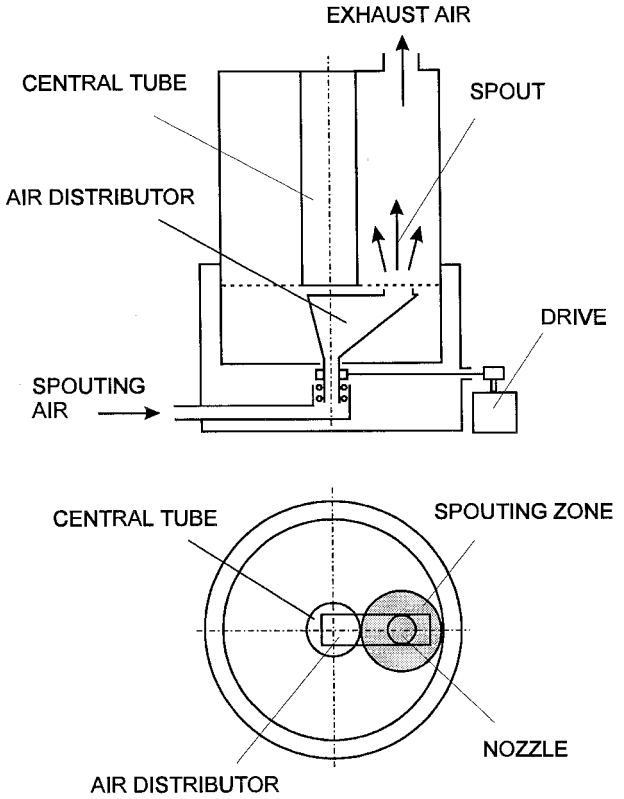

FIGURE 31.14 Schematic diagram of the rotating jet annular spouted bed. (From Devahastin, 1997).

channel, this ratio can be controlled only to a small extent by varying the bed height. Note that it is possible to use multiple spouting nozzles in dryers of larger diameter as well as mechanical agitators to enhance mixing in the RJSB. The shortcoming of the rotating jet configuration is its complex construction because of rotating air distributor and small nozzle-to-grid clearance to be maintained to reduce air bypass.

The interested reader can find more information about the design, hydrodynamics, drying characteristics, and modeling of the rotating jet spouted bed in the literature (Jumah, 1995; Gong et al., 1997; Jumah et al., 1997; Devahastin, 1997; Devahastin et al., 1999).

31.7 DRYING WITH SOL-GEL TRANSFORMATIONS

Because of the noncontact transfer of electromagnetic energy, microwave heating can be advantageous in the technology of high-purity substances. In fact, microwave processing of metalsiloxane sols allowed higher-purity homogeneous products to be obtained than by using traditional methods of heating. Moreover, syneresis of the resulting gels that greatly reduces product quality was practically eliminated (Bessarabov, et al., 1994; Gluhan et al., 1983). In addition, water–alcohol-based multicomponent sols belong to the class of lossy dielectrics (dielectric loss factor in the order of 30 to 50) in contrast to the preferred materials of construction such as quartz glass, fluoroplastics, and most ceramics. It allows design of the microwave apparatus with significant wall thickness without affecting the heating characteristics of the product. Here we present the original design of a microwave rotary processor (Bessarabov et al., 1999) that allows several sequential batch operations to be performed for continuous production of high-purity multicomponent materials.

As reported by Bessarabov et al. (1999), multicomponent sols can be produced by hydrolysis of ultrapure silica and titanium ethers by acidified aqueous solutions of salts (nitrates of potassium, sodium, aluminum, and lead) and boric acid. The hydrolyzates represent complex multicomponent liquid-phase systems containing the products of incomplete saponification of ethoxy groups, dissociation products of salts of alloying components that did not react with the intermediate hydrolysis products of $Si(O\text{-}Et)_4$ and $Ti(O\text{-}Bu)_4$, ethyl alcohol, butyl alcohol, and water. Experiments carried out at temperatures ranging from 30° to 300°C have revealed that after 8 to 10 min of microwave heating, the sol started to boil and then passed into a gellike state. Further moisture evaporation proceeded as a series of vapor blasts of various intensity that dispersed and mixed the gel. When drying is nearly complete, a highly porous structure with practically no resistance to vapor flow is established. At the same time the material temperature starts to increase while the mass of the material tends to stabilize. The material is considered dry when the final moisture content is about 7% to 10% w.b.

Based on the physical phenomena observed during drying, the following stages were identified (see Figure 31.15) (Bessarabov, 1999):

1. Heating-up and evaporation of moisture from the sol of initial moisture content X_0 down to the moisture content X_1 at which gelation of sol starts

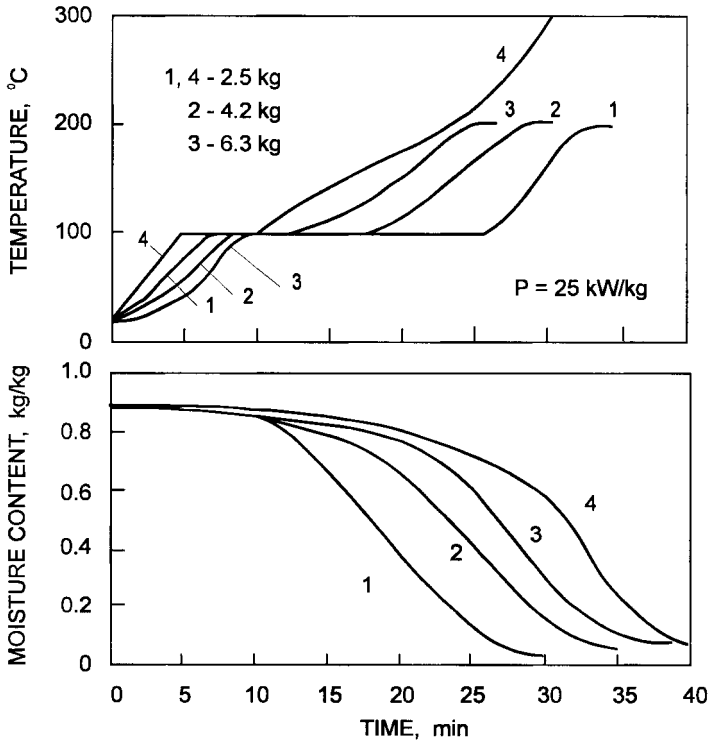

FIGURE 31.15 Drying and temperature curves for selected sols. 1–3: SiO_2, 4: SiO_2-B_2O_3-Na_2O-Al_2O_3. (From Bessarabov et al., 1999.)

2. Gelation of sol with further increase of material temperature to the boiling point and decrease of the material moisture content to X_2 at which the entire volume of sol is transformed into gel of porous structure caused by local eruptions of vaporized moisture
3. Drying of a porous gel structure at constant temperature and constant drying rate—evaporation of free moisture
4. Drying of a porous gel structure at a falling rate period with continuous increase of material temperature (evaporation of structural moisture)

The product in the process of thermal treatment of polycomponent sols transforms from a nonviscous liquid through a high-viscosity liquid to a gel, and

finally to a xerogel. To avoid clinkering, caking, and agglomeration, it is desirable to separate the processes of sols' boiling, gelation, and gel–xerogel drying. This can be done when combining the features of batch and continuous processing in a single apparatus, allowing simultaneous mixing and microwave heating.

The pilot-scale microwave dryer designed by Bessarabov et al. (1999) (Figure 31.16) is a cylindrical microwave resonator (3) equipped with a coaxial quartz drum (5) with four internal spiral inserts (4, 7). The resonator is slightly inclined toward one end; the slope of inclination can be adjusted. The upper end of the inclined chamber is connected to the feeder of initial sol, the system for vapor condensation and discharge (8, 15, 16). The water load (9) prevents unabsorbed microwave energy from being reflected back to the magnetron. The lower end of the chamber is fitted with a waveguide that supplies microwave energy from the generator (2), a variable-speed drive (1) to control and reverse drum rotation, and a Teflon container for dry product (10) screened from the chamber-resonator by a microwave filter. The drum has a sectioned spiral insert attached to the drum wall, which transports the drying material along the drum during its rotation. Each spiral insert has inverse angle of the spiral winding with respect to the preceding one. This makes it possible to run the dryer continuously while performing batch processes in each section of the chamber by simply periodically reversing the rotation of the drum.

The procedure for microwave processing of sols is as follows: a metered amount of sol is fed into the rotating drum with microwave energy set to the required power. Because winding of the first segment of the spiral insert is opposite liquid flow, it hinders transportation of the sol along the first section of the drum so the sol hold-up increases in the course of feeding. After a certain period the sol starts to flow over the spiral insert. When the feeding is over, the sol practically fills the bottom part of the first section of the drum. In this most stretched section, batch microwave drying is performed in the following sequence of processes: sol is heated to the boiling point so the moisture is evaporated practically at a constant rate. Because of progressive moisture removal, viscosity increases, and the sol loses its fluidity. At this moment, rotation of the drum is reversed so the viscous sol is transported to the second section of the drum while the first section is again fed with a new portion of the sol to maintain continuous operation of the dryer. Further evaporation of moisture in the second section of the drum results in such an increase of sol viscosity that the sol starts to adhere to the dryer wall and to the spiral insert. Then it moves inside this section of the drum much more like a thin rotating cylinder of gel. Since the evaporation rate is maintained at the same level but the gel has a higher resistance to vapor flow, the steam generated blasts the

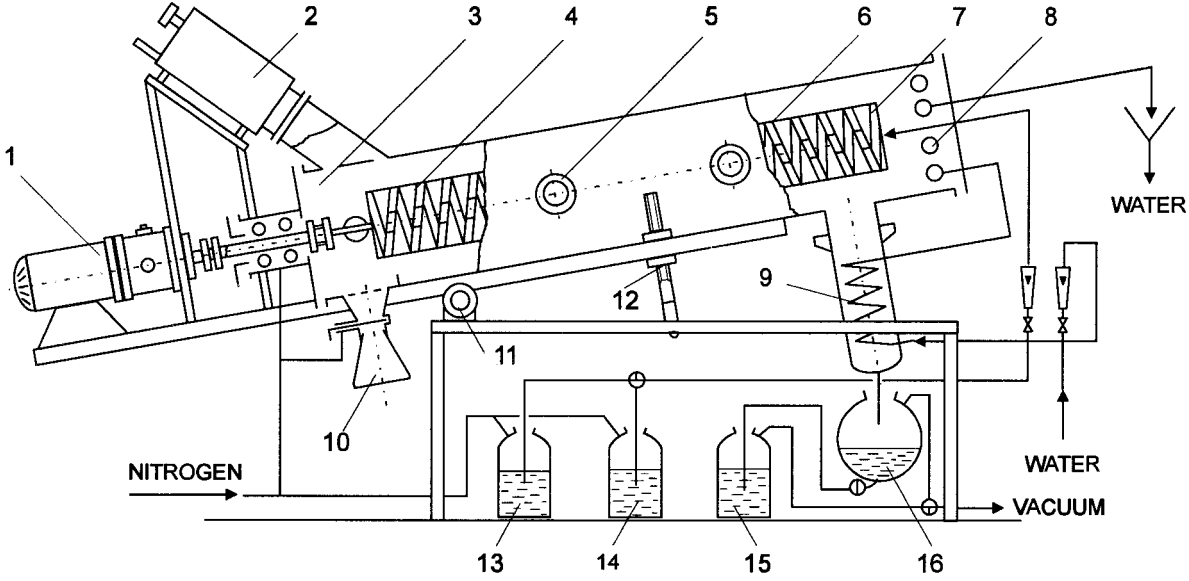

FIGURE 31.16 Schematic of the experimental microwave dryer: 1—motor, 2—MW generator, 3—resonance tube, 4—spiral insert (IV section), 5—viewport, 6—quartz drum, 7—spiral insert (I section), 8—water load, 9—condenser, 10—product tank, 11—swivel, 12—slope adjuster, 13—sol tank, 14—distilled water, 15—condensate tank, 16—condensate discharge. (From Bessarabov et al., 1999.)

gel. Finally, the original solid gel is changed into a bed of still wet but transportable lumps. This completes the second step of processing.

In the third step of processing, rotation of the drum is reversed again so the granular gel is transported by the spiral insert to the fourth section of the drum, where it is dried at a constant temperature and a constant drying rate. Further reversing of the drum rotation transports the essentially loose granules of xerogel to the fourth section of the drum where bound moisture is removed. Because the temperature of the xerogel at the end of the falling rate period may increase to 570 to 650 K, the spiral insert in this section of the drum is made of the quartz ceramics.

The pilot-scale rotary microwave processor (0.08 m in diameter and 1.4 m long) was designed and tested for various power levels up to 2 kW. The maximum evaporation rate was 1.5 kg of water per hour, and the product moisture content was kept within the required limit from 0.12 to 0.15 kg/kg.

Interested readers can find detailed information about the drying kinetics, dielectric properties, and design calculation for this novel rotary microwave processor in the paper by Bessarabov et al. (1999).

31.8 SUPERCRITICAL FLUID TECHNOLOGY TO PRODUCE DRY PARTICLES

Micron, submicron, and ultra-fine particles find increasing applications in pharmaceutical drug delivery. Conventional methods of powder production such as freeze- and spray drying have certain limitations. Freeze-drying produces a broad particle-size distribution requiring downstream milling and sieving operations. Spray drying can produce particles of controlled size but may involve degradation for highly heat-sensitive products as used in the pharmaceutical industry. Supercritical fluid technology offers an efficient but expensive approach to produce high-purity, micron-sized particles of the desired morphological structure in one step.

Several processes utilizing supercritical fluids for materials processing have been reported in the literature although their commercial use is not well documented. Among the well-known processes are rapid expansion of supercritical solutions (RESS) (Phillips and Stella, 1993), the gas antisolvent process (GAS) (Yeo et al., 1993), aerosol solvent extraction system (ASES) (Bleich and Muller, 1996), a precipitation with compressed antisolvent process (PCA) (Brennecke, 1996), and solution-enhanced dispersion by supercritical fluids (SEDS) (Sarup et al., 2000). The first four processes are for products that are soluble in the supercritical fluid or in an organic solvent. Biomolecules such as proteins or nucleic acids cannot be dissolved, and for such processes

the SEDS technique has been shown to work technically, but it results in loss of activity. Sarup et al. (2000) have described the process and presented results for two antibody fragments using isopropanol as a co-solvent in supercritical carbon dioxide. Unfortunately, their results showed a loss of activity due to the presence of the organic solvent. It appears that the choice of temperature and antisolvent is critical in reducing the magnitude of damage during SEDS processing of the antibody fragment. More work is needed before this process can be understood better for such special applications.

Symbols

CHAPTER 4

c	specific heat, J/(kgK)
c_H	humid heat, J/(kgK)
D	diameter, mm
H	height, m
ΔH	latent heat of evporation, J/kg
k	heat utilization factor
m	mass, kg
P	pressure, Pa
Q	heat flow rate, W
R	gas constant, J/(kgK)
t	time, s
T	temperature, °C, K
u	superficial velocity, m/s
v	specific volume, m^3/kg
V	volume, m^3
w	volumetric evaporation rate, $kg/(m^3s)$
W	mass flow rate, kg/s
X	moisture content, %, kg/kg

Greek Letters

β	mass transfer coefficient, m/s
φ	coefficient, kg/m^2
ρ	density, kg/m^3

Subscripts

a	active
A	accumulation
c	cone
d	dynamic
eq	equilibrium
f	final
g	gas
HT	heat transfer
i	initial
in	inlet
mf	minimum fluidization
M	mechanical
p	inert particle
st	static
w	cylinder
0	ambient
1	inlet
2	outlet

Acronyms

QLR	quality loss risk
TRM	three-region model

CHAPTER 5

d_p	particle diameter, m
c	heat capacity, J/(kgK)
D	duct diameter, m
F	force, N
g	acceleration due to gravity, m/s^2
h	heat transfer coefficient, W/(m^{2}K)
H	distance between accelerating ducts, m

k	thermal conductivity, W/(m K)
L	dimensionless distance
ΔP	pressure drop, Pa
t	time, s
T	temperature, K (°C)
u	velocity, m/s
W	mass flow rate, kg/s
x	coordinate, m
X	moisture content (dry basis), kg/kg

Greek Letters

β	volumetric concentration, m^3/m^3
μ	dynamic viscosity, kg/(m s)
ν	kinematic viscosity, m^2/s
ρ	mass density, kg/m^3
ζ	friction factor

Subscripts

cr	critical
g	gas
p	particle (droplet)
s	solid (suspension)
t	terminal
max	maximum
0	initial/flow duct
1	inlet
2	outlet

Superscripts

*	dimensionless parameter

Dimensionless Numbers

$Eu = \Delta P/(u^2\rho)$	Euler number
$Gu = (T\text{-}T_p)/T$	Gukhman number
$Nu = hd_p/k$	Nusselt number
$Pr = c\mu/k$	Prandtl number
$Re = u_0D/\nu$	Reynolds number
$Re_p = u_0d_p/\nu$	Particle Reynolds number

$Re_r = (u \pm u_p)\, d_p/\nu$	Reynolds number (based on relative velocity)
$Re_t = u t_p^d/\nu$	Reynolds number (based on terminal velocity)

CHAPTER 6

d	particle diameter, m
f	frequency of pulsation, 1/s
F	bed cross-sectional area, m^2
g	acceleration due to gravity, m/s^2
H	bed height, m
K	constant, 1/s
K	parameter in Eq. (6.3), Pa
m	mass, kg
N	number of chambers
ΔP	pressure drop, Pa
t	time, s
u	superficial velocity, m/s
X	material moisture content, kg/kg
ε	bed voidage
φ	shape factor
μ	viscosity, kg/(ms)
ρ	density, kg/m^3

Subscripts

b	bulk
bd	bulk (dry)
bw	bulk (wet)
e	equivalent
eq	equilibrium
g	gas
m	material
mf	minimum fluidization
pf	pulsed fluidization
s	solid
st	static
0	reference, initial

Superscripts

d	developed (upper)
i	incipient (lower)

Dimensionless Numbers

$$\mathrm{Ar} = \frac{g d_e^3(\rho_s - \rho_g)}{\mu^2}$$ Archimedes number

$$\mathrm{Re} = \frac{u d_e \rho}{\mu}$$ Reynolds number

CHAPTER 7

d.b.	dry basis
h	heat transfer coefficient, W/(m^{2}k)
ΔH	latent heat of vaporization, kJ/kg
q	heat flux, W/m^2
w_D	drying (evaporation) rate, kg/(m^{2}s)
w.b.	wet basis

Subscripts

s	surface
ss	steam (superheated)
wb	wet bulb

Acronyms

BOD	biological oxygen demand
COD	chemical oxygen demand
SSD	superheated steam drying
TMP	thermo-mechanical pulping
TOC	total organic carbon
VCE	vapor compression-evaporation
VOC	volatile organic compound

CHAPTER 9

A	coefficient, kg/(m^{3}s)
B	coefficient, kg/m^4
C_m	mobilizing orifice discharge coefficient
d_m	diameter (size) of the mobilizer base, m
D	diameter (size) of the mobilizer top, m
D_e	effective diffusion coefficient, m^2/s
E_a	activation energy, J/kmol
g	acceleration due to gravity, m/s^2

F_p	force due to pressure gradient, N
F_y	upward force from momentum balance, N
l	half-thickness of the lamina, m
m	mass of tobacco, kg
n	number of mobilizing orifices
ΔP	pressure drop, Pa
Q_i	volumetric flow rate in each zone of the mobilizer, m^3/s
R	gas constant, J/(kmol K)
t	time, s
T	temperature, K
V	mobilizing flow rate, m^3/s
X	moisture content, kg/kg
X_0	initial moisture content, kg/kg
X_e	equilibrium moisture content, kg/kg
y	upward distance from the base of the mobilizer, m
α	angle,^{0}
ε	bed voidage
ρ	gas density, kg/m^3
ρ_b	bulk density, kg/m^3

CHAPTER 10

A	constant [Eq. (20.6)]
c	specific heat, kJ/(kgK)
d, D	diameter, m
f	frequency, Hz
F	heat transfer area, m^2
G	dryer throughput (wet material), kg/h
h	heat transfer coefficient, $W/(m^2K)$
ΔH	latent heat of vaporization, kJ/kg
I	enthalpy, kJ/kg
k	thermal conductivity, W/(mK)
K	constant [Eq. (20.2)]
L	length, m
m	mass, kg
n	the order of a harmonic frequency
n	number
N	rotational speed, rpm
Q	heat rate, W
RH	relative humidity, %
s	stroke length, m
S	surface area, m^2

t	time
T	temperature, °C
ΔT_e	equivalent temperature difference, °C
u	velocity, m/s
v	sound velocity, m/s
v_H	humid volume, m^3/kg
V	volume, m^3
V	volumetric flow rate, m^3/s
W	mass flow rate, kg/s
X	moisture content, % w.b.
Y	air humidity, kg/kg
Z	constant, [Eq. (20.3)]
β	flooding coefficient
ϕ	heat loss factor
γ	cone angle,^{0}
μ	dynamic viscosity, kg/(ms)
ρ	density, kg/m^3

Subscripts

c	piston (cylinder)
ch	chamber
d	dispersed
f	final (outlet)
g	gas
h	heater
i	initial (inlet)
l	liquid
m	material
M	median
p	particle (droplet)
r	resonance
s	solid
sV	surface-volume
S	spot
t	tube
w	water
$w.b.$	wet bulb
0	ambient
$\mathrm{Nu} = \frac{hd_p\rho_g}{\mu_g}$	Nusselt number

CHAPTER 12

a	sorption capacity, kg/kg
a^*	dimensionless sorption capacity
c	heat capacity at constant pressure, J/(kgK)
C	concentration, kg/kg (kg/m^3)
D	diffusion coefficient, m^2/s
h	particle heat transfer coefficient, W/(m^{2}K)
H	Henry's constant
ΔH	heat of sorption/desorption, J/kg
k	thermal conductivity, J/(kgK)
K	relative sorption capacity
m	mass, kg
n	sorbent renewal rate, 1/batch
R	radius, m
t	time, s
T	temperature, K
u	velocity, m/s
x	distance, m
X	moisture content, kg/kg
α	thermal diffusivity, m^2/s
δ	thermogradient coefficient, 1/K
ε	phase change coefficient
η	reduced drying efficiency

Subscripts

C	corn
c	contact
f	final
i	initial
k	elementary k-layer
0	reference state
r	reference material
s	sorption
S	sorbent
max	maximum

Superscripts

d	delay
m	material

s	sorbent
*	dimensionless

CHAPTER 13

A	amplitude, m
c	specific heat, kJ/(kgK)
C	concentration, kg/m^3
d	diameter, m
d.b.	dry basis
dB	decibel
D	diffusion coefficient, m^2/s
E	enhancement ratio
f	frequency, Hz
g	acceleration due to gravity, m/s^2
I	sound intensity, W/m^2
L	length, m
L	relative level, dB (Figure 13.3)
P	pressure, N/m^2
P	pressure drop, N/m^2
r	radius, m
S	surface area, m^2
t	time, s
T	temperature, ^{0}C, K
u	gas velocity, m/s
v	sound velocity, m/s
w_D	drying rate, kg/(m^{2}s)
W	power, W
x	distance, m
X′	moisture content (wet basis), kg water/kg wet material
α	absorption coefficient, l/s
λ	wavelength, m
ν	viscosity, m^2/s
ρ	density, kg/m^3
ω	angular frequency, rad/s

Subscripts

a	acoustic
cr	critical
e	equivalent
g	gas

s	surface
0	incident

CHAPTER 15

c	heat capacity, kJ/(kgK)
E	energy, W
E_F	energy for fans, W
G	mass flow, kg/s
g	acceleration due to gravity, m/s^2
ΔH	latent heat of vaporization, kJ/kg
n	consecutive number
P	pressure
Q	heat rate, kJ/kmol
Q_o	refrigeration capacity, kW
R	energy consumption ratio
T	temperature, ^{0}C, K
W	mass flow rate, kg/s
Y	absolute humidity, kg water/kg dry air
δY	absolute air humidity difference, kg H_2O/kg dry air

Subscripts

A	air
B	material
c	convective
D	drying
ev	evaporation
g	gas
H	high-temperature side
in	inlet
L	low-temperature side
M	medium-temperature side
R	releasing step
s	solid
S	storing step
0	initial (ambient)
1, 2	consecutive stage

Acronyms

CHP	chemical heat pump
CHPD	chemical heat-pump dryer

CFC	chlorofluorocarbon (freon)
COP	coefficient of performance
HPDE	heat-pump dryer efficiency
PID	proportional-integral-derivative
SMER	specific moisture extraction rate

CHAPTER 18

t	time
TWA	time weighted average

CHAPTER 21

a_w	water activity
a_{wa}	water activity at reference temperature
A	transfer area, m^2
A_r	constant
b	thickness of the dried layer, m
B_r	constant
D_w	diffusivity of water vapor in the dried layer, m^2/s
M	molar mass, kg/mole
M_a	molar mass of the adsorbent, kg/mole
p	partial pressure of water vapor at saturation, Pa
p_c	partial pressure of water vapor in the fluidized bed, Pa
P	operating pressure, Pa
R	gas constant, J/(K mole)
t	time, s
T	temperature, K
X	adsorbent moisture content, kg/kg
α	external heat transfer coefficient, $W/(m^2K)$
β	external mass transfer coefficient, m/s
ΔH_s	latent heat of sublimation, J/kg
ΔH_v	latent heat of vaporization, J/kg
λ	thermal conductivity of the dried layer, W/(mK)

CHAPTER 22

E	electric field strength, V/m
f	frequency, Hz
H	magnetic field strength, A/m
P	electromagnetic power, W
$\tan \delta$	loss tangent

λ	wavelength, m
ε'	dielectric constant
ε''	loss factor
ε_0	permittivity of free space, F/m

Acronyms

MW	microwave
RF	radio frequency

CHAPTER 23

Acronyms

COP	coefficient of performance
RF	radio frequency
SMER	specific moisture extraction rate

CHAPTER 25

P	pressure, Pa
P'	specific microwave power, W/kg dm
T	temperature, ^{0}C
u	superficial velocity, m/s

References

Adamiec J, Kaminski W, Markowski A, Strumillo C. Drying of biotechnological products. In: Mujumdar AS, ed. Handbook of Industrial Drying. 2nd ed. New York: Marcel Dekker, 1991, pp 775–808.

Adamiec J, Kudra T, Strumillo C. Conservation of bio-active materials by dehydration. In: Mujumdar AS, ed. Drying of Solids. Meerut-New Delhi: Sarita Prakashan, 1990, pp 1–16.

Akao T. Applications of pressurized superheated steam to food processing. In: Shimizui S, ed. Chemical Engineering Symposium Series 1. Tokyo, pp 239–240.

Akao T, Furukawa T, Watanabe H. Superheated steam drying for deodorization. In: Proc. 3rd International Drying Symposium, Birmingham, Great Britain, 1982, pp 285–294.

Alikhani Z. Zeolite as particulate medium for contact heating and drying of corn. Ph.D. thesis, McGill University. Montreal, 1990.

Alikhani Z, Raghavan GSV. Simulation of heat and mass transfer in cornzeolite mixtures. Intl. Comm. Heat Mass Transfer 18:791–804, 1991.

Alikhani Z, Raghavan GSV, Mujumdar AS. Adsorption drying of corn in zeolite granules using a rotary drum. Drying Technology 10(3):783–797, 1992.

Alves-Filho O, Strømmen I. Performance and improvements in heat pump dryers. In: Strumillo C, Pakowski Z, eds. Drying '96, Proc. 10th Intl. Drying Symposium (IDS'96), Krakow, Poland, 1996, pp 405–416.

Alves-Filho O, Strømmen I, Aasprong A, Torsveit AK, Boman HC, Hovin W. Heat pump fluidised bed drying for lactic acid suspensions using inert particles and freeze drying. In: Akritidis CB, Marinos-Kouris D, Saravakos GD, eds, Drying '98, Proc. 11th Intl. Drying Symposium (IDS'98), Halkidiki, Greece, 1998, pp 1833–1840.

Alves-Filho O, Thorbergsen E, Strømmen I. A component model for simulation of multiple fluidized bed heat pump dryers. In: Akritidis CB, Marinor-Kouris D, Saravakos GD, eds. Drying '98, Proc. 11th Intl. Drying Symposium (IDS'98), Halkidiki, Greece, 1998, pp 94–101.

Amazouz M, Benali M. Thermal processing of meat rendering sludge in a jet spouted bed of inert particles: Effect of additives. Coumans WJ, Kerkhof PJAM, eds. Proc. 12th Intl. Drying Symposium (IDS 2000). Noordwijkerhout, The Netherlands. Paper 418, 2000.

Amazouz M, Benali M, Kudra T. Drying of value added liquid wastes in a spouted bed of inert particles. CHISA'2000. Praha, Czech Republic, 2000.

Amelot MP. Spray drying with plasma-heated water vapor. M.Sc. thesis. McGill University. Montreal, 1983.

Amelot MP, Gauvin WH. Spray drying with plasma-heated water vapor. In: Mujumdar AS, ed. Drying '86. Washington: Hemisphere Publishing Corp. 1986, pp 285–290.

Anderson JD Jr. Modern compressible flow. New York: McGraw-Hill, 1982. Anon. Technical information. Institute of Chemical Engineering, Warsaw Technical University. Warsaw, 1980 (in Polish).

Anon. The benefits and advantages of a TRSA spouting bed spray dryer. Report by Technical & Research Services Australia PTY, Ltd., Australia, 1986.

Anon. Drying and thermal treatment of wet materials. Minsk, Belarus: Nauka i Tekhnika, 1990a (in Russian).

Anon. Drying and thermal processing of wet materials. Minsk, Belarus: Nauka i Tekhnika, 1990b (in Russian).

Anon. Microwave vacuum drying of particulate foodstuffs. In: Fraunhofer Institute for Food Process Engineering and Packaging. ILV. Annual Report, Munchen, Germany, 1990c, pp 151–153 (in German).

Anon. Filtration and drying systems. Tech Update. Charlotte, NC: Rosenmund Inc., 1990d, 2(3):1–2.

Anon. Nutsch-Dryer TNT. Technical information. 2.0B. Florence: Krauss-Maffei Corp., 1991.

Anon. Drying equipment and installations: Catalogue. Moscow: CINTIHIMNEFTEMASH, 1992a (in Russian).

Anon. The microGas dryer and the food industry. Bellevue: Energy International Inc., 1992b.

Anon. Technical brochure. El Cajon: KETEMA Process Equipment, 1992c.

Anon. Paper sludge—from a disposal problem into a valuable product. DTI's Environmental Management Options Scheme. Project Information Brochure No 3, 1994a.

Anon. Crux vacuum drying system—technical information. Micron Powder Systems-Hosokawa Micron Group, 1994b.
Anon. Technical information. Bellevue: Energy International Inc., 1994c.
Anon. Crux Vacuum Drying System. Bulletin Cl. Orient Chemical Ind. Ltd. Hosokawa Micron Group, 1995a.
Anon. Gas-fired convective-microwave industrial dryer. Tech Profile. Chicago: Gas Research Institute, 1995b.
Anon. Technical information. Surrey, UK: Toshiba Electronics UK Ltd. 1995c.
Anon. Radio frequency dryer 50 Ω technology for paper converting industry. Technical information. Vaulx-en-Velin, France: SAIREM, 1997.
Anon. RF 50 Ω technology applied to the wood industry. Vaulx-en-Velin, France: SAIREM, 1998.
Anon. Technical information. Crescent Valley, BC: HeatWave Drying Systems Ltd, 1999.
Anon. Filtermat spray drying system. Technical information. Fond du Lac, WI: Niro Filtermat, 2000a.
Anon. Technical information. Bietigheim-Bissingen, Germany: Heinkel AG, 2000b.
Anthony, D. Evaporate and crystallize waste brines. Chem Eng 96:138–144, 1989.
Bal S, Musialski A, Swierczek R. Coal gasification in a laboratory plasmo-chemical spouted bed reactor. Koks-Smola-Gas 5:123–128, 1971 (in Polish).
Barre L, Masini M. Drying residues at ambient temperature with the DRY-REX dryer. 50th Canadian Chemical Engineering Conference, Montreal, 2000.
Barrett N, Fane A. Drying of liquid materials in a spouted bed. In: Mujumdar AS, Roques M, eds. Drying '89. New York: Hemisphere Publishing Corp. 1989.
Bartolome LG, Hoff JE, Purdy KR. Effect of resonant acoustic vibrations on drying rates of potato cylinders. Food Technology 23:47–50, 1969.
Belik L. Drying of granular materials by fluidization. Chemie-Ing.-Technik 23(4):253–257, 1960 (in German).
Bellows RJ, King CJ. Freeze-drying of aqueous solutions: Maximum allowable operating temperature. Cryobiology 9:559–561, 1972.
Benstead R. Steam compression drying. In: Proc. 3rd Intl. Drying Symposium, Birmingham, Great Britain, 1982, pp 274–284.
Bernstein S, Tridball R, Groten B. microGas—a combined microwave and convection dryer for industrial processes. Powder and Bulk Solids Conference and Exhibition, Chicago, 1993.
Besemfelder ER. German Patent No. 261,240, 1910.
Bessarabov A, Shimichev V, Menshutina N. Microwave drying of multicomponent sols. Drying Technology 17(3):379–394, 1999.
Bessarabov AM, Lisenko AU, Ivanov MY, Diakonov SS. Studies on heating stages in technology of production of barium, neodymium and samarium titanates. Khimicheskaya Promyshlennost 2:29–32, 1994 (in Russian).
Bezzubov AD, Garlinskaya EI, Fridman VM. Ultrasound and Its Application in Food Industry Moscow: Pishchevaya Promyshlennost, 1996. (in Russian).

Billet R. Evaporation Technology: Principles, Applications, Economics. VCH Verlagsgesellschaft, 1989.

Blacha-Jurkiewicz J, Gawrzynski Z, Glaser R. Drying of granular material in pulsofluidized bed. In: Mujumdar AS, Ed. Drying '87. Washington: Hemisphere Publishing Corp., 1987, pp 109–114.

Blasco R, Diaz G, Reyes A. Pneumatic suspension drying. In: Strumillo C, Pakowski Z, eds. Drying '96, Proc. 10th Intl. Drying Symposium (IDS'96), Krakow, Poland, 1996, pp 427–434.

Bleich J, Muller BW. Production of drug loaded micro-particles by the use of supercritical gases with the aerosol solvent extraction system (ASES) process. J. Microencapsulation 13(2):131–139, 1996.

Bond J-F. Drying paper by impinging jets of superheated steam: Drying rates and thermodynamic cycles. Ph.D. thesis, McGill University, Montreal, 1991.

Borisov Yu Ya, Ginin VN. An acoustic drum dryer. Russian Patent No. 184, 651, 1967.

Borisov Yu Ya, Gynkina NM. On acoustic drying in a standing sound wave. Soviet Physics-Acoustics 8(1):129–131, 1962.

Borisov Yu Ya, Gynkina NM. Experiments on acoustic drying. Ultrazvukovaiya Tekhnika 5(3):38, 1967 (in Russian).

Borisov Yu Ya, Gynkina NM. Acoustic drying. In: Rosenberg LD, ed. Physical Principles of Ultrasonic Technology. Vol. 2. New York: Plenum Press, 1973, pp 381–473.

Borisov Yu Ya, Statnikov Yu G. Flow streams generated in an acoustic standing waves. Akust. Zhurnal 11(1):35–38, 1965 (in Russian).

Bosisio RG, Chan Tang TW, Lamontagne PB. Microwave plasma process for gelatin coating on polyester and cellulose triacetate film bases. J. Applied Polymer Sci. 25:711–716, 1980.

Bosisio RG, Weissfloch CF, Wertheimer MR. The large volume microwave plasma generator (LMP™): A new tool for research and industrial processing. J. Microwave Power 7(4):325–346, 1972.

Bosisio RG, Wertheimer MR, Weissfloch CF. Generation of large volume microwave plasmas. Journal of Physics, E: Scientific Instruments 6:628–630, 1993.

Bosse D, Valentin P. The thermal dehydration of pulp in a large scale steam dryer. In: Proc. 6th Intl. Drying Symposium (IDS'88), Versailles, France, 1988, pp 337–343.

Bott R. Hi-Bar® filtration: The continuous pressure and steam pressure filtration. Bokela: Karlsruhe, Germany, 2000.

Boucher RMG. Drying by airborne ultrasonics. Ultrasonic News. Second Quarter: 8–16, 1959.

Bramlette TT, Keller JO. Acoustically enhanced heat exchange and drying apparatus. U.S. Patent No. 4,805,318, 1989.

Brandreth DA, Johnson RE Jr. Displacement drying. In: Mujumdar AS, ed. Drying'80. Vol. 1. Washington: Hemisphere Publishing Corp. 1980, pp 304–307.

Brennecke JF. New applications of supercritical fluids. Chemistry and Industry 12: 831–834, 1996.

Brun E, Boucher RMG. Research on the acoustic air-jet generator. J. Acoustical Society of America 29:573–583, 1957.

Buchkowski A, Kitchen J. Pulse combustion flash dryer. Technical Report. Hastings, Canada: Novadyne Ltd, 1995.

Buchkowski AG. The development of a pulse combustion flash dryer. Proc. Combustion '96, Ottawa, Canada, 1996.

Buchkowski AG. Pulse combustion dryer development for drying wood waste. EXFOR '99, Montreal, 1999.

Buchkowski AG, Kitchen JA. Drying wood waste with a pulse combustion drying. Proc. First Biomass Conf. of the Americas. Vol. 1. Burlington, 1993, pp 730–735.

Buchkowski AG, Kitchen JA. Drying and burning wood waste using pulse combustion. The Second Biomass Conference of the Americas, Portland, 1995.

Burgess BW, Chapman SM, Seto W. The Papridryer process, Part I—The basic concept and laboratory results. Pulp and Paper Magazine Canada 73:64–73, 1972.

Burgess BW, Seto W, Koller E, Pye IT. The Papridryer process, Part II— Mill trades. Pulp and Paper Magazine Canada 73:73–81, 1972.

Cao CW, Liu XD. Experimental study on impinging stream drying of particulate materials. In: Coumans WJ, Kerkhof PJAM, eds. Proc. 12th Intl. Drying Symposium (IDS'2000). Noordwijkerhout, The Netherlands. Paper No 76, 2000.

Carlson RA, Farkas DF, Curtis RM. Effect of sonic energy on the air drying of apple and sweet potato cubes. J Food Sci 27:793–794, 1972.

Carrington CG, Bannister P, Bansal B, Sun Z. Heat pump dehumidification of timber: Process improvements. Proc. Conf. Institution of Professional Engineers, Vol. 2, Part 1, Dunedin, New Zealand, 1996a, pp 73–77.

Carrington CG, Barneveld NJ, Bannister P. Development of the ECNZ electric heat pump dehumidifier drier pilot plant. Proc. Conf. Institution of Professional Engineers, Vol. 2, Part 1, Dunedin, New Zealand, 1996b, pp 68–72.

Chandrasekaran SK, King CJ. Retention of volatile flavor components during drying of fruit juices. Chem Eng Prog Symp Ser 67(108):122–130, 1971.

Chandrasekaran SK, King CJ. Volatiles retention during drying of food liquids. AIChE J. 18(3):520–526, 1972a.

Chandrasekaran SK, King CJ. Multicomponent diffusion and vapor-liquid equilibria of dilute organic components in aqueous sugar solutions. AIChE J. 18(3):513–520, 1972b.

Chou SK, Hawlader MNA, Ho JC, Chua KJ. On the study of a two-stage heat pump cycle for drying of agricultural products. Proc. ASEAN Seminar and Workshop on Drying Technology. Phitsanulok, Thailand, Paper H:1–4, 1998.

Chua, KJ, Chou SK, Hawlader MNA, Ho JC. A two-stage heat pump dryer for better heat recovery and product quality. J. Institute of Engineers of Singapore 38(6): 8–14, 1998.

Chua KJ, Mujumdar AS, Chou SK, Hawlader MNA, Ho JC. Heat pump drying of banana, guava and potato pieces: Effect of cyclical variations of air temperature

on convective drying kinetics and color change. Drying Technology 18(5):907–936, 2000.

Ciborowski J, Kopec J. Method of drying flat materials with small thickness and apparatus for drying such materials. Polish Patent No. 126,843, 1979.

Clark TD. The current status of radio frequency post-baking drying technology. 72th Annual Technical Conference of the Biscuit and Cracker Manufacturers' Association, Forth Worth, Texas, 1997.

Crotogino RH, Allenger V. Mathematical model of the Papridryer process. Trans. Techn. Section CPPA 5(4):TR84–91, 1979.

Csukas B, Pataki K, Ormos Z. Investigation of drying on the inert bodies in fluidized bed. Proc. 5th Heat and Mass Transfer All Union Conference. Minsk, Belarus, Vol. 6, 1976, pp 178–187.

Cui WK, Mujumdar AS. A novel steam jet and double-effect evaporation dryer; Part I—Mathematical model. In: Mujumdar AS, ed. Drying '84. Washington: Hemisphere Publishing Co., 1984, pp 468–473.

Cui WK, Mujumdar AS, Douglas WJM. Superheated steam drying of paper—effects on physical strength properties. In: Mujumdar AS, ed. Drying '86 Vol. II, Washington: Hemisphere Publishing Co., 1986, pp 575–579.

David M. Exploratory study of effect of superheated steam drying on properties of paper. M.Eng. thesis, McGill University, Montreal, 1987.

Dencs B, Ormos Z. Recovery of solid content from ferment liquor concentrates in fluidized bed spray granulator. Proc. V Conference on Applied Chemical Unit Operations and Processes, Balatonfired, Hungary, 1989.

Dengying L, Xiulan H, Zuyi, L, Qun M, Xiaoming C. Experimental investigation on the flow and drying characteristics of two stage semicircular impinging stream dryer. Proc Asian-Australian Drying Conference, Bali, Indonesia, 1999, pp 652–659.

Devahastin S. Flow and drying characteristics of a novel rotation jet annular spouted bed. M.Sc. thesis, McGill University, Montreal, 1997.

Devahastin S. Mujumdar's Practical Guide to Industrial Drying. Montreal: Exergex Corp., 2000.

Devahastin S, Mujumdar AS, Raghavan GSV. Spouted beds research at McGill University. Proc. Intl. Conf. Food Industry Technology and Energy Applications, Bangkok, 1996, pp 22–29.

Devahastin S, Mujumdar AS, Raghavan GSV. Hydrodynamic characteristics of a rotating jet annular spouted bed. Powder Technology 103:169–174, 1999.

Devine T. Displacement drying with fluorocarbon solvents: a status report. In: Mujumdar AS, ed. Drying '80. Vol. 2. Washington: Hemisphere Publishing Corp., 1980.

Djurkov TG. Modeling of bed pressure drops in rotation-pulsed fluidized bed dryer. In: Akritidis CB, Marinos-Kouris D, Saravacos GD, eds. Proc. 11th Intl. Drying Symposium (IDS'98), Halkidiki, Greece, 1998, pp 160–167.

Dmitriev VM, Rudobashta SP, Kormiltsin GS, Tarova LS. Inert carrier for drying of suspensions and pastes. Russian Patent No. 1,760,834, 1989.

Donsi, G, Ferrari G, Matteo, PDi. Atmospheric and vacuum freeze-drying kinetics of shrimps. Proc. 12th Intl. Drying Symposium (IDS '2000), Amsterdam The Netherlands, Paper 279, 2000.

Dostie M, Navarri P. Preliminary study on drying rate effects in radio frequency drying. In: Rudolph V, Keey RB eds. Drying '94, Proc. 9th. Intl. Drying Symposium (IDS'94), Gold Coast, Australia, 1994, pp 607–614.

Douglas WJM. Drying paper in superheated steam. Drying Technology 12(6):1341–1355, 1994.

Droue MG. Plasma Technology: Review of the State-of-the Art and Its Potential in Canada. Canadian Electrical Association. Report No 126U322, 1984.

Durance T. Vacuum microwave drying for functional and medicinal foods. Seminar on Preservation Technologies for Food, Feed and Fibre, Winnipeg, Canada, 1999.

Durance T, Wang L. Canadian Inst. Food Science & Technology Annual Conference, Kelowna, Canada, 1999.

Dürr H. Direct drying of pasty media, sludge, filter cake, etc. Eirich Information No 1106-1-e. Hardheim, Germany: Machinenfabrik Gustav Eirich, 1996.

Dürr H. Production of ferrite granules according to the vacuum hot steam process (VHSP). J. Phys. IV France 7:C1-57–C1-58, 1997.

Dürr H. Economic drying and gentle processing of filter cake and sludges with superheated vacuum steam. Hardheim, Germany: Machinenfabrik Gustav Eirich, 1998.

Elenkov VR, Diurkov TG. Rotating pulsed fluidized bed dryer for high moisture content bioproducts. In: Mujumdar AS, ed. Drying '92. Amsterdam: Elsevier Science Publishers, 1992, pp 1636–1641.

Elenkov VR, Djurkov TG, Kondov PS. Fluidized bed device. Bulgarian Patent No. 47,977, 1989.

Ellwood EL Gottstein JW, Kauman WG, Wright GW. Vapour drying: A summary of research studies. Australian Forestry 13(1):4–16, 1953.

Elperin IT, Meltser VL. Apparatus for thermal treatment of dispersed materials. Russian Patent No. 596,792, 1978.

Elperin IT, Enyakin YuP, Meltser VL. Experimental investigation of hydrodynamics of impinging gas-solid particles streams. In: Luikov AV, Smolsky BM, eds. Heat and Mass Transfer. Minsk, Belarus, 1968, pp. 454–468 (in Russian).

Elperin IT, Meltser VL, Pavlovskij DL, Enyakin YuP. Transfer Phenomena in Impinging Streams of Gaseous Suspensions. Minsk, Belarus: Nauka i Tekhnika, 1972 (in Russian).

Ensminger DE. Acoustic dewatering. pp 321–334. In: Muralidhara HS, ed. Advances in Solid-Liquid Separation. Columbus, OH: Battelle Press, 1986, pp 321–334.

Ensminger DE. Ultrasonics: Fundamentals, Technology, Applications. New York: Marcel Dekker, 1988.

Erdesz K. Bibliography of literature on fundamentals and applications of vibration in particle processing. In: Mujumdar AS, ed. Drying of Solids. Meerut, New Delhi: Sarita Prakashan 1990, pp 326–338.

Erdesz K, Ormos Z. Drying of paste-like materials in vibro-fluidized bed of inert pack-

ing. In: Mujumdar AS, ed. Drying '86. Washington: Hemisphere Publishing Corp., 1986, pp 177–182.

Faber EF, Heydenrych MD, Seppa RUI, Hicks RE. A techno-economic comparison of air and steam drying. In: Mujumdar AS, ed. Drying 86, Vol. II. Washington: Hemisphere Publishing Corp. 1986, pp 588–594.

Fagernas L, Wilen C. 1988. Steam drying for peat and their organic condensates. Proc. 8th Intl. Peat Congress, Leningrad, 1988, pp 14–20.

Fairbanks HV. Acoustic drying of ultrafine coal. Mining Eng. 22(12):49–50, 1970.

Fairbanks HV, and Chem WI. Influence of ultrasonics upon liquid flow through porous media. Ultrasonics 7(3):195–196, 1969.

Feather LE. Drying and oil impregnation of power transformer insulation. Proc. 6th Electrical Insulation Conf. New York, Paper 32C3-8, 1965, pp 65–69.

Fedorovich NV, Chizhik KG, Syskova MG. Promising use of the combined methods of drying of dispersed materials. CHISA'90, Praha, Czechoslovakia, Paper 998, 1990.

Finzer JRD, Kieckbusch TG. Performance of an experimental vibro-spouted bed dryer. In: Mujumdar AS, '92 ed. Drying Amsterdam: Elsevier Science Publ. 1992, pp 762–772.

Flick D, Lenoir P, Gibert H. Drying of liquids on inert particles circulating in a cyclone device. IDS'90, Praha, Czechoslovakia, 1990.

Foster R. Innovation—The Attacker's Advantage. New York: Summit Books, 1986.

Fridman VM. Ultrasonic Chemical Equipment. Moscow: Mashinostroyennie, 1967 (in Russian).

Furutera M, Origane T, Sawada T, Kunugi Y, Kashiwagi T, Takei T, Aizawa M, Mori H. Advanced absorption heat pump cycles. Proc Intl. Absorption Heat Pump Conf. Montreal, 1996, pp 109–119.

Gauvin WH. A novel approach to spray drying using plasmas of water vapor. Can J Chem Eng 59:697–704, 1981.

Gawrzynski Z. Apparatus for generation of a pulsed fluid bed swirling inside a chamber. Polish Patent No. 150,412, 1987.

Gawrzynski Z, Glaser R. Drying in a pulsed-fluid bed with relocated gas stream. Drying Technology—special issue on progress in drying technologies, Mujumdar AS, Kudra T, eds. 14(5):1121–1172, 1996.

Gawrzynski Z, Glaser R, Kudra T. Drying of powdery materials in a pulsed fluid bed dryer. Drying Technology 17(7&8):1523–1532, 1999.

Gawrzynski Z, Glaser R, Zgorzalewicz J. Drying of granular material in pulsofluidized bed. Hungarian Journal of Industrial Chemistry 17: 245–255, 1989.

Gawrzynski Z, Glaser R, Stanislawski J, Poirier M, Kudra T. Drying of P&P sludge in a pulsed fluid bed dryer. Drying Technology (in press).

Geeraert B. Air drying by heat pumps with special reference to timber drying Heat Pumps and Their Contribution to Energy Conservation. NATO Advanced Study Institute, Series E: Applied Sciences 15:219–246, 1975.

Geldart D. 1973. Types of gas fluidization. Powder Technology 7:285–292, 1973.

Ghate SR, Chinnan MS. Pecan drying with silica gel. Energy in Agriculture 2:11–20, 1983.

Glaser R. Possibilities for drying of sliced vegetables in a pulsed fluid bed. In: Proc. VII Drying Symposium, Lodz, Poland 1991, pp 147–154 (in Polish).

Glaser R, Gawrzynski Z. Drying of sliced vegetables in the pulsed fluid bed. Scientific papers of Wroclaw Academy of Economics. Volume: Technology 528:71–87, 1990 (in Polish).

Gluhan RI, Shimichev VS, Bessarabov AM, Ryabenko EA, Shalumov, BZ. Modelling of MW treatment of sol systems. Proc. Scientific-Technical Conf. on Application of Ultra High Frequency Energy in Technological Processes of National Economy, Saratov 1983 (in Russian).

Goetz V, Elie F, Spinner B. The structure and performance of single effect solid-gas chemical heat pumps. Heat Recovery Systems & CHP 13(1):79–96, 1991.

Goldberger WM, Baroch CJ. Method of coating solids particles. U.S. Patent No. 3,247,014, 1963.

Gong ZX, Devahastin S, Mujumdar AS. A two-dimensional finite element model for wheat drying in a novel rotating jet spouted bed. Drying Technology 15(3):575–592, 1997.

Gray RR. Pulse combustion drying apparatus for particulate materials. U.S. Patent No. 4,695,248, 1987.

Grbavcic ZB, Arsenijevic ZL, Zdanski FK. Drying of suspensions in fluidised bed of inert particles. In: Akritidis CB, Marinos-Kouris D, Saravakos GD, eds. Drying '98. Proc. 11th Intl. Drying Symposium (IDS'98), Halkidiki, Greece, 1998, pp 2090–2097.

Greguss P. Drying by airborne ultrasonics. Ultrasonic News 5:7–11, 1961.

Greguss P. The mechanism and possible applications of drying by ultrasonic irradiation. Ultrasonics 1:83–86, 1963.

Guy C, Benali M, Ostigny E. Free radical oxidation process and installation for treating liquid effluents contaminated by organic substances. U.S. Patent No. 5,641,412, 1997.

Guyon, J. Example of the application of the heat pump incorporated in the malt drying process. PAC Industrie Electricité de France Publication 14:1–15, 1980.

Hamdi H, Jurewicz J. Plasma spouted bed reactor for treatment of solid waste. Electrochemical Society Proc. Vol. 97–39, High Temperature Chemistry IX, 1997, pp 324–331.

Hanni PF, Farkas DF, Brown GE. Design and operating parameters for a continuous centrifugal fluidized bed dryer (CFB). J Food Science 41:1172–1176, 1976.

Hayashi K, Nakamura K, Kanagawa Y, Yasujima M. Improvement of dryability and its distribution in square timber by local steam explosion. Proc. 4th IUFRO Intl. Wood Drying Conference, Rotorua, New Zealand, 1994, pp 359–369.

Heindl A. Microwave assisted vacuum convection drying. Ph.D. thesis, Technical University of Munchen, Munchen, Germany 1993 (in German).

Heindl A, Holley W, Rehmann D. Microwave vacuum convection drying of foodstuffs.

Intl. J Food Technology, Marketing, Packaging and Analysis 44(6):320–327, 1993 (in German).
Hirose Y, Hazama H. A suggested system for making fuel from sewage sludge. Kagaku-Kogaku Ronbunshyu 9:583–586, 1983.
Hosseinalipour SM, Mujumdar AS. A model for superheated steam drying of particles in an impinging stream dryer. In Turner I, Mujumdar AS, eds. Mathematical Modeling and Numerical Techniques in Drying Technology. New York: Marcel Dekker, 1996, pp 537–574.
Hosseinalipour SM. Transport processes in laminar and turbulent opposing jet contactors. Ph.D. thesis, McGill University. Montreal, 1996.
Houpert JM. Artificial Drying of Timber by Dehumidification. Bordeaux: Comité Francais d'Electrothermie, 1978.
Howard WG, Guile BR. (eds.). Profiting from Innovation. New York: Free Press, 1992.
Hudson MS. Drying lumber by the vapor process. Proc. Amer. Wood Pres. Ass. 46: 209–243, 1950.
Hudson MS, Spartanburg SC. Treating wood and wood products. U.S. Patent No. 2,273,039, 1942.
Hudson MS, Spartanburg SC. Apparatus and method for drying wood. U.S. Patent No. 2,435,218, 1948.
Hulkkonen S. Technical information. Vantaa, Finland: IVO Technology Center, 1997.
Hulkkonen S, Parvio E, Raiko M. An advanced fuel drying technology for fluidized bed boilers. In: Heinschel KJ, ed. Proc. 13th Intl. Conf. Fluidized Bed Combustion. ASME. Book No. H0937A-1995, 1995, pp 391–403.
Huxsoll CC, Hall CW. Effects of sonic irradiation on drying rates of wheat and shelled corn. Trans. ASAE 13(1):21–24, 1970.
Iwotech Limited. Technical Bulletins on Moldrup Process. Brande, Denmark: Iwotech Limited, 1993.
Jahkola A, Isonierni M, Wilen C. Improving performance and economy of heating power plants by steam-fluidized bed drying of fuels. Symposium on Low-Grade Fuels, Helsinki, Finland, 1989.
Jensen AS. Pressurized drying in a fluid bed with steam. In: Mujumdar AS, ed. Drying '92, Part B. Amsterdam: Elsevier Science Publishers, 1992, pp 1593–1601.
Jezowska A. Studies on hydrodynamics of spouted bed with cyclically relocated pulsed air stream. Scientific Papers of Wroclaw Academy of Economics. Volume: Technology. 605:99–107, 1991 (in Polish).
Jezowska A. Kinetics of drying in a cyclically shifted spouted bed. Drying Technology—special issue on spouted beds. Kudra T, Raghavan GSV, eds. 11(2):319–337, 1993.
Jonassen O, Kramer K, Strømmen I, Vagle E. Nonadiabatic two-stage counter-current fluidized bed dryer with heat pump. In: Rudolph V, Keey RB, eds. Drying '94. Proc. 9th Intl. Drying Symposium (IDS'94), Gold Coast, Australia, 1994, pp 511–517.
Jones PL. Heat and mass transfer in a radio-frequency dryer. Ph.D. thesis, Loughborough University of Technology, Loughborough, Great Britain, 1981.

Juai XL, Liu DY, Li CZ, Meng Q. The investigation of combined impinging stream dryer of vertical and sloped semi-circle. Proc. 12th Intl. Drying Symposium (IDS'2000). Coumans WJ, Kerkhof PJAM, eds. Noordwijkerhout, The Netherlands, Paper No 104, 2000.

Jumah RY. Flow and drying characteristics of a rotating jet spouted bed. Ph.D. thesis, McGill University, Montreal, 1995.

Jumah RY, Mujumdar AS, Raghavan GSV. A mathematical model for constant and intermittent batch drying of grains in a novel rotating jet spouted bed. In: Turner I, Mujumdar AS, eds. Mathematical Modeling and Numerical Techniques in Drying Technology. New York: Marcel Dekker, 1997, pp 337–380.

Jurewicz J, Proulx P, Bulos MJ. The plasma spouted bed reactor. Proc. ISPC-7, Eindhoven, The Netherlands, 1989.

Kalwar MI, Raghavan VGS, Mujumdar AS. Bibliography on spouted bed technology. In: Mujumdar AS, ed. Drying of Solids. Meerut, New Delhi: Sarita Prakashan, 1990, pp 343–352.

Kardashev GA. Physical Methods of Process Intensification in Chemical Technologies. Moscow: Khimiya, 1990 (in Russian).

Kardashev GA, Mikhailov PE, Yurchenko, YB. Teoreticheskie Osnovy Khimicheskoi Tekhnologii 4(4):633–636 1972 (in Russian).

Kardum JP, Sander A, Skansi D. Comparison of convective, vacuum and microwave drying of chlorpropamide. Drying Technology (in press).

Keller JO, German RS, and Ozer RW. Fundamentals of enhanced scalar transport in strongly oscillating and/or resonant flow fields as created by pulse combustion. In: Mujumdar AS, ed. Drying '92. Amsterdam: Elsevier Science Publishers, 1992, pp 161–180.

Kentfield JAC. Pulse combustors. In: Kentfield JAC, ed. Nonsteady, One-Dimensional, Internal, Compressible Flows. New York: Oxford Univ. Press, 1993, pp 191–235.

King CJ, Clark JP. System for freeze-drying. U.S. Patent No. 3,453,741, 1969.

Kitchen JA. Pulse combustion apparatus. U.S. Patent No. 4,697,358, 1987.

Kitron A, Buchman R, Luzatto K, Tamir A. Drying and mixing of solids and particles' RDT in four-impinging-streams and multistage two-impinging-streams reactors. Ind Eng Chem Res 26:2654–2641, 1987.

Kobayashi Y, Miura I, Kawai Y. High performance drying using combination of HF and hot air under atmospheric pressure. Proc. 6th IUFRO Intl. Wood Drying Conf., Stellenbosch, South Africa, 1999, pp 18–21.

Kovalev VV, Utkov ZA, Gandzyuk IB, Band MI Tkatch AP, Litvinyuk II, Magalnik FM. Apparatus for drying pasty deposit from waste water. Russian Patent No. 1,495,305, 1989.

Kreibaum J. Plasma spouted bed calcination of lac dore vanadium ore concentrate. M.Sc. thesis, McGill University, Montreal, 1986.

Kudra T, Strumillo C, eds. Thermal Processing of Bio-Materials. Amsterdam: Gordon and Breach Science Publishers, 1998.

Kudra T. Drying Technology—special issue on dielectric drying. 8(5):907–1205, 1990.

Kudra T. Natural gas—fuel of choice in industrial drying. In: Akritidis CB, Marinos-Kouris D, Saravakos GD, eds. Drying '98. Proc. 11th Intl. Drying Symposium (IDS'98), Halkidiki, Greece, 1998a, pp 488–495.

Kudra T. Sound-assisted drying. In: Pan YK, Wang XZ, eds. Novel Drying Technologies. Beijing: China Chemical Engineering Publishing House, 1998b, pp 653–660. (in Chinese).

Kudra T. Drying technologies for clean environment. In: Proc. Asian-Australian Drying Conference (ADC'99), Kamaruddin A, Tambunan AH, Mujumdar AS, eds. Bali, Indonesia, 1999a, pp 81–94.

Kudra T. Drying Technology—special issue on drying and dewatering in energy fields. 17(3):379–654, 1999b.

Kudra T. Phase separation in CANMET hydrocyclone prior to thermal drying. CST Workshop 2000 on Separations in Difficult Conditions, Lappeenranta, Finland, 2000.

Kudra T, Mujumdar AS. Impingement stream dryers for particles and pastes. Drying Technology 7(2):219–266, 1989.

Kudra T, Mujumdar AS. Special drying techniques and novel dryers. In: Mujumdar AS, ed. Handbook of Industrial Drying. 2nd ed. New York: Marcel Dekker, 1995, pp 1087–1149.

Kudra T, Strumillo C, Eds. Thermal Processing of Bio-Materials. Amsterdam: Gordon and Breach Science Publishers, 1998.

Kudra T, Pallai E, Bartczak Z, Peter M. Drying of paste-like materials in screw-type spouted bed and spin-flash dryers. Drying Technology 7(3):583–598, 1989.

Kudra T, Buchkowski AG, Kitchen JA. Pulse combustion drying of white pine. Proc. 4th IUFRO Intl. Wood Drying Conf., Rotorua, New Zealand, 1994, pp 396–403.

Kudra T, Gawrzynski Z, Glaser R. Pulsed fluidized bed. U.S. Patent No. 5,918,569, 1999.

Kudra T, Mujumdar AS, Meltser VL. Impinging stream dryers: Principles, practice and potential. In: Mujumdar AS, ed. Drying of Solids. Meerat, New Delhi: Sarita Prakashan, 1990, pp 17–32.

Kudra T, Mujumdar AS, Meltser VL. Impinging stream dryers. In: AS, Mujumdar AS, ed. Handbook of Industrial Drying. 2nd ed. New York: Marcel Dekker, 1995, pp 539–566.

Kudra T, Shivhare US, Raghavan GSV. 1990. Dielectric drying—a bibliography. Drying Technology 8(5):1147–1160, 1990.

Kumar P, Mujumdar AS. Superheated steam drying—a state-of-the-art survey. In: Mujumdar AS, ed. Drying of Solids. Meerut, New Delhi: Sarita Prakashan, 1990, pp 33–71.

Kutsakova VE, Bogatyriev AN. Intensification of Heat and Mass Transfer in Drying of Food Products. Moscow: Agropromizdat, 1987 (in Russian).

Kutsakova VE, Utkin YV. Drying kinetics of proteineous pastes, emulsions and solutions on fluidized bed of inert particles. Zhurnal Prikladno Khimii 60(5):1143–1148, 1987 (in Russian).

Kutsakova VE, Utkin YV. Drying of egg melange on inert particles in swirling stream dryers with tangential inlet of a heat carrier. Trans. VUZOV. Food Technology 5:92–93, 1989 (in Russian).

Kutsakova VE, Markov NB, Utkin YV, Ivanova MP. Apparatus for drying of liquid materials. Russian Patent No. 2,009,413, 1991.

Kutsakova VE, Romankov PG, Rashkovskaya NB. Some kinetic relationships of the drying process in fluidized and spouted beds. Zhurnal Prikladnoi Khimii. 37(10): 2198–2202, 1964 (in Russian).

Kutsakova VE, Utkin YV, Kupanov BY. Method for drying of liquid materials. Russian Patent No. 1,560,948, 1990.

Kutsakova VE, Zotov VP, Usvyat, YN, Uvayeva AB, Gendrikson VA. Inert particle for fluid bed dryer. Russian Patent No. 1,592,683, 1985.

Kuznetsov, VV, Subbotina NI. An effect of ultrasound on the diffusion of electrolytic hydrogen through the ion membrane. Elektrokhimia 1(9):1096–1098, 1965 (in Russian).

Labidi J, Nikapour D, De-Parolis L. Hybrid absorption/compression heat pump for space application. Proc. Intl. Absorption Heat Pump Conf., Montreal, 1996, pp 489–496.

Lapczynska B, Zaremba A. Adsorption drying of wheat and oat. Proc. VI Drying Symposium, Lodz, Poland, 1987, pp 103–109 (in Polish).

Lazar ME, Farkas DF. The centrifugal fluidized bed (CFB) 2. Drying studies on piece-form foods. J. Food Science 36:315–319, 1971.

Legros R. Processing of vegetable materials in fluidized beds. Ph.D. thesis, University of Surrey. Guildford, Great Britain, 1986.

Legros R, Clift R, Millington CA. Development of a mobilization technique for fibrous materials. Powder Technology 85:105–114, 1995.

Lehtinen J. Condebelt board and paper drying. Drying Technology 16(6):1047–1073, 1998.

Lemoine A, Jurewicz J. Gasification of biomass in plasma spouted bed reactor. Intl. Symposium on Plasma Chemistry, Prague, Czech Republic, 1999.

Leontieva AI, Bryankin KV, Konovalov VI, Utrobin NP. Heat and mass transfer during drying of a liquid film from the surface of a single inert particle. Drying Technology, 2001.

Levental LI, Meltser VL, Baida MM, Pisarik NK. Investigation of solid particle motion in reverse gas-solid suspension. In: Investigation of Transport Processes in Dispersed Systems. Minsk, Belarus: ITMO AN BSSR, 1981, pp 69–76 (in Russian).

Liapis AI, Bruttini R. Freeze drying. In: Mujumdar AS, ed. Handbook of Industrial Drying. 2nd ed. New York: Marcel Dekker, 1995, pp 309–343.

Limaverde JR, Limaverde JR, Finzer JRD. Pastelike materials drying in rotary dryer with inert bed. Proc. 12th Intl. Drying Symposium (IDS'2000). Coumans WJ, Kerkhof PJAM, eds. Noordwijkerhout, The Netherlands, Paper 341, 2000.

Lin TM, Durance TD, Scaman CH. Characterization of vacuum microwave, air and freeze dried carrot slices. Food Research International 31(2):111–117, 1998.

Lin TM, Durance TD, Scaman CH. Physical and sensory properties of vacuum micro-

wave dehydrated shrimp. J. Aquatic Food Product Technology 8(4):41–53, 1999.
Lockwood HN. Pulse combustion energy system. U.S. Patent No. 4,708,159, 1987.
Lockwood RM. Pulse combustion fluidizing dryer. U.S. Patent No. 4,395,830, 1983.
Loo E, Mujumdar AS. A simulation model for combined impingement and through drying using superheated steam as the drying medium. In: Mujumda AS, ed. Drying 84. Washington: Hemisphere Publishing Co., 1984, pp 264–280.
Lopez-Cacicedo CL. Application possibilities for heat pumps in the higher temperature range. Elektrowarme im Technischen Aufbau Edition A 38:281–284, 1980.
Lopez-Cacicedo CL. Electrical methods for drying. In: Mujumdar AS, ed. Drying '86, Vol. 1. Washington: Hemisphere Publishing Corp., 1986, pp 12–21.
Lowe CM, King CJ. Slush evaporation: A new method for concentration of liquid foods. J Food Sci 39:248–253, 1974.
Luikov AV. Heat and Mass Transfer in Capillary Porous Bodies. Oxford: Pergamon Press, 1966.
Luikov AV, Mikhailov UA. Theory of Energy and Mass Transfer. Englewood Cliffs, NJ: Prentice-Hall, 1961.
Lyulin NB. Intensification of drying instant pigments by the use of shock wave generator. Ph.D. thesis, Mendeleyev University of Russia, 1998 (in Russian).
Maekawa Y. Instantaneous vacuum drying system. In: Rudolph V, Keey RB, eds. Drying '94. Proc. Intl. Drying Symposium (IDS'94), Gold Coast, Australia, 1994a, pp 359–366.
Maekawa Y. Processing Possibility by Vacu Jet Drying System. Osaka, Japan: Hosokawa Micron Corp., 1994b.
Magnussen OM, Strømmen I. Heat pump drying of heavily salted codfish. Nordic Refrigeration Meeting, Copenhagen, 1981.
Makarov AP, Polyanskii KK, Karnaukh VI. Studies on acoustic vibrations for intensification of lactic sugar drying. Izvestiya Vuzov. Pishchevaya Tekhnologiya 4: 181–183, 1972 (in Russian).
Manohar H, Gleit CE. Fluidized plasma: Solid reactions. In: Flinn JE, ed. Engineering, Chemistry and Use of Plasma Reactors. Chem. Eng. Prog Symp. Series 67(112), 1971, pp 55–59.
Marchevski VN. Technology for continuous drying of casein. Bulletin of Kiev Technical Institut, 1998 (in Russian).
Markowski A, Kaminski W, Strumillo C, Kudra T. Apparatus for heat and mass transfer. Polish Patent No. 100,376, 1977.
Markowski A, Kaminski W, Strumillo C, Kudra T. New design of spouted bed dryer with inert particles. Proc. III Drying Symposium, Lodz, Poland, 1978 (in Polish).
Markowski AS. Drying characteristics in a jet-spouted bed dryer. Can J Chem Eng 70(10):938–944, 1992.
Markowski AS. Quality interaction in a jet-spouted bed dryer for bio-products. Drying Technology 11(2):369–387, 1993a.
Markowski AS. Quality losses risk during drying of bio-products in a jet-spouted bed

dryer. Meeting of the EFCE Drying Working Party. Utrecht, The Netherlands, 1993b.

Marshall MG, Metaxas AC. Modeling the radio frequency electric field strength developed during the RF assisted heat pump drying of particulates. Intl. Microwave Power Institute 33(3):167–177, 1998.

Marshall MG, Metaxas AC. Radio frequency assisted heat pump drying of crushed brick. Applied Thermal Engineering 19:375–388, 1999.

Marziniak R. Kinetic of acoustic drying process. Acustica 27:122–131, 1972 (in German).

Mashkova TL. Acoustic drying. In: Application of Ultrasonics in Processes of Chemical Engineering. Moscow: TINTIEPP Publishing House, 1960, pp 196–201 (in Russian).

Mason RL, Blarcom AV. Drying macadamia nuts using a heat pump dehumidifier. Proc. Development and Application of Heat Pump Dryer, Brisbane, Australia, 1993, pp 1–7.

Mathur KB, Epstein N. Spouted Beds. New York: Academic Press, 1974.

Matsuo K, Senshu T, Hayashi M, Kokuba H. How can heat pumps be made more cost competitive? Proc. Intl. Energy Agency Heat Pump Conf., Graz, Austria, 1984, pp 87–96.

Mbaye M, Aidoun Z, Valkov V, Legault A. Analysis of chemical heat pumps (CHPS): Basic concepts and numerical model description. Applied Thermal Engineering 18(3):138–146, 1997.

McConvey IF, Shering P. Microwave assisted pressure filter drying of pharmaceutical compounds. Trans Ichem E 78(Part C):97–100, 2000.

Meltser VL, Pisarik NK. Interphase heat transfer in impinging single and two-phase streams. Proc XI All Russian Conference on Heat and Mass Transfer. Minsk, Belarus, Vol. VI, Part 1 1980, pp 132–135 (in Russian).

Meltser VL, Tutova EG. Drying of crystalline lysine in reversing impinging streams. Biotekhnologia 2:70–74, 1986 (in Russian).

Meltser VL, Gurevich GL, Starovoitenko EI, Deryugin AI. The calculation method of thermal processing of wet particles in reversing gas-solid streams. In: Heat and Mass Transfer Investigations in Drying and Thermal Processing of Capillary-Porous Materials. Minsk, Belarus: ITMO AN BSSR, 1985, pp 131–138 (in Russian).

Meltser VL, Kudra T, Mujumdar AS. Classification and design considerations for impinging stream dryers. Proc. Intl. Forum on Heat and Mass Transfer—Intl. Drying Symposium. Vol. 1. Kiev, Ukraine 1992, pp 181–184 (in Russian).

Menshutina NV, Tsoukanov VA, Kudra, T. Definition of hydrodynamic stability for a jet spouted bed of inert particles. Proc. 12th Intl. Drying Symposium (IDS'2000), Coumans WJ, Kerkhof PJAM, eds. Noordwijkerhout, The Netherlands, Paper 264, 2000.

Metaxas AC. Foundations of Electroheat; a United Approach. Chichester, England: John Wiley & Sons, 1996.

Metaxas AC, Meredith RJ. Industrial Microwave Heating. Stevenage, UK: Peter Peregrinus Ltd., 1983.

Meunier J, Munz, RJ. Flash drying with superheated steam—a mathematical model. In: Mujumdar AS, ed. Drying '86. Vol. 1. Washington: Hemisphere Publishing Corp., 1986, pp 580–587.

Meyer JP, Greyvenstein GP. The drying of grain with heat pumps in South Africa: A techno-economic analysis. Intl. J Energy Research 16:13–20, 1992.

Miller DG. Application of dielectric heating to the seasoning of wood. Proc. Forest Products Research Society National Annual Meeting, Vol. 2, 1948, pp 235–241.

Miller DG. Combining radio-frequency heating with kiln-drying to provide fast drying without degrade. Forest Products Journal 21(12):17–21, 1971.

Minchev AD, Romankov PG, Rashkovskaya NB. Studies on drying of pastelike materials in the spouted bed. Zhurnal Prikladnoj Khimii 41(4):1249–1250, 1968 (in Russian).

Moeller AL. The Ecal Process—a novel dehydration process. In: Spicer A, ed. Advances in Preconcentration and Dehydration of Foods. New York: Elsevier, 1974, pp 499–504.

Moy JH, DiMarco GR. Exploring airborne sound in a nonvacuum freeze drying process. J Food Sci 35:811–817, 1970.

Mujumdar AS. Recent developments in drying. Annual Conf. Indian Institute of Chemical Engineering, Madras, India, 1981.

Mujumdar AS. Spouted bed technology—a brief review. In: Mujumdar AS, ed. Drying '84. New York: Hemisphere-McGraw-Hill, 1984, pp 151–157.

Mujumdar AS. Recent developments in spouted bed drying. Conf. Transport Processes in Porous Media, Sao Carlos, Brazil, 1989.

Mujumdar AS. Superheated Steam Drying—Principles, Practice and Potential for Use of Electricity. Canadian Electrical Association Report 817 U 671. Montreal, 1990.

Mujumdar AS. Drying technologies of the future. Drying Technology 9(2):325–347, 1991.

Mujumdar AS. Superheated steam drying of paper: Principles, status and potential. In: Mujumdar AS, ed. Drying of Solids. New York:International Science Publisher, 1992, pp 208–220.

Mujumdar AS, ed. Handbook of Industrial Drying. 2nd ed. New York Marcel Dekker, 1995.

Mujumdar AS. Classification and selection of dryers. In: Devahastin S, ed. Mujumdar's Practical Guide to Industrial Drying. Brossard, Canada: Exergex, 2000, pp 23–36.

Mujumdar AS, Menon AS. Drying of solids: principles, classification, and selection of dryers. Vol. 1. In: Mujumdar AS, ed. Handbook of Industrial Drying. 2nd ed. New York: Marcel Dekker, 1995, pp 1–39.

Mujumdar AS, Passos ML. Drying: Innovative technologies and trends in research and development. In: Mujumdar AS, Suvachittanont S, eds. Developments in Drying. Bangkok: Kasetsart University Press, 2000, pp 235–268.

Mujumdar AS, Huang B. Impingement drying. In: Mujumdar AS, ed. Handbook of Industrial Drying. 2nd ed. New York: Marcel Dekker, 1995, pp 489–501.

Munz R, Mersereau O. A plasma spout-fluid bed for the recovery of vanadium from vanadium ore. Chem. Eng. Sci. 45(8):2489–2495, 1990.

Muralidhara HS, Ensminger D. Acoustic drying of green rice. Drying Technology 4(1): 137–143, 1986.

Muralidhara HS, Lokhard, NC, eds. Combined field separation techniques for dewatering. Drying Technology—Theme Issue 6(3):361–569, 1985.

Muralidhara HS, Chauhan SP, Senapati N, Beard R, Jirjis B, Kim BC. Electro-acoustic dewatering (EAD): A novel approach for food processing, and recovery. Separation Science and Technology 23(12&13):2143–2158, 1988.

Muralidhara SH, Senapati N, Beard RB. A novel electroacoustics separation process for fine particle suspensions. In Muralidhara HS, ed. Advances in Solid-Liquid Separation. Columbus, OH: Battelle Press, 1986.

Muranov VA, Lyulin NB, Ryzhukhin OA, Bykov AE, Tarakanova EE. Spray drying of pasty pigments. Lakokrasochnye Materialy 12:18–21, 1997 (in Russian).

Nassikas AA, Akritidis CB, Mujumdar AS. Close-cycle heat pump dryer using superheated steam: An application to paper drying. In: Mujumdar AS, ed. Drying '92. Amsterdam: Elsevier Science Publishers, 1992, pp 1085–1098.

Newber GJ. Energy efficient drying, evaporation and similar processes. Heat Recovery Systems 5(6):551–559, 1985.

Nikitina LM. Thermophysical Parameters and Mass Transfer Coefficients for Wet Materials. Moscow: Energia, 1968 (in Russian).

Ogura H, Mujumdar AS. Proposal for a novel chemical heat pump dryer. Drying Technology 18(4&5):1033–1053, 2000.

Ogura H, Fujimoto S, Iwamoto H, Kage H, Matsuno Y. Thermal energy conversion of night electricity to high/low-temperature heat by $CaO/H_2O/Ca(OH)_2$ chemical heat pump unit. Proc. Int. Conf. on Fluid and Thermal Energy Conversion '97, Yogyakarta, Indonesia, 1997, pp 309–314.

Ogura H, Nagura A, Matsuda H, Hasatani M, Yanadori M, Hiramatsu, M. Studies on heat transfer augmentation in chemical heat pump composed of $CaO/Ca(OH)_2$ reversible reaction and evaporation/condensation of water. In: Proc. Intl. Conf. on the Analysis of Thermal and Energy Systems, Athens, Greece, 1991, pp 665–676.

Ogura H, Shimojyo R, Kage H, Matsuno Y, Mujumdar AS. Simulation of hydration/dehydration of $CaO/Ca(OH)_2$ chemical heat pump reaction for cold/hot heat generation. Drying Technology 17(7&8):1579–1592, 1999.

Oliveira WP, Freire JT. Analysis of evaporation rate in the spouted bed zones during drying of liquid materials using a three region model. In: Strumillo C, Pakowski Z, eds. Drying '96. Proc. 10th Intl. Drying Symposium (IDS'96), Krakow, Poland, 1996, pp 504–512.

Oliveira WP, Silveira AM, Freire JT. Analysis of the drying of pastes in conical spouted beds. In: Rudolph V, Keey RB, eds. Drying '94. Proc. 9th Intl. Drying Symposium (IDS'94), Gold Coast, Australia, 1994, pp 495–502.

Olorunmaie JA, Kentfield JAC. Numerical simulation of waveless pulsed combustors. Acta Astronautica 19(8):669–679, 1989.

Otsuka T, Purdum H, Fairbanks H. Drying of temperature sensitive materials with a heated ultrasonically vibrated chute. Proc. Ultrasonic Intl. Conf. Brighton, Great Britain, 1977, pp 91–95.

Ozer RW. Review of operating data from pilot plant and field pulse combustion drying systems. Proc. Powder and Bulk Solids Conference/Exhibition, Chicago, 1993, pp 407–419.

Ozer RW, Lockwood H, Kimball GJ, Pikus I. Pulse combustion drying system. U.S. Patent No. 5,252,061, 1993.

Paakkonen K, Havento J, Bertalan G, Pyykkonen M. Infrared drying of herbs. Agricultural and Food Science in Finland 8:19–27, 1998.

Pajunen J, Salin J-G, Vihavainen T. Chemical Drying of Wood. VTT Research Report 523, 1988 (in Finnish).

Pakowski Z, Mujumdar AS, Strumillo C. Theory and application of vibrated geds and vibrated fluid beds for drying processes. In: Mujumdar AS, ed. Advances in Drying. Vol. 3. Washington: Hemisphere, 1984, pp 245–306.

Pallai E, Szentmarjay T, Mujumdar AS. Spouted bed drying. In: Mujumdar AS, ed. Handbook of Industrial Drying. 2nd ed. New York: Marcel Dekker, 1995, pp 453–488.

Pan YK, Li JG, Zhao LJ, Ye WH, Mujumdar AS, Kudra T. Drying of a dilute suspension in a vibrated fluidized bed of inert particles. Proc. 12th Intl. Drying Symposium (IDS '2000), Coumans WJ, Kerkhof PJAM, eds. Noordwijkerhout, The Netherlands, Paper 266, 2000.

Pan YK, Pang JZ, Li ZY, Mujumdar AS, Kudra T. Drying of heat-sensitive bio-products on solid carriers in vibrated fluid bed. In: Rudolph V, Keey RB, eds. Drying 194. Proc. 9th Intl. Drying Symposium (IDS'94), Gold Coast, Australia, 1994, pp 819–824.

Pan YK, Pang JZ, Li ZY, Mujumdar AS, Kudra T. Drying of photosynthetic bacteria in a vibrated fluid bed of solid carriers. Drying Technology 13(1&2):395–404, 1995.

Pannu KS, Raghavan GSV. A continuous flow particulate medium grain processor. Can. Agricultural Engineering 29(1):39–43, 1987.

Passos ML, Mujumdar AS, Raghavan VGSV. Spouted bed for drying: Principles and design considerations. In: Mujumdar AS, ed. Advances in Drying. Vol. 4. Washington: Hemisphere Publishing Corp., 1987, pp 359–398.

Perry EJ. Drying by cascaded heat pumps. Inst. of Refrigeration Management, 1981, pp 1–8.

Perry RH, Green DW, Maloney JO eds. Perry's Chemical Engineers' Handbook. 7th ed. New York: McGraw-Hill, 1997.

Petrucci VE, Clary CD. Vacuum microwave drying of food products. Report No. 2897-3. California State University at Fresno, 1989.

Pham QT. Behaviour of a conical spouted-bed dryer for animal blood. Can. J. Chem. Eng. 61(6):426–434, 1983.

Phillips EM, Stella VJ. Rapid expansion from supercritical solutions: application to pharmaceutical processes. Int. J. Pharmaceutics 94:1–10, 1993.

Pikus IF, Kuts PS, Tutova EG, Bogdanov VM. Apparatus for drying of solutions and suspensions. Russian Patent No. 445,808, 1975.

Piper PM, Alimpic M. Possibilities of maize seed drying by adsorption method. CHISA'93. Praha, Czechoslovakia, Paper 13.38, 1983.

Pluenneke KA, Crumm CJ. An innovative drying process with diverse applications. In: Mujumdar AS, ed. Drying '86. Vol. 1. Washington: Hemisphere Publishing Corp., 1986, pp 617–624.

Poirier N. The effect of superheated steam drying on the properties of paper, Ph.D. thesis, McGill University. Montreal, 1991.

Potter OE, Beeby C. Modeling tube-to-bed heat transfer in fluidized bed steam drying. In: Mujumdar AS, ed. Drying '86. Vol. II. Washington: Hemisphere Publishing Corp., 1986, pp 595–603.

Potter OE, Guang LX. Some design aspects of steam-fluidized heated dryers. Proc. 6th Intl. Drying Symposium (IDS'88), Versailles, France, 1988, pp 321–323.

Prasertsan S, Saen-saby P, Prateepchaikul G, Ngamsritrakul P. Heat pump dryer. Part 3: Experiment verification of the simulation. Intl. J Energy Research 21:1–20, 1997.

Prasertsan S, Saen-saby P. Heat pump drying of agricultural materials. Drying Technology 16(1&2):235–250, 1998.

Rafson HJ. Odor and VOC Control Handbook. New York: McGraw-Hill, 1998.

Raghavan GSV, Pannu KS. Method and apparatus for drying and heat treating of granular materials. U.S. Patent No. 4,597,737, 1986.

Rakotozafy H, Louka N, Therisod M, Therisod H, Allaf K. Drying of baker's yeast by a new method: dehydration by successive pressure drops (DDS). Effect on cell survival and enzymatic activities. Drying Technology 18(10):2253–2271, 2000.

Rasev AI. Particular features of dielectric and vacuum wood drying. Proc. 6th IUFRO Intl. Wood Drying Conference, Stellenbosch, South Africa, 1999, pp 37–41.

Re MI, Freire JT. Drying of pastelike materials in spouted beds. In: Mujumdar AS, Roques M, eds. Drying '89. Washington: Hemisphere Publishing Corp., 1989, pp 426–432.

Reger EO, Romankov PG, Rashkovskaya NB. Drying of paste materials on inert substances in spouted beds. Zhurnal Prikladnoi Khimii 40(10):2276–2280, 1967 (in Russian).

Rheinlander PM. Filtermat—the 3-stage spray dryer from DEC. In: Ashworth JC, ed. Proc. 3rd Intl. Drying Symposium. Vol. 1. Birmingham, England, 1982, pp 528–534.

Richards MK. Demonstration of the Sonotech, Inc., frequency-tunable pulse combustion system (CELLO pulse burner). SITE Program Fact Sheet, U.S. Environmental Protection Agency, Cincinnati, April 1–4, 1994.

Rippenger S. Advanced concentration of suspensions and sludges. IEA Workshop on Separation Technologies. Mainz, Germany, 1998.

Roberts RL, Carlson RA, Farkas DF. Preparation of a quick-cooking brown rice product using a centrifugal fluidized bed dryer. J Food Sci 45:1080–1081, 1980.

Rosen HN. Drying of wood and wood products. In: Mujumdar AS, ed. Handbook of Industrial Drying. 2nd ed. New York: Marcel Dekker, 1995, pp 899–920.

Rosen HN, Bodkin RE, Gaddis KD. Pressure dryer for steam seasoning lumber. U.S. Patent No. 4,343,095, 1982.

Rosenberg LD, ed. Physical Principles of Ultrasonic Technology. Vols. 1 and 2. New York: Plenum Press, 1973.

Rossi SJ, Neves LC, Kieckbusch TG. Thermodynamic and energetic evaluation of a heat pump applied to drying of vegetables. In: Mujumdar AS, ed. Drying '92. Amsterdam: Elsevier Science Publishers, 1992, pp 1475–1484.

Rozsa AN. Dielectric vacuum drying of hardwoods. Proc. 4th IUFRO Intl. Wood Drying Conf., Rotorua, New Zealand, 1994, pp 271–278.

Ruf J, Stahl W. The hot filter-press: The new technology of vapor pressure dewatering. In: Baumann ER, Weisert L, eds. Advances in Filtration and Separation Technology. Vol. 11. Boston: American Filtration & Separations Society, 1997, pp 558–562.

Ruf J, Korger V, Stahl W. Proc. 7th World Filtration Congress, Budapest, 1996.

Rysin AP, Ginzburg AS. Theory and technology of food product drying in fluidized vibrated bed. In: Mujumdar AS, ed. Drying of Solids. New York: International Science Publisher, 1992, pp 86–124.

Rysin AP, Zaitsev VM, Shymkov YG, Gusyev AA, Smirnov OS. Method of drying of pasty products. Russian Patent No. 1,024,668, 1981.

Saad, MA. Compressible Fluid Flow. Englewood Cliffs, NJ: Prentice Hall, 1992.

Saito S, Sulaiman IB. Radiofrequency vacuum (RF/V) drying of small diameter Keruing. Proc. 6th Intl. Wood Drying Conf., 1999, p. 234.

Salin JG. Steam drying of wood particles for particleboard. In: Mujumdar AS, ed. Drying '86, Vol. II. Washington: Hemisphere Publishing Corp., 1986, pp 572–574.

Salin JG. Steam drying of wood for improved particleboard and lower energy consumption. Paper and Timber 9:806–810, 1988.

Salin JG. Solvent drying of wood—some results. In: Mujumdar AS, Filkova I, eds. Amsterdam: Elsevier Science Publ., 1991, pp 529–534.

Sanga E, Mujumdar AS, Raghavan GSV. Microwave drying: Principles and applications. In: Mujumdar AS, Suvachittanont S, eds. Developments in Drying, Vol. I. Food Dehydration. Bangkok: Kasetsart Univ. Press, 2000, pp 112–141.

Sanio MR. Economic considerations for dielectrically enhanced heating. In: Electromagnetic Heating—Short Course Workbook. Clifton: IMPI, 1989, pp 57–68.

Sanio MR, Schmidt PS. A procedure for estimating capital and operating costs of dielectric heating equipment. Report TSDD-89-011. Ontario Hydro of Canada. Toronto, 1989.

Sarup L, Servistas MT, Sloan R, Hoare M, Humphreys GO. Investigation of supercritical fluid technology to produce dry particulate formulations of antibody fragments. Trans. IchemE. 78 (Part C): 101–104, 2000.

Schetz JA, Fuhs AE, eds. Handbook of Fluid Dynamics and Fluid Machinery. New York: John Wiley & Sons, Inc., 1996.

Schiffmann RF. Microwave and dielectric drying . In: Mujumdar AS, ed. Handbook of Industrial Drying. 2nd ed. New York: Marcel Dekker, 1995, pp 345–372.

Schneider T, Bridgewater, J. Drying of solutions and suspensions in spouted beds. In: Mujumdar AS, Roques M, eds. Drying '89. New York: Hemisphere Publishing Corp., 1989, pp 421–425.

Shafick H. Solid-liquid separation of fine particles. Proc. Progress in Dewatering of Fine Particle Conference, University of Alabama, 1981, pp 1–32.

Shah RM, Goyel SK. Drying characteristics of tea fluidized on a vibrating bed (Part 1). In: Mujumdar AS, ed. Drying '80. Vol. 2. Washington: Hemisphere Publishing Corp., 1980, pp 176–181.

Shapiro AH. The Dynamics and Thermodynamics of Compressible Fluid Flow. New York: Ronald Press, 1953.

Shatalov AL. Sound-assisted microwave drying. Elektronnaya Obrabotka Materialov 3:37–38, 1976 (in Russian).

Shibata H, Iwao Y, Ide M. Combined superheated steam and microwave drying of sintered glass beads. Proc. 12th Intl. Drying Symposium (IDS'2000). Coumans WJ, Kerkhof PJAM, eds. Noordwijkerhout, The Netherlands, Paper 363, 2000.

Shibata H, Mada J, Shinohara H. Drying mechanism of sintered spheres of glass beads in superheated steam. Ind. Eng. Chem. Res. 27(12):2353–2362, 1988.

Simonyan SG. Low-temperature drying of free-flowing materials. Trudy VNIINSM 2(10):34, 1965 (in Russian).

Smith WB, Smith A, Neauhauser EF. Radio-frequency/vacuum drying of red oak: energy, quality, value. Proc. 4th IUFRO Intl. Wood Drying Conference, Rotorua, New Zealand, 1994, pp 263–270.

Soloff RS. Sonic drying. J. Acoustical Soc. America 36(5):961–965, 1964.

Soloviev MI. Suspending and transportation of granular materials in horizontal ducts. Inzhenerno Phyzicheski Zhurnal 7(10): 62–67, 1964 (in Russian).

Song X. Low temperature fluidized bed drying with temperature program. Ph.D. thesis, The Norwegian Institute of Technology, Division of Refrigeration Engineering. Trondheim, Norway, 1990 (in Norwegian).

Sotocinal S. Design and testing of a particulate medium thermal processor. Ph.D. thesis, McGill University, Montreal, 1998.

Sotocinal SA, Alikhani Z, Raghavan GSV. Heating/drying using particulate medium: A review (parts I and II). Drying Technology 15(2):441–475, 1997.

Speirs BC. An experimental optimization of a large aerovalved, multiple inlet pulse combustor. M.Sc. thesis, University of Calgary, 1989.

Spitzner N PI, Freire JT. Evaluation of models on the drying of pastes in spouted beds with inert particles. Akritidis CB, Marinos-Kouris D, Saravakos GD, eds. Drying '98. Proc. 11th Intl. Drying Symposium (IDS'98), Halkidiki, Greece, 1998, pp 2009–2016.

Stadnik BN, Kazanskii MF. Effect of sound on the intensity of drying capillary-porous materials. In: Investigation of Heat and Mass Transfer in Technological Processes and Equipment. Minsk; Belarus: Nauka i Tekhnika, 1966 (in Russian).

Stahl WH. Synergetic effects by mechanical hybrid processes and process combinations. IEA Workshop on Separation Technologies, Mainz, Germany, 1998.

Stewart CR, Lemieux PM, Zinn BT. Application of pulse combustion to solid and hazardous waste incineration. Proc. Intl. Symposium on Pulsating Combustion. Monterey, CA, Paper B-21, 1991.

Strømmen I. Drying of heavily salted codfish. Ph.D. thesis, The Norwegian Institute of Technology, Division of Refrigeration Engineering. Trondheim, Norway, 1980 (in Norwegian).

Strømmen I, Jonassen O. Performance tests of a new 2-stage counter-current heat pump fluidized bed dryer. In: Strumillo C, Pakowski Z, eds. Drying '96. Proc. 10th Intl. Drying Symposium (IDS'96), Krakow, Poland, 1996, pp 563–568.

Strømmen I, Kramer K. New applications of heat pumps in drying process. Drying Technology 12(4): 889–901, 1994.

Strumillo C, Kudra T. Drying: Principles, Applications and Design. New York: Gordon and Breach Science Publishers, 1986.

Strumillo C, Michalowski S, Grochowski J, Adamiec J. Evaporation drying. Inzynieria i Aparatura Chemiczna 10(4):16–17, 1971 (in Polish).

Strumillo C, Jones PL, Zylla R. Energy aspects in drying. In: Mujumdar AS, ed. Handbook of Industrial Drying. 2nd ed. New York: Marcel Dekker, 1995, pp 1241–1275.

Strumillo C, Kaminski W, Markowski A. Scaling-up of dryers with a spouted bed of inert bodies. In: Mujumdar AS, ed. Drying '80. Vol. 1. Developments in Drying. Washington, D.C.: Hemisphere Publishing Corporation, 1980, pp 180–183.

Strumillo C, Kuts PS, Zbicinski I. The analysis of swirl-impact dryer hydrodynamics. In: Strumillo C, Pakowski Z, eds. Drying '96. Proc. 10th Intl. Drying Symposium (IDS'96), Krakow, Poland, 1996, pp 569–576.

Strumillo C, Markowski A, Kaminski W. Modern developments in drying of paste materials. In: Mujumdar AS ed. Advances in Drying. Vol. 2. Amsterdam: Hemisphere Publishing Corp., 1983, pp 193–232.

Stubbing TJ. Method and apparatus for energy efficient drying. U.K. Patent No. 2,209,383, 1987.

Stubbing TJ. Airless drying process saves energy and reduces emissions. Paper Technology June:36–39, 1990.

Stubbing TJ. Airless drying: Its invention, method and application. Trans. IChemE. Part A 71 (A5):488–495, 1993.

Stubbing TJ. Sludge disposal: Moist incineration or dry combustion—a preliminary comparison. Bitterley, Great Britain: Heat-Win Ltd., 1994a.

Stubbing TJ. Airless drying. In: Drying '94. Proc. 9th Intl. Drying Symposium (IDS'94), Gold Coast, Australia, 1994b, pp 559–566.

Stubbing TJ. Airless drying for reducing the cost of drying materials, reducing the cost of sludge processing and reducing the cost of drying paper. The DEMOS Progress Seminar on Paper Pulp Sludge from a Disposal Problem into a Valuable Product. Leicester, Great Britain. Feb. 8, 1994a.

Stubbing TJ. Method and apparatus for continuous drying in superheated steam. U.S. Patent No. 7,711,086, 1998.
Stubbing TJ. Airless drying-development since IDS'94. Drying Technology 17(7&8): 1639–1651, 1999.
Stuchly SS, Stuchly MA. Microwave drying: potential and limitations. In: Mujumdar AS, ed. Advances in Drying. Vol. 2. New York: Hemisphere Publishing Corp., 1983, pp 53–71.
Sun Z, Carrington CG, McKenzie C, Bannister P, Bansal B. Determination and application of characteristic drying-rate curves in dehumidifier wood drying. Proc. 5th IUFRO Conf., Quebec, 1996, pp 495–503.
Suslick KS, ed. Ultrasound: Its Chemical, Physical and Biological Effects. New York: VCH Publishers, 1988.
Sztabert Z, Przybyla J, Grzelczyk Z. Method for generating a fluidized bed of granular materials. Polish Patent No. 92,255, 1978.
Szuba J, Wasilewski P, Mikolajska U, Bal S, Swierczek R. Method and apparatus for thermo-chemical conversion of coal. Polish Patent No. 83,271, 1976.
Tamir A. Vertical impinging streams and spouted bed dryers: Comparison and performance. Drying Technology 7(2):183–204, 1989.
Tamir A. Impingement streams (ISD) and their application to drying. In: Mujumdar AS, ed. Drying '92. Amsterdam: Elsevier Science Publishers, 1992.
Tamir A. Impinging-Stream Reactors: Fundamentals and Applications. Amsterdam: Elsevier, 1994.
Tamir A, Grinholtz M. Performance of a continuous solid-liquid two-impinging-streams (TIS) reactors: Dissolution of solids, hydrodynamics, mean residence time, and holdup of the particles. Ind. Eng. Chem. Res. 26(4):726–731, 1987.
Tamir A, Shalmon B. Scale-up of two-impinging streams (TIS) reactors. Ind. Eng. Chem. Res. 27:238–242, 1988.
Tang JX, Wang ZG, Huang LX. Recent progress of spray drying in China. Drying Technology 17(9):1747–1757, 1999.
Technical Bulletin. Cello Hi-Efficiency Burners. Atlanta, GA: Sonotech Inc., 1992.
Technical Bulletin. Portland, OR: Pulse Drying System Inc., 1999.
Tessier S, Raghavan GSV. Performance of a sand medium dryer for shelled corn. Trans. ASAE 27(4):1227–1232, 1984.
Thijssen HAC. Falvor retention in drying preconcentrated liquid foods. J. Appl. Chem. Biotechnol. 21:372–377, 1971.
Thomas WJ. RF Drying Provides Process Savings: New systems optimise radio frequency drying for the ceramic and glass fibre industries. Ceramic Industry Magazine April:30–34, 1996.
Tutova EG. Fundamentals of contact–sorption dehydration of labile materials. Drying Technology 6(1):1–20, 1988.
Tutova EG, Kuts PS. Drying of Microbiological Products. Moscow: Agropromizdat, 1987 (in Russian).
Tutova EG, Slizhuk DS. Technology of contact-sorption dewatering of lactic acid and

nitrogen fixing cultures. Trans. ITMO. Minsk, Belarus. Paper UDK 663.15.047, 1990 (in Russian).
Tutova EG, Feldman RI, Meltser AV. Method of contact dewatering of capillary porous materials. Russian Patent No. 1,170,245, 1985.
Tutova EG, Kuts PS, Dushin VV, Bogdanov VM, Kruglov NA, Rusnak MN, Korolev VA. Method of treatment of fodder micro-biological preparations. Russian Patent No. 685,886, 1979.
Tutova EG, Kuts PS, Slizhuk DS, Temlyak FC, Nikiforova LA, Kuznetsov EV, Vasilyev VM. Method of obtaining the lactic acid bacterial preparates. Russian Patent No. 1,325,070, 1987.
Unligil HH. Penetrability and strength of white spruce after ponding. Forest Products Journal 22(9):92–99, 1972.
van Gogh F. Mechanical vapor compression for the pulp and paper industry. Appita 38:372–376, 1985.
Westinghouse Engineer Transformer. Transformer windings dried quickly and uniformly. 25(4):126, 1965.
Wolff E, Gibert H. Atmospheric freeze-drying. Part 1: Design, experimental investigation and energy-saving advantages. Drying Technology 8(2):385–404, 1990a.
Wolff E, Gibert H. Atmospheric freeze-drying. Part 2: Modelling drying kinetics using adsorption isotherms. Drying Technology 8(2):405–428, 1990b.
Wolff E, Gibert H. Freeze-drying under vacuum and in an adsorbing fluidized bed: influence of operation pressure on drying kinetics. In: Mujumdar AS, Filkova I, eds. Drying '91. Amsterdam; Elsevier Science Publishers, 1991, pp 237–240.
Woodford R, Morrison JC. The diffusion of sennoside A through a cellulose membrane. J Pharm Pharmacol. 21(9):602–606, 1969.
Woods B, Husain H, Mujumdar AS. Techno-economic assessment of potential superheated steam drying applications. Canadian Electrical Association Report 9138U888. Montreal, 1994.
Woods BG. Electrical load reduction via infrasonic enhancement of process heat transfer and drying. Ontario Hydro Research Division. Report 91-68-K. Toronto, 1991.
Woods BG. Sonically enhanced heat transfer from a cylinder in cross flow and its impact on process power consumption. Intl. J Heat Mass Transfer 35(10):2367–2376, 1992.
Yamato Y. Aeration-type rotary dryers. U.S. Patent No. 4,656,759, 1987.
Yamato Y. A novel rotary dryer with through air combination. In: Strumillo C, Pakowski Z, eds. Drying '96. Proc. 10^{10} Intl. Drying Symposium (IDS'96), Krakow, Poland, 1996, pp 627–630.
Yamato Y. Application of a novel rotary dryer (TACO). Tokyo: Yamato Sanko Mfg. Co. Ltd., 1998.
Yamato Y, Terada K, Nakamura B. Drying and incinerating furnaces. U.S. Patent No. 3,824,935, 1974.
Yeo SD, Lim GB, Debenedetti PG, Berstein H. Formation of microparticulate protein

powders using a supercritical fluid antisolvent. Biotechnology and Bioengineering 41:341–346, 1993.

Yongsawatdiguul J, Gunasekaran S. Microwave vacuum-drying of cranberries. J Food Process Preserv. 20:145–156, 1996.

Yoshida T, Hoydo T. Superheated vapor as a drying agent in spinning fiber. Ind. Eng. Chem. Proc. Design and Development 2:53–56, 1963.

Yousif AN, Scaman CH, Durance, TD, Girard B. Flavor volatiles and physical properties of vacuum-microwave- and air-dried sweet basil (*Ocimum basilicum* L.). J Agric Food Chem 47: 4777–4781, 1999.

Zayas Y, Pento V. Drying of thermally labile solutions in acoustic field. Myasnaya Industriya 6:31–33, 1975 (in Russian).

Zbicinski I, Smucerowicz I, Strumillo C, Kasznia J, Stawczyk J, Murlikiewicz K. Optimization and neural modeling of pulse combustors for drying applications. Drying Technology; theme issue on drying and dewatering in energy fields. Kudra T, ed. 17(3):609–633, 1999.

Zgorzalewicz J, Glaser R. Hydrodynamics of a pulsed fluid bed of coarse materials. Chemical and Process Engineering 1:3–21, 1989 (in Polish).

Zinn BT. Tunable pulse combustor. U.S. Patent No. 4,770,626, 1988.

Zinn BT, Dubrov E, Rabhan AB, Daniel BR. Application of resonant driving to increase the productivity and thermal efficiency of industrial processes. Proc. Intl. Symposium on Pulsating Combustion, Monterey, CA, Paper F-4, 1991.

Index